SHORT AND LONG CHAINS AT INTERFACES

Sponsored by:

CEA (Commissariat à l'Energie Atomique)/ DSM
DGA (Ministère de la Défense)
Elf-Atochem
IFP (Institut Français du Pétrole)
Unilever UK
CNRS (Centre National de la Recherche Scientifique)

XVth Moriond Workshop
Villars sur Ollon, Switzerland - January 21-28, 1995

Short and long chains at interfaces
Series: Moriond Condensed Matter Physics

ISBN 2-86332-177-3

EDITIONS FRONTIERES
B.P. 33
91192 Gif-sur-Yvette Cedex - France

Printed in Singapore

Proceedings of the XXXth RENCONTRES DE MORIOND
Series: Moriond Condensed Matter Physics
Villars sur Ollon, Switzerland January 21 - 28, 1995

SHORT AND LONG CHAINS AT INTERFACES

Edited by

J. Daillant
P. Guenoun
C. Marques
P. Muller
J. Trân Thanh Vân

EDITIONS
FRONTIERES

XVth Moriond Workshop on:
Short and long chains
at interfaces

was organized by

J. Trân Thanh Vân (Orsay)

with the active collaboration of :

D. Andelman *(Tel-Aviv)*
M. E. Cates *(Cambridge, UK)*
M. Cohen-Stuart *(Wageningen)*
Y. Couder *(Paris)*
J. Daillant *(Saclay)*
P. Guenoun *(Saclay)*
J-F. Joanny *(Strasbourg)*
C. M. Knobler *(Los Angeles)*
C. Marques *(Strasbourg)*
H. Möhwald *(Mainz)*
P. Muller *(Strasbourg)*
G. Porte *(Montpellier)*
H. Ringsdorf *(Mainz)*
C. Safinya *(Santa Barbara)*
R. K. Thomas *(Oxford)*
M. Tirrell *(Minneapolis)*
E. B. Zhulina *(Saint-Petersbourg)*

95' RENCONTRES DE MORIOND

The XXXth Rencontres de Moriond were held in 1995 in Villars-sur-Ollon, Switzerland, and in Les Arcs 1800, Savoie, France.

The first meeting took place at Moriond in the French Alps in 1966. There, experimental as well as theoretical physicists not only shared their scientific preoccupations but also the household chores. The participants in the first meeting were mainly French physicists interested in electromagnetic interactions. In subsequent years, a session on high energy strong interactions was also added.

The main purpose of these meetings is to discuss recent developments in contemporary physics and also to promote effective collaboration between experimentalists and theorists in the field of elementary particle physics. By bringing together a relatively small number of participants, the meeting helps to develop better human relations as well as a more thorough and detailed discussion of the contributions.

This concern of research and experimentation of new channels of communication and dialogue which from the start animated the Moriond meetings, inspired us to organize a simultaneous meeting of biologists on Cell Differenciation (1970) and to create the Moriond Astrophysics Meeting (1981). In the same spirit, we have started a new series on Condensed Matter Physics in January 1994. Common meetings between biologists, astrophysicists, condensed matter physicists and high energy physicists are organized to study the implications of the advances in one field into the others. I hope that these conferences and lively discussions may give birth to new analytical methods or new mathematical languages.

At the XXXth Rencontres de Moriond in 1995, four physics sessions, one astrophysics session and one biology session were held :

* January 21-28	"Dark matter in cosmology, Clocks and Tests of fundamental laws"
	"Short and long chains at interfaces"
* March 11-18	"Electroweak Interactions and Unified Theories"
	"Clustering in the universe"
* March 19-26	"QCD and High Energy Hadronic Interactions"
	" Rencontre de Biologie - Méribel "

I thank the organizers of the XXXth Rencontres de Moriond :

- E. Adelberger, R. Ansari, G. Chardin, T. Damour, O. Fackler, G. Fontaine, G. Gerbier, Y. Giraud-Héraud, G. Greene, B. Guiderdoni, E. Hinds, J. Kaplan, for the session Dark matter in cosmology, Clocks and Tests of fundamental laws,

- J. Daillant, P. Guenoun, C. Marques, P. Muller for the Condensed Matter Physics session,

- P. Binetruy, A. Blondel, R. Cahn, G. Coignet, L. Fayard, P. Fayet, J.-M. Frère, L. Krauss, L. Moscoso, C. Savoy and C. Verzegnassi for the Leptonic session,

- C. Balkowski, A. Blanchard, S. Maurogordato, M. Moniez, C. Tao for the Astrophysics session,

- E. Augé, P. Aurenche, E. Berger, A. Capella, D. Denegri, L. Montanet, B. Pietrzyck, D. Schiff, and C. Voltolini for the Hadronic session,

- M. Fellous, F. Michel, K. Tran Thanh Van, H. Vaucheret, J.-L. Rossignol and H. Denis for the Biology meeting,

and the conference secretaries : G. Ambonati, C. Andrews, N. Bachala, L. Besson, R. Bilhaut, J. Cordier, A. Jacquet, C. Julliard, A. Lecoeur, I. Mac Leod, D. Loncaric, H. Mauger, F. and N. Osswald, H. Pham, J. Plancy, J. Raguideau, C. Renaud, A. M. Renault-Perrin and N. Romain.

I am also grateful to Mrs S. Müller, Ms B. Gautron, Mr. E. Rocca-Serra, Ms. C. Dufourny, Ms. S. Kovalevsky who contributed through their hospitality and cooperation to the well-being of the participants enabling them to work in a relaxed atmosphere.

These Rencontres were sponsored by the Centre National de la Recherche Scientifique (INSU, SPM and FP), the Institut National de Physique Nucléaire et de Physique des Particules (IN2P3), the Commissariat à l'Energie Atomique (DAPNIA, DRECAM), the Ministère de l'Enseignement Supérieur et de la Recherche (programme ACCESS) and the International Science Foundation. The workshop on Dark matter in cosmology, Clocks and Tests of fundamental laws was also sponsored by the National Science Foundation, the meeting on Short and Long Chains at Interfaces by DGA, Elf-Atochem, IFP, Unilever-UK and the Moriond Astrophysics meeting by the Observatoire de Paris-Meudon, the Université de Paris VII and the Centre National d'Études Spatiales. I would like to express my thanks to their encouraging support.

I sincerely wish that a fruitful exchange and an efficient collaboration between the physicists, the astrophysicists and the biologists will arise from these Rencontres as from the previous ones.

J. Trân Thanh Vân

FOREWORD

Both short and long chain amphiphiles create fascinating and yet ill-understood structures at interfaces. However, approaches are often different when dealing with one or the other compounds and it seemed advantageous to organize some kind of meeting such as this, which has tried to bring together the two communities of soft condensed matter physicists dealing with surfactants and polymers. In addition to the presentation of the most recent results in each field, new interesting subjects which involve chains at interfaces, whatever their length, like mixed systems of chains, biological materials or drag reduction in flows by addition of chain molecules were also extensively debated in this meeting.

Polymers present numerous interfacial conformations according to the nature of interfaces and bulk phases. Charged species in solution have recently received lots of interest for grafted configurations as well as adsorbed/depleted ones. This interest comes both from applied problems (charged species are water soluble) and fundamental questions of coupling between the elasticity of the chain and the distributions of monomeric charges and counterions. Such results are directly related to the questions of polymer adsorption, colloidal protection or chemical synthesis in presence of polymers. Melt systems of diblocks or grafted chains, often cast in the form of thin films, can be also strongly distorted by the proximity of an interface. As a result, many experimental situations lead to local ordering or peculiar monomeric distributions which can be described by scaling or field theories (*Interfacial properties of polymer solutions and polymer melts*). The behaviour of chain molecules at interfaces is also essential in wetting and adhesion phenomena. Effects of flow confinement in ultra-thin films and the adhesive properties of polymers were discussed in a series of papers (*Wetting, adhesion and friction*).

A somewhat different situation arises for short chains at the air-solution interface (Langmuir films) where the number of defects in each chain can be very low. The positional or orientational order is now currently assessed by grazing incidence x-ray diffraction, neutron reflection and Brewster angle microscopy. Large instrument facilities are more and more essential to these investigations. The now very precise experimental results can be compared with weak crystallization Landau approaches and simulations. Theory and simulations are indeed more and more precise and therefore increasingly important. More complex systems (several chains per head, coupling between heads and chain ordering, effects of chirality) are now being also investigated. The better understanding of simple species films allows new original investigations of their mechanical and elastic properties. In particular recent developments enable in-situ manipulation of nano-structures at interfaces (*Two-dimensional assemblies of amphiphilic molecules and macromolecules, Langmuir films, membranes, copolymers...*).

Mixed systems are currently studied as the perturbation of a host phase of short chains by another compound which can be a polymer chain. Another approach of this problem - possibly complementary- is a better understanding of the polydispersity in systems constructed of mixtures of diblock copolymers (*Mixed polymer-surfactant systems*). Of course biological systems always present mixtures of short and long chains which are now studied in this respect. For instance the behaviour of membrane proteins raises many interesting questions. A very different aspect is the understanding of molecular motors where a biological system involving a variety of chain molecules can be understood by using the theoretical tools of statistical physics (*Short and long chains in biology*).

Finally, another aim of the meeting was to direct attention to the problem of chains in hydrodynamic flows (*Hydrodynamics and polymers: turbulence, rheology...*). This question, although rather old, is generally not addressed by people of the polymer and surfactant communities. However examples such as long chains extended in strong flows seem more and more important to people dealing with either friction at interfaces or biological molecules (stretching of DNA molecules for instance).

J. Daillant, P. Guenoun, C. Marques, P. Muller

Contents

I. INTERFACIAL PROPERTIES OF POLYMER SOLUTIONS AND POLYMER MELTS

II. TWO-DIMENSIONAL ASSEMBLIES OF AMPHIPHILIC MOLECULES AND MACROMOLECULES (LANGMUIR FILMS, MEMBRANES, COPOLYMERS,...)

III. MIXED POLYMER SURFACTANT SYSTEMS.

IV. WETTING AND ADHESION.

V. SHORT AND LONG CHAINS IN BIOLOGY.

VI. HYDRODYNAMICS AND POLYMERS (TURBULENCE, RHEOLOGY).

1

INTERFACIAL PROPERTIES OF POLYMER SOLUTIONS AND POLYMER MELTS

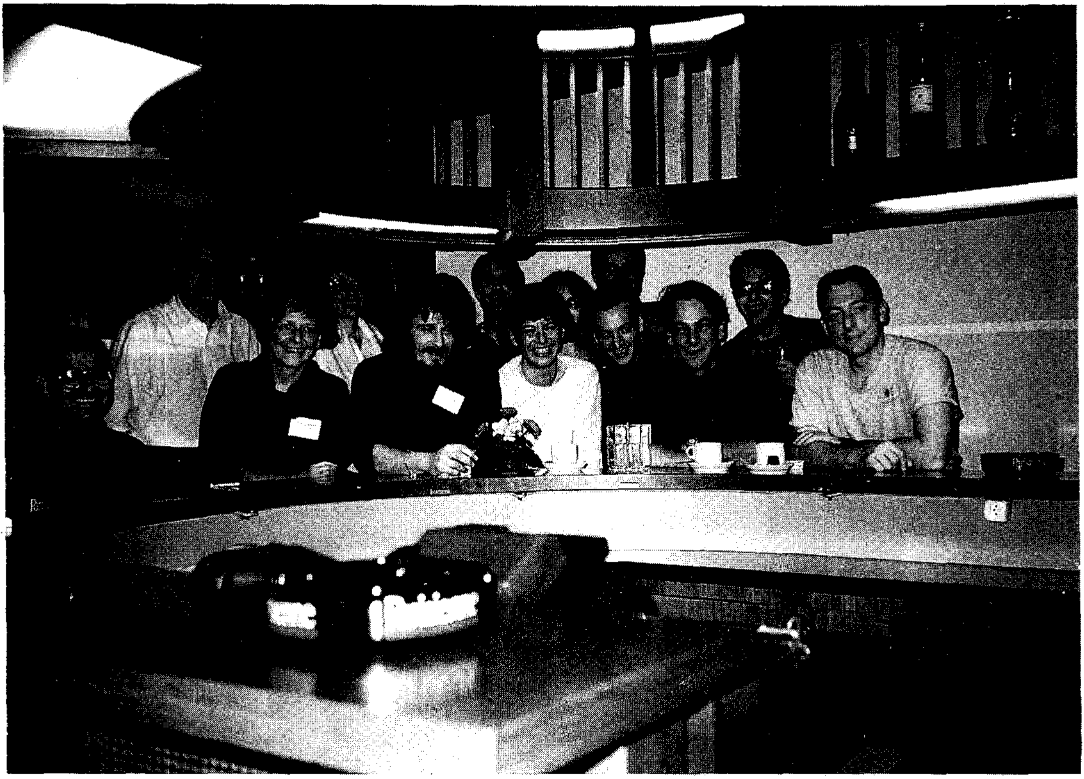

POLYELECTROLYTES ON SOLID SURFACES

M.A. Cohen Stuart

Laboratory for Physical and Colloid Chemistry
Dreijenplein 6, 6703 HB Wageningen,
The Netherlands

ABSTRACT

The simplest way to consider the adsorption of polyions on charged surfaces is as a kind of ion exchange process. Starting from this simplifying viewpoint, some results are deduced that, at first sight, are in reasonable agreement with experimental data. Moreover, a mean-field theory taking chain conformations into account corroborates the picture to a large extent. On closer inspection, however, some data cannot be accounted for in these simple terms. In particular, we discuss pure electrosorption of a polycation on a (net) positive surface, as well as the overcompensation of surface charge that is almost always found in practical systems. Ion correlation effects, as well as kinetically limited adsorption seem to be responsible for these findings.

INTRODUCTION

When charges are present in a macromolecular solution near a surface, several features show up that do not play a role in uncharged systems. If the polymer is charged, the mutual repulsion between the segments opposes accumulation of polymer segments in the surface region. If, in addition, the surface carries a charge, there is an electrostatic contribution to the segment-surface interaction that either promotes or counteracts the adsorption, depending on the sign of the charges. Since electrostatic forces are screened by electrolyte, the salt concentration becomes an important variable. So does the pH if the polyelectrolyte (or the surface groups) are weakly dissociating.

In this paper we shall focus upon systems where polyelectrolytes are attracted to a solid surface by electrostatic forces only. We shall start by taking the viewpoint that this attraction leads to a kind of ion exchange, whereby the small ions that are initially confined to the electrical double layer near the surface are liberated because polyions take their place. We shall investigate the consequences of this viewpoint and check it against experimental observations, in order to find out what shortcomings it has.

ION EXCHANGE

Suppose that a polyelectrolyte chain can be modeled as a rigid polyion of charge Z. Its concentration in solution is c_Z. The solution also contains small ions (concentration c_i) , and we have a surface with a total charge density σ_0 compensated to a large extent by counterions in the double layer; their surface concentration (adsorption) is Γ_i. Consider now the exchange equilibrium between adsorbed polyions (surface density Γ_Z) and small ions at the surface; this will be governed by a Boltzmann factor:

$$\frac{\Gamma_i}{\Gamma_Z}=\frac{c_i}{c_Z}\frac{\exp(e\psi/kT)}{\exp(Ze\psi/kT)} \tag{1}$$

Furthermore, we have an electroneutrality condition, which may be written (neglecting expelled coions):

$$z\Gamma_Z+\Gamma_i=\frac{\sigma_0}{F} \tag{2}$$

Eliminating Γ_i from (1) and (2) we obtain:

$$\Gamma_Z=\frac{\sigma_0}{F}\frac{1}{\frac{c_i}{c_Z}\exp(x-Zx)+Z} \tag{3}$$

where $x = e\psi/kT$.

This equation is extremely crude and ignores many important aspects, such as the strong modification of the charge distribution in the double layer by the polyelectrolyte, the flexibility of the polymer, the contribution of the counterions of the polyelectrolyte, the non-ideality of the electrolyte solution, etc. Nevertheless, it brings out qualitative features that are instructive. Firstly, it shows that the driving force for adsorption is to a large extent entropic: it is accompanied by the liberation of bound counterions from both the surface and the polyion. Secondly, it predicts adsorbed masses as a function of the polymer charge as presented in fig. 1. In this diagram we plot the surface density of monomer units (normalized by the density of elementary surface charges) as a function of the charge on the polymer.

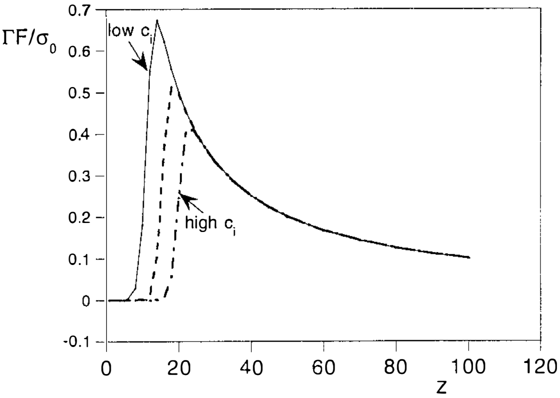

Fig. 1. Normalized adsorbed amount of polymer $\Gamma_z F/\sigma_0$ as a function of the number of charges Z per polymer molecule, calculated on the basis of complete ion exchange (eq. 3), for three different salt concentrations c_i.

As expected, the uncharged polymer does not adsorb, because it cannot exchange any ions with the surface. As soon as Z becomes somewhat larger than unity, however, the polyion density in the surface rises quickly; eventually, it replaces all small counterions. At that point, adsorption cannot rise any more because the number of exchangeable counterions is exhausted. As a consequence, the adsorption follows a line of constant adsorbed charge, i.e. Γ_Z scales like Z^{-1}, the exponential factor in eq. (3) being negligible. We also see that higher concentrations of added electrolyte can shift the complete exchange situation somewhat to higher Z, but when the polyion becomes sufficiently strongly charged, it will always dominate in the surface.

Experimental data seem to corroborate this behaviour. When the charge on the polyion is increased (either by changing pH or by introducing more charged monomers in a random copolymer) the adsorbed amount first rises steeply and then decreases, just as sketched in fig. 1 [1-3].

We can now try to improve on eq. (3) by using a more sophisticated calculation. This is the mean-field polyelectrolyte adsorption theory developed by Böhmer *et al* [4a] on the basis of the lattice formalism for chains at interfaces developed by Scheutjens and Fleer. In this theory, ion concentrations can vary in the direction normal to the interface, and both small ions and polyions can contribute to that density. In addition, the charge density on weak polyions is related to the local proton concentration, whereby it becomes a function of the local potential and the pH in the solution. Within the approximations of this model, the free energy minimum is exactly calculated.

It turns out that the model gives results that are qualitatively very similar to the ion-exchange picture. An example is presented in fig. 2, for 4 different concentrations of monovalent salt. In particular at low ionic strength it is clear that the pattern is strongly analogous to what eq. (3) predicts.

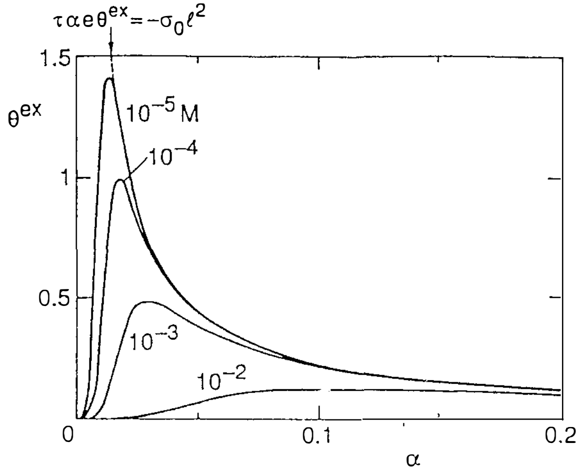

Fig. 2. Adsorbed amount θ^{ex} of a weak polacid consisting of 100 segments as a function of the degree of dissociation of the charged groups, for four different salt concentrations. The arrow denotes the adsorption expected on the basis of ion exchange. Calculated with the mean-field adsorption theory of Böhmer *et al.* [4a], and taken from Van de Steeg *et al.* [4b].

One important consequence of the ion-exchange model is that adsorbed polyelectrolyte layers, though saturated, are much less dense than layers formed by neutral polymers. Part of the surface area remains accessible to neutral polymers, i.e., they form layers with "holes". It should thus be possible to fill the holes in a polyelectrolyte layer with neutral polymer, to an extent depending on the surface charge density, and the polymer charge density. Such mixed adsorption layers have now been observed. In contrast, mixed adsorption layers formed by two different neutral polymers are not stable: one of the polymers will usually adsorb slightly more strongly and displace the other polymer [5-8].

A further consequence of the "layer with holes" picture is that it is difficult to form a brush by adsorption of a diblock copolymer with a charged anchor block. If there is only the slightest tendency for the (neutral) buoy block to adsorb, it will easily do so because the charged anchor block leaves plenty of holes. The adsorbed layer thus formed is thin, and does not provide the steric barrier that is often wanted to overcome long range Van der Waals attraction between surfaces. With neutral diblock copolymers, brush formation can probably be achieved more easily.

COMPLICATIONS

From the discussion above, we are tempted to conclude that our ion-exchange model seems to be able to describe polyelectrolyte adsorption quite well. We have, however, overlooked a number of important complications.

First of all, the charge densities on polymer and surface are not always constant. Many surfaces get their charge from reversible ion transfer processes which are strongly influenced by the surface potential. Therefore the charge can be considerably modified by screening effects. The same applies to weak polyelectrolytes. As a result, the surface + polyelectrolyte system tends to regulate charge, by expelling or taking up protons. Such effects have been studied experimentally, and can be taken into account theoretically in the Böhmer theory.

Another observation which is not so easily accounted for in terms of the mean-field theory is that pure electrosorption of polyelectrolytes can also occur in spite of an average repulsive potential. For example, we have observed that poly(dimethylaminoethyl) methacrylate, a cationic polymer, can adsorb onto positively charged titanium dioxide. Yet, the neutral form of this polymer cannot adsorb, which proves that the polymer-surface interaction is of an electrostatic nature [9]. The data are shown in fig. 3.

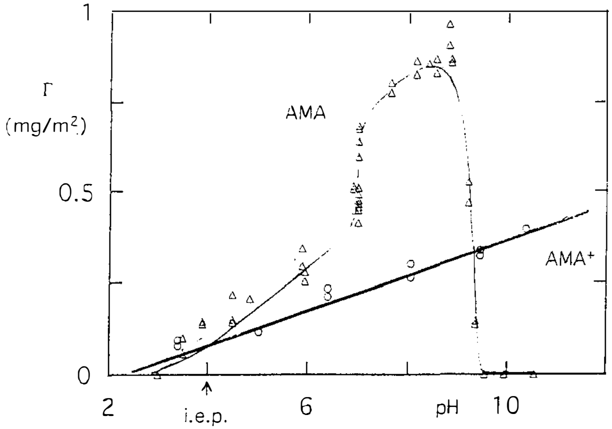

Fig. 3 Adsorbed amount of poly(dimethylaminoethyl methacrylate) on TiO_2 from 0.005 M salt solution, as a function of pH. The point of zero charge of the solid is indicated. For comparison data for the

adsorption of poly (trimethylammoniumethyl methacrylate), which has pH -independent charge, are also shown.

In order to explain this result, we must realize that the net charge on the surface comes from both positive and negative sites. There is one particular pH value (the point of zero charge) where these two populations give contributions to the total charge that are exactly equal, so that the sum is zero. Under other conditions, however, there is no such compensation and there is a net surface charge. There are still both positive and negative sites, though, and this implies that a polymer coming very close to such a heterogeneous surface will see both attracting and repelling sites. Several theoretical studies have dealt with polymers and heterogeneous surfaces. It was found that polymers can readily bind to surfaces which have a net zero adsorption field, and possibly even when the average potential is weakly repulsive [10-12].

OVERCOMPENSATION OF SURFACE CHARGE

With the refinements discussed above taken into account, it would seem that we can construct a fairly succesful theory of polyelectrolyte adsorption. Upon closer inspection of experimental data, however, we discover a major shortcoming. This has to do with the fact that the ion-exchange picture, even when sufficiently refined, is based on the fact that the charge in the adsorbed polymer is equal to the surface charge. This implies that polyelectrolyte adsorption brings the surface close to neutrality, and then stops altogether. Experiments, however, show that polyelectrolytes tend to overcompensate the charge. For a quantitative discussion it is useful to define a stoechiometric factor Q as the ratio between the adsorbed polyelectrolyte charge and the surface charge. Available data suggest that for strongly charged polyelectrolytes Q is always larger than unity, typically by 10-15%, sometimes even much more. In one extensive study on adsorption of random copolymers with charged and neutral monomers, adsorbing on latex particles with fixed charges, it was found that Q depends in a complicated way on the primary structure of the polymer and on the density of charged groups on the surface [13]. The minimum value for Q was found for the case where the average distance between charges on the surface matched that between charges on the polymer. An example, taken from this work, is given in fig. 4. Clearly, the formation of ion pairs is the dominating factor here, and a mean-field description is inappropriate.

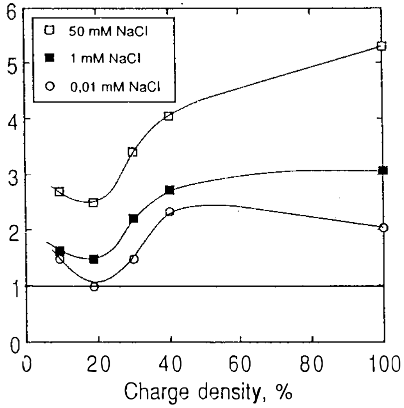

Fig. 4. Ion exchange stoechiometric coefficient Q (= adsorbed charge/surface charge) for cationic copolymers adsorbing on negatively charged polystyrene latex as a function of the fraction of charged monomers per chain (in %), for three different concentrations of added salt (indicated). Taken from ref. 13.

The conclusion that overcompensation of charge is the rule for polyelectrolyte adsorption is further corroborated by the finding that it is possible to deposit positive and negative polyelectrolytes on a surface in alternating order in a perfectly periodic fashion. Such multilayers have been reported notably by Decher *et al.* [14-16].

If we accept the fact that it is not the net surface charge which determines the adsorption, but rather the possibility to form ion pairs between polymer and surface groups, we are led to conclude that aspects like surface and polymer structure are perhaps more important than the net surface charge. Why then do the adsorbed amounts seem to follow the compensation rule at least in an approximate way?

KINETIC FACTORS

The most likely solution of this paradox is that the adsorption is simply kinetically limited by electrostatic repulsion. As long as the surface charge is not compensated, the chains have easy access to the surface, where they can adsorb by ion pair formation. However, as soon as the total charge reverses sign, a repulsive barrier builds up at the solution side of the adsorbed layer which lowers the rate of polymer attachment. As a result, the rate of adsorption falls. It is not difficult to imagine a barrier which almost entirely suppresses adsorption. When this barrier has developed, the adsorbed amount cannot rise any more, even though the situation of lowest free energy has not been reached. This situation is somewhat analogous to the the well-known stability of lyophobic colloids, which consist of charged particles that attract by long range Van der Waalsforces, but cannot aggregate because of an electrostatic barrier. Addition of salt lowers the barrier and induces coagulation. In the same way, addition of salt lowers the barrier to polyelectrolyte adsorption, so that adsorption goes up. Reversing the condition of salt concentration (or pH) does not bring the system back to its initial situation; the process is irreversible.

A quite striking example of this situation is given in fig. 5 where we plot adsorption data for carboxymethylcellulose (CMC) onto hematite (Fe_2O_3) . CMC is a rather stiff molecule that adsorbs tenaciously onto hematite, presumably by means of its hydroxyl groups. When the adsorption is measured at various pH values, a curve is obtained that decays sharply with increasing pH in the range where most of the CMC carboxyl groups dissociate, just as expected for the ion exchange model. However, when the pH is increased after adsorption, no desorption takes place at all, indicating that the adsorption capacity of the surface is much higher than what one obtains during spontaneous adsorption. The most likely explanation is that when the adsorption process stops, this is not because the free energy has come to a minimum, but because the molecules are simply prevented from making contact with the surface by the electrostatic barrier created by the polyelectrolytes already attached.

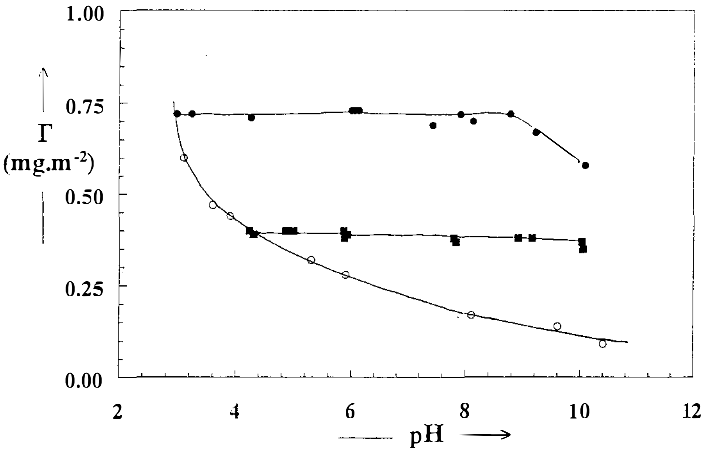

Fig. 5. Amount of carboxymethylcellulose on hematite in 0.01 M NaCl as a function of pH, both directly after adsorption at a given pH, and after adsorbing at a given pH and subsequently increasing the pH. The point of zero charge for hematite is at pH 9.

If kinetic limitation is determining the adsorbed amount, one expects that adsorption will always proceed until a certain surface potential is reached, irrespective of the history of the sample or the nature of the surface. Desorption, however, may occur at a very different potential (or not at all). Hence one expects to find a characteristic adsorption potential, namely the one that is just high enough to stop further adsorption. If polymer is adsorbed in a state of low charge density, and subsequently charged by changing the pH, a higher surface potential is expected. This idea was tested for the AMA /TiO_2 case and found to hold.

CONCLUSIONS AND OUTLOOK

In order to develop more understanding of polyelectrolyte adsorption, the fact that solid surfaces carry charge in the form of discrete ionic groups (which may be more or less mobile) deserves more attention. Correlation effects for heterogeneous surfaces become very important due to the very low energy of ion pairs. Models based upon average potentials, and on electric fields that are homogeneous in a direction parallel to the surface will not be adequate. Some Monte Carlo calculations have treated the adsorbing polyelectrolytes in terms of discrete charges, but the surface charge in terms of an average potential [17]. It should be useful to extend this taking discrete surface charges into account. In addition, the kinetics of the adsorption process must be considered. Barford *et al* [18] developed a theory of polymer adsorption in terms of non-equilibrium configurations, based on the idea that virtually irreversible (ionic) bonds are formed between the surface and charged polymer segments. However, these authors did not consider the kinetics explicitly. New dynamic models such as, e.g., the one developed by Fraaije *et al.* [19] can hopefully cope with this problem in the near future.

ACKNOWLEDGEMENT

The author wants to acknowledge N. Hoogeveen and C.W. Hoogendam for allowing him to make use of their results and for very useful discussions.

REFERENCES

1. T.K.Wang, R. Audebert, *J. Colloid Interface Sci.* **121,** 32-41 (1988).
2. G. Durand, F. Lafuma, R. Audebert, *Prog. Colloid Polymer Sci.* **76,** 278-282 (1988).
3. G. Durand-Piana, F. Lafuma, R. Audebert, *J. Colloid Interface Sci.* **119**, 474-480 (1987)
4a. M.R. Böhmer, O.A. Evers, J.M.H.M. Scheutjens, *Macromolecules* **23** 2288-2301 (1990).
4b. H,G,M, Van de Steeg, M.A. Cohen Stuart, A. de Keizer, B.H. Bijsterbosch, *Langmuir* **8**, 2538-2546 (1992).
5.C. Thies, *J. Phys. Chem.,* **70,** 3783 (1966).
6. H.E. Johnson, S. Granick, *Science* **255**, 966 (1992).
7. P. Frantz, S. Granick, *Langmuir* 8, **1176** (1992).
8. J.C. Dijt, M.A. Cohen Stuart, G.J. Fleer, *Macromolecules* **27**, 3229-3237 (1993).
9. N. G. Hoogeveen, M.A. Cohen Stuart, G.J. Fleer, *Faraday Discuss.* **98**, (in press, 1994).
10. D.Andelman, J.F. Joanny, *Macromolecules* **24**, 6040-6042 (1991).

11. J.F. Joanny, D. Andelman, *Makromol. Chemie, Makromol. Symp.* **62**, 35-41 (1992)

12. D. Andelman, J.F. Joanny, *J.Phys. II France* **3**, 121-138 (1993).

13. L. Eriksson, B.Alm, P. Stenius, *Colloids Surfaces A* **70**, 47-60 (1993).

14. G. Decher, J.D. Hong, *Ber. Bunsenges. Phys. Chem.* **95**, 1430-1431 (1991).

15. G. Decher, J.D. Hong, J. Schmitt, *Thin Solid Films* **210**, 831-835 (1992).

16. Y. Lvov, G. Decher, *Langmuir* **9**, 481-486 (1993).

17. Å. Waltermo. E. Blomberg, P.M. Cleasson, L. Sjöström, T. Åkeson, B. Jönsson, *J. Phys. Chem.* **97**, 11769-11775 (1993).

18. W. Barford, R.C. Ball, C.M.M. Nex, *J. Chem. Soc. Faraday Trans. I* **82**, 3233-3244 (1986).

19. J.G.E.M. Fraaije, *J. Chem. Phys.* **99** , 9202 (1993).

POLYELECTROLYTE SOLUTIONS BETWEEN TWO CHARGED SURFACES

Itamar Borukhov, **David Andelman**(†)
School of Physics and Astronomy
Raymond and Beverly Sackler Faculty of Exact Sciences
Tel Aviv University
Ramat Aviv, Tel Aviv 69978, Israel
and
Henri Orland(*)
Service de Physique Théorique
CE-Saclay
91191 Gif-sur-Yvette, Cedex, France

We investigate the distribution of polyelectrolytes in solution between two charged walls. Such a situation arises, for example, in colloidal suspensions where the polyelectrolytes affect both the aggregation and the stability of the colloidal particles. We consider the case of a good solvent, i.e. in the presence of excluded volume interactions among the monomers. The system is confined between two infinite flat charged walls, making the problem effectively one dimensional. The polyelectrolytes are weakly charged, and several models for the charge distribution are considered. We use a mean field approach to derive two coupled differential equations: a modified *Poisson-Boltzmann* equation for the electrostatic potential, and a *self consistent field* equation for the polymer concentration. The equations are solved numerically. As an example we present a case of competing surface interactions: electrostatic attraction vs. chemical repulsion resulting in a non–monotonic concentration profile. We discuss also the difference between a polymer with a uniform "smeared" charge and one in which the charges are annealed and can redistribute themselves at thermodynamical equilibrium.

(†)Also at: Groupe de Physico-Chimie Théorique, E.S.P.C.I., 10, rue Vauquelin, 75231 Paris Cedex 05, France

(*)Also at: Groupe de Physique Statistique, Université de Cergy–Pontoise, 95806 Cergy–Pontoise, Cedex, France

1 Introduction

We consider an aqueous solution containing charged polymers (*polyelectrolytes*) and small ions (electrolyte) between charged surfaces (Fig. 1). The polymers are positively charged, while the surfaces can be either positive or negative. In addition to electrostatic interactions, we consider excluded volume repulsion between the monomers, and short range (chemical) interactions of the monomers with the surfaces, which can be either attractive or repulsive.

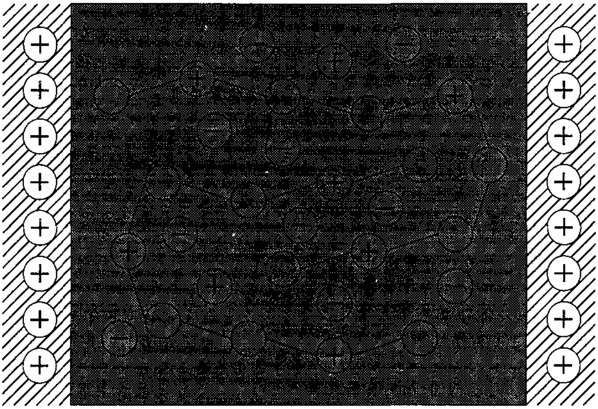

Figure 1: Schematic view of the system.

The motivation for such systems comes from two main sources. The first related system is a colloidal suspension [1, 2, 3], that is, solid particles immersed in an aqueous solution. Polymers may be added to the solution in order to modify the inter-colloidal forces. Some processes, such as waste water treatment and mineral processing, require attraction between the colloids, while other processes, such as ink and paint stabilization, require repulsion [3]. Another related system is a biological one in which proteins (charged macromolecules) affect the interactions between lipid bilayer (biological membranes).

The electrostatics of an *electrolyte* solution between two flat and charged surfaces has been investigated extensively in the frame work of the Gouy–Chapman theory [4], whose starting point is the Poisson–Boltzmann equation. On the other hand, the adsorption (depletion) of *neutral* polymers to (from) one surface and between two surfaces has been also investigated thoroughly, and good understanding was reached [5, 6, 7]. The combination of electrostatic interactions, together with the connectivity of the polymer chain [8], proves to be a complex problem due to the interplay between the short range "chemical" interactions, the polymer conformations (entropy) and the long range (though often screened) electrostatic interactions.

2 Model

We describe the system in a mean field approach through the local electrostatic potential $\psi(\vec{r})$ and the polymer order parameter $\phi(\vec{r})$, related to, $\rho(\vec{r})$, the polymer concentration by $\rho(\vec{r}) = \phi^2(\vec{r})$ [10, 11, 12].

The electrostatic potential is determined by the *Poisson–Boltzmann equation.* For a monovalent electrolyte solution assumed here it can be written as:

$$\nabla^2\psi(\vec{r}) = -\frac{4\pi}{\varepsilon}q(\vec{r}) = \frac{8\pi e}{\varepsilon}c_b \sinh(\beta e\psi) \tag{1}$$

where $q(\vec{r})$ is the charge density determined by the Boltzmann distribution for ions in an electric potential $\psi(\vec{r})$; c_b is the bulk electrolyte concentration, $\beta = 1/k_BT$ where k_B is Boltzmann constant and T is the temperature; e is the elementary charge unit, and ε is the dielectric constant of the solution. Charged polymers and their counter-ions will appear as additional terms on the right hand side of equ. (1).

One way of deriving the Poisson–Boltzmann equation is by writing the free energy as a sum of the electrostatic and entropy of mixing contributions, and then performing a variational procedure [13, 14]. The advantage of this approach is that one can also add the polymer contribution to the free energy and perform the same variational procedure on the total free energy.

At the surfaces, the electrostatic boundary conditions are chosen as fixed surface charge density σ: $\psi'|_s = -\frac{4\pi}{\varepsilon}\sigma$. In a similar way, and depending on the system in mind, one can also choose fixed surface potential as the electrostatic boundary conditions. The effect of the surfaces is screened on a length scale of the Debye–Hückel screening length κ^{-1} (proportional to $1/c_b^{1/2}$), due to the presence of the electrolyte.

For a semidilute solution of polymers the local free energy of the system can be described by [11, 12]:

$$\beta f_{pol}(\vec{r}) \;=\; \frac{a^2}{6}|\nabla\phi|^2 + V(\phi^2) - \mu_p\phi^2 \tag{2}$$

The first term represents the connectivity of the polymer chains, where a is the effective length of one monomer and is roughly of the order of a few Angstroms. The second term represents the polymer interactions. It includes the electrostatic interaction as well as the excluded volume repulsion $\frac{1}{2}v\phi^4$, where $v > 0$ has units of volume and is the excluded volume parameter in good solvent conditions. The last term represents the contact of the system with a polymer reservoir and μ_p is the chemical potential of the polymers.

A variation of the free energy yields the *self consistent field* equation for *neutral* polymers:

$$\frac{a^2}{6}\nabla^2\phi(\vec{r}) = v(\phi^3 - \phi_b^2\phi) \tag{3}$$

where ϕ_b^2 is the bulk polymer concentration. The Edwards correlation length of neutral polymer solutions, as is apparent from equ. (3), is equal to $a/\sqrt{3v\phi_b^2}$ and characterizes the polymer concentration variations in the solution (e.g., close to the wall).

At the surfaces, we use the Cahn boundary conditions [5] to represent the non-electrostatic interaction of monomers with the surface:

$$\frac{1}{\phi}\phi'\bigg|_s = \frac{1}{D} \tag{4}$$

The adsorption length D is inversely proportional to the strength of the surface interaction and is negative (positive) for attractive (repulsive) surfaces.

We return now to the problem of polyelectrolytes where all the contributions to electrostatic and polymer free energy are included. Details are given elsewhere [13, 14].
The contributions of the polymer charges are computed for three models:

- *Smeared*: The charges are uniformly distributed (hence the name "smeared") over the polymer chains. Each monomer has a fractional charge equal to pe. In this case the contribution to the free energy is

$$f_{el}^{(s)} = p\phi^2 e\psi \tag{5}$$

- *Annealed*: Each monomer has a probability p to carry one elementary charge e (and $1-p$ to be neutral). The monomers can ionize or de-ionize dynamically, and thus adjust to the local electrostatic potential [9]. Tracing over the monomer charge degrees of freedom in the partition function results in the following contribution to the free energy:

$$f_{el}^{(a)} = -k_B T\phi^2 \log(1 - p + p\mathrm{e}^{-\beta e\psi}) \tag{6}$$

- *Quenched*: As in the annealed case, each monomer has a probability p to be charged. However, the distribution of the polymer charged is "frozen" (quenched). We will not further discuss here this more difficult case [14] but in many respects we expect this case to be intermediate between the smeared and the annealed cases.

From a variational procedure performed on the full free energy, two coupled equations for the electrostatic potential ψ and polymer order parameter ϕ can be obtained and will replace equ. (1) and equ. (3).

In the smeared case, for example, the Poisson–Boltzmann and the self consistent field equations are modified to become:

$$\nabla^2\psi(\vec{r}) = \frac{8\pi e}{\varepsilon} c_b \sinh(\beta e\psi) - \frac{4\pi e}{\varepsilon}\left(p\phi^2 - p\phi_b^2 \mathrm{e}^{\beta e\psi}\right) \tag{7}$$

$$\frac{a^2}{6}\nabla^2\phi(\vec{r}) = v(\phi^3 - \phi_b^2\phi) + pe\psi\phi \tag{8}$$

Similar equations have been derived for the quenched and annealed cases [14].

3 Results and Discussion

We present two numerical examples of polymer concentration profiles. As our model is effectively one dimensional, the only spatial coordinate left is the distance from the surfaces x whose origin is taken at the mid-plane between the two surfaces.

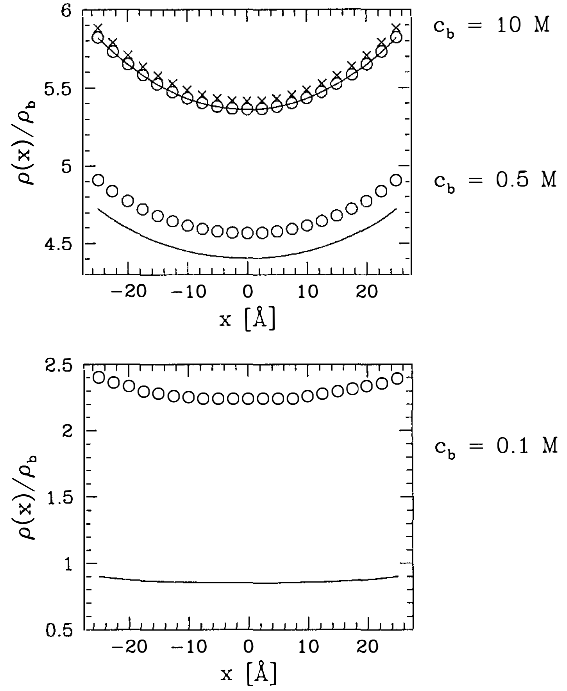

Figure 2: Polymer profiles (rescaled by their bulk value $\rho_b = \phi_b^2$) of the smeared (solid line) and the annealed (circles) cases as function of x, the distance from the surfaces. The three pairs of profiles correspond to three salt concentrations: $c_b = 0.1\,\mathrm{M}$, $0.5\,\mathrm{M}$ and $10\,\mathrm{M}$. The figure is divided into two parts because of the difference in the vertical scales. The line of X's on the top part represents the neutral polymers profile, which is independent of the salt concentration. The polymer parameters used here are: $a = 5\text{Å}$, $v = 125\text{Å}^3$, $\phi_b^2 = 10^{-6}\text{Å}^{-3}$ and $p = 0.001$. The inter-surface distance is 50Å, so that the two surfaces are located at $x = \pm 25\text{Å}$. The surface charge density $\sigma = 1e/500\text{Å}^2$ and the polymer adsorption length $D = -300\text{Å}$.

In the first example (Fig. 2) we compare the polymer concentration profiles of the smeared model (solid line) and annealed model (circles) for three salt concentrations measured in units of mole/litter [M]. The top two pairs of profiles in the figure correspond to high salt concentrations (strong electrostatic screening) while the bottom pair corresponds to a lower salt concentration (weaker electrostatic screening). Beside the three different values of c_b, all other phenomenological parameters used to evaluate the profiles are the same (their values are given in the figure caption). For comparison, we show also at the top of Fig. 2, the profile of neutral polymers with the same adsorption characteristics but which, obviously, is independent of the salt concentration, c_b.

The parameters of Fig. 2 are chosen such that the electrostatic potential is affected only in a negligible way by the presence of polymers [13]. This can be demonstrated by comparing the Debye–Hückel screening length, which varies between 1Å and 10Å, to the Edwards correlation length equal to 260Å. Thus, in this example we concentrated on the effects of the electrostatic potential on the polymer concentration.

The differences between the smeared and annealed models comes from the electrostatic contribution to the polymer part of the free energy (Sec. 2). At low charge density ($p << 1$) and low potentials ($\beta e\psi << 1$), one can expand the annealed free energy in powers of $\beta e\psi$:

$$f_{el}^{(a)} \approx k_B T p\phi^2(\beta e\psi) - k_B T p\phi^2(\beta e\psi)^2 = f_{el}^{(s)} - k_B T p\phi^2(\beta e\psi)^2 \tag{9}$$

Note that the difference between the two free energies is second order in ψ and makes the annealed free energy *lower* than the smeared one. This can be understood simply by observing that the annealing of the polymer charges adds a new effective degree of freedom to the system. Those charge degrees of freedom can adjust according to the local electrostatic potential, and allow a better optimization of the free energy.

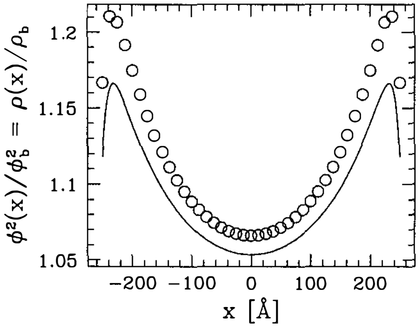

Figure 3: Polymer concentration profiles (rescaled by their bulk value $\rho_b = \phi_b^2$) as function of x, the distance from the surfaces. The smeared (annealed) cases is denoted by solid line (circles). The repulsive short ranged monomer–surface interactions (D = 300Å) competes with the attractive electrostatic monomer–surface interaction ($\sigma = -1e/5000\text{Å}^2$). The polymer parameters used in this example are: a = 5Å, $v = 125\text{Å}^3$, $\phi_b^2 = 10^{-6}\text{Å}^{-3}$ and $p = 0.01$. The bulk salt concentration is c_b = 0.1 M and the inter-surface distance is 500Å so that the two surfaces are located at $x = \pm 250$Å.

In the second example (Fig. 3) we show the result of a competition between short range (chemical) repulsive interactions ($D > 0$) and electrostatic attractive interactions (negative surface charge). We observe a depletion layer near the surface, whereas at larger distances the surface induces an effective adsorption. In this case too, the model parameters have been chosen in such a way so that the electrostatic profile is barely affected by the presence of charged polymers.

Since the difference between the smeared and annealed models is only minor (see Fig. 3), we can consider the simpler smeared case. The polymer behavior can be understood by considering the one dimensional self consistent field equation, equ. (8):

$$\frac{a^2}{6}\phi''(x) = v(\phi^3 - \phi_b^2\phi) + pe\psi\phi \tag{10}$$

As the left hand side of equ. (10) represents the convexity of the profile, the change of behavior should be accompanied by a change of sign in the right hand side of equ. (10). Near the surface the sign of the first derivative of the polymer concentration $\rho(x)$ (which is the same as the sign of the polymer order parameter $\phi(x)$) is determined through the Cahn boundary condition, equ. (5) by the sign of D. For a depletion case, $D > 0$ and $\phi'(x) > 0$ near the left surface. The electrostatic potential is negative at the negatively charged surface, and decays exponentially on a length scale of $\kappa^{-1} = 10$Å. At short distances from the surface the electrostatic part dominates the right hand side of equ. (10) which becomes negative. Thus the profile is convex near the surface as can be seen in Fig. 3. Further away from the surface the electrostatic potential becomes vanishingly small, the polymer part dominates the right hand side of equ. (10), and the profile becomes concave. At the mid-plane between the surfaces the first derivative is zero due to the symmetry of the two surfaces. If the distance between the two surfaces had been much smaller, the profile would have remained convex.

4 Conclusions

In this work, we have investigated concentration profiles of charged polymer chains between two surfaces. We have introduced three models for the charge distribution along the chain. The simplified smeared model is used extensively in the literature as it is easier to handle analytically, but the annealed and quenched models provide a more realistic description of experimental systems. At low electrostatic potentials ($\beta e\psi << 1$) the smeared model provides a good approximation for the annealed model. However, at high electrostatic potentials the difference between the models become significant (see Fig. 2) and should be taken into account. Generally speaking, the annealed charges are less sensitive to the electrostatic conditions, as they can redistribute themselves over the chains according to the local electrostatic potential. The quenched model is considered in more detail elsewhere [14].

We have also investigated the interplay between electrostatic and other interactions such as excluded volume effects in the bulk and short-range interactions between the polymers and the surfaces. In particular, the effect of competing repulsive short-ranged interactions vs. attractive electrostatic interactions has been explored (Fig. 3). We have also seen that further away from the wall the electrostatic interactions dominate as long as they are not screened.

Some possible future directions of research can follow the present study. For example, the osmotic pressure between the two surfaces can be calculated [14] from the local free energy as was done for neutral polymers [6], and compared with experiments. One might also want to extend this work to non-flat geometries, in order to improve the modeling of polyelectrolyte adsorption on colloidal particles. We have considered here fixed surface charge densities, having in mind charged colloids or surfaces. One can also consider situations where the surface potential is externally fixed and induces a variable surface charge density. Finally, it will be interesting to look at polyelectrolyte solutions in a potential gradient (e.g., electrophoresis or electro-osmosis).

Acknowledgments: Partial support from the German-Israeli Foundation (G.I.F.) under grant No. I-0197 is gratefully acknowledged. One of us (IB) would like to thank the Service de Physique Théorique (CE-Saclay) for its hospitality.

References

[1] E. Dickinson and L. Eriksson, *Adv. Coll. Interface Sci.* **34**, 1 (1991) and references therein.

[2] J. F. Joanny, L. Leibler and P. G. de Gennes, *J. Pol. Sci.* **17**, 1073 (1979).

[3] B. Cabane, K. Wong, T. K. Wang, F. Lafuma and R. Duplessix *Coll. and Pol. Sci.* **266**, 101 (1988).

[4] For general references see, for example: J. N. Israelachvili, *Intermolecular and Surface Forces, 2nd ed.* (Academic, London, 1990); E. J. W. Verwey and J. Th. G. Overbeek, *Theory of the Stability of Lyophobic Colloids* (Elsevier, N.Y., 1948); D. Andelman, *Electrostatic Properties of Membranes* in *Handbook of Physics of Biophysical Systems: Structure and Dynamics of Membranes*, Vol. 1, (Elsevier Science B. V., Amsterdam, 1995), pg. 559-602.

[5] P.G. de Gennes, *Macromolecules* **14**, 1637 (1981).

[6] P.G. de Gennes, *Macromolecules* **15**, 492 (1982).

[7] For a review see e.g.: G. J. Fleer, M. A. Cohen Stuart, J. M. H. M. Scheutjens, T. Cosgrove and B. Vincent, *Polymers at Interfaces* (Chapman (Chapman & Hall, London, 1993), chapter 11.

[8] R. Varoqui, A. Johner and A. Elaissari, *J. Chem. Phys.* **94**, 6873 (1991); R. Varoqui, *J. Phys. II France* **3**, 1097 (1993).

[9] E. Raphael and J. F. Joanny, *Europhys. Lett.* **13**, 623 (1990).

[10] S. Edwards, *Proc. Phys. Soc.* **85**, 613 (1965).

[11] P. G. de Gennes, *Scaling Concepts in Polymer Physics* (Cornell Univ., Ithaca, 1979).

[12] J. des Cloizeaux and G. Jannink, *Polymers in Solution: Their Modeling and Structure* (Oxford Univ., Oxford, 1990)

[13] I. Borukhov, *M.Sc. Thesis* (Tel-Aviv University, 1994), unpublished.

[14] I. Borukhov, D. Andelman and H. Orland, to be published.

ANNEALING EFFECTS IN POLYELECTROLYTE BRUSHES

E.B.Zhulina, T.M.Birshtein, O.V.Borisov
Institute of Macromolecular Compounds Russian Academy of Sciences
199004 St.-Petersburg, Russia

Abstract

Scaling analysis is used to consider the effect of pH on the equilibrium behaviour of ionisable polymer brush. It is shown that under the conditions when the local pH' is noticeably smaller than the bulk pH value, the brush thickness H scales as $H \sim s^{1/3}$, where s is the grafting area per chain. For the base-added solutions both pH and H increase rapidly with increasing concentration of sodium ions in the bulk solution. Addition of acid (HCl) does not noticeably effect the brush characteristics provided that $pH' < pH$.

1 Introduction

Due to the long-range character of electrostatic interactions, even weakly charged polyelectrolytes can exhibit qualitatively new features with respect to neutral systems. Typical example is a polymer brush formed by weak polyacids or polybases. The adjustment (annealing) of the degree of ionisation of polymer chains in such brushes to the variation of the external conditions (pH and/or the ionic strength of solution) can manifest itself in peculiar behaviour of the system. The most spectacular effect of charge annealing is the non-monotonic dependence of the brush thickness on the grafting density and/or the ionic strength of the solution.

Theoretical investigations of the annealed vs. quenched polyelectrolyte brushes are based on the scaling type analysis$^{1,2)}$ and the self-consistent field approaches$^{3-5)}$. The scaling analysis$^{1)}$ provides the asymptotical power law dependencies for the averaged brush properties (the degree of ionisation, the brush thickness, etc) on the parameters of the system (molecular weight and the grafting density of the chains in the brush, the bulk degree of ionisation and the ionic strength of solution). The more refined self-consistent field approaches$^{3-5)}$ provide more detailed information about the distributions of polymer units and the mobile ions in the system, as well as the corresponding electrostatic potential. These publications demonstrate that in a certain range of parameters variation (increase) of ionic strength of solution, J, results in an increase in the degree α of brush ionisation and corresponding increase in the brush thickness. The same holds for the variation (decrease) of the grafting density $1/s$; brushes with the higher value of the area per chain s can have higher values of the brush thickness H. Such behaviour is quite different from the conventional behaviour of the quenched systems; at the fixed degree of ionisation quenched polyelectrolyte brushes can only diminish their thickness with increasing J and s. These publications demonstrate also that the most pronounced difference in the behaviour of the quenched and the annealed brushes is expected when the degree of chain ionisation in the bulk solution is high, $\alpha_b \simeq 1$, whereas the chains in the brush are only weakly charged, so that their degree of ionisation $\alpha << 1$. In this paper we focus on this situation and use the scaling type analysis, to consider the effect of pH on the equilibrium brush behaviour. (Our previous work$^{1)}$ was focused mainly on the effect of ionic strength of solution, some preliminary scaling results on the pH effect are reported in the forthcoming publication$^{2)}$).

2 Model

We consider a layer formed by homopolyacid chains $(HA)_N$ consisting of $N >> 1$ symmetrical units of the size a grafted at one end onto impermeable planar surface with the grafting density $1/s$ chains per unit area (Figure 1). The chains are assumed to be flexible, so that the Kuhn segment of a chain, l, is equal to a, and the Bjerrum length $l_B = e^2/\epsilon kT$

is approximately the same as a chain unit length, $l_B/a \approx 1$. Here ϵ is the dialectric constant of water and kT is the thermal energy. Throughout this paper we use the box model of the brush[6)], according to which all the chains in the brush are stretched homogeneously and their free ends are localised at the outer boundary of the brush.

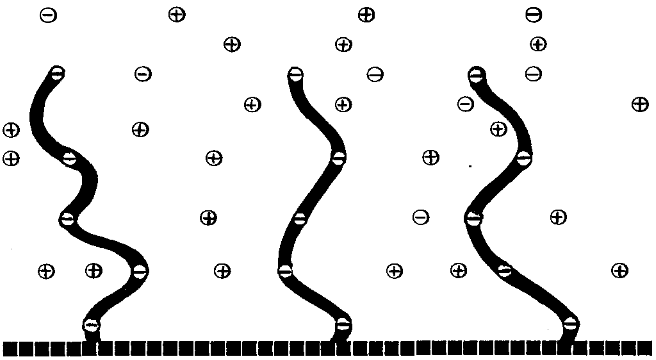

Figure 1. Polyelectrolyte brush immersed in water solution.

The brush is immersed in a water solution of the low molecular weight acid (HCl) or the base (NaOH). Variation of the acid or base content in the bulk solution provides the corresponding variation of the $pH = -log(C_H)$ of the solution, where C_H is the concentration of the mobile protons. For pure water $C_H = C_* = 10^{-7}$. The dissociation of the acid groups in the bulk solution

$$AH \longleftrightarrow A^- + H^+ \tag{1}$$

is determined by the dissociation constant k and the concentration of protons C_H,

$$\frac{\alpha_b}{1-\alpha_b} = \frac{k}{C_H} \tag{2}$$

We assume that $k = const$ is independent of the degree of acid ionisation α_b and determines the value of $pK = -log(k)$. Variation of $pH > pK$ provides high values of the degree of ionisation, $\alpha_b \simeq 1$. We assume also that $pK < 7$ and, thus, in pure water the polyacid chain is highly charged. Let C_{Na} and C_{Cl} be the fixed concentrations of positively and negatively charged ions originating from the dissociation of the added base NaOH or acid HCl. Addition of the sodium ions $C_{Na} > C_*$ shifts the ionisation equilibrium to the higher values of α_b: the concentration of mobile protons diminishes as

$$C_H \approx \frac{C_*^2}{C_{Na}} \tag{3}$$

whereas the addition of acid leads to a corresponding increase in C_H as

$$C_H \approx C_{Cl} \tag{4}$$

However, for the range of $pH > pK$ we can ignore the variation of α_b with pH and consider $\alpha_b \approx 1$.

The degree of ionisation of the grafted polyacids in the brush is determined by the local concentration of protons inside the brush, C'_H, which is always higher than that in the bulk solution, $C'_H > C_H$. Correspondingly, the value of α determined by the active mass law

$$\frac{\alpha}{1-\alpha} = \frac{k}{C'_H} \tag{5}$$

is always lower than the bulk value, $\alpha < \alpha_b$. When $C'_H > C_H$ and α is only slightly smaller than α_b, the behaviour of the brush is vertually the quenched brush behaviour with $\alpha \approx 1$. As it was shown previously⁷⁾, the scaling behaviour of such systems is rather primitive; the chains are nearly totally stretched and strongly oriented normaly to the surface, so that the brush thickness $H \approx aN$. This scaling dependence holds for a wide range of grafting densities comprising the range of individual grafted polyions ($s > a^2N^2$), where the weakening of the orientational effects diminish H by the numerical factor of the order of unity. However, when $C'_H \gg C_H$ and $\alpha \ll \alpha_b$, the degree of the brush ionisation starts to depend on the parameters of the system via C'_H, and one finds the much more varied annealed brush behaviour which is the subject of the present consideration.

3 Charge Balance

The interconnection of C'_H with the parameters of the system is determined by the particular regime of the polyelectrolyte brush. As was demonstrated previously⁸⁾, within the scaling approximation one can distinguish between two electrostatically different states of the brush: the brush can be either electroneutral (the so called⁷,⁸⁾ osmotic brush regime (OsB)), or barely charged (the so-called⁷⁾ Pincus brush regime PB and the regimes of individual charged chains which we refer here as CC regime). The first (electroneutral) state of the brush is attained at relatively high surface charge $\alpha N/s$ when high electrostatic potential due to the charged grafted chains prevents mobile protons from leaving the brush. The electroneutrality condition implies

$$C'_H + C'_{Na} = \alpha C + C'_{OH} \tag{6}$$

for the base added solution, and

$$C'_H = \alpha C + C'_{Cl} + C'_{OH} \tag{7}$$

for the acid added solution. Here $C = N/sH$ is the concentration of polymer units and $C'_{OH} = C_*^2/C'_H$ is the concentration of OH groups in the brush. The interconnection between C'_i and C_i $(i = Na, H, Cl)$ is given by the Donnane rule:

$$\frac{C'_H}{C_H} = \frac{C'_{Na}}{C_{Na}} = \frac{C_{Cl}}{C'_{Cl}} \tag{8}$$

Thus, one obtains from eqs.(6),(8), (3) and (4),

$$\alpha C \approx C'_H \frac{C_{Na}^2}{C_*^2} \qquad \alpha C \gg C_{Na} \tag{9}$$

and

$$\alpha C \approx C'_H \qquad \alpha C \gg C_{Cl} \tag{10}$$

for the base and the acid added solutions, correspondingly. Equations (9) and (10) relate the degree of the brush ionisation α with the polymer concentration C and the concentration of the mobile protons C'_H in the brush under the conditions of the OsB regime. Together with the active mass law, eq.(5), they give

$$\alpha \approx \frac{C_{Na}}{C_*}\sqrt{\frac{k}{C}} \qquad \alpha C \gg C_{Na} \tag{11}$$

and

$$\alpha \approx \sqrt{\frac{k}{C}} \qquad \alpha C \gg C_{Cl} \tag{12}$$

for the base and the acid added solutions, correspondingly. As is seen from eq.(12), α is not sensitive to the diminishing of pH of the solution in the range $\alpha C \gg C_{Cl}$. This is due to the fact that an increase in the bulk concentration of protons slightly effects the local concentration of protons in the brush, $C'_H \gg C_H$. However, even small addition of the sodium ions $C_{Na} > C_*$ in solution induces rapid increase in α according to eq.(11) due to the substitution of protons by sodium ions inside the brush and increasing the local pH'.

The second (charged) state of the brush is attained at relatively weak surface charge $\alpha N/s$, when nearly all mobile ions leave the brush forming together with the negatively charged brush the electric double layer of characteristic thickness

$$\lambda = \frac{s}{l_B \alpha N} \gg H \tag{13}$$

Under these conditions only the small fraction of all mobile protons is localised inside the brush and one should apply the electroneutrality condition to the whole double layer. This leads to the substitution of the term $\alpha C = \alpha N/sH$ in eqs.(6),(7) and (9) by the term $\alpha N/s\lambda = l_B\alpha^2 N^2/s^2$, and one obtains

$$\frac{l_B \alpha^2 N^2}{s^2} \approx C'_H \frac{C_{Na}^2}{C_*^2} \tag{14}$$

and

$$\frac{l_B\alpha^2N^2}{s^2} \approx C'_H \tag{15}$$

for the base and the acid added solutions, correspondingly. With the account of eq.(8) we have finally

$$\alpha \approx (\frac{ks^2C^2_{Na}}{l_BN^2C^2_*})^{1/3} \tag{16}$$

$$\alpha \approx (\frac{ks^2}{l_BN^2})^{1/3} \tag{17}$$

Equations (16) and (17) determine the degree of the brush ionisation α in the PB and the CC regimes.One can see the same tendency as discussed earlier: decreasing pH does not effect the degree of brush ionisation, eq.(17), whereas increasing the content of the sodium ions leads to rapid increase in α, eq.(16).

4 Force Balance

In order to obtain the equilibrium dimensions of the brush we consider the balance of various forces applied to the grafted chains: the elastic force f_{conf} arising in the stretched chains, the force f_{conc} due to the nonelectrostatic (volume) interactions and the electroatatic force f_{elec}. Both f_{elec} and f_{conc} tend to stretch the brush, whereas f_{conf} opposes this stretching. Thus, the force balance implies

$$f_{conf} = f_{conc} + f_{elec} \tag{18}$$

For simplicity, we restrict ourselves with consideration of rather sparse brushes where the short-range nonelectrostatic interactions can be neglected with respect to the electrostatic repulsion between polymer units, and , thus,

$$f_{conf} \approx f_{elec} \tag{19}$$

Assuming Gaussian elasticity for the grafted chains one gets

$$f_{conf}/kT \simeq \frac{H}{a^2N} \tag{20}$$

As was shown earlier[7,8)], the value of the electrostatic force is goverened by the ratio H/λ. At $H/\lambda \ll 1$ when the brush is virtually electroneutral, f_{elec} is determined by the difference in osmotic pressures of the mobile ions inside and outside the brush (OsB regime),

$$f_{elec}/kT \simeq \alpha CS \tag{21}$$

At $H/\lambda \gg 1$ when the brush is nearly barely charged and the intermolecular repulsion dominates over the intramolecular interactions (PB regime), f_{elec} can be calculated as[7)]

$$f_{elec}/kT \simeq \frac{l_B\alpha^2N^2}{s} \tag{22}$$

However, when the brush splits into separate nonoverlapping polyions and the intramolecular electrostatic repulsion becomes the dominating factor in the chain stretching (CC regime),

$$f_{elec}/kT \simeq \frac{l_b\alpha^2N^2}{H^2} \tag{23}$$

where H is the end-to-end distance of a polyion and the characteristic brush thickness at low grafting densities $s \gg H^2$. We do not consider the CC regime here and restrict ourselves with the OsB and PB regimes only.

Force balance together with the equations (11), (12), (16) and (17) provides the final expressions for the equilibrium brush thickness H and the degree of ionisation α.

ACID ADDED SOLUTION

As is seen from the eqs.(12),(17), decreasing $pH < 7$ does not effect the brush ionisation with respect to the pure water case: α is determined by the local $pH' = -log(C'_H) < pH$. Depending on the molecular weight of the grafted polyacids, one can find the two main electrostatic regimes OsB and PB. In the OsB regime the force balance (eqs.(21) and (20)) gives

$$H \simeq a\alpha^{1/2}N \qquad C \simeq \alpha^{-1/2}/as \tag{24}$$

where α is given by eq.(12). Correspondingly,

$$H \simeq a^{4/3}(ks)^{1/3}N \tag{25}$$

$$\alpha \simeq (aks)^{2/3} \tag{26}$$

In the PB regime (eqs.(20),(22)) one has

$$H \simeq \frac{\alpha^2a^3N^3}{s} \tag{27}$$

and using the equation (17) for α one gets

$$H \simeq \frac{k^{2/3}s^{1/3}N^{5/3}}{l_B^{2/3}} \tag{28}$$

It is interesting to note that in both OsB and PB regimes H and α scale with s in a similar way: $H \sim s^{1/3}$ and $\alpha \sim s^{2/3}$. This means that the boundary between the two regimes does not depend on s, but is determined by the parameters k and N; at $a^4kN^2/l_B \gg 1$ the brush is in the OsB regime, whereas at $a^4kN^2/l_B \ll 1$ the brush is found in the PB regime. Increasing area per chain s leads to an increase in the local pH' in both regimes and, thus, the range of s where the peculiar dependence $H \sim s^{1/3}$ can be expected, is limited from above. It is also limited from below, since at small s the nonelectrostatic interactions provide the quasineutral behaviour of the brush with $H \sim s^{-\beta}$ where $\beta > 0$[7].

BASE ADDED SOLUTION

As was already mentioned above, even small addition of NaOH in the bulk solution leads to noticeable increase of the brush ionisation. Under the conditions of the OsB regime where H and α are given by eqs.(24) and (11), one gets

$$H \simeq a^{4/3}(ks)^{1/3}N\frac{C_{Na}^{2/3}}{C_*^{2/3}} \tag{29}$$

$$\alpha \simeq (aks)^{2/3}\frac{C_{Na}^{4/3}}{C_*^{4/3}} \tag{30}$$

In the PB regime one gets from eqs.(27) and (16)

$$H \simeq \frac{k^{2/3}s^{1/3}N^{5/3}}{l_B^{2/3}}\frac{C_{Na}^{4/3}}{C_*^{4/3}} \tag{31}$$

$$\alpha \simeq (\frac{ks^2C_{Na}^2}{l_BN^2C_*^2})^{1/3} \tag{32}$$

It is interesting to note that in the PB regime H increases with C_{Na} more rapidly than in the OsB regime. Thus, by varying the concentration of NaOH in the bulk solution, it is possible not only to affect the brush thickness, but also change the elecrostatic state of the brush. However, due to rapid increase in pH' and α with increasing C_{Na} , the dependencies (29)-(32) are expected to be valid in a rather limited range $pH' < pH$. At $pH' \approx pH$ the annealing effects disappear and the brush maintains the quenched type behaviour with $\alpha \approx \alpha_b$.

5 Conclusions

Using scaling type analysis we have demonstrated that variation of pH of the bulk solution can affect considerably the ionisation equilibrium in the brush. Unusual behaviour of the brush thickness ($H \sim s^{1/3}$)is expected when the local pH' in the brush is noticeably lower than the bulk pH value. Under these conditions the decrease in pH due to addition of acid into the bulk solution does not affect considerably pH' and the brush behaviour;α decreases only slightly ($\alpha \sim C_{Cl}^0$ in both OsB and PB regimes). For base added solutions even small addition of sodium ions leads to rapid increase in pH', $\alpha \sim C_{Na}^{4/3}$ and $\alpha \sim C_{Na}^{2/3}$ for the OsB and PB regimes, correspondingly. As was demonstrated earlier$^{1)}$, addition of small amounts of salt molecules (NaCl) into the bulk solution also shifts the ionisation equilibrium in the brush: α scales with $C_{Na} = C_{Cl}$ as $\alpha \sim C_{Na}^{2/3}$ and $\alpha \sim C_{Na}^{1/3}$ in the OsB and PB regimes, correspondingly. This increase in α is less rapid than for the base added solutions. The origin of an increase of the brush ionisation is due to the fact, that though salt molecules do not affect the pH bulk value, sodium ion substitute partially protons in the brush similarly to the case of the base added solutions. The effect is, however, less strong.

It is interesting to note that addition of small amounts of very different substances (acid, base and salt) does not affect universal scaling of the brush thickness H with the grafting density, $H \sim s^{1/3}$. Increasing s and diminishing concentration of immobilised charge αC in the brush always leads to an increase in the local pH', additional brush ionisation and corresponding additional swelling.

The annealing effects considered in this paper are of rather general character. They are possible in various polymer systems with immobilised charge, such as, for example, polyelectrolyte gels, charged micelles, cells etc. One can formulate the general requirements to the systems where the described annealing effects can be expected:

- The system can be subdivided into two subsystems separated by a "membrane" which is permeable for the mobile ions and the solvent, but is impermeable for the immobilised charge. The two subsystems are in the thermodynamic equilibrium with each other;
- Presence of the immobilised charge within one of the subsystems. The value of the immobilised charge is not fixed, but is determined by the equilibrium requirements for both subsystems;
- The membrane is flexible and permits variation of the subsystem dimensions. The geometry and dimensions of the subsystem with the immobilised charge provide its electroneutrality.

Though particular scaling laws will be different for different systems, the sign of the predicted annealing effects is expected to be invariant with respect to the physical nature of the system.

6 Acknowledgement

This work was partially supported by the Russian Fund of Fundamental Research (grant N93-03-5797) and International Science Foundation (grant NT8000).

7 References

1. E.B.Zhulina, T.M.Birshtein, O.V.Borisov Macromolecules 1995,**28**, 1491.
2. T.M.Birshtein, E.B.Zhulina, O.V.Borisov Polymer Science USSR, (in press).
3. R.Israels, F.A.M.Leemakers, G.J.Fleer Macromolecules 1994,**27**, 3087.
4. S.Misra, S.Varanasi J.Coll.Int.Sci. 1991,**146**, 251.
5. Yu.V.Lyatskaya, F.A.M.Leemakers,G.J.Fleer, E.B.Zhulina, T.M.Birshtein Macromolecules 1995 (in press).
6. S.J.Alexander J.Physique 1977,**38**, 983.
7. O.V.Borisov, T.M.Birshtein, E.B.Zhulina Macromolecules 1994,**27**, 4795.
8. P.Pincus Macromolecules 1991,**24**, 2912.

ADSORPTION OF CHARGED DIBLOCK COPOLYMERS ON SILICA FROM AQUEOUS SOLUTIONS

Catherine Amiel *
Laboratoire de Physico-Chimie des Biopolymères, CNRS, 2-8 rue H. Dunant, 94320 Thiais France.

Mohan Sikka, James W. Schneider, Matthew Tirrell
Department of Chemical Engineering and Material Science, University of Minnesota, Minneapolis, MN 55455, USA.

Jimmy W. Mays
Department of Chemistry, University of Alabama at Birmingham, Birmingham, AL 35294.

* To whom correspondance should be addressed

ABSTRACT

We have studied the adsorption of a water soluble diblock copolymer, poly(t-butylstyrene)-sodium poly(styrene sulfonate) (PtBS-NaPSS), on silica surfaces in aqueous solutions. The block copolymers used were compositionally assymmetric, with large, hydrophilic, PSS blocks and small, hydrophobic, PtBS blocks in order to ensure their water solubility. Materials with molecular weights of 87,000 and 160,000 g/mol were used. Kinetics of adsorption and adsorbed amounts were measured by in situ ellipsometry.

Adsorption could not be observed in pure water without added salt (NaCl). When the NaCl concentration was increased to 1M, adsorption could be readily observed. The adsorption behaviors of NaPSS homopolymers and PtBS-NaPSS copolymers of approximately the same PSS size have been compared: copolymer adsorbed amounts at equilibrium were significantly higher than for the homopolymers. Moreover, homopolymers completely desorb in pure water whereas no desorption in pure water was oberved for the copolymers. This demonstrates the role of the uncharged block in anchoring the diblock at the solid surface. The kinetics of adsortion showed a two stage process: an initial diffusion-limited stage, followed by a slower buildup of surface coverage in a brush-limited stage.

INTRODUCTION

Polymer brushes, i.e structures formed when polymer chains are tethered by one end to a solid surface, are extensively studied either theoretically and experimentally since the last ten years. The behavior of neutral brushes under various conditions is rather well understood [1] . At the contrary, polyelectrolyte brushes have been investigated to a lesser extent than neutral ones [2, 3]. Long range electrostatic interactions have then to be taken into account. The relative locations of the brush counterions define roughly two different types of behaviors: strongly charged brush when the counterions are located outside the brush or quasi neutral brush when the counterions are trapped inside the brush. The number of parameters that have to be considered is larger than in the neutral case: besides the classical ones which are the chain length and the grafting density, there are the parameters associated with the charge state of the chains: degree of charge and charge statistics along the chain (annealed or quenched charges) and the salt concentration of the aqueous solution.

Only few experimental works have been done in this area. Different pathways can be choosen for the synthesis of a charged brush: - synthesizing a neutral brush and post-ionizing the mobile chains, - grafting charged chains to the surface or - adsorbing diblock copolymers where one part is hydrophobic and is playing the role of an anchor by collapsing on the solid surface and the other polyelectrolyte. We have chosen the latter pathway with the use of poly(t-butylstyrene)-sodium poly(styrene sulfonate) copolymers. The aim of the present work is to study the conditions of their adsorption on silica surfaces. An ellipsometric set-up allows to measure the adsorbed amounts and to follow the kinetics of adsorption.

MATERIALS AND METHODS

Diblock copolymers of poly(t-butylstyrene)-sodium poly(styrene sulfonate) (PtBS-NaPSS) have been synthesized using methods described elsewhere [4]. These diblock copolymers are compositionnaly assymetric, with a small hydrophobic block and a large hydrophilic tail in order to ensure their water solubility. A NaPSS homopolymer of molecular weight 10^5 g/mol was also used. It was purchased from Polysciences Inc. The molecular characteristics of the polymers used in this study are summarized in table 1.

Sample	M_w (g/mol)	M_w/M_n	% sulfonated on PSS block	N_{NaPSS}	N_{PtBS}
MT2	87 000	1.03	89	404	26
MT3	160 000	1.04	87	757	27
NaPSS	100 000	1.1	90	485	---

Table 1: Polymer Molecular characteristics

Polymer solutions were prepared by dissolution in distilled water and equilibration for at least one week before any adsorption experiment. To avoid dust particles, they were filtered through 0.6 or 0.8 μm polycarbonate membrane filters from Nuclepore Inc. prior to each use.

Silica surfaces for adsorption were prepared from polished silicon wafers (Virginia Semi conductor Co). Dense oxide layers of ca 1500 Å have been thermally grown on these wafers and the surfaces were cleaned of any organic contamination using an UV lamp before each experiment.

The experimental set up which is described in detail elsewhere [4] was using a SOPRA ES4G spectroscopic ellipsometer. The experiments were performed using a specially built quartz cell, allowing in situ adsorption measurements. The wavelength and angle of incidence were held at a fixed value $\lambda = 589.9$ nm and $\theta = 75.5$ °. The ellipsometer readings Δ and Ψ correspond to the change, on reflection, of the relative phase and amplitude of the p and s components of the light wave. Data are analyzed assuming a homogeneous layer for the polymer film (figure 1).

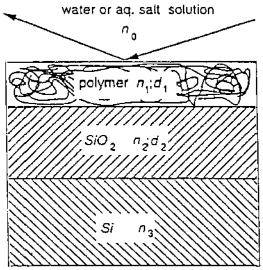

Figure 1: Multilayer model of adsorbed homogeneous polymer layer

The refractive index n_l and the layer thickness d_l are determined from the basic eqution of the ellipsometry:

$$\tan(\Psi)\, e^{(i\,\Delta)} = f(n_0, n_1, d_1, n_2, d_2, n_3, \lambda, \theta) \qquad (1)$$

n_2, d_2 and n_3 were measured prior to any experiment. The refractive index of the solution n_0 was estimated from the contribution of all solution components. The equation (1) is a complex non linear equation which is impossible to invert directly. Rather, an iterative procedure has been used to determine the family of solutions $\{n_1, d_1\}$ which agreed to the experimental values. Since the contrast between the refractive indices of the solution and the polymer layer is low and taking into account the uncertainty in the ellipsometric angles (0.1°), unique values of n_1 and d_1 could not be found for any data set. However, their product, which is related to the adsorbed amount of polymer A was found to be invariant:

$$A = d_1 * (n_1 - n_0) / (dn/dc)_P \qquad (2)$$

$(dn/dc)_P$ is the refractive index increment of the polymer solution.

RESULTS

The adsorption experiments have been conducted in the following way: as soon as the polymer solution was introduced in the cell containing the silica surface, the ellipsometric measurements were taken as a function of time until an equilibrium was attained (constancy of the optical readings). The polymer solution was then drained and replaced with pure water. Ellipsometry measurements were taken again during ca 10 hours in order to check a possible desorption in pure water. Again the pure water was replaced by an aqueous solution having the same salt concentration as the initial polymer solution and measurements were taken. Experimental data were then analyzed and adsorbed amounts were calculated. The average associated error was about 10%.

Adsorbed amounts at equilibrium: the adsorbed amounts at equilibrium are reported on table 2 for each of the polymer system studied.The following observations can be made from these results:

- No adsorption can be observed in pure water, for any of the polymers studied (homopolymer or copolymers). All of them have a polyelectrolyte moiety which should be highly charged because electrostatic screening is very weak in pure water. The repulsion between the charged groups along the chains seems to inhibit the accumulation of the polymers on the solid surface. Moreover, there should exist also a weak repulsion between the polymers and the surface because the silica surfaces are slightly negatively charged under the experimental conditions.

- At a NaCl salt concentration of 1 M, non negligible adsorbed amounts are measured in all the cases. The Debye screening length associated with this salt concentration is of the order of 3 Å at 25 °C. This value is comparable to the monomer length (NaPSS moieties are almost 100% sulfonated) and lower than the Bjerrum length (~ 8 Å). This means that the electrostatic repulsions between the charged groups along the chains are screened. The conformational and aggregation properties of the polyelectrolyte arms should resemble those of a neutral chain in moderate-to-good solvent conditions.

Polymer sample	Adsorption medium	Concentration (ppm)	Adsorbed amounts before rinsing (mg/m^2)	Adsorbed amounts after rinsing with water (mg/m^2)
NaPSS	water	60	—	—
NaPSS	1 M (NaCl)	60	0.45	0.45
MT2	water	60	—	—
MT2	1 M (NaCl)	60	2.1	1.9
MT3	water	60	—	—
MT3	1 M (NaCl)	60	1.8	1.9
MT3	1 M (NaCl)	300	1.8	1.8

Table 2: Adsorbed amounts for polymers

- Adsorbed amounts are 4-5 times higher for MT2 than for NaPSS homopolymer of molecular size comparable to that of the charged block in MT2, for adsorption of a 60 ppm solution in 1 M salt. This indicates that the short, hydrophobic, PtBS block in MT2 plays a role in anchoring the block copolymer to the silica surface. This can be interpreted as a collapse of the hydrophobic blocks onto the solid surface in order to minimize their unfavourable contact with the aqueous solution.
- No influence of the polymer concentration on the final adsorbed amounts were observed for MT3 by increasing the initial polymer concentration from 60 ppm to 300 ppm.
- The adsorbed amounts calculated for the block copolymers stay unchanged, within experimental error, before and after 10 hours contact with pure water. This absence of desorption in pure water shows that the adsorption energy of the hydrophobic block is large enough to compensate for the repulsive polymer surface interactions due to electrostatic repulsions between the charged groups.

It is interesting to see how those first results compare with model predictions. N. Dan et al have developped a scaling model for the adsorption of a charged-neutral copolymer on solid surfaces in aqueous solutions ^{5}. This model applies in a range of moderatly high salt concentrations, allowing a description similar to the one initially developped for neutral copolymers ^{6} except that an additional length has to be introduced : the electrostatic persistence length of the charged chains. The total free energy of the chains involves the adsorption energy of the hydrophobic blocks, the free energy of the grafted polyelectrolyte blocks and the chemical potential of the polymer solution. Experimental data show that the adsorbed amounts at saturation seem to be insensitive to the polymer concentration in the reservoir. This leads us to assume that the chemical potential contribution in the total free energy is negligible. The minimization of this energy with respect to the number density of chains on the surface σ gives:

$$\sigma = \phi_S{}^{4/5} \ (\delta / N_B)^{6/5} \qquad (3)$$

where ϕ_S is the salt concentration, δ is the energy per chain due to the attachment of the hydrophobic block on the surface and N_B is the number of segments in the polyelectrolyte block. The adsorbed amount A, which can be approximated as the product $\sigma * N_B$ (the hydrophobic block is short) expresses as:

$$A = \phi_S{}^{4/5} \ (\delta)^{6/5} / (N_B)^{1/5} \qquad (4)$$

Experimental results have been obtained at the same salt concentration (1 M) for two different copolymers MT2 and MT3 having the same sizes of PtBS blocks but sizes of NaPSS blocks being in a ratio of about 2. Equation 4 predicts that the MT2 adsorbed amount should be ca 13% higher than the MT3 adsorbed amount. This is well in agreement with the experiments, taking into account the 10 % associated error of the measurements. Moreover, equation 3 predicts that the ratio of the number of chains per unit area should be in the ratio 2:1 for MT2 versus MT3. This is the results that is seen experimentally, well outside the bounds of experimental errors.

Kinetics of adsorption. Recent adsorption studies of neutral diblock copolymers ^{7} have shown that two regimes of growth of the adsorbed layer can be expected: - a first transport limited regime where the growth rate is controlled by the diffusion of the adsorbing species toward the surface. The adsorbed amount should vary as:

$$A(t) = (2/ (\pi)^{1/2} .) \ * C_0 .* (D\ t)^{1/2} \qquad (5)$$

where C_0 is the concentration in diffusing species and D their diffusion coefficient. When the surface is filled up, adsorbed chains start to overlap and to adopt a brushy conformation. Then a slower growth rate is expected because the further chains have to penetrate the brush layer. This process involves rearrangement and deformation of already adsorbed chains. In this brush limited regime, the adsorbed amount has been predicted to vary as [8]:

$$A(t) = (A_{sat} - A_c).(1 - e^{-kt}) + A_c \qquad (6)$$

where k is the rate constant and A_c indicates the adsorbed amount to be reached for the exponential law to be valid.

Adsorbed amounts variations for MT2 and MT3 at a polymer concentration of 60 ppm and 1 M NaCl have been reported on figure 2 as a function of the square root of the time. A first regime of linear variation is observed for both copolymers, consistently with a transport limited regime.

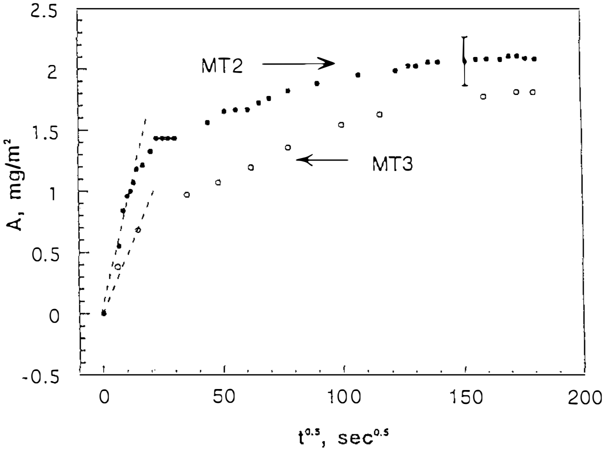

Figure 2: Mass adsorbed amounts, A, versus the square root of time in seconds. Transport limited regimes are seen in the early stage.

It should be interesting to deduce the diffusion coefficients D from the slope values. This leads us to ask the question of the nature of the diffusing species. Recent investigations of the solution properties of these copolymers [9] have shown that the cmc are lower than the polymer concentrations used in our experiment. This means that both micelles and free polymers are present in solution. Two arguments seem to be in favor of a micellar nature of the diffusing species: the free polymer concentration should be very low (of the order of the cmc) and the molten state of the micellar cores (PtBS) should make their desaggregation a slow process. However, it is impossible to give a definite conclusion from the experimental data because of the large number of unknown parameters and the lack of precision of the slope values.

The end of the diffusion limited regime should correspond to the time where the chains start to overlap. The average spacings between the chains Σ_{diff} at this time have been calculated from the adsorbed amount values and compared in table 3 to the radius of giration of the polyelectrolyte block R_g in 1 M solution. R_H values of the micelles determined in solution [9] are also given for comparison. Table 3 shows that Σ_{diff} has a value between R_g and $2R_g$, in agreement with a regime of non interacting adsorbed macromolecules. At the contrary, the average spacings between chains at saturation of adsorption Σ_{sat} are slightly lower than R_g , showing that brush formation should be involved in the second part of the kinetic.

Polymer sample	Rg (A°)	Σ_{diff} (A°)	Σ_{sat} (A°)	R_H micelle (A°)
MT2	100	125	90	160
MT3	150	210	130	450

Table 3: Molecular parameters for the adsorption of MT2 and MT3

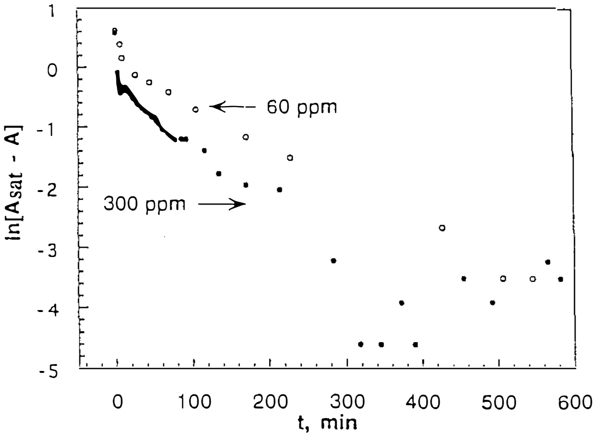

Figure 3 : Long time behavior of the adsorption for MT3, at two different polymer concentrations.

The exponential behaviors predicted by equation (6) for the brush limited regime have been represented on figure 3 for MT3 adsorbed in 1M salt, at two different polymer concentrations 60 and 300 ppm. The rate constants k deduced from these fits are increasing with the polymer concentration: $k=1.1*10^{-4}\ s^{-1}$ for a polymer concentration of 60 ppm and $k= 1.7*10^{-4}\ s^{-1}$ for 300 ppm. This can simply be explained because the statistical number of molecules hitting the surface at any given time is an increasing function of the polymer concentration, leading to a faster rate of growth of the adsorbed layer.

CONCLUSION

The first experimental results have shown that assymetric diblock copolymers PtBS-NaPSS do adsorb on silica surfaces from aqueous solutions but this process requires strong screening of the charged groups of the copolymers by the addition of salt in the adsorption medium. The enhanced adsorption of the copolymers compared to that of NaPSS homopolymers, as well as their absence of desorption in pure water, have demonstrated the anchoring role of the PtBS block in the adsorption process.The adsorbed amounts at saturation are compatible with a brush structure of the adsorbed layer, the PtBS block being collapsed at the solid surface and the NaPSS blocks extending in solution. Kinetics of adsorption have shown a two stage process, with a first initial diffusion limited stage followed by a brush limited regime where the growth rate of the layer has been slowed down. Scaling model [5] of the adsorption of charged diblock copolymers predict variations of the adsorbed amounts and grafting densities with the charged block size which are in good agreement with the experimental results. More experiments need to be done in order to confirm the scaling laws agreement, not only by varying the PtBS and NaPSS block sizes but also by studying the salt concentration dependance. Indeed, scaling models and mean field models are in disagreement with the exponent of the salt concentration.

REFERENCES

1- Halperin, A.; Tirrell, M.; Lodge, T. P.; *Adv. Polym. Sci.*, **1992**, 31, 100.
2- Pincus, P.; *Macromolecules*, **1991**, 24, 2912.

3- Israels, R.; Leermaker, F. A. M.; Fleer, G. J.; Zhulina, E. B.; *Macromolecules*, **1994**, 27, 3249.
4- Amiel, C.; Sikka, M.; Schneider, J. W.; Tirrell, M., Mays, J.; to be published in Macromolecules.
5- Dan, N.; Tirrell, M.; *Macromolecules*, **1993**, 26, 4310.
6- Marques, C.; Joanny, J. F.; Leibler, L.; *Macromolecules*, **1988**, 21, 1051.
7- Motschmann, H.; Stamm, M.; Toprakcioglu, Ch; *Macromolecules*, **1991**, 24, 3681.
8- Ligoure, C., Leibler, L.; *J. Phys. France*, **1990**, 51, 1313.
9- Guenoun, P.; Davis, H. T.; Tirrell, M., Mays, J., submited to Macromolecules.
 - Guenoun, P.; Lipsky, L.; Tirrell, M.; Manuscrpt in preparation.

MICELLE FORMATION AND ADSORPTION AT THE SOLID-WATER INTERFACE OF PS-PEO DIBLOCK COPOLYMERS

A.JADA, J.HOFFSTETTER and B. SIFFERT
CNRS-CRPCSS
24 Avenue du Président Kennedy 68200 Mulhouse-France

Abstract

AB diblock copolymers in a highly selective solvent, good for B and poor for A, exhibit amphiphilic behavior.

Micelle formation in water in the concentration range 10^{-7}-10^{-2} M by copolymers composed of polystyrene as the A block and polyoxyethylene (PEO) as the B block having Mn values in the range 1000 and 1000-5000 respectively was investigated by fluorescence probing method.

Furthermore adsorption from water onto titanium dioxide particles were made with copolymer initial concentration ranging up to 10^{-3} M. The stability behavior of the copolymer covered TiO_2 particles as function of copolymer concentration was investigated by absorbance, sedimentation and zeta potential measurements .

The behavior of polymeric surfactants in water and in the presence of solid particles was found to depend on their molecular characteristics.

Introduction

Copolymers having hydrophobic sequence such as polystyrene (PS) and hydrophilic sequence such as poly(ethylene oxide) (PEO) form micelles in dilute aqueous solutions1-4) and are used as stabilizers in solid-liquid5,6) dispersion and in the preparation of aqueous latex particles. Fluorescence probing (FP) refers to the use of a variety of neutral molecules, simple and complex ions which upon proper photoexcitation emit light whose characteristics are sensitive to the immediate environment of the probe. The dissolution of pyrene as fluorescent probe in aqueous surfactant solutions leads, at the CMC, to the sharp decrease in the I_1/I_3 ratio, I_1 and I_3 are repectively the intensities of the first and the third vibronic peaks in the pyrene fluorescence emission. In the present work, slow and rapid decreases of the I_1/I_3 ratio were observed, depending on the characteristics of the copolymer. Thus for these reasons, the onset concentration at which the I_1/I_3 ratio remains constant will be called, the apparent critical concentration (Capp) rather than CMC.

In this paper, the study of micelle formation and adsorption at solid-solution interface of a series of PS-PEO block copolymers in aqueous solutions is reported.

Experimental

The titanium dioxide (TiO_2, P25) used was purchased from Degussa. The surface area S measured by the BET method was 52 m^2 g^{-1} and the average size measured by sedimentation was 0.6 mm, at pH value of 5.5.

Fluorescence probing method :

Fluorescence emission spectra, made at 25 °C, of aqueous copolymer solutions containing 10^{-6} M pyrene were recorded on a Shimadzu RF-5001PC spectrophotofluorimeter over the range 350-500 nm, with the excitation wavelength at 335 nm.

Preparation of suspensions

A mixture (0.015%) of the solid sample and deionized water was ultrasonicated for few minutes and agitated at room temperature for 48 hours. A known volume of standard aqueous copolymer solution was then added and the resulting dispersion was shaken for further 2 days, the final pH value of the dispersion was about 5.5 ± 0.1.

Microelectrophoresis, optical density and sedimentation:

The microelectrophoresis was performed with a Lazer Zee meter, Model 500, purchased from Pen Kem Inc. The Optical density of the dispersion was measured at 500 nm. The same dispersion was placed in a calibrated tube to settle colloidal particles and the amount of the sediment was measured each five minutes during five hours.

Adsorption isotherms

Each aqueous TiO_2 suspension containing known amount of copolymer was centrifuged at 14,000 rpm to settle copolymer covered TiO_2 particles. After centrifugation, the supernatant was removed, mixed with D_2O and analysed for its residual copolymer concentration (Ce), using 250 Mhz proton NMR on a Bruker AC 250-F spectrometer.

Results and discussion

The structures, compositions, and molecular weights of the copolymer samples are presented in Table1. All the samples contain at least 50 wt% of PEO.

Table 1

Characteristics of non ionic copolymers : M_n is the copolymer number molecular weight, m, the repeating units of the PS , n, the repeating units of the PEO block and Capp is the apparent critical micelle concentration at 25°C.

	Triblock PEO-PS-PEO (see Ref 2)				Diblock PS-PEO			
Sample	**TB1**	**TB2**	**TB3**	**TB4**	**SE 10-10**	**SE 10-20**	**SE 10-30**	**SE 10-50**
M_n (g/mol)	17800	12100	15700	13200	2000	3000	4000	6000
m	27	23	36	35	10	10	10	10
n	2*170	2*110	2*135	2*108	23	46	69	115
Capp*10^5 (M)	<0.01	<0.01	<0.01	<0.01	1.0	1.4	1.6	2.5

The plots of I_1/I_3 ratio against copolymer concentration for SE samples are shown in Fig 1.

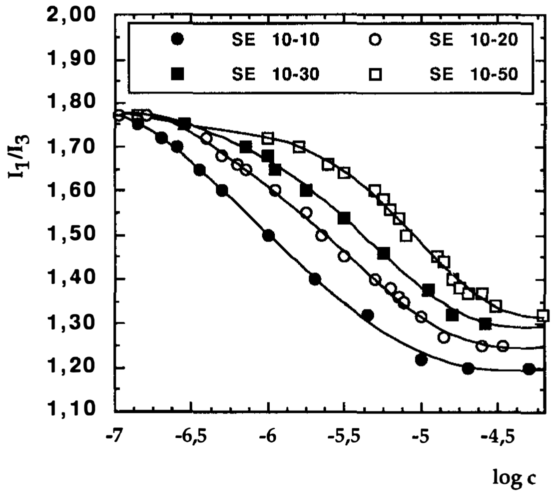

Figure 1.Variation of fluorescence intensity ratio of pyrene solubilized in various diblock copolymer aqueous solutions vs. copolymer concentration C (mol/l).

It can be seen that the I1/I3 ratio decreases over more than one decade for SE 10-10, SE 10-20, SE 10-30 samples. However, the I1/I3 ratio decreases over less than one decade for SE 10-50. The value of C_{app} increases with the PEO chain length for diblock SE series and is independent of the PEO chain length for the triblock series as shown in Table 1. It should be emphasized that C_{app} is a measure of the copolymer association efficiency in water. The increase of C_{app} with PEO chain length for SE series is explained by an increase of copolymer hydrophilicity. The slow decrease of I1/I3 ratio observed for SE 10-10, SE 10-20 and SE 10-30 was also observed for triblock series2) and this behavior can be explained by the partition of pyrene between water and polymolecular aggregates.

Adsorption isotherms for diblock copolymers SE series are shown in Fig 2.

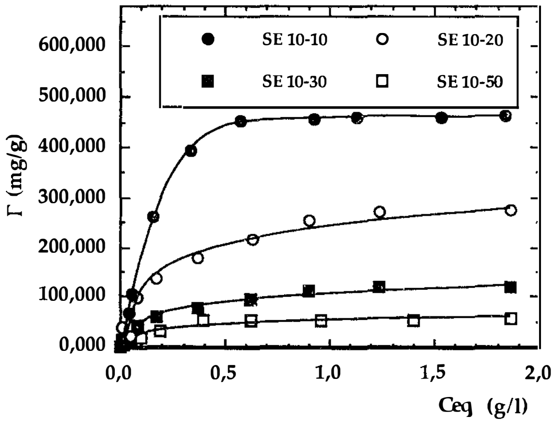

Figure 2. Adsorption isotherms of diblock copolymers from water onto TiO_2 particles.

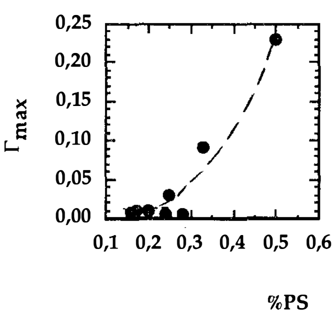

Figure 3. Variation of the plateau level Γ_{max} (in mmol/g) vs. the weight fractions of PS block.

It can be observed that the adsorption at the plateau level Γ_{max} increases with decreasing PEO chain length. Figure 3 shows the variation of the plateau level Γ_{max} vs. the weight fractions of PS block, for di and triblock copolymers.

The results shown in Fig.3 clearly indicates that the adsorption is governed by the PS content of the copolymer. The adsorption of PS-PEO onto TiO_2 particles influences some surface characteristics, such as the ζ-potential of the particle by shifting the position of the plane of the shear away from the particle surface. The ζ-potential of TiO_2 particles decreases with increasing copolymer concentration C and reaches a plateau value. The ζ-potential measured for TiO_2 dispersions in the absence of copolymer is equal to 30 ± 4 mV and the values found for various copolymers at higher concentration are given in Table 2. Stable suspensions were obtained when appreciable ζ-potential values resulted.

Further, the stabilization effect of the block copolymers upon TiO_2 dispersions was determined by measuring the optical density (OD) and the sedimentation rate (k) as a function of C. In the absence of polymer the OD and k values measured for TiO_2 dispersion were equal to 0.4 ± 0.1 and 0.05 ± 0.005 ml/mn respectively. In the presence of the polymer the optical density increases for SE 10-10 and then remains constant at higher C. However OD varies slightly with C, , within the error range for SE 10-20, SE 10-30, SE 10-50 and PEO-PS-PEO triblock copolymers. The sedimentation rate decreases slowly for SE 10-10 and steeply for SE 10-20, SE 10-30 and SE 10-50.This implies that stabilization using block copolymers is more effective with samples having higher weight fractions of PS.

Table 2

Experimental properties of aqueous dispersions made with TiO_2 particles in the presence of non ionic copolymers: Γ_{max} is the plateau adsorption level of the copolymer onto TiO_2 particles. OD is the optical density measured at 500 nm, k is the rate of sedimentation and $|\zeta|$ is the magnitude of zeta potential, measured at high copolymer concentration of TiO_2/copolymer/water dispersions.

Sample	Γ_{max} (mg/g)	k (ml/mn)	OD	$\lvert\zeta\rvert$ (mV)
SE 10-10	460	0.01	1.75	15
SE 10-20	276	0.02	0.35	7
SE 10-30	120	0.02	0.40	6
SE 10-50	55	0.02	0.3	4

In Table 3 are listed values of surface density σ_{exp} for various copolymers. The results shown in Table 3 indicate that σ_{exp} decreases with increasing the repeating units of the

PEO block (decrease in adsorption). However the adsorption is governed by the size of the PS block. Thus, reducing the size of PS chain leads to a reduction in the area occupied per molecule, indicating that the PEO chain can be more closely packed and stretched at the interface.

Table 3

Experimental surface densities of aqueous dispersions made with TiO_2 particles in the presence of non ionic diblock and triblock copolymers.

	Triblock PEO-PS-PEO				Diblock PS-PEO			
Sample	**TB1**	**TB2**	**TB3**	**TB4**	**SE 10-10**	**SE 10-20**	**SE 10-30**	**SE 10-50**
σ_{exp} (nm^{-2})	**0.078**	**0.110**	**0.065**	**0.070**	**2.670**	**1.065**	**0.347**	**0.106**

Conclusion

The Capp of PS-PEO copolymers increases with the PEO chain length and it has very small value for PEO-PS-PEO triblock copolymers. Further, these copolymers when adsorbed at TiO_2-water interface can prevent coagulation or enhance flocculation of the the colloidal particles, depending on the spatial extension of the polymer from the solid surface. Thus for SE10-10 the PS chain is adsorbed onto the surface and the PEO chain is fully extended and is in contact with the surrounding aqueous medium, forming a stabilizing layer, such behvior gives a stable dispersion. When the PEO chain length increases, the decrease in surface densities observed indicate folding of the PEO which can lead to the formation of individual monomolecular units (internal PS segment coil surrounded by less extended PEO segments). Such individual monomolecular units lead to the formation of bridged TiO_2 particles and enhance the coagulation of dispersion. The behavior of the polymeric surfactants in water depends on their molecular characteristics. More quantitative investigations on the thickness of the copolymer adsorbed amount and comparaison with the model proposed by Marquès7) et al, for adsorption of neutral diblock copolymers from a selective solvent for one block, are underway.

References

(1) Khan, T. N.; Mobbs, R. H.; Price, C.; Quintana, J. R. Eur. Polym. J. 1987, 23, 191.
(2) Jada, A.; Siffert, B.; Riess, G. Colloids and Surfaces. 1993, 75, 203.
(3) Tuzar, Z.; Kratochvil, P. Adv. Colloid Interface Sci. 1976, 6, 201.
(4) Riess, G.; Hurtrez, G.; Bahadur, P. Encyclopedia of Polymer Science and Engineering, 2nd ed.; Wiley: New York, 1985, Vol. 2, p 324.
(5) Napper, D. H. Polymeric Stabilization of Colloidal Dispersions, Academic press, New York, 1983.
(6) Tadros, Th. F. Adv Colloid Sci. 1980, 12, 141.
(7) Marquès, C. M.; Joanny, J. F.; Leibler, L. Macromolecules. 1988, 21, 1051.

MULTIBLOCK COPOLYMERS AT INTERFACES.

E. Leclerc (*), R. Douillard (**), M. Daoud(*)
(*) Laboratoire Léon Brillouin (C.E.A.-C.N.R.S.)
C.E. Saclay F 91191 Gif/Yvette
(**) Laboratoire de Biochimie et de technologie des proteines.
I.N.R.A. La Géraudière B.P. 527 44026 Nantes Cedex

Abstract.

We consider the configurations and the various regimes when an alternating, symmetric, multiblock copolymer made of successive sequences of A and B monomers with equal length Z is at the interface between two immiscible solvents that are respectively good for one of the sequences and poor for the other one. We find two semi dilute regimes, when the copolymers overlap. For monomer concentrations below Γ^{**}, we find a first range where the thickness of the copolymers is constant and equal to the radius of a sequence. For concentrations larger than Γ^{**}, a second regime appears, where the sequences stretch out and adopt a conformation similar to what was reported for grafted polymers.
Finally at a concentration Γ_{sat}, the interface is completely saturated, and the copolymers form micelles in the bulk: it becomes energetically more favorable to have copolymers in the bulk than at interface.

I. Introduction.

A large effort has been devoted these last few years to understand the structure of polymers at interfaces[1-23]. More recently, the structure and ordering of diblock copolymers in the vicinity of a surface was also considered in the opposite limit of melts[24]. There is another interesting case that was extensively studied. This is the case of the structure of a multiblock copolymer at an interface. We will consider in what follows the case of an alternating multiblock, where respective polymerisation index Z_a and Z_b are constants, and equals. This is by contrast with the more general case, when they are random. Because each of the sequences is soluble in only one of the solvents, the copolymer is forced to remain in the vicinity of the interface. Solvents will be assumed to be good solvents of their respective part. The structure of the copolymer in dilute solution will be considered in section 2. Section 3 will deal with the concentration effects, when the interface is progressively covered with polymers. Because of the excluded volume effects, as concentration is increased, the loops are forced to extend in the direction orthogonal to the surface. Finally, in section 4 , we find that for large concentrations it becomes energetically more favorable to form micelles in the bulk rather than to increase the surface concentration. Thus the interface is saturated in this regime. The structure of the micelles is studied in the simple case where one copolymer may form one micelle.

2. The dilute case.

Let us first consider the case of a single multiblock copolymer made of N successive sequences of two different chemical species. Each sequence is made of Z monomers, and the copolymer is regular. We also assume that both monomer species have identical size a. The two components are not soluble in a single solvent, but in two immiscible solvents. As a result, the copolymer may either remain at the interface between the solvents or form micelles in either solvents. Such micelles would have flower like shape, with the insoluble part in the center and the soluble sequences forming loops from this core. The latter solution however implies a high free energy and would only take place when the surface is completely saturated with copolymers. Therefore the chain is localized in the vicinity of the interface, the junction points between sequences are assumed to be located in the interface. The resulting structure is as shown on figure one. The interface is assumed to be flat on the scale of the copolymer, and we neglect completely any roughness of the interface. Because each part is in a good solvent, the characteristic sizes $R_\perp$ and $R_{||}$ respectively orthogonal and parallel to the surface are

$$R_\perp \approx Z^{3/5}a \qquad (1)$$

and

$$R_{//} \approx N^{3/4}Z^{3/5}a \qquad (2)$$

In the former relations, several assumptions are made. The first one is that the structure of a loop, that is of one sequence, is basically the same as that of a polymer in the bulk of a solution. In relation (2) we assumed that the structure of the copolymer is a two dimensional self avoiding walk[1 25] in the plane. This explains the exponent 3/4 that is the Flory approximation to a two dimensional self avoiding walk.

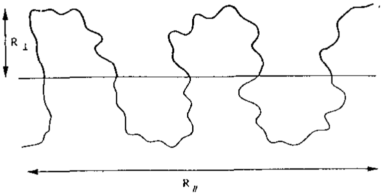

Figure 1.- The structure of a copolymer at the interface Every sequence is soluble in one of the immiscible solvents and has isotropic conformation. The various sequences extend on the surface as a two-dimensional chain.

The surface pressure of the solution in the dilute regime is merely

$$\Pi \approx \frac{\Gamma}{NZ} \qquad (3)$$

where Γ is the total number of monomers, per unit area, irrespective of the chemical nature, and the surface pressure is measured in units of kT. This dilute regime holds as long as the various chains are far apart from each other on the surface. This implies that the surface concentration Γ is smaller than an overlap concentration Γ^*:

$$\Gamma^* \approx \frac{NZ}{R_{//}^2} \approx N^{-1/2}Z^{-1/5}a^{-2} \qquad (4)$$

For larger concentrations, the polymers overlap, and the surface becomes semi-dilute.

3. Semi-dilute surface regimes.

For concentrations larger than Γ^*, the various copolymers start overlapping. We expect a different behavior for the chains, and the appearance of a second characteristic length ξ, related to the screening of the excluded volume interactions[26]. Excluded volume interactions are present inside a blob, and are screened at larger distances. As we will see, two different cases are to be considered depending on the relative values of the screening length ξ and the orthogonal radius $R_\perp$.

3.1. The constant width regime.

For concentrations slightly above Γ^*, the copolymers start overlapping. Because of this, the excluded volume interaction are screened at large distances[26 1]. This implies that the longitudinal conformation of a chain is identical to the one in the dilute regime for distances smaller than this length. For larger distances , chains are gaussian, if one takes the screening length as a unit. This introduces blobs with size ξ, made of g_d sequences. The latter number may be estimated using relation (4) :

$$g_d \approx \left(\Gamma a^2 Z^{1/5}\right)^{-2} \tag{5}$$

and, generalizing relation (2), we get

$$\xi \approx g_d^{3/4} Z^{3/5} \approx \left(\Gamma a^2\right)^{-3/2} Z^{3/10} a \tag{6}$$

For larger distances, because the excluded volume interactions are screened, we have

$$R_{//} \approx \left(\frac{N}{g_d}\right)^{1/2} \xi \approx N^{1/2} \left(\Gamma a^2\right)^{-1/2} Z^{1/2} a \tag{7}$$

The surface pressure may be estimated by a classical scaling assumption. The pressure is due to the contact between blobs, we expect the pressure to become independent of the number N of sequences. We find

$$\Pi \approx \left(\Gamma a^2\right)^3 Z^{-3/5} \tag{8}$$

Note that this result may be interpreted as giving a unit energy per unit surface.

3.2. The quasi-brush regime.

In the semi-dilute regime that was discussed in the previous section, the screening length ξ is larger than the radius of one sequences $R_\perp$. As concentration is increased, ξ decreases and becomes of the same order as $R_\perp$ for a concentration Γ^{**}. Comparing relations (1) and (6), we get

$$\Gamma^{**} a^2 \approx Z^{-1/5} \tag{9}$$

For larger concentrations, we get a second semi-dilute regime. The blob size becomes smaller than the radius of a sequence. As a consequence, each sequence is forced to adopt a stretched configuration, and the orthogonal width $R_\perp$ of the layer increases. The various distances may be obtained by scaling arguments. Assuming that ξ is independent of Z and is a function of concentration only, or that $R_\perp$ depends linearly with Z. We get

$$\xi_\perp \approx \left(\Gamma a^2\right)^{-3} a \qquad (10)$$

and
$$R_\perp \approx Z\left(\Gamma a^2\right)^2 a \qquad (11)$$

In the direction parallel to the interface, the length is defined by a non-avoiding walk. This gives

$$R \approx N^{1/2}\xi \approx N^{1/2}\left(\Gamma a^2\right)^{-3} a \qquad (12)$$

Finally, the surface pressure may be evaluated by a scaling argument, calculated by the requirement that the surface pressure be independent of Z in this regime. Using relations (8), and (9), we find

$$\Pi \approx \left(\Gamma a^2\right)^6 \qquad (13)$$

Note that the structure of the polymers in this concentration range is the same as that for grafted chains[27-28], this may be checked for instance by eliminating Γ between relations (10) and (11). The resulting structure is shown on figure 2.

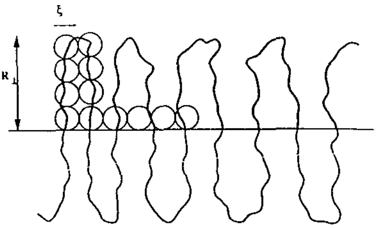

Figure 2. - In the concentrated regime, the chains adopt an extended configuration similar to grafted polymers. The distance between "graft points" is determined here by concentration.

4. Micelles.

So far we discussed only the configuration of the copolymers at the interface. We did not consider the possibility that they be in the bulk of the solution. This is what we consider in this section. Because of the copolymeric nature of the macromolecules, micelles are formed. On either side of the interface, one of the component is in a poor solvent and tends to segregate. Sequences in bad solvent conditions aggregate and form the core of the micelle. While sequences, in good solvent, form the corona of the micelle.

In order to calculate the structure of such micelles, we assume that it is similar to that of diblock copolymers[29-30]. This is a reasonable assumption when the sequences are long. The usual assumption for diblock micelles is that they have the same structure as a star polymer[31-32].

The number of diblocks in a micelle is determined by minimizing the free energy of a micelle:

$$F_m \approx N\left(\frac{R_c}{R_o}\right)^2 + N^{3/2}\ln\left(\frac{R_c}{R_m}\right) + \gamma R_c^2 \qquad (14)$$

where the first term is the energy of the core, assumed to be purely elastic, the second one the energy of the corona, and the last one is the interfacial contribution. Here R_c, R_o and R_m are respectively the radius of the core, the unperturbed radius of a sequence, and that of the micelle. Usually, the contribution of the core may be neglected. Minimizing this free energy with respect to N gives the number N_o of diblocks in a micelle. It was found:

$$N_o \approx Z^{4/5}\left(\gamma a^2\right)^{6/5} \qquad (15)$$

In the following, we will always assume that we are in the simple case where the number N of sequences in the multiblock is equal to N_o, and thus that a copolymer may form only one micelle.

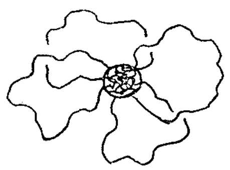

Figure 3. - The structure of a multiblock copolymer in a highly selective solvent. We assume that a copolymer can form one micelle.

The partition between interface and bulk is, at equilibrium, defined by the equality of the chemical potentials on the surface and in the bulk. Clearly, when the free energy of a micelle becomes smaller than that of a chain at the interface, any added copolymer will preferentially go in the bulk. This implies that the surface becomes saturated. This may happen only in the quasi-brush regime: both in the semi-dilute and in the dilute ranges, the free energy of the copolymer at the surface is smaller than that of a copolymer in the bulk. Minimization of relation (14) leads to the free energy F_m of a copolymer in a micelle. We find

$$F_m \sim N_o^{3/2} \qquad (16)$$

with N_o given by equation (15). In the brush regime, the free energy F_S of a copolymer on the surface is very similar to that of grafted polymers. It is made of two contributions. The first one corresponds to the excluded volume interactions between monomers and is proportional to the number of blobs. The second one is an elastic contribution due to the stretching of the sequences in the direction orthogonal to the surface. Thus we have

$$F_S \approx N_o\left[\left(\frac{R_\perp}{\xi_{//}}\right) + \left(\frac{R_\perp}{R}\right)^2\right] \qquad (17)$$

where $R_\perp$ is the normal extension of the layer, and R the radius of an ideal chain made of blobs with g monomers. Minimizing the free energy with respect to $R_\perp$, we find :

$$F_s \approx NZ\Gamma^5 \tag{18}$$

Comparing relation (18) with the free energy of the copolymer in the micelle, relation (16), we find the surface saturation concentration :

$$\Gamma_{sat} \approx \left(\gamma a^2\right)^{3/25} Z^{-3/25} \tag{19}$$

For larger bulk concentrations, the thickness and the size parallel to the interface and surface pressure become roughly constant because the surface is saturated and any added copolymers goes preferentially to the bulk.

5. Conclusion.

We discussed the structure of regular symmetric copolymers made of N successive sequences of Z monomers each. These sequences are soluble in two immiscible solvents. We assumed that the interface between the latter is flat, and that the junction point between any two sequences is located in the interface. As a function of the monomer concentration, we found four regimes. In the dilute range, the copolymers are far from each other and extend on the interface. The width of the layer is the radius of a sequence. Their dimension on the surface may be considered as a two dimensional self avoiding walk. For concentrations larger than Γ^*, but smaller than Γ^{**}, the polymers overlap. In this concentration range, surface pressure increase with concentration while width of the layer is constant.

For larger values of Γ, because of the excluded volume interactions, each sequence adopts an extended configuration normal to the interface. The resulting structure is similar to what was found for grafted polymers. Therefore the width of the layer increases with concentration, and the surface pressure is the same as for a semi dilute solution.The various regimes for the surface pressure are sketched on figure 4.

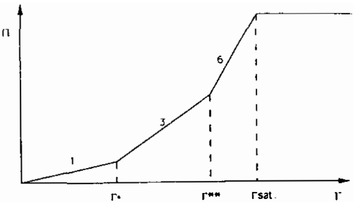

Figure 4. - Logarithmic plot of the surface pressure as a function of surface concentration in the various regimes. Slopes are indicated in each range

For larger bulk concentrations, the surface tends to saturate. So any added copolymer forms preferentially a micelle in the bulk. We considered only the special case where the number of sequences is such that a micelle is made of only one copolymer. In this case there is no CMC, so that this is very different from diblock copolymers, or of multiblocks with a number of sequences smaller than this special number N_0. The various regimes should be observable by neutron reflectometry, ellipsometry and hydrodynamic measurements. Although our results are in reasonable agreement with recent experiments, several improvements may be done. In the present approximation, it would be interesting to study the cases when the number of sequences is different from N_0, that we considered here. For large values of N, there is the possibility of forming a branched multimicellar structure, and eventually a gel. This is presently under investigation

References.

1. P.G. de Gennes, Scaling concepts in polymer physics, Cornell ,University Press, (1979).
2. J. Eisenriegler, K. Kremer, K. Binder, J. Chem. Phys. 77, 6296, (1982).
3. T. Ishinabe, J. Chem Phys. 76, 5589(1982); J. Chem. Phys. 77, 3171, (1983).
4. E. Bouchaud, M. Daoud, J. Physique 48, 1991, (1987).
5. M. Kawaguchi, M. Mikura, A. Takahashi, Macromolecules 17, 2063, (1984).
6. R. Varoqui, P. Dejardin, J. Chem. Phys. 66, 4395, (1977)
   E. Pefferkorn, A. Carroy, R. Varoqui, J. Pol. Sci., Pol. Phys. Ed.,23, 1997, (1985).
7. J.M. Bloch, M. Sansone, F. Rondelez, D.G. Peiffer, P.
   M.W. Kim, P.M. ,Eisenberger, Phys. Rev. Lett. 54, 1039, (1985).
8. K.G. Barnett, T. Cosgrove, B. Vincent, D.S. Sissons, M. Cohen Stuart, Macromolecules 14, 1018, (1981).
9. C.M. Marques, J.F. Joanny, Macromolecules, 22, 1454, (1989).
10. A. Halperin, J.F. Joanny, J. Physique, II, 1, 623, (1991).
12. A. Johner, J.F. Joanny, J. Physique, II, 1, 181, (1991).
13. L. Auvray, J.P. Cotton, Macromolecules 20, 202, (1987).
14. J. Klein, J. Chem. Soc. Faraday Trans. 79, 99 (1983).
15. J.N. Israelachvili, M. Tirrell, J. Klein, Y. Almog, Macromol. ,17, 204, (1984).
16. S. Granick, S. Patel, M. Tirrell, J. Chem. Phys. 85, 5370, (1986).
17. G. Rossi, P. Pincus, Europhys. Lett. 5, 641, (1988).
18. E. Dickinson, D.S. Horne, J.S. Phillips, R.M. Richardson, Langmuir,9, 242, (1993).
19. A. Chakrabarti, P. Nelson, Phys. Rev. A46, 4930, (1992).
20. C. Yeung, A.C. Balazs, D. Jasnow, Macromolecules, 25, 1357, (1992).
21. A.C. Balazs, Acc. Chem. Res.,26, 63, (1993).
22. X. Sun, E. Bouchaud, A Lapp, B. Farnoux, M. Daoud, G. Jannink, Europhys. Lett. 6, 207, (1988).
23. D. H. Ou-Yang, Z. Gao, J. Physique,
24. T.P. Russel, A. Menelle, S.H. Anastasiadis, S.K. Satija, C.F. Majkrzak, Prog. Coll. Pol. Sci., 91, 88, (1991).
25. P.J. Flory, Principles of polymer chemistry. Cornell Univ. press , (1953) .
26. S. F. Edwards , Proc. Phys. Soc. 88 , 265 , (1966) .
27. S. Alexander, J. Physique, 38, 983, (1977).
28. P.G. de Gennes, Macromolecules, 13, 1069, (1980).
29. C. Marques J.F. Joanny L. Leibler Macromolecules, 21, 1051, (1988).
30. A. Johner J.F. Joanny, Macromolecules,23, 5299, (1990),26
31. A. Halperin, Macromolecules,20, 2943, (1987).
32. M. Daoud J.P. Cotton, J. Physique,43, 531, (1982).

Autophobic behavior of polymers at interfaces

Günter Reiter[*], **Philippe Auroy**[+], **Loïc Auvray**
Laboratoire Léon Brillouin, CEN Saclay, F-91191 Gif-sur-Yvette Cedex, France
[*]present address: Centre de Recherches sur la Physico-Chimie des Surfaces Solides,
C.N.R.S., 24 Avenue du Président Kennedy, F-68200 Mulhouse, France
[+]present address:Insitut Curie,Section de Physique et Chimie, URA 448 du C.N.R.S.,
11, rue Pierre et Marie Curie, 75231 PARIS, Cedex 05, France

ABSTRACT

We investigated the stability and wetting behavior of thin films of polystyrene on layers of end-functionalized polystyrene molecules grafted onto silicon wafers. The "brush-like" layers entropically repelled the non-grafted but otherwise identical molecules. Thus, thin polystyrene films on top of dense polystyrene brushes were unstable and dewetted the brush by the growth of cylindrical holes. We studied this dewetting process in detail as a function of grafting density. The contact angle formed by the non-grafted molecules on top of the brush, and also the dewetting velocity, increased significantly with increasing grafting density. Embedding a few longer molecules into a brush had little effect on the contact angle but drastically slowed down the dewetting process. Implications of these results on adhesion or stabilization of thin liquid films are discussed.

1. Introduction

From experiments with bulk samples we know that identical molecules are compatible and mix. At an interface, however, we may experience a different behavior because molecules are exposed to additional interactions and constraints. Therefore, molecules in contact with another medium may exhibit properties deviating from the bulk. At the ultimate, such molecules may even "dislike" molecules of their own kind. Chemically identical molecules can become incompatible and, e.g. the same molecules do not wet a monolayer of adsorbed molecules. Such behavior was observed for small molecules on high energy surfaces already more than 40 years ago by W.A. Zisman1) and denoted as "autophobic". No proven explanation was offered at that time but it was speculated that orientation or packing constraints due to adsorption were responsible for this effect. Theoretically a similar phenomenon was predicted for polymeric liquids2,3). Anchoring many chain-like molecules to an interface by one end induces steric constraints causing stretching of the molecules4,5) Stretching, in turn, results in entropic repulsion for non-grafted macromolecules. Consequently, grafting many molecules onto an interface leads to the formation of a distinct "new" interface between grafted and non-grafted molecules with a non-zero interfacial tension. Under such conditions it is expected to observe the striking phenomenon that a polymer melt does NOT wet a "brush" of molecules of its own kind. Here we provide experimental evidence that a thin polymer film forced onto a layer of grafted but otherwise fully identical molecules dewets this layer.

End-functionalized polymers which were able to interact physically with the substrate have also been used to stabilize nonwetting liquid films6). Intuitively, the stabilizing effect was attributed to the strong interaction of the grafted molecules with the substrate and the interpenetration of grafted and free molecules. Thus, one would expect that the more molecules are anchored to the substrate the more stable the films are. Here, however, we will show that increasing the number of grafted molecules on the substrate leads to the counterintuitive effect of de-stabilization.

A related problem of interaction between grafted and non-grafted molecules is also encountered in the context of improvement of adhesion between a polymer and a solid substrate or between incompatible polymers. Commonly, end-functionalized polymers or block copolymers are used to increase the adhesive energy between the two bodies one wants to "glue" together7,8) It is not yet answered completely if an increasing number of such molecules at the interface between the two bodies would always improve adhesion9,10).

Experimental indications of autophobic behavior for identical polymers of different molecular weight were observed previously by Mourran, Chatenay and coworkers11) and Liu et al.12). Non-spreading drops or dewetting was found for systems where the melt on top of a chemically identical brush consisted of significantly longer molecules. In ref. 12 films thinner than the radius of gyration were put on top of the grafted layers so that it cannot be excluded that confinement effects as observed earlier[13)] have at least partially caused dewetting.

The effect of steric repulsion preventing the penetration of a brush has been demonstrated directly[14)] in a related experiment. However, in that case *two* layers of grafted polymers *in solution* were interacting. Here we will describe consequences of increasing grafting density on the wettability of the brush.

2. Experimental Section

For our studies we used layers of polystyrene end-attached onto silicon wafers coated with thin films (thickness (d) approx. 1000Å) of chemically identical molecules. Two different molecular weights of deuterated polymers were synthesized in our laboratory, split into two batches, and either terminated by a methyl group or by a monochloro-silane group. Methyl terminated protonated polystyrene was also synthesized. Molecular characteristics of the polystyrenes used are given in Table I. The silicon wafers were irradiated by UV-light in a water saturated oxygen atmosphere (UV-ozone treatment). Thin films were prepared by spincoating a dilute polymer solution onto these wafers.

Table I: Molecular characteristics of polystyrenes used

Sample	Weight-averaged molecular weight [g/mol]	M_w/M_n	radius of gyration [Å]	End-group
PS-S-R	9 300	1.04	25	monochloro-silane
PS-S-N	9 300	1.04	25	methyl
PS-L-R	43 500	1.03	55	monochloro-silane
PS-L-N	43 500	1.03	55	methyl
PS-p1-N	43 000	1.09	56	methyl
PS-p2-N	1 120 000	1.24	288	methyl

The first four samples are deuterated, the last two are protonated (abbreviated by p). The monochloro-silane endgroup is reactive and allows for grafting chemically onto the silicon surface. The methyl endgroup is non-reactive. The abbreviations have the following meaning: PS for polystyrene, S and L for short and long, respectively, and R and N for reactive and non-reactive endgroups, respectively.

For a systematic study of the dependence of dewetting on the grafting density of the brush we performed our experiment in two stages. First, we prepared a grafted layer, and, second, we covered this layer with a thin film of non-reactive polymer by spincoating a dilute polystyrene solution of non-reactive molecules directly onto the brush. For the grafted layer we spincoated an approximately 1000Å thick film of end-functionalized polymers onto the UV-treated silicon substrates. After different times of annealing at temperatures well above the glass transition temperature (T_g) the samples were put into a bath of toluene to wash off all non-grafted molecules.

The thicknesses of the layers remaining after washing and drying (=brushes) were determined by ellipsometry. The brush thickness increased rather fast at short annealing times but then only very slowly at later times, probably with the logarithm of annealing time once the thickness is larger than about two times the radius of gyration. Such a slow increase in the grafting density was expected theoretically15) and is attributed to the difficulties to penetrate an already existing brush to reach the substrate for grafting.

3. Results

First, we wanted to show that dewetting is indeed the consequence of the formation of a brush16). Therefore we prepared two films, one with short non-reactive (sample A, PS-S-N) and the other with short end-functionalized (sample B, PS-S-R) molecules. Subsequently, both samples were annealed at 160°C for 200min. (T_g is about 100°C). The behavior of the two samples was strikingly different (see Fig.1). Sample B showed numerous cylindrical holes which grew upon further annealing characteristic for dewetting initiated by a fundamental instability of the film17,18,19). Rupture of film B was the result of an exponential growth of surface modulations with a characteristic wavelength depended on film thickness. This instability is the consequence of a competition of surface tension of the film - which tries to keep the film flat - and attractive long range forces - which try to make the films thinner. Reactive molecules which did not have a chance to graft onto the substrate dewetted a brush formed by identical molecules. Increased annealing of sample A did not lead to any signs of such dewetting behavior. However, sample A became extremely "rough". For the shorter molecules (PS-S-R) autophobic behavior was already visible after 30min annealing at 160°C. For the longer molecules (PS-L-R), however, we had to anneal more than 40 hours at 160°C in order to observe first indications of dewetting.

The two polymers came from the same synthesis and differed only in their termination. All other steps of the sample preparation procedure were identical and performed simultaneously. Thus, the observed dewetting behavior of sample B could only be attributed to reactive end-groups which led to the formation of a grafted layer on the substrate. The existence of such a layer was indeed confirmed by ellipsometry, X-ray and neutron reflectometry after washing sample B in a container of toluene. The thickness (h) of the remaining polymer layer was about 60Å which has to be compared with the radius of gyration of 25Å.

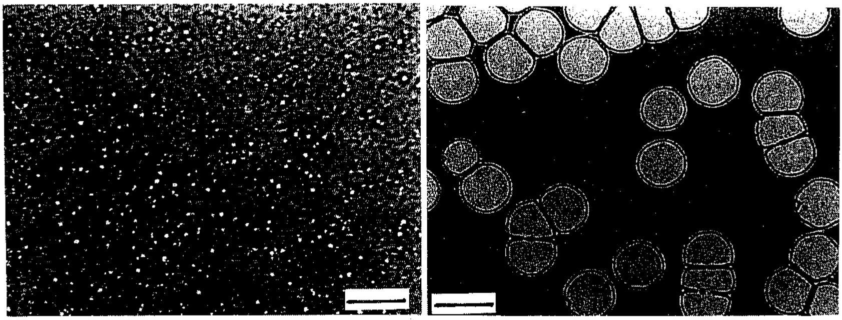

Fig. 1: Optical micrographs of two 1000Å thick polystyrene films (Mw = 9 300 g/mol) on silicon wafers after annealing for 200min at 160°C. Both samples were identical except that the molecules of sample A were methyl terminated while for sample B they had a monochloro-silane group at one end. The white disks visible on the right micrograph represent cylindrical holes. The length of the bar is 500 µm.

To investigate the influence of grafting density on the dewetting process we coated several wafers with 100nm thick films of reactive polymer (PS-S-R)[20]. The samples were annealed for various times in order to obtain layers of variable grafting density[15]. After washing off the non-grafted molecules these brushes were coated with non-reactive polymer and annealed again. In the following we focus only on samples with a sufficiently dense grafted layer which showed dewetting.

Contact angles (θ) have been determined from balancing the volume of a hole of diameter D_H (for D_H of the order of 100µm) and a depth equal to the initial film thickness (d) with the volume of the rim of diameter D_R using the following equation[21] predicted for slippage of a polymer on a solid substrate:

$$\theta = (D_H \cdot d)/(4 \cdot D_R^2 \cdot s) \qquad (1)$$

Due to the specific break-up mechanism all holes had a fairly uniform size. The parameter s takes into account that the shape of the rim is asymmetric. s has a value of about 0.1. If the shape of the rim is symmetric the equation for the equilibrium contact angle reads:

$$\theta = \sqrt{2} \cdot (D_H^2 \cdot d)/(D_R^3 + D_H \cdot D_R^2) \approx \sqrt{2} \cdot (D_H \cdot d)/D_R^2 \qquad (2)$$

The approximation is valid if D_H is much larger than D_R. For large holes equ. (1) and (2) differ only by a constant factor of about 1.8. In the case of very thick rims we could determine the contact angles directly from the interference fringes. The results compared better with the values obtained from equ. (1).

The higher the grafting density was, the larger was θ formed by polystyrene melt on top of a polystyrene brush. In correlation with θ, the dewetting velocity increased also with grafting density. Plotting the averaged velocity (v) as a function of contact angle shows that v increased with θ. (The values of v are averages - accounting for the non-constant growth rate - over approximately the first 100μm of hole growth). This increase was faster than linear, but significantly slower than the θ^3-dependence (Tanner's law) of the dewetting velocity on ideal solid surfaces[17,22].

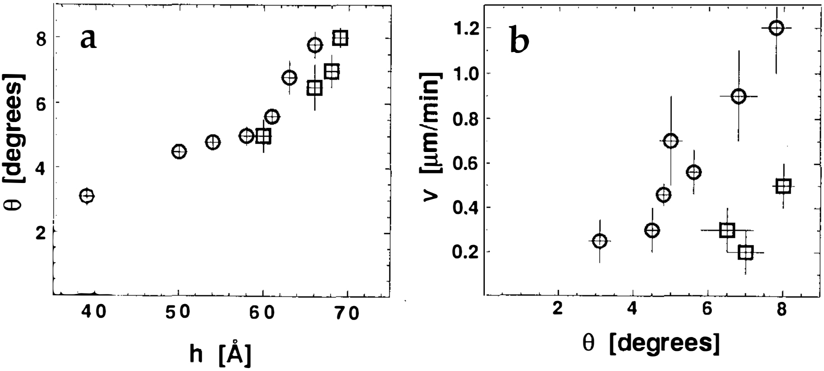

Fig.2 a) Contact angles (θ) of polystyrene (PS-p1-N, M_W = 43 000 g/mol) on a polystyrene brush (circles: PS-S-R, M_W = 9 300 g/mol; squares: PS-S-R brushes with a few PS-L-R molecules, Mw = 43 500 g/mol, see Table II) as a function of thickness of the washed and dried brush. The thickness of the initial films was approximately 900Å.
b) Averaged dewetting velocity (v) as a function of θ for the same data as in a).

Covering layers of grafted molecules with non-reactive polymer of much higher molecular weight favored dewetting as was expected from theory[2,3] and was already shown experimentally[12]. We have also performed a brief study. PS-L-R brushes with a thickness of 80Å, 100Å and 125Å, respectively, showed no signs of dewetting when coated with PS-L-N. However, when coated with the much longer molecules of PS-p2-N all except the sample with the 80Å brush showed the formation of holes indicating that these brushes could not be wetted by the longer molecules.

We determined the width of the interface between a PS-S-R brush and a film of PS-p1-N on top using neutron reflectometry[23]. For a 900Å thick film of PS-p1-N on a PS-S-R brush we found that the width of the interface as approximated by an error-function varied between s = 12±2 and s = 18±2Å for brush thicknesses between 63 and 50Å, respectively. This means that significant penetration occurred only at the outer part of the brushes and only very few molecules could reach the substrate. Details will be published elsewhere[24].

In a few cases we prepared brushes from mixtures of short and long *reactive* molecules (PS-S-R and PS-L-R). The concentration of the long molecules was varied. The samples were annealed at 160°C until small holes became visible. While under the same conditions we needed only a few minutes to create holes in a sample of just small reactive molecules (PS-S-R) we had to anneal for more than one day to see first indications of dewetting for a sample containing about 28% long molecules. The bi-modal brushes were then washed and coated with a film of PS-p1-N molecules. Neutron reflectometry was used to determine the interface of such bimodal brushes in contact with a polymer melt. Conditions of preparation and some results are given in Table II.

Table II: Bi-modal brushes

name	% of long molecules [min]	grafting time	h_o [Å]	h_{core} [Å]	contact angle [degrees]	averaged velocity [µm/min]
A	15	1080	72±1	60±2	~5	not measured
B	3.5	315	74±1	68±2	7±0.5	0.2±0.1
C	12	870	78±1	69±2	8±0.3	0.5±0.1
D	28	5650	76±1	66±2	6.5±0.7	0.35±0.1

Contact angles and averaged velocity were determined for a polystyrene film (PS-p1-N, approximately 900Å thick) on top of the resulting brushes for an annealing temperature of 160°C. The brush thickness h_o was determined by neutron reflectometry measurements of the washed and dried brushes before coating. h_{core} reflects only the thickness of the inner part of the bi-modal brush consisting mainly of short molecules as determined from the mid-point of the steep region of the density profile seen by neutron reflectometry.

In Fig. 3 we show typical neutron reflectivity results for a bi-modal system. In the main part we have plotted the reflectivity curves for the system after washing and drying (without a top layer, curve A) and compared it with curve B obtained after the brush was coated with a 1030Å thick layer of PS-p1-N and short annealing of 100min at 160°C. The inset shows part of the corresponding scattering length density profiles - focusing the brush region - used for the best fit of the data. We want to point out several aspects. First curve B differs only slightly from the curve A. The additional interference fringes originate from the thickness of the protonated layer on top of the brush. The whole curve B is lower than curve A. This already indicates that the brush-film interface is less steep, i.e. some free polymers can penetrate the brush a little (see also inset). Nonetheless, one can clearly see that curve B has a similar minimum as curve A. Thus the brush thickness has not changed much. In particular, the brush is not swollen by the free molecules. The position of the minimum shifted slightly to higher wavevectors indicating that the thickness of the brush layer has decreased. This decrease is attributed to the few longer grafted molecules which are floating on top of a brush of shorter molecules as predicted theoretically$^{25)}$. It is also visible from Fig. 3 that there are not too many long molecules embedded in the brush of shorter molecules.

4. Discussion and Conclusions

It is certainly not at all obvious that the observed dewetting behavior of our brush/melt system should be similar to the behavior of a simple polystyrene film on a non-wettable silicon wafers. In a qualitative sense, however, concerning rupture the behavior of the two cases did not differ. All holes had very much the same size and preliminary tests showed that the average distance between holes decreased significantly with decreasing film thickness. As all molecules, both in the brush and in the film, were polystyrene molecules it seems to be reasonable to assume that the brush layer has no (significant) effect on the long range van der Waals forces acting on the surface of the polymer film. Quantitatively, we expect however that the influence of the brush-layer should affect the thickness-dependence of the average distance between initial holes and the related size of the final droplets.

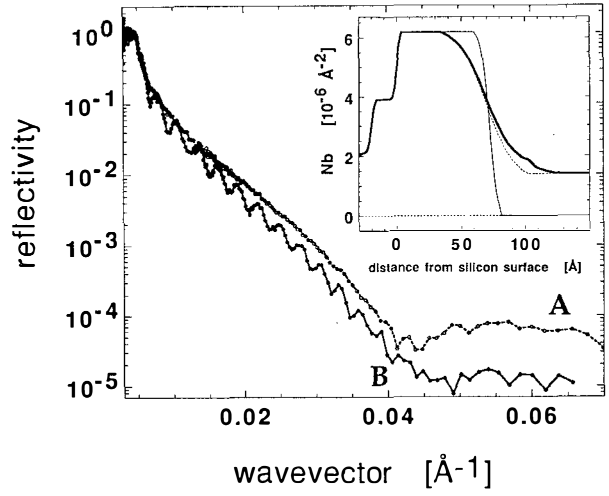

Fig. 3: Neutron reflectivity versus wavevector for the system A of Table II. Curve A is the result for the bare brush. Curve B shows the result for the same brush after coating it with a 1030Å thick PS-p1-N film and annealing for 100min at 160°C. The inset shows the corresponding scattering length density profiles (only the part relevant for the brush is shown). The thin solid line corresponds to curve A, the thick solid line to curve B, and the dotted line represents only the steep part of the profile (the interface is smeared with an error function) without the tail which is attributed to the longer brush molecules.

Although our free molecules were of finite length, we nonetheless compared our results with the theoretical prediction for the contact angle (θ). θ should vary according to the following relation:

$$\theta \cong (3kT/2a\gamma)^{1/2} \cdot (\pi^4 h/12N^2 a^4)^{1/6} \qquad (3)$$

k is the Boltzmann constant, T temperature, a the statistical segment length, γ the "chemical" surface tension of the brush/air interface, N the degree of polymerization of the grafted molecules, and h the thickness of the grafted layer. It is easily visible that for increasing N the degree of stretching (defined as $h/N^{1/2}a$) has to increase with $N^{3/2}$ in order to obtain the same contact angle. For the short and long reactive molecules in our experiments this means that the longer molecules have to be about 10 times more stretched than the shorter ones. This could explain why it is more difficult to observe dewetting for long grafted molecules.

We observed the predicted trend of equ. (3) only qualitatively. A quantitative comparison revealed severe discrepancies. According to equ. (3) θ should not vary much with h, while experimentally a strong increase of θ with h was observed. However, our experimental conditions deviate from the assumptions made by theory.

There is still significant interpenetration between the free molecules and the brush, especially in the outer region of the brush. Thus, we have two competing effects. Entropic repulsion of the free molecules by the inner region of the brush molecules. But we have to account also for the interaction between the outer layer and the free molecules. We speculate that this interaction may play a dominant role for brushes of long molecules in the sense that it can prevent dewetting even on a non-wettable brush. The parts of the grafted molecules situated in the outer region may act as "connectors" between the free molecules and the inner brush region. The length and area density of these "connectors" can control dewetting. In order to have dewetting these "connectors" have to be pulled out of the melt of free molecules. This pull-out force26) has to be at least compensated by the driving force, the balance of the interfacial forces at the three-phase contact line.

Our experiments with bi-modal brushes seem to support this concept. The dewetting velocity depends sensitively on the number of long molecules embedded in a brush of shorter ones. For the same contact angle, i.e. the same driving force, we observed a significantly lower dewetting velocity in the case of bi-modal brushes (see Fig. 2b).

These investigations are relevant also for brush/elastomer systems. Grafted molecules are used to improve adhesion of the elastomer to a solid. The optimal grafting density for maximum adhesion is currently investigated9,10). Interaction between the brush and the elastomer may be limited by the necessary swelling of the elastomer in order to allow penetration by the brush molecules. Our results indicate a second limiting constraint. It is difficult to penetrate brushes of high grafting density with non-crosslinked polymers. One can imagine that it will be even more difficult for an elastomer. We therefore conclude that brushes with very high grafting density are never useful for the purpose of improving adhesion.

It is preferable to use rather long molecules for the grafted layer in order to stabilize liquid films or to improve adhesion. The unfavorable formation of a brush of high grafting density is extremely slow for long polymers. To observe the same autophobic behavior the degree of stretching has to be larger for longer molecules. However, although different times scales apply, even for long polymers, for high enough grafting energy a brush may be formed which repels even identical molecules.

Acknowledgements:
This work would not have been possible without the help of P. Bassereau, A. Menelle and P. Silberzan. Very helpful and inspiring discussions with M. Aubouy, F. Brochard-Wyart, D. Chatenay, L. Leibler, A. Mourran, and E. Raphaël are gratefully acknowledged.

References:

1 Hare, E.F., Zisman, W.A., J. Phys. Chem.,1955, 59, 335; ibidem: 1955, **59**, 1097
2 Leibler, L., Ajdari, A., Mourran, A., Coulon, G., Chatenay, D., in: *Ordering in Macromolecular Systems,* Teramoto, A., Kobayashi, M., Norisuje, T. , (Eds.), Springer-Verlag, Berlin, 1994, p. 301-311
3 Shull, K., Faraday Discuss., 1994, 98, article #22
4 Alexander, S., J. de Phys., 1977, **38**, 983
5 de Gennes, P.G.; Macromolecules, 1980, **13**, 1069
6 Yerushalmi-Rozen, R., Klein, J., Fetters, L.J., Science, 1994, **263**, 793
7 Creton, C., Brown, H.R., Deline, V.R., Macromolecules, 1994, **27**, 1774
8 Xiao, F., Hui, C.-Y., Washiyama, J., Kramer, E.J., Macromolecules, 1994, **27**, 438
9 Brochard-Wyart, F., de Gennes, P.G.; J. Adhesion, to be published
10 Deruelle, M., Tirrell, M.,Marciano, Y., Hervet, H., Leger, L.; Faraday Discuss., 1994, **98**, article #6
11 Partly in ref. 2 and Chatenay, D., Mourran, A. private communication
12 Liu, Y., et al., Phys. Rev. Lett., 1994, **73**, 440
13 Zhao, W., et. al., Phys. Rev. Lett., 1993, **70**, 1453
14 Klein,J., Perahia,D., Warburg,S., Nature,1991, **352**, 143
15 Reiter, G., Auroy, P., Auvray, L.; Phys. Rev. Lett., submitted
16 Ligoure, C., Leibler, L., J. Phys. (France),1990, **51**, 1313
17 Brochard-Wyart, F., Daillant, J. Can. J. Phys,1990, **68**,1084
18 Sharma, A., Langmuir, 1993, **9**, 861
19 Reiter, G., Phys. Rev. Lett.,1992, **68**, 75; Langmuir, 1993, 9, 1344
20 Reiter, G., Auroy, P., Auvray, L.; Macromolecules, submitted
21 Brochard-Wyart, F., de Gennes, P.-G., Hervet, H., Redon, C., Langmuir,1994, **10**, 1566
22 A linear relation between velocity and inverse viscosity is expected for dewetting on a perfect solid surface as shown experimentally.
See: Redon, C., Brochard-Wyart, F., Rondelez, F.; Phys. Rev. Lett.; 1991, **66**, 715
23 See e.g.: Russell, T.P., Mat. Sci. Rep, 1990, **5**, 171
24 Reiter, G., Auroy, P., Auvray, L.; to be published
25 Dan, N., Tirrell, M.; Macromolecules, 1993, **26**, 6467
26 We assume that there exists a threshold force for pull-out similar to what was predicted for the case of adhesion.
See: Raphaël, E., de Gennes, P.-G., J. Phys. Chem., 1992, **96**, 4002

SURFACE SEGREGATION AND END DISTRIBUTION IN POLYMER BLENDS AND MELTS: INCOMPRESSIBILITY AND BOUNDARY CONDITIONS

David T. Wu and Glenn H. Fredrickson
Department of Chemical Engineering
University of California, Santa Barbara, California 93106

ABSTRACT: The presence of a surface disturbs a polymer melt or blend from its bulk configurations and composition, even in the absence of explicit enthalpic interactions. First, we consider the case of a nearly incompressible melt at a hard wall. We extend the usual ground state analysis of self-consistent field (SCF) theory to describe a) a finite chain in a melt of much longer polymers, and b) a melt of equal length polymers. From this, we find a small excess of ends near the surface, followed by a compensating Gaussian depletion on the R_g length scale.

Second, we examine the surface of a molten blend of two polymers with different flexibilities as characterized by the parameter $\beta^2 = R_g^2/V_{mol}$, where V_{mol} is the molecular volume of a polymer. Our analytic perturbative solutions to the SCF equations indicate that the more flexible component segregates to the surface, in agreement with experiments by Bates *et al.* [Phys. Rev. Lett., **70** 307 (1993)]. The enrichment extends a distance R_g from the surface. For small asymmetries, the magnitude of the segregation scales as $\sqrt{N}$, where N is a mean polymerization index, but for greater conformational asymmetry, we expect saturation at the surface, at a value of $\epsilon = (\beta_A/\beta_B)^2$ for which bulk segregation occurs.

Our presentation derives the effective boundary conditions appropriate for a (nearly) incompressible blend from microscopic considerations. This simplification should be useful for describing blends of polymers with more complex architecture.

I. Introduction

Many applications of polymer materials rely on their interfacial or surface properties, which can differ significantly from corresponding properties in the bulk. In particular, the enrichment at the surface of a particular component in a blend, or of end groups at the surface of a melt, may strongly affect either surface chemistry or physical properties. In this paper we examine how the presence of a neutral hard surface, even without explicit enthalpic interactions, can perturb the distribution and configurations of polymers in a melt or blend.

The distribution and effect of ends at the surface of a polymer melt has been previously considered in numerous experimental,1a) numerical1b) and analytical1c) studies. The distribution of chain ends near a surface may affect physical processes such as polymer welding as well as the molecular weight dependence of surface properties such as the surface tension. We focus here on the role of chain connectivity and present analytic solutions for a finite chain in a melt of much longer chains, and some results for a melt of equal length finite chains.

Evidence for segregation effects in blends and copolymers arising from conformational asymmetry (i.e. components differing in their pure-component parameters $\beta = R_g/\sqrt{V_{mol}}$, where V_{mol} denotes the molecular volume of a polymer) exists from experiments performed with polyolefins in the bulk and at the surfaces of thin films.2) The component with the smaller β was found to be consistently favoured at the surface. While the explanation of these observations has been surrounded by some controversy from a variety of approaches including density functional theory,3a) simulation3b) and liquid-state theory,3c) we use a coarse-grained field theory to focus on the role of conformational asymmetry and compressibility.

For the one-component melt, we confirm that reflecting boundary conditions are appropriate for describing chain configurations, producing a flat profile up to a microscopic length from the wall. While we expect this same density profile in a blend, the composition profile may be nonuniform over a longer length scale and requires nontrivial *constant flux* boundary conditions for this "outer" region. We show how these effective boundary conditions arise from strictly microscopic absorbing boundary conditions.

II. The One-Component Melt: End Effects

We start with a brief summary of the self-consistent field description of a polymer melt near a wall.[4,5,6] Each polymer in our theory consists of N statistical segments of length b and has a configuration described by a function $R(s)$, where s labels the monomer index. Following Helfand,[5] we consider the reduced partition function for observing monomer s on a given polymer at point r (z is the normal component of r measured from the wall, and we assume translational invariance in the x-y plane)

$$Q(z,s) = Z^{-1} \int \mathcal{D}R(s^*) e^{-\{H_0[R(s^*)]+U(R(s^*))\}} \delta(R(s)-r) \tag{2.1}$$

where the path integral is performed over paths $R(s^*)$ with $s^* \in [0,s]$. The quantity Z is a normalization constant equal to $Q(z,s)$ for zero potential ($U(r)=0$) and we have chosen units of energy such that $k_B T = 1$. The object

$$H_0[R(s)] = \frac{3}{2b^2} \int_0^N ds \, (\frac{dR}{ds})^2 \tag{2.2}$$

is the Hamiltonian for a free polymer with Gaussian statistics, and

$$U(r) = v\rho_b[\tilde{\rho}(z) - 1] \tag{2.3}$$

is a mean-field potential with $\tilde{\rho}(z) = \rho(z)/\rho_b$ being the monomer density normalized by its bulk value ρ_b. The interaction parameter v can be thought of as an excluded-volume parameter, but can be considered more generally to control the compressibility of the system. This form for $U(r)$ represents a local harmonic penalty for density fluctuations, the derivation and thermodynamic consequences of which are discussed elsewhere.[5,6] The function $Q(z,s)$ can be shown to satisfy the differential equation and boundary conditions

$$[\partial_s - \frac{b^2}{6}\partial_z^2 + U(z)]Q(z,s) = 0 \tag{2.4a}$$

$$Q(z,0) = 1; \;\; Q(0,s) = 0; \;\; \text{and } Q(\infty,s) = 1 \tag{2.4b}$$

The first of these follows from the definition of $Q(z,s)$, the second from the impenetrability of the wall, and the third from the fact that $U(r) = 0$ in the bulk. The monomer concentration can then be written as

$$\rho(z) = \frac{\rho_b}{N} \int_0^N ds Q(z,s) Q(z, N-s) \tag{2.5}$$

while the concentration of ends is simply $(2\rho_b/N)Q(z,N)$.

The self-consistent equations Eqs. (2.3) - (2.5) can be solved exactly in the limit of infinite N.$^{6)}$ In this limit, the function $Q(z,s)$ reaches a steady-state or "ground-state" value $Q_{GS}(z)$ for large values of s, which corresponds to the loss of memory in the middle of the chain of the position of the chain ends. For such long chains, the monomer density profile is dominated by the distribution of "middle" monomers. At large values of s, the first derivative term in Eq. (2.4a) is negligible, from which one obtains the solution

$$Q_{GS}(z) = \tanh(z/\xi) \quad ; \quad \tilde{\rho}_{GS}(z) = \tanh^2(z/\xi) \tag{2.6}$$

where ξ is the Edwards bulk correlation length$^{4)}$ given by

$$\xi \equiv \frac{\beta}{\rho_b}\sqrt{\frac{2}{v}} = \frac{b}{\sqrt{3v\rho_b}} \tag{2.7}$$

For a melt, ξ is on the order of a monomer size and is proportional to the square root of the compressibility. While in reality the microscopic details reflect liquid-state packing effects, our theory incorporates a microscopic length scale to smoothly control the density rise from the wall in the limit of incompressibility.

The statistics of a chain of length N' placed in a melt of much longer polymers (which produce the ground-state density profile) is then given by the solution $Q_\infty(z,s)$ to the equation

$$[\partial_s - \frac{b^2}{6}\partial_z^2 + v\rho_b(\tilde{\rho}_{GS}(z) - 1)]Q_\infty(z,s) = 0 \tag{2.8}$$

but considered only for $s < N'$. The Green's function for Eq. (2.8) can be evaluated analytically, and so $Q_\infty(z,s)$ follows directly from the definition Eq. (2.1). However, in the regime of physical interest, $\xi \ll z \ll sb^2/\xi$, we find to lowest order in $1/\sqrt{s}$

$$Q_\infty(z,s) \approx \tanh(z/\xi) + 2c_1\frac{\xi}{b}\sqrt{\frac{3}{2\pi s}}\exp(\frac{-3z^2}{2sb^2})[\tanh(z/\xi) + \frac{3z\xi}{sb^2}] \tag{2.9}$$

where $c_1 = 2(1 - \ln(2))$ is a numerical constant. Using the above expression in Eq. (2.5), we find the monomer concentration in the same regime to be

$$\tilde{\rho}_\infty(z) \approx \tanh^2(z/\xi)\ \{1 + \frac{4c_1}{\sqrt{\pi}}\frac{\xi}{R'_g}e^{-z^2/4R'^2_g} - 2c_1\frac{z\xi}{R'^2_g}\operatorname{erfc}(\frac{z}{2R'_g})\} \tag{2.10}$$

to lowest order in ξ/R_g', where $R_g' = \sqrt{N'b^2/6}$ is the radius of gyration of the test chain. Details of these approximations are given in Ref. [6].

The normalized monomer density $\tilde{\rho}_\infty(z)$ and distribution of ends $Q_\infty(z,N)$ are displayed in Fig. 1 and are seen to rise from the wall on the length scale ξ to an excess compared to the bulk which then decays roughly like a Gaussian on the R_g length scale. (The approximations Eqs. (2.9,2.10) are essentially indistinguishable from numerical evaluation of Eqs. (2.3) - (2.5) on the scale of the graph.) Comparing $Q_\infty(z,N)$ to $\tilde{\rho}_\infty(z)$ reveals a preference for ends within the range of ξ, followed by a compensating depletion on the range of R_g.

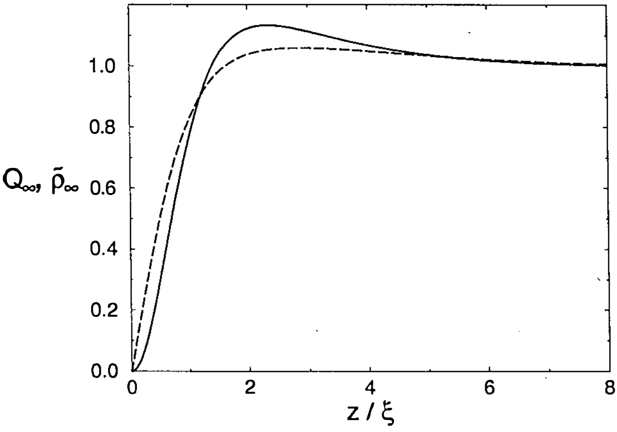

Fig. 1. The normalized density $\tilde{\rho}_\infty(z)$ (solid) and distribution of ends $Q_\infty(z,N)$ (dashed) for a chain with $N = 30$ and $b = \xi$ in a melt of much longer chains.

To describe a melt of equal length chains, however, requires a correction to the potential to satisfy the condition of self-consistency. We proceed by perturbing to linear order in N^{-1} about the exact $N = \infty$ solution:

$$Q(z,s) = Q_\infty(z,s) + N^{-1}\bar{Q}(z,s) \quad ; \quad \tilde{\rho}(z) = \tilde{\rho}_{GS}(z) + N^{-1}\bar{\rho}(z) \qquad (2.11)$$

From Eq. (2.5) we can express the first order change in the normalized density as

$$\bar{\rho}(z) = \frac{2}{N}\int_0^N ds Q_\infty(z, N-s)\bar{Q}(z,s) \approx \frac{2}{N}Q_{GS}(z)\int_0^N ds\bar{Q}(z,s) \qquad (2.12)$$

To leading order, the self-consistent equations become

$$[\partial_s - \frac{b^2}{6}\partial_z^2 + v\rho_b(\tilde{\rho}_{GS}(z) - 1)]\bar{Q}(z,s) = -v\rho_b Q_\infty(z,s)\bar{\rho}(z) \tag{2.13}$$

Integrating the above equation over s and neglecting boundary terms, which are down by an order of N^{-1}, we find

$$[-\frac{b^2}{6}\partial_z^2 + v\rho_b(3\tilde{\rho}_{GS}(z) - 1)][\int_0^N ds\bar{Q}(z,s)] = 0 \tag{2.14}$$

which has as solution $\int_0^N ds\bar{Q}(z,s) \propto \mathrm{sech}^2(z/\xi)$. The perturbation for the density is thus $\bar{\rho}(z) \propto \tanh(z/\xi)\,\mathrm{sech}^2(z/\xi)$, and so from Eq. (2.11), we can write

$$\tilde{\rho}(z) = \tanh^2(z/\xi + c_N N^{-1}) \tag{2.15}$$

for the density profile of a melt of chains of length N, where c_N is a constant we leave here undetermined. In summary, to order N^{-1}, the density profile is merely shifted inwards by a distance scaling as N^{-1}. This is consistent with a linear response estimate$^{6)}$ for the same correction from ground state, which was found to be order N^{-1} near the surface, and only order $N^{-3/2}$ on the R_g scale.

Finally, we note that the surface tension γ can be determined from a knowledge of the monomer density profiles above according to the relation

$$\gamma\sigma = \frac{1}{2}v\int dr[\rho_b^2 - \rho(r)^2] + \frac{1}{N}\int dr[\rho_b - \rho(r)] \tag{2.16}$$

where σ is the surface area. The first term is the surface contribution to the interaction energy (including constraint fields), and the second term can be identified as the surface depletion of polymers.$^{6)}$

III. Conformationally Asymmetric Blend at a Surface

We consider a two-component blend of polymers differing in their β parameters at an (air or hard) surface. Let component $K = A$ or B consist of polymers of N_K monomers having statistical segment length b_K and equal volumes v_m. The conformational asymmetry parameter is defined as

$$\epsilon = (\beta_A/\beta_B)^2 \tag{3.1}$$

where the pure component parameter β_K^2 is given by $\beta_K^2 = b_K^2/6v_m$. We let component A have the higher value of β and thus be considered the stiffer species, while component B is the more flexible (i.e. we choose $\epsilon > 1$).

Having defined (without loss of generality) equal monomer volumes, we can model the effect of finite compressibility by using the total monomer density $\rho(z) = \rho_A(z) + \rho_B(z)$ in the self-consistent field $U(z)$ felt identically by each component. The monomer concentration for component K is given here by

$$\rho_K(z) = \frac{f_K \rho_b}{N_K} \int_0^{N_K} ds Q_K(z,s) Q_K(z, N_K - s). \tag{3.2}$$

where f_K is the bulk K-monomer mole fraction, and the reduced partition functions $Q_K(z,s)$ solve the differential equations

$$[\partial_s - \frac{b_K^2}{6}\partial_z^2 + U(z)] Q_K(z,s) = 0 \tag{3.3}$$

with the same microscopic boundary conditions Eq. (2.4b) as for the melt. As discussed in Ref. [5], this form for the potential involves the additional assumptions of random mixing and a density and compressibilty which are composition independent ($f_A + f_B = 1$), and so should be valid in the incompressible limit.

We expect the composition profiles to depend sensitively on the conformational asymmetry, since small differences in β lead to bulk phase separation.$^{7)}$ We thus analyze our equations within a perturbation theory in $(\epsilon - 1)$ about a reference where the two components are identical, each having a mean value of β given by

$$\beta^2 \equiv (\beta_A^2 + \beta_B^2)/2 \tag{3.4}$$

We write the perturbed quantities (designated by a bar) according to

$$Q_K = Q_0 + (\epsilon - 1)\bar{Q}_K \quad ; \quad \tilde{\rho} = \tilde{\rho}_0 + (\epsilon - 1)\bar{\rho} \tag{3.5}$$

where Q_0 and $\tilde{\rho}_0$ are the unperturbed functions (for which $b_A = b_B = b$), and $(\epsilon - 1)\bar{Q}_K$ and $(\epsilon - 1)\bar{\rho}$ are first-order corrections. From Eq. (2.5), $\bar{\rho}$ is given by

$$\bar{\rho}(z) = \frac{2}{N} \int_0^N ds Q_0(z,s) \bar{Q}_+(z, N - s) \tag{3.6}$$

to lowest order in $(\epsilon - 1)$, and where we have defined $\bar{Q}_+ = f_A\bar{Q}_A + f_B\bar{Q}_B$.

Using the convention for $\pm$ that the plus value corresponds to component A and minus to B, the equations for $\bar{Q}_K$ to first order in $(\epsilon - 1)$ then reduce to

$$[\partial_s - \frac{b^2}{6}\partial_z^2 + v\rho_b(\tilde{\rho}_0 - 1)]\bar{Q}_K = (\pm\frac{b^2}{6}\partial_z^2 - v\rho_b\bar{\rho})Q_0 \tag{3.7}$$

We can expect the density to be relatively unperturbed compared to $\bar{Q}_K$, and so use a ground-state approximation for the density and Q_0. With the Green's function for the ground-state potential, we arrive at analytical solutions for the perturbative equations. Details of the calculation are presented elsewhere.[8)]

In the regime $\xi \equiv (\beta/\rho_b)\sqrt{2/v} \ll z \ll \sqrt{sb^2/6}$, the solution is found to be

$$Q_K(z,s) \approx 1 \pm (\epsilon - 1)\frac{4}{9}(1 - f_K)\frac{\sqrt{s}b}{\xi}\ [\frac{1}{\sqrt{\pi}}\exp(-Z_s^2) - Z_s\,\mathrm{erfc}(Z_s)] \tag{3.8}$$

where $Z_s = z/(2\sqrt{sb^2/6})$. From Eq. (2.5), the density of species K is given by

$$\begin{aligned} \tilde{\rho}_K(z) &\approx f_K \pm (\epsilon - 1)\frac{16}{9\sqrt{6}}f_A f_B\frac{R_g}{\xi}\ F_\rho(z/2R_g) \\ F_\rho(Z) &= (1 + Z^2)e^{-Z^2}/\sqrt{\pi} - (3Z + 2Z^3)\,\mathrm{erfc}(Z)/2 \end{aligned} \tag{3.9}$$

where $Z = z/(2R_g)$. The shape F_ρ of the composition profile is shown in Fig. 2.

The species with lower β is thus found to segregate to the surface, in agreement with experiment. The magnitude of the segregation is proportional to the conformational asymmetry, the radius of gyration, the product of the volume fractions, and increases as the blend is made less compressible. (Segregation effects due to size alone, such as those described above for homopolymer melts, are subdominant, being of order N^{-1}.) The range of the segregation is on the order of R_g of the chains, and decays rapidly, nearly as a Gaussian. From Eq. (3.9), we note also that the surface excess is given by the simple relation

$$f_s \equiv \frac{\rho_A(z = 0^+)}{\rho_B(z = 0^+)} = \frac{f_A}{f_B} + \frac{16}{9\sqrt{6\pi}}\frac{(\epsilon - 1)R_g}{\xi} \tag{3.10}$$

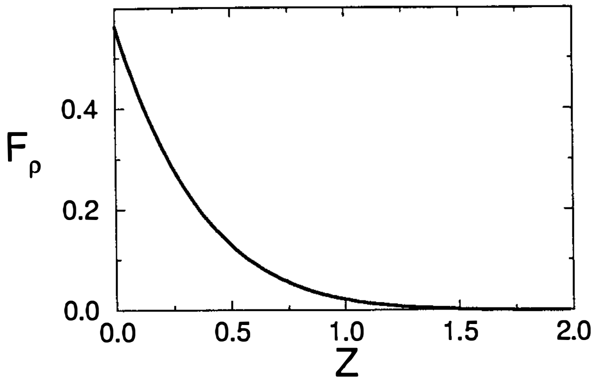

Fig. 2. The function F_ρ entering in the composition profile $\rho_K(z)$.

These results are valid when the perturbation $(\epsilon - 1)\bar{Q}_K$ is small compared to the unperturbed value $f_K Q_0$. This is true when

$$\epsilon - 1 \ll \xi / b_K \sqrt{N_K} \tag{3.11}$$

Since for a molten blend, ξ is on the order of a monomer size b_K, the above criteria is satisfied for the range of validity desired, i.e. before bulk phase separation is produced by conformational asymmetry.[2b,7] For greater conformational asymmetry, we expect saturation at the surface.

IV. Effective Boundary Conditions and deGennes Sum Rule

As noted by de Gennes,[8] the ground state $\tanh^2(z/\xi)$ potential for the homopolymer melt has an integrated attractive strength that precisely cancels the repulsion of the wall, giving rise to eigenfunctions near ground state obeying reflecting boundary conditions. For a melt of finite chains, the statistics are given by reflecting boundary conditions with an effective surface potential for chain ends.[6]

For the blend, however, the potential due to the density profile near the wall is too strong to balance the wall repulsion for component B, and too weak for component A. In effect, the inhomogeneous part of the microscopic differential equation Eq. (3.7) acts as a source (sink) term for probability, producing a nonzero slope just beyond a bulk correlation length from the wall. This property of a finite slope is equivalent to effective *constant flux* boundary conditions

$$\partial_z Q_K(z,s)|_{z=0} = -(2/3)^{3/2}(\epsilon - 1)(1 - f_K)/\xi \tag{4.1}$$

and so the solution Eq. (3.8) for the blend satisfies the free polymer differential equation (i.e., with U(**r**) = 0) subject to Eq. (4.1). Reflecting boundary conditions for a given component are approached as the blend is made either more conformationally symmetric or compressible, or more inflexible or pure in that component.

Acknowledgements: This work was supported by the MRL program of the National Science Foundation under Award No. DMR-9123048. The work herein stems from our collaborations with J. P. Carton, A. Ajdari, and L. Leibler. We also thank David Morse and James Donley for helpful discussions.

References

[1] (a) J. F. Elman *et al.*, Macromolecules, **27**, 5341 (1994); (b) S. K. Kumar, M. Vacatello, and D. Y. Yoon, J. Chem. Phys., **89**, 5206 (1988); (c) P.-G. de Gennes, C. R. Acad. Sc. Paris, **307**, série II, 1841 (1988). Also see Ref. [6] and references therein.

[2] (a) M. Sikka *et al.*, J. de Physique II, **4**, 2231 (1994); (b) F. S. Bates *et al.*, Macromolecules, **25** 5547 (1992).

[3] (a) G. H. Fredrickson and J. P. Donley, J. Chem. Phys., **97** 8941 (1992); (b) A. Yethiraj *et al.*, J. Chem. Phys., **100**, 4691 (1994); (c) K. S. Schweizer *et al.*, to appear.

[4] M. Doi and S. F. Edwards, *The Theory of Polymer Dynamics*, Clarendon, Oxford (1986).

[5] See for example E. Helfand, J. Chem. Phys., **62**, 999 (1975).

[6] D. T. Wu, G. H. Fredrickson, J.-P. Carton, A. Ajdari, and L. Leibler, J. Poly. Sci., Physics Ed., to appear in Dec. 1995.

[7] F. S. Bates and G. H. Fredrickson, Macromolecules, **27** 1065 (1994); G. H. Fredrickson, A. J. Liu and F. S. Bates, Macromolecules, **27** 2503 (1994).

[8] D. T. Wu, G. H. Fredrickson, J. P. Carton, A. Ajdari, and L. Leibler, manuscript in preparation.

[9] P.-G. de Gennes, C. R. Acad. Sc. Paris, **290**, série B, 509 (1980).

SEGMENTAL ORDER IN A GRAFTED POLYMER MELT : NMR INVESTIGATIONS

M. Zeghal [1], B. Deloche [1],and P. Auroy [2]
[1] Laboratoire de Physique des Solides (CNRS-URA D0002)
Université Paris-Sud, 91405 Orsay, France
[2] Institut Curie, Section de recherche (CNRS-URA 448),
11, rue Pierre et Marie Curie, 75231 Paris cedex 05, France

Abstract

Dynamics of polymer chains grafted on a solid substrate are investigated by deuterium NMR. The experiments are performed on end grafted deuterated polydimethylsiloxane in the melt state. The NMR spectra show clearly that chain segments undergo uniaxial reorientations around the normal to the interface. This local order reveals the existence of orientational correlations between chain segments.

Introduction

Grafted polymer layers on a solid substrate are the subject of considerable interest [1,2]. A lot of work has been done in the regime of high grafting density and was mainly devoted to structural studies of polymer layers [3,4]. However, very little is known about chain dynamics in these systems. For that reason we are currently developping deuterium-NMR (^{2}H-NMR) in this field, technique which is known to be very sensitive to the anisotropy of molecular motions [5,6]. Herein we report some ^{2}H-NMR spectra observed on nanolayers made of end-grafted deuterated polydimethylsiloxane (PDMS-D) in the melt state. Clearly for a high grafting density, the spectra reveal an uniaxial segmental order.

Samples

The substrate we used was silica, under the form of porous beads [3] or planar slides. Experiments were performed on PDMS-D chains synthesized via anionic polymerisation (Mn=71000 ; Mw/Mn=1.11). The grafting reaction was described in reference [7]. X-ray reflectivity and neutron scattering data obtained on flat and porous silica respectively show that the thickness of the grafted polymer is 80 Å i.e. close to of the radius of gyration value for the PDMS chains in the corresponding ungrafted melt (Rg~70Å). The mean distance between adjacent grafting junctions is then 40Å.

^{2}H-NMR background

The ^{2}H-NMR approach we used consists of studying how quadrupolar interactions Δ (interaction between the quadrupolar moment of the deuteron with the electronic environment of the C-D bond) affect the magnetic relaxation function M(t) or its Fourier transform. When rapid and anisotropic molecular motions take place in the system ($\tau < 10^{-6}$s), the interaction Δ is partially time averaged $\left(\overline{\Delta} \neq 0\right)$.

$$\overline{\Delta} \propto \nu_Q \; \overline{P_2(\cos\Theta(t))} \qquad (1)$$

where ν_Q denotes the static quadrupolar coupling constant ($\nu_Q \sim 2.10^5$ Hz).Θ(t) in the second Legendre polynomial P_2 is the angle between the C-D bond and the steady magnetic field B. This non-zero interaction $\overline{\Delta}$ leads to a modulation of the function M(t) which may be expressed as

$$M(t) \; = \; M_o \; e^{-t/T_2} \cos(\overline{\Delta} \; t) \qquad (2)$$

or as well, by Fourier transforming eq. (2), to a doublet of Lorentzian lines characterized by a splitting $\overline{\Delta}$. Note that for isotropic motions ($\overline{\Delta}$=0), the resulting spectrum is a single Lorentzian line characterized by a linewidth $\delta\nu$ depending on the relaxation time T_2 only ($\delta\nu \sim T_2{}^{-1}$). In the case of uniaxial motions consisting in fast reorientations around a symmetry axis (denoted by the unit vector **n**), the splitting may be expressed as

$$\overline{\Delta} \propto \; \nu_Q \; |P_2(\cos\Omega)| \; \overline{P_2(\cos\theta(t))} \; = \; \nu_Q \; |P_2(\cos\Omega)| \; S \qquad (3)$$

where Ω and θ are the angles between the symmetry axis **n** with respect to the magnetic field and the C-D bond respectively. The $|P_2(\cos\,\Omega)|$ term, which depends only on the geometry of the experiment, allows us to check the uniaxial character of the molecular motions. The second factor $\overline{P_2(\cos\,\theta(t))}$ depends on molecular dynamics : It is the mean degree of orientational order of the C-D bond relative to the symmetry axis, the so-called order parameter S.

Experimental results

The ^{2}H-NMR spectrum obtained at room temperature on grafted porous silica is characterized by a broad non-Lorentzian lineshape (fig. 1a). The half-height linewidth $\delta\nu$ is large ($\delta\nu$=400Hz) compared with the one obtained on the corresponding ungrafted melt ($\delta\nu \leq$10Hz). Moreover, T_2 measurements performed on the porous system by spin echo method give access to a linebroadening much smaller than the observed one. This suggests that another effect than the T_2 process contributes to the spectral linewidth $\delta\nu$. Actually, this point is corroborated by the response to an appropriate pulse sequence [8], which shows a modulation in the relaxation function, related to a non-zero residual interaction ($\bar{\Delta}\neq 0$): It demonstrates that the molecular motions are anisotropic on the ^{2}H-NMR time scale, though the porous system is macroscopically isotropic. At first sight, from the NMR point of view, the porous system is non uniform since the chain segments may present different axis for the anisotropy and different degrees of orientation. Therefore, the resulting spectrum is expected to be a superposition of various doublets (as defined in eq. 1), which corresponds to an ensemble average.

$$M(t)_{porous} = M_o\left\langle e^{-t/T_2}\cos(\bar{\Delta}\;t)\right\rangle \qquad (4)$$

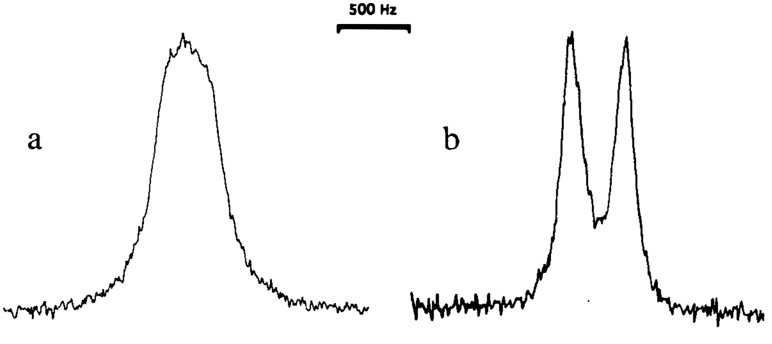

Fig.1: ^{2}H-NMR spectra obtained on -a) Porous silica -b) Planar silica for Ω=90°.

In order to clarify this spatial average, it may be relevant to work on a "monodomain" characterized by one macroscopic symmetry axis for dynamics. For that reason, we carried out an experiment on a sample made of 50 planar slides (parallel and equidistant), stacked in a cylindrical rack (diameter=12mm) [9]. Turning this rack around it's major axis allows us to adjust the angle Ω between the normal **n** to the slides and the magnetic field **B**. Figure 1b shows that the ^{2}H-NMR spectrum obtained for Ω=90° is composed of a resolved doublet. Moreover the doublet spacing depends on the angle Ω and its variation reproduces faithfully the $|P_2(\cos\Omega)|$ function given in eq.3 (fig. 2).

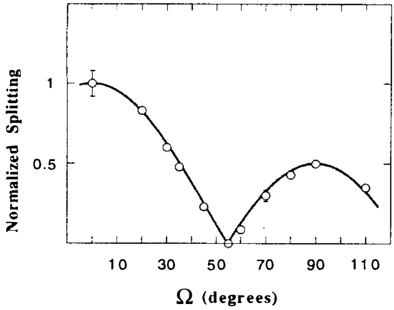

Fig 3: Variation of the normalized splitting $\frac{1}{2}\frac{\Delta\nu(\Omega)}{\Delta\nu(90°)}$ versus the angle Ω.

Discussion

Spectra analysis : The result obtained on the "monodomain" demonstrates that the normal to the grafting plane is a uniaxial symmetry axis for the segment motions, and gives direct access to the mean degree of order S of the chain segments. Additionally, we have observed that the half-height linewidth of the doublet component depends also on the angle Ω and reproduces the $|P_2(\cos\Omega)|$ function [9]. This implies that the linewidth comes from a distribution of order P(S) related to a non uniform segmental orientation along the grafted chains. Hence, the relaxation function observed on the "monodomain" may be expressed as :

$$M_{slide}(\Omega,t) = \int_{-\infty}^{\infty} e^{-t/T_2} \cos(\nu_Q \, |P_2(\cos\Omega)| \, S \, t) \, P(S) \, dS \qquad (5)$$

Consequently, it is clear that the spectrum obtained on porous silica arises from a superposition of various doublets associated with the random angular distribution of **n** (powder spectrum):

$$M(t)_{porous} = \int M(\Omega, t)_{slide} \sin\Omega \; d\Omega \qquad (6)$$

Note that the distribution of order P(S) can then be inferred from the "monodomain" spectrum and eq.(5)

Uniaxial dynamics: The main result of this NMR study is that the chain segments of a grafted melt exhibit an uniaxial reorientational dynamics around the normal **n** to the polymer-silica interface. This property is unambiguously observable on a macroscopically oriented sample ("monodomain") since the normal **n** is a symmetry axis for the system. The observed motional uniaxiality is likely related to the dense anisotropic confinement of the chains. The lateral packing of the chains arising from the high grafting density restricts their conformations. A simple way to visualize the chains' behavior is to consider that the orientational fluctuations take place through an anisotropic fluid medium made of partially aligned chains along the direction normal to the planar substrate. Therefore, the observed spectra are the typical response of an uniaxial fluid characterized by the mean degree of orientational order S. The value of S may be easily deduced from eq.3 (with ν_Q =175 KHz for PDMS methyl group) and from the splitting ($\Delta\nu$=450 Hz). Taking into account the chemical configurations of the PDMS monomer [10] the degree of order of the segment connecting two adjacent oxygen atoms of the chain is $S=2{,}3\times10^{-2}$. This local uniaxial order is typical of tethered flexible macromolecules. In particular, the same kind of motional uniaxiality was observed on amphiphilic molecules of water soap systems, and more recently on diblock copolymers organized in a lamellar structure [6].

Orientational correlations: Our results suggest that a strong local constraint occurs within the polymer layer. However, the observed anisotropy of chains does not necessarily correspond to an elongation of their end to end vector since the observed thickness of the polymer layer is close to the value of the radius of gyration Rg for a regular melt. Whatever the nature of the internal constraint is, the observed segmental ordering is not a single chain process but instead involves orientational correlations due to interactions between chain segments. The presence of such correlations is corroborated by the behavior of the layer upon swelling, at sufficient high degree of dilution. ^{2}H-NMR spectra of the swollen "brush" show a single line typical of an anisotropic dynamics: the orientational correlations between the chain segments are screened by the solvent molecules. These inter-chains effects may determine some physical properties of such nanolayers. For instance the diffusion of homopolymers free chains inside the grafted layer would be prevented by a loss of entropy, due to the orientational correlations. This might be related to some recent observations on dewetting of polymer layers coated by homopolymer melts [11].

Concluding remarks

This study shows that ^{2}H-NMR is a powerful tool for dynamical studies of polymer layers.

The present observations concerning dynamics of end grafted chains in the melt state infer to study the effect of relevant parameters such as the chain length and the grafting density. Besides, it would be interesting to investigate the screening or coupling effects of a swollen "brush" by solvents or homopolymer chains.These experiments have to be performed in association with wetting studies.

[1] S.T. Milner, Science 251, 905 (1991).

[2] G.J. Fleer et al, *Polymers at Interfaces.* (Chapman and Hall, Cambridge, 1993).

[3] P. Auroy, Y. Mir, and L. Auvray, Phys. Rev. Lett. 66, 719 (1991).

[4] A. Karim et al, Phys. Rev. Lett. 73, 3407 (1994).

[5] B. Deloche, M. Beltzung, and J. Herz, J. Phys. Lett. France 43, 763 (1982).

[6] S. Valic et al, Polymer (June, 1995)..

[7] P. Auroy, Ph.D. Thesis, Université Paris Sud (1990).

[8] J.P. Cohen Addad, R Vogin, Phys. Rev. Lett., 33, 940 (1974).

[9] M. Zeghal, P. Auroy and B. Deloche, (to be published).

[10] H. Toriumi et al, Macromolecules 18, 305 (1985).

[11] See for example G. Reiter contribution in these proceedings.

EFFECT OF A LOW MOLECULAR WEIGHT GRAFT COPOLYMER ON THE INTERFACIAL TENSION BETWEEN TWO INCOMPATIBLE POLYMERS.

Gabriel SCHREYECK, Pascal MARIE
Institut Charles Sadron (CRM-EAHP)
6, rue Boussingault
67083 STRASBOURG Cedex
FRANCE

We have studied the effects of a short graft copolymer poly(dimethylsiloxane)-g-poly(ethylene oxide) on the interfacial tension (γ) between poly(dimethylsiloxane) (PDMS) and poly(ethylene oxide) (PEO).

Variations of γ with time show a sharp decrease to a minimum, followed by a slow increase towards an equilibrium tension. The first part of the kinetics of interface formation corresponds to the adsorption of copolymer molecules at the interface. The second one is less expected and has been attributed to an interfacial phase transition.

Interfacial tension at equilibrium decreases linearly with the volume fraction of copolymer and levels off as a certain concentration of copolymer in the PEO phase is reached, in agreement with some theories. Furthermore, the change in the slope may be attributed to the micellisation of the copolymer in the PEO phase.

INTRODUCTION

It is well known that amphiphilic A-B copolymers preferentially segregate to the interface between two incompatible homopolymer phases A and B1)2). They therefore increase the compatibility of homopolymers and reduce the interfacial tension between immiscible polymers. Such amphiphilic copolymers are usually used to modify the physical properties of the interface in order to improve its mechanical strength and to enhance the adhesion between polymer phases. They are also used as a compatibilizing agent in blends, in order to control the stability and morphology of the dispersed phase.

Our aim in this work is to study the adsorption of a low molecular weight graft copolymer at the interface between two incompatible homopolymers (i.e. $\chi N >> 1$, N being the number of monomer per chain and χ the Flory parameter). We are interested in studying the interfacial tension (γ), especially the kinetics of interface formation γ as a function of time (t); the influence of the temperature (T) on γ ; and the influence of copolymer concentration (Φ_{cop}).

EXPERIMENTAL SECTION

Materials

The polymers we have used are poly(dimethylsiloxane) (PDMS) of molecular weight (M_n), $M_n = 22\ 400$ g/mol and poly(ethylene oxyde) (PEO), $M_n = 1\ 000$ g/mol. These polymers are incompatible ($\chi^{80°C} = 0.62$) and different as PDMS is hydrophobic and amorphous whereas PEO is hydrophilic and semi-crystalline.

The copolymer is PDMS-graft-PEO, $M_n = 1\ 200$ g/mol with 67 percent by weight of ethylene oxyde. A NMR ^1H study shows that it has a backbone of 4 dimethylsiloxane monomers on which are graft 2 chains of 9 ethylene oxyde monomers.

Furthermore, we have studied the behavior of the copolymer at the air / water interface at 25°C by measuring the surface tension of aqueous solutions using the DuNoüy ring method. The plot of the surface tension versus log copolymer concentration decreases linearly up to a concentration corresponding to the critical micellar concentration ($\sim 3.10^{-4}$ g/cm^3). The surface area per molecule which can be obtained from the limiting slope of straight line, via the Gibbs' equation, turned out to be 62 Å^2. We have also deduced an interfacial width of about 30 Å. From these data, we can give a schematic conformation of the copolymer molecule (Figure 1) which should not be very different from that of the PDMS / PEO interface.

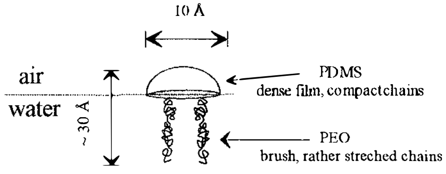

Figure 1 : Schematic conformation of the copolymer at the air / water interface

Interfacial tension measurements

The interfacial tensions were measured by a pendant drop apparatus which uses a video digital image processing technique. A block diagram of the apparatus is shown in Figure 2. A fluid drop of different mixtures of copolymer with PEO was formed, at the tip of a glass capillary tube, in a matrix of the PDMS phase. The digitalized image of the drop is analysed with commercial VISILOG® software to extract the arbitrary coordinate points of the drop profile. The experimental profile is compared to the calculated Laplacian profile with a robust shape comparison algorithm until satisfactory convergence is obtained. The resulting output is the interfacial tension (γ) given with a good accuracy (0.05 mN/m).

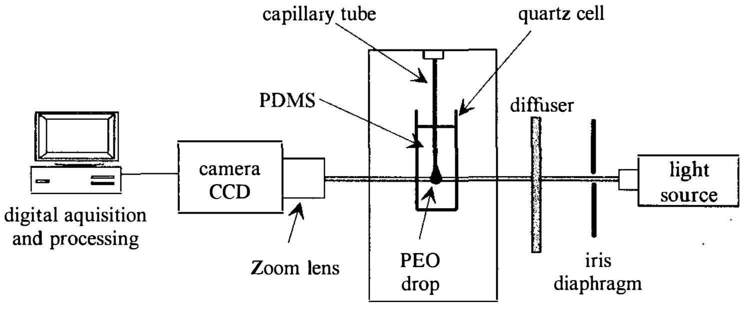

Figure 2 : Schematic representation of the pendant drop apparatus

RESULTS AND DISCUSSION

Kinetics of interface formation

The time dependance of the interfacial tension for the PDMS / PDMS-g-PEO / PEO system is shown in Figure 3.

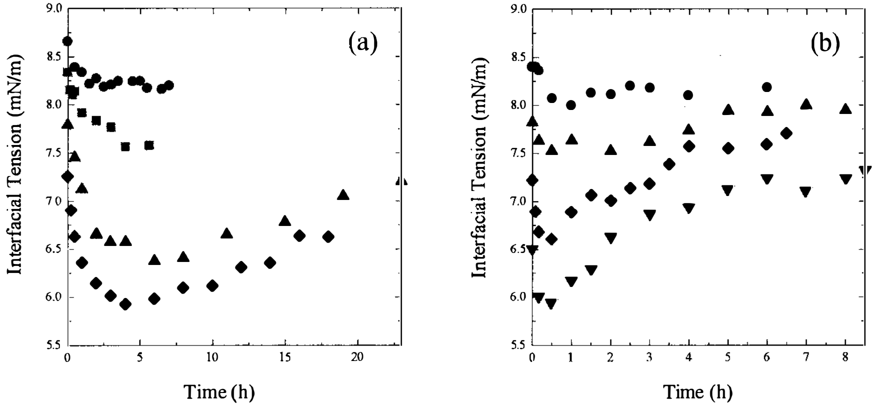

Figure 3 : Time dependance of the interfacial tension for the PDMS/PDMS-g-PEO/PEO system at two temperatures : (a) 80 °C, (b) 140 °C and at different concentrations of copolymer in the PEO phase ● 1% ; ■ 2% ; ▲ 2,5% ; ◆ 5% ; ▼ 7.5%.

We can observe a fast decrease of γ with time to a minimum, followed by a slow increase towards an equilibrium. This behavior is accelerated as the temperature increases from 80 to 140 °C. These kinetics have never been observed before, and can be explained as follows :

- the first part of the curve (sharp decrease) can be attributed to the diffusion of the copolymer to the interface followed by a slow adsorption at the interface with an energy barrier3).
- the second part (increase) is unexpected and may be the result of a surface phase transition. We can imagine, for example, a transition from a hemi-micellar surface phase towards a thin interfacial copolymer film with the expulsion of copolymer molecules from the interface4) (Figure 4). The copolymer cannot go through the interface in the PDMS phase because it is immiscible with the high molecular weight PDMS. Thus, the expulsion has to occur in the PEO phase.

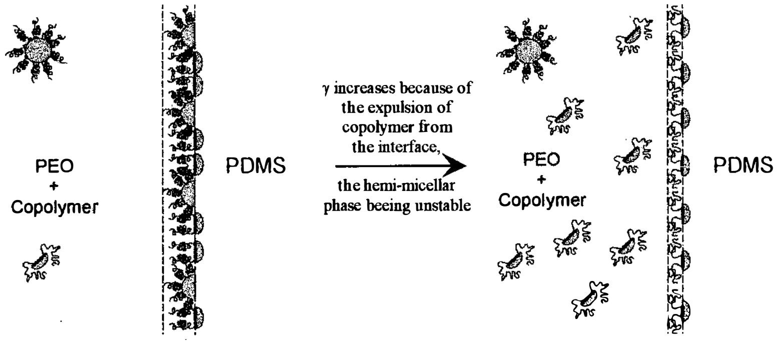

Figure 4 : Schematic interpretation of the unexpected part (increase of γ with time) of the formation kinetics of the PDMS/PDMS-g-PEO copolymer/PEO interface.

Effect of the copolymer concentration

Interfacial tension at equilibrium decreases linearly with increasing copolymer concentration in the PEO phase and levels off beyond a volume fraction of $\Phi_{cop} \sim 0.58$ (Figure 5a). This change in the slope may be attributed to the micellisation of the copolymer in the PEO phase. Thus, the concentration at which it happens can be thought of as a critical micellar concentration (Φ_{cmc}) in the melt. The high value found for this CMC is not very surprising as the copolymer has a very low molecular weight.

The linear decrease before the CMC can be interpreted with the help of the theory of Noolandi5). We obtain, with certains approximations6), the following formula :

$$\gamma \approx \gamma_0 + d\left\{\frac{\chi}{2} + \frac{1}{Z_c}\left(1 - e^{Z_c\chi/2}\right)\right\}.\phi_c \tag{1}$$

where γ_o is the interfacial tension without copolymer, d is the width at the half height of the copolymer profile and Z_c, the degree of polymerisation of the copolymer. For our system, we can deduce an interfacial width of d ~ 8 Å.

We can also interpret the results using Gibbs' equation (Figure 5b). The slope of the linear part gives a surface area per copolymer molecule of 180 $Å^2$ which corresponds to an interfacial width of 10 Å. This value is consistent with the previous analysis.

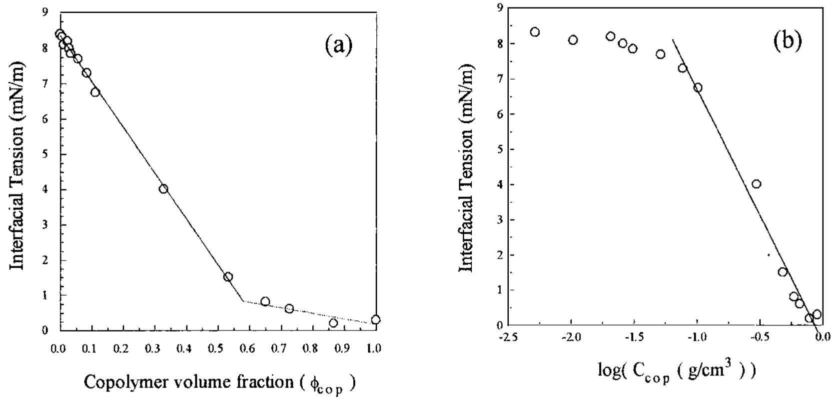

Figure 5 : Equilibrium interfacial tension for the PDMS/PDMS-g-PEO/PEO system as a function of copolymer concentration. (a) The solid line is a linear fit from the theory of Noolandi *et al.*, (b) The solid line is a linear fit from the Gibbs' equation.

CONCLUSION

In this study, the effect of the addition of a low molecular weight PDMS-graft-PEO copolymer in reducing the interfacial tension between PDMS and PEO has been investigated as a function of copolymer concentration. The interfacial tension data demonstrate the surfactant-like behavior of the added graft copolymer. Comparison with predictions have shown an interface rather small compared to the one found in the case of water/air interface. But the most surprising result is the evolution of the interfacial tension with time. Indeed, after the decrease in γ vs time corresponding to the diffusion and adsorption of the copolymer at the interface, we observe an increase in the same curves. This increase has been explained as an interfacial phase transition.

REFERENCES

1) S. Wu, *Polymer Interface and Adhesion*, Marcel Decker, chap.3 (1982).
2) J.T. Koberstein, *Encyclopedia of Polymer Science and Engineering*, Wiley, **8**, p. 237 (1987).
3) J. F. Baret, J. Chim. Phys., **65**, p. 895 (1968).
4) Discussion with C. Ligoure at the XXXth Rencontres de Moriond (1995).
5) J. Noolandi, K. M. Hong, Macromolecules, **17**, p. 1531 (1984).
6) S. H. Anastasiadis, I. Gancarz, J. T. Koberstein, Macromolecules, **22**, p. 1449 (1989).
7) G. Schreyeck et P. Marie, C. R. Acad. Sci. II (submitted).

HOW DO SURFACE FIELDS COUPLE TO BULK ORDERING ? AN EXAMPLE OF SURFACE-INDUCED LAMELLAR ORDERING.

M S Turner*, Cavendish Lab, Madingley Road, Cambridge CB3 0HE, UK.
C M Marques, I.C.S., 6 rue Boussingault, 67083 Strasbourg Cedex, France.
M Rubinstein, Image Research Lab, Kodak Co., Rochester, NY 14650-02116.

We study theoretically the hexagonal phase of diblock copolymer melts and determine to what extent lamellar ordering is induced near a flat surface. For a full account of this work see Ref. 1. In the limit of weak segregation (ordering) we employ a Landau-Ginzburg mean-field theory. In the strong segregation limit we use instead an expansion in derivatives of the lamellar displacement u, with appropriate boundary conditions. The surface field, proportional to the differential affinity of blocks A and B to the surface, couples to the ordering and increases the lamellar character of the ordered structure close to the surface. The extent of the region where this lamellar character predominates diverges logarithmically when the bulk hexagonal-lamellar transition is approached. In the strong segregation limit we find that the lamellar region exists provided that the surface field is larger than some critical value, readily obtainable in experiments. We believe that our approach may prove useful for other systems, including lyotropics.

1. Introduction

It is now well established that, for temperatures below the order-disorder temperature T_{ODT}, diblock copolymers self-assemble spontaneously in the melt to form ordered phases of layers (the lamellar phase), rods (the hexagonal phase), spheres (the cubic phase) as well as others[2]. In the so-called weak segregation limit the excess of one of the species varies smoothly over the sample whilst in the strong segregation limit $T \ll T_{ODT}$ there is a sharp interface between alternate regions of almost pure A or B blocks.

We consider here a monodisperse melt of linear diblock copolymers with total degree of polymerization N, made up of one A-block of N_A monomers joined to one $B-$block of $N - N_A$ monomers. The bulk phase behaviour is sensitive to two parameters[3,4] (i) χN, where χ is the Flory incompatibility parameter between polymer A and B, in $k_B T$ units, and (ii) the molecular asymmetry parameter $f \equiv N_A/N$. For symmetric ($f = 1/2$) copolymers the lamellar phase is formed[3] for temperatures $\chi N > 10.49$. For asymmetric copolymers ($f \neq 1/2$) cubic and hexagonal structures are predicted to form at lower temperatures, *i.e.*, at higher values of χN. Well below the transition temperature, in the so-called strong segregation limit, the phase behaviour is mainly controlled by f. The hexagonal phase is found for $0.12 < f < 0.28$ whereas the lamellar and cubic phases are found for $0.28 < f < 0.5$ and $f < 0.12$ respectively[4]. In the present work we study the extent of surface-induced lamellar ordering in copolymer melts where the stable phase in the bulk is hexagonal.

II. Weak Segregation

We study the interfacial structure close to the ordering transition. In this limit the system can be described by a Landau-Ginzburg expansion of the free-energy as a function of the local average excess content of (say) monomers A, $\psi(\mathbf{r}) = \phi_A(\mathbf{r}) - \langle\phi_A\rangle$

$$F[\psi_q]N = \frac{1}{2!}\int_q NS(q)^{-1}\psi_q\psi_{-q} - \frac{\mu}{3!}\int_q\int_{q'}\psi_q\psi_{q'}\psi_{-q-q'} + \frac{\lambda}{4!}\int_q\int_{q'}\int_{q''}\psi_q\psi_{q'}\psi_{q''}\psi_{-q-q'-q''} \tag{1}$$

where $S(q = |\mathbf{q}|)$ is the Fourier transform of the two-point correlation function in the disordered homogeneous phase, and ψ_q the $q-$Fourier component of the order parameter ψ. Close to the order-disorder transition the susceptibility $S(q)$ is strongly peaked around some vector q_0 and can be approximated by $S^{-1}(q) = \tau + c\,(q^2 - q_0^2)^2$ with an effective temperature $\tau = 2(\chi N)_s - 2(\chi N)$.

The bulk hexagonal phase can be described by a first-harmonic expansion of the order parameter

$$\psi(z,y) = 2a_1\cos\{q_0 z\} + 2a_2\cos\{q_0\frac{\sqrt{3}y - z}{2}\} + 2a_3\cos\{-q_0\frac{\sqrt{3}y + z}{2}\} \tag{2}$$

with $a_1{=}a_2{=}a_3{=}a_h$. Whilst instead the lamellar phase corresponds to $a_1{=}a_l$ and $a_2{=}a_3{=}0$.

The interfacial free-energy excess $\bar{\Omega}$ near an interface is given by

$$\bar{\Omega} = \int_V dV\,[\psi(\mathbf{r})U(\mathbf{r}) + F[\psi(\mathbf{r})] - F[\psi(x,y,z\to\infty)]] \tag{3}$$

Here U is the surface potential, for which we employ $U(z) = -\Delta\gamma\delta(z)$, where $\Delta\gamma = \gamma_{BS} - \gamma_{AS}$ and γ_{AS} and γ_{BS} are the interfacial tensions of polymers A and B with respect to the surface. For a weak enough hexagonal-lamellar transition (which implies a weak enough asymmetry μ) the bulk correlation length can still be large compared to q_0^{-1}, the period of the ordered phases. In this limit we look for solutions of the order parameter $\psi(z,y)$ as in (2) but with $z-$dependent amplitudes. By symmetry only two out of the three amplitudes are independent $a_1(z) \neq a_2(z) = a_3(z)$. The slow variation of the amplitudes on the scale of the crystalline wavelength allows us to make a gradient expansion. We renormalise the distances by $z = t\xi$ with $\xi^2 = 8cq_0^2\lambda/\mu^2$, and the amplitudes by $a_2 = Y\mu/\lambda$ and $a_1 = X\mu/\lambda$, where the bulk equilibrium values of the amplitudes are $X = \sqrt{2\alpha}$ and $Y = \frac{1+\sqrt{1+10\alpha}}{5}$ with $\tau = -\alpha\mu^2/\lambda$. Integrating and minimising with respect to X and Y we obtain the following two coupled differential equations

$$\begin{aligned}\frac{d^2X}{dt^2} &= (-2\alpha + 4Y^2)\,X + X^3 - 2Y^2\\ \frac{d^2Y}{dt^2} &= (-2\alpha - 2X + 2X^2)\,Y + 3Y^3\end{aligned} \tag{4}$$

where $C = 8\Delta\gamma\xi\lambda^2/(3\mu^3)$. These are to be solved subject to the boundary conditions $\frac{dX}{dt}(z=0) = -C$, $\frac{dY}{dt}(z=0) = 0$ and $X(t=\infty) = Y(t=\infty) = \frac{1+\sqrt{1+10\alpha}}{5}$ There is an interesting analogy between our copolymer system and the movement of a classical particle of mass unity moving in (X,Y) space. The solution of (4) corresponds to the trajectory of a particle starting with a speed $-C$ tangential to the $X-$axis and terminating at (X_∞, Y_∞) with zero speed, see Fig. 1a. The positions corresponding to the pure lamellar or hexagonal phases are tops of hills. Above the transition temperature between the hexagonal and lamellar phases the height of the hexagonal hill is larger then the height of the lamellar hill. Because there is conservation of the total energy it is possible to define the curve in the (X,Y) space where the initial point must be located (complete determination of the initial position would require a second integral of motion). This curve is simply the equipotential line at the level $-C^2/2$ from the top of the hexagonal hill.

In Fig. 1a we present a trajectory obtained by numerical integration of the differential equations (4) describing the interfacial structure. For temperatures approaching the transition temperature from above, the trajectories pass increasingly closer to the top of the lamellar hill where they have a small speed. This slowing down, and hence the region of lamellar-like ordering, extends up to a distance l which diverges logarithmically with the distance from the transition tempreature in α units, $\alpha - \alpha_c$ ($\alpha_c = (7+3\sqrt{6})/5 \approx 2.87$)

$$l = aR\log\{bN(\alpha - \alpha_c)\} \tag{5}$$

where a and b are functions of the surface strength $\Delta\gamma$. The logarithmic divergence is characteristic of wetting problems.

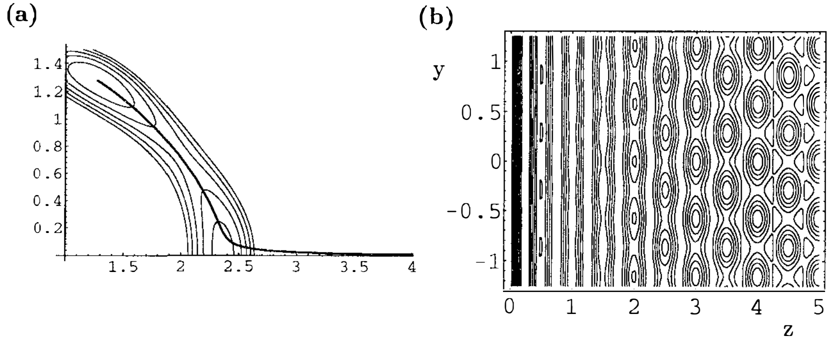

Figure 1 (a) The trajectory of a classical particle according to the "equations of motion" (4), close to the hexagonal-lamellar phase transition ($\alpha = 2.8$, $\alpha - \alpha_c = -0.07$). The reduced surface strength is $C = 20$. The trajectory stops at the top of the hexagonal hill at $t, z \to \infty$. The lamellar metastable point is at $(\sqrt{5.6}, 0)$. Drawn equipotential lines are at levels -0.1, -0.2, -0.3, -0.4, -0.5. **(b)** A contour plot of ψ in the same interfacial region. The correlation distance ξ defined in the text is taken in this case to be equal to $4\pi q_0^{-1}$.

Summarizing the results for the weak segregation case we stress that: (i) The lamellar order appearing close to the surface in our weakly ordered hexagonal phase is induced by the preferential coupling between the surface potential and the wave component perpendicular to the interface. (ii) The extent of the lamellar region diverges logarithmically with the relative decrease in temperature below the lamellar - hexagonal transition.

III. Strong segregation

We assume that a region of lamellar ordering exists in the vicinity of the surface, see Fig. 2. The normal to the solid surface and the axis of symmetry of the hexagonal phase define the z- and x-directions respectively. The local vertical displacement of the lamellar layer is u and we take the continuum limit where u varies smoothly throughout the sample. The energy density of the deformation of the lamellar phase, for $z < \xi$, is[5]

$$F = \frac{B}{2}\left(\frac{\partial u}{\partial z}\right)^2 + \frac{K}{2}\left(\frac{\partial^2 u}{\partial y^2}\right)^2 \tag{6}$$

Here K is the bending or splay modulus and B is the compression modulus.

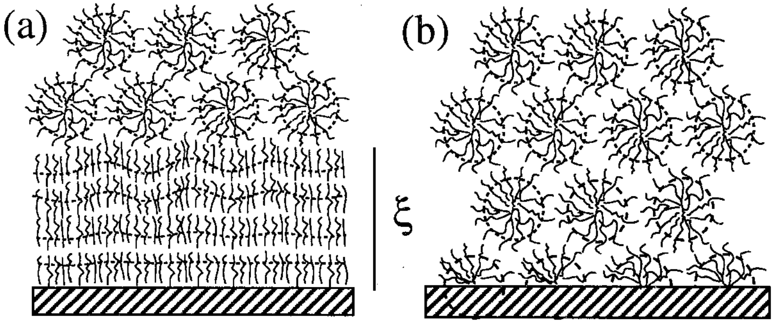

Figure 2 **(a)** Schematic diagram of the lamellar ordering which may be induced at the surface. We see a slice through the y-z plane with symmetry in the x-direction. The dotted circles represent the position of the interfaces between the A and the B-blocks of the copolymers. **(b)** The alternative case that no lamellar ordering exists. Note that both A and B components of the copolymer are in contact with the surface in this case.

We retain only the first fourier component of the lamellar displacement field $a(z)$ with $u = a(z)\cos qy$. The boundary conditions are that the solid surface is flat $a(0) = 0$ and that the undulation of the lamellae must match onto the hexagonal phase at the relevant interface, approximated by $a(\xi) = a_o$. Minimising (6) we find that $a(z) = a_o\frac{\sinh\nu z}{\sinh\nu\xi}$ with ν a characteristic inverse length given by $\nu = q^2\sqrt{K/B}$. By using this result for $a(z)$, integrating over $0 < z < \xi$ and adding the surface and chemical potential contributions we obtain the total free energy excess per unit area

$$\Delta\Omega = \frac{1}{4}a_o^2\sqrt{KB}\,q^2\coth\nu\xi + \Delta F\,\xi - p\Delta\gamma \tag{7}$$

where ΔF is the chemical potential between the hexagonal and lamellar phases and $p(f) \sim 1$ is the proportion of the surface which would be in contact with the unfavourable polymer component if the hexagonal phase existed at the surface, see Fig. 2b. In order to determine the penetration depth ξ we minimise $\Delta\Omega$ with respect to ξ

$$\xi = \frac{1}{\nu}\sinh^{-1}\left(\frac{K\,a_o^2 q^4}{4\Delta F}\right)^{1/2} \tag{8}$$

Which simplifies in the limit $\xi\nu \gg 1$ (many layers) to $\xi = \frac{1}{2\nu}\log\left(K\, a_o^2 q^4/\Delta F\right)$.

We estimate[6] $B = 3\gamma_{AB}/h$ and $K = \gamma_{AB}h/3$ where $h = (\gamma_{AB}/3)^{1/3}N^{2/3}$ is the thickness of a single lamellar layer and $\gamma_{AB} = b\chi^{1/2}$, where b is the monomer size, is the interfacial tension acting at the AB interface[4]. The amplitude and the wavelength of the lamellar undulations at the interface with the hexagonal phase are both of the order of the hexagonal lattice size (repeat distance) which is itself of the order of the lamellar thickness h. Thus the product $\xi\nu$ is the number of layers in the lamellar region, to within a numerical prefactor of order unity. Using these estimates and neglecting numerical factors of order unity, we find

$$\xi/h \simeq \text{const} + \log\frac{\gamma_{AB}}{h\Delta F} \tag{9}$$

This behaviour, where ξ diverges logarithmically as $\Delta F \to 0$, suggests that ξ is rarely very large. An estimate of ΔF may be obtained by comparing the free energy densities of the hexagonal and lamellar phases near the phase boundary[4]. To first order in f we find $\Delta F = \text{const.}(\gamma_{AB}/N)^{2/3}(f_o - f)$ where $f_o \approx 0.28$ is the position of the phase boundary and the constant of proportionality has a numerical value of approximately 3.05.

The lamellar region exists whenever the energy difference $\Delta\Omega$ is negative. Solving $\Delta\Omega = 0$ for $\Delta\gamma$ we find that the lamellar region exists for $\Delta\gamma > \Delta\gamma_c$ where $\Delta\gamma_c \simeq \gamma_{AB}$ in the limit $\xi\nu \gg 1$. Since the magnitude of the surface tensions at a polymer/air interface can be much larger than γ_{AB} it seems likely that this condition may be readily accessible experimentally.

Three main approximations are inherent in the preceding treatment: (i) We ignore the effect of any distortion to the hexagonal phase near the interface with the lamellar region. (ii) We neglect all higher order fourier components of the displacement field u. (iii) We utilise an expansion of the free energy Eq. (6) which is strictly only valid for slowly varying perturbations. However, we do expect our results to remain accurate at the qualitative level.

References

1. Turner, M.S.; Rubinstein, M.; Marques, C.M. *Macromolecules* **1994**, *27*, 4986.
2. Bates, F.S.; Fredrickson, G.H. *Annu. Rev. Phys. Chem.* **1990**, *41*, 525.
3. Leibler, L. *Macromolecules* **1980**, *13*, 1602.
4. Semenov, A.N. *Sov. Phys.-JETP* **1985**, *61*, 733.
5. de Gennes P. G. *J. Phys. Suppl. C4* **1969**, *30*, 65.
6. Turner, M.S.; Joanny, J.F. *Macromolecules* **1992**, *25*, 6681.

POLYMER MATRIX INFLUENCE ON THE KINETICS OF SOME FUNDAMENTAL INORGANIC COLLOIDAL REACTIONS

Rina Tannenbaum
Department of Chemical Engineering and Materials Science
University of Minnesota
Minneapolis, MN 55455, U.S.A.

Among the most useful methods for the preparation of pure metal powders is the thermolysis of metal carbonyl complexes in hydrocarbon solutions. Zero-valent cobalt particles are obtained by the decomposition of $Co_2(CO)_8$. The reaction is primarily governed by diffusion which is strongly dependent on the viscosity of the solution. In a solution containing polystyrene, the viscosity is directly proportional to the concentration of the polymer. To study the variation of the rate constants of this colloidal reaction as a function of the solution viscosity, we examined various polystyrene solutions of different molecular weights and concentrations. The reaction rate increases considerably at polymer content below and at the critical coil overlap concentration. Above this concentration, as the polymer coils become entagled and contracted, the decreased mobility of the molecules due to higher viscositiy and lower diffusion rate, lowers the reaction rate. The influenece of the molecular weight of the polystyrene on the reaction kinetics had a "catalytic" effect on reaction rates and was most dramatic with a $MW_{(avg)}$ of ~120,000. We find that in the dilute polymer regime, below the PS coil overlap threshold, the polymer chains can provide the necessary support for the aggregation of the cobalt particles. Also, in the dilute regime, the mobility of the cobalt molecules is not hindered due to the low solution viscosity. However, there is evidently a critical molecular weight at which the "catalytic" effect of the polymer is at its maximum. These results will be discussed, and possible mechanisms for the polymer-enhanced colloid reactions will be offered.

1. INTRODUCTION

Thermolysis of transition metal carbonyl complexes in solution under an inert atmosphere is a well known technique for the preparation of pure metal powders[1]. The thermal decomposition of $Co_2(CO)_8$ to metallic cobalt and carbon monoxide under an inert atmosphere at temperatures ~90°C, proceeds in two steps[2,3]: the first step is the equilibrium decomposition of $Co_2(CO)_8$ to $Co_4(CO)_{12}$ and the second step is the irreversible decomposition of $Co_4(CO)_{12}$ to $Co^{(0)}$ clusters, whereas CO_g is released in both steps.

$$2Co_2(CO)_8 \rightleftharpoons Co_4(CO)_{12} + 4CO_g \qquad (I)$$

$$Co_4(CO)_{12} \rightleftharpoons Co_4 + 12CO_g \dashrightarrow Co_k^{(0)} \qquad (II)$$

The thermal decomposition reaction of cobalt carbonyl complexes in solutions and in polymer matrices (referred here as solid state) has been thoroughly documented[2,3]. The mechanistic aspects of the solid state decomposition were similar to those found with the solution decomposition, as concluded from the type of intermediates formed in the reaction in both cases, and from the nature of the end-products. The kinetic aspects, however, were quite different for the two media, as the rate constant found for the solid state reaction, was two orders of magnitude smaller than the one found for the solution reaction[4]. Hence, embedding $Co_2(CO)_8$ in a polymeric matrix (high molecular weight polystyrene) significantly slowed down the decomposition process. The decomposition of $Co_2(CO)_8$ to $Co_4(CO)_{12}$ and further to metallic Co is primarily governed by the diffusion of the molecules through the viscous medium. The solid state polystyrene system provides a medium with a considerable increase in viscosity[5,6], thus giving rise to lower reaction rates.

The study of the variation of the rate constants of reactions (I) & (II) as a function of the concentration of the polystyrene moiety in the cobalt carbonyl solutions[7] shows that since reaction (I) is primarily governed by diffusion, the reaction rate decreases with the increase in polystyrene content above the critical coil overlap concentration. Reaction (II), on the other hand, being a colloidal reaction, is greatly facilitated by the presence of the polymer, and the reaction rate increases considerably at polymer content below and at the critical coil overlap concentration. Previous reports[8,9] describe the stabilization of colloidal cobalt particles in dilute polymer solutions, by adsorption of the polymer to the metal particles to form a film that separates the particles sufficiently to keep Van der Waals forces below thermal energy levels. Above the critical coil overlap concentration, as the polymer coils become entagled and contracted, the decreased mobility of the molecules due to higher viscositiy and lower diffusion rate, has the effect of lowering the reaction rate of reaction (II) as well.

The effect of polymer concentration on the decomposition kinetics was examined with polystyrene of $MW_{(avg)}$=250000[7]. In this paper we examine the effect of the variation of molecular weights and concentrations of polystyrene on the kinetics of reaction (II), which seems to be the one "catalyzed" by the presence of polystyrene in the reaction solution.

2. RESULTS AND DISCUSSION

Reaction (II) may be approximated to be a first order reaction, and therefore the rate constant becomes k_{dec} and the rate expression is:

$$\ln x = k_{dec} \cdot t \qquad \text{(III)}$$

(where: $x=[Co_4(CO)_{12}]_t$)

Figure 1 portrays the kinetics of reaction (II) in solutions of polystyrene of various molecular weights and various concentrations. A closer examination of the polystyrene solutions for which k_{dec} reaches its maximal value, reveals that the polystyrene content corresponds to its critical concentration in dilute solutions, c*, a concentration which marks the onset of the coil overlap process between the polymer chains in solution[6]. For polystyrene concentrations [PS]<c*, the polymer coils have infinite dilution radii and do not overlap, while for [PS]=c*, the coils begin to overlap having reached the overlap threshold. At this critical concentration c*, the intrinsic viscosity, $[\eta]$, corresponds to the relationship: $c^* \cdot [\eta]=1$[6]. The intrinsic viscosity is a measure of the polymer's ability to increase solution viscosity in the absence of intermolecular effects, i.e., at infinite dilution. The intrinsic viscosity of polystyrene in toluene may be calculated according to the Mark-Houwink experimental relation: $[\eta]=KM^{a}$, where K and a are specific constants for various polymer/solvent combinations. Table 1 (inserted in Figure 1) lists the coil overlap concentrations, W*(wt%), for the $MW_{(avg)}$ chosen for this study.

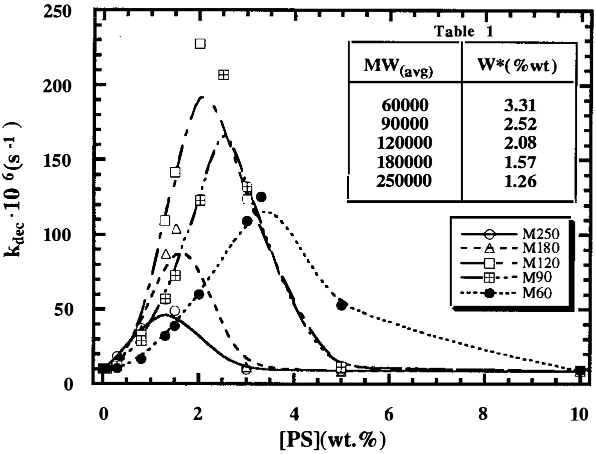

Table 1

$MW_{(avg)}$	W*(%wt)
60000	3.31
90000	2.52
120000	2.08
180000	1.57
250000	1.26

Figure 1: The influence of polystyrene concentrations at different molecular weights on rate coefficients.

The dependence of $k_{dec(max)}$ (at c*) on molecular weight is shown in Figure 2. The rate coefficients for reaction (II) increase with polymer chain size at lower molecular weights, but decrease at higher molecular weights. The "catalytic" effect which the presence of polystyrene has on reaction (II) is most dramatic with a $MW_{(avg)}$ of ~110,000. Previous studies of metal-polymers interactions reveal that under certain conditions (typical for each metal-polymer pair), there are specific coordination bonds which can develop between an electron-deficient metallic species and an organic moiety in the polymer chain containing π molecular orbitals. In reaction (II), the mechanism of decomposition implies the existance of such electron-deficient cobalt species, and therefore it is most likely that they will interact with the π–system of the phenyl rings in the polystyrene molecule[9,10]. Such an interaction creates a driving force which prompts the cobalt molecules to seek the proximity of the polystyrene. On this basis, it is possible to analyze the dependence of k_{dec} on the polymer concentration in solution and on the polymer molecular weight. The rate of reaction (II) is a function of the cobalt concentration associated with

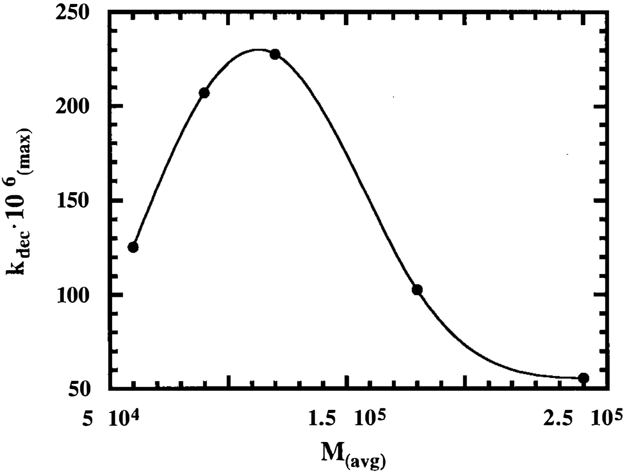

Figure 2: Dependence of rate coefficients on molecular weight of polystyrenε at the corresponding W*.

the polymer chains, the mobility of the cobalt species in solution and the ability of cobalt particles on different chains to interact with each other. As [PS] increases, the cobalt concentration within the polymer increases, but the mobility of the cobalt species decreases due to the increase in solution viscosity, and hence the behavior shown in Figure 1. Furthermore, as [PS] increases, the concentration of the cobalt species within the chains increases, but the excluded volume of each chain increases as well, thus rendering interactions between the chain more difficult and resulting in the behavior shown in Figure 2.

An interesting insight into the mechanism of decomposition can be obtained by the normalization of the results, i.e. their expression as the ratio of k_{dec} and k_{dec} at c* ($k_{dec}/k_{dec(max)}$) as a function of the ratio of polystyrene concentration and c* ([PS]/c*) for that particular molecular weight, as shown in Figure 3. The data points lie on a "universal curve", which implies that the "catalytic" influence which the presence of polystyrene in the solution has on reaction (II) is a general characteristic of this type of systems.

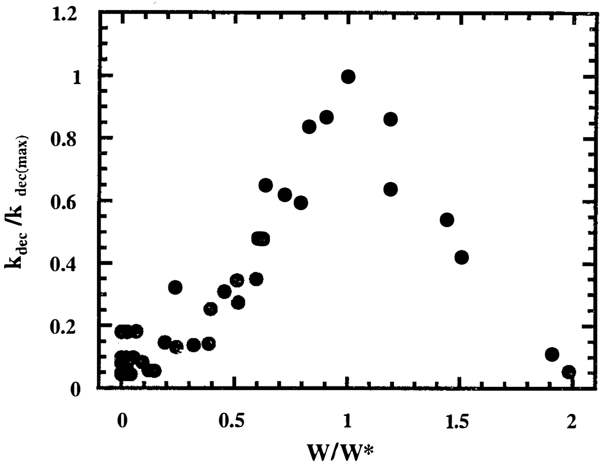

Figure 3: The universal behavior of the rate coefficient dependence on coil overlap concentration at corresponding molecular weights of polystyrene.

References

1. G. F. Emerson, K. Ehrlich, W. P. Giering and D. Ehntholt, *Trans. N.Y. Acad. Sci.*, **30**, 100 (1968).
2. M. F. Mirbach, A Saus, A. M. Krings and M. J. Mirbach, *J. Organometal. Chem.*, **205**, 229 (1981), and pertinent references therein.
3. G. Bor, U. K. Dietler, P. Pino and A. Poë, *J. Organometal. Chem.*, **154**, 301 (1978), and pertinent references therein.
4. R. Tannenbaum, C. L. Flenniken and E. P. Goldberg, *J. Polym. Sci. Phys. Ed.*, **25**, 1341 (1987), and pertinent references therein.
5. R. B. Bird, C. F. Curtis, O. Hassager and R. C. Armstrong, *Dynamics of Polymeric Liquids:* Vol. 2, *Kinetic Theory* , 2nd ed., Wiley, New York, 1987, and pertinent references therein.
6. P. G. deGennes, *Scaling Concepts in Polymer Physics*, Cornell University Press, Ithaca, New York, 1979, and pertinent references therein.
7. R. Tannenbaum, Inorg. Chim. Acta , 227, 233 (1994), and pertinent references therein.
8. P. H. Hess and P. H. Parker, Jr., *J. Appl. Polym. Sci.*, **10**, 1975 (1966).
9. H. Hirai and N. Toshima, Tailored Metal Catalysts , Y. Iwasawa ed., D. Reidel Publishing Company, New York, 1986, and pertinent references therein.
10. R. Tannenbaum, E. P. Goldberg and C. L. Flenniken, *Metal-Containing Polymeric Systems,* C. Carraher, C. U. Pittman and J. Sheats eds., Plenum Press, New York, 1985.

TWO-DIMENSIONAL ASSEMBLIES OF AMPHIPHILIC MOLECULES (LANGMUIR FILMS, MEMBRANES, COPOLYMERS,...)

SYMMETRY AND STRUCTURAL PHASE TRANSITIONS IN LANGMUIR MONOLAYERS

V.M.Kaganer
Institute of Crystallography, Russian Academy of Sciences
Leninskii pr. 59, 117333 Moscow, Russia
e-mail: kaganer@theory.rc.ac.ru

The condensed phases of Langmuir monolayers are treated in the framework of the Landau theory of phase transitions, as a result of successive ordering of the hexatic phase. The phase transitions are due to two degrees of freedom of long-chain molecules: the change of orientation of their long axes causes tilting phase transitions at decreasing surface pressure and the herringbone ordering of their short axes (backbone planes) gives rise to crystallization phase transitions with decreasing temperature. Crystallization occurs in two stages via intermediate 1D crystal phases. The theory describes the upright and tilted hexatic phases at high temperatures, the upright 1D herringbone-ordered crystal and two tilted ones differing in their directions of both tilt and crystallization at intermediate temperatures, and the upright and tilted 2D crystals at low temperatures. Distortions of the unit cell in different phases are treated as induced by the primary order parameters. The experimental data from monolayers of fatty acids with chain lengths from 19 to 22 is analyzed. The distortions due to the tilt of the molecules and ordering of their backbone planes are separated. The structure factor of the hexatic phase is calculated for the Nelson and Halperin model of the hexatic as a two-dimensional crystal containing a gas of interacting dislocations. The ratio of the radial to the azimuthal peak widths decreases considerably when the dislocations interact and depends on the sample size. The experimental data on the diffraction peak profiles in different phases of Langmuir monolayers is discussed.

Phase diagram of Langmuir monolayers. Transitions between condensed phases of Langmuir monolayers were first observed as kinks in the surface pressure — area isotherms more than fifty years ago. Systematic measurements by Stenhagen [1] and Lundquist gave rise to the phase diagrams which were modified since then only in their fine structure. Monolayers of different amphiphiles possess very similar phase diagrams. Although the measurements on any substance are performed in a limited temperature range, a generalized phase diagram can be compiled from isotherm studies of amphiphiles with different chain lengths by matching up regions of the same shape with regular shifts of the temperature axis [3]. Two novel experimental techniques, Brewster angle microscopy [4] and polarized fluorescence microscopy [5] were used to determine the phase diagram of fatty acid monolayers. It contains a new transition line which was not apparent in isotherm measurements, Fig. 1.

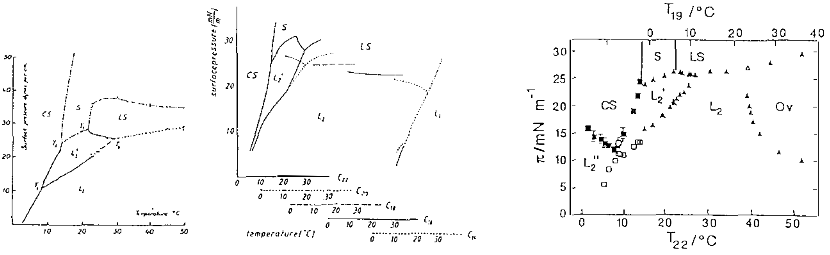

Figure 1: Experimental phase diagrams from Refs. [1, 3, 5]

Interpretation of diffraction data [6]. Recent x-ray diffraction experiments have shown that all kinks in the isotherms observed by Stenhagen and Lundquist are due to structural phase transitions and all regions of Fig. 1 have different structures. Structure determination is based on analysis of diffraction pattern of the monolayer, Fig. 2. The scattering pattern in reciprocal space is given by the product of two factors, the structure factor reflecting translational order of the molecular centers in the plane of the monolayer, and the form factor of the individual molecule. The structure factor of a 2D lattice consists of a set of delta-function discontinuities along lines ("Bragg rods") normal to the monolayer plane. The form factor of a long rod-like molecule takes on large values only on a disk normal to its long axis, which will be called the reciprocal disk of the molecule. The intersections of the first-order Bragg rods with the reciprocal disk give rise to three pairs of diffraction maxima. There is as yet no way of controlling monolayer mosaicity, and the diffraction pattern is always averaged over all domain orientations in the monolayer plane ("powder averaging"), with loss of direct azimuthal information.

If the molecules do not tilt on average, the reciprocal disk and hence all the peaks lie in the plane of the monolayer. In the phase *LS* possessing sixfold symmetry, all six first-order wave vectors have equal length and overlap completely in the powder pattern. The single observed peak is said to be triply degenerate. Because of this degeneracy, the sixfold symmetry of the *LS*

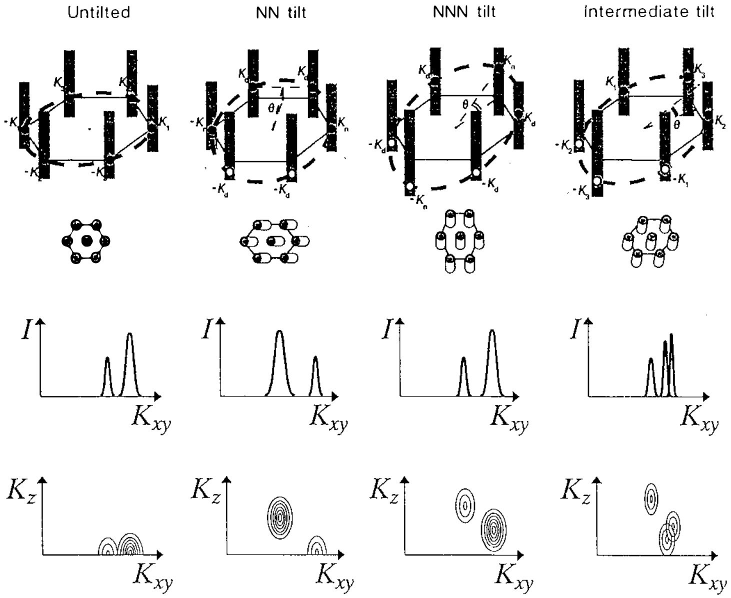

Figure 2: Interpretation of diffraction data

phase cannot be said to have been directly observed on the water surface. The triple degeneracy is lifted in cases where the lattice is distorted from hexagonal, due for example to an ordering of the backbone planes of the molecules, and distinct peaks are revealed.

The degeneracy may also be lifted by molecular tilt. In this case, the peaks move out of the monolayer plane which depends on both the tilt magnitude and its azimuth, or direction. Since the only points of the reciprocal disk to remain in the monolayer plane are those on the line perpendicular to the tilt, diffraction peaks from a tilted phase can only remain in the plane if they lie in this direction. This occurs for one pair when the molecules tilt towards one of their nearest neighbor (NN) molecules. When the molecules tilt to a next-nearest neighbor (NNN) molecule, all the wave vectors move out of the plane. If the tilt azimuth is intermediate between NN and NNN, or if the distortion of the unit cell is asymmetrical, there are three distinct first-order peaks.

Theoretical phase diagram [7, 8, 9]. The theoretical phase diagram, Fig. 3, is constructed to satisfy simultaneously the symmetry requirements of the Landau free energy expansion and the experimental data, both thermodynamical and structural. The nomenclature of the observed phases is preserved; the phase L_2 is subdivided, for symmetry reasons, into two phases, L_{2d} and L_{2h}. All features of the theoretical phase diagram are derived from the unique

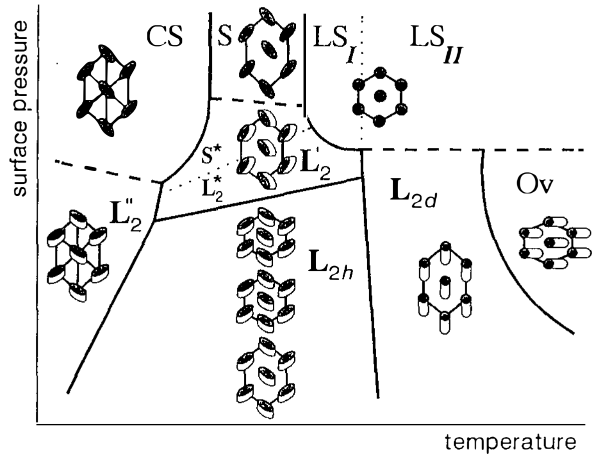

Figure 3: Theoretical phase diagram

free energy expansion invariant with respect to the hexatic symmetry of the most symmetrical phase, LS. Phase transitions are due to two degrees of freedom of long-chain molecules: the change of orientation of their long axes causes tilting phase transitions at decreasing surface pressure and the herringbone ordering of their short axes (backbone planes) gives rise to crystallization phase transitions with decreasing temperature. Crystallization occurs in two stages via intermediate 1D crystal phases. The present theory describes the upright (LS) and tilted (L_{2d} and Ov) hexatic phases at high temperatures, the upright 1D herringbone-ordered crystal (S) and two tilted ones (L'_2 and L_{2h}) differing in their directions of both tilt and crystallization at intermediate temperatures, and the upright (CS) and tilted (L''_2) 2D crystals at low temperatures.

Order parameters and free energy expansions [7, 8, 9]. The tilting phase transitions are described by two-component order parameter (η, β), where β is the azimuthal angle of the collective tilt and $\eta = \sin\theta$, where θ is the tilt angle. The most general expansion of the free energy invariant with respect to the sixfold symmetry of the hexatic phase is

$$\Phi_\eta = A\eta^2 + B\eta^4 - D\eta^6 \cos 6\beta + E\eta^{12} \cos 12\beta. \qquad (1)$$

The first two terms are sufficient to describe the second order phase transition at $A = 0$, provided $B > 0$. The last two terms, small in comparison with the first ones, are the lowest order terms depending on the tilt azimuth β. They give NN tilt ($\beta = 0$) for $D > 0$ and NNN tilt ($\beta = \pi/6$) for $D < 0$. As D varies from positive to negative values, the first order transition NN → NNN occurs for $E < 0$, whereas the second order phase transitions NN → I → NNN with an intermediate tilt azimuth in the phase I is realized for $E > 0$.

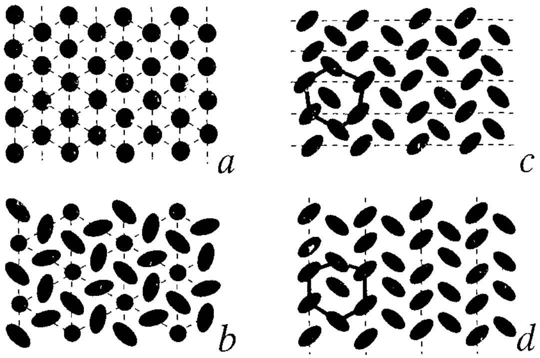

Figure 4: Possible crystallization waves: three waves of density (a) and herringbone order (b) with equal amplitudes, one wave of herringbone order with the wave vector in NN direction (c) and NNN direction (d)

There are two possible types of crystallization waves in 2D hexatic. Consider the transformation of the order parameter on reflection in the symmetry plane containing the wave vector. The order parameter can either remain unchanged, or change sign. The amplitudes of density waves ρ_1, ρ_2, and ρ_3, directed 120° to each other, are scalars which do not change sign on reflection. They give rise to the free energy expansion

$$\Phi_\rho = P\rho^2 + Q\rho_1\rho_2\rho_3\cos(\gamma_1+\gamma_2+\gamma_3) + R\rho^4 + S(\rho_1^4+\rho_2^4+\rho_3^4), \tag{2}$$

where $\rho^2 = \rho_1^2 + \rho_2^2 + \rho_3^2$ and γ_j are the phases of crystallization waves. Minimization gives $\rho_1 = \rho_2 = \rho_3$, i.e., the transition from the hexatic to hexagonal crystal, Fig. 4(a).

The herringbone ordering is described by a three-component order parameter φ_j changing sign on reflection. The free energy expansion does not contain a third-order term since it changes sign on reflection. Then one has

$$\Phi_\varphi = F\varphi^2 + G_1\varphi^4 + G_2(\varphi_1^4 + \varphi_2^4 + \varphi_3^4), \tag{3}$$

where $\varphi^2 = \varphi_1^2+\varphi_2^2+\varphi_3^2$. The minimum with respect to the components φ_j depends on the sign of G_2. For $G_2 > 0$ one has $\varphi_1 = \varphi_2 = \varphi_3$. The ordered phase is a 2D hexagonal crystal with two molecules per unit cell, Fig. 4(b). This phase is chiral. When $G_2 < 0$, the hexagonal symmetry is broken: $\varphi_1 = \varphi$, $\varphi_2 = \varphi_3 = 0$, meaning that crystallization occurs only in one dimension. The ordered phase [Fig. 4(c,d)] consists of equidistantly spaced rows of the molecules, with the order parameter alternating from one row to the next. Within a row, the molecules possess liquid-like order.

The phases shown on Figs. 4(c) and 4(d) give rise to different low-order diffraction peaks. On Fig.4(c), the bonds do not lie in the crystalline rows. This gives broad first-order diffraction peaks, reflecting the liquid-like order. In contrast, the diffraction pattern of the phase shown on Fig. 4(d) shows one narrow peak due to diffraction from the crystalline rows, while the doubly-degenerate peak caused by the short-range translational order within the rows is broad. Comparing these results with the experimental data on the diffraction peak widths, we can attribute Fig. 4(c) to the phases S and L_2' whereas Fig. 4(d) corresponds to the phase L_{2h} possessing considerably different widths of the peaks.

Direct transitions between a hexatic and a herringbone-ordered crystal are not allowed in the Landau theory. The intermediate phase is either 1D crystal or hexagonal crystal. The phase sequences observed in smectic liquid crystals and in Langmuir monolayers contain different intermediate phases, Fig. 5.

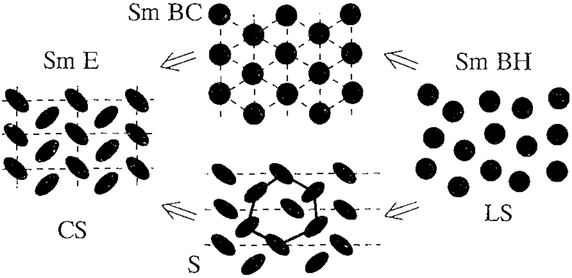

Figure 5: The phase sequences observed in smectic liquid crystals (top) and in Langmuir monolayers (bottom)

Distortions of unit cell in different phases [6]. Figure 6 presents the diffraction data for different isotherm scans of fatty acid monolayers. The high-temperature scan (Fig. 6(a)) traverses the sequence $LS_{II} - Ov - L_{2d}$ for the C_{19} acid [10]. From the positions of the non-degenerate and doubly-degenerate peaks, the magnitude and direction of the tilt were determined as described above. LS_{II} is the hexatic phase and gives a triply-degenerate diffraction peak. On the transition to the Ov phase where the molecules start to tilt in the NNN direction, the peak splits to a non-degenerate one and doubly-degenerate one with the stretching of the unit cell in the tilt direction. At the Ov -- L_{2d} transition the tilt direction changes to NN and the peaks interchange.

Isotherm measurement scans traversing the phase sequence $S - L_2' - L_{2h}$ are presented in Fig. 6(b,c). The transformation of the unit cell shape on lowering surface pressure is illustrated in Fig. 3. The distortion in the S phase is NN due to the ordering of the backbone planes of the molecules. In the L_2' phase, the molecules tilt in an NNN direction normal to the initial stretching, so that the tilt acts to decrease the distortion. When the tilt direction is changed to NN at the $L_2' - L_{2h}$ transition, one might expect a further increase of the stretching under the action of tilt as happens at high temperatures at the $Ov - L_{2d}$ transition. However in fact the unit cell discontinuously shrinks in the NN direction, so that its distortion azimuth jumps to NNN. The subsequent continuous decrease of the distortion in the L_{2h} phase is due to the

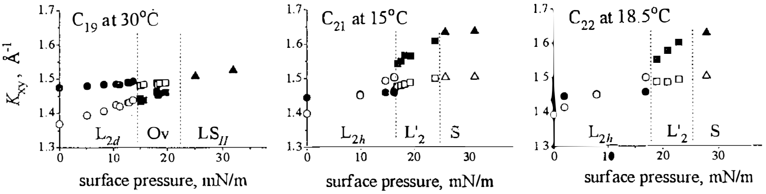

Figure 6: In-plane components of the scattering vectors in different phases of fatty acid monolayers

action of increasing tilt angle. Beyond the intercept where the distortion magnitude reaches zero, its direction is NN. This unexpected behavior indicates that not only the tilt direction but also the packing of the backbone planes of the molecules change discontinuously at the $L_2' - L_2$ transition.

Distortion of the unit cell is described by its magnitude ξ and orientation ω (the angles ω and $\omega + \pi$ are equivalent). The free energy can be expanded in powers of distortion as

$$\Phi_\xi = C\xi^2 - U\varphi^2\xi \cos 2\omega - V\xi\eta^2 \cos 2(\omega - \beta) + W\psi^2\xi \cos 2\omega. \tag{4}$$

Eq. (4) describes the behavior of the observed diffraction peaks in fatty acid monolayers when all its coefficients C, U, V, W are positive. The distortions in the phases L_{2d} and Ov are induced by tilt: $\xi \sim \eta^2$. In the phase S (where $\varphi \neq 0$) the distortion is $\xi = (U/2C)\varphi^2$ with the unit cell stretching to NN ($\omega = 0$), provided that U is positive. In the L_2' phase, the tilt direction is NNN ($\beta = \pi/2$) because of the coupling of the primary order parameters. Here one finds that the distortion $\xi = (U\varphi^2 - V\eta^2)/2C$ decreases continuously with increasing tilt angle η, in agreement with the experimental data. The observed decrease of distortion with increasing tilt angle in the L_2' phase is thus determined given its observed behavior in two neighboring phases, namely, stretching to nearest neighbor due to NN tilt in the L_{2d} phase and, also to nearest neighbor, due to ordering of the backbone planes in the S phase. The distortion in phase L_{2h} is $\xi = |W\psi^2 - V\eta^2|/2C$. It is equal to zero when $\eta^2 = (V/W)\psi^2$, so that the diffraction peaks coincide at a non-zero tilt angle. For smaller tilt angles, the minimum of is achieved at $\omega = \pi/2$, i.e., the unit cell shrinks in the tilt direction. For larger tilt angles one has $\omega = 0$ and the unit cell stretches in the tilt direction. This behavior is observed in the experiment, Fig. 6(b,c).

There are two mechanisms driving unit cell distortion, the tilt and the ordering of the backbone planes. The distortion induced by tilt is proportional to the square of the tilt order parameter $\eta = \sin\theta$. In order to separate the contributions from each of them, the signed distortion parameter $d = \xi\cos 2(\omega - \beta)$ is plotted as a function of $\sin^2\theta$, Fig. 7. The data points from both tilted phases at a given temperature lie on the same line, suggestive of commonality of structure. The L_2 phase data covers a wide range of tilt angles, allowing a more precise determination of the regression line parameters for this phase. At high temperatures the data points for the Ov and L_2 phases of the C_{19} acid lie on one and the same straight line passing

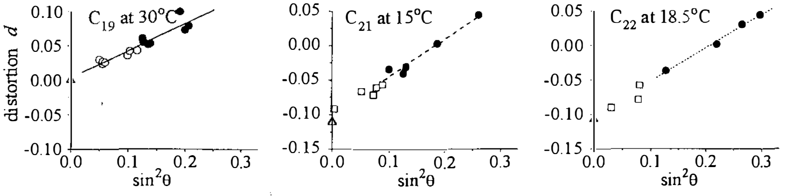

Figure 7: Distortions as a function of $\sin^2\theta$

through the origin. Hence the distortion is induced by tilt only. In contrast, the zero tilt angle intercept of the lower-temperature lines of the C_{21} and C_{22} acids is non-zero. Hence there exists another contribution to the distortion caused by the ordering of the backbone planes of the molecules.

Diffraction peak profile of the hexatic phase [11]. There are three types of translational order which can be distinguished from the qualitatively different patterns to which they give rise. First, the absolute long-range translational order in an ideal three-dimensional crystal results in δ-function diffraction peaks. Secondly, in systems with reduced dimensionality, thermal fluctuations destroy the long-range translational order and cause power-law singularities instead of δ-function peaks. This is the case both for two-dimensional crystals and smectic liquid crystals. Thirdly, Nelson and Halperin [12] found that the melting of a two-dimensional crystal can occur in two stages. The transition from 2D crystal to the intermediate phase, called 'hexatic', is due to the unbinding of thermally excited dislocation pairs. Hexatics contain a concentration of dislocations in thermodynamic equilibrium which interact elastically with each other. As a result, hexatics possess only short-range translational order, but quasi-long-range bond orientational order.

We have determined the shape of the diffraction spots in a dislocated crystal, rigorously taking into account the correlations between dislocations in the hexatic phase. The peak profile is determined by the behavior of the correlation function $< \exp i\boldsymbol{Q}[\boldsymbol{u}(\boldsymbol{r}+\boldsymbol{\rho}) - \boldsymbol{u}(\boldsymbol{r})] >$ at distances ρ comparable to the mean distance between dislocations. The approximations employed below are valid in this range of ρ and cannot be applied in the limit $\rho \to \infty$, essential for analysis of the long-range order in the system. Since the elastic strain caused by a dislocation is long-range, decreasing as $1/r$, the main contribution to the correlation function is from dislocations located at distances r large in comparison with ρ, and comparable to the sample size L. Then the exponent can be expanded over $\rho \ll r$: $\boldsymbol{Q}[\boldsymbol{u}(\boldsymbol{r}+\boldsymbol{\rho}) - \boldsymbol{u}(\boldsymbol{r})] = \boldsymbol{\rho}\frac{\partial}{\partial \boldsymbol{r}}[\boldsymbol{Q}\boldsymbol{u}(\boldsymbol{r})]$. The standard expression for the strain field of a single dislocation with the bare elastic constants should be used here. The diffraction peaks occur Gaussians in the azimuthal direction. The azimuthal and the radial peak widths can be expressed in terms of the elastic moduli and the mean dislocation density and do not involve any phenomenological parameter. The ratio of the radial to the azimuthal peak widths decreases considerably when the dislocations interact and depends on the sample size.

Diffraction peak widths of phases of Langmuir monolayers. At the $LS - S$ transition the single peak of the hexatic phase LS splits into two, one doubly-degenerate and one non-degenerate, both with correlation lengths of about 30 intermolecular distances. This orthorhombic distortion is interpreted as due to the ordering of the short axes (backbone planes) of the molecules. Isotherm scans over the phase sequence $S - L_2' - L_2$ revealed drastic changes in the correlation lengths at the $L_2' - L_2$ transition, see Fig. 8. The correlation lengths for the two peaks in the L_2' phase differ only slightly from those in the S phase, being about 30 intermolecular distances. In the L_2 phase, the non-degenerate peak shows a correlation length of about 60 intermolecular distances whereas for the doubly-degenerate one the correlation length is about 4 times smaller. Essential differences in the correlation lengths of two peaks were found also for the monolayers of the longer-chain fatty acids in an uncompressed state [14].

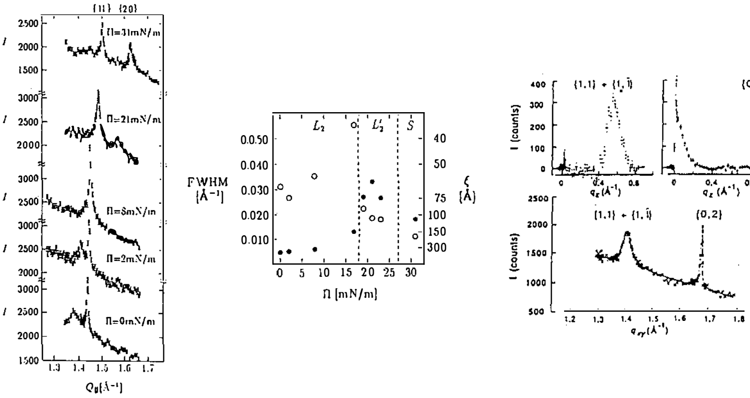

Figure 8: Diffraction peak profiles for the monolayers of behenic (C_{22}) acid at 18.5°C [13] (a,b) and triacontanoic (C_{30}) acid at zero surface pressure and 5°C [14]
(c)

These diffraction patterns have been described by appearance of crystallization waves of herringbone order differing in directions of wave vectors with respect to bonds, Fig. 4(c,d). An alternative explanation may be given in terms of two types of dislocation-mediated melting of anisortopic 2D crystal [15], Fig. 9. When one type of dislocations possess lower core energy than the other two, 2D crystal melts to "1D smectic phase" (destroyed by fluctuations on long range), which gives rise to two diffraction peaks with essentially different widths. However, the transition $L_2' - L_2$ cannot be explained in terms of two types of dislocation-mediated melting of one and the same 2D crystal since, as has been shown above, these phases differ also in packing of backbone planes. Two different crystallization waves allowed by the Landau theory provides an adequate description of the transition.

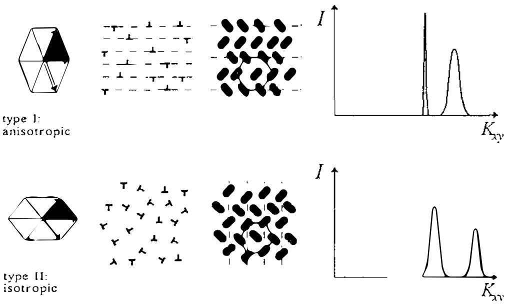

Figure 9: Two types of dislocation-mediated melting of 2D anisotropic crystal [15], two different crystallization waves in the Landau theory, and corresponding diffraction patterns

Acknowledgments. This report is based on researches performed in collaboration with E.B.Loginov, V.L.Indenbom (Institute of Crystallography, Moscow, Russia), I.Peterson, R.Kenn (Institute of Physical Chemistry, Mainz, Germany), P.Dntta, M.Durbin, M.Shih (Northwestern University, Evanston, USA).

References

1. S.Ställberg-Stenhagen and E.Stenhagen, Nature **156**, 239 (1945).
3. A.M.Bibo and I.R.Peterson, Adv.Mater. **2**, 309 (1990).
4. G.A.Overbeck and D.Möbius, J. Phys. Chem. **97**, 7999 (1993).
5. D.K.Schwartz and C.M.Knobler, J. Phys. Chem. **97**, 8849 (1993).
6. V.M.Kaganer, I.R.Peterson, R.M.Kenn, M.C.Shih, M.Durbin, and P.Dutta, J. Chem. Phys., submitted.
7. V.M.Kaganer and V.L.Indenbom, J. Phys. II France **3**, 813 (1993).
8. V.M.Kaganer and E.B.Loginov, Phys. Rev. Lett. **71**, 2599 (1993).
9. V.M.Kaganer and E.B.Loginov, Phys. Rev. E (1995), in press.
10. M.Durbin *et al.*, J. Phys. Chem. **98**, 1753 (1994).
11. I.R.Peterson and V.M.Kaganer, Phys. Rev. Lett. **73**, 102 (1994).
12. D.R.Nelson and B.I.Halperin, Phys. Rev. B **19**, 2457 (1979).
13. R.M.Kenn *et al.*, J. Phys. Chem. **95**, 2092 (1991).
14. F.Leveiller *et al.*, J. Phys. Chem. **96**, 10380 (1992).
15. S.Ostlund and B.I.Halperin, Phys. Rev. B **23**, 335 (1981).

SIMULATING LANGMUIR MONOLAYERS OF FATTY ACIDS

S. Karaborni
Koninklijke/Shell-Laboratorium, (Shell Research BV, Amsterdam)
POSTBUS 38000, 1030 BN Amsterdam, The Netherlands.

Monolayers at the air-water interface exhibit several phase transitions. To a large extent, the role of conformational defects in these transitions has been neglected. Over the last four years, we have developed a model to simulate monolayers at the air-water interface. The model is capable of predicting quantitatively the rich polymorphism seen in x-ray diffraction, fluorescence microscopy and Brewster–angle microscopy. In this manuscript we focus on the delicate relationship between chain conformation and tilting in determining the monolayer behaviour. Results are also shown from novel simulations performed to determine the vapour-liquid coexistence in Langmuir monolayers.

Introduction

Since the early surface tension measurements on oil films by Langmuir [1] and Harkins [2], monolayers of amphiphilic molecules at the air–water interface subsequently, known as Langmuir monolayers, have attracted continuous interest from the research community [3]. In the 1940's the remarkable experiments by three groups. [4] have strongly questioned the simplicity of Langmuir monolayers. Today, there is mounting evidence that monolayers of amphiphilic molecules at the air–water interface display a very complex phase behaviour [5].

The onset of new, powerful experimental techniques such as synchrotron X–ray diffraction has undoubtedly resulted in a molecular understanding of Langmuir monolayers, especially their lattice geometry and molecular tilt order, and the use of fluorescence microscopy has led to the direct observation of domain structure and phase transitions. Similarly, new microscopy techniques that do not use fluorescent probes are being developed to study domain morphology and the order of phase transitions in the absence of probe impurities. Unfortunately, the molecular conformation cannot yet be described quantitatively using the above techniques, but it has to be inferred from other measurable quantities such as the electron density in the nonpolar section of the monolayer [6]. In fact, in all X–ray experiments the chain conformation is believed to play a minor role, thus the molecules are always assumed to be all-trans in the interpretation of the data [6]. These assumptions are in contrast with non–resonance Raman studies of Langmuir monolayers at high density which indicate the presence of gauche defects that grow upon monolayer expansion [7]. In support of the Raman studies, recent X–ray diffraction experiments on fluorinated alkyl acid monolayers show a completely different behaviour from fully hydrogenated acid monolayers as a result of the difference in chain flexibility between fluorinated and hydrogenated alkyl acids [8, 9].

In this manuscript, we describe the use of molecular simulations to investigate (1) finite size effects in Langmuir monolayers, (2) relation between chain conformation and monolayer tilting, (3) role of kink defects in the highly packed phases, (4) Difference between monolayers of C16 and C20 fatty acids, and (5) the vapour–liquid coexistence in pentadecanoic acid monolayers.

Simulation Details

The model used in these simulations to mimic the behaviour of fatty acids at the air-water interface has been described in great detail in Ref. [10]. The most important features of the model include: (1) interactions between chains using the anisotropic united atom model, (2) water-amphiphile interactions are modelled using an external potential developed initially to simulate micelle–water interactions [11, 12]. The external potential allows the movement of headgroups and chain methylenes in and out of the water, and allows the formation of a finite size interface; and (3) the headgroup interactions are purely repulsive. Simulations have been performed on monolayers of C16 and C20 fatty acids at temperatures ranging from 275 to 325 K, and at molecular areas varying from 0.185 to 0.40 nm^2/molecule.

Is system size important?

Over the last five years, several papers on molecular simulations of Langmuir or Langmuir–Blodgett monolayers (for a review on simulation literature see Ref. [13]) self-assembled monolayers [14, 15], and monolayers at oil-water interfaces [16] have appeared. To date there have been only a few studies on size effects in simulations of monolayers [15, 17, 18]. To a large extent, these simulations reported conflicting results.

Table 1: Average results at T=275 K. The errors are standard deviations. N is the number of molecules. t_1 is the number of time steps used for equilibration, and t_2 is the number of time steps used to produce the average properties. $< U_{conf} >$ is the configurational energy. $< R >$ is the average end-to-end distance. $< Z >$ is the average monolayer height. $< \theta >$ is the average tilt angle from the normal to the interface. $< \phi >$ is the average direction of tilt (If $< \phi > =$ 0, 60 or 120 degrees, molecules are tilted towards their next nearest neighbours. If $< \phi > =$ 30, 90, 150 degrees, molecules are tilted towards their nearest neighbours). $< P(T) >$ is the average trans fraction which is the number of dihedral angles in trans conformation divided by the total number of dihedral angles. $< P(D) >$ is fraction of defects which is calculated from Voronoi polygon constructions. $\epsilon = 665$ J/mol and $\sigma = 0.3527$ nm. Exponents indicate last digits of standard deviations from average values.

$\frac{Area}{nm^2}$	N	$\frac{<U_{conf}>}{\epsilon}$	$\frac{<R>}{\sigma}$	$\frac{<Z>}{\sigma}$	$\frac{<\theta>}{degrees}$	$\frac{<\phi>}{degrees}$	$< P(T) >$	$P < D >$
0.23	16	-34^2	6.69^2	5.98^4	27.9^8	91^4	0.980^6	0.03^2
	64	-31^1	6.69^1	6.01^3	26.9^4	86^9	0.971^4	0
	256	-33^1	6.69^1	5.97^3	27.7^3	27^6	0.976^2	0
0.25	16	-27^4	6.63^7	5.58^4	34^1	90^3	0.96^2	0
	64	-25^2	6.63^1	5.61^4	33.3^7	90^3	0.958^5	0
	256	-26.6^5	6.64^1	5.58^2	33.8^2	90^2	0.964^2	0.02^1
0.27	16	-25^1	6.62^4	5.20^2	39.7^4	89^4	0.965^8	0
	64	-26^2	6.63^1	5.19^3	39.7^4	90^3	0.966^4	0.007^6
	256	-18.8^4	6.55^1	5.33^3	36.8^2	107^2	0.949^2	0.22^3

Monolayers comprising 16, 64 and 256 molecules have been simulated. The results of the monolayers at 0.23, 0.25 and 0.27 nm^2/molecule at T= 275 K are summarised in Table I. From the data it is clear that properties, such as tilt angles and average trans fractions, of 16–molecule systems are not significantly different from those of 64–molecule monolayers. The simulations at 0.23 and at 0.25 nm^2/molecule using 64 and 256 molecules do not show any significant difference in any of the properties calculated. However, the simulation at 0.27 nm^2/molecule using 64 molecules shows different degrees of ordering, tilt angle and chain conformation than the 256 molecule monolayer. On average, the tilt angle and the average trans fraction are higher in the 64– monolayer than in the 256–monolayer. The number of defects/molecule, as calculated from Voronoi polygons rises drastically from ≈ 0 to 0.22 defects/molecule with increase in system size, implying a much lower level of ordering in the 256– than in the 64–molecule monolayer. Indeed, snapshots of the 256– molecule monolayer at 0.27 nm^2/molecule show a clear formation of domains. At 0.23 and 0.25 nm^2/molecule, domains do not form even in 256–molecule monolayers. It is likely that the domain sizes are too large to be detected at 0.23 and 0.25 nm^2/molecule in a simulation of only 256 molecules. This is supported by experimental data which predict an increase in domain sizes with increase in density.

We speculate that for non-tilted high–density phases the system size does not play an important role [19]. However, for intermediate–density monolayers the system size is crucial mainly due to the competition between the formation of a large tilt angle and the appearance of domains [18]. Since small system size and periodic boundary conditions favour large tilt angles over disorder, one should be aware that the calculated tilt angles in simulations may be higher than those measured experimentally.

Chain conformation affects the tilting behaviour

In Fig. 1a, the monolayer tilt angle θ is plotted as a function of area per molecule at three temperatures. In general, at any particular area per molecule, tilt angles are higher at lower temperature as in previous simulations [20]. The maximum tilt angle also appears to depend strongly on temperature. It ranges from 40° at 275 K to 10° at 325 K [21]. The strong variations in the maximum tilt angle are an indication of the sensitivity of our model to small changes, by molecular dynamics standards, in temperature. The tilt transition is clear at 275 and 300 K. At both temperatures the monolayers undergo a transition between 0.19 and 0.21 nm^2/molecule [21]. This value is in good agreement with experimental data [22] and recent simulation results of fully hydrogenated monolayers [23]. At 325 K there is no clear transition. The tilt angle does not show any significant upper jump at any of the densities studied, whereas at 275 K there is a big jump in tilt angle from 5.5 to 16.5° which occurs between 0.20 and 0.21 nm^2/molecule [21]. At 300 K the tilt angle jumps from 3.5 to 13.5° also between 0.20 and 0.21 nm^2/molecule. The density in which the tilt transition occurs appears to be largely independent of temperature (It appears that the transition at 275 occurs at a slightly higher density than at 300 K, however only an upper estimate of this difference can be given (0.01 nm^2/molecule)).

The presence of collective tilt in the monolayers is sustained to a higher area per molecule with decreasing temperature. At 325 K, the collective tilt breaks at 0.23 nm^2/molecule, and the monolayer undergoes a first order phase transition to the so–called liquid–expanded (LE) phase [21]. At 300 K, the tilt order breaks at 0.25 nm^2/molecule, at which density the monolayer also undergoes a first order phase transition to a phase exhibited by lateral self-diffusion, lower chain conformational order and a ring in the lateral structure factors [10, 24].

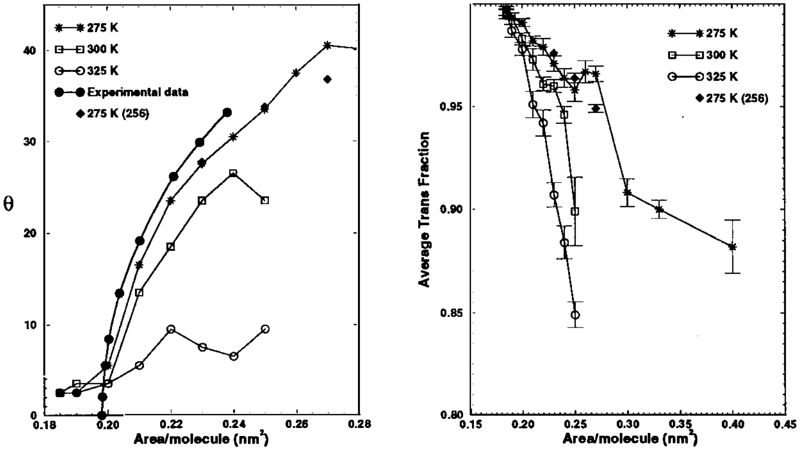

Figure 1: **(right)** Most probable monolayer tilt angle as a function of molecular area at 275 K, 300 K and 325 K. The results are also shown for monolayers consisting of 256 molecules at 275 K, and for X-ray reflectivity results in monolayers of $C_{19}H_{39}COOH$ [6] at 300 K. **(left)** Average trans fraction at 275 K, 300 K and 325 K. Results are also shown for a monolayer consisting of 256 molecules at 275 K.

At 275 K, the molecules are consistently tilted towards their nearest neighbours after the tilt transition in agreement with x-ray diffraction experiments at low temperature [25, 26]. At this temperature, there is no phase transition to a LE phase, however molecules segregate into well-ordered and tilted domains. The appearance of these domains depend highly on the number of molecules. When 64 molecules are used the formation of domains begins at 0.30 nm^2/molecule, whereas monolayers consisting of 256 molecules show the presence of domains at an earlier stage (0.27 nm^2/molecule).

Over the entire density range the tilt angles calculated in the simulations are somewhat similar to the X-ray reflectivity data of Kjaer et al. [6] (Fig. 1). It is clear, however, that the simulations systematically underestimate the value of tilt angles after the tilt transition, and the difference grows with increasing area per molecule. We speculate that this disagreement is due to one or more of the following reasons: (1) Our model is not good enough to reproduce the magnitude of tilt angles. (2) Real amphiphilic molecules are not completely devoid of gauche defects, but ignoring these defects in the interpretation of the experimental data leads to overestimation of the magnitude of tilt angles. (3) The experiments were performed before complete relaxation of the monolayer. While we cannot discount immediately the first hypothesis, we can show that the second and third hypotheses are highly probable. The first obvious analysis is to calculate the conformational defects in the model monolayers. A common measure of chain conformation is the average trans fraction which is the number of dihedral angles in trans conformation divided by the total number of dihedral angles. Fig. 1 shows the behaviour of the chains as a function of area per molecule. At the same area coverage, the average trans fraction is higher at lower temperatures as in previous simulations [20]. At the same temperature the average trans fraction decreases with decreasing density. The chain conformation can not be quantitatively measured using any of the available techniques, and can be obtained only qualitatively using infrared experiments [7, 27]. In cases where this latter technique is used there is a clear decrease in the average trans fraction with decreasing density.

Combining the conformational and tilting results from Fig. 1, it appears that (1) at low temperatures the tilt angles and the average trans fractions are high whereas at high temperatures both quantities are low, and (2) very small differences in the average trans fraction result in large differences in tilt angles. One can see for example at 0.22 nm^2/molecule, that, upon decreasing the temperature from 300 to 275 K, there is a 2% increase in average trans fraction, while the change in tilt angle is 5°. Temperature has additional effects on other properties, beside chain conformation, that could influence the tilt angle. Thus, in order to isolate as much as possible the relation between chain conformation and tilt angle we performed an additional simulation at 300 K, in which the energy barriers to dihedral rotation are twice as large as before. The results from this new simulation show that the trans fraction increases from 0.96 to 0.99 while the tilt angle increases from 18.5 to 23.5°.

Experimental data show that fatty acid monolayers have conformational defects [7, 27], and our simulations results establish a strong relationship between changes in chain conformation with changes in tilt angles. Therefore, models in which it is assumed that molecules have no conformational defects are likely to lead to significant errors in the calculation of tilt angles.

Recent experimental investigations have strongly questioned the validity of lateral pressure measurements in Langmuir troughs [28]. There is now a strong evidence that several measurements performed during compression or expansion of an amphiphilic monolayer do not reflect an equilibrium state [28]. In particular, Buontempo and Rice [27] have shown that the average conformation of the chain relaxes in a much longer time than that usually allocated to usual measurements. To investigate the effect of the chain conformation relaxation on the tilt behaviour, we performed two simulations at 0.20 and 0.22 nm^2/molecule, and at $T = 312$ K [29]. Fig. 2 shows the equilibrium as well as the equilibration part of the simulation at 0.22 nm^2/molecule. From the time evolution, we see that the monolayer initially responds to expansion by a sudden increase in the tilt angle. Over a much longer time-scale the increase in tilt is counteracted by a slow increase in the fraction of gauche defects which in turn leads to a slow decrease in the tilt angle before equilibrium is finally achieved, *i.e.*, the slow changes of the conformational defects are the rate limiting factor for the overall equilibration. These results are in agreement with recent infrared expansion experiments on Langmuir monolayers of alcohols [27].

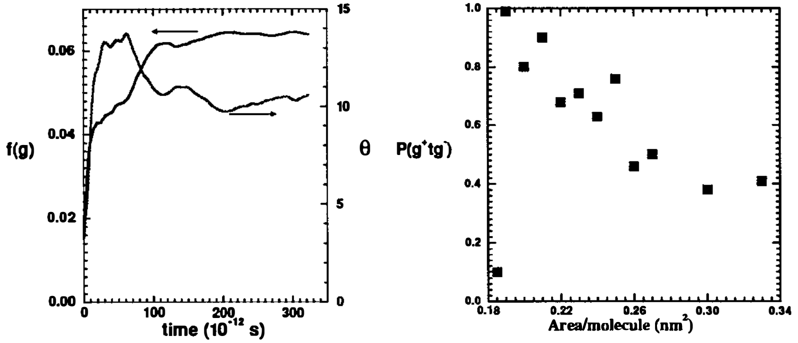

Figure 2: **(left)** Running average tilt angle θ and fraction of torsional angles in a gauche state $f(g)$ at 0.22 nm^2/molecule as a function of time (temperature = 312 K). Time = 0 signals the end of the expansion of the monolayer from 0.20 to 0.22 nm^2/molecule, and signifies the start of the relaxation at 0.22 nm^2/molecule. During the initial 12 picoseconds of the simulation the tilt angle makes a high jump. At the same time the fraction of torsional angles in a gauche state increases only slightly. As the simulation proceeds more gauche defects become part of the monolayer, and the tilt angle decreases. It is clear that the slow changes of the conformational defects are the rate limiting factor for the overall equilibration. **(right)** Probability of finding two gauche angles on one molecule in the kink ($g^{\pm}tg^{\mp}$) conformation

Role of kink defects

It may come as a surprise to some that highly ordered crystalline phases do contain gauche defects. It is intuitively expected that conformational defects will disturb the monolayer crystalline order. We note, from our simulations, that most of the gauche defects are concentrated at the molecular ends especially near the molecular tails, in agreement with other simulations [17, 20, 23]. In addition to these gauche defects, it appears that the central sections of molecules may also contain conformational defects. A close analysis of these defects shows that they are parts of a kink conformation (two gauche angles separated by a trans angle). Kink defects appear at molecular areas as low as .19 nm^2/molecule (see Fig. 2). At larger areas per molecule, other forms of gauche defects appear, that fit with the collective direction of the monolayer, and do not destroy the crystalline order. From a packing point of view kink defects are the most preferred form of chain deformations because the volume created by a kink defected molecule is only slightly higher than the volume of an all–trans molecule, and the overall direction of the chain is preserved. The formation of kink defects is a well known phenomenon in the phase behaviour of long chain n–alkanes crystals [30].

Comparison between different chain lengths

Simulations described up to this point have been performed on C20 fatty acids. Simulations performed at 300 K on C16 acids indicate a difference in tilting and conformational behaviour [12, 31]. For example, C16 acids undergo a less drastic Liquid condensed (LC)–LE transition than C20 acids, and the LC-LE phase transition in C16 monolayers occurs at 0.22 nm^2/molecule in comparison with 0.25 nm^2/molecule for C20 monolayers. In addition, C20 acids undergo a clear phase transition in which the tilt angle increases from 3.5 to 13.5° C at 0.20 nm^2/molecule, whereas C16 acids do not appear to undergo a clear tilt transition. Even in the regime in which the C16 acids are slightly tilted (Area per molecule less than 0.216 nm^2/molecule), It is difficult to calculate a tilt direction. At areas per molecule higher than 0.22 nm^2/molecule the C16 molecules don't exhibit a collective tilt.

Comparisons between the tilt angles and average conformations are given in Figure 3 for C16 and C20 acids. To note, is that the average trans fraction and the most probable tilt angles are higher in C20 than in C16 monolayers. In addition, note the large decrease in the average trans fraction between .24 and .25 nm^2/molecule in C20 monolayers, and compare that with the decrease in the average trans fraction between 0.216 and 0.22 nm^2/molecule (location of the melting of the C16 monolayer).

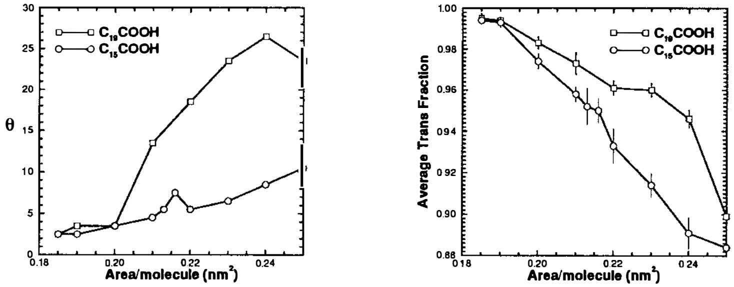

Figure 3: **(left)** Most probable monolayer tilt angle and **(right)** average trans fraction as a function of molecular area for $C_{15}H_{31}COOH$ and $C_{19}H_{39}COOH$ C19COOH monolayers at 300 K.

Does the monolayer model exhibit a vapour-liquid coexistence?

The experimental determination of the phase boundaries and of, if present, the critical points for the co-existence regimes is a very difficult task [32]. Experiments to determine the $\pi - A$ isotherms of monolayers of pentadecanoic acid (PDA) – the systems which has been studied in most detail – have been carried out as early as 1926 [33]. More extensive measurements were later performed by Harkins and co-workers [4]. In the seventies, Kim and Cannell [34] showed that the LE and G phases are connected by truly horizontal isotherms inferring a first-order transition, and calculated a critical point of ≈ 26° C. In the eighties, Pallas and Pethica [35] found markedly different coexisting densities and argued that the critical temperature should be higher than 50° C [35]. Using the fluorescence technique, phase coexistence was observed at temperatures approaching 70° C. [36]

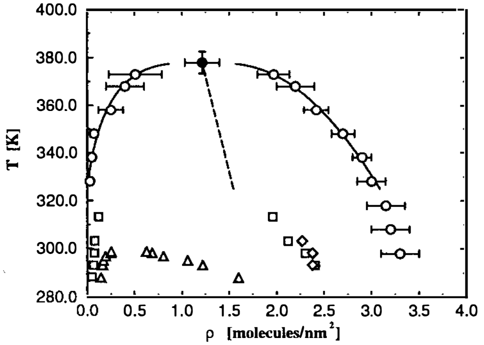

Figure 4: Vapour-liquid coexistences curves for pentadecanoic acid monolayers. The results of the isotherm measurements of Kim and Cannell [34] and Pallas and Pethica [35] are shown as open triangles and squares, respectively. The fluorescence data of Moore *et al.* [36] (only given for the liquid branch) are represented by open diamonds. The simulation data are depicted by open circles. The solid line is the scaling law fit through the simulation data using an exponent of 0.32, the dashed line is obtained from the rectilinear law, and the filled circle is the corresponding critical point.

In principle, computer simulations are an ideal tool to investigate the transitions of the Langmuir monolayers and the coexistence regions in microscopic detail. However, until recently it was considered impossible to calculate the phase diagram of such complex systems using conventional techniques. Even if reliable potential functions for the monolayer were available, direct simulations in the canonical or microcanonical ensemble cannot yield reliable data on the phase coexistence, since phase segregation is dramatically perturbed by the finite size of the simulated systems (usually $N < 100$) [12, 19, 20]. Recent results on the critical behaviour of n-alkanes [37] however, have indicated that the limitations of the conventional techniques can be successfully overcome using a combination of the Gibbs-ensemble Monte Carlo (GEMC) approach and the configurational-bias Monte Carlo (CBMC) method.

The phase diagram of the model PDA monolayer [38] is shown together with the various experimental results in Figure 4. As is clearly evident from the figure, there is no quantitative agreement between the co-existence densities obtained from our simulations and the various experimental data. The densities of the liquid phase of the model monolayer are approximately 25% higher than those obtained experimentally [35, 36], and the critical point seems to be shifted to higher temperatures. The reason for this difference is perhaps due to the absence of attractive forces caused by dispersive interactions between tail segments and water molecules. Including this part in the external potential should substantially lower the heat of vapourisation and thereby reduce the critical temperature. Molecules in the liquid phase should also show a more mushroom-like structure and, thereby, reduce the density of the system. Despite the difference between the simulation and experimental results, one can see that the monolayer model yields a coexistence between a liquid and a vapour phase. It will be of major interest to determine whether the model used throughout this work yields a Liquid Expanded– Liquid Condensed coexistence.

Conclusions

Over the last few years, the phase behaviour of Langmuir monolayers has been studied in great details; thanks in part to developments in synchrotron x-ray and neutron diffraction, fluorescence microscopy and Brewster-angle microscopy. These techniques have added tremendously to our knowledge of lattice structure and tilting behaviour. The chain conformation remains, however beyond, the realm of the above-mentioned techniques. In this manuscript, I have focussed on the role of chain conformation in affecting the phase behaviour of Langmuir monolayers. Extensive simulation results show that (1) an increase in the number of conformational defects induces a decrease in the magnitude of tilt angles, (2) chain conformation plays an important role in determining the location, and even the presence, of the LC-LE transition, (3) kink defects are present in monolayers at densities as high as 0.19 nm^2/molecule. The role of these kink defects in changing the phase behaviour is not well-understood, and (4) at the same temperature and density, short chains exhibit a tendency to favour conformational defects over an uniformly tilted monolayer.

Acknowledgements

I thank A. van Helden, J. I. Siepmann, B. Smit, S. A. Rice, and G. Verbist for many stimulating discussions. I am grateful to the Shell group for allowing the publication of these results.

References

[1] Langmuir, I. *J. Am. Chem. Soc.* **1917**, *39*, 1848.

[2] Harkins, W. D. *J. Am. Chem. Soc.* **1917**, *39*, 354 and 451.

[3] Knobler, C. M. In *Advances in Chemical Physics;* Rice, S. A., Ed.; Wiley: New York, 1988.

[4] Harkins, W. D.; Young, T. F.; Boyd, E. *J. Chem. Phys.* **1940**, *8*, 954. Harkins, W. D.; Boyd, E. *J. Phys. Chem.* **1941**, *45*, 20. Harkins, W. D.; Copeland, L. E. *J. Chem. Phys.* **1942**, *10*, 262. Copeland, L. E.; Harkins, W. D.; Boyd, G. E. *J. Chem. Phys.* **1942**, *10*, 357. Dervichian, D. G. *J. Chem. Phys.* **1939**, *7*, 931. Ställberg–Stenhagen, S.; Stenhagen, E. *Nature* **1945**, *156,* 239.

[5] Bibo, A. M.; Knobler, C. M.; Peterson, I. R. *J. Phys. Chem.* **1991**, *95*, 5591; *Makromol. Chem. Macromol. Symp.* **1991**, *46*, 55. Bibo, A. M.; Peterson, I. R. *Advanced Materials* **1990**, *2*, 309. Peterson, I. R. *Ber. Bunsenges. Phys. Chem.* **1991**, *95*, 1417. Knobler, C. M. *J. Phys.: Condens. Matter* **1991**, *3*, S17.

[6] Kjaer, K.; Als–Nielsen, J.; Helm, C. A.; Tippmann–Krayer, P.; Möhwald, H. *J. Phys. Chem.* **1989**, *93*, 3200.

[7] Kawai, T.; Umemura, J.; Takenaka T. *Chem. Phys. Lett.* **1989**, *162,* 243.

[8] Barton, S. W.; Goudot, A.; Boulassa, O.; Rondelez F.; Lin, B.; Novak, F.; Acero, A.; Rice, S. A. *J. Chem. Phys.* **1992**, *96*, 1343.

[9] Shin, S.; Collazo, N.; Rice, S. A. *J. Chem. Phys.* **1992**, *96*, 1352; Collazo, N.; Shin, S.; Rice, S. A. *J. Chem. Phys.* **1992**, *96*, 4735.

[10] Karaborni, S. *Langmuir* **1993** *9*, 1334.

[11] Karaborni, S.; O'Connell, J. P. *J. Phys. Chem.* **1990**, *94*, 2624. *Langmuir* **1990**, *6*, 911. *Tenside, Surfactants and Detergents* **1993**, *30*, 235.

[12] Karaborni, S.; Toxvaerd, S. *J. Chem. Phys.* **1992**, *96*, 5505.

[13] Karaborni, S. *Tenside Surfactants and Detergents* **1993**, 30, 256.

[14] Hautman, J.; Klein, M. L. *J. Chem. Phys.* **1989**, *91*, 4994; *J. Chem. Phys.* **1990**, *93*, 7483. Hautman, J.; Bareman, J. P.; Klein, M. L. *J. Chem. Soc. Faraday Trans.* **1991**, *87*, 2031.

[15] Siepmann, J. I.; McDonald, I. R. *Mol. Phys.*, **1992**, *75*, 255.

[16] Smit, B., Hilbers, P. A. J., Esselink, K., Rupert, L. A. M., van Os, N. M., Schlijper, A. G. *Nature* **1990**, *348,* 624; *J. Phys. Chem.* **1991**, *95*, 6361. Esselink, K.; Hilbers, P. A. J., van Os, N. M., Smit, B.; Karaborni, S. *Colloids and Surfaces A* **1994**, *91*, 1994. Karaborni, S.; Esselink, K.; Hilbers, P. A. J.; Smit, B. *J. Phys.: Condens. Matter.* **1994**, *6*, A351.

[17] Bishop, M.; Clarke, J. H. R. *J. Chem. Phys.* **1991**, *95*, 540.

[18] Shin, S.; Collazo, N.; Rice, S. A. *J. Chem. Phys.,* **1993**, *98*, 3469.

[19] Karaborni, S. and Siepmann, J, I. *Mol. Phys.* **1994**, *83*, 345.

[20] Bareman, J. P.; Klein, M. L. *J. Phys. Chem.* **1990**, *94*, 5202. Bareman, J. P.; Cardini, G. Klein, M. L. *Phys. Rev. Lett.* **1988**, *60*, 2152.

[21] Karaborni, S. and Verbist, G. *Europhys. Lett.*, **1994**, *27*, 467.

[22] Barton, S. W.; Thomas, B. N.; Flom, E. B.; Rice, S. A.; Lin, B.; Peng, J. B.; Ketterson, J. B. Dutta, P. *J. Chem. Phys.* **1988**, *89*, 2257.

[23] Moller, M. A.; Tildesley, D. J.; Kim, K. S.; Quirke, N. *J. Chem. Phys.* **1991**, *94*, 8390.

[24] Karaborni, S.; Toxvaerd, S. *J. Chem. Phys.* **1992**, *97*, 5876.

[25] Lin, B.; Shih, M. C.; Bohanon, T. M.; Ice, G. E.; Dutta, P. *Phys. Rev. Lett.* **1990**, *65*, 191.

[26] Kenn, R. M.; Böhm, C.; Bibo, A. M.; Peterson, I. R.; Möhwald, H.; Als-Nielsen, J.; Kjaer, K. *J. Phys. Chem.* **1991**, *95*, 2092.

[27] Buontempo, J. T.; Rice, S. A. *J. Chem. Phys.* **1993**, *98*, 5835.

[28] Kato, T.; Akiyama, H.; Tanaka, T. *Chem. Phys. Lett.* **1991**, *184*, 455. Kato, T.; Hirobe, Y.; Kato, M. *Langmuir* **1991**, *7*, 2208. Kato, T. *Langmuir* **1990**, *7*, 870.

[29] Buontempo, J, T.; Rice, S. A.; Karaborni, S.; Siepmann, J. I.; *Langmuir* **1993**, *9*, 1604.

[30] Maroncelli, M.; Qi, S. P.; Strauss, H. L.; Snyder, R. G. *J. Am. Chem. Soc.* **1982**, *104*, 6237. Craievich, A; Denicolo, I.; Doucet, J. *Phys. Rev. B* **1984**, *30*, 4782. Maroncelli, M.; Strauss, H. L.; Snyder, R. G. *J. Chem. Phys.* **1985**, *82*, 2811.

[31] Karaborni, S.; Toxvaerd, S.; Olsen, O. *J. Phys. Chem.* **1992**, *96*, 4965.

[32] Knobler, C. M. *Advances in Chem. Phys.* **1990**, *77*, 397

[33] Adam, N. K.; Jessop, G. *Proc R. Soc. London A* **1926**, *110*, 423.

[34] Kim, M. W.; Cannell, D. S. *Phys. rev. Lett.* **1975**, *35*, 889. *Phys. Rev. A* **1976**, *13*, 411.

[35] Pallas, N. R.; Pethica, B. A. *J. Chem. Soc. Faraday Trans. I* **1987**, *83*, 585.

[36] Moore, B. G.; Knobler, C. M.; Akamatsu, S.; Rondelez, F. *J. Phys. Chem.* **1990**, *94*, 4588.

[37] Siepmann, J. I.; Karaborni, S.; Smit, B. *J. Am. Chem. Soc.* **1993**, *115*, 6454. *Nature* **1993**, *365*, 330. Smit, B.; Karaborni, S.; Siepmann, J. I. *J. Chem. Phys.* **1995**, *102*, 2126.

[38] Siepmann, J. I.; Karaborni, S.; Klein, M. L. *J. Phys. Chem.* **1994**, *98*, 6675.

IMAGING STUDIES OF MONOLAYERS

Charles M. Knobler

Department of Chemistry and Biochemistry
University of California
Los Angeles, California 90095-1569, USA
e-mail: knobler@chem.ucla.edu

The development of two techniques for the visualization of monolayers at the air/water interface, polarized fluorescence microscopy (PFM) and Brewster-angle microscopy (BAM), has had a major impact on our understanding of the physics of these two-dimensional systems. The changes in textures that are observed when phase boundaries are crossed, either along isotherms or surface-pressure isobars, allow the locations of the boundaries to be determined with precision. Such measurements have played an important role in determining the complex phase diagrams of monolayers of simple amphiphiles such as fatty acids, esters and alcohols. The textures also reveal large-scale self organization of the molecular tilt azimuth into regular patterns such as stripes and stars. A Landau-deGennes theory that has been developed for hexatic phases of liquid crystals can describe these textures. It is necessary to take into account the broken symmetry associated with the presence of the interface, the inherent lack of head-tail symmetry in the amphiphiles and the orientation of the amphiphiles at interfaces with isotropic monolayer phases.

Introduction. The considerable progress that has been made in our understanding of the physics of insoluble monolayers at the interface between air and water (Langmuir monolayers) is largely the result of two kinds of experiments: x-ray diffraction and reflectivity measurements, which provide information about the microscopic structures of monolayers; and optical studies by fluorescence microscopy and Brewster-angle microscopy (BAM), which probe the organization at a length scale in excess of 1 μm.

It is now recognized that the phase diagrams of Langmuir monolayers of simple substances such as long-chain saturated fatty acids, esters and alcohols are complex and that there are more than a dozen condensed monolayer phases. Elsewhere in this volume, Kaganer [1] has discussed the phase diagram (see his Figs. 1 and 3) and has cited the experimental and theoretical evidence for it. I will focus instead on the optical textures of monolayers, which, while related to the nature of the underlying phases, probe the nature of self assembly on mesoscopic and macroscopic length scales. Our knowledge of the equilibrium properties of monolayers and the possibility of direct visualization makes it possible to begin examination of the nonequilibrium properties of monolayers. For example, a study of flow of a monolayer through a channel has recently been reported [2].

Visualization methods. The visualization of monolayers by fluorescence microscopy has become a standard technique. Usually a small amount (10^{-2} - 1 mol %) of a fluorescent probe, which is itself an amphiphile, is added to the monolayer under investigation. The contrast between monolayer phases, which allows them to be differentiated in the image, is the result of differential solubility of the probe. Such experiments have been described in several reviews [3-5]. Another visualization method, Brewster-angle microscopy (BAM) has more recently been developed [6,7]. It provides images of the variations in refractive index on the surface and is sensitive to the optical anisotropy, which allows variations in molecular orientation to be observed. Polarized fluorescence microscopy (PFM) also is sensitive to molecular orientation. In a recent comparative study, it has been shown that, with few exceptions, the images obtained by the two methods are equivalent [8].

Changes in textures. The schematic surface pressure-temperature phase diagram shown in Fig. 1 provides a road map for the discussion of some textures; the arrows on the diagram indicate some of the paths along which observations have been made. I will describe the changes in the textures that are observed and then discuss their significance.

Transitions between condensed phases. Diffraction studies [1,3] show that a number of the monolayer phases are *tilted phases*, i.e. phases in which the molecules are uniformly tilted with respect to the surface normal. The textures in such phases are often mosaics, Fig. 2a, composed of domains of uniform reflectivity or fluorescence with sharply defined, jagged grain boundaries. The texture coarsens slowly over time and the boundaries become straighter, with a rate depending on the

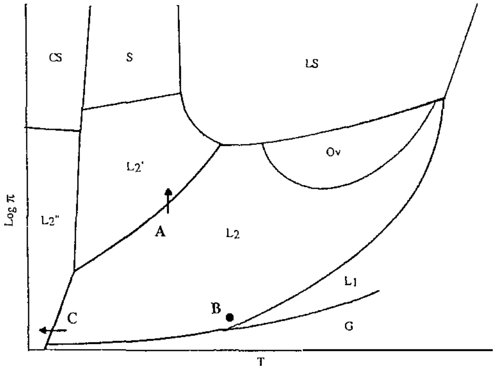

Figure 1: Schematic surface pressure-temperature diagram. The L_1 phase is an isotropic liquid; the G phase is gas. Phases CS, S and LS are untilted phases. L_2, L_2', L_2'' and Ov are tilted phases. In the L_2' and Ov phases the tilt is towards next-nearest neighbors and in L_2 and L_2'' it is toward nearest neighbors. More details can be found in references 1 and 3.

temperature and the chain length of the amphiphile [8]. Path A in Fig. 1 crosses a phase boundary between two tilted phases that can be distinguished by the molecular tilt azimuth. In the lower-pressure (L_2) phase, the molecules point toward their nearest neighbors while in the higher-pressure (L_2') phase the tilt is toward next-nearest neighbors. As the monolayer is brought towards the phase boundary by increasing the pressure at constant temperature, there are no sudden changes in the texture. But when the boundary is crossed, there is a marked alteration in the texture in which the relative reflectivities change and some boundaries are displaced, see Fig. 2b. Similar changes can be

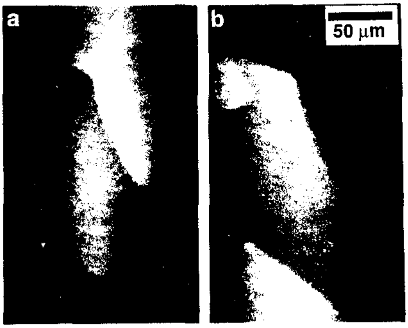

Figure 2: Polarized fluorescence micrograph showing the transition between the L_2 and L_2' phases in arachidic acid at 18 °C and 5.1 mN/m. (a) Image in L_2 phase (b) Image after transition to L_2' phase. [From D. K. Schwartz and C. M. Knobler, J. Phys. Chem. **97**, 8849 (1993)]

observed when the phase boundary is crossed by changing the temperature at constant pressure. In PFM studies of transitions from a tilted to an untilted phase, the transition is seen as a complete loss of texture. With the BAM, however, a faint texture can be observed in the CS and S phases [8].

Striped textures in one-phase regions of fatty acids at low temperature and pressure. Striped textures slowly form when the 14, 15 and 16-carbon saturated fatty acids are brought into a one-phase region close to the triple point with the liquid and gas, point B in Fig. 1 [9,10]. The stripes, Fig. 3, do not represent variations in the density because they cannot be observed with ordinary fluorescence microscopy. They are typically 50 μm in width and can be cm long. A variety of point defects, including Archimedian spirals, may be observed in the texture. If the stripes are disturbed, for example, by stirring, they reform. The stripe width increases with increasing surface pressure along an isotherm and decreases with increasing temperature along an isobar.

Transitions in domains of tilted condensed phases surrounded by an isotropic phase. Domains of tilted condensed phases display a large variety of textures that have been called "star defects" because of their relation to similar textures associated with defects in smectic liquid crystals [10]. A surprising change in such textures was recently reported by Fischer, et al.[12], who studied monolayers of methyl esters of long-chain fatty acids. The path followed in their experiments is labeled C in Fig. 1. Although the path shown connects two condensed phases, isolated domains surrounded by the isotropic liquid phase are metastable and can be studied, as shown in Fig. 4a. Under the initial conditions, each domain has the form of a six-arm star defect in which there are six

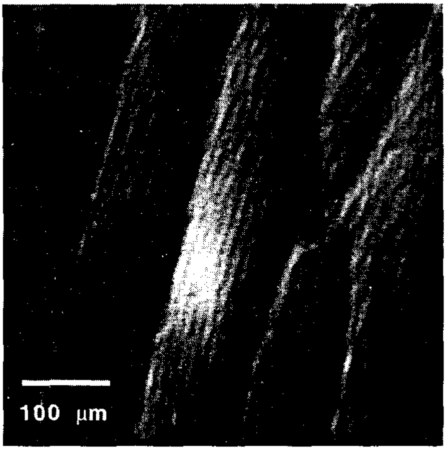

Figure 3: BAM image of a stripe texture in pentadecanoic acid at 2 °C. The image has been enhanced for clarity. A point defect is seen at the right.

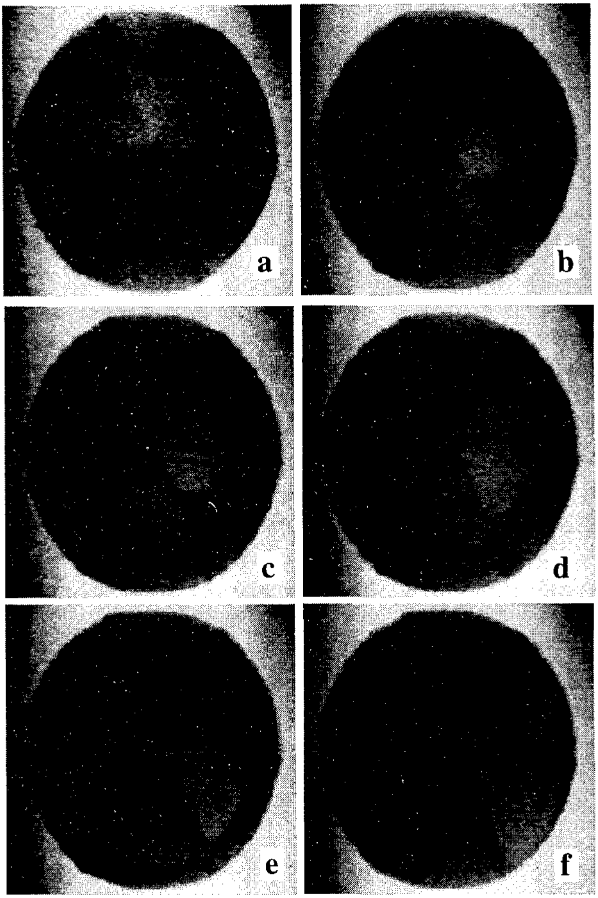

Figure 4: The "blooming" transition in methyl octadecanoate. The PFM images show the evolution of the texture as a single domain surrounded by the isotropic liquid phase is cooled through a transition. The new phase nucleates at the center and then grows to fill the domain. A six-arm star is recovered after the transition, but the fluorescence intensities in each pie-shaped region have been changed. The transition is reversible, but on heating the new phase first appears at the periphery of the domain.

distinct pie-shaped regions. When the phase boundary is crossed by lowering the temperature, a new texture nucleates at the center of the star and spreads over the domain, Figs. 4bcde, a process we have called "blooming". After the transition is complete, Fig. 4f, the domains still have a six-arm star texture, but the relative intensities of fluorescence or the variations in reflectivity have changed. If the system is now heated through the transition, the new texture forms at the boundary with the surrounding isotropic phase and spreads inward until the original star texture is recovered.

Significance of the textures. The variations in the fluorescence intensity and reflectivity that are seen as textures by PFM and BAM represent large-scale organization of the molecular tilt azimuth. The molecular tilt angle is a thermodynamic quantity whose value is set by the density and temperature of the monolayer, but the tilt azimuth is not. The textures arise from the self-organization of the molecules into ordered arrays. In regions of uniform texture, all molecules have the same tilt azimuth; sharp changes in the texture represent essentially discontinuous changes in the tilt azimuth.

Analyses of the textures in Figs. 2-4 show that the tilt azimuths are organized as pictured in Fig. 5. The mosaic texture consists of grains with different tilt azimuths, Fig. 5a. In the transitions between tilted phases, the tilt azimuths within these regions change in response to the changes in molecular orientation. Faint textures in the untilted CS and S phases arise because the molecular cross sections are not circular. Molecules in these phases pack in a herringbone pattern that produces a rectangular unit cell. We believe that the grains are associated with different orientations of the cell [8].

The stripes are *splay* stripes [10]. As shown in Fig. 5b, the tilt azimuth at the stripe center is parallel to the stripe direction, rotates across the stripe, and changes discontinuously at the stripe edge. The tilt may be to the right or to the left and both orientations are observed. Splay textures are also found in the stars seen in the high-temperature phase in the esters [11,12]. The tilt azimuth within each pie-shaped region is uniform and the molecules point towards the interface with the isotropic phase, Fig. 5c. There is a $\pi/3$ change in the tilt azimuth at each boundary between regions. The blooming observed as the temperature is lowered through the phase transition corresponds to the nucleation and growth of a phase in which the tilt azimuth is parallel to the interface, Fig. 5d. Here again, there is a $\pi/3$ change in the tilt azimuth at each boundary. As in the case of the stripes, the tilt may be either towards the left or the right, and equal numbers of both types of domains are observed.

Theoretical treatment. Diffraction studies of Langmuir monolayers have found that in most of the condensed phases the translational correlation length is short: there is no crystalline order [1,3]. On the other hand, the existence of the star and stripe textures in such phases demonstrates that there is long-range orientational order [13]. This suggested to Peterson and coworkers [14] that most of the condensed monolayer phases are *mesophases* and an analysis of the symmetry properties determined from diffraction leads to the conclusion that there is a one-to-one correspondence between

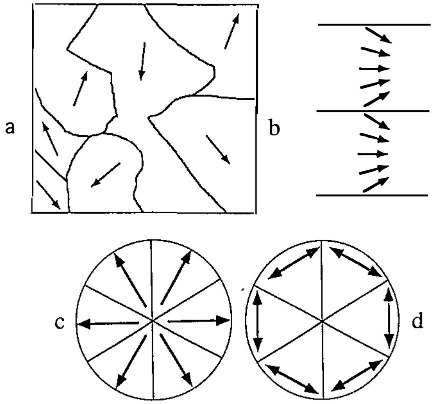

Figure 5: Organization of tilt azimuth in monolayers. (a) Mosaic texture; (b) Splay stripes; (c) Star texture in high-temperature phase of esters; (d) Star texture in low-temperature phase. The double-headed arrows indicate that the tilt can be either clockwise or counterclockwise. Equal numbers of each type of structure are found.

monolayer phases and those of smectic liquid crystals and that some of the phases are tilted hexatics [1,15].

Star defects in tilted hexatic phases have been examined theoretically by Selinger and Nelson [16] and striped textures in chiral smectic films by Langer and Sethna [17] and Hinshaw and Petschek [18], all of whom employed a Landau-deGennes theory appropriate to a continuum elastic medium. Selinger [19] pointed out that the theory for ordinary smectic liquid crystals could not be employed for monolayers without modification because it does not take account of the broken symmetry that results from the presence of the air/water interface and the absence of head-tail symmetry in the amphiphiles.

A free energy density appropriate to tilted hexatic phases in monolayers can be written in terms of an order parameter $\vec{c}$ that is the projection of the molecular axis on the water surface and two fields, the hexatic bond-angle field θ and the tilt-azimuth field φ [20]. Even in its simplest form, the free energy must include many contributions: (1) The deformation energy of a non-uniform 2D hexatic, which is the energy cost of spatial variations in the bond-angle field; (2) The free energy associated with the bend and splay deformation of a 2D nematic liquid crystal; (3) The coupling energy between the bond-angle and tilt-azimuth fields; (4) The bend and the splay of the texture associated with the head-tail asymmetry of the molecules; (5) The effect of the interface with the isotropic phase on the bend and splay energy.

The nature of the textures predicted by the free energy depends on the monolayer phase and on the values of the various material constants. In general, the constants are unknown, so it is only possible to examine the textures that arise in different regimes of the parameter space. Fischer, et al.[19] have shown that the free energy can account for many of the textures that have been observed in domains surrounded by an isotropic phase, including various stars and boojums (which are textures in which the tilt azimuth changes continuously). They also described spiral textures that are a combination of bend and splay. Such textures have not yet been observed in monolayers of simple amphiphiles but have recently been discovered in monolayers of thermotropic liquid crystals [21]. Splay stripe textures also arise quite naturally from the theory [22].

In general, it is observed that there is a tendency for a normal boundary condition for the molecular tilt azimuth at the interface of a domain with an isotropic phase. The theory shows that this condition plays an important role in the stability of the splay stars and boojums. Why then does the parallel boundary condition appear in the low-temperature, low-pressure phase of the methyl esters? Fischer, et al.[12] believed that the blooming transition accompanied a phase transition from the L_2 to the L_2'' phase, which is a transition between two phases in which the tilt is toward nearest neighbors. They attributed the parallel boundary condition to the onset of herringbone order in the L_2'' phase. An examination of the orientations of molecules at the grain boundaries between the six regions of uniform tilt showed that herringbone order is more easily accommodated when there is a parallel orientation. Recently, however, diffraction studies of methyl esters [23] have shown that the higher-temperature phase is L_2', in which the tilt is toward next-nearest neighbors, and not L_2. Thus, in addition to the onset of herringbone order, the molecules undergo a 30° change in tilt direction during the transition. In the underlying modulo $2\pi/6$ hexatic order, such a change is also accomplished by the 90° rotation that is observed.

Acknowledgment. The work described here is the result of collaborations with a large number of people, many of whose names appear with mine in the references. It has been carried out with the support of the U.S. National Science Foundation.

References

1. V. M. Kaganer, XXXth Rencontres de Moriond, Villars sur Ollon, Switzerland, 1995.
2. D. K. Schwartz and C. M. Knobler and R. Bruinsma, Phys. Rev. Lett. **73**, 2841 (1994).
3. C. M. Knobler and R. C. Desai, Annu. Rev. Phys. Chem.**43**, 207 (1992)
4. H. M. McConnell, Annu. Rev. Phys. Chem. **42**, 171 (1991)
5. C. M. Knobler, Adv. Chem. Phys. **77**, 397 (1990).
6. S. Hénon and J. Meunier, Rev. Sci. Instrum. **62**, 936 (1991).
7. D. Hönig and D. Möbius, J. Phys. Chem. **95**, 4590 (1991).

8. S. Rivière, S. Hénon, J. Meunier, D. K. Schwartz, M.-W. Tsao and C. M. Knobler, J. Chem. Phys. **101**, 10045 (1994).

9. J. Ruiz-Garcia, X. Qiu, M.-W. Tsao, G. Marshall, C. M. Knobler, G. A. Overbeck, and D. Möbius, J. Phys. Chem. **97**, 6955 (1993).

10. D.K. Schwartz, J. Ruiz-Gracia, X. Qiu, J. V. Selinger and C. M. Knobler, Physica A **204**, 606 (1994).

11. X. Qiu, J. Ruiz-Garcia, K. J. Stine, C. M. Knobler, and J. V. Selinger, Phys. Rev. Lett. **67**, 703 (1991).

12. B. Fischer, M.-W. Tsao, J. Ruiz-Garcia, T. M. Fischer, D.K. Schwartz and C. M. Knobler, J. Phys. Chem. **98**, 7430 (1994).

13. Or more precisely, quasi-long range order because long-range order cannot exist in two dimensional systems.

14. R. M. Kenn, C. Böhm, A. M. Bibo, I. R. Peterson and H. Möhwald, J. Phys. Chem. **95**, 2092 (1991).

15. A. M. Bibo, C. M. Knobler and I. R. Peterson , J. Phys. Chem. **95**, 5591 (1991).

16. J.V. Selinger and D.R. Nelson, Phys. Rev. A **39**, 3135 (1989).

17. S. A. Langer and J. P. Sethna, Phys. Rev. A **34**, 5035 (1986).

18. G. A. Hinshaw and R. G. Petschek, Phys. Rev. A **39**, 5914 (1989).

19. J.V. Selinger, in *Complex Fluids*, edited by E.B. Sirota, D. Weitz, T. Wittten and J. Israelachvili (Materials Research Society, Pittsburgh, 1992), p. 29.

20. T. Fischer, C. M. Knobler and R. Bruinsma, Phys. Rev. E **50**, 413 (1994).

21. J. A. Mann, Jr., XXXth Rencontres de Moriond, Villars sur Ollon, Switzerland, 1995; M. N. G. de Mul and J. A. Mann, Jr., Langmuir **10**, 2311 (1994).

22. J. V. Selinger, Z.-G. Wang, R. F. Bruinsma and C. M. Knobler, Phys. Rev. Lett. **70**, 1139 (1993).

23. W.J. Foster, M. C. Shih and P. S. Pershan, preprint.

PHASE SEPARATION IN LANGMUIR MONOLAYERS

M. Seul, AT&T Bell Laboratories, Murray Hill, NJ 07974, U.S.A.

Abstract

Langmuir films, composed of suitable amphiphiles adsorbed at an air-water interface, facilitate the realization of a two-dimensional binary mixture. Late-stage coarsening in such a system, subjected to rapid isothermal expansion, has been investigated via direct imaging and extensive pattern analysis. This analysis yields a description of the domain coarsening dynamics, as well as an elucidation of spatial correlations and topological properties of the evolving droplet patterns. The latter provide evidence for a prominent role of entropy maximization in the selection of pattern configurations, in close analogy to the behavior of cellular structures, or "froths". In this note, I summarize our principal results with reference to current theory and simulations and identify topics of interest for future research.

I Introduction

The evolution of a binary mixture to its new equilibrium state subsequent to a field or temperature quench has been the subject of extensive theoretical, numerical and experimental research [1]. The point of departure for much of the theoretical analysis is the classic mean-field theory of late-stage coarsening, or Ostwald ripening, in an infinitely dilute system [2]. The extension of this single droplet theory to systems of finite volume fraction of minority phase requires the inclusion of interdroplet correlations in the evolution dynamics [3]. Extensive theoretical and numerical analysis, particularly for two-dimensional (2D) systems, predicts the preservation of an asymptotic scaling state in multidroplet coarsening. As with the single droplet dynamics, this state is characterized by a growth exponent of 1/3 for the mean droplet radius; however, the shape of the normalized, scaled droplet radius distribution is significantly modified from that of the Lifshitz-Slyozov (LS) distribution [4]. Quantitative experimental tests of the theoretical predictions for 2D systems are now beginning to appear [5].

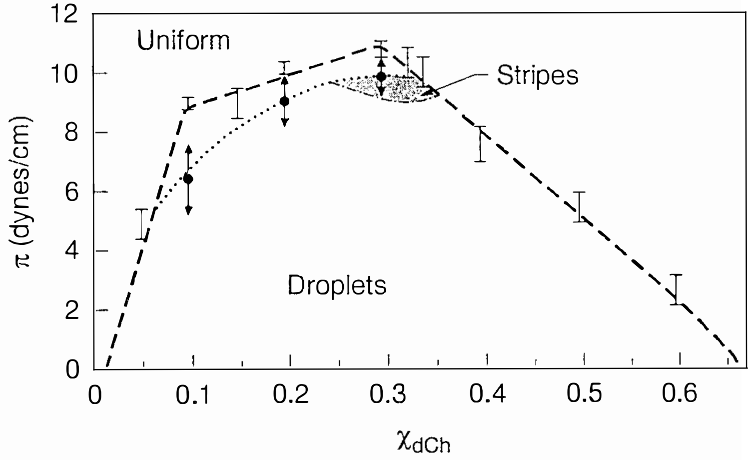

Fig. 1 - Schematic Phase Diagram – Phase boundary between a uniform state and (droplet and stripe) domain phases in Langmuir films, composed of dimyristoylphosphatidylcholine (DMPC) and dihydrocholesterol (dCh); π denotes surface pressure, χ_{dCh} represents mole fraction of dCh. The dashed line and error bar symbols, adapted from Benvegnu and McConnell [9], pertain to room temperature measurements. The solid symbols, connected by a dotted line to guide the eye, mark transitions identified by Morgan and Seul [10], based on the isothermal compressibility of (fluorophore-free) mixtures at $T = 19°C$. The hashed region is occupied by a stripe liquid phase, further investigated by Seul [10].

In addition to diffusion-mediated interdroplet correlations, coarsening in many experimental situations proceeds in the presence of a variety of long-ranged interactions which can fundamentally alter the coarsening dynamics [6]. This is so particularly for a class of systems which adopt equilibrium configurations in the form of stripe or droplet ("bubble") patterns; these are stabilized by the competition of short-ranged attractive and long-ranged repulsive interactions whose ratio determines the characteristic scale of the patterns [7]. The effect of repulsive dipolar interactions on the coarsening dynamics of a 2D system with conserved order parameter has been recently investigated by Sagui and Desai [8].

Langmuir monolayers facilitate the experimental realization of a 2D binary mixture subject to competing interactions [9]. We have relied on mixed Langmuir monolayers composed of the phospholipid dimyristoylphosphatidylcholine (DMPC) and dihydrocholesterol (dCh) to study, via direct imaging, the late-stage coarsening behavior of such a mixture subsequent to a rapid isothermal expansion [10]. In the following two sections, I summarize our principal observations. A schematic surface pressure - composition phase diagram of this system is depicted in Fig. 1.

II Coarsening of Droplet Domains: Dynamic Scaling

Following an initial regime dominated by the fastest growing unstable composition mode, the evolution of the 2D binary mixture, of composition $\chi_{dCh} = 0.2$ and corresponding (nominal) area fraction $\Phi \simeq 0.25$, exhibits dynamic scaling over the entire range of experimental time scales accessible to us. As shown in Fig. 2, the scaling regime is characterized by an exponent of ~ 0.28 for the mean droplet radius and by a normalized, scaled droplet radius distribution, $P(R/\langle R\rangle)$, which is virtually symmetric and thus well approximated by a Gaussian. From the point of view of a maximum entropy analysis we have developed for droplet patterns, the Gaussian represents an approximation to the slightly skewed line shape produced by the theory. Systems of lower (nominal) area fraction display a distinct skewness in $P(R/\langle R\rangle)$.

The competition of long-range repulsive and short-range attractive interactions is expected to lead to a cross-over in the coarsening dynamics when the droplet size, $\langle R\rangle$, reaches the scale of the equilibrium length, $R_{eq} \sim \Phi^{1/2}\Lambda$. We attribute our failure to observe this cross-over to the fact that the characteristic cross-over time, $t^* = t(\langle R\rangle = R_{eq})$ exceeds our observation time, a likely consequence of the fact that dipolar coupling in our system is exceedingly weak. In fact, while a cross-over does manifest itself in simulations of strongly coupled systems, weak coupling appears to move the cross-over time out of reach, in analogy to experimental observations; in fact, the analysis of Sagui and Desai actually leaves open the possibility that, for thin films with weak coupling, $t^* = \infty$. At the finite temperatures pertinent to experiment, an intriguing alternative possibility would allow for an intrinsically disordered ground state. Simulations (at zero temperature) of weakly coupled systems closely approach the numerical value reported here [8]. Interestingly, the coarsening of the stripe liquid phase of near-critical DMPC/dCh mixtures attains its equilibrium length scale on microscopic time scales, given the predominance of dipolar repulsion over attractive interactions in that phase, as discussed by Seul [10].

The primary role of electrostatic interactions in the coarsening of the binary Langmuir films investigated here appears to be the stabilization of droplet patterns against coalescence so that the pattern evolution must proceed via evaporation and condensation [2].

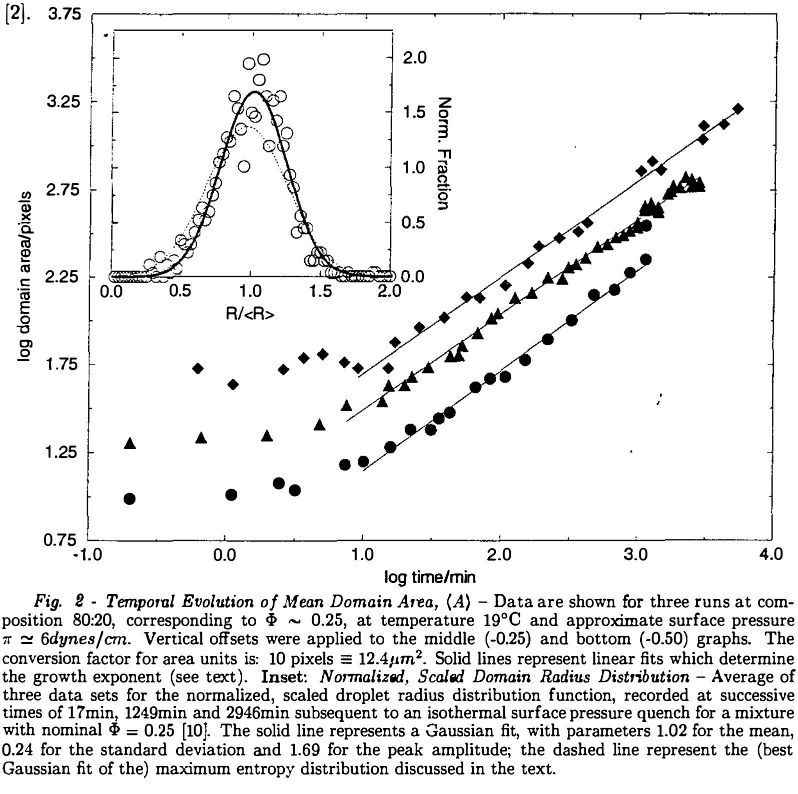

Fig. 2 - Temporal Evolution of Mean Domain Area, $\langle A \rangle$ – Data are shown for three runs at composition 80:20, corresponding to $\Phi \sim 0.25$, at temperature 19°C and approximate surface pressure $\pi \simeq 6 dynes/cm$. Vertical offsets were applied to the middle (-0.25) and bottom (-0.50) graphs. The conversion factor for area units is: 10 pixels $\equiv 12.4 \mu m^2$. Solid lines represent linear fits which determine the growth exponent (see text). **Inset:** *Normalized, Scaled Domain Radius Distribution* – Average of three data sets for the normalized, scaled droplet radius distribution function, recorded at successive times of 17min, 1249min and 2946min subsequent to an isothermal surface pressure quench for a mixture with nominal $\Phi = 0.25$ [10]. The solid line represents a Gaussian fit, with parameters 1.02 for the mean, 0.24 for the standard deviation and 1.69 for the peak amplitude; the dashed line represent the (best Gaussian fit of the) maximum entropy distribution discussed in the text.

III Spatial Correlations: Entropy Maximization

The Voronoi diagram of droplet centroids represents a (space-filling) graph uniquely associated with a given coarsening droplet pattern [11]. Analysis of such graphs (see left-hand panel of Fig. 3) reveals topological characteristics of the underlying pattern, notably in the form of the two plots contained in the right-hand panels of Fig. 3. These depict (empirical) correlations that are well known in the context of cellular patterns ("froths") [12].

The Lewis law, $a_n = 1 + \lambda_a C$ (and analogously for x_n, see Fig. 3), describes a linear correlation between the mean area of n-fold coordinated droplets (or that of n-sided polygons), a geometrical quantity, and their topological charge, $C \equiv n - 6$, a topological quantity. Here, $a_n \equiv \langle A_n \rangle / \langle A \rangle$ and $x_n \equiv \langle A_{Vp_n} \rangle / \langle A_{Vp} \rangle$, respectively represent the average area of an n-fold coordinated droplet, normalized by the mean droplet area, $\langle A \rangle$, and the average area of an n-sided Voronoi cell, normalized by the mean cell area, $\langle A_{Vp} \rangle$.

The Aboav-Weaire (AW) law describes the tendency toward compensation of topological charge at the N(earest) N(eighbor) level, given a finite overall density of (topological) charge. That is, for given $\mu_2 \equiv \sum_{n \geq 3} p_n C^2 > 0$, the AW law states that $C + n\overline{C}_{NN} = (1 - a)C + \mu_2$ where C denotes the charge of an n-sided cell and $\overline{C}_{NN}$ represents the average charge of its n nearest neighbors; the degree of charge compensation is measured by the correction term, $(1 - a)C$. In view of the Euler-Poincaré law, $\langle C \rangle = 0$, this parametrization ensures validity of the exact relation $\langle C + n\overline{C}_{NN} \rangle = \mu_2$ [12]. Note that, with $\langle C \rangle = 0$, the AW law may be rewritten in the conventional, but far less intuitive, form $nm(n) = (6 - a)n + 6a + \mu_2$.

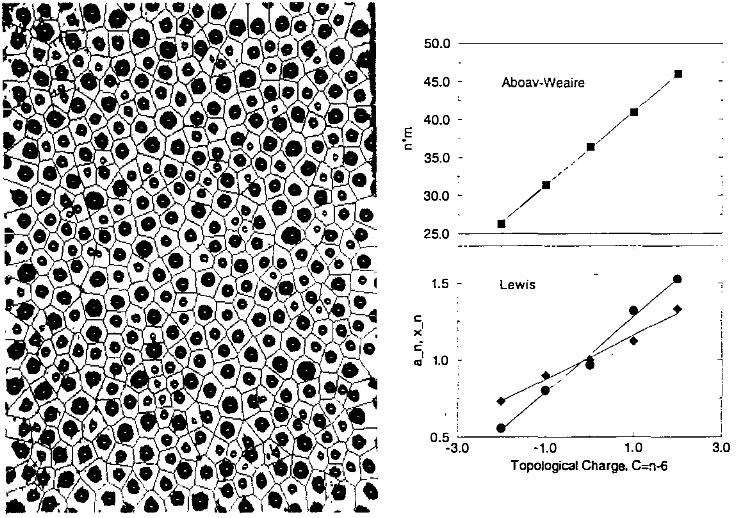

Fig. 3 - Voronoi Analysis of Droplet Pattern - **(Left Panel)**: Superposition of a flat-fielded domain pattern and the corresponding Voronoi diagram of droplet centroids which are also indicated. The image shows a droplet domain pattern in a Langmuir film of DMPC and dCh, with mole fraction $\chi_{dCH} = 0.2$ [10]; the pattern was recorded after 1249 min of coarsening, at 19°C, following a surface-pressure quench. The vertical dimension of the field of view is 1500μm. **(Right Panel)**: Geometrical and topological statistics in the form of plots (with linear fits) corresponding to Lewis law (bottom) for droplet pattern (solid circle) and corresponding Voronoi diagram (diamond) and Aboav-Weaire law (top), as discussed in the text where a_n and x_n are defined; $\langle A \rangle_{nn}$, n and m respectively denote the average area of droplets in the NN shell of a given droplet, the droplet coordination number and the average coordination number of droplets in the NN shell of an n-fold droplet.

The parameters, μ_2, λ_a (λ_x) and a, serve to classify cellular patterns. Typical values extracted from the Voronoi analysis of coarsening droplet patterns reveal them to be in a class with equilibrated random Voronoi lattices. In their most recent contributions, Sagui and Desai have performed a Voronoi analysis of numerically generated patterns and find, for weakly coupled systems, virtually identical results.

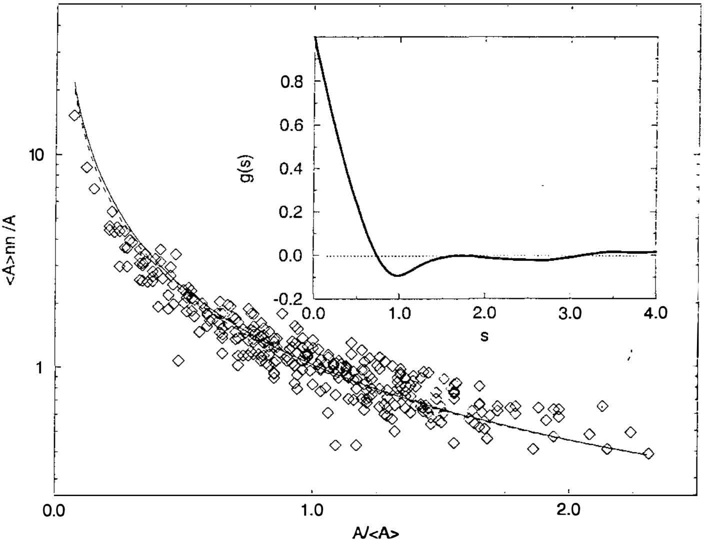

Fig.4 - Area Correlations between NN Domains – Spatial correlations in the area values assumed by adjacent domains, for the pattern in Fig. 4. The solid line represents the model discussed in the text, with parameters $\mu_2 = 0.75$, $\lambda = 0.25$ and $a = 1.1$; the dashed line corresponds to the limit of setting $\mu_2 = 0$ and $a = 1$, as discussed by Sire and Seul [10]. **Inset**: *Topological Charge Correlation Function* – $g(s) = \langle C(r+s)C(r)\rangle_S / \langle C(r)C(r)\rangle_S$, with $C \equiv n - 6$ and distance s measured in units of the average NN centroid distance, $s = \sqrt{\langle A_{Vp}\rangle}$, where $\langle A_{Vp}\rangle$ represents the average Voronoi cell area.

Beyond facilitating assignments to a particular class of cellular pattern, the close analogy between the coarsening droplet patterns and cellular patterns suggests a prominent role for entropy maximization in the selection of droplet configurations. Explicit analysis reveals the density of topological defects in the coarsening patterns to remain unchanged throughout the scaling regime. This is equivalent to setting the energy scale so that minimization of the free energy must proceed under this additional constraint, in addition to those first applied in the maximum entropy analysis of space-filling cellular patterns by Rivier [12].

The tendency toward complete charge compensation at the NN level, expressed in the form of the AW law, manifests itself in a pronounced anti-correlation of the corresponding geometrical quantity, namely the droplet area. This is depicted in Fig. 4.

IV Outlook

I close by enumerating topics of interest for future research.

Living Droplets - As discussed by Morgan and Seul [10], large scale inhomogeneities in coverage, Φ, appear during the coarsening process. Timasheva and Singer, in unpublished work, have found that electrostatic interactions are capable of destabilizing uniform droplet patterns if the mean droplet radius, $\langle R\rangle$, is allowed to adjust itself according to the locally prevailing Φ. An assembly of such "living droplets" would be able to approach equilibrium, on a local scale, by adjusting the locally prevailing coverage, Φ, to match $\langle R\rangle$, in accordance with the expected equilibrium behavior [13]. This intriguing picture raises the possibility that a second phase separation, between regions of respectively low ("gas") and high ("liquid") values of Φ, and subsequent coarsening process of such regions of different Φ, may occur concomitantly with the droplet coarsening. This clearly is an interesting issue to pursue in an experiment monitoring the appearance of large-scale structure.

Two-Time Correlations - Recent theoretical analysis of coarsening has focused on the evaluation of time-dependent two-point correlation functions of the order parameter (see e.g. Bray in [1]). It has been conjectured that the decay of the temporal autocorrelation (or two-time correlation) function, evaluated for a given patch of sample, is governed by a new dynamic exponent, λ, whose value is related to spatial dimensionality. Experimental measurements of λ are scarce. The Langmuir films investigated here may well be suitable to provide a detailed experimental test in 2D.

Tunable Structural Dissimilarity - Analysis of DMPC/cholesterol pressure-area isotherms by Hirshfeld and Seul[9] suggests that DMPC may assume differing molecular configurations in coexisting regions of different composition. This would not be altogether surprising in view of the rather dissimilar molecular structures of the constituents whose mixtures, in the form of vesicular dispersions, are known to exhibit rather unusual phase behavior. Thus, it would be interesting to study mixed Langmuir films of molecules whose structural dissimilarity may be altered in a controlled fashion. Possible examples may be mixtures of fatty acids or alcohols with hydrocarbon and with partially fluorinated alkyl chains, or mixtures of phospholipids with choline and with ethanolamine headgroups. The latter system would also provide for the option to alter the dipolar coupling via control of bulk pH and ionic strength.

Acknowledgements

The work described here represents the result of a delightful collaboration with Nicole Morgan and Clèment Sire. It is a pleasure to acknowledge fruitful interactions with Rashmi Desai, John Marko, Celeste Sagui and Sherwin Singer.

References

[1] J.D.Gunton. M.San Miguel and P.S.Sahni in*Phase Transitions and Critical Phenomena, vol.8*, edited by C.Domb and J.L.Lebowitz (Academic Press 1983); S. Komura, Phase Transitions **12**. 3 (1988); A. J. Bray, NATO Adv. Study Inst. *Phase Transitions and Relaxation in Systems with Competing Energy Scales*, Geilo, Norway (1993).

[2] I.M. Lifshitz and V.V. Slyozov, J. Phys. Chem. Solids **19**, 35 (1961); C. Wagner. Z. Elecktrochemie **65**. 581 (1961).

[3] T. Imaeda and K. Kawasaki, Physica **164A**, 335 (1990); N. Akaiwa and P. W. Voorhees, Phys. Rev. **E49**, 3860 (1994).

[4] J. A. Marqusee and J. Ross, J. Chem Phys. **80**, 536 (1984); J. A. Marqusee, ibid. **81**. 976 (1984); P.W. Voorhees, J. Stat. Phys. **38**, 231(1985); M. Marder, Phys. Rev. **A36**, 438 (1987); Q. Zheng and J.D. Gunton, Phys. Rev. **A39**, 4848 (1989); T.M. Rogers and R.C. Desai, Phys. Rev. **B39**, 11956 (1989); J. H. Yao, K. R. Elder, H. Guo and M. Grant, Phys. Rev. **B47**, 14110 (1993).

[5] O. Krichevsky and J. Stavans, Phys. Rev. Lett. **70**, 1473 (1993); Phys. Rev. E, submitted.

[6] T. Ohta and K. Kawasaki, Macromolecules **19**, 2621 (1986); K. Kawasaki and Y. Enomoto, Physica **150A**, 463 (1988); M. Bahiana and Y. Oono, Phys. Rev **A41**, 6763 (1990); P. W. Voorhees, Ann. Rev. Mater. Sci **22**, 197 (1992); L.Q. Chen and A.G. Khachaturyan, Phys. Rev. Lett. **70**, 1477 (1993).

[7] M. Seul and D. Andelman, Science **267**, 476 (1995).

[8] C. Roland and R.C. Desai, Phys. Rev. **B42**, 6658 (1990); C. Sagui and R.C. Desai, Phys. Rev. Lett. **71**, 3995 (1993); Phys. Rev. **E49**, 2225 (1994); Phys. Rev. Lett. **74**, 1119 (1995); preprints (1995).

[9] C. L. Hirshfeld and M. Seul, J. Physique **51**, 1537 (1990); H.M. McConnell, Annu. Rev. Phys. Chem. **42**, 171 (1991); D. J. Benvegnu and H. M. McConnell, J. Phys. Chem. **96**, 6820 (1992).

[10] M. Seul, N. Y. Morgan and C. Sire, Phys. Rev. Lett. **73**, 2284 (1994); M. Seul, Europhys. Lett. **28**, 557 (1994); N. Y. Morgan and M. Seul, J. Phys. Chem. **99**, 2088 (1995); C. Sire and M. Seul, J. Physique I **5**, 97 (1995).

[11] M.O. Magnasco, Phil. Mag. **B65**, 895 (1992); ibid, **B69**, 397 (1994).

[12] D. Weaire and N. Rivier, Contemp. Phys. **25**, 59 (1984); H. Flyvbjerg, Phys. Rev. **47**, 4037 (1993); J. Stavans, Rept. Prog. Phys. **56**, 733 (1993).

[13] M. M. Hurley and S. J. Singer, J. Phys. Chem. **96**, 1938 and 1951 (1992).

MORPHOLOGY TRANSITIONS IN THE GROWTH OF DOMAINS IN SURFACTANT MONOLAYERS

E. Scalas[1], G. Brezesinski[1], H. Möhwald[1,2]
1) Universität Mainz, Institut für Physikalische Chemie, Germany
2) Max Planck Institut für Kolloid- und Grenzflächenforschung, Germany
and
G. Indiveri, A.C. Levi, A. Gliozzi
Università di Genova, Dipartimento di Fisica, Italy

ABSTRACT

Results of extensive computer simulations of domain growth are presented. The simulations are able to reproduce the tip-splitting transition observed in real systems including surfactant monolayers at the air-water interface. In the transition region clusters with hybrid morphologies appear. The presence of such hybrid clusters seems to suggest that, at least in the case of our simulation, there is a gradual cross-over from dendritic to tip-splitted clusters as the lateral coupling βJ varies through the transition region.

1. INTRODUCTION

After some recent important results on dendritic growth1), the attention of researchers from various fields has focused on the problem of morphology transitions in the shape of diffusion-driven far-from-equilibrium growing crystalline (or liquid-crystalline) structures.

Although the selection problem in dendritic growth can be considered satisfactorily solved, the nature of the so-called tip-splitting transition, where the tip of a growing branch splits into two or more parts, is not yet clear. Among the various explanations proposed for the tip-splitting transitions there are variational theories2,3). Other authors tried to explain morphology transitions in analogy to the bifurcation path to chaos4). It is not even clear whether it is possible to use the word *transition* or if it is better to think of a gradual *cross-over* between the two morphologies.

Most of these ideas have been developed for two-dimensional systems, therefore surfactant monolayers at the air-water interface also known as *Langmuir monolayers* (one of the best approximations to Abbott's *Flatland* we know) are suited to test them. In monolayers, clusters of a condensed phase growing at the expense of a fluid (or liquid-expanded) phase can be observed by means of fluorescence microscopy or Brewster-angle microscopy when the coexistence surface pressure is reached.

Here we shall briefly review results obtained by a computer simulation of domain growth described in detail elsewhere5), and we shall present some new results based on extensive simulations in the region of the tip-splitting transition.

2. MORPHOLOGY TRANSITIONS IN LANGMUIR MONOLAYERS

During domain growth in Langmuir monolayers several different morphologies appear, depending on the growth conditions (temperature and disequilibrium) and on the nature of the surfactant molecules. Here we shall restrict ourselves to the analysis of the transition between dendritic and tip-splitted clusters.

Even if in Langmuir monolayers it is difficult to control disequilibrium locally, it is possible to obtain morphology diagrams by varying temperature and compression rate6). In the transition region between dendritic and tip-splitted growth, clusters of hybrid morphology appear6).

Domains in monolayers of triple-chain isomeric phospholipids growing under similar conditions can show different growth morphologies depending on the position of the branched chain with respect to the glycerol backbone7). In this case it was possible to prove by grazing incidence X-ray diffraction that for dendritic domains the chains are more tilted, the deviation from hexagonal symmetry is more pronounced and hence the lattice anisotropy is larger[8]).

3. DIFFUSION-LIMITED GROWTH

The "Standard Model"[9]) for domain growth is a diffusive model where there is a field: $u(\mathbf{r}, t)$, representing temperature, or, better in our case, impurity concentration, and obeying the diffusion equation:

$$\frac{\partial u}{\partial t} = D\nabla^2 u \tag{1}$$

where D is the collective diffusion coefficient. There are two boundary conditions at the interface. The Stefan condition is a statement of mass conservation. If we neglect diffusion in the condensed phase we have:

$$v_n = -D\left[(\nabla u)_{exp}\right] \cdot \hat{\mathbf{n}} \tag{2}$$

where v_n is the growth velocity normal to the interface and $\hat{\mathbf{n}}$ is the unit vector normal to the interface and pointing towards the liquid expanded phase. The other boundary condition, the Gibbs-Thomson one, is a statement of local equilibrium at the interface:

$$u_s = -d_0 K \tag{3}$$

where u_s is the value of the diffusive field at the interface, K is the local curvature of the interface and d_0 is the capillary length, proportional to the interface stiffness[5]): the sum of the interface tension and its second derivative with respect to the angle between the normal to the interface and a fixed direction in the plane. To complete our Standard Model, we have to add a boundary condition far from the growing cluster. Indeed in a two dimensional geometry one has to choose this boundary condition on a circle far from the growing cluster, let say at a distance R much greater than the cluster radius, and not at infinity, in order to avoid logarithmic divergence in the solutions:

$$u(R) = -\Delta \tag{4}$$

where Δ is the supersaturation at long distance.

Even if this model does not take into account some important effects such as convection, there are no analytical solutions available. Therefore computer simulations can help to improve our understanding of morphology transitions. One of the advantages of computer simulations is that it is possible to account for the basic microscopic physical processes.

In our simulation diffusion, condensation, evaporation, and rearrangement at the interface compete with each other giving rise to different growth morphologies as a function of the model parameters.

Particles are sent in from the outside, as in DLA10): they move randomly on a triangular lattice until they either stick to the growing cluster or are lost. At the same time other particles detach from the cluster boundary and they perform a random walk either sticking into another position or evaporating.

The energy E of the cluster is given by the lattice-gas formula:

$$E = -J \sum_{\langle i,j \rangle \in \mathrm{cluster}} n_i n_j \tag{5}$$

where $\langle \cdot,\cdot \rangle$ denotes the sum over nearest-neighbour sites and n_i is 1 for a cluster particle and 0 for an empty site. The probability of condensation or evaporation is:

$$p = \frac{1}{\exp\left[\beta\left(\Delta E - \mu_{eq}\Delta N\right)\right] + 1} \tag{6}$$

where μ_{eq} is the chemical potential for solid-vapour coexistence, ΔE and $\Delta N = \pm 1$ are the variations of energy and number of particles, respectively. The growth rate dN/dt is, by construction, equal to $\exp(\beta\Delta\mu) - 1$ (Wilson-Frenkel's growth rate5)). The time unit of the simulation is then the inverse of the growth rate.

4. RESULTS AND CONCLUSIONS

Perhaps one of the most interesting features of the growth model discussed in the previous section is that computer simulations are able to reproduce the tip-splitting transition observed in real systems. The transition occurs for $4 < \beta J < 5$ at all investigated disequilibria ($3 < \beta\Delta\mu < 6$). For $\beta J \geq 5$ the clusters are dendritic, whereas for $\beta J \leq 4$ the tips become unstable and split. In the case of dendrites, the simulation reproduce realistic results, for instance a constant velocity of the branches is reached after a transient decrease.

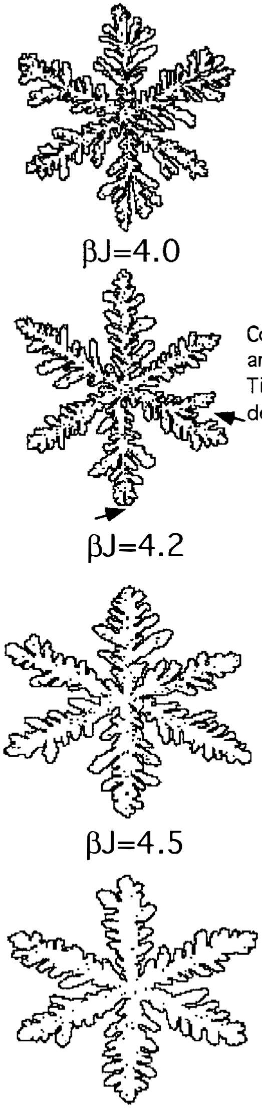

$\beta J=4.0$

Coexistence of dendritic arms and tip-splitting. Tip-splitting events are denoted by arrows.

$\beta J=4.2$

$\beta J=4.5$

$\beta J=4.8$

Fig. 1

We have investigated the transition region in detail for high growth rate ($\beta\Delta\mu = 6$). Simulations lasting 3000 time units and leading to clusters with more than 10^6 particles have been carried out for lateral couplings $\beta J = 4.0$, 4.2, 4.5, 4.8. In Fig.1 we report the results of the simulation for t=1800. As can be observed by direct inspection of Fig.1, hybrid morphologies, observed also in experiments on monolayers6), appear at $\beta J = 4.2$, whereas at $\beta J = 4$ the tip splitting events become so numerous that they are hard to identify. Moreover the box fractal dimension of the perimeter of the clusters monotonically decreases towards 1 with increasing lateral coupling. These findings suggest that we do not observe a sharp transition, but rather a gradual cross-over between the two morphologies.

5. ACKNOWLEDGMENTS

This work was supported by the Bundesministerium für Forschung und Technologie (BMFT), the Deutsche Forschungsgemeinschaft (DFG) and the Human Capital and Mobility Program of the EC. One of the authors (E.S.) was put in condition to perform this work by a grant afforded by Genoa University, Italy (borsa di studio per perfezionamento all'estero).

REFERENCES

1) For a review see: E. Ben-Jacob and P. Garik, Nature, **343**, (1990), 523.
2) O. Shochet and E. Ben-Jacob, Phys. Rev. E, **48**, (1993), R4168.
3) A. Hill, Nature, **348**, (1990), 426.
4) Y. Sawada, Physica A, **140**, (1986), 134.
5) A. Gliozzi, A.C. Levi, M. Menessini, and E. Scalas, Physica A, **203**, (1994), 347.
6) S. Akamatsu, Thèse de doctorat de l'Université Paris VI, 1992.
7) A. Dietrich, H. Möhwald, W. Rettig, and G. Brezesinski, Langmuir, **7**, (1991), 539.
8) A. Dietrich, G. Brezesinski, H. Möhwald, B. Dobner, and P. Nuhn, Il Nuovo Cimento, in press.
9) J.S. Langer, Rev. Mod. Phys., **52**, (1980), 1.
10) T.A. Witten and L.M. Sander, Phys. Rev. Lett., **47**, (1990), 1400.

BREWSTER ANGLE MICROSCOPY STUDY OF CHIRAL DISCRIMINATION IN LANGMUIR MONOLAYERS

D. Vollhardt, G. Emrich, V. Melzer, G. Weidemann and U. Gehlert
Max-Planck-Institut für Kolloid- und Grenzflächenforschung, Rudower Chaussee 5,
D-12 489 Berlin, Germany

Abstract

The morphological variety of chiral discrimination in condensed phase domains of Langmuir monolayers is outlined by selected chiral amphiphiles from the type of amino acid derived amphiphiles, amphiphilic aldonamides, amphiphiles with different structured head groups containing amide bondings, alkanoyl monoglycerol esters, and phospholipids. A comparison of BAM micrographs with the corresponding π - A isotherms demonstrates the higher sensitivity of the morphological studies to the specific stereochemistry. The main features of shape and inner structure of racemic and enantiomeric monolayers are presented and in the most cases, striking differences of both types are visualised. Based on the effective interaction between the enantiomeric forms two main categories of 1:1 enantiomer mixtures are discussed (i) a conglomerate-like type (homochiral discrimination) and (ii) the formation of a racemic compound (heterochiral discrimination). Examples without chiral discrimination effects are found in the free rotating limit.

Introduction

The recent interest in monolayers of long chain amphiphiles with a chiral polar head group has the following main reasons: (i) the chiral nature of the natural phospholipids is of importance for interactions and thus transport processes at biological membranes and (ii) the analysis of chiral forces is less complicated for two-dimensional arrangements than for the three-dimensional crystalline structure.

Chiral monolayers provide a unique system to study chirality-dependent interactions under defined conditions. The interactions of enantiomers to form racemic or diastereomeric mixtures can be examined over a wide range of specific monolayer states. Therefore surface pressure (π)- area (A) isotherms were used to demonstrate that amphiphilic amino acid derivatives show chiral discrimination between the isotherms of enantiomeric amphiphiles and their 1:1 enantiomer mixtures[1,2].

With the recent development of Brewster angle microscopy (BAM)[3], an effective method is available to visualise the morphology of amphiphilic monolayers on microscopic scale without requirement of probe molecules. A further advantage of the method is based on the possibility to obtain information on the orientational order of the condensed monolayer phases.

In the present paper, a short review is given on the variety of chiral discrimination effects in the monolayer morphology.

Chiral Discrimination in Morphology of Langmuir Monolayers

In the simplest case, a chiral molecule has an asymmetric carbon atom connected to four different chemical groups, so that permutations of any pair of these groups leads to the mirror image of the original molecule. For a chiral amphiphile of a Langmuir monolayer, Andelman[4] constructed a tripod model at which three groups are anchored on the water surface, while the fourth group representing the aliphatic chain points up to the air. For such tripod amphiphile, two stereomers can be formed where the sequence of the three anchoring groups can be arranged clockwise or counterclockwise. Unfortunately, all chiral amphiphiles available to us deviate more or less from this construction principle.

For the understanding of the chiral discrimination effects, two categories of 1:1 enantiomer mixtures are distinguished in chiral monolayers, namely a conglomerate-like type and the formation of a racemic compound. In the case of the conglomerate-like type, the effective interaction between the same enantiomers is more favourable; hence corresponding to homochiral discrimination ($E_{D\text{-}D}$ or $E_{L\text{-}L} > E_{D\text{-}L}$), while the tendency to form a racemic compound is an indication that heterochiral interaction is preferred over the homochiral interactions ($E_{D\text{-}D}$ or $E_{L\text{-}L} < E_{D\text{-}L}$).

Finally it is worth mentioning that no chiral discrimination is expected in the free rotating limit, where $V_{ij} << k_BT$ (V_{ij} - van der Waals interaction).

Now, according to these categories representative examples are presented for chiral discrimination in the monolayer morphology.

Figure 1: Seven-fold domain of R-mono-palmitoyl-glycerol formed in the plateau region of the π - A isotherm (20 °C). The bar of all BAM micrographs represents 100 μm.

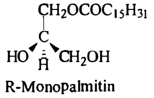

R-Monopalmitin

For alkanoyl monoglycerolester monolayers[5,6], due to the free rotating limit no chiral discrimination effects have been observed over a large temperature range. Conspicuous features are demonstrated by the circular condensed phase domains of R-1-monopalmitin (Fig. 1) which are subdivided into seven segments. They are formed in the two-phase coexistence region of the main transition. The segments meet at a centre and are separated by sharp straight lines at which the chain tilt azimuth jumps by a defined angle (Fig. 1). For the understanding of the slight efficiency of chiral centre, recent BAM and Grazing incidence X-ray diffraction measurements have revealed that a pronounced chiral effect exists for 1-monostearin at low temperatures only[13].

Morphological studies of the most important phospholipids, such as cephalines and lecithines demonstrate that chirality affects both the shape and the inner structure of the domains[7,8]. For example, the enantiomeric DPPE monolayers evolve chirally wound dendritic growth pattern, while the corresponding racemic structures are straight dendrites (Fig. 2b and c). The compact DMPE domains (Fig. 2a) observed show distinct chiral structural elements. On the other hand, the energetic differences between the enantiomeric and racemic forms are so small that no differences in the thermodynamic behaviour could be observed.

The chiral discrimination of the homologous N-alkyl-γ,δ-dihydroxy-pentanoic acidamide monolayers is based on the dominant effect of the hydrogen bonding system of the -NH-CO- group. Both enantiomeric N-tetradecyl-γ,δ-dihydroxy-pentanoic acidamide (TDPAA) monolayers show straight needle-like structures based on two axes. The enantiomeric structures have a striking stereomeric mirror image relation of the intersection angle (about 152 ^{0}) between a main and a minor growth direction (Fig. 3a and b), while the racemic structures evolve no preferred growth for the two growth direction with intersection angles up to 180°. In spite of the conspicuous chiral discrimination effects in the long range orientational order, differences in the π -A isotherms of these amphiphiles have not been found.

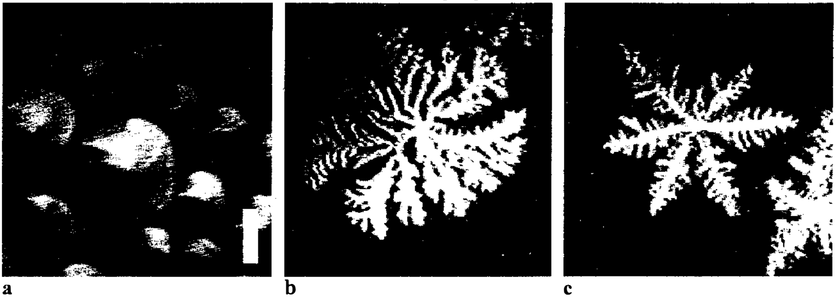

Figure 2: a) L-DMPE domain (T = 25°C). The segment boundaries of all domains are wound. The bowing of the segment boundaries is clockwise in all domains. b) L-DPPE domain (T = 43°C). A main arm of a dendrite corresponds to a segment. Consequently the bowing of all dendrite arms is also clockwise for all domains. c) DL-DPPE (T = 43°C) domain. The lattice at the air water interface is not chiral and the dendrite arms are straight.

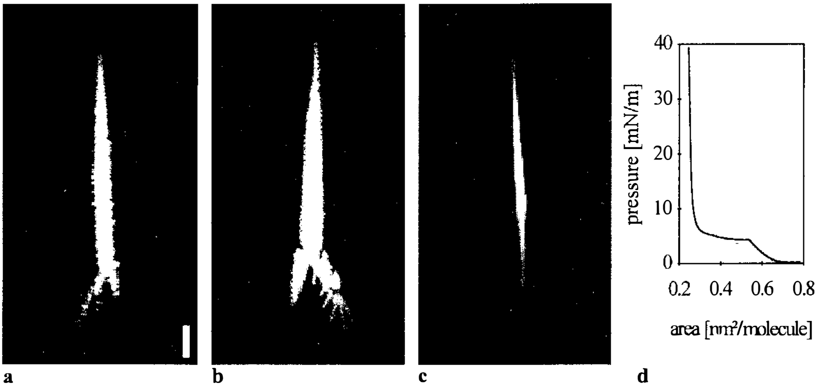

Figure 3: Chiral discrimination of the condensed phase textures of N-tetradecyl-γ,δ-dihydroxy-pentanoic acidamide monolayer ($0.35\ nm^2\ molecule^{-1}$, $9\ mN\ m^{-1}$, 10 °C).
a) S-enantiomer, b) R-enantiomer, c) 1:1-R,S racemate, d) isotherm

R-TDPAA

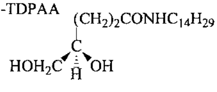
$(CH_2)_2CONHC_{14}H_{29}$—C(H)(HOH_2C)(OH)

The morphological discrimination of amino acid derived amphiphiles is of special interest because of their biological relevance. In the most cases, there are homochiral differences in the isotherms [4,5]. Here N-stearoylserine methyl ester (SSME) monolayers are discussed in order to emphasise some general features of the amino acid amphiphiles. On compression, both enantiomeric SSME monolayers evolve dendritic crystals with front propagation and straight growth directions. However,

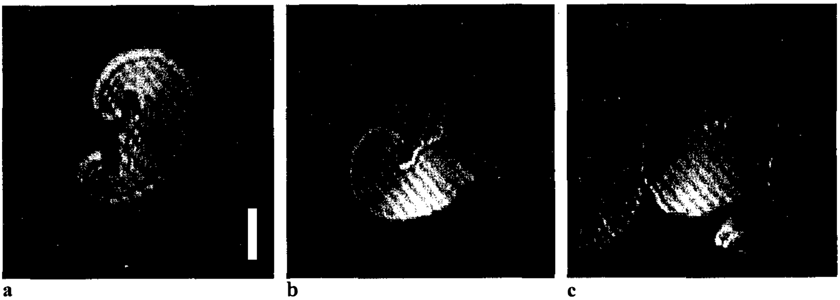

Figure 4: Time-dependent change of condensed phase domains of 1:1 racemic N-stearoylserine methyl ester (24 °C, 0.55 nm^2 molecule^{-1}). a) Two arms are evolved in opposite direction, b) the arms grow together and encircle two holes, c) as a result of coalescence, circular structures are formed with irregular periphery and surrounding a small hole.

R-SSME

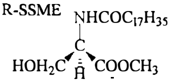

these non-equilibrium structures change with time if the monolayer compression is stopped. Then, corresponding with the chiral centre, the side arms tend to be curved clockwise (R-SSME) and counterclockwise (S-SSME), respectively. It is informative to observe the transformation kinetics of the condensed phase domains of racemic 1:1-R,S-SSME monolayers (24 °C, 0.55 nm^2 molecule^{-1}) (Fig. 4). At the beginning the compact domains evolve two arms curved in opposite directions (Fig. 4a) and growing one against the other. In this state, a mirror symmetry of the domain structure is obvious. Then, the arms grow together and encircle two holes. Coalescence of the condensed phase leads finally to circular structures with an irregular periphery which surround a small hole.

N-dodecyl-gluconamide (Glu)[11,12] and N-dodecyl-mannonamide (Man) monolayers are representative two-dimensional systems with striking differences in the π - A isotherms of the enantiomeric and racemic forms, namely in the first case with heterochiral discrimination and in the second one with homochiral discrimination. The corresponding differences in the dendritic crystallisation are presented in Fig. 5. D- and L- Glu form identical dendritic crystals. The dendrites grow anisotropically with straight main axes and numerous straight side branches (Fig. 5a). The corresponding racemic monolayers form isotropically distributed structures below the microscopic scale (Fig. 5b). The morphology of Man monolayers is very different. The enantiomers form featherlike crystals with clockwise curvature for the D-form and counterclockwise curvature for the L-form (Fig. 5c). The Man-racemate exhibits similar growth patterns, but curvature of the side branches in both directions (Fig. 5d). The chiral discrimination of the monolayer morphology can be related to the stereospecific configuration and conformation of the sugar head groups of the aldonamides, in particular to the development of an intermolecular hydrogen bonding cycle.

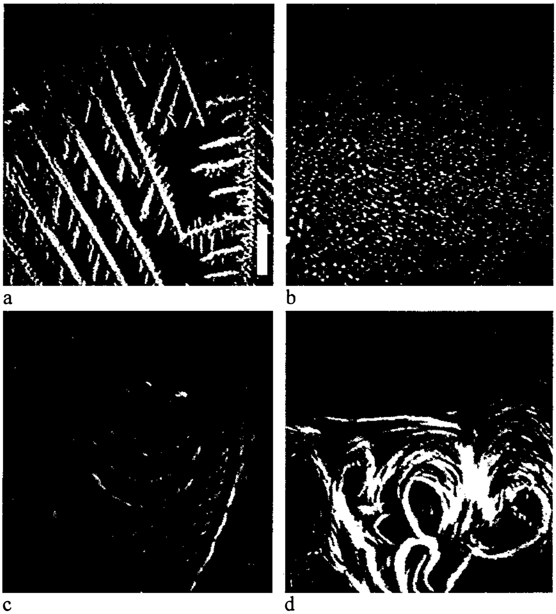

Figure 5: a) Dendritic crystallisation in a L-N-dodecylgluconamide monolayer(20 °C, 3 mN m^{-1}, 0.23 nm^2 molecule^{-1}) and b) short range orientational order for the racemic mixture with isotropic aggregation at microscopic scale (20 °C, 4 mN m^{-1}, 0.22 nm^2 molecule^{-1})

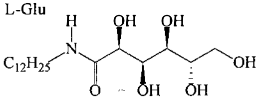

c) Morphology of condensed phase structures of D-N-dodecyl-mannonamide (30 °C, 0.2 mN m^{-1}, 0.5 nm^2 molecule^{-1}) and d) of the racemic mixture (30 °C, 0.5 mN m^{-1}, 0.5 nm^2 molecule^{-1})

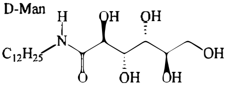

Acknowledgements

Financial assistance from the Deutsche Forschungsgemeinschaft (Sonderforschungsbereich SFB 312) and the Fonds der Chemischen Industrie is gratefully acknowledged.

References

1) E. M. Arnett, N.G. Harvey, P.L. Rose, Acc. Chem. Res. 22(1989)131
2) J.G. Heath, E.M. Arnett, J. Am. Chem. Soc. 114(1992)4500
3) S. Henon, J. Meunier, Rev. Sci. Instrum. 62(19991)936
4) D. Andelman, J. Am. Chem. Soc. 111(1989)6536
5) G. Weidemann, U. Gehlert, D. Vollhardt, Langmuir, 1995 in press
6) U. Gehlert, G. Weidemann, D. Vollhardt, J. Colloid Interface Sci., 1995 in press
7) G. Weidemann, D. Vollhardt, Colloids Surf., 1995 in press
8) G. Weidemann, D. Vollhardt, Thin Solid Films, 1995 in press
9) K.J. Stine,J.Y.-J. Uang, S.D. Dingman, Langmuir 9(1993)2112
10) D.P. Parazak, J. Y.-J. Uang, B. Turner, K.J. Stine Langmuir 10(1994)3787
11) D. Vollhardt, T. Gutberlet, G. Emrich, J.-H. Fuhrhop, Langmuir, 1995 in press
12) G. Emrich, D. Vollhardt, T. Gutberlet, B. Kling, J.-H. Fuhrhop, Prog. Colloid Polym. Sci., 98(1995) in press
13) U. Gehlert, D. Vollhardt, H. Möhwald, G. Brezesinski, in preparation

SURFACE CRYSTALLIZATION IN NORMAL-ALKANES AND ALCOHOLS

M. Deutsch[a], B.M. Ocko[b], X. Z. Wu[c,d], E.B. Sirota[d], and S.K. Sinha[d]
[a]*Physics Department, Bar Ilan University, Ramat Gan 52900, Israel*
[b]*Physics Department, Brookhaven National Laboratory, Upton, NY 11973, U.S.A.*
[c]*Physics Department, Northern Illinois University, DeKalb, IL 60115, U.S.A.*
[d]*Corporate Research Science Laboratory, Exxon Research and Engineering Co.,*
Route 22 East, Annandale, NJ 08801, U.S.A.

Abstract

A new, rare surface freezing phenomenon is observed in molten normal-alkanes and their derivatives (alcohols, thiols, *etc.*). X-ray and surface tension measurements show the formation of a crystalline monolayer on the surface of the liquid alkane at temperatures up to 3°C above the bulk solidification temperature, T_f. For alcohols, a single *bilayer* is formed. In both cases, the molecules in the layer are hexagonally packed and oriented normal to the surface for short chain lengths, and tilted for long ones. In both cases the isngle layer persists down to T_f. In terms of wetting theory, this constitutes a very limited partial wetting of the liquid surface by the crystalline layer. The new surface phase is obtained only for chain lengths $14 < n \leq 50$ in alkanes, and $16 < n < 30$ in alcohols. The measurements are satisfactorily accounted for within a simple theory based on surface energy considerations.

1 Introduction

Molecules residing at the free surface of a liquid or solid are less confined than those in the bulk. Their higher entropy renders the melting temperature of the surface *lower* than that of the bulk. This effect, called surface melting, is a general result of statistical mechanics and was observed in numerous materials ranging from molecular crystals[1], through water[2], to semiconductors[3] and metals[4]. The opposite phenomenon, that of surface melting, i.e. the ordering of the surface at temperatures *higher* than that of the bulk is a very rare phenomenon, detected until recently only in liquid crystals[5, 6]. Even there the order is not crystalline but smectic. We review here our recent work, which revealed true surface freezing in normal-alkanes and their derivatives. The simplicity of these molecules and their interactions, as compared to liquid crystals, indicates that surface freezing is a fundamental consequence of the inherently anisotropic interactions in chain molecules.

Liquid n-alkanes and alcohols, which are linear hydrocarbon chains, [CH_3-$(CH_2)_{n-2}$-CH_3, or, in short, Cn for alkanes and CH_3-$(CH_2)_{n-2}$-CH_2OH, denote CnO for alcohols], are basic structural units of many organic and biological molecules including lipids, surfactants, and liquid crystals, and determine their properties to a large extent[7, 8]. As they are the major constituents of oils, fuels, polymers, and lubricants they also have an immense industrial importance. Their surface properties, which remain largely unexplored, are important to applied as well as basic science. Recent x-ray scattering[9, 10], surface tension[9, 10, 11], optical[12], and simulation studies[13] have shown that these chain molecules exhibit remarkable behavior at the free surface.

In our x-ray scattering and surface tension measurements the abrupt formation of a crystalline monolayer on the surface of n-alkanes is observed at temperatures of up to 3°C above their bulk melting temperatures, for a range of chain lengths $14 < n \leq 50$. For alcohols, the same phenomena are observed. Here, however, a bilayer is formed over a smaller temperature range of up to 1°C and a chain length range of $16 < n < 30$. These appear to be the simplest systems in which surface-induced 2D crystalline ordering has been observed. The vanishing of the surface layer for the short chain end of the range can possibly be interpreted as the first observation of a transition from surface freezing to surface melting behaviour. The vanishing of the layering at the long chain end of the range is likely due to the proliferation of conformational distortions in the individual chains.

The next sections describe the experiments, the main body of results and our conclusions.

2 Experimental.

The samples, purchased from either Sigma, Aldrich or Fluka, were of purity > 99% and used as received. A small amount was placed on a 3 inch silicon wafer, forming a ~0.5mm thick film after melting. The wafer was placed inside a sealed cell whose temperature was regulated and uniform to within a few mK. The free surface of the samples was studied as a function of temperature by X-ray reflectivity (XR), X-ray grazing incidence diffraction (GID), and Bragg-rod (BR) measurements using the Harvard/BNL Liquid Surface Diffractometer at beamline X22B, NSLS, Brookhaven National Laboratory, with a typical wavelength λ= 1.54Å. XR yields information on the electron density profile *normal* to the surface, such as the thickness and density of a surface film. Here, the formation at the surface of a layer of electron density different from that of the bulk results in an oscillatory modulation on the otherwise monotonically varying reflectivity curve. The GID measurements provide information on the structure of a film within the surface plane. A surface crystalline layer yields sharp Bragg peaks in the diffraction curve. The orientation of the molecular chains is obtained from the Bragg-rods (BR), i.e. the surface-normal dependence of the scattered intensity at the position of each in-plane GID peak. These techniques are able to resolve the surface structure on an Å level both in-plane and perpendicular to the surface. For a full review we refer the reader to Ref. [14].

We have also carried out surface tension (ST) measurements, using the Wilhelmy plate method, in a cell similar to that used for the x-ray measurements. These provide information on the excess free energy of the molecules at the surface over those in the bulk. The formation of the layer at T_s is seen here as sharp change from a negative to a positive slope in the surface tension $\gamma(T)$ curve. The temperature was scanned at a rate ≤0.3 mK/sec to ensure ample thermal equilibration. For further details see Refs. [10, 15].

3 Results and Discussion.

Reflectivity curves above and below the solid monolayer formation temperature T_s for C18 and C18O are shown in Fig. 1 . Note the smooth monotonic decrease of both curves for $T > T_s$ which is typical of liquid surfaces broadened by capillary wave roughness[16]. These surfaces

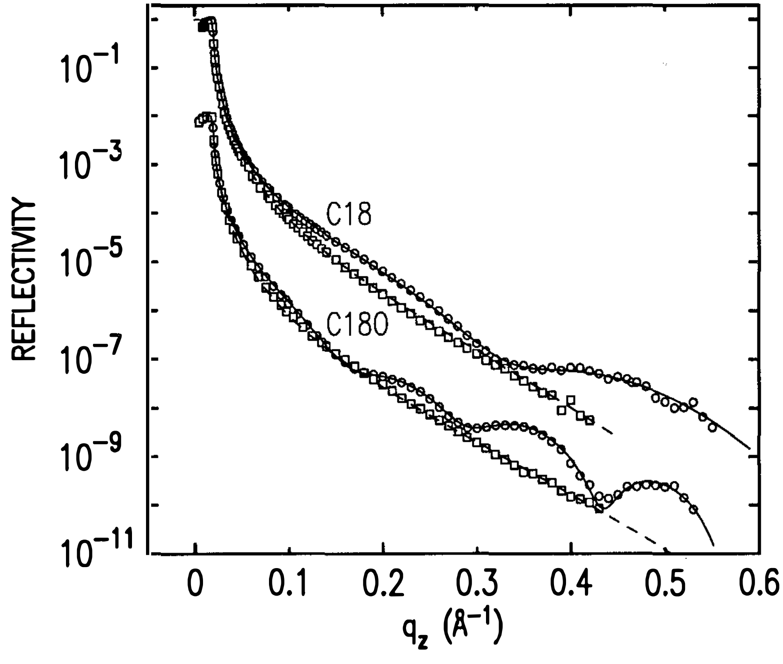

Figure 1: X-ray reflectivities for C18 and C18O in the liquid surface phase (circles) and the surface monolayer phase (squares). The solid and dashed lines are fits to the data, corresponding to the density profiles shown in Fig. 2.

are modeled well by an Error-function-like density profile with a Gaussian width parameter of $\sigma \approx 4.3$Å. Since for capillary wave dominated surface roughness σ scales as the square root of the surface tension ratio, this value is in good agreement with the $\sigma_{H_2O} = 2.8$Å measured for water[17]. The reflectivity at $T < T_s$ shows an oscillatory modulation indicative of a surface layer, as discussed above. Note, however, that the periods of the oscillations differ by a factor of two for the alkane and the alcohol, indicating a twofold thicker surface layer for the alcohols.

To obtain quantitative information on the density profile a simple multiple slab model is used in which the interfacial broadening between neighboring slabs is accounted for by a Gaussian roughness factor. The densities, thicknesses and the Gaussian roughness factors are determined by fitting the Fourier transform of the model to the normalized reflectivity curve, R/R_F, where R_F is the universal Fresnel reflectivity curve of Optics[14, 18]. Such a fit for the C18 alkane, shown as a solid line in Fig. 1, requires only two slabs, and provides an excellent representation of the data. The corresponding density profile is shown in Fig. 2. For all chain lengths below $n \leq 30$, the layer thickness obtained is very close to the extended length of the molecule and the density is ~15% higher than that of the underlying liquid. We consider, therefore, the layer to be a densely packed (solid) mono-molecular layer of vertically aligned molecules. The GID measurements[9] show a single resolution-limited peak for $T < T_s$, indicating that the

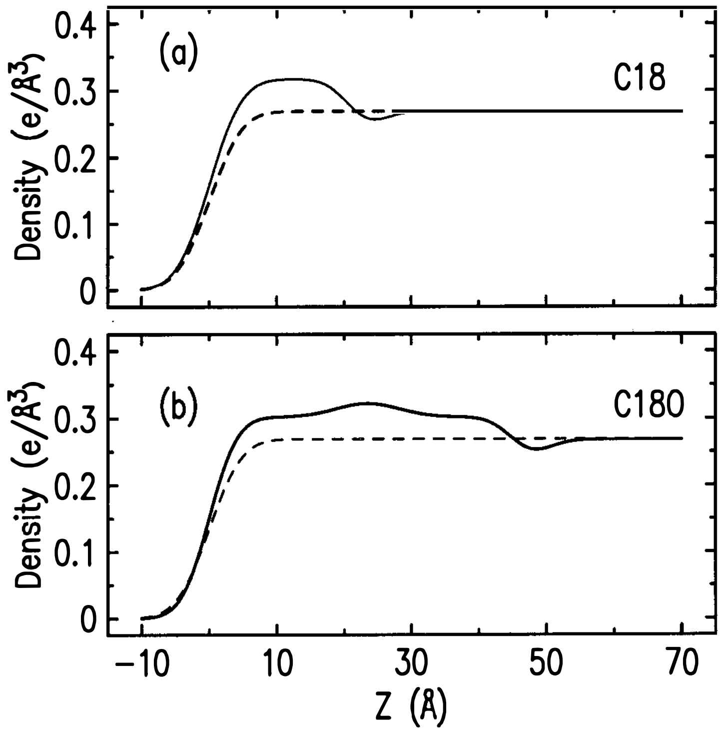

Figure 2: Electron density profiles for C18 and C18O corresponding to the solid and dashed lines in Fig. 1. Note the dense solid monolayer in C18 and bilayer in C18O on top of the less dense liquid. The higher and lower density regions in C18O are discussed in the text.

monolayer is an hexagonally packed crystal, with a nearest neighbour distance of 4.76Å and an in-plane crystalline coherence length exceeding a few thousand Å. This structure is very similar to the bulk rotator R_{II} phase[7]. For chains longer than $n \approx 30$ the molecules start tilting, with the tilt angle increasing with chain length and reaching 16° for C36. The BR measurements show the tilt to be in the nearest neighbour direction. The crystalline coherence length for the monolayers of the tilted molecules is considerably smaller than that of the vertical ones: a few hundred Å, in agreement with the increased disordering tendency of the longer chains. The structure of the alcohol surface layer is significantly different from that of the alkane. Here the twofold shorter modulation period of R/R_F indicates a twofold thicker layer: a bi-, rather than a mono-, layer. A slab model now requires a thin, high-density slab to be added at the center of the wide slab representing the bilayer, as well as a small depression near the bilayer-liquid interface, as shown in Fig. 2. As the density of the OH group is higher, and that of the CH_3 is lower, than that of the CH_2 group comprising the main body of the chain, the central slab is interpreted as a layer of the OH head groups, while the low density depression is due to a layer of terminal CH_3 groups. We thus find that the molecules in the upper layer are oriented with their

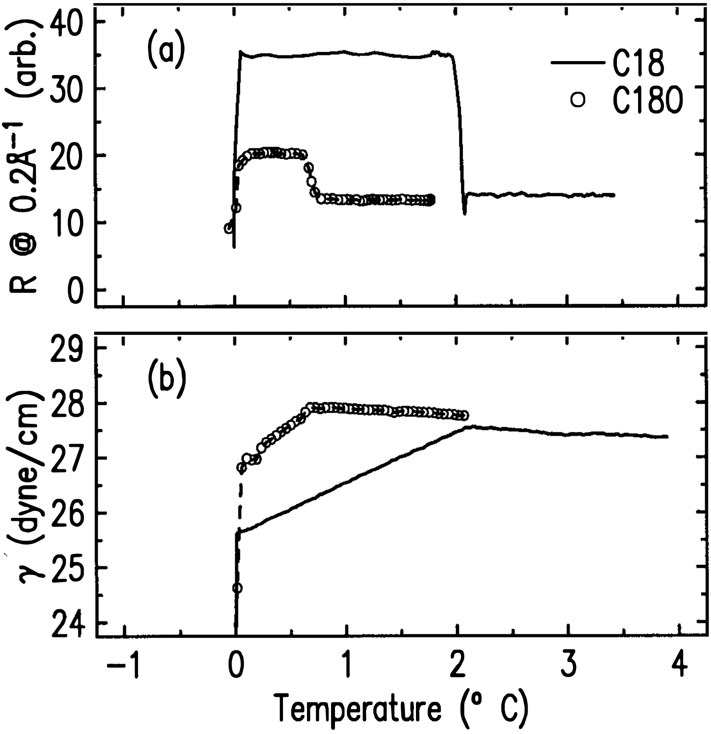

Figure 3: (a) Temperature scan of the reflectivity of C18 and C18O at a fixed q_z=0.20 Å^{-1}. Note the abrupt changes on solidification at T_f and the surface layer formation, at T_s. (b) Surface tension of C18 and C18O in cooling. Note the slope changes discussed in the text.

head groups at the bottom, while those in the lower layer have theirs at the top. The GID and BR measurements show an in-plane crystalline structure, where the molecules are hexagonally packed in each layer with vertical molecules for $n \leq 22$ and tilted ones for $n \geq 24$. The tilt angle increases with n and reaches 22° for $n = 26$. However, unlike long chain alkanes, the tilt direction here is towards *next*- nearest neighbours. Furthermore, the hexagonal lattice of the upper layer is shifted in the next-nearest-neighbour direction by two-thirds of a layer spacing, putting each molecule in the upper layer at the center of the equilateral triangle formed by three adjacent molecules in the lower layer. This results in an efficient packing which minimizes the free volume in the bilayer. Fig. 1 shows that the reflectivity changes considerably upon the formation of the monolayer phase. Temperature scan at a fixed $q_z = 0.2$Å^{-1} (judiciously chosen from Fig. 1) are shown in Fig. 3(a) for C18 and C18O. The formation of the surface layer at T_s and the bulk freezing at T_f are clearly seen. No further transitions are observed. In statistical mechanics terms, the formation of the solid monolayer is a wetting effect and the solid layer is said to wet the liquid surface[19]. The lack of growth of more layers as the bulk critical point is approached renders the wetting in this case strongly incomplete. Similar incomplete wetting was observed for the smectic surface layer on the bulk liquid for the 12CB liquid crystals[6]. However, the number of layers there increases to 5 as the critical temperature is approached, so that the wetting is less incomplete.

The surface tension scans for C18 and C18O are shown in Fig. 3(b). First note the sharp break in the slope, indicating the formation of the monolayer. The lack of any further breaks indicates, again, that no additional layers are formed. Since the surface tension γ is the *excess* free energy of the surface over that of the bulk, and since the free energy is given by $F = U - TS$, we obtain that $d\gamma/dT = -(S_s - S_b)$, where S is the entropy, and s, b denote surface and bulk, respectively. For $T > T_s$ the surface is liquid and, as discussed above, $S_s > S_b$ so that a negative slope is observed. However, the ordering of the surface at $T < T_s$ reduces S_s considerably so that $S_s < S_b$ and the slope becomes positive. The sharp change at T_s here, as well as in Fig. 3(a), indicate that within our temperature resolution of a few mK the transition is first order. However, unlike for the bulk freezing-melting effect, no hysteresis is observed in T_s. The slope change of C18O is about twice that of C18, indicating a twofold gain in entropy, in accord with the formation of a bilayer rather than a monolayer.The x-ray and surface tension measurements were repeated for a wide range of chain lengths n and temperatures T. We now discuss the chain length dependence found in these experiments.

For both alkanes and alcohols [9, 10, 20, 21] we find that the slope $d\gamma/dT$ at $T > T_s$ is practically n- independent and for alkanes it is equal to -0.09±0.01 dyne/cm/°C, in agreements with literature values[7]. For $T < T_s$ the slope is linearly increasing with n, and the slope is about twice larger for alcohols than for alkanes. This can be accounted for by chain-conformational entropy arguments[10, 20].

The measured temperature range of existence of the surface layer, $\Delta T = T_s - T_f$, is plotted in Fig. 4(a). Note that the range for alcohols is much smaller, both in n and ΔT, than that of alkanes, indicating a much reduced tendency for surface ordering. The shape of these curves can be rationalized using the following simple thermodynamical arguments. Since $d\gamma/dT = -(S_s - S_b)$, we have[10] $\Delta T = (\gamma_{T_s} - \gamma_{T_f})/(S_b - S_s)$. The measurements show that γ_{T_s} is practically independent of n. Using the known relations[7] $(S_b - S_s) \sim n$, and[22, 21] $\gamma_{T_f} \sim n^{-2}$, we obtain:

$$\Delta T = a/n - b/n^3, \tag{1}$$

where $a < b$ are positive proportionality constants[21]. Eq. (1) clearly shows that for small n, ΔT is negative, and hence the surface layer is always disordered at temperatures above the bulk freezing temperature T_f. For very large n, the entropy reduces the ordered surface phase $\Delta T \rightarrow 0$ for $n \rightarrow \infty$. Only for intermediate n does an ordered surface phase exist with a significant temperature range ΔT. This simple surface energy model accounts for the vanishing of the ordered surface phase for low n. The transition from positive to negative ΔT can be interpreted as a transition from surface freezing to the common surface melting behaviour. Fitting Eq.(1) to the measured alkane data yields a satisfactory agreement, as shown by the solid lines in Fig. 4 (a). The faster-than-predicted falloff in the figure for large n is due to other disordering mechanisms, not accounted for in our simple model. These are most likely the internal degrees of freedom of the molecules such as the proliferation of *gauche* transformations and the associated loss of the average linearity of the molecule. For alcohols, additional interactions must be included to describe ΔT versus chain length[21].

Finally, the surface layer thickness and nearest neighbour distances are shown in Fig. 4 (b,c). The monolayer thickness D for alkanes (and bilayer half-thickness for alcohols) vary linearly with n, as expected. As the average slope of this variation is slightly smaller than the canonical 1.27Å per carbon found in bulk alkane crystals, small deviations from a fully extended, vertical chain conformation are likely to exist. A small but clear decrease of slope

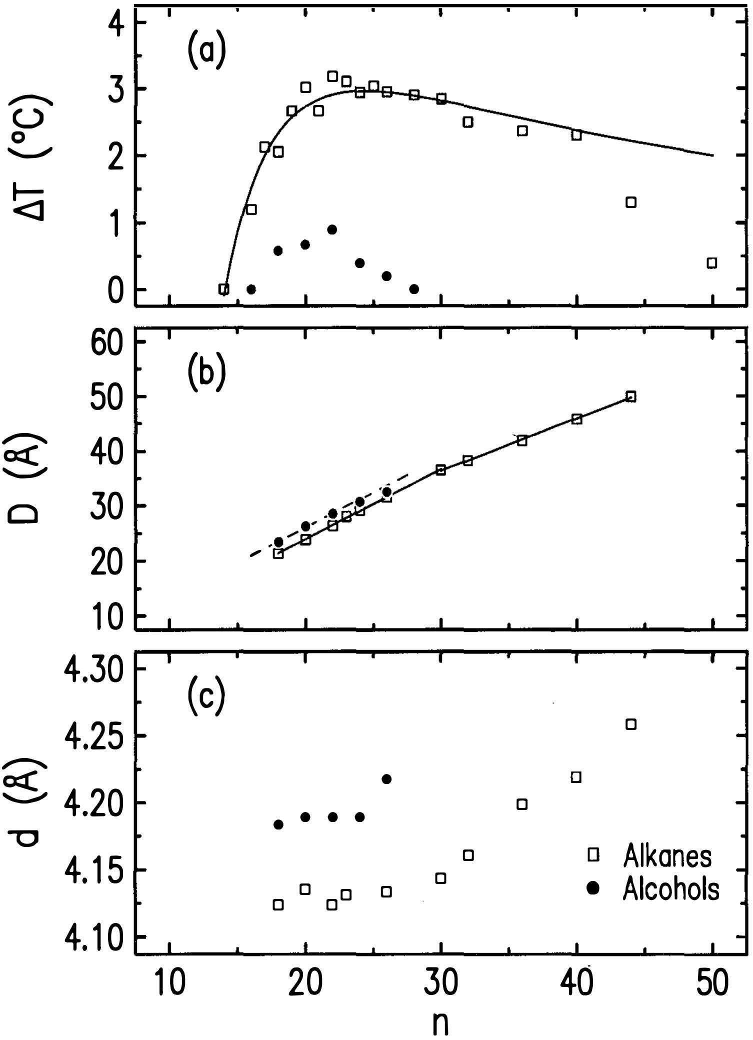

Figure 4: (a) The measured range of existence $\Delta T = T_s - T_f$ for the crystalline surface phase for alkanes and alcohols. The solid lines are fits to the theoretical expression in Eq. (1). (b) The reflectivity- measured monolayer thickness D for alkanes and half of the bilayer thickness of alcohols. (c) The GID-measured lattice spacing d of the hexagonally packed surface layer. the slope changes in (c) and (d) are discussed in the text.

is observed for $n \approx 30$ in alkanes and $n \approx 22$ in alcohols. At the same n we observe in Fig 4(c) the onset of a linear increase in the in-plane lattice spacing d, which is constant for smaller n. This marks the onset of a molecular tilt, while the onset of conformational disorder occurs for alkanes at a higher $n \approx 40$, destroying eventually the crystalline order. The BR measurements done on both substances clearly show the tilt for $n \geq 30$ in alkanes and $n > 22$ in alcohols. The existence or otherwise of an increased conformational disorder at these n can not be determined, however, by these methods. It is therefore possible that the proliferation of *gauch* defects in the chains above these n increases their average cross sections and decreases their average length as compared to the fully extended chains, thus contributing to the observed increase in d and the decrease in D, caused mainly by the tilt. This is an earlier, less developed, stage of the mechanism which is most likely responsible for the fast falloff in ΔT for large n in Fig 4(a). However, since ΔT is not a direct structural quantity it may not be as sensitive to conformational disorder as D and d. This may explain why the onset of the falloff in ΔT occurs only at $n \approx 40$ for alkanes and $n \approx 26$ for alcohols. A determination of the relative contributions of these effects will probably require additional GID and BR study using significantly higher resolutions than used for the present ones. An undulator source and a crystal analyzer will be required for these studies.

4 Conclusion

The novel surface phase, freezing and partial wetting effects presented here are not restricted to n-alkanes and alcohols. First measurements indicate that they exist in thiols and halogenated alkanes as well. Indeed they may be characteristic of a large class of molecules. Measurements on alkane mixtures also show a rich and unexpected surface phase behaviour[23]. At present no microscopic theory is available to account for the observed phenomena. It is hoped that further studies of related but progressively more complex chain molecules may reveal not only the origins of the surface behaviour detailed above, but also those of the surface behaviour of molecules incorporating such chains, like liquid crystals, and shed new light on the surface freezing *vs.* surface melting behaviour in condensed matter in general.

Acknowledgements: M.D.'s work is supported by the U.S-Israel Binational Foundation, Jerusalem. Brookhaven National Laboratory is supported by the Division of Materials Research, U.S. Department of Energy under contract No. DE-AC02-76CH00016.

References

[1] S. Chandavarkar, R. M. Geertman and W. H. de Jeu, *Phys. Rev. Lett.* 69 (1992) 2384.

[2] M. Elbaum and M. Schick, *Phys. Rev. Lett.*, 66 (1991) 1713 .

[3] A. W. Denier van der Gon, J. M. Gay, J. W. M. Frenken, and J.F. van der Veen, *Surf. Sci.* 241 (1991) 335 .

[4] J. W. M. Frenken and J. F. van der Veen, *Phys. Rev. Lett.* 54 (1985) 134 ; H. Dosch, T. Höfer, J. Peisl and R. L. Johnson, *Europhys. Lett.* 15 (1991) 527.

[5] E. B. Sirota, P. S. Pershan, S. Amador and L. B. Sorensen, *Phys. Rev. A* 35 (1987) 2283 ; B. D. Swanson, H. Strager, D. J. Tweets and L. B. Sorensen, *Phys. Rev. Lett.* 62 (1989) 909 ; P. S. Pershan, *Structure of Liquid Crystal Phases* (world Scientific, Singapore,1988)

[6] B.M. Ocko, *Phys. Rev. Lett.* 64 (1990) 2160 ; B.M. Ocko, A. Braslau, P.S. Pershan, J. Als-Nielsen, and M. Deutsch, *Phys. Rev. Lett.* 57 (1986) 94 .

[7] An excellent summary of the properties of n-alkanes can be found in D. M. Small, *The Physical Chemistry of Lipids*, (Plenum, NY, 1986)

[8] E. B. Sirota, H. H. King, Jr., D. M. Singer and H. Shao, *J. Chem. Phys.* 98 (1993) 5809 .

[9] X. Z. Wu, E. B. Sirota, S. K. Sinha, B. M. Ocko, and M. Deutsch, *Phys. Rev. Lett.* 70 (1993) 958 .

[10] X. Z. Wu, B. M. Ocko, E. B. Sirota, S. K. Sinha, M. Deutsch, B. H. Cao, and M. W. Kim, *Science* 261 (1993) 1018 .

[11] J. C. Earnshaw and C. J. Hughes, *Phys. Rev. A* 46 (1992) R4494 .

[12] G. A. Sefler, Q. Du, P. B. Miranda, and Y. R. Shen *Chem. Phys. Lett.* 235 (1995) 347.

[13] T. K. Xia, J. Ouyang, M. W. Ribarsky and U. Landman, *Phys. Rev. Lett.* 69 (1992) 1967 ; L. Askadskaya and J. P. Rabe, *Phys. Rev. Lett.* 69 (1992) 1395 .

[14] P. S. Pershan, Faraday Disc. Chem. Soc. 89 (1990) 231 ; A. Braslau, P.S. Pershan, G. Swislow, B.M. Ocko, and J. Als-Nielsen, *Phys. Rev. A* 38 (1988) 2457 ; J. Als-Nielsen and K. Kjaer in *Phase Transitions in Soft Condensed Matter* ed. T. Riste and D. Sherrington (Plenum,N.Y., 1989)

[15] G. L. Gaines, *Insoluble Monolayers at the Liquid Gas Interface* (Wiley, NY, 1966).

[16] B. M. Ocko, X. Z. Wu, E. B. Sirota, S. K. Sinha and M. Deutsch, *Phys. Rev. Lett.* 72 (1994) 242.

[17] A. Braslau, M. Deutsch, P.S. Pershan, A. Weiss, J. Als- Nielsen and J. Bohr, *Phys. Rev. Lett.* , 54 (1985) 114 ; S. K. Sinha, E. B. Sirota, S. Garoff and H. B. Stanley, *Phys. Rev. B*, 38 (1988) 2297 ; A. Braslau, P. S. Pershan and G. Swislow, *Phys. Rev. A*, 38 (1989) 2457.

[18] M. Born and E. Wolf, *Principles of Optics*, (Pergamon,Oxford,1975)

[19] P. G. deGennes, *Rev. Mod. Phys.*, 57 (1985) 827 .

[20] M. Deutsch, X. Z. Wu, E. B. Sirota, S. K. Sinha, B. M. Ocko and O. M. Magnussen, *Europhys. Lett.*, in press.

[21] X.Z. Wu, E. B. Sirota, S. K. Sinha, B. M. Ocko, and M. Deutsch (to be published).

[22] X. Z. Wu, B. M. Ocko, E. B. Sirota, S. K. Sinha and M. Deutsch, *Physica A*, 200 (1993) 751 .

[23] X. Z. Wu, B. M. Ocko, H. Tang, E. B. Sirota, S. K. Sinha, and M. Deutsch, *Phys. Rev. Lett.* , submitted.

TILTED MONOLAYER PHASES OF CHIRAL DIOLS

E. Scalas1), G. Brezesinski1), W.G. Bouwman2), K. Kjaer2) and H. Möhwald1,3)
1) Universität Mainz, Institut für Physikalische Chemie, Welder Weg 11, D-55099 Mainz
2) Physics Department, Risoe National Laboratory, DK-4000 Roskilde
3) Max-Planck Institut für Kolloid- und Grenzflächenforschung, Rudower Chaussee 5, D-12489 Berlin

ABSTRACT

The influence of chirality on the structure of condensed monolayer phases of an 3-alkoxy-propane-1,2-diol was investigated by Synchrotron x-ray diffraction at the air/water interface. At 20 °C the pure enantiomers exhibit at all lateral pressures investigated an oblique lattice. The tilt angle decreases continuously with increasing pressure. The tilt direction changes from close to NN at lower pressure to close to NNN at higher pressure. The racemate forms a centred rectangular lattice with a molecular tilt similar to that of the enantiomer. A transition occurs at 18 mN/m from a rectangular phase with NN tilt and NN distortion to a rectangular phase with NNN tilt and NNN distortion. These observations can be explained by slightly preferred heterochiral interactions at least at lower lateral pressures.

1. INTRODUCTION

The investigation of the influence of chirality on the monolayer behaviour is of considerable interest because in nature many processes are influenced by chiral molecules. Phospholipid monolayers on water are appropriate systems to study the influence of chirality on the structure1). In order to understand the interactions between tails and head group region at the atomic level it may become helpful to resort to simpler model compounds. 3-Alkoxy-propane-1,2-diols may be considered as the parent compounds of the large family of phosphatidylcholines. 1-Hexadecyl-glycerol ($C_{16}H_{33}$-O-CH_2-CHOH-CH_2OH) consists of one C16 hydrocarbon tail and a glycerol head containing an asymmetric tetravalent carbon. On the other hand diol derivatives are of interest because they exhibit both thermotropic and lyotropic liquid crystalline behaviour. The occurrence of liquid crystalline phases is strongly dependent not only on the chain length but also on the heteroatom that links the alkyl chain to the diol head group2). Monolayers of a racemic mixture and of the pure S- and R-enantiomers have been investigated by fluorescence microscopy3) on water and using transmission electron diffraction4) on Formvar substrates. On solid support the racemic diol forms an orthogonal rotator phase with an unit cell area of 0.20 nm^2. The aim of this work was to study the influence of chirality on the structure of condensed monolayer phases at the air/water interface.

2. MATERIALS AND METHODS

3-Hexadecyloxy-propane-1,2-diol was kindly synthesized by C. Tschierske (Institut of Organic Chemistry, University of Halle, Germany). In all monolayer experiments the subphase was ultrapure water purified using a Millipore desktop unit. The substance was spread from a chloroform solution. The pressure-area isotherms were recorded using a film balance with continuous Wilhelmy-type pressure measuring system. The measurements of the local structure of monolayers at 20 °C were carried out using the liquid surface diffractometer on the undulator X-ray beam line BW1 at HASYLAB, DESY, Germany. The monochromated X-ray beam strikes the surface at grazing incidence5-7). A vertical linear position-sensitive detector mounted behind a Soller collimator was moved horizontally to measure the diffraction of the monolayer. As the monolayers are 2-D powders, consisting of 2-D crystallites randomly oriented in the plane, Bragg rod scattering can be found merely by mapping the (Q_{xy}, Q_z)-space. The lattice spacings d_{hk} are related to the horizontal component of the scattering vector at maximum intensity Q^m_{xy} according to $d_{hk} = 2\pi/Q^m_{xy}$. The Bragg rods in addition yield the tilt angle t and the tilt azimuth8).

3. RESULTS

The diol forms stable monolayers on water. The pressure-area isotherms at 20°C show a clearly pronounced break in the slope corresponding to the main transition from a liquid-expanded state to an ordered phase (Fig. 1). The transition pressure of the pure enantiomers is at this temperature about 1 mN/m higher than that of the racemate. The temperature dependence of the isotherms shows that there are pronounced differences between the racemate and the pure enantiomers. For the racemate we estimated a critical temperature (above which a condensed phase can not be formed on compression) of 48 °C, whereas for the enantiomers it amounts to 39 °C.

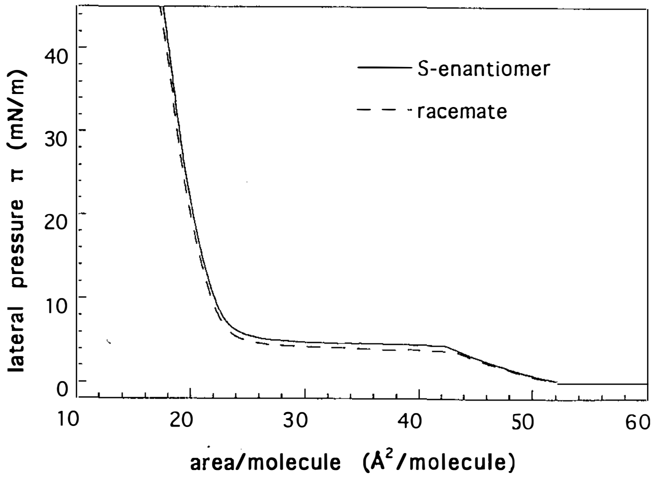

Fig. 1. Pressure-area isotherms of the racemate and the S-enantiomer at 20 °C

Fig. 2 shows some contour plots of the corrected x-ray intensities as a function of the in-plane scattering vector component Q_{xy} and the out-of-plane scattering vector component Q_Z of both the racemate and the pure enantiomer at different surface pressures Π (indicated). The pure enantiomers exhibit at all pressures investigated three diffraction peaks although two of them are barely resolved at higher lateral pressures, whereas the racemic mixture exhibits at all pressures only two diffraction peaks. Below 18 mN/m the single (non-degenerate) peak of the racemate has the maximum intensity at the horizon ($Q_Z = 0$ Å^{-1}) and for the twofold degenerate peak the maximum is at higher Q_Z. Above 18 mN/m both peaks have their maximum intensity above the horizon. Comparing the positions of the two peaks in Q_{xy} one observes that below 18 mN/m the twofold degenerate peak occurs at lower Q_{xy} and above 18 mN/m at higher Q_{xy} values.

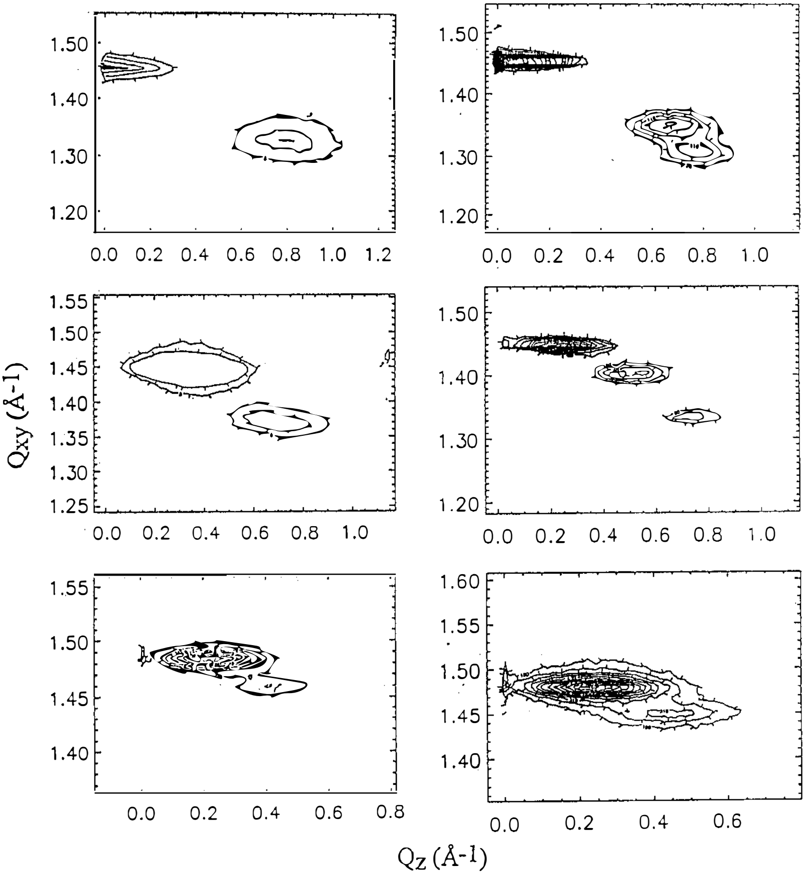

Fig. 2. Contour plots of the corrected x-ray intensities from monolayers of both the racemate (*left*) and the enantiomer (*right*) versus in-plane and out-of-plane scattering vector components Q_{xy} and Q_z at different surface pressures (racemate: 14, 30, and 45 mN/m; enantiomer: 12, 20, and 41 mN/m (*from top to bottom*)) and 20 °C.

4. DISCUSSION

The diol investigated possess a chiral centre at the C2 carbon atom of the glycerol backbone. Therefore, we could expect a chiral phase for the pure enantiomers. Indeed the three distinct peaks observed at all pressures indicate an oblique lattice. The tilt angle decreases continuously with increasing pressure (Fig. 3 left). At the lowest surface pressure investigated the molecules are tilted close to the nearest neighbour (NN) direction. With increasing pressure the tilt direction continuously changes towards a next-nearest neighbour (NNN) direction.

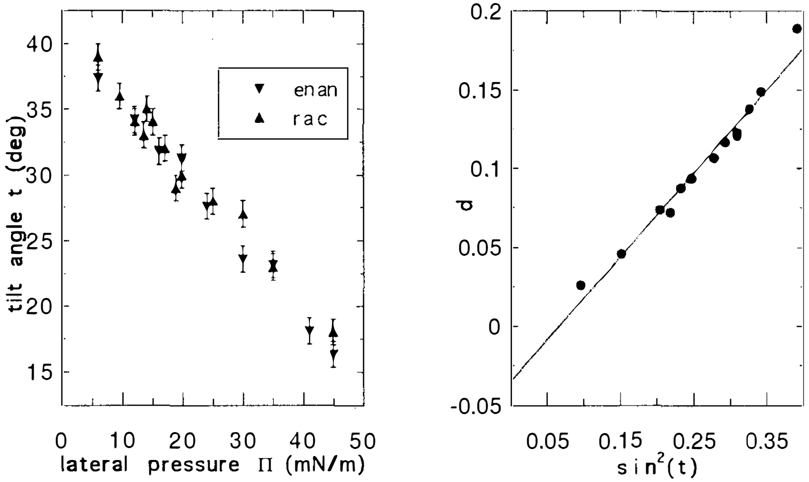

Fig.3. (Left) Tilt angle t as a function of lateral pressure Π for both the racemate (rac) and the enantiomer (enan). (Right) Corrected lattice distortion d as a function of $\sin^2(t)$

The two diffraction peaks of the racemate indicate a rectangular unit cell. The tilt angle decreases continuously with increasing pressure (Fig. 3 left). Within the experimental errors both the racemate and the enantiomer exhibit the same tilt angle at the same surface pressure. The different rectangular phases of the racemate can be described in terms of tilt and distortion azimuths. The observed x-ray intensity distribution in Q_z can be explained by a tilt of the chains towards their next neighbours (NN) at lateral pressures below 18 mN/m and by a tilt towards their next-nearest neighbours above 18 mN/m.

The lattice distortion is defined to be $\xi = (a^2 - b^2)/(a^2 + b^2)$ where a and b are the major and minor axes of the ellipse passing through all six nearest neighbours of a given molecule[9). If the in-plane component of the scattering vector of the degenerate peak is smaller than that of the non-degenerate peak the distortion is in the NN direction, whereas in the opposite case the distortion is in the NNN direction[10).

Therefore, at the transition pressure of the racemate (18 mN/m at 20 °C) both the tilt azimuth ω and the distortion azimuth β change their direction from NN ($\omega=\beta=60°$) to NNN ($\omega=\beta=90°$). This transition is similar to the L_{2d} - Overbeck (Ov) phase transition in fatty acid monolayers[10). However, in the case of L_{2d} and Ov-phases the lattice distortion is only due to the tilt of the molecules ($d=\xi\cos[2(\omega-\beta)] = A\sin^2(t) + B$, with $B = 0$) whereas in the case of the racemic diol $B < 0$ showing an additional contribution to the lattice distortion (see Fig. 3 (right)).

The phase behaviour of the racemate is different from that of the enantiomer. This can be explained assuming slightly preferred heterochiral interactions which could lead to a compound formation. Therefore, the occurence of spirals with opposite handedness observed by fluorescence microscopy3) points to a dynamic separation of the enantiomers. At higher lateral pressures the phase structures of both the racemate and the enantiomers are very similar pointing to a weakening of the chiral discrimination.

ACKNOWLEDGMENTS

This work was supported by the Bundesministerium für Forschung und Technologie (BMFT), the Deutsche Forschungsgemeinschaft (DFG), the Danish Natural Science Research Council, and the EC Human Capital and Mobility program. We thank HASYLAB at DESY, Hamburg, Germany, for beam time and for providing excellent facilities and support. One of the authors (E.S.) was put in condition to perform this work by a grant of Genoa University. Useful discussion with V.M. Kaganer is gratefully acknowledged.

REFERENCES

1) C. Böhm, H. Möhwald, L. Leiserowitz, J. Als-Nielsen, K. Kjaer, Biophys. J. **64** (1993) 553

2) C Tschierske, G. Brezesinski, S. Wolgast, F. Kuschel, H. Zaschke, Mol. Cryst. Liq. Cryst. Letters 7 (1990) 131

3) R. Rietz, G. Brezesinski, H. Möhwald, Ber. Bunsenges. Phys. Chem. **97** (1993) 1394

4) T. Moenke-Wedler, G. Förster, G. Brezesinski, R. Steitz, I.R. Peterson, Langmuir **9** (1993) 2133

5) J. Als-Nielsen, K. Kjaer in: T. Riste, D. Sherrington (Eds.), *Phase Transitions in Soft Condensed Matter*, NATO Series B, **211** (1989) Plenum Press, New York and London, pp. 113

6) J. Als-Nielsen, H. Möhwald in: S. Ebashi, M. Koch, E. Rubenstein (Eds.), *Handbook on Synchrotron Radiation*, Elsevier/North-Holland, Amsterdam, pp. 1

7) J. Als-Nielsen, D. Jacquemain, K. Kjaer, M. Lahav, F. Leveiller, L. Leiserowitz, Phys. Rep. **246** (1994) 251

8) K.Kjaer, Physica B **198** (1994) 100

9) E.B. Sirota, H.E. King, D.M. Singer, H. Shao, J. Chem. Phys. **98** (1993) 5809

10) V.M. Kaganer, I.R. Peterson, R.M. Kenn, M.C. Shih, M. Durbin, P. Dutta, J. Chem. Phys. *submitted*

STRUCTURES OF BRANCHED CHAIN KEPHALINE MONOLAYERS AT THE AIR/WATER INTERFACE

F. Bringezu[1], G. Brezesinski[2], H. Möhwald[2,3], P. Nuhn[1]

[1] *Universität Halle, Institut f. Pharm. Chemie, Weinbergweg 15,,D - 06120 Halle, Germany*
[2] *Universität Mainz, Institut f. Physikal. Chemie, Welder Weg 11, D-55099 Mainz, Germany*
[3] *Max-Planck-Institut f. Kolloid- und Grenzflächenforschung, Rudower Chaussee 5, D-12489 Brlin, Germany*

Abstract

Phosphatidylethanolamines (PEs) with α-branched fatty acids linked to position C1 of the glycerol backbone have been synthesized. Monolayers at the air/water interface have been investigated using Synchrotron Grazing Incidence Diffraction (GID). Kephalines with short side-branches exhibit strongly tilted monolayer phases. Triple chain PEs form at lower surface pressures rectangular monolayer phases, and at higher lateral pressure hexagonal phases occur. At zero pressure self-aggregation in a hexagonal packing of untilted hydrocarbon chains has been observed if all three chains have the same length. For a quadruple chain kephaline at zero pressure a rectangular phase with tilted chains and at higher pressure a hexagonal phase with vertical arranged hydrocarbon chains could be observed.

1. Introduction

Phospholipid monolayers at the air/water interface have been widely investigated by means of several techniques due to their importance as suitable model systems for biological membranes [1,2]. However, among measurements of thermodynamical parameters, surface potential and fluorescence microscopy only Synchrotron Grazing Incidence Diffraction (GID) measurements allow to determine the structure of the monolayer at an atomic level. Branched chain phospholipids provide interesting model systems because they enable investigations of principle features determining the structures of membranes and thin films [3]. Varying the positions and the length of hydrophobic side branches intermolecular interactions as well as the relative sizes of hydrophilic and hydrophobic moieties can be changed to a large extent. Indeed, for phosphatidylcholines (PCs) we could show that side branches exhibit a strong influence on both the thermodynamical and structural behavior of the monolayers.

In this work we present the first results on the structure of monolayer phases of branched chain phosphatidylethanolamines (PEs).

2. Materials and Methods

2.1. Synthesis

The preparation of 1-acyl-2-O-hexadecyl-glycero-3-phosphoethanolamines was started with acylation of rac. 1-benzyl-2-O-hexadecylglycerol, which was obtained by reductive ring opening from 2-hexadecyl-1,3-benzylidenglycerol. The resulting acyl-benzyl-glyceroles were purified using column chromatography. Following steps were the catalytic removing of the benzyl group and phosphorylation of the obtained glycerol derivatives with bromoethyldichlorophosphat. The resulting bromoesters were transformed into the final products using EtOH / ammonia. The 1,2- diacyl-glycero-3-phosphoethanolamines were synthesized using nearly the same procedure as described but starting with 1-benzylglycerol.

All lipids were purified using column chromatography on silica gel. The characterization of the compounds was performed by analytical HPLC, FAB-MS and ^{1}H-NMR.

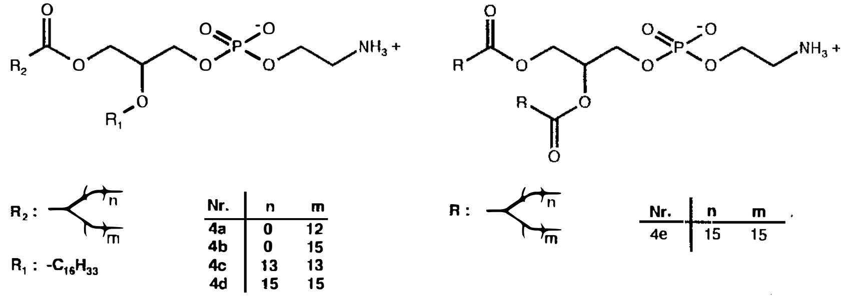

Nr.	n	m
4a	0	12
4b	0	15
4c	13	13
4d	15	15

Nr.	n	m
4e	15	15

Figure 1: Synthesized branched-chain phosphatidylethanolamines

Synchrotron Grazing Incidence X-ray Diffraction (GID) experiments were performed using the liquid-surface diffractometer at the undulator beamline BW1 at HASYLAB, DESY (Hamburg, FRG). The measurement set-up has been described previously$^{4)}$.

3. Results

3.1. Double chain PEs with short branched chain fatty acids

The hydrophobic region of the molecules was modified by introduction of a methyl side group in the acyl chain at C1 position of the glycerol backbone. Furthermore the length of the main acyl chain was varied. In the case of compound **4a** the branched acyl chain is shorter and in **4b** the branched acyl chain is longer than the unbranched hexadecyl residue at C2 position of the glycerol. At 20 °C **4a** displays three distinct Bragg peaks indicating molecular tilt in a non-symmetry direction and hence the absence of mirror symmetry. The unit cell dimensions can be determined by indexing the peak at highest Qz as (1,0), at lower Qz as (0,1) and at lowest Qz as $(1,\bar{1})$. The lattice parameters a,b and γ as well as the tilt angle t and the area per chain Axy are presented in table I.

Increasing the length of the acyl chain leads to compound **4b**. The GID measurements were performed at 20°C and at different surface pressures Π. In contrast to **4a** the diffraction spot profiles parallel and perpendicular to the surface yield at all lateral pressures investigated two peaks. The condensed monolayer phase of **4b** consists of a centred rectangular unit cell with strongly tilted molecules. The cell dimensions for the lattice of the chains can be deduced by indexing the peak at high Qz as the coinciding (1,1) and (1,$\bar{1}$) reflections and the peak at low Qz as (0,2) reflection. The data are presented in table I.

substance	Π (mN/m)	a (Å)	b (Å)	γ (°)	t (°)	A_{xy} (Å^2)
4a	26	5,31	5,01	117,2	27,7	23,7
4a	41	5,27	4,99	118,0	24,4	23,2
4b	12	5,55	5,04	117,0	35,3	24,9
4b	26	5,41	4,99	117,5	31,4	23,9
4b	41	5,31	4,99	118,0	25,6	23,4
4c	4	4,90	4,90	120,0	0	20,8
4c	40	4,86	4,86	120,0	0	20,4
4d	0	4,91	4,91	119,5	9,5	21,0
4d	4	4,90	4,90	119,5	8,9	20,9
4d	15	4,91	4,91	120,0	0	20,9
4d	37	4,82	4,82	120,0	0	20,1
4e	0	4,94	4,94	119,1	14,6	20,6
4e	4	4,93	4,93	119,2	10,3	20,9
4e	15	4,89	4,89	119,7	7,2	20,8
4e	20	4,87	4,87	120,0	0	20,5
4e	27	4,84	4,84	120,0	0	20,3
4e	41	4,84	4,84	120,0	0	20,3

Table I. Lattice parameters a,b, angle γ, tilt angle t and area per chain Axy for different surface pressures.

3.2. Triple chain PEs with long chain branched fatty acids

In the case of the triple-chain PE **4d** a condensed phase could be observed already at zero lateral pressure. The diffraction profile indicates two peaks. One peak has its maximum at Qz = 0 Å^{-1} and the other one at Qz = 0.2 Å^{-1}. The corresponding maxima in Qxy are 1.48 Å^{-1} and 1.47 Å^{-1}, respectively. The tilt angle can be calculated to 9.5°. The chains are tilted towards their nearest neighbours. Between 10 mN/m and 15 mN/m a phase transition is observed. At a lateral pressure of 15 mN/m only one sharp Bragg peak occurs, indicating a hexagonal packing of the hydrocarbon chains. The maximum intensity in the Qz resolved scan was found in the plane of the water surface ($Qz \approx 0$ $Å^{-1}$). Therefore, a nearly vertical chain orientation can be deduced.

The kephaline **4c** exhibits two acyl chains and an unbranched ether residue of almost the same length. In this case only one sharp diffraction peak could be observed at all pressures investigated indicating a hexagonal packing. At a surface pressure of 40 mN/m (Fig. 2) the diffraction peak perpendicular to the surface has a maximum at $Qz \approx 0$ $Å^{-1}$. Therefore vertical chain orientation can be deduced.

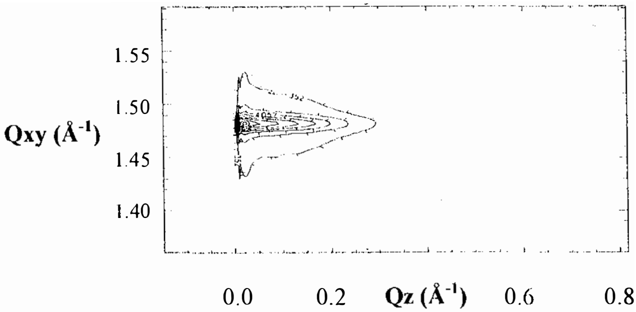

Figure 2: Corrected X-ray intensities as a function of the in-plane component Qxy and the out-of-plane component Qz of the scattering vector of **4c** at 40 mN/m, T = 15°

The investigation at zero lateral pressure and high molecular area shows that **4c** spontaneously forms a highly ordered monolayer phase. The final result of the self aggregation is a hexagonal phase with nearly vertical arranged hydrocarbon chains.

3.3. Quadruple chain PE with long chain branched fatty acids

At lower lateral pressures and even at zero pressure the quadruple-chain kephaline **4e** displays two diffraction peaks indicating a rectangular unit cell. The chains are tilted towards their nearest neighbours (NN). Above 20 mN/m a hexagonal condensed phase with vertical arranged chains occurs.

4. Conclusion

Racemic DPPE as a double chain kephaline exhibits a rectangular phase with tilted molecules towards their nearest neighbours (NN) up to 35 mN/m and above this lateral pressure a hexagonal phase with vertical arranged hydrocarbon chains occurs $^{5)}$.

The introduction of a methyl branched fatty acid at the C1 position of the glycerol (compounds **4a** and **4b**) leads to a disturbance of the lateral interactions. As a consequence an oblique (chiral) lattice with strongly tilted chains appears. The larger tilt of **4a** compared to that of **4b** could be due to the difference of the chain length between acyl and ether residue. This means that the tendency to optimise the hydrophobic interactions between chains of different length leads to a tilting of the molecule. The same behavior could be observed for triple chain PEs. If the three chains have almost the same length (**4c**) than a hexagonal phase with vertical arranged molecules is observed. In compound **4d** the branched fatty acid chain is longer than the ether residue and therefore a rectangular phase with tilted chains towards NN is formed. Only at higher surface pressures a hexagonal phase has been observed.

The kephaline **4e** with four chains of almost the same length forms at zero pressure a rectangular phase with tilted chains. This could be an indication for a bending of the C2 acyl chain (described for several double chain phospholipids) which leads to an effective difference in the chain length.

Acknowledgements

We wish to thank K. Kjær and W.G. Bouwman for helpful discussions and technical support. This work was supported by the Deutsche Forschungsgemeinschaft (DFG).

References

1) H. Möhwald (1993) in: *Phospholipids Handbook*, G. Cevc (Ed), M. Dekker, N.Y., 579 - 602
2) J. Als-Nielsen and H. Möhwald (1991) in: *Handbook on Synchrotron Radiation*, S. Ebashi, M. Koch, E. Rubenstein (Eds.), North Holland, Amsterdam, 1 - 53
3) A Dietrich, H. Möhwald, W Rettig, and G. Brezesinski (1991) Langmuir 7, 539 -546
4) J. Als-Nielsen, D. Jaquemain, K. Kjaer, M. Lahav, F. Leveiller, L. Leiserowitz (1994) Phys. Rep. **246**, 251 - 321
5) C. Böhm (1993) Ph. D. thesis, Universität Mainz

DECOUPLING OF CHAIN- AND HEAD GROUP ORDERING IN PHOSPHOLIPID MONOLAYERS

H. Baltes*, M. Schwendler*, C. A. Helm*, H. Möhwald*#
B. Struth*, E. Scalas*, G. Brezesinski*

* Johannes Gutenberg - Universität
Institut für Physikalische Chemie
Jakob-Welder-Weg 11
D-55099 Mainz / Germany

\# Max Planck Institut für
Kolloid- und Grenzflächenforschung
Rudower Chaussee 5
D-12489 Berlin / Germany

The order/disorder transition of the phospholipid 1,2-dihexadecyl-sn-glycero-3-phosphocholine and ethylene oxide spacered derivatives was studied by X-ray reflection and thermodynamic measurements. We find that increasing the length of an ethylene oxide spacer (zero to three EO groups) between the phosphate group and the glycerol backbone (i) induces a slight shift of the main transition, (ii) reduces the influence of the head groups on the chain lattice (iii) increases the head group length and promotes its hydration. For DH(EO)3PC in the ordered phase we find that the small phosphate groups (which are the main source of contrast in X-ray reflectivity) are almost homogeniously distributed within the head group region. In the fluid phase the phosphate groups are preferentially oriented towards the air/water interface.

Introduction

Phosphatidylcholine monolayers are well established model systems for monolayer studies at the air/water interface.

The order of the aliphatic tails of phosphatidylcholine monolayers was extensively studied by X-ray grazing incidence diffraction (GID). It was found that the chains exhibit a very large tilt angle which is presumably due to the bulky head group.

To obtain a better understanding of the influence of the head groups on the chain order we introduced ethylene oxide spacers of variable length between the glycerol backbone and the phosphate group. The behavior of these spacers is also of general interest since they are widely used hydrophilic moieties of non-ionic tensides.

Again, we investigated the chain order with GID. However, the head groups are less ordered than the chains and the head group contribution cannot be distinguished. Therefore, we used specular X-ray reflection (XR) to investigate the head group arrangement perpendicular to the interface. This method is especially susceptible to the position of the phosphate group within the head group region.

Materials

1,2-dihexadecyl-sn-glycero-3-phosphocholine (DHPC) was obtained chromatographically pure from Fluka, Switzerland. The racemic one to three spacer derivatives DH(EO)$_1$PC, DH(EO)$_2$PC and DH(EO)$_3$PC were kindly synthesized by B. Rattay at the Institute of Pharmaceutical Chemistry, Martin Luther University Halle, Germany. They are chromatographically pure. The chemical structure of the molecules is given in Fig. 1.

In the following communication the aliphatic chains are referred to as "tails", while the rest of the molecule is called "head".

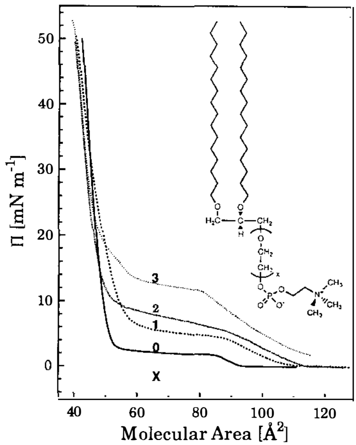

Fig. 1: Structure formula and isotherms of DH(EO)$_x$PC

X-ray Details and Analysis

GID measurements were performed using the liquid surface diffractometer on the synchrotron X-ray beam line BW1 at HASYLAB, DESY, Hamburg. The in-plane peaks of the Qxy scans were assumed to be powder pattern Bragg peaks of a two dimensional

lattice. The tilt angle of the molecular long axis with respect ot the normal, t, was calculated from the peak position of the Bragg rods /1/.
XR measurements are performed at our institute by means of a home made θ/θ set-up with slit collimation, conventional Cu-Anode (λ=1.54Å), graphite secondary monochromator and NaI detector /2/. The data are background-subtracted and normalized to the Fresnel reflectivity of a sharp air/water interface. For the analysis reasonable models of the electron density are computed and model parameters are derived by curve fitting to the experimental data. We checked some models and found almost identical electron density profiles. For the further discussion we divide the film into four slabs, one representing the aliphatic tails and the other representing the head group. The reflectivity of the resulting layer system is computed by a modification of the Parratt formalism, which is also able to handle smeared interfaces.
To reduce the number of free fit parameters we assume that the aliphatic tails are not hydrated, resulting in a fixed number of 129 electrons per chain. The molecular area A is taken from the isotherms, which are normalized at the highest pressure Π=41mN/m to the area measured by means of GID to eliminate inweight errors. Then, the electron density of the tails and their lengths are closely related $\rho_{Tail} = N^e_{Tail} / (A\ l_{Tail})$. The smearing parameters of all boxes and the water subphase are assumed to be identical. Past it, the three head boxes are set to identical lengths, giving rise to only two free lengths within this model.

Results and Interpretation

Fig. 1 compares pressure/area isotherms of the phospholipids with different EO spacer lengths. The pressure corresponding to the onset of the main transition increases with the number x of spacers, i.e. the EO group inhibits ordering. Accordingly the EO group also causes monolayer expansion in the LE phase comparing films at constant lateral pressure. This behaviour contrasts to that in the LC phase where diffraction studies have demonstrated a higher lateral density with increasing x at a fixed pressure /1/ (Fig. 2).

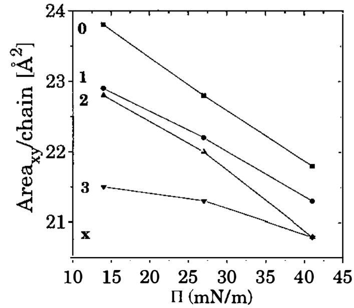

Fig. 2: Molecular Area per chain of DH(EO)$_x$PC

Fig. 3 gives X-ray reflectivity data for DH(EO)$_3$PC with increasing surface pressure from bottom to top. In the LC phase ($\pi \geq 20$mN/m) one observes a strong increase of contrast with pressure. This essentially means that the density of the electron richest part of the monolayer increases. This would be achieved if water is squeezed out of the head group region or/and if the phosphorous atoms would be confined in a plane parallel to the surface.

Fig. 4 gives two representative electron density profiles for the LE phase ($\pi \leq$ 10mN/m) and for the LC phase. For the LC phase the tail electron density is 93-98%, which is reduced on going to lower pressures as expected. For the head group density one realizes a narrow and symmetrical profile in the LC phase, whereas in the LE phase the distribution is broad and asymmetrical. The latter finding is independent of possible errors in ρ_{Tail}. One can easily verify that the asymmetry and broadness of the head group profile would be recovered even if 20% higher values of ρ_{Tail} would be subtracted from the total density profile to determine ρ_{Head}. We estimated an error in ρ_{Tail} of ± 14% for the LE phase and ± 1% for the LC phase at 41mN/m.

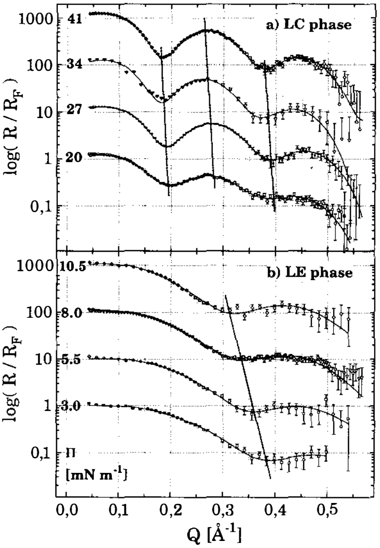

Fig. 3: X-ray reflectivity of DH(EO)$_3$PC

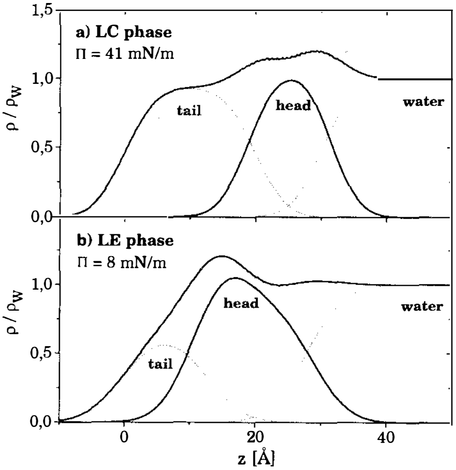

Fig. 4: Electron density profiles of DH(EO)$_3$PC

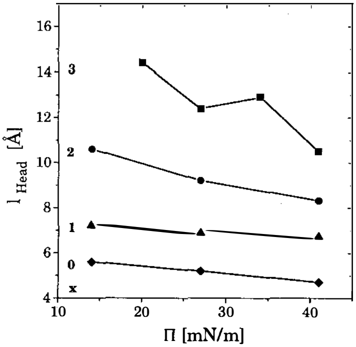

Fig. 5: Head length of DH(EO)$_x$PC

Fig. 5 compares the lengths of the head group extensions for different spacer lengths. One realizes a decrease in l_{Head} with pressure and an increase with spacer length. For the most reliable data, those at high pressure, the thickness increase is about 2Å per EO group, which is in good agreement with other systems /3/.

In order to quantify the asymmetry observed in Fig. 4b Fig 6 gives the deviation of the position of maximum electron density from the head group center. This distance is close to zero for the LC phase and deviates considerably in the LE phase. The fact that values derived independently from various measurements in these phases scatter only little shows the consistency of the analysis.

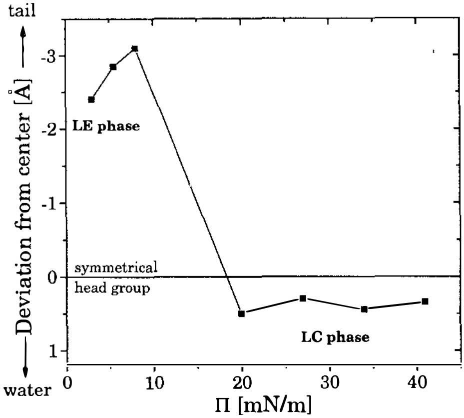

Fig. 6: Head group asymmetry

Discussion and Conclusions

We separated the electron density profile into an aliphatic region and a head group, the latter consisting of an EO spacer of almost 100% and of phosphorous acid groups of about 150% water electron density. Looking at our model we would expect an asymmetric head group density profile with a maximum towards the water for a completly stretched head group in the LC phase. This, however, is not encountered suggesting that the plane containing the phosphorous acid is further shifted towards the tail/head interface. The phosphorous groups are not (completely) homogeneously distributed, but seem to be preferentially oriented towards the head group center (a homogeneous distribution cannot explain the high intensity of the third peak in Fig. 3).

With these general remarks we will now justify the model of the arrangement in the two phases displayed in Fig. 10: In the LC phase the aliphatic tails are ordered as shown previously by diffraction measurements. Even at the highest pressure the tails are tilted with the tilt angle decreasing continuously with x (t=21° for x = 0 to t = 12° for x = 3), which means that the influence of the bulky head group is decreasing. The cross-sectional area of the chains amounts to (20.2±0.2)Å^2, a typical value for rotator phases. The phosphocholine head can pack denser with increasing x, but this group still determines the packing density. This indicates that the phosphocholine is arranged within a plane parallel to the surface, but can be shifted along the normal by some small distance.

The reflectivity analysis in this work suggests that this shift is symmetrical with respect to the maximum along z and increased monotonically from below 3Å to below 5Å, on going from x=0 to x=3. The reduction of l_{Head} on compression in the LC phase then can be understood as partial ordering of the head groups. The fact that the total head group length and also the film thickness measured from hydrocarbon/air interface to the electron density maximum (PO_4) increases by about 2Å per EO group, but the length of the stretched EO group is about 3.8Å, proofs that the EO group is not fully stretched.

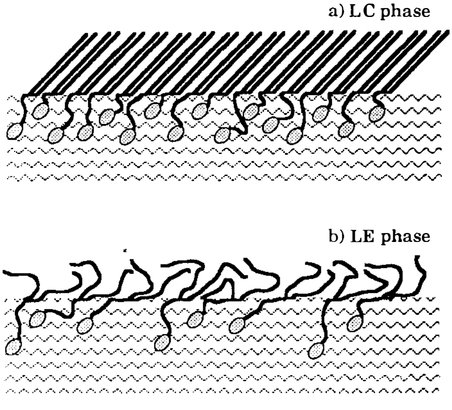

Fig. 7: Model structure of $DH(EO)_3PC$

For the LE phase we realize an asymmetric electron density profile with a shoulder about 6Å from the maximum towards water (for x=3). This suggests a bimodal phosphocholine arrangement with a predominant distribution towards the hydrocarbon/head interface. This is understood as a preferential EO arrangement parallel to the interface. In accordance with this one measures an additional contribution of the EO groups to the lateral pressure in the isotherms for the LE phase. The calculation of the 2D radius of gyration of three EO groups is in good agreement with the onset of interaction at about 100Å^2 per molecule.

Acknowledgement

This work was supported by the Deutsche Forschungsgemeinschaft (DFG), the Bundesministerium für Forschung und Technologie (BMFT), the Fonds der Chemischen Industrie, the Human Capital and Mobility Program (EG) and the Graduiertenkolleg "Physik und Chemie supramolekularer Systeme".

/1/ B. Struth, E. Scalas, G. Brezesinski, H. Möhwald, F. Bringezu, W. G. Bouwman, K. Kjaer "Influence of a hydrophilic spacer on the structure of a phospholipid monolayer", submitted to Il Nuovo Cimento

/2/ H. Baltes, M. Schwendler, C. A. Helm. H. Möhwald, "Tail and Head Group Interactions in Phospholipid Monolayers", submitted to J. Coll. Interf. Sci.

/3/ J. R. Lu, Z. X. Li, R. K. Thomas, E. J. Staples, L. Thompson, I. Tucker and J. Penfold, J. Phys. Chem. 98, 6559-6567 (1994)

LECITHINS WITH SHORT AND LONG BRANCHED FATTY ACIDS: X-RAY DIFFRACTION AND MISCIBILITY OF DIFFERENT GEL PHASES

G. Förster[a], G. Brezesinski[b], B. Dobner[c]
[a]Institute of Physical Chemistry, Martin-Luther-Universität Halle-Wittenberg,
[b]Institute of Physical Chemistry, Johannes-Gutenberg-Universität Mainz,
[c]Institute of Pharmaceutical Chemistry, Martin-Luther-Universität Halle-Wittenberg

Poster presented by G. Förster

Despite of the complex molecular structure of lecithins with (i) two fatty acid chains, (ii) ester or ether linkage to the glycerol forming the surface between the hydrophilic and hydrophobic parts of the bilayer, and (iii) the phosphatidylcholine headgroup, usually only few informations are available from powder diffraction patterns in lecithin / water dispersions.
In an overview the diffraction patterns of lecithins modified in the hydrophobic part are presented. The observed phases are classified on this basis into crystalline, subgel, and gel structures.

This work was supported by the Deutsche Forschungsgemeinschaft (SFB 197). The triple bond lecithin was a gift of H. Rührup. Thanks for contributions to Astrid Brandt, Martina Mannová, Norbert Pietschmann, Bernd Rattay, Sabine Wolgast and Ina Zimmermann and for technical assistence to Christa Helbig and Barbara Elsner.

Experimental

DPPC and DHPC were commercial products (Fluka, Sigma) and were used without further purifications (for abbreviations see Fig.1 and Fig.3). Other lipids are synthesized as described elsewhere[1)2)3)]. Aqueous dispersions (50 wt%) of the lipid in excess water were measured at definite temperatures with CuKα radiation in transmission techniques registrating the scattered intensity continously in the range $2\theta = 0.4°...40°$ ($s = 0.045...4.160\ nm^{-1}$)[1)].

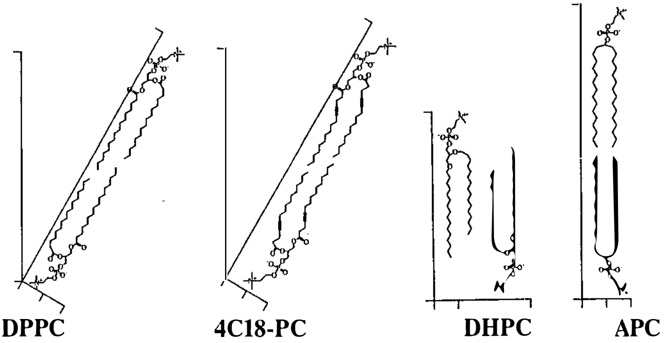

Fig.1 Chemical structure and schematic conformation of unbranched lipids
DPPC: 1,2-dipalmitoyl-*sn*-glycero-3-phosphocholine, **4C18-PC**: 1,2-dioctadec-4-ynoyl-*sn*-glycero-3-phosphocholine, **DHPC**: 1,2-dihexadecyl-*sn*-glycero-3-phosphocholine, **APC**: 1-pentadecyl-hexadecyl-phosphocholine

DPPC as Reference Substance

The diffraction pattern of solvent crystallized monohydrate **DPPC** sample represents the scattering of a 3D crystalline phase (Fig.2A). After crystallization from the melt only those spacings remain in the pattern, which correspond to the most strong reflections of the crystalline phase. This indicates that only a short range order appears in both, the lateral as well as the bilayer packing. In **DPPC** samples with excess water a subgel phase Lc' is build after annealing at 4 °C (Fig.2C). The spacings in the wide angle region of the powder pattern were indexed according to a subcell HS1[4)]. The 2D unit mash describes the molecular packing of the lecithins within bilayers seperated by water (water halo at $s \sim 3.0\ nm^{-1}$). At the transition temperature into the gel phase Lβ' this molecular order disappears, and only the scattering of the chain packing is detected. A 2D deformed hexagonal lattice of tilted chains exists in which the differences in the line width of the (11) and (20) peaks are interpreted with a NN tilt direction (Fig.2N)[5)6)]. The formation of the subgel phase Lc' from Lβ' on cooling becomes more easily by the introduction of a triple bond in both chains near the glycerol backbone. In the case of **4C18-PC** (Fig.2E) a Lc' phase is formed spontaneously, and the phase is stabilized up to temperatures near the main transition temperature[7)].

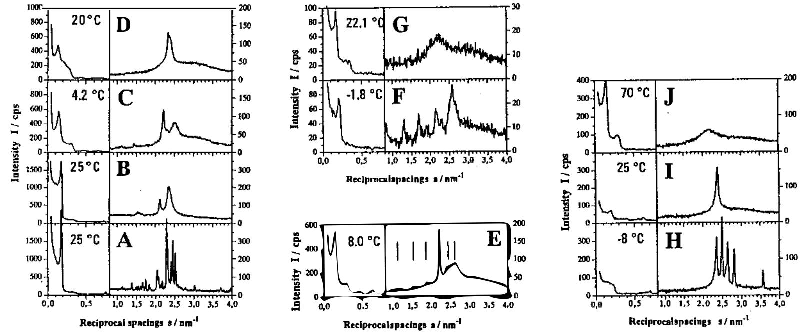

Fig.2 Diffraction pattern of unbranched lecithins
A: **DPPC** monohydrate, solvent crystallized, **B**: **DPPC** monohydrate, melt crystallized, **C**: **DPPC** hydrated, Lc', **D**: **DPPC** hydrated, $L\beta'$, **E**: **4C18-PC**, Lc', **F**: **APC**, new subgel phase, **G**: **APC**, $L\alpha$, **H**: **DHPC**, $L\rho_a$+ice, **I**: **DHPC**, $L\beta_a$, **J**: **DHPC**, $L\alpha$, **K**.. **W** see below

Alkyl-Phosphatidylcholine and Alkyl-Phosphocholine

A branched fatty acid is favorably introduced in **DPPC** together with an ether linkage at the other carbon atom of the glycerol to prevent a migration of the fatty acids. Surprisingly, the gel phase structures of mixed8) and double ether linkaged lecithins9)10) are different from that of **DPPC**. In all cases antiparallel arranged lipid molecules are forming the bilayer with a hexagonal packing of untilted chains ($L\beta_a$). On cooling **DHPC** (Fig.2H) a splitting of the short spacing is observed, but no additional peaks appear at $s < 2.0\ \mathrm{nm}^{-1}$. The character of the phase $L\rho_a$ looks more like a gel phase with a dense. packing of the chains than a subgel phase. No molecular order is reached even as a ratio of four chains per head group exists in an antiparallel packed bilayer.

In the alkyl phosphocholine **APC** two long branched fatty acids directly are bound at the same carbon atom with the phosphatidylcholine headgroup. This direct coupling gives rise to a crystallization from a liquid crystalline phase directly into a new type of subgel phase (Fig.2F).

C1 Branched Lecithins

Corresponding to the well established asymmetric conformation of lecithins11) the introduction of a Me branching in similar positions of the fatty acids gives rise to different packing conditions within the hydrophobic part. Lecithins with short branchings in C1 position of the glycerol show gel phases $L\beta_i$ with interdigitated chains within bilayers. In binary phase diagrams the differences in the phase structures $L\beta'$ **(DPPC)** / $L\beta_i$ **{(3MeP)HPC}** and $L\beta_i$ **{(2PropP) HPC}** / $L\beta_a$ **(DHPC)** is confirmed by thermodynamical studies: a miscibility gap exists between the corresponding gel phases (Fig.4).

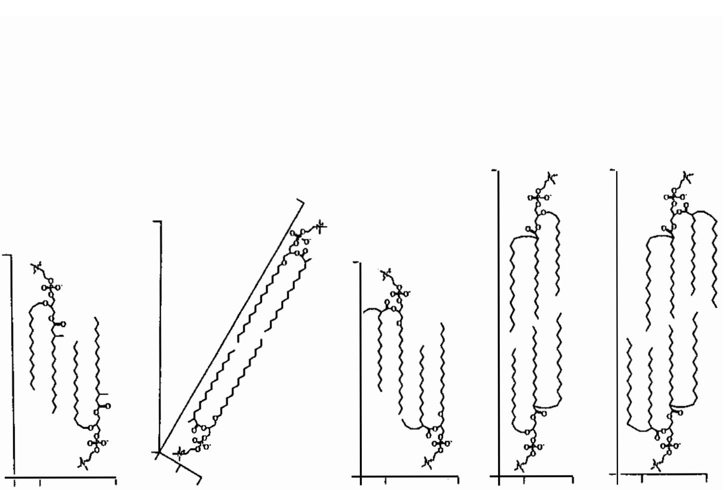

Fig.3 Chemical structure and schematic conformation of branched lipids
(3MeP)HPC: 1-(3-methyl-palmitoyl)-2-hexadecyl-*sn*-glycero-3-phosphocholine, **H(2MeP)PC**: 1-hexadecyl-2-(2-methyl-palmitoyl)-*sn*-glycero-3-phosphocholine, **H(2ButP)PC**: 1-hexadecyl-2-(2-butyl-palmitoyl)-*sn*-glycero-3-phosphocholine, **(2TetradecP)HPC**: 1-(2-tetradecyl-palmitoyl)-2-hexadecyl-*sn*-glycero-3-phosphocholine, **D(2TetradecP)PC**: 1,2-di-(2-tetradecyl-palmitoyl)-*sn*-glycero-3-phosphocholine

On cooling **(3MeP)HPC** the appearence of ice peaks and a splitting of the short spacings according to the subcell O⊥ is observed in the pattern (Fig.2L). It characterizes the phase $L\rho_i$ as a gel phase without order of the whole molecules, although a ratio of three chains per one headgroup exist.

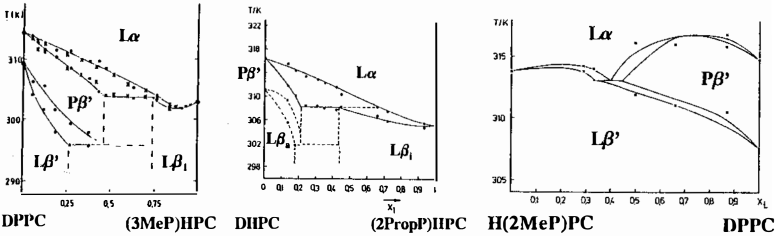

Fig.4 Quasi binary phase diagrams (50 wt% water) demonstrating miscibility gaps (i) between the gel phases Lβ' and $L\beta_i$ (left) as well as (ii) between $L\beta_a$ and $L\beta_i$ (middle), but (iii) miscibility in Lβ' phases (right)

C2 Branched Lecithins

Short branchings in the C2 position of the glycerol {**H(2MeP)PC**} reconstructs the Lβ' phase in comparison to $L\beta_a$ of the unbranched **HPPC**[3]. The observed profile of the diffraction pattern and a complete miscibility of the gel phases in the binary phase diagram (Fig.4) show, that the same structure exists in **H(2MeP)PC** and **DPPC** gel phases. This findings imply that short chains in C2 position cross over the interface to the hydrophilic headgroup region. Otherwise, characteristic differences exist in the polymorphism between **H(2MeP)PC** (Lρ' →Lβ'→Lα) and **DPPC** (Lc'→Lβ'→Pβ'→Lα)[12)]. The temperature dependence of the lamellar repeat distance (Fig.5) shows for the branched lecithin a "soft" transition behavior and unusual high values in the Lα phase. Surprisingly no molecular order could been reached in the low temperature phase Lρ'. A comparison of the line profiles in the X-ray diffraction pattern (Fig.2O) implies from the broadening of both short spacings that in contrary to **DPPC** a NNN tilt direction[5)] may exist in Lρ' of **H(2MeP)PC**.

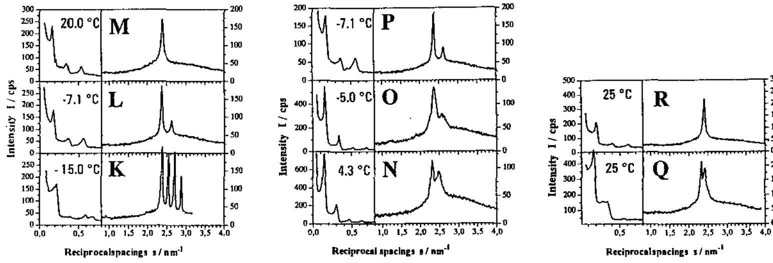

Fig.2 Diffraction pattern of short branched lecithins
A...J: see above, **K**: **(3MeP)HPC**, $L\rho_i$+ice, **L**: **(3MeP)HPC**, $L\rho_i$, **M**: **(3MeP)HPC**, $L\beta_i$, **N**: **DPPC**, Lβ': tilt to NN, **O**: **H(2MeP)PC**, Lρ': tilt to NNN, **P**: **(3MeP)HPC**: $L\rho_i$: no tilt, **Q**: **H(2PropP)PC**, Lβ', **R**: **H(2ButP)PC**, $L\beta_1$, **S...W**: see below

In the homologeous series up to **H(2PropP)PC** the phase Lβ' is stable and from the decrease of the bilayer repeat distance an increasing tilt angle is deduced (Fig.2Q)[3)]. In the **H(2ButP)PC** a new gel phase was detected (Fig.2R), and a model for room temperature with interdigitated chains $L\beta_i$ is proposed.

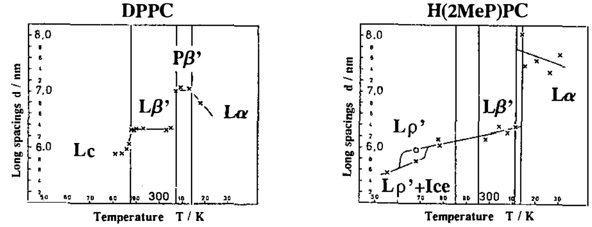

Fig.5 Temperature dependence of the long spacings of an unbranched and branched lecithin with the same gel phase (i) stepwise melting, (ii) soft melting mode

Triple and Quadruple Chain Lecithins

A long branched fatty acid in one position of the glycerol results in a triple chain lecithin. A gel phase Lβ is observed in **(2TetradecP)HPC** with untilted chains, oppositely arranged in bilayers (Fig.2S). On cooling a gel phase Lρ appears with an $O_\perp$ subcell without indications of a molecular order.

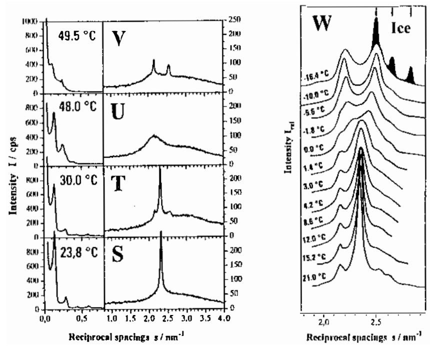

Fig.2
Diffraction pattern of long branched lecithins **A...R**: see above, **S**: **(2TetradecP)HPC**, Lβ without headgroup lattice, **T**: **(2TetradecP)HPC**, Lβ with headgroup lattice, **U**: **(2TetradecP)HPC**, Lα without headgroup lattice, **V**: **(2TetradecP)HPC**, Lα with headgroup lattice, **W**: **D(2TetradecP)PC**, reversible transition from the gel to a subgel phase

During annealing quite below the main transition temperature T_m = 42 °C a recrystallization of the sample is induced. Two additional short spacings are observed in all phases measured indicating a strong interaction of adjusted headgroups. The transition temperatures as well as the bilayer repeat distance are not affected. A reconstuction of the first polymorphic behavior was only possible with a new preparation after dissolving in organic solvent.

The comparison of this behavior with the gel phase structure of the quadruple chain lecithin **D(2TetradecP)PC** with two ester linkaged long chain branched fatty acids shows the outstanding conditions for headgroup crystallization in the triple chain lecithin (three chains per head group). The quadruple chain lecithin has a Lβ gel phase like the triple chain lecithin[1]. The subgel phase also shows additional spacings and transforms reversible into the gel phase (Fig.2W).

Conclusions

This overview about different occuring bilayer types and chain packing modes gives an idea of the selection of DPPC as the main lipid component with certain value of (i) headgroup size, (ii) surface building conditions, and (iii) chain matrix multiplicity, which prevent it optimal from crystallization.

References

[1]P. Nuhn, G. Brezesinski, B. Dobner, G. Förster, M. Gutheil, H.-D. Dörfler, Chem. Phys. Lipids 39 (1986) 221-236, [2]G. Brezesinski, B. Dobner, H.-D. Dörfler, M. Fischer, S. Haas, P. Nuhn, Chem. Phys. Lipids 43 (1987) 257-264, [3]B. Rattay, G. Brezesinski, B. Dobner, G. Förster, P. Nuhn, Chem. Phys Lipids 75 (1995) 81-91, [4]S. Abrahamsson, B. Dahlén, H. Löfgren, I. Pascher, Progr. Chem. Fats Other Lipids 16 (1978) 125-143, [5]A. Tardieu, V. Luzzati, F.C. Reman, J. Mol. Biol. 75 (1973) 711-733, [6]V.M. Kaganer, A.M. Osipov, I.R. Peterson, J. Chem. Phys. 98 (1993) 3512-3527, [7]M. Mannová, G. Brezesinski, G. Förster, J. Rührup, in preparation, [8]N.S. Haas, P.K. Scripada, G.G. Shipley, Biophys. J. 57 (1983) 241-244, [9]J.T. Kim, J. Mattai, G.G. Shipley, Biochemistry 26 (1987) 6592-6598, [10]P. Laggner, K. Lohner, G. Dergovics, K. Müller, A. Schuster, Chem. Phys. Lipids 44 (1987) 31-60, [11]H. Hauser, I. Pascher, R.H. Pearson, S. Sundell, Biochim. Biophys. Acta 650 (1981) 21-51, [12]H.H. Füldner, Biochemistry 20 (1981) 5707-5710

MOLECULAR REARRANGEMENTS IN LIPID MONOLAYERS: A STUDY ON PHASE TRANSITIONS

J. Sánchez-González, M.A. Cabrerizo-Vílchez, and M.J. Gálvez-Ruiz*
Departamento de Física Aplicada, Universidad de Granada
18071 Granada, ESPAÑA

ABSTRACT

The behavior of three different long chain lipids, at the air-water interface, has been studied as a function of temperature.

In order to analyze the influence of the molecular structure on this behavior, the lipids distearoylphosphatidylcholine (DSPC), distearoylphosphatidylethanolamine (DSPE) and Sphingomyelin (Sph) have been chosen, since DSPC and Sph molecules have the same polar group and DSPC and DSPE molecules show identical hydrocarbon part.

Experimental isotherms surface pressure (π)-molecular area (A), obtained by compressing simple and mixed monomolecular layers of these lipids have been performed.

The monolayer properties of these compounds are influenced by the temperature bringing about important changes in both interaction characteristics and the stability of the monolayers. These changes are mainly attributed to a decrease in the van der Waals type attractive forces between the hydrophobic regions, in case of the DSPE lipid, also to an increase of the dehydration effect.

Moreover, the occurrence of the liquid extended (LE)-liquid condensed (LC) phase transition during the compression of these systems depends strongly on temperature. Only the films formed by DSPC, Sph or a mixture on both of them undergo this phase transition.

The transition surface pressure values corresponding to the beginning and the end of the phase have been calculated by analyzing the successive derivatives of the experimental isotherms.

A performance of the phase transition has been carried out by a thermodynamic study of the experimental results.

---

* To whom correspondence should be sent

INTRODUCTION

The study of mixed monolayers under different experimental conditions, is of great interest because it enables us to gain a much better understanding of the interactions between the monolayer compounds. In addition, superficial processes are strongly dependent on those interactions. In the present work we have focused our attention on the thermodynamic study of the liquid expanded (LE)-liquid condensed (LC) phase transition for monolayers formed by the lipids distearoyl phosphatidylcholine (DSPC) and Sphyngomyelin (Sph).

The surface pressure values corresponding to the beginning and the end of the transition have been calculated as it is explained next.

Following a suitable thermodynamic formulation(1,2), the apparent molar entropy, enthalpy and internal energy changes during the LE-LC phase transition have been evaluated.

MATERIALS AND METHODS

In all the experiments the subphase used was water (Milli-Q), the final conductivity and pH were $\leq 10^{-4}\ \Omega^{-1}\ cm^{-1}$ and 5.5-6.0, respectively.

The three lipids forming the monolayers, Distearoyl-L-α-Phosphatidylcholine (DSPC), Distearoyl-L-α-Phosphatidylethanolamine (DSPE) and Sphyngomyelin (Sph) were supplied by SIGMA. The solvents used for spreading the films were a 4:1 (v/v) mixture of n-hexane and ethanol for the DSPC and Sph lipids and a 5:1 (v/v) mixture of chloroform and methanol for the DSPE lipid.

The experimental device employed to perform the surface pressure-molecular area (π-A) isotherms has been previously described(3-5), as well as experimental condition.

In order to carry out a thermodynamic study of the LE-LC phase transition, the surface-pressure values corresponding to the beginning and the end of this transition have been calculated as in previous studies(4,6), based on other works(7,8).The followed method is shown in fig. 1. In that, a computer simulated isotherm and its successive derivatives are represented. We can observe that the searched for points (the start and the end of the transition) corresponding with an inflection point in the first derivative and therefore, with a minimum and a maximum in the second derivative, respectively, consequently with a third vanishing derivative.

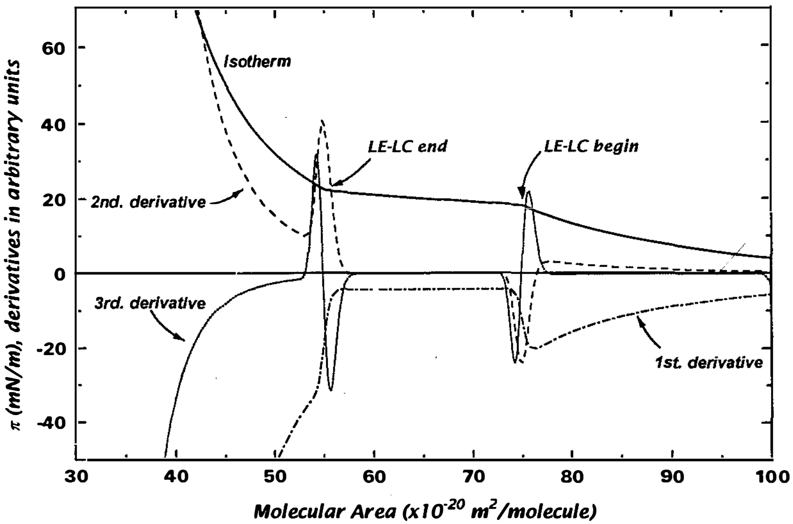

Figure 1. Model of isotherm and its sucessive derivatives.

RESULTS AND DISCUSSION

We have studied the π-A experimental isotherms corresponding to the compression of simple and mixed monolayers formed by the lipids DSPC, DSPE or Sph, or by a mixture of two of them, under different temperatures (298.2, 303.2, 308.2 and 313.2 K).

As main result we reveal that out of all the studied monolayers, only films composed by Sph and/or DSPC undergo the LE-LC phase transition under some conditions of temperature. These cases are represented in Figs. 2-4. The rest of the experimental isotherms do not show this phase transition. In some cases the monolayers are at the LE state and others, i.e. the DSPE films, are at the LC state.

In Fig. 2 the π-A isotherms, corresponding to the compression of Sph films that undergo the LE-LC phase transition, are represented. As expected the transition surface pressure increases with temperature. At higher temperatures, the simple monolayers remain in LE state.

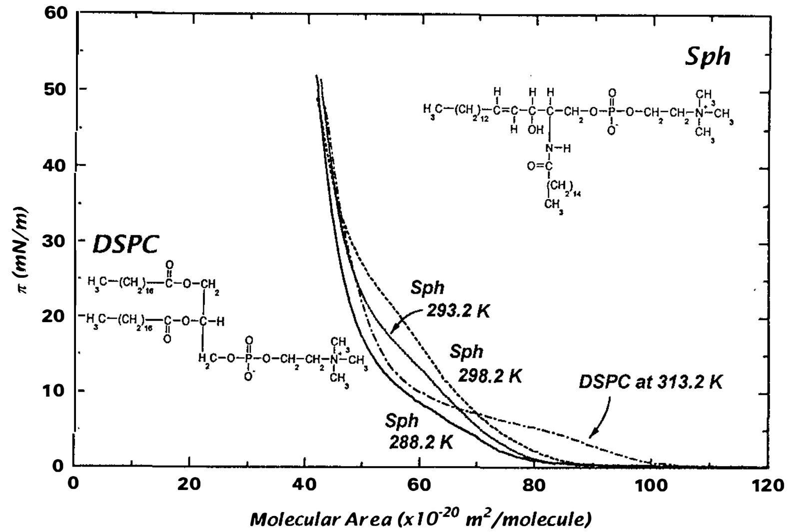

Figure 2. Compression isothems for monolayers of Sph and DSPC.

The only film formed by DSPC that suffers the LE-LC phase transition is the film compressed at 313.2 K and shown in Fig. 2. At different temperatures, the DSPC monolayers are in the LC state, except for the higher temperature (313.2 K), which provokes an increase of the hydrocarbon chains mobility, showing this transition.

The mixed monolayers of DSPC and Sph arise a somewhat intermediate behavior compared with that shown by pure components. The characteristic of the isotherms is a progressive condensation as the condensed structure of DSPC is approached. Therefore, when the proportion of DSPC is high in the mixed monolayers, the behavior is similar to that shown by the pure DSPC monolayers. As we can observe in fig. 3, only few mixed monolayers suffer the LE-LC phase transition.

Comparing the behavior with that show in the three dimensions for different systems, are more plausibly explained by conformational changes or molecular reorientation than by phase changes, properly speaking.

In the table 1, the surface pressure and molecular area corresponding to the beginning and the end of the LE-LC phase transition that undergo our films are represented, included the experimental conditions of temperature. Comparing these values, we observe that for monolayers containing DSPC, the LE-LC phase transition appears at lower surface pressure values. In these cases, there is a less important molecular reorientation compared with the monolayers formed by Sph.

As expected, apparent molar entropy, enthalpy and internal energy changes during the transition, have negative values. This means that during the LE-LC phase transitions, the molecules in monolayer become more ordered and the transition is exothermic. The lipids with high molecular asymmetry suffer a higher molecular reorganization when they are compressed as monolayers, for this reason, the transition is observed, mainly in monolayers containing Sph.

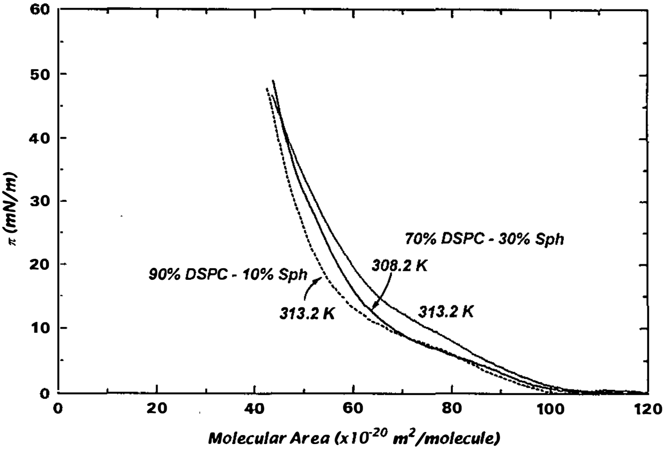

Figure 3. Compression isotherms for mixed monolayers

Table 1. Phase transition points and thermodynamics. a^e, a^c are molecular areas of expanded and condensed states in 10^{-20} m^2/molecule, π in mN/m, Δs, Δh and Δu in kJ and W (compression work) in J/mol. Systems: A=Sph, B=70% DSPC-30% Sph, C=90% DSPC-10% Sph and D=DSPC.

SYSTEM	T(K)	a^e	π^e	a^c	π^c	Δs	Δh	Δu	W
A	288.2	64.1	6.7	47.0	24.1	-160	-45.1	-52.0	1280
A	293.2	60.9	12.5	47.2	28.9	-130	-36.8	-41.8	1530
A	298.2	56.2	20.3	45.7	34.6	-96	-28.7	-32.0	1660
B	308.2	86.8	4.2	59.5	16.6	-180	-54.8	-65.7	1410
B	313.2	78.3	8.8	62.7	16.9	-100	-31.8	-37.5	1170
C	313.2	80.3	5.9	49.1	27.7	-	-	-	2350
D	313.2	82.5	4.9	49.3	23.2	-	-	-	1910

The general trend is that an increase in temperature provokes an decrease in the thermodynamic quantity changes. For these systems, the temperature effect on the difference between expanded and condensed areas is less important than that on the transition surface pressure values. It supports the idea that, during the transition, the lipids suffer a change in inclination with respect to the surface, and not important molecular orientation, for this reason when the temperature increases, the entropy changes are lower, due that mobility of hydrocarbon chains in our molecular systems also increases.

One possible way of assaying this hypothesis is to calculate the work involved from the area below the quasi-isobaric zone in the diagrams π-A (LE-LC transition zone), according to the method described by Abraham et al.[9)]. These results are presented ,also, in the table 1.

More remarkable is that the calculated compression works during the transition have similar values for all the monolayers. This fact confirm us that the molecular reorientation in the air-liquid interface is similar for both type of lipid, even when the films are mixed. Only as the temperature is high and the monolayers is formed by DSPC or with very high proportion of this lipid, the work values increase respect to the others, again due to higher mobility of the hydrocarbon chains in this molecules comparing with the structure more rigid of the Sph molecules.

Acknowledgment: *This work has been financially supported by the Comisión Interministerial de Ciencia y Tecnología (CICYT), project no. 94-0560.*

REFERENCES

1. K. Motomura, K. Sekita, and R. Matuura, *J. Colloid Interf. Sci.* **49**: 319 (1974).
2. K. Motomura, T. Yano, M. Ikematsu, M. Matuo, and R. Matuura, *J. Colloid Interf. Sci.* **69**: 209 (1979).
3. M.J. Gálvez-Ruiz and M.A. Cabrerizo-Vílchez, *Colloid Polym. Sci.* **269**: 77-84 (1991).
4. M.J. Gálvez-Ruiz and M.A. Cabrerizo-Vílchez, *Thin Solid Films* **210/211**: 127 (1992).
5. J. Sánchez-González and M.J. Gálvez Ruiz, Accepted for publication in *Progr. Colloid Polym. Sci.* (1995).
6. M.J. Gálvez-Ruiz and M.A. Cabrerizo-Vílchez, *Colloids and Surfaces*, **58**: 61-72 (1991).
7. H.L. Brockman, G.M. Jones, C.J. Schewebke, J.M. Smaby, and D.E. Jarvis, *J. Colloid Interf. Sci.* **78**(2), 502 (1980).
8. O. Albrecht, M. Gruler and E. Sackmann, *J. Colloid Interf. Sci.* **79**: 319 (1981).
9. B.M. Abraham and F. Behroozi, *J. Colloid Interf. Sci.* **127**: 346 (1989).

PENDENT DROP TECHNIQUE FOR STUDIES OF DYNAMIC PROPERTIES OF SOLUBLE ADSORPTION LAYERS AND INSOLUBLE MONOLAYERS

R. Miller[1], J.B. Li[1], R. Wüstneck[2], J. Krägel[2], D. Clark[3] and A.W. Neumann[4]
1 Max-Planck-Institut für Kolloid- und Grenzflächenforschung, Berlin, Germany
2 University of Potsdam, Department of Solid State Physics, Potsdam, Germany
3 Institute of Food Research, Norwich Laboratory, Colney, Norwich, UK
4 University of Toronto, Department of Mechanical Engineering, Toronto, Canada

Abstract

Axisymmetric drop shape analysis (ADSA) of pendant drops is a methodology which may be applied to a large variety of dynamic and equilibrium studies of adsorption layers of soluble surfactants and proteins as well as monolayers of insoluble molecules. Adsorption kinetics measurements of protein solutions have been performed with the technique. The measurements allow us to determine the mechanism controlling the adsorption kinetics, which is rather complex for solutions of protein and protein/surfactant mixtures. At low protein concentration and short adsorption time, no surface tension changes are observed. This induction interval has been observed for other proteins as well, but a reasonable theoretical model explaining this phenomenon has not been proposed so far. As a consequence the effective diffusion coefficients determined under these conditions are much higher than expected. At higher concentration and longer adsorption times the calculated values for the effective diffusion coefficient agree well with expected values.

1. Introduction

The pendant drop technique, based on video image acquisition and Axisymmetric Drop Shape Analysis (ADSA), is a novel methodology with many applications [1-5]. It has been used to study dynamic and static adsorption processes of surfactants [1] or proteins [2, 3] as well as mixtures and insoluble monolayers [4,5]. All these studies can be performed at the liquid/air and liquid/liquid interfaces. It has also been applied to investigations of dilational rheology and exchange studies of surfactant and protein adsorption layers [1, 2].

The aim of the present study is to demonstrate application of the pendant drop method to aqueous protein solutions. The method allows measurement of the dynamic surface tension of aqueous - lactoglobulin and -casein solutions and highlights peculiarities in the adsorption behaviour of these proteins.

2. Experimental set-up and materials

A schematic of the pendant drop apparatus used in this study is shown in Fig. 1. The method is based on video-enhanced detection of drop shape coordinates from which the surface or interfacial tension can be obtained through a fitting procedure employing the Gauss-Laplace equation. The main features of the apparatus are a light source (L), a video camera (CCD) with objective, frame grabber (D) and a PC. The shape coordinates of the drop, formed at the tip of a capillary (C) attached to a syringe (S) are determined using a grey-level analysis on the PC.

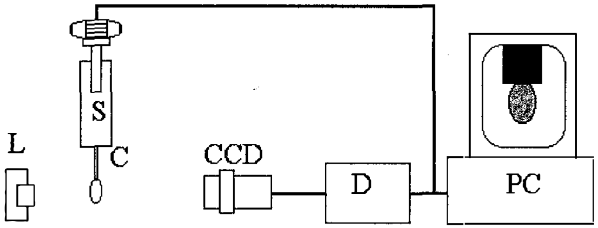

Fig. 1 Schematic of a pendent drop set-up

The surface tension γ is the only variable parameter in the fitting procedure used in the ADSA software [6]. The accuracy of the γ-measurements is of the order $\pm 0.1\,\mathrm{mN/m}$. ß-casein, a sample from bovine milk (SIGMA C-6905, Lot 12H9550), and ß-lactoglobulin (SIGMA L-0130, Lot 91H7005) were used without further purification. The molecular weight of ß-casein and ß-lactoglobulin were 24,000 and 18,400, respectively. All experiments were performed in phosphate buffer solution, prepared from Na_2HPO_4 and NaH_2PO_4. The surface tension of a 10 mM buffer at pH=7 was 72.7 mN/m.

3. Determination of the adsorption from dynamic surface tensions measurement

Dynamic surface tensions is the most accessible parameter for determination of the adsorption mechanism of surface active material at liquid interfaces. There are quantitative theories that describe the adsorption kinetics of surfactants, but for polymers in general and proteins in particular, no such models exist [7 - 9]. In this paper we apply a diffusion-controlled adsorption model to experimental data for aqueous protein solutions. The diffusion coefficients (D_{eff}) obtained in this way are only effective values, but they can be used to derive information about the mechanism of the adsorption layer formation. Values of D_{eff} much smaller than physically sensible values indicate that additional processes hinder the adsorption, for example, rearrangements of adsorbed molecules at the interface. Much larger D_{eff}-values indicate that additional assumptions are necessary to explain a process apparently faster than diffusion. Such process could be a fast surface spreading of adsorbed molecules at comparatively low surface coverages.

The slopes at $t \rightarrow 0$ and $t \rightarrow \infty$ can be used as good approximations for the determination of diffusion coefficients from $\gamma(t)$-dependencies . At $t \rightarrow 0$ and for low protein concentrations, no special prerequisites (such as an adsorption isotherm) are necessary and diffusion coefficients can be determined directly from the $\gamma(t)$-dependencies. However, use of the long time approximation procedure requires knowledge of the thermodynamic equilibrium state of the adsorption layer.

An effective diffusion coefficient can be determined from a short time approximation [10] using the following

$$D_{eff} = \frac{\pi}{4}\left[\frac{1}{RTc}\left(\frac{d\gamma}{d\sqrt{t}}\right)_{t \to 0}\right]^2 \qquad (1)$$

where R is gas constant, T the temperature and c the bulk concentration.

The surface tension at t=0 cannot be measured but extrapolation from the data leads to $\gamma = \gamma_0$ where γ_0 is the surface tension of the solvent. Only if this prerequisite is fulfilled can Eq. (1) yield reasonable values of D_{eff}.

In the long time approximation, the following equation can be derived [10] from the adsorption isotherm,

$$D_{eff} = \pi \frac{\left(\frac{d\gamma}{d\ln c}\right)^4}{\left(RTc\left[\frac{d\gamma}{d(1/\sqrt{t}}\right]_{t \to \infty}\right)^2} \qquad (2)$$

Further theoretical models and a review of experimental examples on various protein systems have been described for example in [11].

4. Results and discussion

The time dependency of surface tension for ß-lactoglobulin and ß-casein is shown in Figs 2 and 3. It can be easily seen that the shape of the $\gamma(t)$-dependencies relates strongly to the protein concentration. In particular, the initial slopes at low adsorption times exhibit a behaviour which is obviously different for lower and higher protein concentrations.

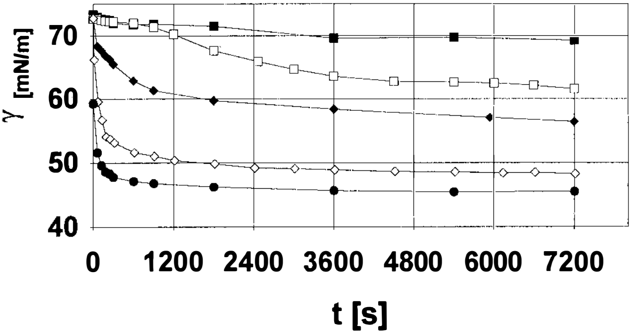

Fig. 2 $\gamma(t)$-dependency of ß-lactoglubulin in phosphate buffer at pH=7; $c=10^{-8}$ (■), 10^{-7} (□), 10^{-6} (◆), $5 \cdot 10^{-6}$ (◇), $2 \cdot 10^{-5}$ (●) mole/l,

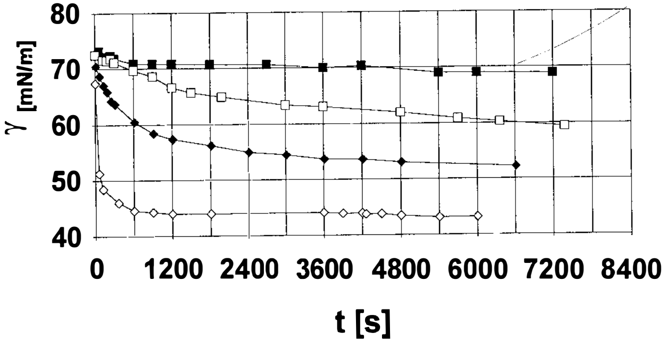

Fig. 3 $\gamma(t)$-dependency of ß-casein in phosphate buffer at pH=7, $c=10^{-8}$ (■), 10^{-7} (□), 10^{-6} (◆), 10^{-5} (◇) mole/l,

At short adsorption times and low protein concentrations, the surface tension may even exceed 72.7 mN/m. This effect is not understood but an even more pronounced effect was observed with other protein systems [12]. An induction period is evident were the surface tension remains nearly constant. This has also been reported by other authors [2, 13 -16]. A possible explanation for this specific effect with proteins could be a varying adsorption layer thickness. At the beginning of adsorption, molecules spread and form a very thin layer until a primary coverage has been established. In this state no significant surface tension changes appear. Then further adsorption leads to an increase in the layer thickness which is accompanied by a noticable surface tension change. This change in layer thickness is only the consequence of molecular conformations and does not imply a multilay formation. There is no theoretical model so far which describes this process sufficiently.

The effective diffusion D_{eff} of the two proteins at pH=7, calculated from Figs 2 and 3 using the short and long time approximations Eqs. (1) and (2), are summarised in Table 1. Values obtained during the induction period are neglected. The short time approximation yields values much too large so that an additional process at low surface coverage must be assumed.

However, the D_{eff}-values obtained at higher concentration and longer adsorption time agree well with physically expected values, so that a diffusion-controlled process is likely. A better model including the adsorption during the induction period and possible changes of the adsorption layer thickness needs to be developed.

Table 1: Efficient diffusion coefficients D_{eff} for ß-lactoglobulin and ß-casein at pH=7 calculated from a short time and long time approximation, respectively

Protein	concentration [mole/l]	D_{eff} from Eq. (1) [m²/s]	D_{eff} from Eq. (2) [m²/s]
ß-Lactoglobulin	$2\cdot10^{-5}$	$1.19\cdot10^{-8}$	$8.41\cdot10^{-11}$
	$1\cdot10^{-6}$	$2.15\cdot10^{-8}$	$5.32\cdot10^{-10}$
	$5\cdot10^{-6}$	$1.21\cdot10^{-8}$	$3.19\cdot10^{-10}$
	$1\cdot10^{-7}$	$9.46\cdot10^{-9}$	$9.28\cdot10^{-8}$
	$1\cdot10^{-8}$	$2.72\cdot10^{-6}$	$5.01\cdot10^{-5}$
ß-Casein	$1\cdot10^{-5}$	$9.42\cdot10^{-9}$	$6.73\cdot10^{-10}$
	$1\cdot10^{-6}$	$2.81\cdot10^{-8}$	$2.50\cdot10^{-8}$
	$1\cdot10^{-7}$	$4.29\cdot10^{-8}$	$1.31\cdot10^{-6}$
	$1\cdot10^{-8}$	$1.48\cdot10^{-6}$	$4.9\cdot10^{-3}$

5. Conclusions

The pendent drop technique is a methodology applicable to a large variety of dynamic and equilibrium studies. It is applicable to adsorption layers of soluble surfactants and proteins as well as monolayers of insoluble molecules. The adsorption kinetics of the protein solutions studied here show some peculiarities: at low concentration and short adsorption time, a negative surface pressure is observed. This effect has been observed for other proteins as well, but so far it is not understood.

The determined effective diffusion coefficients for low protein concentrations and short adsorption times are much higher than expected, suggesting that there is an additional mechanism acting at low surface coverage. This could be for example a fast surface spreading process of molecules arriving at an almost bare interface. At higher concentration and longer adsorption times the calculated diffusion coefficients values are physically realistic.

6. Acknowledgements

The work was financially supported by a project of the European Community (HCM/ERBCHRXT930322), the DFG (Wu 187/3-1), the Medical Research Council of Canada (grant no. MT-5462), and the Fonds der Chemischen Industrie (RM 400429).

7. References

1. Miller, R., Sedev, R., Schano, K.-H., Ng, C. and Neumann, A.W., Colloids & Surfaces, 69(1993) 209
2. Miller, R., Policova, Z., Sedev., R. and Neumann, A.W., Colloids & Surfaces, 76(1993)179
3. M.A. Cabrerizo-Vilchez, Z. Policova, D. Kwok, P. Chen and A.W. Neumann, Colloids & Surfaces B, Biointerfaces, in press
4. Kwok, D.Y., Vollhardt, D., Miller, R., Li, D. and Neumann, A.W., Colloids & Surfaces A, 88(1994)51
5. Li, J.B., Miller, R., Wüstneck, R., Möhwald, H. and Neumann, A.W., Colloids & Surfaces A, in press
6. Cheng, P., Li, D., Boruvka, L., Rothenberg, Y. and Neumann, A.W., Colloids & Surfaces, 43(1990)151
7. Graham, D.E. and Phillips, M.C., J. Colloid Interface Sci., 70(1979)403
8. Douillard, R. and Lefebvre, J., J. Colloid Interface Sci., 139(1990)488
9. Serrien, G., Geeraerts, G., Ghosh, L., and Joos, P., Colloids and Surfaces, 68(1992)219
10. Fainermann, V.B., Makievski, A.V. and Miller, R., Colloid and Surfaces A, 87,61(1994)
11. S.S. Dukhin, G. Kretzschmar and R.Miller, "Dynamics of Adsorption at Liquid Interfaces", in "Studies of Interface Science", D.Möbius and R. Miller (Eds), Elsevier, Amsterdam, Vol. 1, 1995
12. Neumann, A.W., Workshop "Dynamics of Adsorption at Liquid Interfaces", Nov. 1994, Wageningen, The Netherlands
13. Wei, A.P., Herron, J.N. and Andrade, J.D., in "From Clone to Clinics", D.J.A. Crommelin and H.Schellekens (Eds), Kluwer Academic Publishers, The Netherlands, (1990)305
14. de Feijter, J., Benjamins, J. and Tamboer M., Colloids & Surfaces, 27(1987)243
15. Douillard, R., Daoud, M., Lefebvre, J., Minier, C., Lecannus, G. and Coutret, J., J. Colloid Interface Sci., 163(1994)277
16. Xu, S. and Damodaran, S., Langmuir, 10(1994)427

PHASE TRANSITIONS AND ADSORPTION CHARACTERISATION OF PHOSPHOLIPID MONOLAYERS AT AIR/WATER, DODECANE/WATER AND CHLOROFORM/WATER INTERFACES

J.B. Li[1], R. Miller[1], D. Vollhardt[1], A.W.Neumann[2] and H.Möhwald[1]

1 Max-Planck-Institut für Kolloid- und Grenzflächenforschung, Berlin, Germany

2 University of Toronto, Department of Mechanical Engineering, Toronto, Canada

Abstract

Two phospholipid compounds, DPPC and DMPE, have been used to investigate phase transitions and monolayer behaviour at air/water and dodecane/water interfaces and their adsorption behaviour at chloroform/water interface by using the axisymmetric drop shape analysis (ADSA) technique. The pressure-area isotherms of Langmuir monolayers of such phospholipids obtained by ADSA show good agreement with conventional LB balance measurements.

Adsorption processes of DPPC and DMPE monolayers at the chloroform/water interface depend on the concentrations of solutions and adsorption time. In the concentration range of 0.0004 to 1 mM/l and the time interval of 1000s to 50s adsorption layers do not undergo clear phase transitions when increasing the interfacial pressure via increasing bulk concentration. The adsorption isotherms reflect a typical adsorption behaviour up to a critical concentration of aggregation of the phospholipids.

1. Introduction

The axisymmetric drop shape analysis (ADSA) was developed as a methodology to study dynamic and thermodynamic properties of surfactant and protein adsorption layers [1-4]. Recently ADSA was used as a film balance to study the surface pressure/area isotherm of an octadecanol monolayer [5, 6].

ADSA as a film balance to study fundamental characteristics of phase behaviour of assembled monolayers at liquid/fluid interfaces has several advantages: homogeneity of temperature, surface pressure, surface concentration, symmetry of area changes.

The main objective of the present work is to test the capacity of ADSA as a film balance in a larger molecular area variation interval at the air/water interface and to demonstrate the applicability to monolayers at a liquid/liquid interface. In addition to the monolayer behaviour the adsorption behaviour of the phospholipids, DPPC and DMPE, at the chloroform/water interface was studied.

2. Theory, Materials and Experiments

From the shape of an axisymmetric pendent or sessile drop the interfacial tension can be determined by fitting the Gauss-Laplace equation to the experimental drop coordinates,

$$\gamma\left[\frac{1}{R_1}+\frac{1}{R_2}\right]=\Delta P.$$

Here γ is the interfacial tension, R_1,R_2 are the two principal radii of curvature, ΔP is the pressure difference across the interface, $\Delta P=\Delta P_0+(\Delta\rho)gz$, and ΔP_o is the reference pressure at an arbitrary reference plane, $\Delta\rho$ is the density difference between the fluids, g is the accelaration due to gravity, z is the vertical height above the reference plane.

The experimental set-up of the pendent drop used in the present studies has been described in another paper of this book [7]. The experiments can be performed for very different systems, as shown in Fig. 1. In the simplest case a) the surfactant is dissolved in the liquid, for example water, and the change of the drop shape with time yields the adsorption process of the surfactant at the drop surface. The technique works in the same way when the surfactant is dissolved in both liquid phases, or when two different surfactants are present in the two liquid phases (case b). By spreading an insoluble surfactant, dissolved in a solvent, on the surface of a drop, even insoluble monolayers can be studied with the pendent drop technique. Compressions and expansions of the monolayer are performed by changing the drop volume (case c) [5].

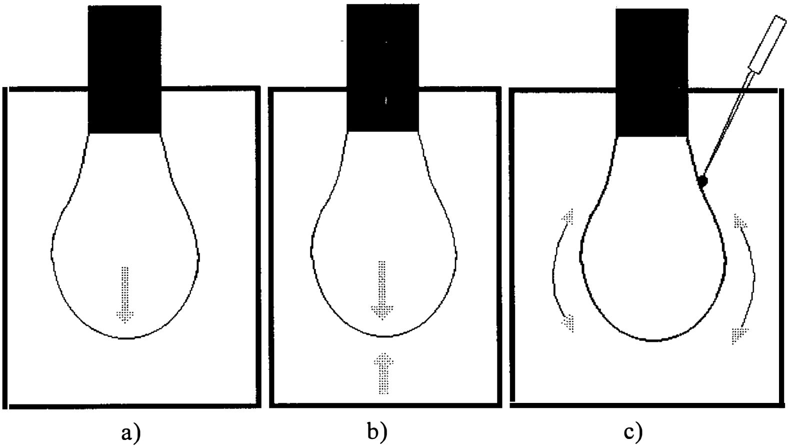

Fig. 1 Schematic of pendent drop experiments; a - adsorption at a liquid/gas interface, b - adsorption layer formed from both sides at a liquid/liquid interface, c - monolayer at a liquid/gas interface

A study of an insoluble monolayer at the liquid/liquid interface is readily possible, in contrast to experiments with a conventional Langmuir trough. First the monolayer is spread on the surface of a water drop. After the solvent has evaporated from the surface (at least 10 min) the drop is gently immersed into the second liquid, in the present example into n-dodecane. Then, compression and expansion of the monolayer is produced again by drop volume changes. As ADSA provides drop volume and area data in addition to the surface tensions, the absolute interfacial area is well known at any time of the experiment.

The lipids DPPC and DMPE (99%+purity) from Sigma were used without further purification. For spreading they were dissolved in chloroform with a concentration of 0.0001 mM/L. Chloroform and n-dodecane with 99% purity were purchased from MERCK and Sigma, respectively. Chloroform for adsorption measurements was saturated with Millipore water for about a week. Then the saturated chloroform was used to prepare a series of phospholipid solutions, and the saturated water was used to produce the chloroform/water interface. The water used in all experiments was prepared in a Millipore apparatus.

3. Experimental Results

The compression isotherm of a DPPC film on a water surface is shown in Fig. 2. The surface area of the pendent drop has a rather large variation from about 0.23 to 0.58 cm^2 during compression, necessary to vary the pressure from 0 to 51.0 mN/m. A first order phase transition occurs at 82 Å^2/molecule which leads from the LE to LC phase. The following coexistence region of LE and LC is between 82Å^2 and 58Å^2 and the surface pressure is above 6 mN/m in the LC phase. Comparing the whole process of phase transition, ADSA shows results consistent with the conventional film balance measurements.

The $\pi(A)$-isotherm reaches pressure values up to about 55 mN/m as the film is compressed. This value is very high and was not reached so far on usual Langmuir troughs.

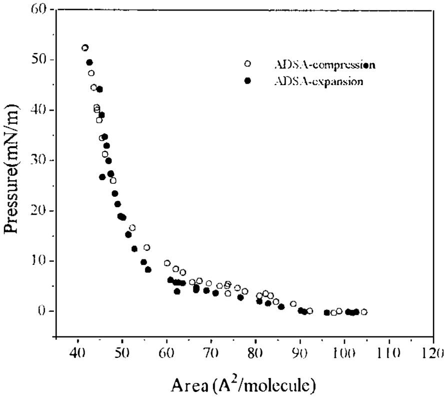

Fig. 2 Isotherms ofDPPC at Air/Water interface at 20°C

In addition to the above DPPC film measurements, a second monolayer, DMPE with a small head group, was investigated. Although the two phospholipids are very similar in their structure they show different phase behaviour. For example the DMPE monolayer exhibits a region of small slope changes at higher surface pressures. Our results with ADSA show a less pronounced phase transition and the pressure is somewhat higher than expected. The reason could be a comparatively fast compression so that equilibrium conditions were not fulfilled.

Unlike films at the air/water interface, the isotherm of DPPC at the water/dodecane interface firstly shows a gaseous phase with a plateau region [8] beginning near 100 Å^2/molecule indicating the coexistence of an isotropic fluid and a liquid condensed phase. For molecular areas below 70 Å^2/molecule the film is almost completely in the condensed phase. Similar phase behaviour was also observed for another phospholipid in the same interface system [9]. Our results for DPPC from ADSA are in good agreement with the LB balance measurements. The same good agreement was obtained for DMPE monolayers.

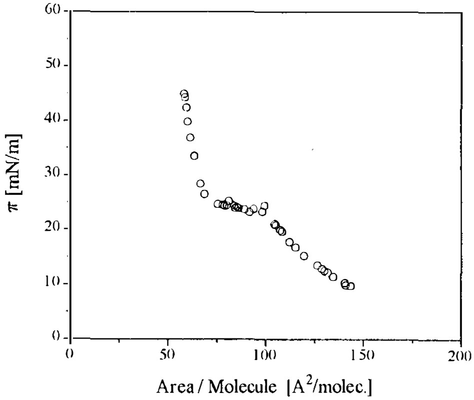

Fig. 3 Isotherm of DPPC at the water/n-dodecane interface at 22 °C

In a third series of experiments the phospholipids were dissolved in chloroform and studied at a water/chloroform interface. In this case the phospholipids adsorb from the chloroform phase at the interface and an adsorption isotherm can be obtained by measurements in a certain bulk concentration interval [10]. The results for DMPE are shown in Fig. 4.

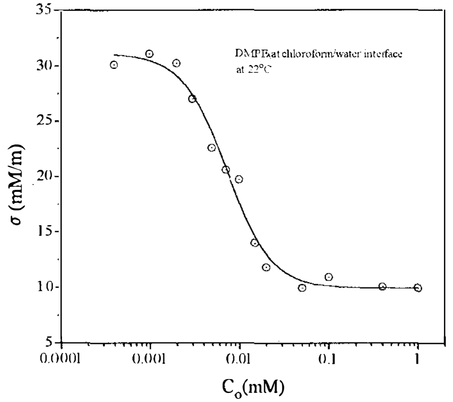

Fig. 4 Dynamic adsorption behaviour of DMPE at the chloroform/water interface at 22°C

No significant phase transitions or coexistence regions are observed. From the slope of the adsorption isotherm the area per molecule can be calculated. The values for both DPPC and DMPE are about 45Å²/molecule, which is very close to the molecular area values for an insoluble monolayer.

4. Conclusions

The experimental results show that ADSA allows measurements of adsorption layer and monolayer isotherms in a very broad molecular area interval without any set-up modifications. Compared with the conventional LB trough the ADSA technique has several advantages: easy monolayer studies at the liquid/liquid interface, uniform temperature, concentration and pressure, less external disturbances, high temperature measurements. A disadvantage is less accuracy of the amount spread on the surface and the so far rather high compression rates.

Adsorption studies of soluble phospholipid layers at a chloroform/water interface by using the pendent drop technique exhibit a diffusion controlled adsorption behaviour, like typical surfactants. Unlike the insoluble monolayer, no phase transitions are observed within a wide concentration range within the time interval studied.

6. Acknowledgements

The work was financially supported by a project of the Medical Research Council of Canada (grant no. MT-5462), and the Fonds der Chemischen Industrie (RM 400429).

7. References

1. Cheng, P., Li, D., Boruvka, L., Rothenberg, Y. and Neumann, A.W., Colloids & Surfaces, 43(1990)151
2. Miller, R., Sedev, R., Schano, K.-H., Ng, C. and Neumann, A.W., Colloids & Surfaces, 69(1993) 209
3. Miller, R., Policova, Z., Sedev., R. and Neumann, A.W., Colloids & Surfaces, 76(1993)179
4. M.A. Cabrerizo-Vilchez, Z. Policova, D. Kwok, P. Chen and A.W. Neumann, Colloids & Surfaces B, Biointerfaces, in press
5. Kwok, D.Y., Vollhardt, D., Miller, R., Li, D. and Neumann, A.W., Colloids & Surfaces A, 88(1994)51
6. Li, J.B., Miller, R., Wüstneck, R., Möhwald, H. and Neumann, A.W., Colloids & Surfaces A, in press
7. R. Miller, J.B. Li, R. Wüstneck, J. Krägel, D. Clark and A.W. Neumann, Pendent drop technique for studies of dynamic properties of soluble adsorption layers and insoluble monolayers, Proceedings of the "Long and Short Chains at Interfaces" meeting, Villars-sur-Ollon, 1995
8. C.A. Helm, L. Laxhuber, M. Lösche and H. Möhwald, Coll. Polymer Sci., 264(1986)46.
9. M. Thoma and H. Möhwald, J. Colloid Inteface Sci., 162(1994)340.
10. S.S. Dukhin, G. Kretzschmar and R.Miller, "Dynamics of Adsorption at Liquid Interfaces", in "Studies of Interface Science", D.Möbius and R. Miller (Eds), Elsevier, Amsterdam, Vol. 1, 1995

KINETICS OF POLYMERISATION IN LANGMUIR MONOLAYERS OF n-ALKYLTRIMETHOXYSILANE

P. FONTAINE, F. RONDELEZ
Institut Curie, Laboratoire P.S.I., 11, Rue Pierre et Marie Curie, 75231 PARIS CEDEX 05,
FRANCE

ABSTRACT

Molecules of Octadecyltrimethoxysilane ($CH_3-(CH_2)_{17}-Si(OCH_3)_3$), OTMS as current abbreviation, are amphiphiles and readily form Langmuir monolayers at the air water interface. Indeed the long alkyl chain insures the insolubility of the molecule in the aqueous subphase, whereas the polar head group, which consists of a silicon atom bonded to three methoxy groups ($-OCH_3$), provides the anchoring onto the interface. Upon contact with water, the methoxy groups hydrolyse into hydroxyl groups. It initiates a polymerisation process characterised by an in-plane condensation of the neighbouring hydroxyl groups. The presence of siloxane bonds (Si-O-Si) between molecules has been established by Okahata & al[1], based on F.T.I.R. measurements. So far however, neither the process, nor the structure of the polymerised monolayer, have been carefully investigated. In this study, we have unravelled the kinetics of the two steps of the polymerisation process (hydrolysis and condensation). For the hydrolysis, this was achieved through macroscopic π-A measurements which detect the change of molecular area associated with the replacement of the bulky methoxy groups by smaller hydroxyl groups. We show that adjusting the pH of the bulk water allows to control the rate of hydrolysis. As for the condensation, epifluorescence microscopy enables us to follow the apparition of the polymerised domains (typical area 100µm^2) within the monolayer. At long times (2 hours on pH=2 water subphase), one reaches a two dimensional sheet of molecular thickness about 25 Å and covering areas as large as several mm^2.

Introduction :

Silane molecules with long alkyl chains are frequently used as surface modifiers. For instance, Octadecyltrichlorosilane ($CH_3 - (CH_2)_{17} - SiCl_3$, OTS for short) is very well known to form self-assembled monolayers on natural oxides (silica, alumina ...), when the substrate is dipped into a dilute solution of OTS in hydrocarbon solvent. Following deposition, the oxide surface, which is naturally hydrophilic becomes strongly water repellent. A possible mechanism of formation of the organic monolayer is based on the presence of a nanometer thick, physisorbed film of water onto the solid substrate. The silane molecules adsorb on the aqueous film through their polar trichloro head groups, whereas the chains are oriented towards the organic solvent. The adsorption process stops since the substrate is covered with a dense outer layer of non-reactive methyl groups. Upon contact with water, the head groups hydrolyse, and the chlorine atoms are progressively replaced by hydroxyl (-OH) groups. This allows intermolecular condensation, and the formation of an in-plane 2D siloxane network (Si-O-Si). Finally, following the removal of the water film by heat treatment, some of the unreacted hydroxyl groups may couple to the silanol groups (Si-OH) of silica, thus providing a covalent grafting of the film to the substrate[2].

In order to better understand the interaction between the organosilane molecules and the aqueous film, we have turned to a model system, namely a Langmuir film[3] of n-alkylsilane molecules spread at the surface of water. Since those molecules can be considered as amphiphiles, a monolayer is readily formed. We have studied these monolayers by surface pressure isotherms and epifluorescence microscopy. These two complementary techniques allow to monitor respectively the hydrolysis and the condensation steps of the chemical reactions. We have selected Octadecyltrimethoxysilane ($CH_3 - (CH_2)_{17} - Si(OCH_3)_3$) rather than OTS in order to decrease the hydrolysis rate and to bring it into a convenient experimental range.

Kinetics of the hydrolysis :

Fig. 1 shows the reaction scheme for the hydrolysis of the methoxy groups. This reaction is associated, as pointed out by the figure, to a sharp decrease of the molecular cross section of the head group. According to CPK molecular models, the cross section of the head drops from 40Å^2 for the original trimethoxysilane group to 20Å^2 for the fully hydrolysed trihydroxylsilane group. On the other hand, the cross section of an alkyl chain in the all-trans extended conformation is known to be smaller than 20Å^2. The molecular area occupied by the molecule is therefore governed by the head group cross-section.

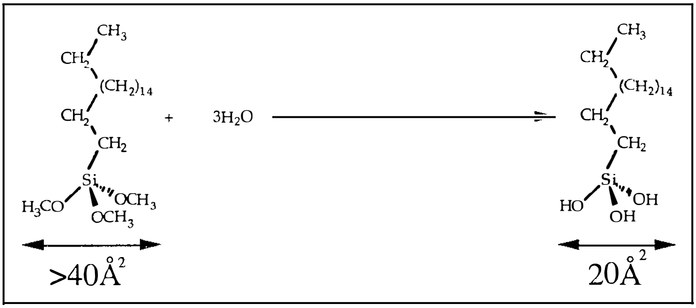

fig. 1: Hydrolysis of the trimethoxysilane head group.

Surface pressure - area per molecule measurements are well suited to detect such a decrease in molecular cross section. In order to follow continuously the chemical evolution of the monolayer, we have monitored the time evolution of the area per molecule at constant surface pressure ($\pi = 10 \mathrm{mNm}^{-1}$) and temperature ($T = 20°C$). As shown in fig. 2-a, the expected decrease of the area per molecule from $40 \pm 5Å^2$ to a limit value of $20 \pm 1Å^2$ is obtained over a period of 1000±300 minutes.

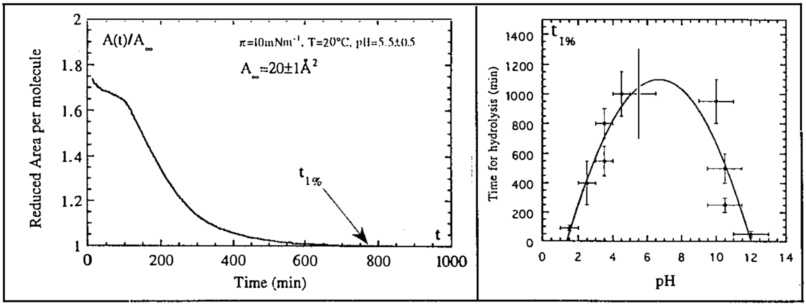

fig. 2-a- fig. 2-b

fig. 2-a- Temporal evolution of the area per molecule at constant surface pressure. b- Influence of the pH of the aqueous subphase on the time to complete hydrolysis.

A somewhat surprising feature of this curve is the abrupt change of slope separating two different regimes. At first, the hydrolysis rate is slow but it markedly accelerates after about 150±50 minutes. The most plausible explanation is that the model of a simple hydrolysis for all three methoxy groups is oversimplified. Once a methoxy group has been replaced by an hydroxyl group, the remaining methoxies become more sensitive to hydrolysis. Therefore one has to assume different rate constants for the first, second and third hydrolysis respectively[4]. Secondly, the pH at the interface has decreased and the hydrolysis is known to be catalysed by acidic conditions. Thirdly, the cleavage of the methoxy groups may be caused not only by hydrolysis but also by direct coupling with hydroxyls located on neighbouring molecules : $\equiv Si-OCH_3 + HO-Si\equiv \rightarrow \equiv Si-O-Si + CH_3OH$. The combination of all these effects is quite sufficient to explain the complexities of the observed kinetics[4].

A convenient definition of the hydrolysis rate is to use the time $t_{1\%}$ at which the average area per molecule has dropped to 1% of the asymptotic value. For pH=5.5, $t_{1\%}$ equals 1000±300 minutes. Fig. 2-b displays the dependence of $t_{1\%}$ versus the pH of the water subphase. The longest time is obtained at pH=7 and exceeds one day. On the other hand, at pH below 2 and above 12, it becomes shorter than the response time of the system (10 minutes). This variation is consistent with the fact that hydrolysis is catalysed both by protons and hydroxide with acidic and basic media respectively. A similar curve has been reported for the hydrolysis of Tetraalkoxysilanes ($Si(OR)_4$, with R an alkyl group) in three dimensional sol-gel processes[5,6]. This strong pH dependence provides us a simple way to adjust the hydrolysis step in a time range convenient for the observation of the subsequent network formation.

Kinetics of intermolecular condensation :

CPK molecular models indicate that the cross section of the head group does not change during the condensation reaction, ($\equiv Si-OH + HO-Si\equiv \rightarrow \equiv Si-O-Si\equiv + H_2O$). Thus, surface pressure measurements cannot be used to monitor the polymerisation step. On the other hand, X-ray diffraction experiments[4,7] have given evidence that the molecules are highly condensed in the final stages of the reaction of polymerisation. This suggests to use direct visual observation to follow the growth of polymerised domains. Indeed if one mixes the OTMS molecules with a small amount of fluorescent markers, the dye molecules will have a tendency to be expelled from the densest close packed regions of the monolayer. We should therefore be able to observe the formation of dark domains within the monolayer, if the polymerisation process is controlled by a nucleation and growth process. This is achieved by using epifluorescence microscopy, with a lateral resolution of a few micrometers

In order to follow the condensation, we have dissolved 0.5mol% of NBD-ODA (4-octadecylamino-7-nitrobenz-2-oxa-1,3-diazole) with OTMS molecules before spreading the monolayer on the aqueous subphase at neutral pH. For an area per molecule of 60Å^2/molecule, the film exhibits a homogeneous uniform grey phase (fig.3-a), in agreement with the π-A isotherm which indicates that at such surface concentration, the monolayer should be in its liquid expanded phase[4]. To launch the condensation process, we then quickly lower the pH to an acidic value of 2±0.5. As discussed above, the time to complete the hydrolysis at this pH is one hour. 20-30 minutes after lowering the pH, black domains appear within the monolayer (fig. 3-b). By expanding and compressing the film, we checked that once formed, these domains are irreversible. Therefore they do not correspond to the gaseous bubbles, nor to the liquid condensed islands, which are frequently observed in the coexistence regions of the phase diagram of amphiphilic monolayers[3-b]. The irreversibility strongly suggests that intermolecular condensation has occurred within the domains and that a 2D gel phase has been formed over macroscopic distances.

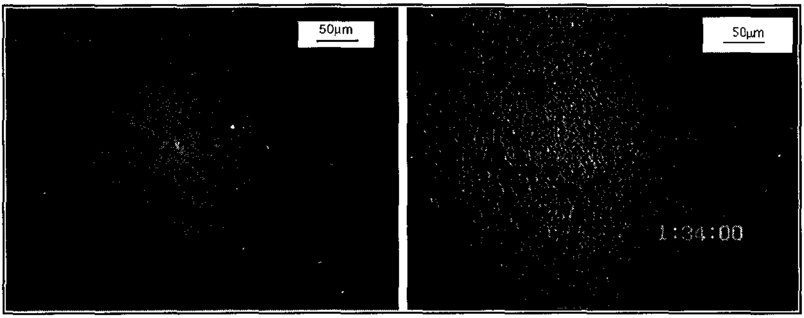

fig 3-a fig 3-b

fig. 3 : Epifluorescence images of an OTMS monolayer at 60Å^2/molecule just after pH lowering (fig 3-a) and 20-30 minutes after (fig 3-b).

During the next 30 minutes, more black domains appear at random places within the monolayer and each domain grows up to a limiting size of 100±50μm^2. After one hour, no further evolution is discernible. The final monolayer is composed of black domains surrounded by a grey phase, which itself is floating into a dark gas-like phase. The apparition of this latter phase is due to the fact that the surface pressure is not held constant in this experiment. Thus the free surface created by the shrinkage of the molecular area discussed previously is not compensated by the compression of the film. The grey phase is not fluid, possesses sharp, irregular edges, and inhomogeneities of the dye concentration within the phase are clearly visible. All this suggest that the grey phase is partially polymerised at least at the macroscopic level.

Our experiments show that hydrolysis and most of the condensation take place simultaneously. This is markedly different from the case of Tetraalkoxysilanes 3D solgels, for which the condensation is much slower that the hydrolysis : more than one week as compared to one hour at pH=2. The reasoning leading to the higher condensation rate in 2D is the higher probability of contact when the molecules diffuse over a surface rather than within a volume. In addition condensation reactions are topochemically favoured in Langmuir monolayers, first because of the pinning of the reactive head groups in the plane of the water interface, second because of the high surface density.

Conclusion :

By studying separately the hydrolysis and condensation kinetics of n-alkyltrialkoxysilane at the air water interface, we have shown that the time scales are the same for the two processes. As soon as hydroxyl groups are formed within the monolayer, the molecules start to condense. This is in agreement with the fact that cross-linking reactions are topochemically favoured. The rates of hydrolysis and condensation can be controlled over two orders of magnitude by adjusting the pH of the subphase. This has enabled us, in a separate work, to study the microscopic structure of the polymerised monolayer by Grazing Incidence X-Ray Diffraction[4,7].

Acknowledgement :

We gratefully acknowledge the financial support of IFCPAR-CEFIPRA, the Indo-French Centre for the Promotion of Advanced Research, under contract # 907-2-94-2036.

References :

1) K. Ariga, Y. Okahata, J. Am. Chem. Soc.,111, (1989) 5618.
2) J.B. Brzoska, N. Shahidzadeh, F. Rondelez, Nature, 360, (1992) 719.
A. Parikh, D.L. Allara, F. Rondelez, J. Phys. Chem., 98, (1994) 7577.
3) a- G.L. Gaines, Insoluble monolayers at Liquid Gas interfaces, Wiley, New York 1966.
b- H. Möhwald, Ann. Rev. Phys. Chem., (1990) 441.
4) P. Fontaine, R.M. Kenn, F. Rondelez, to be published.
5) R. Aelion, A. Loebel, F. Eirich, J. Am. Chem. Soc., 72, (1950) 5705.
6) F. Devreux, J.P. Boilot, F. Chaput, A. Leconte, Phys. Rev. A, 41, (1990) 6901.
7) P. Fontaine, M. Goldmann, F. Rondelez, in preparation.

POLYMERIZABILITY OF LINOLEIC ACID MONOLAYERS AT THE GAS/LIQUID INTERFACE

Jouko P.K. Peltonen, Mika Linden and Jarl B. Rosenholm
Department of Physical Chemistry, Åbo Akademi University
Porthansgatan 3-5, FIN-20500 Turku, Finland

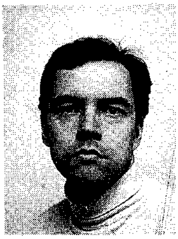

The effect of varying the subphase composition on the polymerization kinetics of linoleic acid Langmuir monolayers was investigated. The pH of the $TbCl_3$ subphase was found to have a dramatic influence on the compressibility of the monolayer. The appearance of a condensed-like phase at pH's beyond a critical value was interpreted in terms of the formation of a monohydroxy complex of Tb metal ions and its interaction with the ionized monolayer. The condensation was highly specific to the metal ion, Al, Pb and Zn were studied for comparison. By tuning the condensation of the monolayer a pronounced increase of the polymerization rate was observed. A model for the reaction kinetics is presented. The fit of experimental data to the model implied that the reaction was of first order. The temperature dependence of the reaction was observed to be very weak and actually the Arrhenius plot could not be applied to accurately determine the activation energy. The insensitivity of the reaction of linoleic acid towards oxygen as well as the little temperature dependence of the reaction rate strongly suggest that the reaction follows the ionic polymerization mechanism.

Introduction

Langmuir-Blodgett (LB) technique offers an illustrative possibility to study the polymerization processes of reactive amphiphilic monomers at the gas/liquid interface.$^{1-8)}$ We have recently studied the reactivity of some unsaturated fatty acids with either one or two nonconjugated double bonds in the middle of the hydrocarbon chain.$^{6,7,9,10)}$ The kinetics can be followed in real time and the rate of the reaction may be determined within the proposed model. The intermolecular distance can be controlled by adjusting the surface pressure. Furthermore, the molecular arrangement of surfactants having an ionizable headgroup can be tuned by varying the subphase composition.$^{11-13)}$ By a certain choice of the subphase composition and pH, the processability of even an initially expanded film may be enhanced decisively.

The surfactant used in this work, cis-9,12-octadecadienoic (linoleic) acid (LA), was obtained from FLUKA and used without further purification. The substance was dissolved in n-hexane to form a solution with a concentration of 1 mg/ml. Until spreading, the solution was protected against light and stored in a refrigerator. $TbCl_3$, $AlCl_3$ (FLUKA), $Pb(NO_3)_2$ and $ZnSO_4$ (Merck) were used as the subphase salts and were PA-grade. The pH was adjusted by the addition of 0.1 M NaOH or HCl.

A KSV LB-5000 Langmuir trough (KSV-Instruments, Helsinki, Finland) with a Wilhelmy balance was used for the monolayer formation. Monolayers were obtained by spreading the solutions on a thermostated (20 °C) subphase containing the metal ions. The Milli Q filtration system (Millipore Corp., USA) was used to purify the water for the subphase having a resistance of 18 MΩ cm.

The monolayer irradiation was carried out using a 30 W low pressure mercury lamp placed 0.15 m above the monolayer. The reaction kinetics of the monolayer was monitored as a change in the barrier speed and mean molecular area while simultaneously keeping the surface pressure constant. The Langmuir trough was protected against natural UV-light with an absorbing yellow semitransparent plastic sheet.

The phase behaviour and polymerization kinetics

Figure 1 shows the compression isotherms of linoleic acid at various pH of the $TbCl_3$ subphase. At low pH the compression leads to a pure liquid-expanded (LE) monolayer with a collapse pressure of ca. 32 mN/m. At this pH the monolayer is fully nondissociated and thus no interaction with the metal ions takes place. With increasing pH the degree of dissociation of the monolayer increases giving rise to the interaction with the Tb-ions. Despite the decrease of the mean molecular area (fig. 1, curves 1-3) the Tb^{3+}-ions are not able to fully condense the monolayer. Increasing the pH further accelerates the formation of $Tb(OH)^{2+}$ complexes. The interaction of these complexes with the ionized acid molecules leads to an energetically and sterically most preferable packing structure and the monolayer now appears in the solid-expanded (SE) state (fig. 1, curves 4-5). The same kind of phase transition can be generated by using Al-ions, even so that the LE-SE transition takes place already at pH-interval 3.5-4.7. However, no phase transition was observed for the subphases

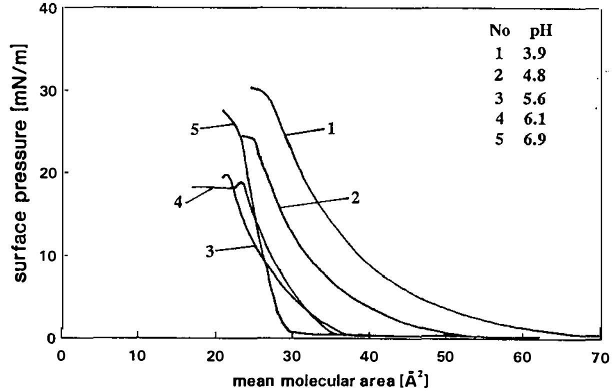

FIGURE 1. Compression isotherms of linoleic acid monolayers measured on a 10^{-4} M $TbCl_3$ subphase.

containing either Pb or Zn. As a crude rule it may be concluded that divalent ions, even if they form monohydroxy complexes, are not able to condense monolayers of cis-type unsaturated fatty acids. For the hydrolysed trivalent ions this is evidently possible. However, the condensing mechanism in the Al-linoleic acid and Tb-linoleic acid systems seems to be different. Tb forms only monohydroxy complexes while within the rather complex solution chemistry of Al it seems to be the dihydroxy complex ($Al(OH)_2^+$) that is responsible for the best packing arrangement in the linoleic acid monolayer.[10)]

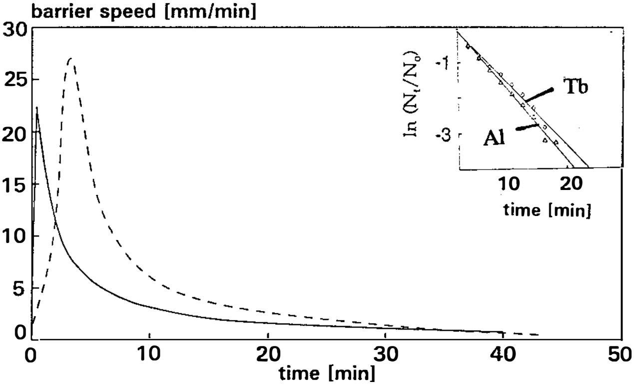

FIGURE 2. The barrier speed vs. time of a linoleic acid monolayer during the UV-irradiation. The UV-light was switched on at time t=0 min. The measurements were carried out in normal air on a 10^{-4} M $TbCl_3$ subphase (- - -) of pH 6.9 and $AlCl_3$ subphase (——) of pH 4.8 and under a constant surface pressure of 15 mN/m. Inset is the decrease of the monomer concentration as a function of time (eqs. 4 and 5).

As a results of the ability to control the phase behaviour of linoleic acid monolayers, a pronounced increase in the monolayer reactivity could be obtained compared with earlier reports.[6,7)] Typical kinetic curves of linoleic acid monolayer polymerization at the Tb (pH 6.9) and Al (pH 4.8) subphase are shown in figure 2. The time t=0 min corresponds to the switching on of the UV-lamp and the reaction-induced area contraction of the monolayer gives rice to the barrier movement. It is clearly seen that the initiation of the reaction differs for the two systems. The curve measured on the Al-subphase follows almost an ideal first order kinetic curve whereas a delayed increase of barrier speed in the curve corresponding to the Tb-subphase indicates that some initiation process preceding the polymerization reaction takes place. In both cases the reaction-induced decrease of the mean molecular area was ca. 7.5-8.5 Å^2.

The reaction kinetics model is based on the assumption that for each reaction step the UV-irradiation-induced change in mean molecular area,

$$\Delta\langle a\rangle = \langle a\rangle_0 - \langle a\rangle_\infty \,, \tag{1}$$

is equal. $\langle a\rangle_\infty$ corresponds to the completion of the reaction and can be read from the kinetic reactivity curve if taking into account the initial monolayer instability.[9)] The mean molecular area at time t can be written as

$$\langle a\rangle_t = \langle a\rangle_0 - ((N_0-N_t)/N_0)\Delta\langle a\rangle = \langle a\rangle_0 - x\Delta\langle a\rangle \,, \tag{2}$$

where N_0 is the number of spread molecules, N_t is the number of monomer molecules at time t, and x is the fraction of reacted monomers. The speed of the macroscopic area contraction relates to the average speed of the compressing barrier which can be further correlated to the reaction rate at the molecular level.[9)] Assuming a first order reaction, the reaction rate law is given by

$$dN/dt = -kN_t \,, \tag{3}$$

where k is the reaction rate constant. The integration of (3) from the initial boundary values ($t = 0$, $N = N_0$) to that corresponding to time t ($N = N_t$) leads to

$$\ln (N_t/N_0) = -kt \,, \tag{4}$$

which can be directly applied to the experimental kinetic curve since

$$N_t/N_0 = (\langle a \rangle_t - \langle a \rangle_\infty)/\Delta\langle a \rangle \ . \qquad (5)$$

Inserted in fig. 2 is a plot of equation (4) according to the shown reactivity curves and the relation given in equation (5). The linear fit indeed implies that the reaction is of first order. This concerns especially the case of Al-subphase. The values of k obtained as the slope of the curve are $k = 3.0 \bullet 10^{-3}\ s^{-1}$ for Al-LA and $k = 2.8 \bullet 10^{-3}\ s^{-1}$ for Tb-LA at the given temperature (20°C) and surface pressure (15 mN/m). The temperature dependence of the reaction has been found to be very weak.9) The reaction was also insensitive to oxygen.9) This indicates that the reaction follows the ionic polymerization mechanism rather than radical polymerization.14-16)

References

1. Dubault, A.; Casagrande, C.; Veyssie, M. *J. Phys. Chem* **1975**, 79, 2254.
2. Rabe, J.P.; Rabolt, J.F.; Brown, C.A.; Swalen J.D. *Thin Solid Films* **1985**, 133, 153.
3. Tamura, H.; Mino, N.; Ogawa, K. *Thin Solid Films* **1989**, 179, 33.
4. Meller, P.; Peters, R.; Ringsdorf, H. *Colloid Polym. Sci.* **1989**, 267, 97.
5. Duran, R.S.; Zhou, H.C. *Polymer* **1992**, 33, 4019.
6. Peltonen, J.P.K.; He, P.; Rosenholm, J.B. *Thin Solid Films* **1992**, 210/211, 372.
7. Peltonen, J.P.K.; He, P.; Rosenholm, J.B. *Langmuir* **1993**, 9, 2363.
8. Bodalia, R.R.; Duran, R.S. *J. Am. Chem. Soc.* **1993**, 115, 11467.
9. Peltonen,J.; He, P.; Linden, M.; Rosenholm J.B. *J. Phys. Chem.* **1994**, 98, 12403.
10. Linden, M.; Peltonen, J.; Rosenholm J. *Colloids Surfaces*, **1995**, submitted.
11. Peltonen, J.P.K.; He, P.; Rosenholm, J.B. *J. Am. Chem. Soc.* **1992**, 114, 7637.
12. Peltonen, J.P.K.; Linden, M.; Györvary, E.; Fagerholm, H.; Eriksson, F. *Thin Solid Films* **1994**, 242, 88.
13. Linden, D.J.M.; Peltonen, J.P.K.; Rosenholm, J.B. *Langmuir* **1994**, 10, 1592.
14. Barraud, A.; Rosilio, C.; Ruaudel-Teixier, A. *J. Colloid Interface Sci.* **1977**, 62, 509.
15. Cemel, A.; Fort,Jr., T.; Lando, J.B. *J. Polym. Sci.* **1972**, 10, 2061.
16. Puterman, M.; Fort,Jr., T.; Lando, J.B. *J. Colloid Interface Sci.* **1974**, 47, 705.

MEASUREMENTS OF THE ELASTIC TENSOR OF A CRYSTALLINE MONOLAYER ON WATER SURFACE BY X-RAY DIFFRACTION

A. Renault, J.F. Legrand[1], C. Zakri, J.P. Rieu, F. Graner and B. Berge
Laboratoire de Spectrométrie Physique, URA08, BP87, 38402 ST Martin D'Hères-France
G. Grübel
European Synchrotron Radiation Facility, BP 220, 38043 Grenoble- France

Recently, two methods[1,2] have been developped to study the two-dimensional shear modulus of insoluble monolayers at the air-water interface. Abraham & al.[1] used direct method where the shear is applied to a solid monolayer, with an apparatus of about one centimeter, thus probing a polycrystalline structure. Their analysis gives a very low value for μ, the shear modulus : $\mu<0.1$ mN/m, for $C_{20}H_{41}OH$. On the contrary, Bercegol & al.[2], by bending an isolated 2D monocristal, obtain a very different value (~3000 mN/m, for the Young modulus of a monolayer of NBD stearic acid).

We present in this paper a third method which permits to determine the elastic constants using X-ray diffraction. It is well known that in 2D systems[3], the Bragg peaks are replaced by power-law singularities:

$$I \propto |Q-Q_0|^{-(2-\eta)} \qquad (1)$$

where the power law exponent is directly related to the Lamé coefficients λ and μ by the following relation[4] for hexagonal symetry:

$$\eta = ((k_BT/4\pi\mu)(\lambda+3\mu)/(\lambda+2\mu))Q_0^2 \qquad (2)$$

Recent progress[5] on high resolution grazing incidence diffraction at the ESRF allows to determine η, in the interesting range for monolayers. In addition, the high resolution enables also to measure the static monolayer compressibility modulus K, by studying the Bragg peak position Q_0 versus lateral pressure ($K= -1/2Q_0\, d\pi/dQ_0$). K is related to the Lamé coefficients λ and μ by the relation :

$$K= \lambda + \mu. \qquad (3)$$

With the two experimental determinations of η and K, we thus can use the two equations (2) and (3) to obtain λ and μ.

---

[1] second adress: ESRF, BP 220, 38043-Grenoble Cedex

We have studied a 1-decanol ($C_{10}H_{21}OH$) monolayer at the air-water interface. After deposition of a drop of solutions in dodecane with different concentrations (25%, 50%, 60%, 75% et 100% and alcohol in alkane) on the water surface, the drop gets spontaneously surrounded by a monolayer of pure alcohol6). Surface tension measurements show that the lateral pressure decreases of about 10 mN/m with the dilution of the alcohol in the range of the above mentioned concentration7).

Figure 1 shows the raw diffraction data for 1-decanol monolayer at T=4°C and 11°C. For each temperature, one displays two peaks with change in lateral pressure of 4.8mN/m. The melting transition is weakly first order at 14.3 (± 0.3)°C. The crystalline structure of the alcohol monolayer is hexagonal, the long axis of the molecules being vertical on average. We just recall that each point on diffraction data corresponds to the intensity integrated over 360 deg rotation of the trough. This was necessary to smooth the grain crystalline texture because the 2D crystals are very large5).

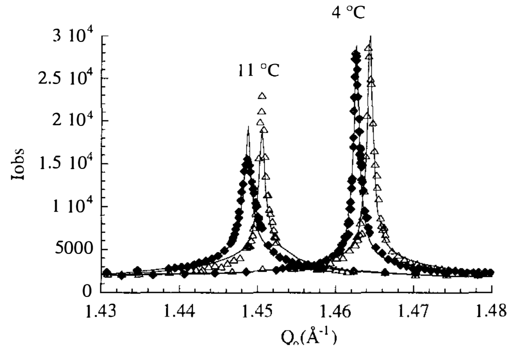

Figure1: Evolution of powder diffractogramms of 1-decanol monolayers at 4°C and 11°C with lateral pressure. Lines are the best fits. Δ: datas for pure decanol; ◆: datas for decanol in dodecane (50/50)

In Figure 1, one observes large shifts of the Bragg peaks with temperature and small shifts due to pressure changes. All Bragg peaks are analysed with a power law shape (continuous lines on fig.1). The best fit gives the position Q_0, the amplitude and the power-law exponent $-(2-\eta)$ (details in reference 4). Fig.1 reveals a clear broadening starting a few degrees below the melting transition.

Consequently, η increases with temperature. This indicates a softening of the lattice prior to melting. Table1 gives the results for η at 4°C and 11°C.

Figure 2 displays the position of the Bragg peak centers Q_0 versus surface tension at two temperatures 4°C and 9°C.

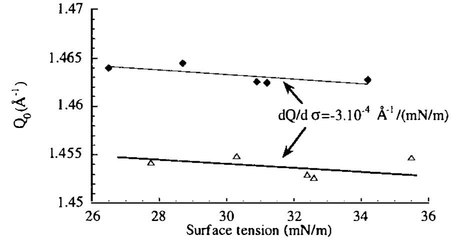

Figure 2: Position of the Bragg peak centers versus the surface tension at constant temperature (4°C and 9°C). Lines are the best fits. ◆: at 4°C; Δ : at 9°C

We expect a linear compressibility and the slope is equal to $dQ_0/d\sigma=-(3.10^{-4}+/-.510^{-4})$Å^{-1}/(mN/m). It appears that this value does not change appreciably between 4°C and 11°C, in the range of the uncertainty of our experiment. We can extract the modulus of compressibility K. Then knowing K and η, we can deduce λ and μ which determines completely the elastic tensor for this hexagonal 2D system. Table 1 shows the results at two different temperatures (4°C and 11°C).

T °C	η	K(mN/m)	μ(mN/m)	λ(mN/m)	E(mN/m)
4°C	0.36 ± .05	2440± 300	200 ± 80	2220 ±400	720 ± 300
11°C	0.41 ± .05	2420 ± 400	170 ± 50	2250± 400	630 ±200

Table 1: Results of η and elastic constants values obtained for 1-decanol monolayers at two temperatures (4°C and 11°C). K is the compressibility modulus, λ and μ the Lamé coefficients and E the Young modulus.

The values obtained for Young modulus in the 1-decanol monolayer (720± 300 mN/m at 4°C and 630± 200 mN/m at 11°C) are of the same order of magnitude as those measured by Bercegol &al.[2)] in NBD stearic acid monolayer (3600 ± 1300 mN/m), a chain with 18 carbons. Our results are compatible with the existence of a 2D crystal within the framework of 2D melting theories. The value of K is similar to the one we deduce from X-ray data by Barton &al.[8] in heneicosanol monolayers in the hexagonal phase. If we estimate the volumic compressibility (K'=K/l where l is a chain length =13.5Å), we found $K'=2.10^9$ Pa. This value agrees with different works on chain compounds like fluorinated chains oligomers constrained by hydrostatic pressure ($3\ 10^9$ Pa, see refence 9).

With the example of the 1-decanol, we have shown that high resolution X-ray studies associated with surface tension measurements, enable to determine the elastic constants of monolayers at the water-air interface. The precision of this method relies mainly on the quality of the spatial caracteristics of the X-ray beam and on the high coherence of the 2D crystalline lattice. This method could be increased with the use of channel-cut monochromator and analyser and may also be applied to structures of lower symetry.

BIBLIOGRAPHY

1) B.M. Abraham, K. Miyano, J.B. Ketterson and S.Q. Xu, J. Chem. Phys., 78,4776 (1983); B.M. Abraham, K. Miyano, J.B. Ketterson and S.Q. Xu, Phys. Rev. Lett., 51, 1975 (1983)

2) H. Bercegol and J. Meunier, Nature, 356, 226 (1992)

3) B. Jancovici , Phys. Rev. Lett. 19, 20 (1967), L. Gunther , Y. Ymry and J. Lajzerowicz, Phys. Rev. A 22, 1733 (1980).

4) D.R. Nelson, in "Phase Transitions and Critical Phenomena", Vol 7 (ed by C. Domb and J.L Lebowitz Acad. Press, 1983). K.J. Strandburg, "Two-dimensional melting" Rev. Mod. Phys. 60, 161 (1988).

5) B. Berge, O. Konovalov, J. Lajzerowicz, A. Renault, J.P. Rieu, M. Vallade, J. Als-Nielsen, G. Gruebel and J.F. Legrand, Phys. Rev. Lett., 73, 1652 (1994)

6) It was shown by Neutron reflectivity that the alkane does not come in the monolayer and stays in the reservoir drop: A. Renault, J.F. Legrand, J. Webster, D. Bucknall and J. Penfold, private communication.

7) A. Renault, O. Schultz, O. Konovalov and B. Berge, Thin Solid Films, 248, 47(1994)

8) S.W. Barton, B.N. Thomas, E.B. Flom, S.A. Rice, B. Lin, J.B. Peng, J.B. Ketterson and P. Dutta, J. Chem. Phys., 89, 2257 (1988)

9) E.Bellet- Amalric, J. F. Legrand, M. Stock-schweyer and B. Meurer Polymer 3 (1994)

EXPERIMENTAL STUDY OF THE BREAKAGE OF A TWO-DIMENSIONAL CRYSTAL

L.Pauchard, J.Meunier
Laboratoire de Physique Statistique de l'E.N.S.
(URA 1306 du CNRS, associé aux Universités PARIS VI et VII)
24 rue Lhomond 75231 Paris Cedex 05 France

In this short review, we summarize a study of the mechanical properties of two-dimensional crystals obtained in a Langmuir monolayer. Crystal shape and elasticity have allowed use to measure the Young's modulus of a single monocrystal, and also observe the coexistence between an instantaneous and a time-lag crystal-breaking mode when stress is applied.

The Kosterlitz-Thouless-Halperin-Nelson's predictions for two-dimensional solids, based on the idea of melting by dislocation unbiding, give a lower limit for Young's modulus. Langmuir monolayers are well adapted to compare real two-dimensional systems with this theory. The monolayers, we study at the free surface of water, are made of an insoluble amphiphilic molecule (stearic acid) including a fluorescent group (NBD) attached to the twelfth carbon of the aliphatic chain. The variation of the area accessible to the monolayer reveals a first order phase transition 1). Hence, during compression of the water surface, we observe, by fluorescence microscopy, a solid phase (area per molecule≈30 Å^2) coexisting with a liquid expanded phase (83 Å^2/molecule). In the liquid state, the molecule lies flat on the water surface, quenching the fluorescence of the NBD group, on the contrary an intense fluorescence is obtained when the NBD groups are lifted out of the water in the solid state. Recently, x-ray diffraction revealed a crystalline structure of this solid phase 2).

In the absence of impurities due to oxydation of the molecule, crystals are long rodlike with two parallel sides (more than 1mm long and 5 to 50 µm wide) 3). Such a shape allows micromechanical measurements on a single crystalline rod. Using 3 silanised glass fibers (10 µm diameter), perpendicular to the water surface and 0.5mm separated, it was possible to isolate then to apply a force to a rod. Bending a crystal in the plane of the water, then relaxing the constraint, the rod becomes instantaneously straight again. This absence of plastic deformation allows us to deduce the Young's modulus of the two dimensional NBD-stearic crystal from several plots of the extend of bending versus the applied force 4). The value obtained, 3660±1300mN/m, is in agreement with the Kosterlitz-Thouless theory on the melting of a two dimensional crystal, which predicts a lower value for the Young's modulus (for our crystal 700mN/m) 5,6).

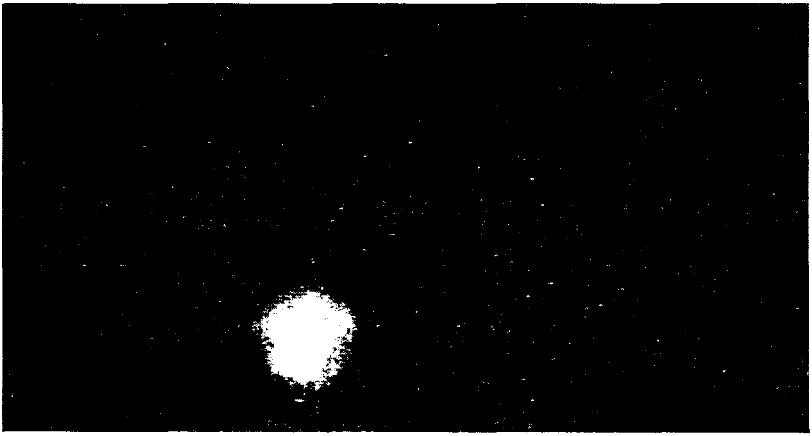

Figure 1: fracture of a rod (50 µm wide) after a 3 points flexion.

During these measurements, it was found that a rod under a bending stress breaks after a delay time t_B (Fig.1). To study the breakage time, statistics were done by measuring t_B for different strains τ or rates of extensions of the external line of the rods under bending 7). The different breaking times measured for a given value of τ are grouped around their mean value $\overline{t_B}$. Since, most of the observed dispersion on the experimental values of t_B results from the low experimental accuracy in τ, the time-lag breaking appears to be a well-defined function of the applied stress. The breakage time $\overline{t_B}$ versus $1/\tau^2$, on a semi-logarithmic scale, is shown in Fig.2. The plot is linear except for large $\overline{t_B}$ because of an experimental artefact 7,8). At high strain, the time-lag breaking remains however we also observe instantaneous breaking 7). Moreover, it has been observed that a rod keeps the memory of the applied strain that is, if the strain is released after a time $t_1<t_B$ and then applied again after a duration of t_3, the rod will break after a delay t_2 independent of t_3 and such that $t_1+\overline{t_2}=\overline{t_B}$.

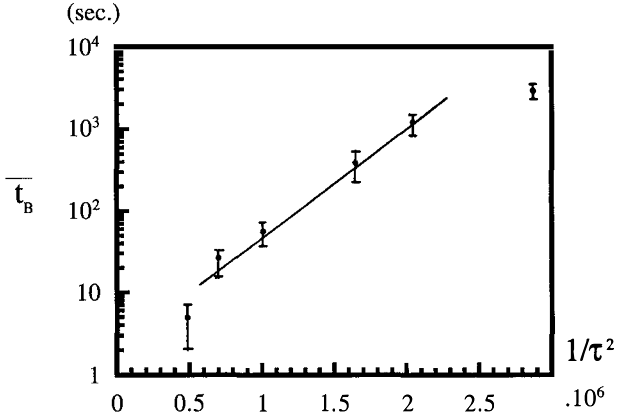

Figure 2: mean time-lag breaking $\overline{t_B}$ versus $1/\tau^2$ on a semilogarithmic scale. A point on this figure corresponds to a statistic where about 20 rods were broken.

The complexities of the mechanisms of fracture and the enormous variety of material dependent effects has not yet allowed for the formulation of a universally encountered fracture behaviour. Several explanations can be given to understand our phenomena.

First, the linear plot in Fig.2 is in agreement with a calculation of Pomeau [9)], suggesting that the time-lag breaking results from the time of nucleation of a crack. This nucleation time is proportional to $\exp(-c^d/\tau^d)$, with d=2 for a two-dimensional model and d=4 in a three-dimensional model (c being a molecular constant). The large exponent for three-dimensional crystals indicates that the range of strain giving observable times of nucleation is too small to be observed, contrary to the case of a two-dimensional crystal. However, the nucleation of a crack is due to a thermal process. Consequently, within the Pomeau's theory, the mean value of the time for nucleation is t_n but the probability of nucleation is given by a Poisson law. We do not observe this law in our experiments: the breaking time is well-defined, suggesting that the breaking results from the percolation of a large number of cracks, N. According to the Poisson law, the distribution width for the time of nucleation of one crack is t_n. ;However a crack percolation model predicts a width, $t_n/\sqrt{N}$. Our experimental results are best explained by the later, with N>>100.

Another way to explain the breaking mechanism considers the migration of point defects (vacancies, impurities) towards the region of largest stress, through the constraint yield. This assumption implies a plastic deformation which we did not observe, within the 1 μm resolution of the microscope.

Finally, another suggestion results from considering the very anisotropic growth and optical properties of the solid domain. The appearance of a solid domain melting under the effect of a prolongated illumination, suggests that a solid domain is made of long fibers, the molecular forces being very different in the direction of the length and in the perpendicular direction. Considering this fibrous structure at the molecular scale, the process leading to the breaking is probably a succession of a large number of elementary processes. The elementary process could be the breaking of a fiber under stress, producing the progress of a crack from the edge of the domain. When the size of this crack reaches the critical size satisfying the Griffith critical condition, it propagates quickly [10)].

In addition, we have been interested in the effects of a prolongated bright light beam focused on a crystal. We have noticed that, for a rod in which the pressure remains constant, illumination implies the nucleation of local volumes of liquid at some points distributed at random inside the solid, leading to the process of melting (Fig.3). Whereas, for a crystal under a bending stress (i.e. corresponding to an inside stress gradient) melting occurs along the neutral axis of the rod (Fig.4), which seems paradoxical with the Lifschitz's theory 11). However, our phenomenon seems to require the formation of impurities, in the crystal, generated by light and the presence of oxygen in the air . In this case, strictly two-dimensional theories of melting 12) can not be applicable here. Experiments are in progress to find the mechanism explaining these observations.

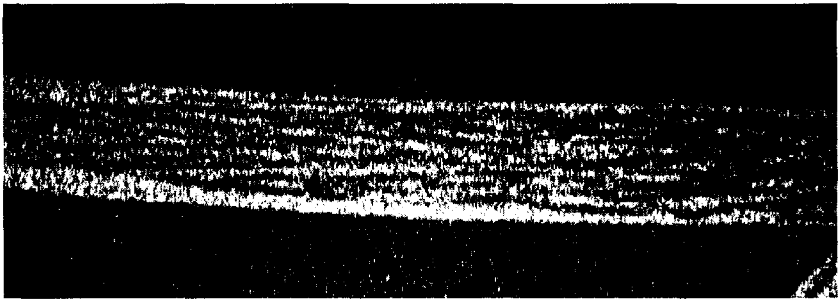

Figure 3: melting of a rod (about 20 μm wide) without stress.

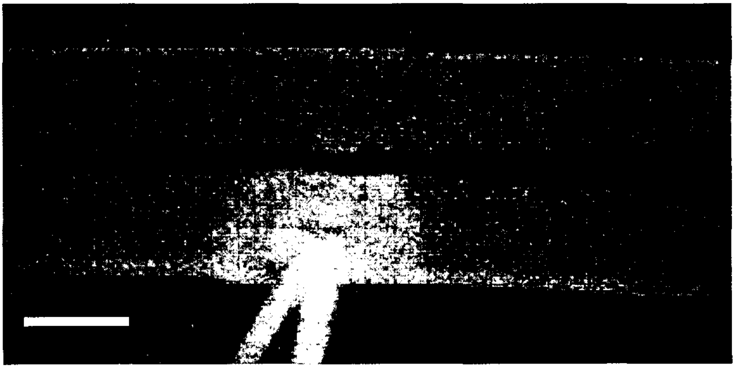

Figure 4: melting of a rod under a bending stress: a volume of liquid has been nucleated within the solid, along the neutral axis of the crystal (bar=20 μm)

References
1- H.Bercegol, F.Gallet, D.Langevin, J.Meunier, J.Phys.(Paris) **50** (1989) 2277
2- C.Flament, K.Graf, F.Gallet, H.Riegler, Thin Solid Films **243** (1994) 411
3- H.Bercegol, J.Phys.Chem. **96** (1992) 3435
4- H.Bercegol, J.Meunier, Nature (London)**356** (1992) 226
5- D.R. Nelson, B.I. Halperin, Phys. Rev. B **19** (1979) 2457
6- D.R. Nelson in "*Phases transitions and critical phenomena* " Vol7 (eds C. Dombs and J.L. Lebowitz, academic, London, 1983)
7- L.Pauchard, J.Meunier, Phys.Rev.Lett. **70** (1993) 3565
8- L. Pauchard, J. Meunier, Progr. Colloid. Polym. Sci. **98** (1995), in press.
9- Y. Pomeau, C.R. Acad. Sci. (Paris) **314** (1992) 553
10- A.A. Griffith, Philos.R.Soc.London A **221** (1920) 163
11- I.M. Lifschitz, L.S. Gulida, Dokl. Akad. Nauk. (USSR), **87** (1952) 377
12- J.M. Kosterlitz, D.J. Thouless, J.Phys.C **6** (1973) 1181
- B.I. Halperin, D.R. Nelson, Phys.Rev.Lett. **41** (1978) 121
- A.P.Young, Phys.Rev.B **19** (1977) 1855

LIGHT SCATTERING FROM A BUCKLED BIDIMENSIONAL SOLID

Arnaud SAINT-JALMES, François GRANER(*), Michel ASSENHEIMER
and François GALLET
Laboratoire de Physique Statistique de l'Ecole Normale Supérieure
(U.R.A. 1306 associée au C.N.R.S. et aux Universités Paris 6 et Paris 7)
24, rue Lhomond - 75231 Paris cedex 05 - France
(*) C.N.R.S. URA 8, Laboratoire de Spectrométrie Physique,
Université Joseph Fourier, BP 87, 38402 Saint-Martin d'Hères Cedex, France

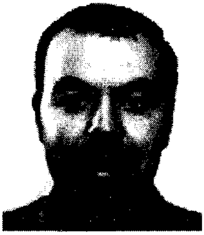

Abstract

Above a surface pressure threshold Π_c, we detect a buckling instability in the low temperature solid phase of a C_{18}-C_{18} phosphocholine monolayer spread at the air-formamide interface. Light scattering provides measurements of the threshold value $\Pi_c = 7\ mN.m^{-1}$, and of the instability wavelength ($\lambda \approx 38\ \mu m$) and amplitude ξ (a few nm). We report also preliminary results on temporal evolution of this phenomenon. The spectrum of this deformation shows several diffraction peaks. From their intensities and their positions, we conclude that these peaks are odd harmonics of a non-sinusoidal deformation. Main results of a theoretical model taking into account dipolar interactions and stress anisotropy are also presented.

1. Introduction

Comparing Langmuir film behaviour on different liquids gives information about the effective role of the substrate on the microscopic film structure and on specific interactions between the polar heads and the substrate molecules.

Amongst other liquids, formamide can be used as an alternative non-aqueous solvent to support amphiphilic monolayers [1-3]. Advantages are its high polar moment and dielectric constant, respectively 3.4 Debye and 109.5 at 20°C (versus 1.85 and 80.2 for water). Its solvation properties, hydrogen bonds, surface tension (58.2 $mN.m^{-1}$ at 20°C, versus 73 $mN.m^{-1}$ for water), and molecular stability make it as suitable as water for spreading

Langmuir films. Recently, the phase diagram of 1,2-Distearoyl-sn-Glycero-3-Phophatidylcholine (DSPC) on formamide has been determined from surface isotherms and fluorescence microscopy observations 4). One recovers the same variety of phases as on water (gas, liquid, solid and mesophases).

A feature specific to a DSPC film spread on formamide is the spontaneous buckling of the low temperature solid phase above a surface pressure threshold Π_c 5). This undulation has never been observed on water except on a polymerized monolayer 6).

Grazing incidence X-ray diffraction was performed to determine the structure of this solid phase 7). The chains are organized on an oblique lattice, and their tilt, measured from Bragg rod scans, is about 35°. No structural change is observed when the surface pressure is varied from 1 to 38 $mN.m^{-1}$. In the solid phase, the area per molecule is $A=46$ $Å^2$, and the compression modulus $\kappa = -A d\Pi / dA = 3500$ $mN.m^{-1}$ is very large compared to water ($\kappa = 500$ $mN.m^{-1}$). Two consequences of this specific behaviour must be pointed out : no phase transition can interfere with the buckling instability and the high rigidity of this phase seems to be an important ingredient for the occurence of the instability.

The typical wavelength of buckling (a few μm) makes light scattering experiments relevant to characterize this deformation. Here we present first results of these experiments showing scattered peaks and dynamical evolution of the instability. Elements of theory and discussion which have been presented elsewhere 5) are briefly recalled.

2. Direct observation of buckling

Figure 1 is a scheme of the experimental set-up showing our home-made Langmuir trough with its two barriers symmetrical compression system. The surface pressure is measured with a filter paper suspended from a Wilhelmy balance.

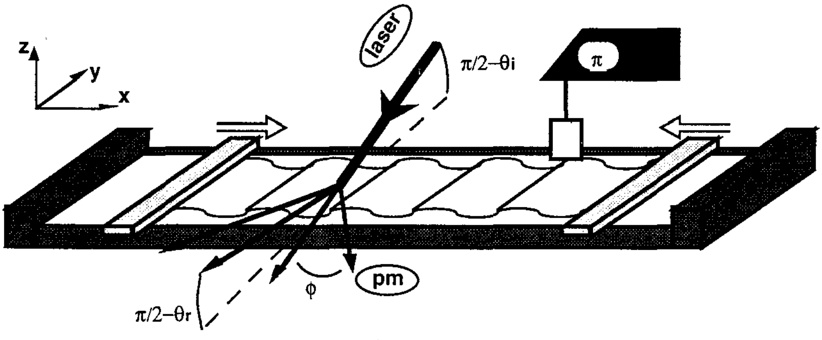

Figure 1. Sketch of the experimental set-up.

In the solid phase (T<19°C), uniaxial compression creates above the pressure threshold Π_c an undulation roughly parallel to the orientation of the barriers and constant both in space and time. This buckling instability is directly visible by shadowgraphy (fig. 2) with an intensified camera (SIT 68, Dage-MTI) and a standard x20 or x40 objective : the roughly periodic deformation of the surface acts as a serie of alternate convergent and divergent dioptres. A characteristic length scale appears on these images of the orders of 10 μm and the deformation amplitude is a few nm (estimated from the distance between focalisation planes).

However, extracting precise information from these images is delicate and more quantitative analysis will come from light scattering.

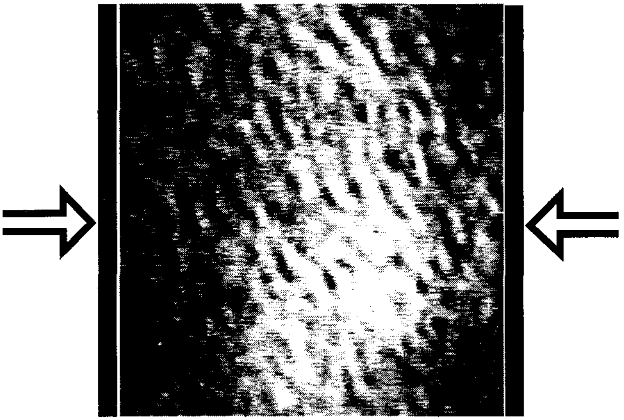

Figure 2 . Shadowgraphic image of buckling. The Field is 100x100 μm. Arrows indicate the direction of compression.

3. Light scattering experiments

Using the buckled film as a grating, we measure the spectrum of the undulation by scattering the $\lambda_0=488$ nm line of a 35 mW argon laser. The beam, driven through a monomode optical fiber, hits the horizontal xy -plane with incident angles $\theta_i=35^\circ$ and $\phi=0^\circ$. We detect the signal scattered by the monolayer with a photomultiplier placed off the specular reflection, at $\theta_r=35^\circ$ and $\phi \neq 0$.

At $\phi \ll 1$, the intensity scattered per unit solid angle $dI/d\Omega$ is related to the amplitude of the deformation z by [8-9]:

$$\frac{1}{I_r}\frac{dI}{d\Omega} = S\left|\xi_q\right|^2 \frac{k^4}{4\pi^2}\cos^3\theta_i \quad \text{where } z = \xi(x,y) = \sum_q \xi_q \exp(i\vec{q}.\vec{r})$$

k is the incident wavevector, q is the transfer wavevector ($|q| = \frac{4\pi}{\lambda_0}\sin\frac{\phi}{2}\sin\theta_i$) and I_r the specular reflected intensity.

All the experiments were performed at T=10°C.

a) Dynamical properties

First, the photomultiplier is set-up in a fixed position (ϕ=4°, q=7360 cm^{-1}). We exert small compression steps ($\Delta A \approx 1$ Å^2 during a few seconds) and we detect the scattered intensity I_{scat} above a pressure threshold Π_c^{exp}. Figure 3 shows the temporal behaviour of I_{scat} during and after a compression step. From a peak value reached at the end of compression, I_{scat} relaxes and two regimes can be separated in this relaxation. In the first minutes, I_{scat} quickly decreases, probably due to rearrangements of solid domains. After this fast decay, I_{scat} slowly decreases on a longer time scale. After 10 hours, I_{scat} reaches a quasi-equilibrium plateau value. Between 10 hours and 60 hours, the variation of I_{scat} is 35 %. Note that this may not be directly related to buckling relaxation (it may be due to evaporation, degradation or solubility of the monolayer...)

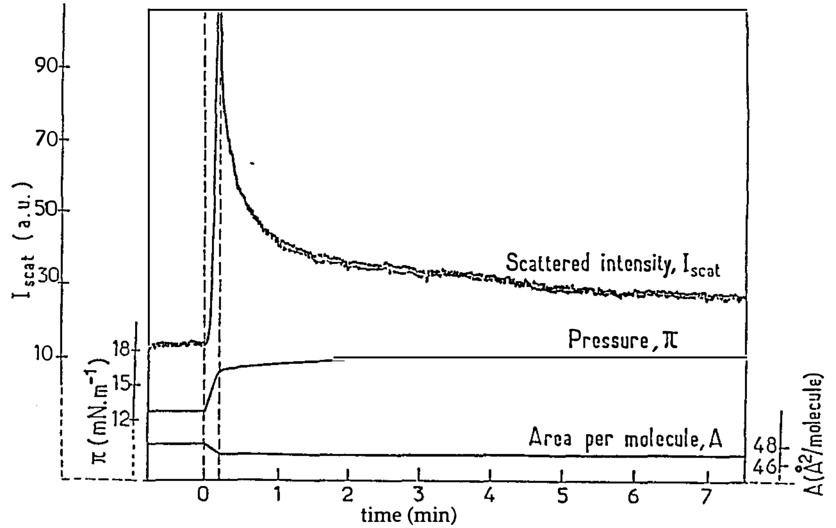

Figure 3 . Pressure Π, scattered light intensity I_{scat} and area per molecule A versus time t during and after a compression step.

This plateau value is zero for 4 $mN.m^{-1} < \Pi < 7\ mN.m^{-1}$ and strictly positive for $\Pi > 7$ $mN.m^{-1}$. Thus the threshold for permanent buckling is about 7 $mN.m^{-1}$.

These dynamical properties are strongly influenced by the history of the layer and especially by the relaxation time between two successive compression steps. For a same compression step, the peak value and relaxation time scale are smaller if the monolayer has previously relaxed for a longer time. However, the plateau value is roughly the same. Also, after decompressing the monolayer to $\Pi \approx 0$ $mN.m^{-1}$ and waiting a few hours before recompression, the plateau is reached faster than for the "fresh" monolayer. We conclude that some peculiar rearrangements occur during the first hours. Further compression and recompresssion lead to reproducible results. In the following experiments, the monolayer has been allowed to relax long enough to get reproducible results.

In figure 4, we plot the scattered intensity versus the surface pressure Π for different relaxation times Δt after each compression step. The time interval between two successives steps is 3h30. I_{scat} is a linear function of Π and the fit crosses the Π-axis at the same value $\Pi_c^{exp}=7\pm1$ $mN.m^{-1}$, whatever Δt. This can be extrapolated to infinite time and agrees that $\Pi_c^{exp}=7\pm1$ $mN.m^{-1}$ is the threshold value for permanent buckling.

Since I_{scat} is continuous at Π_c^{exp}, we believe that this instability is second-order.

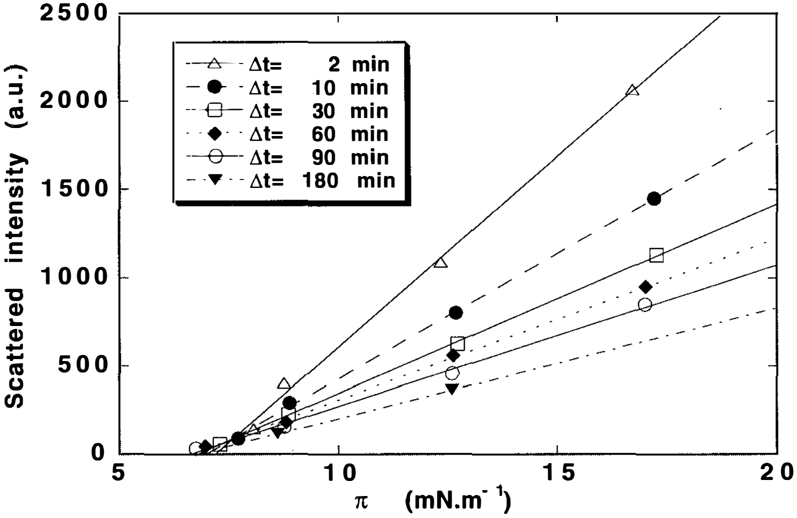

figure 4. Scattered intensity vs π at various relaxation time Δt.

b) Spectrum

The spectrum of the buckled deformation is obtained by varying ϕ when the intensity has reached its equilibrium value. A reference scan is performed in the solid phase at $\Pi \approx 0 mN.m^{-1}$. This reference is reproducible and is substracted from scans at higher pressures. Because of specularly reflected light at small angles, we cannot explore the $|q| \leq 2.5\ 10^3\ cm^{-1}$ region. Figure 5 shows a typical scan at $\Pi=8.6\ mN.m^{-1}$.

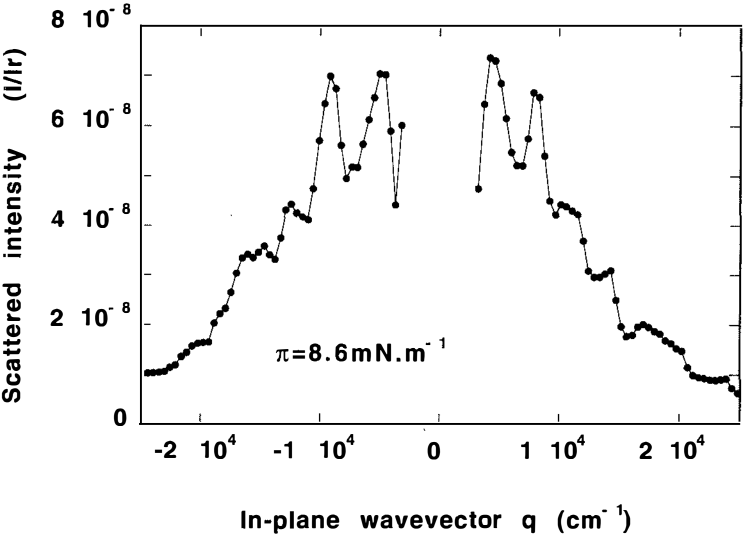

figure 5. Scattered intensity vs in-plane wavevector q at $\pi=8.6\ mN.m^{-1}$.
Line shown to guide the eye.

Over a symmetrical decrease, we see roughly periodic modulations in the intensity ratio I/I_r. Rather than succesive diffraction orders, we believe that these peaks correspond to harmonics of a non sinusoidal deformation above the threshold. By plotting the peak positions versus peak rank, it appears that they are odd harmonics of a fundamental mode at $q_1 \approx 1650\ cm^{-1}$ (peak positions averaged on many spectrums are $q_3 \approx 5100\ cm^{-1}$, $q_5 \approx 8650\ cm^{-1}$, $q_7 \approx 11600\ cm^{-1}$, $q_9 \approx 14700\ cm^{-1}$, $q_{11} \approx 18000\ cm^{-1}$). No clear dependence of these positions nor of the spectrum shape can be detected by varying the pressure.

From these scans, it is possible to extract a wavelength and an amplitude of the buckled state : λ_{exp}=38 μm and $\sqrt{<\xi^2>}$ = 2 nm at π=8.6 mN.m^{-1}. These values have the same magnitude as those estimated from direct microscopy.

3. Theoretical approach : dipolar interactions and anisotropic effects

Here, we recall the main results of a theoretical model and discussion which has been presented elsewhere 5).

Milner et al. 10) have shown that, in a fluid phase, buckling is a first-order instability and should always occur for a negative surface tension threshold γ_C. We have modified their model by adding vertical destabilizing effects of dipolar interactions to classical stabilizing effects of gravity and surface tension (bending energy can be neglected) and we have shown that for a single-mode deformation of small amplitude, buckling is a second-order instability and occurs at a positive surface tension threshold γ_C.

We calculated γ_C= 6 mN.m^{-1}, i.e Π_c^{theo}=52 mN.m^{-1} for formamide. Considering that the dipoles are locally normal to the buckled surface or vertical along the *z* direction does not noticeably change these predictions.

This theoretical pressure threshold is much larger than Π_c^{exp}=7 mN.m^{-1}. These two values can be reconciled by introducing stress anisotropy : in a solid phase, we can no longer use the isotropic concept of pressure and we must define a 2D-surface stress tensor Π_{ij} which has its principal directions along the x and y direction 5,11). In its minimum energy position, the filter paper is more sensitive to Π_{yy} while the theoretical value for the threshold corresponds to Π_{xx}. We expect $\Pi_{yy} < \Pi_{xx}$, which is consistent with $\Pi_c^{exp} < \Pi_c^{theo}$.

The predicted wavelength at the threshold λ_{theo}= 24 μm is smaller than the measured one. Note that a possible wavelength variation close to the threshold is not considered here.

A complete theory should also take into account, for example, the presence of different solid domains with various orientations and non linear coupling between all unstable modes.

4. Conclusions and perspectives

A DSPC monolayer spread on formamide at T<19°C is in a crystalline phase. In this phase, strong interactions between formamide and polar heads lead to a high stability of the monolayer and a large compression modulus. As a consequence, buckling occur before collapsing.

Although buckling is directly observable by microscopy, light scattering is more adapted for a quantitative characterization. We have shown that dynamical properties of buckling depend on molecular rearrangements at short and long time scale. Threshold, wavelength and amplitude are measured by this method. We also conclude that detected diffraction peaks are odds harmonics of a fundamental mode of a non-sinusoidal deformation.

A simple theoretical model introducing vertical destabilizing effects of dipolar interactions and stress anisotropy is consistent with experimental results.

We are optimizing the experimental set-up to scan smaller q with better resolution. We expect to understand the onset of the instability (q-dependence), the evolution during compression and the high pressure region (transition to the collapsed state).

To test the validity of the model, we plan to measure the stress anisotropy by exciting capillary waves in two orthogonal directions. Preliminary results show that the surface pressure is different in this phase from the one measured by a Wilhelmy balance. It is larger in the direction of compression than in the perpendicular one.

1) S.P. Weinbach, K. Kjaer, J. Als-Nielsen, M. Lahav and L. Leiserowitz, J. Phys. Chem. 97 (1993) 5200.

2) S.P. Weinbach, D. Jacquemain, F. Leveiller, K. Kjaer and L. Leiserowitz, J. Am. Chem. Soc. 115 (1993) 11110.

3) S.P. Weinbach, K. Kjaer, W. Bouwman, G. Grübel, J.F. Legrand, J. Als-Nielsen, M. Lahav and L. Leiserowitz, Science 264 (1994) 1566.

4) F. Graner, S. Perez-Oyarzun, A. Saint-Jalmes, C. Flament et F. Gallet, J. Phys. II France 5 (1995) 313-322

5) A. Saint-Jalmes, F. Graner, F. Gallet, B. Houchmandzadeh, Europhys. Lett. 28(1994) 565.

6) L. Bourdieu, J. Daillant, D. Chatenay, A. Braslau, and D. Colson, Phys. Rev. Lett. 72 (1994) 1502.

7) A. Saint-Jalmes, F. Graner, F. Gallet, P. Nassoy, M. Goldmann, submitted to Chem. Phys. Lett.

8) D. Langevin in *Light scattering by liquid surface and complementary techniques* , edited by D. Langevin. Surfactant science series volume 41 (M. Dekker) (1992) p. 20 and references therein.

9) P. Croce , J. Optics (Paris) 8 (1977) 127-139.

10) S.T. Milner, J.-F. Joanny and P. Pincus, Europhys. Lett. 9 (1989) 495.

11) L. Landau and E. Lifchitz, Theory of Elasticity, Pergamon Press, Oxford 1984.

Phase diagram and collapse of a diacetylenic Langmuir film.

C. Gourier[†], J. Daillant[†], G. Zalczer[†], D. Chatenay[††,*] and A. Braslau[†]
[†]*Service de Physique de l'Etat Condensé, CEA-Saclay*
F-91191 Gif-sur-Yvette Cedex, FRANCE
[††] *Institut Curie, Section de Physique et Chimie, Laboratoire PSI*
UA CNRS 1379 et Université Paris VI,
11, rue Pierre et Marie Curie, F-75321 Paris Cedex 05, FRANCE

I. INTRODUCTION.

Amphiphilic monolayers spread at the air-water interface and compressed to beyond the equilibrium spreading pressure of coexistence with the bulk phase (ESP), are metastable and "collapse". Despite considerable effort neither the role of dimensionality and of the range of interactions on molecular ordering nor the mechanisms of collapse have been fully elucidated. The most likely routes to the bulk phase are a slow nucleation and growth process above a pressure $\Pi_{collapse}$ [1] (intermediate trilayer and multilayer states have been observed [2,3]) and, if the compression rate is high, a fracture process at $\Pi_{fracture} > \Pi_{collapse}$. The formation of trilayer structures has been suggested to arise from the buckling and folding of the monolayer [4], although the corresponding energies [5] and wavelengths are probably too large [6]. If a nucleation and growth process is to be retained, the solid bulk phase can either form at defects already present in the monolayer [5], or by homogeneous nucleation [1]. The rate of collapse depends, in particular, on the temperature, the pH [7] and the nature and concentration of the cations in the subphase [8]. The collapse is expected to be strongly dependent on the initial state of the monolayer, and the choice of the solvent as well as the deposition procedure are essential in obtaining reliable results.

10,12 pentacosadiynoic acid (PCA) is a diacetylenic amphiphile that can be polymerized under U.V. irradiation [9]- [11]. Polymerizable diacetylenic films have attracted much attention since the work of Wegner [12] due to their potential applications. In the present context, the PCA presents the advantage of forming at low pressures on water very stable trilayers that can be studied in detail. The film can also be stiffened by polymerization. In this latter case, the much more stable monolayer buckles. All the collapse processes can therefore be studied with this same material.

Collapsed films are highly inhomogeneous. Ignoring this inhomogeneity can lead to serious misinterpretations. In this study we used Brewster angle microscopy (B.A.M.) to image the texture of the films in situ, and atomic force microscopy (A.F.M.) on transferred films when a better resolution was desirable (with the risk of structure or texture change during transfer), together with pressure-area isotherm and x-ray scattering measurements.

II. THE 10-12 PENTACOSADIYNOIC FILM ON A BASIC BUFFER SUBPHASE.

A basic subphase stabilizes the monolayer with respect to tri- or multi-layer growth (see below) [11]. Isotherms of PCA spread on a sodium tetraborate buffer (pH=7.5) at different temperatures ranging between $17°C$ and $30°C$ are given in fig.1. An expanded phase is formed at a high molecular area. The pressure in the expanded phase starts to increase slowly at about $0.80nm^2/molecule$ to reach a plateau of transition (first order transition) towards a more condensed phase. At a molecular area of about $0.3nm^2/molecule$, the pressure increases again in the condensed phase. Finally the monolayer collapses at a pressure higher than $30mN/m$. X-ray reflectivity experiments have been performed at room temperature in the expanded phase: the overall thickness of the monolayer is $1.76nm$, with $0.70nm$ for the upper alkyl section, $0.26nm$ for the lower alkyl section, $0.4nm$ for the diacetylenic rod, and $0.4nm$ for the headgroup thickness. The expanded phase appears to be rather disordered.

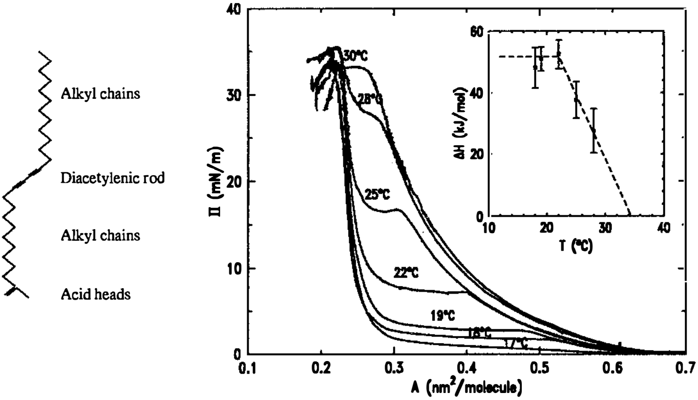

fig.1: *left: schematic of the PCA molecule; right: surface pressure - molecular area isotherms for PCA on a basic buffer and a 1:9 ethanol hexane mixture as spreading solvent at different temperatures Insert: enthalpy of transition.*

The chain thickness in the condensed phase ($2.1nm$) is larger than in the expanded phase. The nucleation and growth of long (up to $600\mu m$), narrow, ramificated domains can be observed by Brewster angle microscopy. Some of the domains appear to grow from a bright nucleus (fig.2 left). By carefully controlling the pH and the temperature, and using the 1:9 ethanol/hexane spreading solvent mixture, a condensed film with very long range order ($1mm$) is systematically observed (fig.2 right). This highly ordered condensed film is ideal for the polymerization.

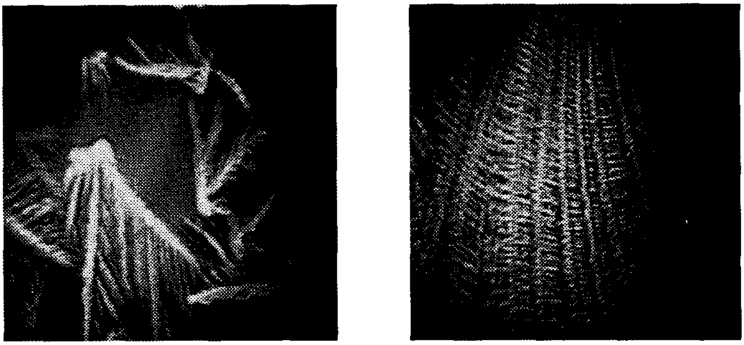

fig.2: *Brewster angle microscopy image on the expanded condensed transition plateau. left: nucleation of domains, right: highly ordered domains at the low area end of the plateau. The image size is* $600\mu m \times 600\mu m$.

III. POLYMERIZATION ON A BASIC BUFFER.

The PCA was exposed to U.V. radiation both in the expanded phase and in the condensed phase. To avoid ozone oxidation (leading to a pressure increase after a few minutes exposure) the polymerization was performed under an Argon atmosphere. In contrast to the expanded phase, a long range polymerization is evidenced in the condensed phase. This suggests that the film has to be condensed and organized enough for polymerization. This is in some way in agreement with the often quoted topochemical nature of the polymerization reaction [9]-[11].

The film area at constant pressure diminishes (about 10%) upon polymerization suggesting a molecular rearrangement, in agreement with the x-ray measurements. The polymerized film can be compressed without collapsing to a much higher pressure than the unpolymerized film ($> 40mN/m$). Grazing incidence x-ray scattering has been performed on a polymerized film compressed to $15mN/m$. A broad peak at $q_x = 4 \times 10^{-4} nm^{-1}$ can be attribuated to the buckling of the film in the third dimension [6] which has been observed with other polymerized systems and should be characteristic of such covalently tethered films without intrinsic tension.

IV. COLLAPSE OF THE 10-12 PENTACOSADIYNOIC FILM ON PURE WATER.

Surface pressure - molecular area isotherms for PCA film on a pure water subphase at room temperature using chloroform as spreading solvent are shown in fig.3 for different speeds of compression. The first domains of condensed phase, appearing into the gas phase at the very large molecular area of $20nm^2/molecule$, could be observed by B.A.M.. The pressure starts to increase at $0.32nm^2/molecule$ up to a bump at a molecular area of $0.256 \pm 0.005nm^2$. The pressure of the bump depends on the speed of compression. Moreover, for pressures below the bump pressure. the film is not stable. If the compression stops, the pressure slowly decreases due to collapse. The existence of trilayer domains in the gas - condensed phase coexistence region has been demonstrated using x-ray reflectivity experiments, atomic force microscopy and optical microscopy images even at molecular areas higher than $0.32nm^2/molecule$. X-ray reflectivity has been performed at the constant pressure $\pi = 3mN/m$, and a molecular area slowly decreasing from $0.29nm^2/molecule$ to $0.22nm^2/molecule$ during the 12 hour long experiment. The thickness of the film ($6.75nm$) is consistent with a trilayer. The corresponding χ^2 value of the fit is however rather high (11). This is because the film is not uniform, as can be observed on A.F.M. images (fig.4) obtained on a film deposited at $5mN/m$, but rather consists of rectangular trilayer domains.

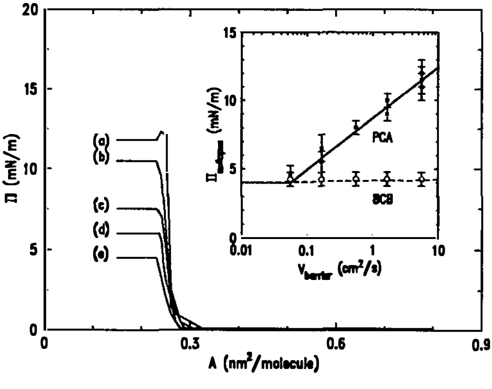

fig.3: *Surface pressure - molecular area isotherms for PCA on pure water subphase at room temperature using chloroform as spreading solvent. The compression velocity is (a)* $0.17nm^2/molecule/s$, *(b)* $0.051nm^2/molecule/s$, *(c)* $0.017nm^2/molecule/s$, *(d)* $0.051nm^2/molecule/s$, *(e)* $0.0017nm^2/molecule/s$. *Insert: The pressure of collapse as a function of velocity for PCA and for the liquid-crystal 4-cyano-4'-n octylbiphenyl (8CB).*

The χ^2 value can be significantly improved by including a coexistence with a monolayer in the model. Trilayers could also be obtained by deposition of 3-dimensional PCA crystals (no spreading solvent) on water. In the latter case, we do not observe a monolayer, suggesting that the trilayer is the stable phase in equilibrium with the crystal at very low pressure, i.e. the monolayer would always be metastable. A.F.M. images shown in fig.4 obtained respectively at higher and lower pressure than that of the bump, show very different domains. In particular, after the bump (for an area $0.2nm^2/molecule$), the domains are smaller and thicker. This indicates that the collapse occurs at the bump which corresponds to the activation barrier necessary to create multilayer nuclei from the trilayers. Indeed, the smaller size and wide thickness distribution of the multilayer nuclei suggest that their origin is the break or folding of the previously observed trilayers.

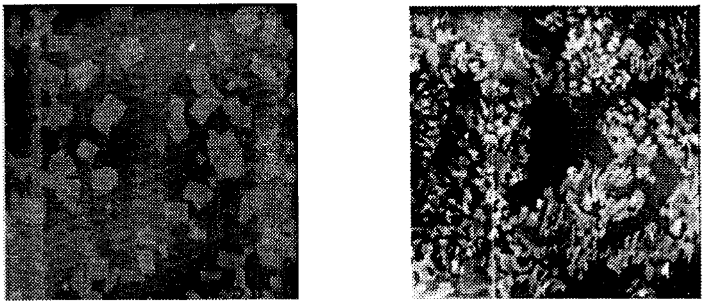

fig.4: *Atomic force microscopy image of the trilayer (left) and the collapsed film (right) deposited on a silicon wafer. The image size is* $100\mu m \times 100\mu m$.

The collapse pressure of PCA is given in fig.3 as a function of the compression velocity. Remarkably, the collapse pressure is linear in the logarithm of the compression velocity:

$$\Pi = \Pi_0 + \theta lnV \qquad (1)$$

with $\theta = (1.63 \pm 0.13)mN/m$. Interestingly, another material forming trilayers at the air-water interface, the liquid crystal 4-cyano-4'-n octylbiphenyl (8CB) does not exhibit any speed dependence of the collapse pressure. 8CB is in a smectic A phase at room temperature. This suggests that in the case of 8CB the trilayer domains can form and/or grow freely whereas the formation and/or growth of "solid" multilayer domains of PCA requires to overcome some additional energy. Briscoe and Evans [13] have studied the sliding friction between two monolayers of fatty acid deposited on molecularly smooth mica substrates using a friction apparatus. They also found $P = P_0 + \alpha lnV$ where P is the pressure applied to the film and $\alpha = 0.42MP$, close to the pressure in the monolayer obtained by dividing the surface pressure θ by the monolayer thickness ($0.77MP$). A possible interpretation is therefore that the growth of multilayers gives rise to a sliding frictional force between layers which is more important at higher velocities. The dependence of the collapse pressure on V can also be due to the nucleation of more and more multilayer islands with increasing velocity.

V. CONCLUSION.

In this study, different processes by which an overcompressed monolayer escapes into the third dimension have been identified. Compressing the polymerized network, buckling in the third dimension was observed at a surface pressure $\pi = 15mN/m$ and irreversible collapse at $\pi > 40mN/m$. With an unpolymerized film and pure water as subphase, intermediate trilayer domains have been evidenced at very low pressure ($< 1mN/m$). This trilayer is the stable phase in equilibrium with the crystal. Upon further compression the film breaks into multilayer fragments, with a logarithmic dependence of the collapse pressure on the compression velocity. We aim at describing this process in detail, and in particular the possible role of structural defects during the growth.

* Present address: LUDPC Institut de Physique, 3 rue de l'université, F67084 Strasbourg.
e-mail: gourier@amoco.saclay.cea.fr, daillant@amoco.saclay.cea.fr

REFERENCES

[1] R.D. Smith and J.C. Berg, J. Colloid Interface Sci. **74** 273 (1980).
[2] M. Lundquist, Chem. Script.**1** 197 (1971).
[3] J. Daillant, L. Bosio, B. Harzallah, and J.J. Benattar, J. Phys. II **1** 149 (1991).
[4] H.E. Ries, Jr. Nature **281** 287 (1979).
[5] E.S. Nikomarov, Langmuir **6** 410 (1990).
[6] L. Bourdieu, D. Chatenay, J. Daillant and D. Luzet, J. Phys. France **4**, 37 (1994).
[7] R. Aveyard, B.P. Binks, N. Carr, and W.A. Cross, Thin Solid Films **188** 361 (1990).
[8] E. Pezron. P.M. Claesson, J.M. Berg, and D. Vollhardt, J. Colloid Interface Sci. **138** 245 (1990).
[9] D.Day and J.B. Lando, macromolecules **13** 1483 (1980).
[10] C.A.J. Putman,H.G. Hansma, H.E. Gaub, and P.K. Hansma, Langmuir **8**, 3014 (1992).
[11] B.M.Goettgens, R.W. Tillmann, M. Radmacher and H.E. Gaub, Langmuir **8** 1768 (1992).
[12] G. Wegner, Z. Naturforshc. **24B** 824 (1969).
[13] B.T. Briscoe and D.C.B. Evans, Proc. R. Soc. Lond. A **380**, 389 (1992).

MIXED POLYMER SURFACTANT SYSTEMS

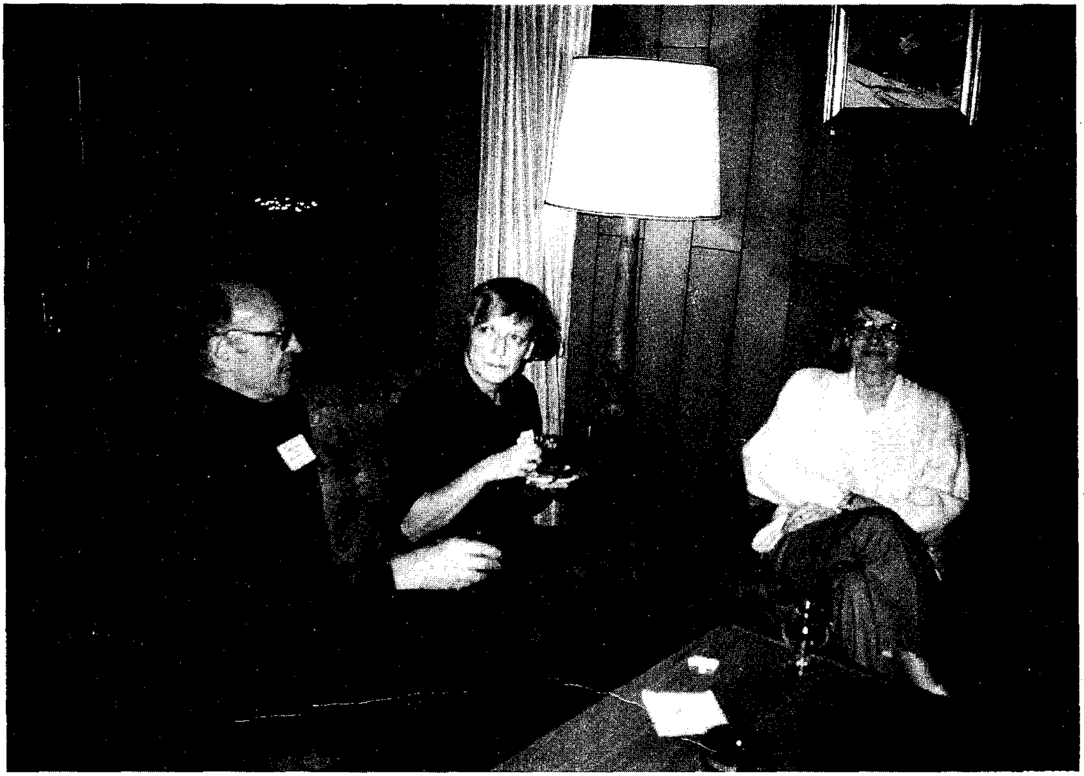

SOLUBILIZATION OF AN ADSORBING POLYMER IN A LYOTROPIC LAMELLAR PHASE : EFFECT OF POLYMER MOLECULAR WEIGHT

M.F. FICHEUX, T. RILEY, A.M. BELLOCQ, F. NALLET

Centre de Recherche Paul Pascal – CNRS
Avenue du Dr. A. Schweitzer – 33600 Pessac (France)

Abstract : We examine the effect of the molecular weight (M_W) of polyethyleneglycol PEG on the stability of the lamellar phase made of sodium dodecylsulfate-octanol-water. This L_α phase can incorporate up to 30 % of PEG. The degree of solubilization is nearly independent of the size of PEG in the range M_W: 3350–22600, and is weakly dependent on the smectic period. For some polymer and bilayer concentrations PEG with M_W=8000 and 22600 generate a two-phase region where two lamellar phases coexist. The extent of this region , that might be bounded by two critical points, is polymer size dependent. Finally addition of PEG to L_α results in a thinning of the bilayers which increases with M_W.

In the past few years, the effects of polymer on surfactant flexible layers begun to be investigated theoretically ($^{1-3}$) and experimentally in lamellar phases (^{4,5}) and microemulsions (^{6}). In this paper as well as in a previous one (^{7}) we examine the effect of a water-soluble neutral polymer, polyethyleneglycol (PEG) on the stability of a lamellar phase made of charged surfactant bilayers consisting of sodium dodecylsulfate and octanol. In the first paper we found that the lamellar structure still exists when pure water is replaced with aqueous solutions of PEG (M_W=22600 g/mol). Large amounts of PEG can be solubilized in the electrostatically lamellar phase, however for intermediate polymer concentrations and layer spacings, adding polymer generates a closed-loop smectic-smectic miscibility gap that might be bounded by two critical compositions. The comparison with the polymer-free reference system reveals that PEG gets partially associated to the octanol-SDS bilayer and makes the interactions between the bilayers less repulsive. They even become attractive enough to promote the phase separation between two lamellar phases, with the possible existence of critical points. In the present paper, using X-ray scattering we study the effect of the molecular weight of PEG on the phase diagram of the above mixed system.

–

Experimental part: Three polyethyleneglycols with molecular weights of 22600, 8000 and 3350 were obtained from Fluka and used without purification. The radius of gyration of isolated macromolecules and the overlap concentration C^* for PEG 22600 and PEG 8000 were obtained from neutron and light scattering experiments [PEG 22600: Rg=29 Å, C^*-35 g/l ; PEG 8000: R_g=16 Å, C^*=85 g/l]. The corresponding values for PEG 3350 were estimated as Rg ~ 9 Å, C^*=180 g/l. Preparation of spatially homogeneous samples at thermal equilibrium and the X-ray measurements were performed as described before (^{7}).

Results and discussion

***Phase diagrams*:** The extent of the lamellar phase of the ternary system water-octanol-SDS at constant temperature and pressure can be described by two composition variables: the membrane composition defined as the molar octanol to SDS ratio R and the membrane weight fraction c_m. The lamellar phase exists with R comprised between 1.2 and 2.9 and c_m between 5 and 60 % so that the thickness of the water layer can be continuously varied from 15 to 500 angströms. In the preceeding paper we have investigated in detail the section of the phase diagram of the quaternary system water-PEG (22600)-octanol-SDS where the ratio R is hold constant and equal to 2.7. This type of diagram allows to follow the solubility of the polymer in the lamellar phase made with bilayers of a given composition as a function of the lamellar spacing d.

Figure 1 shows the resulting pseudoternary phase diagrams defined by R=2.7 for the different chain length polyethyleneglycols. All of them present a lamellar phase. The first remarkable fact is that the boundaries of this region are within the experimental accuracy slightly dependent on the polymer molecular weight in the range 3350-22600, they only depend on the monomer units concentration. The solubility of PEG in L_α is almost independent on the smectic period d; indeed it follows a plateau for c_m comprised between 0.25 and 0.6. At large d, for c_m below 0.25, the solubility continuously falls from 30 % to 0 %. Thus, up to one half of the water of the mesophase can be replaced with PEG.

In the preceeding paper we have seen that PEG 22600 produces at intermediate membrane and polymer-concentrations a closed-loop two-phase region where two lamellar phases of different periods coexist (region L_α/L_α). Figure 1 shows that the extent of this area depends strongly on the chain length of the polymer. This area exists only in presence of PEG 22600 and PEG 8000.

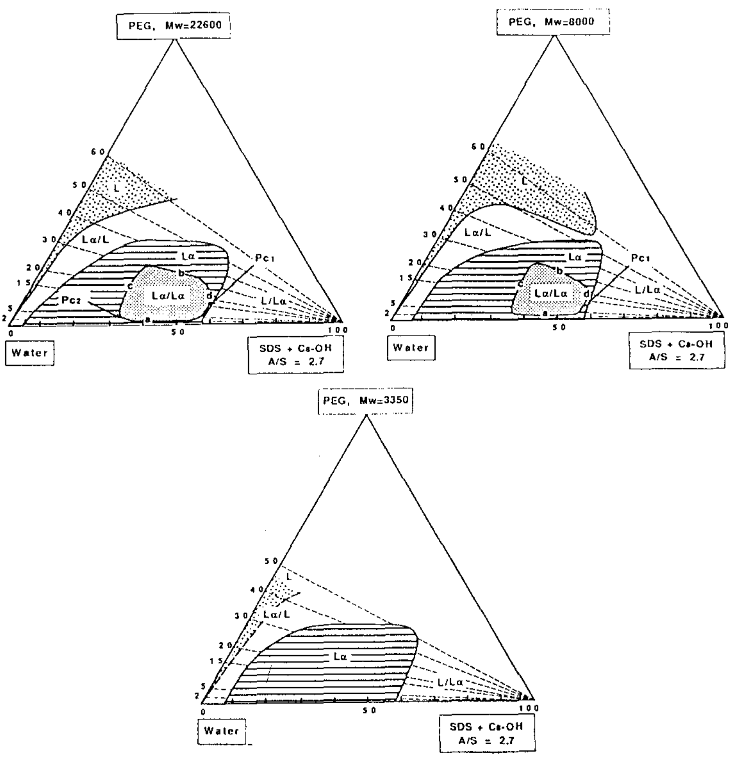

Figure 1: Sections at constant bilayer composition (R=2,7) of the quaternary phase diagram water-octanol-SDS-PEG with PEG 22600, PEG 8000, PEG 3350 (T=25°C).

Lamellar phase: We have studied for each polymer, the X-ray spectra of monophasic lamellar samples located along dilution lines defined by a constant concentration of polymer in water (c_p). The spectra are characteristic of lamellar phases. Depending upon c_m, they indeed exhibit one, two or three orders of Bragg diffraction at q_0, $2q_0$, $3q_0$. Whatever M_w and c_p varying from 0 to 0.4 a linear behavior of the smectic period d with the inverse of the membrane volume fraction is observed. Figure 2 gives as an example results obtained for PEG 8000 along the line c_p=0.02. This classical swelling law is still relevant for monophasic samples located along both sides of the demixing area (line c_p=0.3). The geometric thickness of the bilayers δ as deduced from the swelling law: $d=\delta/\phi m$ depends on both the polymer content c_p and the polymer size. As shown in figure 3, δ decreases as c_p increases and this effect is all the more larger as M_w is higher.

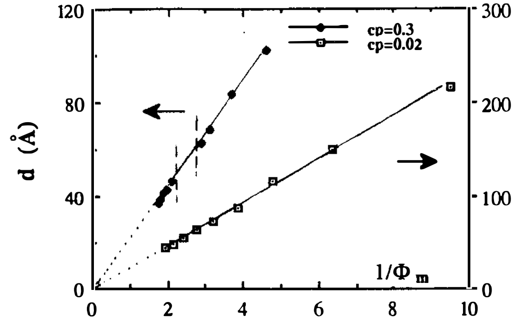

Figure 2: Smectic period d versus $1/\phi_m$ *along the dilution lines* $c_p=0.02$ *and* $c_p=0.3$

The decrease of δ reveals the adsorption of PEG on the SDS bilayers and suggests a slight increase of the average area per polar head of the surfactant. It also shows that this interaction is enhanced as the length of the PEG chains increases. Similar effects have been observed in SDS micellar solutions in presence de PEG (8). There are indeed many evidences that SDS and ethylene oxide polymers strongly interact mainly via the polar head of the surfactant when the polymer molecular weight is larger than 4000 (9). An alternative interpretation can be considered however; the observed decrease of the smectic period d at constant alcohol + surfactant concentration may also arise from a partial solubilization of PEG in the bilayer. At this stage we cannot draw definite conclusions about the polymer partitionning between solvent and bilayers.

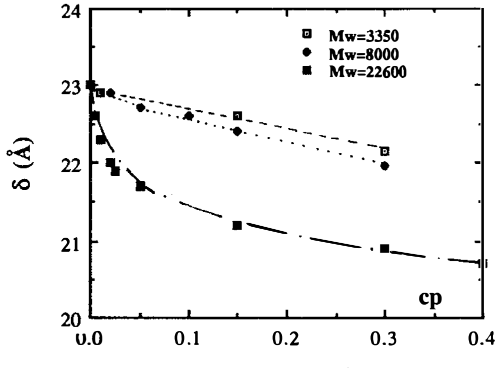

Figure 3: Evolution of the membrane thickness δ *with the polymer fraction* c_p.

L_α–L_α ***two-phase région***: As already mentioned, two-phase equilibria involving two lamellar phases are found in presence of PEG 22600 and PEG 8000. Their identification rests upon the analysis of X-ray spectra which display two sets of Bragg peaks, each characteristic of a lamellar phase. For both polymers, the lower (a) and upper (b) boundaries of the two-phase region follow closely dilution lines at constant c_p. Similarly the left (c) and right (d) boundaries correspond to lines at constant c_m, meaning that along these lines the phase separation occurs at almost constant thickness of the water layer. The limits (a) and (c) change with the molecular weight while the two others at high c_m (line d) and high c_p (line b) are less sensitive to the size of the polymer. As M_w decreases, the boundary (c) shifts to higher c_m from $c_m=0.3$ for PEG 22600 to $c_m=0.35$ for PEG 8000 and the boundary (a) to higher c_p from $c_p=0.01$ for PEG 22600 to $c_p=0.03$ for PEG 8000. These changes appear to be strongly related to the size and the overlap concentration of the polymer. For both polymers, the phase separation along line (c) occurs when the thickness of the water layer is of the order of the diameter of isolated macromolecules (PEG 22600 d_ω~50 Å; $2R_g=58$ Å; PEG 8000: d_ω~40 Å; $2R_g=32$ Å). Following this trend, in the case of the smaller polymer (PEG 3350) line (c) would be expected to be located very close to line (d). This is consistent with the disappearance of the two-phase region for this polymer. Similarly, the lower boundary (a) appears to be connected with the overlap concentration C^*.

Unfortunately direct evaluation of the composition of the coexisting phases is impossible: we cannot achieve macroscopic phase separation. Therefore, the precise compositions of the coexisting phases – and in particular the polymer partitioning between the two lamellar phases – remain unknown. However, some indications can be deduced from the splitting $\Delta q \equiv |q_2 - q_1|$ between the Bragg peak positions of the coexisting two lamellar phases. Large splittings are associated to strongly different lamellar phases while $\Delta q \rightarrow 0$ signals lamellar phases with negligible differences in smectic period, as should occur at a critical point. For PEG 22600 we found two strong minima of Δq precisely located on the boundary of the two-phase domain, respectively at $\phi_m=0.58$, $c_p=0.15$ and at $\phi_m=0.32$, $c_p=0.038$. These two points, denoted P_{c1} and P_{c2} in figure 1, have been ascribed to critical points. This statement is in line with the strong decrease of the layer compression modulus $\overline{B}$ (equivalent to the diverging osmotic compressibility in isotropic solutions), evidenced by dynamic light scattering and neutron scattering measurements, in the vicinity of P_{c2} (7). Similarly, in the case of PEG 8000, measurements of Δq along the border of the L_α/L_α region suggest the existence of two critical points, one, P_{c2} is in the membrane rich region at $\phi_m=0.57$, $c_p=0.15$, the second P_{c1} found at low ϕ_m and c_p has not been so precisely located (P_{c1}: $\phi_m=0.36$, $0.25<c_p<0.05$).

In conclusion our study shows that the lamellar phase made of sodium dodecylsulfate-octanol-water can incorporate up to 30 % of the water soluble polymer PEG. This degree of solubilization is nearly independent of the molecular weight of PEG in the range M_W 3350-22600 and is weakly dependent on the smectic period d. Moreover for intermediate polymer and bilayer concentrations, the polymers PEG 22600 and PEG 8000 generate a closed-loop smectic-smectic miscibility gap that might be bounded by two critical points. Two of the boundaries of this L_α-L_α domain are size-polymer-dependent, one is related to the radius of gyration Rg, the other one to the overlap concentration. In presence of PEG the repeat distance shrinks slightly. This results from a thinning of the bilayer or a partial penetration of the polymer within it, or a combination of both effects. These effects are enhanced when the concentration and molecular weight of the polymer are increased.

References

(1) De Gennes P.-G., J. Phys. Chem. **94** (1990) 8407

(2) Brooks J.T., Marques C.M. and Cates M.E., J. Phys. II France **1** (1991) 673

(3) Brooks J.T. and Cates M.E., J. Chem. Phys. **99** (1993) 5467

(4) Singh M., Ober R. and Kléman M., J. Phys. Chem. **97** (1993) 11108

(5) Ligoure C., Bouglet B. and Porte G., Phys. Rev. Lett. **71** (1993) 3600

(6) Lal J. and Auvray L., J. Phys. II France **4** (1994) 3119

(7) Ficheux M.F., Bellocq A.M. and Nallet F., J. Phys. II France **5** (1995) 823

(8) Cabane B. and Duplessix R., J. Phys. 43 (1982) 1529; J. Phys. **48** (1987) 651

(9) Goddard E.D., *Interactions of surfactants with polymers and proteins*, Goddard E.D. and Ananthapadmanabhan K.P. Eds (CRC Press, Boca Raton, 1993)

POLYMER IN A LYOTROPIC LAMELLAR PHASE: POSSIBLE MODEL FOR PROTEINS IN MEMBRANES

Ewa Z. Radlinska(1,2), Tadeusz Gulik-Krzywicki(3), Françoise Lafuma(1),
Dominique Langevin(4), Wladimir Urbach(4), Claudine E. Williams(2)
and Raymond Ober(5)

(1)Laboratoire de Physico-Chimie Macromoléculaire, Université Paris VI, CNRS URA 278, ESPCI, 10, rue Vauquelin, 75231 Paris, France
(2)LURE, Centre Universitaire Paris-Sud, 91405 Orsay, France
(3)Centre de Génétique Moléculaire, CNRS, 91190 Gif-sur-Yvette, France
(4)Laboratoire de Physique Statistique, ENS, 24, rue Lhomond, 75231 Paris, France
(5)Laboratoire de Physique de la Matière Condensée, Collège de France, 75231 Paris, France

Abstract

We study the lamellar phase of a ternary system comprised of a non-ionic surfactant, a charged polymer and water. The polymer, a water soluble random copolymer of styrene and styrene sulfonate, can be incorporated in the system up to several weight percent and its behaviour can be varied by adjusting the proportion of hydrophobic to hydrophilic monomers. Surface tension measurements clearly indicate a surfactant-polymer interaction over a wide surfactant concentration range. Using freeze fracture electron microscopy we demonstrate that the polymer molecules are confined inside the surfactant bilayers. The system offers a simple model for the protein interactions in biological membranes.

Introduction

The polymer solubilisation into lyotropic surfactant phases has been a subject of numerous studies1-9). It is well known that changes resulting from the polymer-surfactant interactions can affect both the bulk and surface properties of solutions10-11). Therefore, the mixed polymer-surfactant systems have found broad applications1). These systems are also of fundamental interest for understanding physics governing the modification of surfactant self-assembly in the presence of large molecules and the behaviour of polymer molecules in confined environment. In particular, the smectic lamellar phase formed by surfactants in water solutions is of special interest in the studies of aqueous polymer/surfactant mixtures6-8).

The interaction of proteins with amphiphilic molecules has been extensively studied for over half a century1). This activity has been motivated by a need to understand, at the molecular level, the basics of biological functions of proteins as the main building blocks of biological structures, in particular of cells. However, the fact that both proteins and cell membranes are of a very complex physico-chemical nature makes it difficult to gain a clear insight into the observed processes and to model them theoretically. Therefore, a need arises to find alternative molecular systems that could be used to study the role of specific aspects of protein-phospholipid interactions. Here we describe a ternary system composed of a surfactant, water and polyelectrolyte. Using various experimental techniques, in particular freeze fracture electron microscopy and small angle x-ray scattering12), we show that the polymer molecules are incorporated into the surfactant bilayers, in full analogy to biological cells.

Results and analysis

We study a ternary system of a non-ionic surfactant, n-dodecyl pentaoxyethylene glycol ether ($C_{12}E_5$), a water-soluble polymer, poly(styrene-co-styrene sulfonate) with degrees of sulfonation ranging from 30% to 90% and water. Poly(styrene-co-Na styrene sulfonate) (abbreviated as $PS_{1-x}NaPSS_x$, x being the degree of sulfonation or charge content) is a random copolymer of highly hydrophobic polystyrene units and hydrophilic polystyrene sulfonate ones. It was obtained by postsulfonation of a polystyrene with a molecular weight of 250000 and a polydispersity (M_w/M_n) of 213). The behaviour of poly(styrene-co-styrene sulfonate) in semi-dilute water solutions was characterised elsewhere14,15). In order to probe the interactions between polymer and surfactant molecules in solution we used the simple method of surface tension measurements.

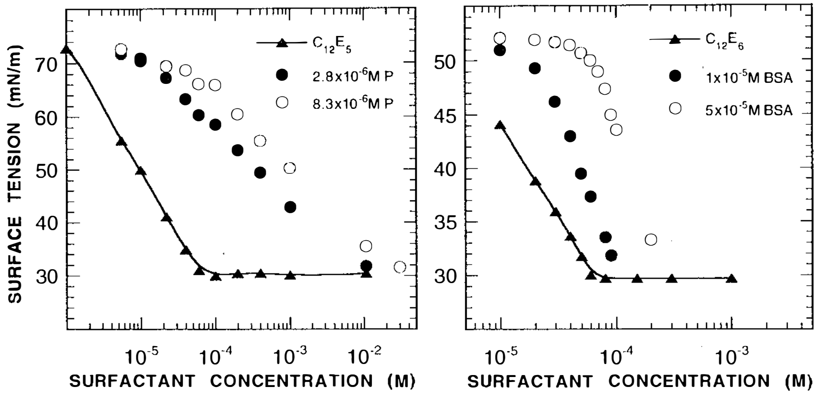

Figure 1. a) Surface tension of the $C_{12}E_5$/water /$PS_{1-x}NaPSS_x$ (x=0.45) system measured using the Wilhelmy Plate Method at room temperature. Data for the binary $C_{12}E_5$/water system are shown with full triangles, full circles correspond to 2.8×10^{-6} moles/l of polymer and empty circles to 8.3×10^{-6} moles/l of polymer. b) Surface tension of the $C_{12}E_6$/water /bovine serum albumin system (after Nishikido et al.[16]). Data for the binary $C_{12}E_6$/water system are shown with full triangles, full circles correspond to 1×10^{-5} moles/l of BSA and empty circles to 5×10^{-5} moles/l of BSA.

Unlike other water soluble polymers, $PS_{1-x}NaPSS_x$ has a high affinity for non-ionic surfactants as shown by our experimental data. The value of surface tension is a measure of the number of free surfactant molecules in the mixed system, which in turn depends on the interplay between the processes of self-assembly, surfactant-to-polymer binding and surface activity. For small charge content there is a clear indication of a surfactant-polymer interaction over the concentration range 10^{-6}M to 10^{-2}M of $C_{12}E_5$ (Figure 1a), which is similar to the attraction of bovine serum albumin (BSA), a widely studied hydrophilic protein with a hydrophobic pocket, to the hexa(oxyethylene) dodecyl ether ($C_{12}E_6$) non-ionic surfactant[16] (Figure 1b). The surface tension curves shown in Figure 1a for the concentration of polymer of 2.8×10^{-6} M and 8.3×10^{-6} M suggest that the addition of polymer depletes the surface of surfactant molecules which bind to the polymer in the solution.

The surface tension results indicate that the basic structure of $PS_{1-x}NaPSS_x$ may offer a very simplified model of protein, in which the several hundred different units found in proteins have been replaced by just one hydrophilic and one hydrophobic type of monomer. The numerical proportion of hydrophobic to hydrophilic units in proteins determines their behaviour in solution, and this can be modelled by varying the degree of sulfonation in poly(styrene-co-styrene sulfonate).

The phase diagram of $C_{12}E_5$/water system is well known[17)]. We concentrate on a region of high surfactant content where a liquid crystalline lamellar mesophase (L_α) exists at room temperature. Recently we have shown that the characteristic SAXS spectra of the lamellar phase are affected by the presence of polymer molecules: shift and broadening of the Bragg lines as well as emergence of small-Q scattering background were observed[12)].

Freeze fracture electron microscopy can be used to directly observe the polymer-induced structural changes in the lamellar phase. In this method, a small droplet of sample is placed on a copper holder, covered with a copper plate and rapidly quenched in liquid propane. Then, the frozen sample is fractured at -125°C inside the vacuum chamber of a Blazer Model 301 freeze etching apparatus ($p<10^{-6}$ Torr). The exposed fracture face is shadowed by a platinum-carbon layer at an angle of 35°. Examples of the TEM micrographs of the replicas are shown in Figure 2. All of the pictures clearly demonstrate a well defined lamellar structure and the interlayer distance is in very good agreement with the SAXS-determined values[12)]. The surfaces exposed by cleavage (and visible on the FFEM images) are mid-sections through the hydrophobic centre of the bilayer[18)]. These surfaces appear smooth for the binary $C_{12}E_5$/water mixture (Figure 2A). For the ternary $C_{12}E_5$/water /polymer systems additional objects are clearly visible on the images (Figure 2B-D). Because of the cleavage properties of the freeze-fractured bilayers the objects seen cannot be attached to the hydrophilic surfaces of the lamellae but have to be enclosed inside the bilayers[19)]. We conclude that those objects are the images of molecules of $PS_{1-x}NaPSS_x$ confined inside the bilayers. A deeper analogy may exist between the system studied by us and the biological membranes since proteins are basically amphoteric, complex, unbranched polymers[1)]. It seems that for the present system this analogy extends also to the structural position of the polymer molecules relative to the bilayer.

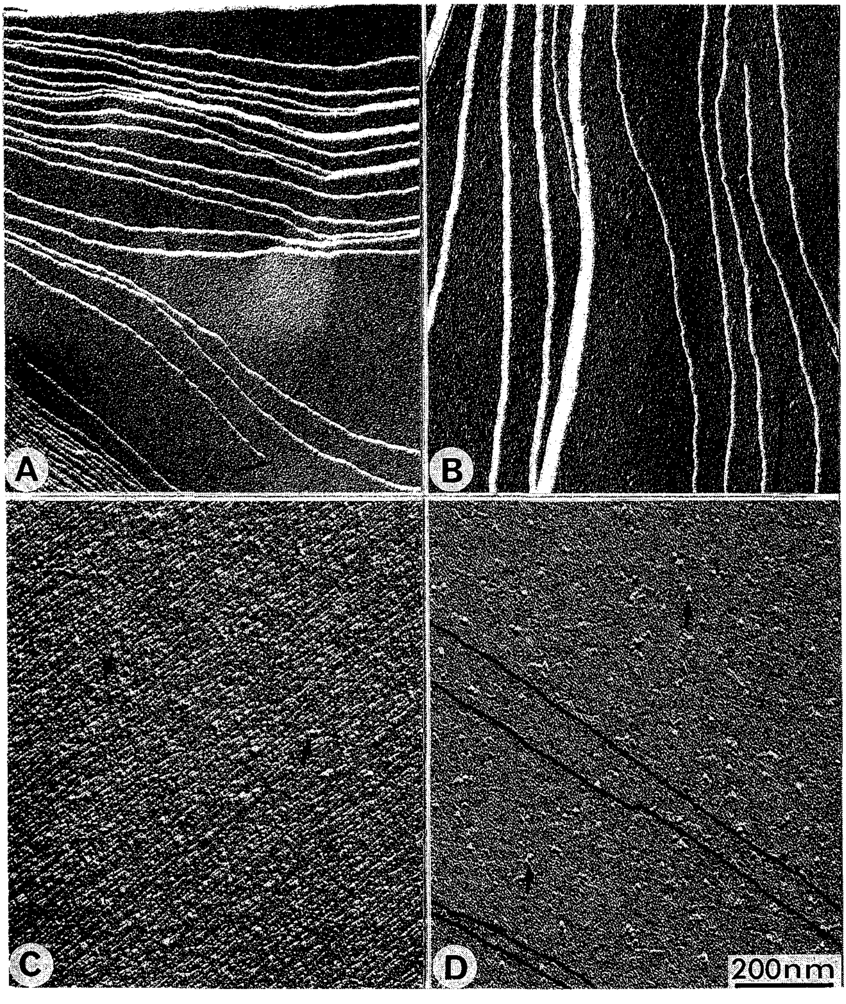

Figure 2. Freeze fracture electron microscopy images for samples of surfactant-to-water ratio 3.39 with and without polymer. The sulfonation degree of the polymer is x=0.30. A: binary $C_{12}E_5$/water system, 77.2 wt% of surfactant. The concentration of polymer is 0.2 wt% (B) and 2.3 wt% (C: side view and D: top view). Arrows indicate positions of the polymer molecules.

Conclusions

We have presented experimental evidence showing that in the ($C_{12}E_5$)/water/poly(styrene-co-styrene sulfonate) system there is a pronounced polymer-surfactant interaction (surface tension data). Freeze fracture electron microscopy results unequivocally demonstrate that in the lamellar phase the polymer molecules enter the bilayers and remain incorporated as isolated entities inside them. The system is a particularly simple model for the protein interactions in biological cell membranes.

Acknowledgements

We thank L. Bon Nguyen for the preparation of polymer and J. C. Dedieu for excellent technical assistance in electron microscopy. We express our gratitude to C. Safinya, P. Pincus, J. Israelachvili, E. Sackmann, T. Zemb, M. Waks and I. Iliopoulos for useful discussions.

References

[1] *Interactions of Surfactants with Polymers and Proteins*, edited by E. D. Goddard and K. P. Ananthapadmanabhan (CRC Press, Inc., Florida, USA, 1993).
[2] K.Seki and D. A. Tirrell; *Macromolecules* , **17,** 1692 (1984).
[3] J. C. Brackman and J. B. F. N. Engberts; *Langmuir*, **7,** 46 (1991).
[4] C. Petit, Th. Zemb, and M. P. Pileni; *Langmuir*, **7,** 223 (1991).
[5] C. Quellet, H. F. Eicke, and W. Sager; *J. Phys. Chem.*, **95**, 5642 (1991).
[6] C. Ligoure, G. Bouglet, and G. Porte; *Phys. Rev. Lett.*, **71**, 3600 (1993).
[7] M. Singh, R. Ober, and M. Kleman; *J. Phys. Chem.*; **97**, 11108 (1993).
[8] P. Kekicheff, B. Cabane, and M. Rawiso; *J. Colloid Interface Sci.*, **102**, 51 (1984).
[9] I. Iliopoulos, and U. Olsson; *J. Phys. Chem.*; **98**, 1500 (1994).
[10] P. G. de Gennes; *J. Phys. Chem.*, **94**, 8407 (1990).
[11] J. T. Brooks and M. E. Cates; *J. Phys. Chem.*, **99**, 5467 (1993).
[12] E. Z. Radlinska, T. Gulik-Krzywicki, F. Lafuma, D. Langevin, W. Urbach, C. E. Williams and R. Ober; *Phys. Rev. Lett.*, in press.
[13] H. S. Makowski, R. D. Lundberg, and G. S. Singhhal; *US Patent 3870841*, 1975, EXXON Research and Engineering Company.
[14] W. Essafi, F. Lafuma, and C. E. Williams; *Am. Chem. Soc. ACS Symposium Series 548,* 278 (1994).
[15] W. Essafi, F. Lafuma, and C. E. Williams; *Macromolecules,* in press.
[16] N. Nishikido, T. Takahara, H. Kobayashi, and M. Tanaka; *Bull. Chem. Soc. Jpn.*, **55**, 3085 (1982).
[17] R. Strey, R. Schomäcker, D. Roux, F. Nallet, and U. Olsson; *J. Chem. Soc. Faraday Trans.*, **86**, 2253 (1990)
[18] J. P. Sergrest, T. Gulik-Krzywicki, and C. Sardet; *Proc. Nat. Acad. Sci. USA,* **71**, 3294 (1974).
[19] T. Gulik-Krzywicki; *Biochimica et Biophysica Acta,* **415**, 1 (1975)

VESICLE FORMATION FROM NEUTRAL AMPHIPHILIC BILAYERS DOPED BY AN IONIC SURFACTANT

C. Ligoure, C. Couve, J. Oberdisse, J. Appell, J-F. Berret and G. Porte
Groupe de Dynamique des Phases Condensées (URA CNRS 233), Université
Montpellier II, C.C.026, place Eugène Bataillon, F-34095 Montpellier Cedex 05, France

ABSTRACT

We investigate the modifications in the phase behavior of a non ionic ternary surfactant system (Triton X100/octanol/water) after addition of small amounts of an ionic amphiphile (Cetylpyridiniumchloride). From neutron scattering, we show that, the birefringent L_α lamellar phase disappears completely and is replaced by two different isotropic phases, depending on the total membrane concentration: a dilute phase of small unilamellar vesicles, and an "elastic" phase, consisting of densely packed big onions (multilamellar vesicles) having unique rheological properties, at higher surfactant concentration. We interprete the spontaneous formation of vesicles by investigating the bending elasticity of fluid bilayers consisting of two amphiphilic species. We have shown that the corresponding composition degree of freedom couples to the curvature, playing a crucial role in the bending properties of mixed membranes. This can be quantified in terms of the bending moduli of the individual consisting monolayers, provided that these are calculated at fixed chemical potential and not at fixed composition. This general approach is applied to the specific case of dilute initially neutral membranes weakly charged by addition of a small amount of an ionic surfactant. The calculated electrostatic contribution to the rigidities may well be sufficiently negative as to explain the observed spontaneous bending.

INTRODUCTION

One of the characteristic feature in ternary phase diagrams of surfactants/cosurfactants and water is the large region of the L_α phase which consists of a regular stacking of very large bilayers parallel to each other. The resulting lamellar phase is birefringent and shows quasi long range smectic order. Increasing attention is presently focusing on the spontaneous formation of vesicles and liposomes from surfactant bilayers membranes. Most of these systems involve at least two amphiphilic compounds, so that the membranes are in fact mixed bilayers. For instance, Hoffmann et al 1) have studied a ternary system consisting of a non ionic surfactant (tetradecyldilethylaminoxide) and a non ionic cosurfactant (hexanol) in pure water. They have added to this neutral system a small proportion of ionic surfactant (tetradecylmethylammoniumbromide) and show that the lamellar birefringent phase disappears and is replaced by a stable liposome phase, as revealed by freeze fracture electron microscopy. However, very low concentrations (few mM) of added salt is actually sufficient to wipe out the effect of the ionic dopant and the phase diagram goes back to its initial geometry (corresponding to the inital non ionic situation).

We have studied a similar dilute neutral surfactant/cosurfactant mixture in pure water. This system exhibits a very classical phase diagram, but it is profoundly affected by addition of a small amount of a cationic surfactant. The lamellar phase disappears and is replaced by two distinct isotropic phases, depending on the total membrane volume fraction. Using small angle neutron scattering technique (SANS), we have characterized the structure of these two phases. The experimental results are developed in the first section of this article.

Dealing with the experimental facts, the problem is to understand the spontaneous tendency for symmetrical bilayers to bend so as to form vesicles.The basic idea, first suggested by Safran et al 2) is to consider explicitely the coupling between the local curvature and the local composition of the membrane. We summarize in section II a simple but quite general thermodynamical formalism3), which allows to calculate the relevant bending moduli of mixed bilayers as well as the stability criteria. This general framework is then applied to the more specific present experimental situation: a single neutral bilayer doped with an ionic amphiphile. The calculated electrostatic contribution to the bending rigidity of the bilayer may well be sufficiently negative so as to explain the spontaneous bending observed by Hoffmann et al and ourselves.

I EXPERIMENTS

The initial system considered, consists of Triton X100 (non ionic commercial surfactant) and octanol in pure water. It exhibits a very classical phase diagram (see figure 1a). Increasing the alcohol upon surfactant weight ratio, we observe the following sequence of phases : micelles (L_1), lamellar phase (L_α), and finally a thin region of existence of the sponge phase (L_3). Adding a small amount (3.5% in weight of the membrane) of a cationic surfactant (cetylpyridiniumchloride) leads to great changes (see figure 1b): the lamellar phase disappears completely (as well as the sponge phase), and is replaced by two isotropic phases separated by a two phases coexistence domain. We have performed small angle neutron scattering experiments in the Laboratoire Leon Brillouin in Saclay in order to analyze the structure of these two isotropic phases, and we have chosen for all samples a high alcohol/surfactant ratio ($w=M_{octanol}/M_{TX100} > 0.4$), so that the initial non doped samples are lamellar.

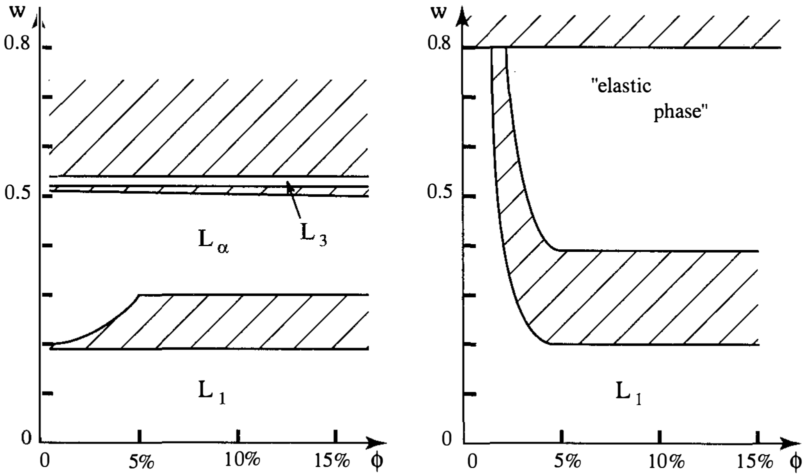

Fig. 1 a

Fig. 1 b

Figure1: Phase diagrams of the systems: Fig. 1a:TX100/octanol/ water; Fig.1b:TX100/octanol/water with 3.5% of CPCL(in weight of surfactant and cosurfactant)added.. X axis: weight fraction of octanol plus TX100; Y axis: octanol weight upon TX100 weight

The dilute phase (L_1), corresponding to a total volume fraction of alcohol and surfactant $\phi<1.5\%$, with $w>0.4$ is transparent, isotropic, fluid,sligthly bluish and does not show any shear induced birefringence. On figure (3), the scattered intensity times q^2 (the scattering vector) of one sample ($\phi = 1\%$, $w=0.5$) is plotted as a function of q . The first maximum at low q's ($q=0.02$ A^{-1}) is the correlation peak due to the electrostatic interaction between the individual objects separated by a mean distance of about 50 nm.

In the high q range, the scattering patterns of the neutral and doped samples are identical, meaning that both consist of bilayers with $\delta=3$ nm dry thickness. The oscillations in between correspond to the form factor of the objects: their relative positions indicate unilamellar vesicles of average diameter D=17nm.

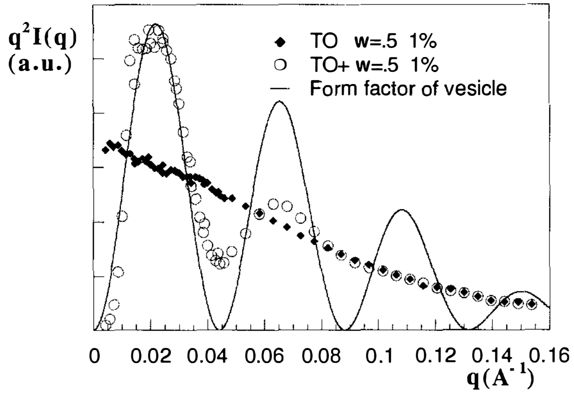

Figure 2: Neutron scattering pattern ($q^2I(q)$ versus q) of two dilute samples (ϕ=1%, w=0.5): diamonds: non doped sample; open circles: doped sample (3.5% CPCL in weight of the membrane added); full line: form factor of a vesicle (external diameter D=8.5 nm and thickness δ=3nm)

The more concentrated phase (ϕ>3%, w>0.3), we have called "elastic phase" is isotropic, transparent, very viscous, and shows extremely strong flow birefregence. Furthermore, small bubbles remain trapped over months, suggesting a finite yield stress as confirmed by rheological measurements of the elastic modulus G. The scattered intensity (see fig.3) by the doped sample (ϕ=5% w=0.5), reveals the existence of two Bragg singularities at q_B = 0.105 A^{-1} and 2 q_B, characteristic of a local smectic order with a periodicity d = 60 nm. The consistent picture of the elastic phase is the following: it is that of close packed spherical onions (glass of soft balls).; each onion has a mean diameter of about 600 nm and consists of about ten bilayers, with an interlamellar spacing of 57 nm and a dry membrane thickness of 3 nm. The average size of the onions is derived from the correlation bump observed in light scattering at q=0.001 A^{-1}. However, it should be noticed that the existence of this correlation bump seems to depend on the history of the sample. Our scattering results are in good agreement with the FFEM pictures obtained on a similar system 1).

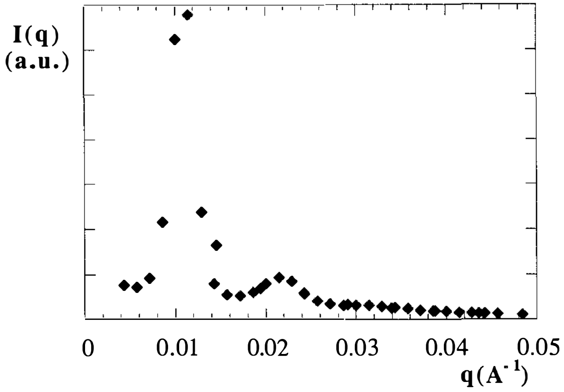

Figure3: Scattered intensity of a concentrated doped sample ("elastic phase"): ϕ=5%, w=0.5

II MODEL OF BENDING INSTABILITY IN MIXED CHARGED BILAYERS

Using the Hefrich's classical phenomenological approach for the bending energy of a fluid membrane, bending instability and spontaneous formation of vesicles in surfactant bilayers occurs as soon as the bending modulus of the corresponding monolayer $\tilde{\kappa} = \kappa + 1/2\bar{\kappa}$ becomes negative, where κ and $\bar{\kappa}$ are respectively the elastic mean and gaussian curvature bending moduli of gaussian curvature of the monolayer. However, in the case of mixed bilayers, such as those presented in section I, an additional degree of freedom must be considered as well, namely the chemical composition of the membrane. Actually, the local composition certainly couples to the local curvature of the bilayer therefore playing a crucial role in the spontaneous bending. The basic idea, first developped by Safran et al$^{2)}$ is that, in mixed surfactant membranes, amphiphilic molecules can exchange from the upper to the lower monolayer. Upon bending the bilayer, the curvatures experienced by the two monolayers have opposite signs. So, in general, their chemical compositions will change respective to one an another. If the coupling between curvature and composition is strong enough symmetry breaking and spontaneous bending occur.

In order to extend these ideas to various experimental situations, we have shown that symmetry breaking and spontaneous formation of vesicles from mixed surfactant bilayer membranes are controlled by the sign of the bending modulus of mixed monolayers at constant chemical potential $\tilde{\kappa}_{\mu}$, rather than the usuall one $\tilde{\kappa}_{\psi}$ at fixed composition3). This expresses simply the fact that amphilic molecules can exchange from the upper to the lower leaflet. We have also shown how $\tilde{\kappa}_\mu$ can be derived from $\tilde{\kappa}_\psi$. As a result it appears that $\tilde{\kappa}_\mu$ is lower than $\tilde{\kappa}_\psi$, meaning that the composition degree of freedom of the mixed bilayer induces a softening of its bending rigidity.

We apply now these general results to the following situation: an initially neutral bilayer to which we progressively add increasing amounts of an ionic surfactant. This is relevant, we think to the situation investigated by Hoffmann et al1) and by ourselves in section I. We would like to focus more specifically on the electrostatic effect: so, we assume that the ionic dopant has the same packing requirements as the neutral amphiphile (i-e. the same molecular structure apart from the ionic charge); in particularly, both amphiphiles have the same packing contribution to the bending modulus $\tilde{\kappa}$. For charged bilayers in water, the upper and lower electrical double layers contribute to the bending elasticity4)· We focus on very dilute lamellar systems, so that we can neglect the inter membranes interaction. The two important characteristics lengths are: the Debye screening length λ and the Gouy-Chapman length l_c 5). We have at room temperature the Bjerrum length $l_B = 0.72$ nm. Using our general results, 3), and the calculations of Lekkerkerker6), we obtain for the electrostatic contribution to the bending properties 3):

$$\Delta\tilde{\kappa}_\psi = \tilde{\kappa}_\psi - \tilde{\kappa} = \frac{2\,T\,\lambda}{\pi\, l_B} L(p) \text{ where: } L(p) = \frac{(q-1)(q+2)}{q\,(q+1)} - \mathrm{dilog}\left(\frac{2}{1+q}\right) \qquad (1)$$

$$\Delta\tilde{\kappa}_\mu = \tilde{\kappa}_\mu - \tilde{\kappa} = \frac{2\,T\,\lambda}{\pi\, l_B} H(p) \text{ where: } H(p) = L(p) - \frac{4\,p^3}{q\,(q+1)^2(2\,p+q)} \qquad (2)$$

where the following notations are used:

$$p = 2\,\pi\, l_B\, \lambda\, \psi = \frac{\lambda}{l_c}\,;\; q = \sqrt{1+p^2} \text{ and } \mathrm{dilog}(x) = \int_1^x \frac{\ln(t)}{1-t}\,dt$$

p is the reduced area surface charge density (ψ denotes the ionic dopant area density), T is the temperature.

So the charge contributions $\Delta\tilde{\kappa}_\psi$and $\Delta\tilde{\kappa}_\mu$to the bending rigidities $\tilde{\kappa}_\psi$ and $\tilde{\kappa}_\mu$ are controlled by the mathematical properties of the functions L(p) and H(p) which only depend on the dimensionless reduced area charge density p.

These functions are plotted on figure (4). L(p) is a non monotonic function positive at low charge density but negative at higher p's (p> 6.7). At very high p, L(p) asymptotically reaches its lowest negative value: $1-\pi^2/6$. So, charging a bilayer7) up to a sufficient area density may well lead to spontaneous bending provided that the molecular packing contribution $\tilde{\kappa}$ to $\tilde{\kappa}_\psi$is smaller than $2T\lambda\,(\pi^2/6 - 1) / \pi l_B$. Interestingly, taking λ= 100 nm (a reasonnable value for our experimental situation in absence of added salt) the asymptotic negative value of $\Delta\tilde{\kappa}_{\psi}$ of the order of -50 T is reached for ψ of the order of $2.10^{-1}\mathrm{nm}^{-2}$ (i-e when roughly 10% of the neutral surfactant is replaced by the ionic dopant). Since for most common single chain surfactants ($\tilde{\kappa}$ = 1 to 10 T typically) the packing contribution to the rigidity is by far smaller than 50 T , we do expect spontaneous bending in our situation as is indeed observed..If now we remember that the surface charge density is not a conserved quantity, we must consider rather $\Delta\tilde{\kappa}_{\mu}$ and therefore the properties of H(p). The variations of H(p) are also represented in figure (4) so that they can be compared to those of L(p). We note that at low charge density, H(p) is significantly smaller than L(p) (softening effect due the composition degree of freedom) which means that the spontaneous bending is expected even sooner upon charging progressively the membrane (H(p) becomes negative as soon as p is larger than 3.4). However at high charge density, the asymptotic values of L(p) and H(p) are simply identical. This means that the composition degree of freedom plays no role in the high charge regime. Furthermore, adding salt at fixed area density ψ decreases the value of p (which is proportionnal to the Debye screening length λ), and therefore increases the bending rigidity of the bilayer. This explains why, the formation of liposomes or vesicules, seen in the absence of added salt, is suppressed after addition of quite small amounts of salt.

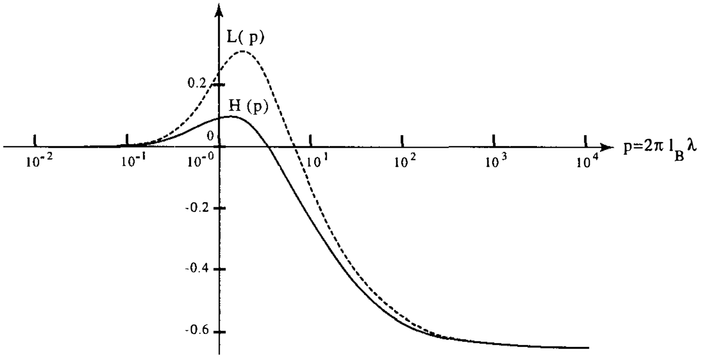

Figure 4:Variation of the function L(p) (dotted line) and H(p) (full line). Note that lin versus log units have been used for the vertical and horizontal scales respectively.

CONCLUSION

We have given experimental evidences of spontaneous unilamellar or multilamellar vesicles formation in dilute mixed surfactant bilayers solution,built up from neutral bilayers doped with small amounts of an ionic amphiphile. The bending instability has been interpreted in terms of the bending moduli at fixed chemical potential of each monolayer: the calculated electrostatic contribution may well be sufficiently negative so as to explain the spontaneous bending we observed.

REFERENCES

1-H. Hoffmann, U. Munkert, C. Thunig, and M. Valiente, Journal of Coll. Interface Sci. **163**, (1994), 217

2- S. A. Safran, P. A. Pincus, D. Andelman and F. C. Mac Intosh, Phys. Rev. A, **43**,(1991), 1071.

3- G. Porte and C. Ligoure, J. Chem. Phys, **102**, (1995), 4290.

4- D. Andelman, in Handbook of Physics of Biological Systems, Volume 1, Chapter 12, edited by R. Lipowsky, 1994, Elsevier Science B. V.

5- P. A. Pincus, J.F. Joanny, and D. Andelman, J.Europhys. Lett **11**, (1990), 763

6- H. N. W. Lekkerkerker, Physica A, **140**, (1989), 319.

7- M. Winterhalter and W. Helfrich, J. Chem. Phys.**96**, (1992), 327
M. Winterhalter and D. Lasic, Chemistry and Physics of Lipids, **64**, (1993),35

THEORETICAL STUDIES OF DIBLOCK COPOLYMER MIXTURES

An-Chang Shi and Jaan Noolandi
Xerox Research Centre of Canada
2660 Speakman Drive
Mississauga, Ontario, Canada L5K 2L1

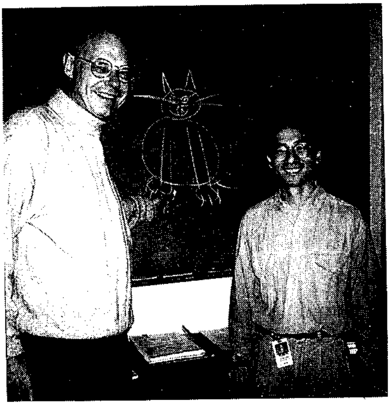

ABSTRACT

The phase behavior of mixtures of two monodisperse diblock copolymers made up of A and B monomer units is investigated using self-consistent mean-field theory. Due to the large number of controlling parameters (two molecular weights, two chemical compositions, temperature, and polymer volume fractions), a very rich phase behavior is expected. Two extreme cases are studied: (**1**) mixtures of small amount of short diblocks with long diblocks, and (2) mixtures of diblocks with equal lengths. For the case of short and long mixtures, we found that the addition of small amount of short diblocks has large effects on the phase boundaries of the system. For the case of equal length diblocks, several new phases including an inversed spherical phase and a bilayer phase are predicted. Our studies demonstrate that the phase behavior of binary mixtures of diblock copolymers is controlled by the interfacial curvature and the segregation of the diblocks.

One of the ultimate goals in studies of block copolymers is the development of methods to determine polymer morphology for materials applications. The phase behavior of diblock copolymers can be controlled by synthesizing precisely tailored diblock copolymers. Another route to control block copolymer morphologies is through polymer blending, in which two or more copolymers with different morphologies are mixed together to get a desired morphology. Furthermore, mixtures of diblock copolymers are interesting because of their potential to form new types of ordered phases, and as a testing ground for theoretical models which have been developed for one-component systems. What has been lacking on the theoretical side is a systematic attempt at understanding the phase behavior of even a simple system such as a binary mixture of two types of monodisperse diblock copolymers composed of A and B monomer units. Due to the large number of controlling parameters (the four degrees of polymerization Z_{1A}, Z_{1B}, Z_{2A}, Z_{2B}, the tatal volume fractions of the copolymers, and the A-B interaction parameter χ), a very rich phase behavior is expected for these binary mixtures. We have launched a systematic study of the phase behavior for diblock copolymer mixtures using the self-consistent mean-field theory. Specifically, we have studied two extreme cases: Mixtures of long diblock copolymers with a small amount of short diblock copolymers 1), and mixtures of diblock copolymers of equal lengths 2). A general observation from these studies is that the phase behavior of binary mixtures of diblock copolymers is controlled by the interfactial curvature, which is proportional to the average chemical composition of the diblock copolymers at the interfaces, and the segregation of the diblocks to the interfaces.

The model system is a binary mixture of two types of AB diblocks, with chemical compositions $f_1 = Z_{1A}/Z_1$, $f_2 = Z_{2A}/Z_2$, and a Flory-Huggins interaction parameter χ between the A and B units. Here Z_1 and Z_2 are the degrees of polymerization of the two diblock copolymer chains and Z_{1A} and Z_{2A} are degrees of polymerization of the A blocks for the first and second components. The binary mixture itself is composed of two monodisperse components, with $1 - \phi$ as the volume fraction of the first component and ϕ as the volume fraction of the second component. The phases of diblock copolymer melts are well described by mean-field theory. Many methods have been developed to solve the mean-field equations for single component diblock copolymer melts. The methods are usually applicable for either the strong segregation limit 3) or for the weak segregation limit 4), both involving specific assumptions about the polymer density profiles. An exact approach, which neither involves a priori assumptions about the shape of the equilibrium density profiles nor truncates the free energy, corresponds to solving the mean-field equations numerically 5). For the binary mixtures of diblock copolymers, an analytic theory in the strong segregation limit has been developed and applied to the lamellar and cylindrical phases of the mixtures $^{6)}$. The model system is studied by using the self-consistent mean-field theory described in $^{1)}$. For a given set of parameters $\{\chi, Z, f_1, f_2, \phi\}$, the self-consistent field theory is solved for the lamellar, cylindrical, and spherical structures. The equilibrium structure is determined by minimizing the free energy density with respect to the domain sizes of the structure. This procedure is repeated for all values of f_1, f_2, and ϕ. The phase diagram is then constructed by analysing the free energies of the different structures.

For the case of mixtures of long and small amount of short diblock copolymers $(Z_1 >> Z_2, \phi << 1)$ $^{1)}$, our studies demonstrated that the addition of a small amount of the short diblocks has quite large effects on the phase boundaries, as exemplified in Figure 1. The fact that we can change the phase boundary by blending a small amount of short diblocks into the long diblock melt provides a novel method to control the phase behavior of the system.

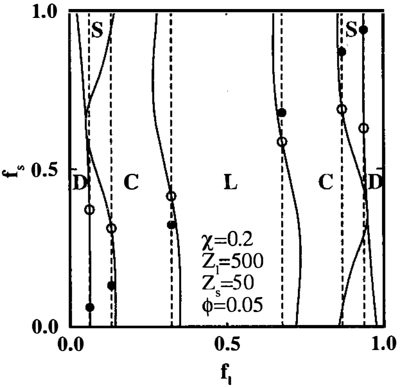

Figure 1 Calculated phase diagram for binary mixtures of long and a small amount of short diblock copolymers, showing the shift of the phase boundaries between the lamellar (L), cylindrical (C), spherical (S), and the disordered (D) phases.

For the case of mixtures of equal lengths diblock chains$^{2)}$, the phase diagram is complicated by the appearance of several new phases and a phase separation region, as exemified in Figure 2. When one of the diblock copolymers is highly asymmetric, *e.g.* $f_1 \sim 0$ or 1, two new phases, a bilayer diblock lamellar phase and an inversed spherical phase, are stablized in the system. The density profile for the inversed spherical phase is shown in Figure 3, indicating a spherical phase with homopolymers localized inside the spheres. Some possible applications of this novel phase have been suggested $^{2)}$.

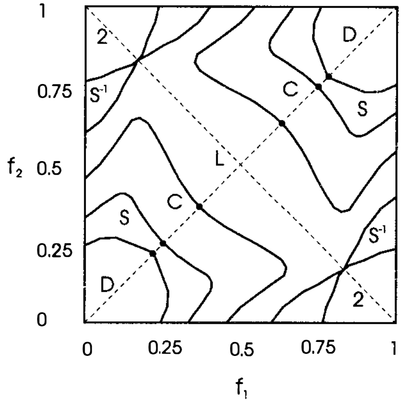

Figure 2 Calculated phase diagram for binary mixtures of diblock copolymers of equal lengths. The phase separation region is indicated by 2 and the inversed spherical phase is indicated by S^{-1}.

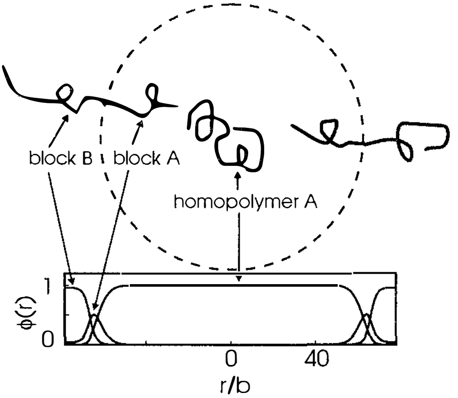

Figure 3 Structure-density profile diagram for a mixture of a homopolymer and an asymmetric diblock copolymer resulting in inverse spherical domains containing the homopolymer.

The calculated phase diagram can be understood in terms of the interfacial spontaneous curvature and the segregation of the diblocks. The spontaneous curvature of the interfaces is determined by the chemical compositions of the diblocks at the interfaces. If the diblocks are completely segregated, the spontaneous curvature is proportional to the total chemical composition $f = (1-\phi)f_1 + \phi f_2$, and the phase boundaries will be determined by f only, *i.e.*, the phase boundaries will be parallel to each other. The segregation of the diblocks is determined by the chemical compositions f_1 and f_2. Figure 4 shows the calculated density profiles for the mixtures of long and short diblocks.

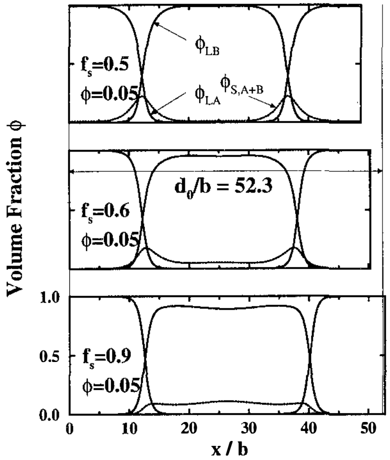

Figure 4 Calculated lamellar concentration profiles for $Z_l = 500$, $Z_s = 50$, $f_l = 0.5$, $\phi = 0.05$, (a) $f_s = 0.5$; (b) $f_s = 0.95$. The long chain profiles are plotted as solid lines and the short chain profiles are represented by the shaded areas. The equilibrium domain spacing of the pure diblock system (d_0) is indicated in the middle. For symmetric short diblocks (top panel) the small molecules localize at the interfaces. For asymmetric short diblocks (bottom panel) the small molecules localize in the domains. All distances are expressed in terms of the Kuhn's length b.

When f_1 and f_2 are close to 0.5, the diblocks are segregated to the interfaces. This explains the approximately parallel phase boundaries in the interior of the f_1-f_2 phase diagrams. On the other hand, when either f_1 or f_2 is close to 0 or 1, the highly asymmetric diblocks are localized in the middle of the domains, as will be demonstrated in the next section, and the interfacial spontaneous curvature is no longer determined by the total chemical composition f. For example, when $f_1 = 1$, the spontaneous curvature of the interfaces is determined by f_2. The appearance of the spherical, bilayer lamellar, and inverse sperical phases can be attributed to the change of the interfacial curvature with f_2.

In summary, a systematical study of the doblock copolymer binary mixtures has been launched using the self-consistent mean-field theory. The results for the two extreme cases, mixtures of long and short diblocks and mixtures of equal length diblocks, demonstrate that the phase behavior of the diblock blends is controlled by the interfacial curvature, which is determined by the average chemical composition of the diblocks at the interfaces, and the segregation behavior of the diblocks. The calculated phase diagram provides a useful tool for the design of diblock blends with specific microphases. A number of new phases are predicted, and possible applications of these new phases are explored.

REFERENCES

1. Shi, A.-C.; Noolandi, J. *Macromolecules* **1994**, 27, 2936.
2. Shi, A.-C.; Noolandi, J. *Macromolecules* , , In press.
3. Leibler, L. *Macromolecules* **1980**, 13, 1602.
4. Semenov, A. N. *Sov. Phys. JETP* **1985**, 61, 733.
5. Vavasour, J. D.; Whitmore, M. D. *Macromolecules* **1992**, 25, 2041. Matsen, M. W.; Schick, M. *Phys. Rev. Lett.* **1994**, 72, 2660.
6. Zhulina, E. B.; Lyatskaya, Yu. V.; Birshtein, T. M. *Polymer* **1992**, 33, 332.

MIXED MICELLISATION IN A BIDISPERSE DIBLOCK COPOLYMER SOLUTION

P. Sens,
Institut Charles Sadron,
6 rue Boussingault, 67083 Strasbourg Cedex, France

Abstract

We discuss theoretically aggregation in a solution of diblock copolymers of two different sizes. The free energy of one aggregate is calculated as a function of the proportion of short and long chain in the micelle. We use the Doud-Cotton model to calculate the energy of the micelle as a function of the aggregation number of each component. The two parameters that caracterize the asymmetry of the blocks are the ratio of the insoluble part of the diblock n and an other parameter b which depends on the sizes of the soluble parts of the diblocks. Mixed micelles are found only in an intermediate range of n and b, which shows that diblock copolymers with a very different asymetry do not mix. In a certain range of asymetries, the small copolymers are incorporated discontinously into the micelles formed by the larger copolymers. This leads to two different types of aggregates coexisting in the solution: micelles containing only large copolymer, and mixed micelles.

1- Introduction

A diblock copolymer is a long flexible chain composed of two different polymers chemically attached together. Imersed in a selective solvent which is a bad solvent for one of the blocks and solubilizes the other block, the insoluble part shrinks while the soluble part is swollen. At sufficiently high copolymer concentration, a surfactant-like aggregation process called micellisation is observed[1]. The purpose of this work is to study this aggregation in a bidisperse solution composed of long and short copolymers. The soluble part (or hydrophilic part if the solvent is polar) is supposed to be much longer than the insoluble part for the two biblocks, so that the aggregates are always spherical[2] and can be described by the Daoud-Cotton model.

2- Daoud-Cotton model for the mixed micelle

A spherical micelle is decomposed in three parts. An outer corona formed by the long and short hydrophilic blocks and characterized by the length of each swollen blocks h_l and h_s, a spherical core of radius R formed by the melt of insoluble blocks, and the interface between them, characterized by a interfacial tension γ (see Fig. 1). For a bidisperse micelle, the blob model due to Daoud and Cotton gives the

---

[1] Israelachvili, J.N. *Intermolecular and Surface Forces,* Academic, London (1992)

[2] Izzo, D.; Marques, C.M. *Macromolecules* **1993,** 26, 7189

following expression for the energy of the corona[3] :

$$E(p_l,p_s)=(A-B)p_l^{3/2}+B(p_l-p_s)^{3/2} \qquad (1)$$

where pl and ps are the number of long and small block in the micelle, and A and B caracterize the asymetries of the blocks: $A=\log(h_l/R)$ and $B=\log(h_s/R)>$ A and B are considered as roughly constant ($h_l>h_s>R$) [3]. In the following, the ratio is denoted by $b=B/A$ ($0<b<1$). The micelle is sketched qualitatively in figure 1.

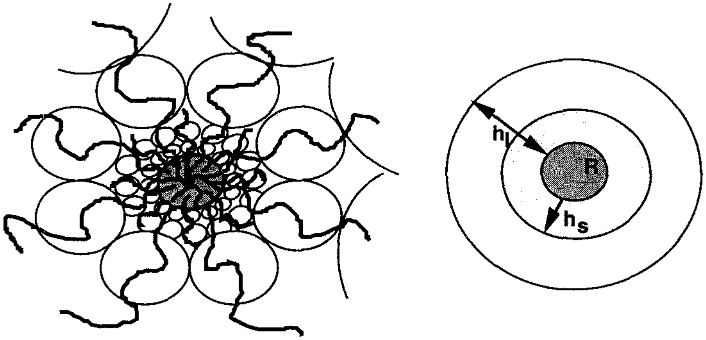

Fig.1 Schematic representation of the Daoud-Cotton model for a bidisperse micelle.the outer corona is formed by the long chains and the interne corona is formed by long and short chains

3- linearisation near the one component limit

To determine the critical micellar concentration (cmc) and the aggregation number of each species, the following set of conditions has to be satisfied (see [4] for detailed calculation)

$$\mathcal{F}=0 \qquad \partial_{pl}\mathcal{F}=0 \qquad \partial_{ps}\mathcal{F}=0 \qquad (2.a)$$

where $\mathcal{F}$ is the free energy of the aggregates that has to be minimized

$$\mathcal{F}=E(p_l,p_s)+\gamma(N_lp_l+N_sp_s)^{2/3}-\mu_lp_l-\mu_sp_s \qquad (2.b)$$

N_l and N_s are the degree of polymerization of the insoluble part of the long and short copolymer. The ratio of the polymerization indices $n=N_s/N_l$ ($0<n<1$). In the free energy, the interfacial energy has been expressed as a function of the aggregation number by using the volume conservation of the core, and the elastic energy of the core has been neglected since for spherical micelles it is much lower than the energy of the corona[4]. A chemical potential has been introduced for each species (μ_l, μ_s) to take into account the exchange between the micelle and the bulk. Below the cmc,

---

[3] Daoud,M.; Cotton, J.P. *J. Phys. (Paris)* **1982,** *43,* 531

[4] Sens,P.; Marques, C.M. ; Joanny, J.F. *In preparation*

each chemical potential increases as the logarithm of the bulk concentration of the copolymer. Once aggregation occurs, the chemical potentials are roughly constant[1].

In order to simplify these equations, we investigate the perturbation caused by a small amount of small copolymer $\delta\mu_s$ added to a solution of long copolymers. This problem can be solved by an expansion near the solution of equation (2) for $p_s=0$, which gives the cmc and the aggregation number of a monodisperse solution of long copolymers: $p_l^0=(2\gamma/3A)^{6/5}N_l^{4/5}$ and $\mu_l^0=(2\gamma/3)^{3/5}(AN_l)^{2/5}$ (the equivalent expression for the small copolymer p_s^0 and μ_l^0 are straightforward).

The linear expansion is performed with $p_l=p_l^0+\delta p_l$, $p_s=\delta p_s$, $\mu_l=\mu_l^0+\delta\mu_l$, $\mu_s=\mu_s^*+\delta\mu_s$ and shows that a minimal chemical potential (or concentration) of short chain in the bulk $\mu_s^*=(3b+n)/5(bn)^{2/5}\mu_s^0$ is needed for the mixed micelles to be formed. Mixed micelle form only if the short diblocks are incorporated in the large micelle before they can aggregate by themselves. This statement require that $\mu_s^*<\mu_s^0$, which limit the difference in asymmetry of the two types of diblock:

$$3b+2n<5(bn)^{2/5} \qquad (4)$$

Once this condition is fullfiled, the linearisation gives the number of small copolymer incorporated in the large micelle $\delta p_s/p_l^0 \approx \delta\mu_s/(D\mu_l^0)$ with

$$D=5b-9b^2+8bn-4n^2 \qquad (5)$$

One easily sees that the solution is non physical for values n and b such that D<0. It has been shown [4] that this range of parameters correspond to a situation where the number of short diblocks in the micelle jumps discontinously from zero to a finite value as one increases the concentration. In this case, micelles of two different compositions can be found in equilibrium in the solution, as shown in figure 2 where the probability distribution of finding a micelle with a given composition is plotted. The distribution exhibit two distinct peaks, one for mixed micelles and one for micelles of long copolymer.

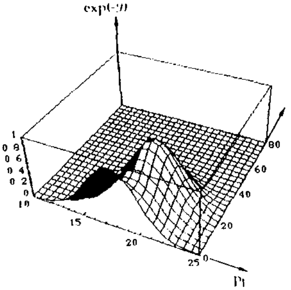

Fig.2 Probability distribution of finding a mixed micelle in function of its composition of short (p_s) and long (p_l) diblock in the case of discountinous incorporation of small diblock in the large micelle. Two different types of micelle exist at equilibrium.

Furthermore, one can see from equation (4) and (5) that mixed micellisation can occurs only in intermediate range of the parameters (n,b), and that the discontinous behaviour mentionned above can be observed in the limit of this range.

4- Evolution of the critical micellar concentrations

One can go beyond the linear expansion by solving numerically the set of equations (2). The result is presented in figure 3 in a (μ_s-μ_l) diagram.

Two possible trajectories at fixed concentration of short copolymers are presented. (1) The concentration of small copolymers is below μ_s^0 (the lowest chemical potentiel compatible with mixed micellisation). In this case the concentration of small copolymers is not high enough to allow mixed micellisation. As the concentration of large copolymers increase, the chemical potential of the large copolymers μ_l increase until it reaches its critical value μ_l^0, where the monodisperse micellisation of large copolymers starts. In this case, the small copolymers are left in the solution. (2) In the second trajectory the concentration of small copolymers is high enough to allow the mixed micellisation ($\mu_s^{(2)}>\mu_s^*$). The mixed micellisation occurs for a concentration $\mu_l^{(2)}$ of large copolymers.

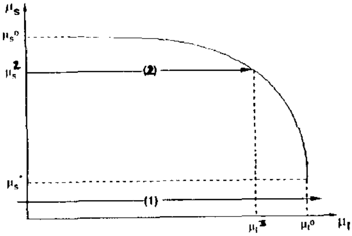

Fig.3 Evolution of the critical micellar chemical potential of long copolymer μ_l with the concentration of small diblocks. the mixed micellisation is possible if $\mu_s>\mu_s^*$

5- Conclusion

This work is a short version of a more complete study of the possibilities of mixed micellisation in a solution of diblock copolymers of two different sizes and asymmetries. We have also derived a phase diagram for the mixed micellisation where one can see that very different copolymer do not mix. By very different, we mean very different values of the two parameter n and b. Two copolymers of very different sizes but same asymmetry can mix in our model. The coexistence of micelles of two different composition is found in a certain range of asymmetry. The detailed calculation has been presented elsewhere[4], where we also discus a brush model which might apply to mixing of copolymer and surfactant.

DYNAMIC LIGHT SCATTERING STUDIES ON THE NEW SURFACTANT CETYL TRIMETHYL AMMONIUM HYDROXY NAPHTHALENE CARBOXYLATE (CTAHNC)

B.S.Valaulikar, W. Urbach and D.Langevin
Laboratoire de Physique Statistique,
Ecole Normale Superieure,
24 Rue Lhomond, 75231, PARIS, FRANCE
P.A.Hassan and C.Manohar,
Chemistry Division, Bhabha Atomic Research Centre, Trombay,
BOMBAY-400 085, INDIA

The surfactant CTAHNC forms worm-like micelles at low concentration. Surface tension measurements show two CMC's at very low concentration of the surfactant. The second CMC at 0.025mM corresponds to the formation of giant micelles. At higher concentration of the surfactant liquid crystalline phases form and the solution shows flow birefringence indicating the presence of rod-like micelles.

Dynamic light scattering measurements are done to obtain the diffusion coefficient as a function of the concentration of the surfactant. The diffusion coefficient is also measured as a function of temperature. The effect of the addition of salt on the diffusion coefficient is also studied. The hydrodynamic radius is obtained from the diffusion coefficient and the results are discussed in terms of the shape and size of the micelles.

INTRODUCTION

In the past few years there has been a considerable interest in surfactant systems which form worm like micelles[1-3], the most studied being Cetyl trimethyl ammonium bromide (CTAB) with Sodium Salicylate (NaSal). These systems form worm like micelles at very low concentrations of about a few mM and form networks. The network properties are different from similar systems of polymers in view of the finite life time of the long micelles and play a decisive role in controlling the rheological properties[4,5]. The ability of these systems to show the interesting properties at low concentrations has been traced to the surface activity of NaSal molecules which results in strong adsorption on to micellar surface of CTAB transforming it into a giant worm like micelle[6]. Since the surface activity of the molecule plays an important role an attempt was made to enhance the surface activity by incorporating an extra benzene ring into NaSal to obtain Sodium Hydroxy Naphthalene Carboxylate (SHNC)[7,8]. The addition of SHNC to CTAB solutions not only produced two viscoelastic gel phases but it also showed two liquid crystalline phases (possibly nematic) thus indicating the close connection between the two structures. The viscoelastic gel also showed strong flow birefringence. This motivated us to prepare CTAHNC - a new surfactant obtained by removing NaBr from CTAB +SHNC mixture. This enabled us to investigate a two component system instead of the multicomponent CTAB+SHNC system. Such two component systems are studied by Hoffmann et al[2]. The surfactant CTAHNC has been not studied upto now and we report here the preliminary results of Dynamic Light scattering (DLS) studies on this surfactant. Our results indicate that the surfactant forms long micelles at very low concentrations.

MATERIALS AND METHODS

CTAB was obtained from sigma chemicals and the SHNC was a gift from Atul Chemicals. SHNC was purified by methods mentioned earlier[7]. CTAHNC was prepared by taking equimolar solutions of CTAB and SHNC in water and filtering the resulting precipitate. The precipitate was washed several times with water to remove the NaBr and was dried. The surface tension was measured by Du Nouy ring method. The DLS experiments were performed on the instrument built in our laboratory.

OBSERVATIONS

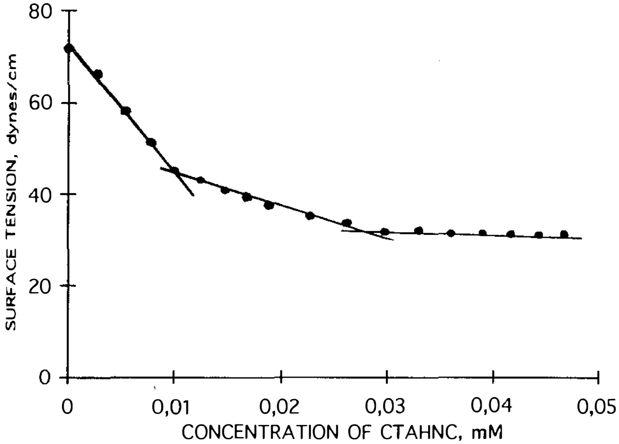

Figure 1: Surface tension of the CTAHNC solution as a function of its concentration.

Figure 1 shows the plot of surface tension versus concentration of CTAHNC and it is seen that there is change in slope of the plot at two different concentrations of CTAHNC. The first change of slope occurs at 0.01mM (cmc1) and the second at 0.028mM (cmc2). Such changes in the physical properties are seen in some surfactant systems due to the change in the shape of the micelles from spherical to rod shape[9)]. Hence, CTAHNC micelles can be said to have spherical shape from cmcl to cmc2 and cylindrical shape above cmc2. These values are typical of nonionic surfactants and this correspondence indicates that CTAHNC behaves like a uncharged surfactant. This suggests that one can look upon CTAHNC as a double chain surfactant one with a long chain and the other with a short chain. The packing considerations show that one can expect to form long cylindrical micelles out of such double chain surfactants [10)].

The diffusion coefficients were measured by obtaining the Intensity-Intensity autocorrelation function g(t) at several angles and fitting the data with a polydispersity fit using the relation:

$$g(t)=A\ (\exp(-t/\tau) + p/2\ (t/\tau)^2)^2$$

where τ is the correlation time of the decay and p is the polydispersity index which is related to the width of the size distribution[11]. The measured decay correlation times τ were inversely proportional to q^2 where $q = \frac{4\pi n}{\lambda}\sin\frac{\theta}{2}$, n being the refractive index of water, λ being the wavelength of the laser and θ is the sctttering angle. The plot of 1/τ versus q^2 is linear and the slope of this plot gives the diffusion coefficient. The polydispersity index p is in the range of 2 to 4%.

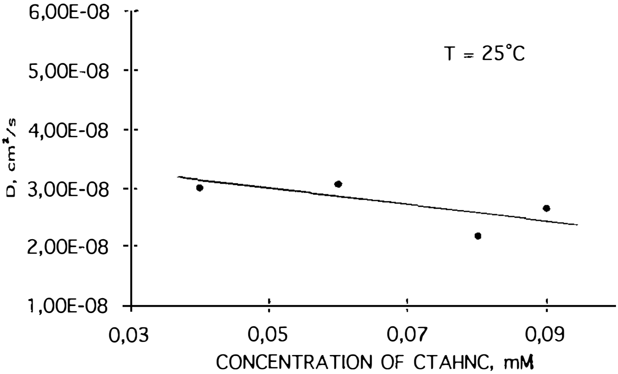

Figure 2: Difffusion coefficient of CTAHNC solution as a function of its concentration.

Figure 2 shows the diffusion coefficient (D) as a function of the concentration of CTAHNC. The concentration range is from 0.04mM to 0.09mM. The samples below 0.025mM showed very low intensity and hence the D value could not be obtained at low concentrations. As seen in figure 2 the diffusion coefficient decreases as the concentration of CTAHNC increases. This indicates that the micellar size increases with increase in concentration of the surfactant.

Viscoelastic gels are known to be sensitive to temperature changes. Hence the diffusion coefficients are measured as a function of temperature. Figure 3 shows the diffusion coefficients measured for two concentrations, 0.04mM and 0.08mM both above the cmc2 as a function of temperature T. The temperature is changed from 20° C to 35° C. The diffusion coefficient increases with an increase in the temperature of the solution.

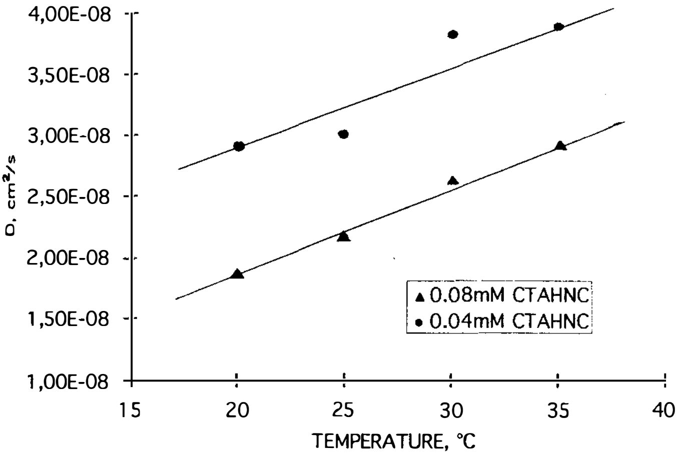

Figure 3: Difffusion coefficient of CTAHNC solution as a function of temperature.

The diffusion coefficient is also measured in presence of salts like KCl, NaCl, ammonium carbonate. This is essential as ammonium carbonate is added to the system to change the pH in FRAP (Fluorescence Recovery After Photobleaching) experiments. The diffusion coefficient is found to decrease in presence of very small amounts (0.2mM) of the electrolyte. The further addition of the electrolyte increases the diffusion coefficient. At higher concentration of the electrolyte (above 1mM) some particles appear in the solution. The appearance of small particles makes the measurement of D inaccurate. The study suggests that the addition of electrolyte decreases the solubility of the surfactant and the surfactant is salted out of the solution.

DISCUSSION

In DLS experiments, the diffusion process observed depends upon the lengths probed (L) and the q value. In dilute solutions L is the hydrodynamic radius R whereas in concentrated solutions L represents the correlation length ξ. For qL<<1, the process observed is the centre of mass diffusion and τ is given by $\tau^{-1} = Dq^2$ where $D = \frac{k_B T}{6\pi\eta R}$, k_B being the

Boltzman constant and η is the viscosity of water at temperature T. For qL>>1, the contribution from the internal modes of the micelles is added and τ is given by: $\tau^{-1}= Dq^{g}$. For qL>4.2 Adam et al[12)] found that g=2.8. The qL values for CTAHNC samples are in the range 1.12 to 2.66. Thus, a mixing of the two diffusion processes is observed. Since there is no deviation from the relation $\tau^{-1}= Dq^{2}$, the contribution of internal modes is small and one can get an idea of the dimension of the micelle using the relation $D=\frac{k_B T}{6\pi\eta R}$.

The calculated R values are in the range of 700 Å to 1000 Å. Since the micelles of this size are expected to be non-spherical, the actual longer dimension of the micelle is greater than 1000 Å. If the volume of the sphere with radius R is equated to the volume of a cylinder with radius 20 Å (approximate length of the CTAHNC chain) then the length of such a cylinder is of the order of 10^{6} Å. However such large lengths are expected to be in coiled form and the actual length will be less than 10^{6}Å. It is decided to use some other technique to confirm the findings of this study. The increase in D with the increase in temperature is due to the decrease in ηR value. The hydrodynamic radius calculated using the proper value for viscosity of water showed a decrease with increase in temperature.

CONCLUSION

The DLS experiments indicate the formation of giant micelles in the solution of the surfactant CTAHNC at very low concentration. The hydrodynamic radius of the micelle is in the range of 700 Å to 1000 Å. The diffusion coefficient of the micelle increases with the increase in the temperature of the system. The diffusion coefficient is also sensitive to the presence of the electrolytes in the system.

ACKNOWLEDGEMENTS

We would like to thank Dr.S.D.Samant for SHNC samples and for advice regarding purification method. This work was supported financially by Indo-French Center for Promotion of Advanced Research (IFCPAR) grant for project 1007-1 . We are grateful to Director, IFCPAR for all the administrative support.

REFERENCES

1) M.E.Cates and S.J.Candau, J.Phys.Condens.Matter. 2 6869(1990)
2) H.Rehage and H.Hoffmann, Molecular Phys. 74 933(1991)
3) H.Rehage, I.Wunderlich and H.Hoffmann, Prog.Colloid. Interface. Sc. 72 1986(1986)
4) M.E.Cates, Macromolecules, 20 2289(1987)
M.E.Cates, Macromolecules, 21 256(1988)
5) S.J.Candau, F.Merikhi, G.Watson and P.Lemarechal, J.Physique, 51 977(1990)
6) C.Manohar, U.R.K.Rao, B.S.Valaulikar and R.M.Iyer, J.Chem.Soc. Chem.Comm. 379 (1986)
7) B.K.Mishra, S.D.Samant,P.Pradhan, S.B.Mishra and C.Manohar, Langmuir 9 894(1993)
8) S.Mishra, B.K.Mishra, S.D.Samant, J.Narayanan and C.Manohar, Langmuir 9 2804(1993)
9) H.Hoffmann, G.Oetter, B.Schwandner, Prog.Colloid.Polym.Sci., 73 95(1987)
10) S.Mishra, B.K.Mishra, D.K.Chokappa, D.O.Shah and C.Manohar; Bull.Mat.Sci. (To be published).
11) P.N.Pusey, Photon Correlation and Light beating spectroscopy, Eds. H. Z.Cummins and E.R.Pike, Plenum, 1973, NY.
12) M.Adam and M.Delsanti, Macromolecules 10 1229(1977).

WETTING AND ADHESION

Spreading of chain molecules via molecular dynamics

by

Joël De Coninck
Modélisation Moléculaire
Université de Mons-Hainaut
20, Place du Parc
7000 - Mons
Belgium

1.Introduction

Wetting and spreading are important phenomena for many practical purposes and their study is mainly based on Young's equation, already established a few centuries ago. Rather recently however, new powerful techniques have been used to get a microscopic description of these processes using for instance ellipsometry, AFM/STM,... Very surprising properties have been observed at that scale and many research groups are trying to get a clear understanding of these phenomena.

In this paper, we study the dynamics of the spreading of liquid drops of chain molecules on a solid substrate using complementary microscopic approaches.

Section 2 will be devoted to the presentation of some experimental observations. In Section 3, we will present the status of the related effective models and we will complete this "tour" by new results using Molecular Dynamics in Section 4. Some perspectives are given in Section 5.

2. Some experimental observations.

Remarkable ellipsometric techniques with a very high resolution normal to the substrate have been used in particular by A.M. Cazabat, M.P. Valignat... in the Collège de France to observe the time dependent profile of sessile drops of polymeric fluids in a complete wetting regime. [1]

Different profiles of a drop of polydimethylsiloxane on top of silicon wafer covered by a grafted layer of trimethyl groups are presented for instance in figure 1.

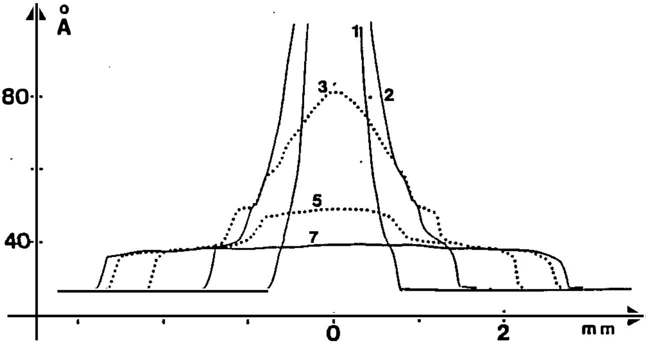

Figure 1: Ellipsometric thickness profiles of a polydimethylsiloxane as a function of the time. The profiles are recorded every 24 hours.

These results show clearly the existence of layers of molecular thickness (of the order of 7 Å). Plotting the radius of these layers as a function of the time, there appears one regime in $\sqrt{t}$ for the short-times. Moreover, when the second layer becomes empty, there appears a second regime in $\sqrt{t}$ for the first layer.

More information on experimental observations can be found in Valignat's contribution to this book or in [2-3].

The origin of this $\sqrt{t}$ behaviour is far from being clear : is it related to substrate or chain effects for instance? Moreover, the details of the mechanism of spreading cannot be observed at that scale.

3. Some effective models

One of the first related model is due to de Gennes and Cazabat [4] and is based on hydrodynamical considerations. Assuming viscous frictional forces for the contact with the wall, this model leads to a good description of the data.

Several research were devoted to a molecular description of these spreading properties. Two main ingredients are required to define such model.

Once we have described the energy of interaction between the atoms of the liquid and the atoms of the solid, it remains to define the dynamics to describe the displacement of the atoms as a function of the time, starting from a sessile drop.

A first series of numerical simulations were based on Monte-Carlo dynamics with a local conservation of matter [5].

Let us consider a lattice $\mathbf{Z}^3$ at each site i of which we consider a variable n_i which may take two values : +1 if there is an atom and 0 otherwise. The substrate is given by the half infinite lattice $\mathbf{Z}\mathrm{x}\mathbf{Z}\mathrm{x}\{n\in\mathbf{Z}\,|\,n\leq 0\}$. The energy of interaction is of the form

$$H(n_1,\ldots,n_N) = \sum\nolimits_{i,j} v_{ij} n_i n_j + \sum\nolimits_i A(i) n_i \tag{1}$$

where v_{ij} is the pairwise interaction energy, which is taken for simplicity equal to v if i and j are nearest neighbours and 0 otherwise. The term A(i) describes the liquid/substrate interaction. It is given by A/d^3 where d is the distance between the atom i and the substrate whenever $d>1$ and some constant B whenever $d=1$ in lattice units. Within this model, we consider an initial configuration of occupied sites and let the system evolve according to a Monte-Carlo dynamics which preserves locally the number of occupied sites.

At each step, the atoms (n_i,n_j) can interchange positions according to the Kawasaki's algorithm [6], i.e. with a transition probability P given by

$$P[(n_i,n_j)\rightarrow(n_j,n_i)] = \frac{1}{1+e^{-[H(n_i,n_j)-H(n_j,n_i)]/kT}} \tag{2}$$

with all the other sites of the system being kept fixed; k is the Boltzmann's constant and T is the temperature.

The advantage of these models is that they allow to recover all the experimentally observed properties. For instance, we can interpret the origin of the diffusive growing in terms of random displacements of the molecules on top of the first layer; these molecules will then find the wall once there appear some vacancies in their vicinity within the first layer due to thermal fluctuation.

This model also lead to a simple interpretation of the origin of the second √t regime observed for the first layer.

We have indeed to consider for the initial drop a temperature T below the critical temperature, in a three dimensional space (d=3), $T_c^{d=3}$. Once all the molecules belong to the first layer, the system becomes a two dimensional system on top of the substrate, and it is known that $T_c^{d=2} \leq T_c^{d=3}$ [7]. If the considered temperature T is such that

$$T_c^{d=2} \leq T \leq T_c^{d=3} \tag{3}$$

we will then observe a second diffusive regime for the first layer, once the second layer become empty [5], and the associated gas phase.

Another interpretation has been proposed within this context by taking into account possible heterogeneities on top of the substrate [8].

However for these models, it is not possible to justify the choice of the dynamics except perhaps in some coarse grained sense.

The only possibility to do that microscopically is to consider the associated Molecular Dynamics technique.

4. Molecular dynamics for chain molecules.

Let us consider a set of atoms interacting via some classical L-J potentials, the dynamics of the system being given by the classical Newton's equations relating the forces acting on this atom i to its acceleration $\mathbf{a}_i$.

$$\sum_j F_{ij} = m_i a_i \tag{4}$$

This technique has been previously used for simple molecules (mono and bi-atomic molecules) by Yang, Koplik and Banavar [9] and by Nieminen, Abraham Kartienen and Kaski [10]. The two groups considered respectively two different plane: one modeled by five layers of atoms and the other by an idealized flat substrate. Both type of simulations lead to the existence of a precursor film but they disagree on the time dependence of the radius of the first layer $R_1(t)$: the first group got $\sqrt{\log (t)}$ and the second group, t.

Recently [11,12], we have considered chain molecules within this context.

The pair interactions are given by classical L-J potentials of the form

$$V_{ij}(r) = \frac{C_{ij}}{r^{12}} - \frac{D_{ij}}{r^6} \tag{5}$$

where i and j refer to a liquid or a solid atom and where r is the distance between the two atoms. Moreover, the fluid atoms are subject to some confining potential of the form

$$V_{mol}(r) = D_{mol} r^6 \tag{6}$$

between adjoining atoms belonging to the same molecule. It should be noted that this new potential considerably reduce the volatility of the liquid and is chosen to mimic the properties of the polymeric fluids.

The solid is made by two layers of atoms and we cut the interacting potential for distances r>2.5 in units of the fluid size. To incorporate the long range effects, we add some potential of the form

$$V_{tail}(r)=\frac{A}{(r+u)^3} \tag{7}$$

where u is the unit height of the solid lattice.

For our simulations, we have chosen $C_{ff} = D_{ff} = C_{sf} = D_{sf} = 1$ and $C_{ss} = 36.45$, $D_{ss} = 5$. The parameters which control the wetting behaviours are C_{sf} and D_{sf}. If for instance we lower C_{sf} and D_{sf} , we can obtain a partial wetting regime.

We have considered fluid drops made of 864, 4000, 16384 and 32000 atoms in chains of length 8 and 16 on top of a solid of 147456 atoms.

The initial configuration is given by an equilibrated sphere of liquid which is given a small downward velocity to reach the substrate. During the spreading, the temperature of the solid alone is maintained fix.

The results indicate the existence of a precursor film, the radius of which grows with an asymptotic power law compatible with $\sqrt{t}$ as reproduced in figure 2.

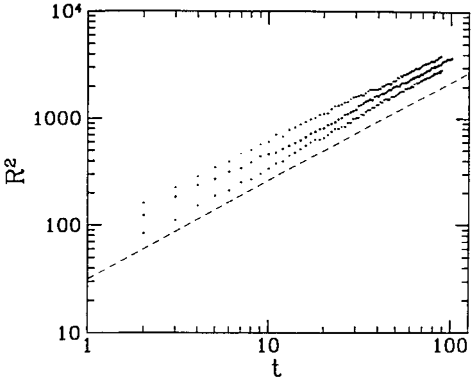

Figure 2 : The squared radius of the first layer as a function of the time t for different drops with chains with 16 and 8 atoms, the straight line shown for reference has a slope of 0.92.

To compute this radius R, at a given time t, we use the same procedure as the experimentalists. We plot the density of atoms of the first layer ρ as a function of the radius r and we define R_1, as the radius at which $\rho(r)$ is equal to 0.5.

On the basis of these results, we are also interested by the molecular details of the spreading : how are the molecules approaching the substrate?

To study this displacement, we have plotted in particular the radius R where the atoms of the second layer enters the first layer normalized by the radius of the second layer at the same time R_2, over 100 units of time to increase the statistics. The results are given in figure 3.

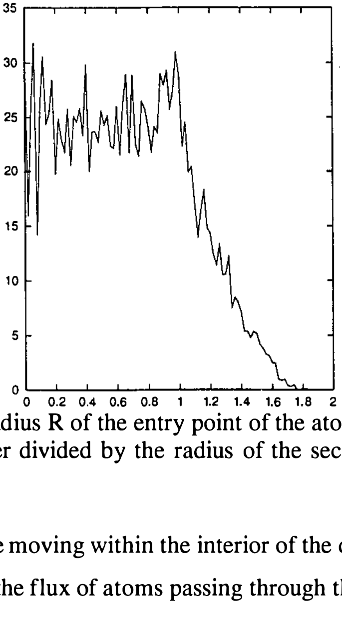

Figure 3: Histogram of the radius R of the entry point of the atoms of the second layer going into the first layer divided by the radius of the second layer at that time, during 100 time steps.

This indicates that the atoms are moving within the interior of the drop. To clarify the situation, we have also studied the flux of atoms passing through the plane separating the first and the second layer. By weighting by +1 the atoms moving downward and by -1 the others, we have obtained the distributions plotted in figure 4 as a function of the reduced radius R/R_2. To improve the statistics, we have again considered averages over successive time intervals of 100 units. We easily observe that the flux is much reduced in the central region.

This picture supports the de Gennes-Cazabat prediction of the existence of a permeation rubber near the edges of the drop, the atoms at the interior moving in fact oftenly up and down.

5. Concluding remarks.

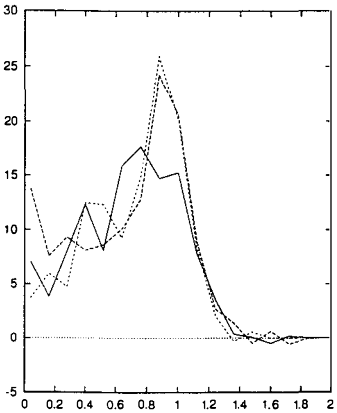

Figure 4: The average flux over 100 time steps per unit area of atoms of a 2000 16-atoms drop going from the second layer into the first layer as a function of R/R_2 for three different starting times.

The introduction of chain molecules combined with very large systems have allowed us to reproduce satisfactorily the experimental observations of spreading for ideal substrates. More realistic substrates are now under investigation and will probably lead to a detailed understanding of these remarkable phenomena.

Acknowledgements

This research is supported by the Belgian Program on Interuniversity Poles of Attraction, initiated by the Belgian state, Prime Minister's Office, Science Policy Programming and by the Région Wallonne.

References

[1] F. Heslot, A.M. Cazabat and P. Levinson, Phys.Rev.Let. **62**, 1286 (1989).

[2] M.P. Valignat, N. Fraysse and A.M. Cazabat, Langmuir **9**, 601 (1993).

[3] M.P. Valignat, N. Fraysse and A.M. Cazabat, Langmuir **9**, 3255 (1993).

[4] P.G. de Gennes and A.M. Cazabat, C.R. Acad. Sci. **310**, 1601 (1990).

[5] J. De Coninck, N. Fraysse, M.P. Valignat and A.M. Cazabat, Langmuir **9**, 1906 (1993).

[6] K. Kawasaki, in Phases Transitions and Critical Phenomena, vol. 2 edited by C. Domb and M.S. Green (Academic, London, 1972).

[7] R.B. Griffiths, in Phases Transitions and Critical Phenomena, vol. 1 edited by C. Domb and M.S. Green (Academic, London, 1972).

[8] A.M. Cazabat, J. De Coninck, S. Hoorelbeke, M.P. Valignat and S. Villette, Phys. Rev. E **49**, 4149 (1994).

[9] J.X. Yang, J. Koplik and J.R. Banavar, Phys. Rev. Lett. **67**, 3539 (1991).

[10] J. Nieminen, D. Abraham, M. Karttienen and K. Kaski, Phys. Rev. Lett. **69**, 124 (1992).

[11] J. De Coninck, U. D'Ortona, J. Koplik and J.R. Banavar, Phys. Rev. Lett. **74**, 928 (1995).

[12] U. D'Ortona, J. De Coninck, J. Koplik and J.R. Banavar, to appear in Phys.Rev.E.

MOLECULAR EFFECTS IN ULTRA-THIN LIQUID FILM SPREADING DYNAMICS

S.Herminghaus, U.Sigel, U.Albrecht, P.Leiderer
Fakultät für Physik, Universität Konstanz, 78434 Konstanz,
Federal Republic of Germany

The Spreading Dynamics of Silicon Oil Films at thicknesses in the monolayer regime is studied by monitoring the evolution of the coverage profile with optically excited surface plasmons. While for thicknesses above one monolayer the observed profiles agree well with the theory of viscous flow spreading, strong deviations are observed at smaller coverages which point to a diffusivity which decreases with decreasing coverage. This can be qualitatively explained in the framework of the excluded area interaction of the chain molecules. When the coverage decreases, the configurational entropy of the individual molecules changes strongly, leading to a substantially enhanced apparent viscosity for submonolayer films.

The spreading dynamics of oil films on solid surfaces has been studied intensively during the last decade, mainly because of its importançe for lubrication and coating applications [1,2]. An extensive theoretical treatment of the spreading of nonvolatile liquids has been set up [3] assuming viscous flow and neglecting the effect of the molecular structure of the oil. Within this framework, many experimental observations could be quantitatively predicted. More recently, one has started to focus on the impact of the molecular structure on the film profiles. In the monolayer regime, a tendency of layering was also observed with chainlike molecules in experiments [4,5] as well as in molecular dynamics simulations [6-8]. In the present work, we investigate the regime of molecular diffusion in the submonolayer regime for chainlike molecules. In experiments with poly(dimethylsiloxane) (PDMS) films on metal surfaces, we monitored the emerging film profiles optically by means of surface plasmons, as described before [4]. It is observed That the continuum model breaks down quite abruptly at a film thickness corresponding to the backbone diameter of the molecules, crossing over to submonolayer diffusion. This is the regime we want to focus on in the present paper.

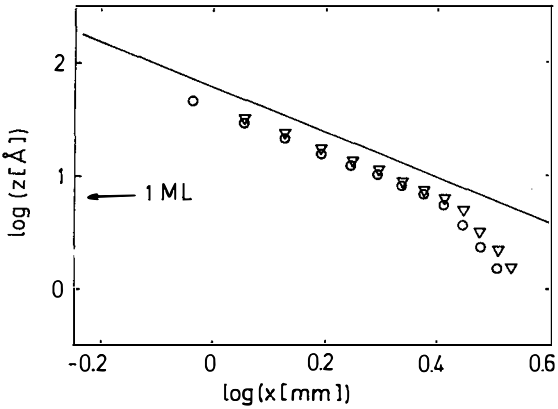

Fig.1. Log-log plot of precursor film profiles of PDMS on an evaporated gold film, measured in vertical rise geometry. Above a thick-ness of 7Å, the profiles agree well with the scaling law predicted for viscous flow (represented by the straight line only the slope of which is significant). Below 7Å, which corresponds to one densely packed layer, significant deviations are observed.

Fig.1 shows a set of typical data obtained for a vertical-rise geometry. The profiles obtained are plotted on a log-log scale in order to compare with the theoretical prediction that the precursor film thickness d should scale as the inverse square of distance, $d \sim x^{-2}$ [2]. The slope of the straight line is -2, demonstrating the good aggreement of theory with the profiles found experimentally, at least for film thicknesses exceeding 7 Å. This is just the diameter of the PDMS backbone and corresponds to the thickness of one monolayer (ML) of densely packed molecules lying flat on the surface. Below this thickness, significant deviations from the scaling law are observed. Qualitatively, a steeper profile is needed to produce the creep velocity of the precursor film, which points to a reduction of diffusivity for coverages less than one ML.

This is supported by similar data obtained with spreading microdroplets, which have been published before [4]. It was found both experimentally and in Mote-Carlo (MC) simulations that the profile of sub-monolayer 'droplets' was quite well represented by a spherical cap, instead of a gaussian distribution expected for diffusing single monomers with hard-core interaction. It was shown by MC simulation that the experimental profiles could be well explained by assuming that the chain molecules were lying flat on the surface. If these data are reanalyzed in the framework of the diffusion equation, grad[D(c) grad c] $-$ $\partial_t c = 0$, one can extract the diffusivity D(c), which is plotted in fig.2. (c denotes the coverage, with c=1 corresponding to one ML). It is clearly seen that D(c) increases with increasing coverage for submonolayer films. At first glance, this seems to be a puzzle, since one would expect the mobility of the molecules to *decrease* as they become more densely packed, thus mutually hindering their motion. It will now be shown that although this effect is present, there is also an influence of the conformational entropy of the chains which acts in the opposite direction, overcompensating the former effect. As a result, one obtains, from purely analytical considerations, a simple picture which accounts for the observed behaviour of the diffusivity.

Fig.2. The diffusivity vs. the coverage in the submono-layer regime as derived from the data of ref. [4] (Monte Carlo Simulations). It is clearly seen that the diffusivity increases within the analyzed range of coverage by about a factor of four.

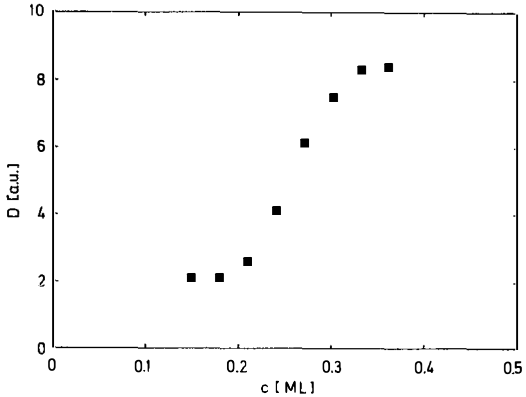

We write the molecular mass current j (in the plane) as [9]

$$j = c \langle v \rangle = c\, m\ \mathrm{grad}\mu(c) = c\, m\ d\mu/dc\ \mathrm{grad}\, c \tag{1}$$

where c is the coverage, <v> is the mean drift velocity of the molecules, $\mu(c)$ is the chemical potential and m is the mobility of the molecules. From the diffusion equation we have j = D(c) grad c and thus

$$D(c) = c\, m\ d\mu/dc \tag{2}$$

For independent monomers, $\mu = kT \ln c$, and D becomes constant, as expected. For chain molecules, we have an additional term $-TS_c$ in the chemical potential which is connected to the conformational entropy S_c of the chains. This can be written as -kT ln w, where w is the number of possible configurations of the chain. This depends on the coverage c, namely on how many near sites are already occupied by monomers belonging to other molecules. We thus have for the chemical potential

$$\mu(c) = kT\ (\ln n - \ln w) \qquad (3)$$

where n = c/l is the number of chain molecules per unit area and l is the number of monomers per chain (i.e., the degree of polymerization). For the diffusivity we thus get

$$D(c) = m\ kT\ \{ 1 - c\ (d \ln w/dc)\} \qquad (4)$$

For further evaluation, we have to find expressions for m and w, which are both affected by neighboring molecules.

We are interested in the coverage dependence of D, whereby we want to compare with the diffusivity D_o of a free (single) chain molecule diffusing alone on the surface. For the latter, there is also a finite coverage being seen by the monomers, namely the other monomers belonging to the same chain molecule. This gives, for instance, rise to the fact that for the conformation of the single chain, only self avoiding random walks (SAW) are to be taken into account (not the 'phantom chain' configurations). Further reduction of the number of possible conformations is effected only by *other* chain molecules. Similarly, the mobility m of the molecule is effectively (with respect to the mobility of a 'lonely' molecule) reduced only by monomers belonging to other chains, not by those belonging to the same one.

In what follows, we denote the probability that a site next to the chain under consideration is occupied by a monomer belonging to a neighboring chain as c_n. For the mobility, we simply write $m = m_o(1 - c_n)$. Here m_o plays the role of an attempt frequency for jumps to neighboring sites of the substrate, and c_n is the probability that a jump is not successful because the target site is occupied by a monomer belonging to another chain. Next, we have to derive an expression for the number of conformations of the chain, w. This is given by the number of SAWs possible under the condition that there is a certain density of forbidden (occupied) sites. For zero coverage on a square lattice, we can approximate this by w 3^l, since a bond can continue either straight, bend 90 degree to the left, or bend 90 degree to the right (three possibilities). This represents a walk which is self-avoiding only in the first consecutive step, but we will take this as an approximation for the sake of simplicity.

What happens if some of the sites are occupied? In the case that all nearest neighbour sites are occupied, there remains only a single conformation, namely the one which is already realized. Generally, there are $2(1-c_n)+1$ possibilities for a single bond, where again we need to know the foreign occupation of the sites next to the chain. We thus have for the number of conformations

$$w \cong \{ 3 - 2c_n)\}^l \qquad (5)$$

and for the diffusivity D(c)

$$D(c) = m_o k\ T\ (1-c_n) \times\{ 1 + [2c\ l\ /(3 - 2c_n))] \times (dc_n/dc)\ \} \qquad (6)$$

To obtain an expression for c_n, we first calculate the blob size ξ of the chains, along the lines of standard scaling theory. To do this, we first recall that the end-to-end distance R as derived from Flory's theory of swelling scales as

$$R \sim l^{3/(d+2)} \tag{7}$$

where d is the dimension of the system. For 3D, this leads to the well known law $R \sim l^{0.6}$. The critical concentration (or coverage, respectively) c* for mutual penetration of the chains is approximately given by the self-density, $c^* \cong l/R^2$ (in two dimensions). For coverages larger than c*, the blob size ξ should not depend on l, since the chains are then longer than the blob diameter. On the other hand, for $c \leq c^*$ we have $\xi = R$. Thus for $c \geq c^*$ we can write a scaling law for ξ:

$$\xi \cong R\,(c^*/c)^m \tag{8}$$

where m is still to be determined. This obviously behaves as

$$\xi \sim l^{(3-2m)/4} \tag{9}$$

where we have used equation (7). To cancel the l-dependence, we have to demand that $3 - 2m = 0$ or, since we are interested only in the c-dependence,

$$\xi \sim c^{-m} = c^{-3/2} \tag{10}$$

Viewed from the chain whose motion is to be examined, the concentration of foreign monomers $c_f(r)$ increases up to the total coverage c within a distance $r \cong \xi$ (r is the distance to the chain, measured in units of bond length). The probability $c_f(1)$ that a site next to the chain is occupied by a monomer belonging to another chain is thus roughly given by

$$c_f(1) \equiv c_n \cong c/\xi \sim c^{m+1} \tag{11}$$

The prefactor must be unity, because when c=1, the probability c_n to have a nearest neighbour site (which would else be free) occupied is equal to one. Consequently, we have $c_n = c^\lambda$. Inserting this into equation (6), we obtain for the diffusivity D(c)

$$D(c) = D_o(1-c^\lambda)\,\{1 + 3\lambda\, c^\lambda\, l/(3-2c^\lambda)\} \tag{12}$$

where $D_o = m_o\, k\, T$ and $\lambda = m + 1 = 5/2$.

The central result of this paper is shown in fig.3, where we plotted $D(c)/D_o$ vs. c for different values of l. For l=10, which is a typical length of the polymers used in our experiments, an increase in the diffusivity similar to the observed one is seen. The small full circles on the curves indicate the estimated limiting concentrations, $c^* = l^{-1/2}$. They correspond in each curve to an increase in D of roughly a factor of two, aside from the 'pathological' case l=1. This case, which should yield $D/D_o \equiv 1$ [10], is also described rather well by the theory as long as one does not approach c=1 too closely. The intersection of all curves at (1;0) corresponds to the fact that when the molecules are lying densely, their mobility is equal to zero. For a polymer diffusing on a surface, this case is of course never observed since as $c \to 1$ (from below), it becomes entropically favourable for monomers to leave the first layer, and the model breaks down.

This work was supported by the Deutsche Forschungsgemeinschaft (SFB 306).

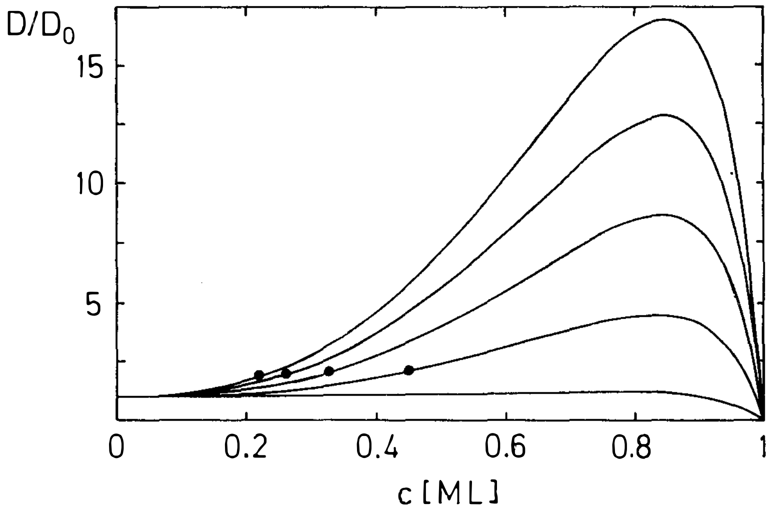

Fig.3. D/D_0 vs. the coverage according to eq.(12) for chain lengths 1, 5, 10, 15 and 20. The maximum value is monotonically increasing with chain length. The qualitative behaviour is obviously similar to what is shown in fig.2

[1] L.Leger, M.Erman, A.M.Guinet-Picard, D.Ausserre, C.Strazielle; *Phys. Rev. Lett.* **60** (1988) 2390.

[2] A.M.Cazabat; *Adv. Colloid Interface Sci.* **34** (1991) 73.

[3] J.F.Joanny, P.-G.deGennes; *J. Physique* **47** (1986) 121.

[4] U.Albrecht, A.Otto, P.Leiderer; *Phys. Rev. Lett.* **68** (1992) 3192.

[5] J.P.Rabe, S.Buchholz; *Phys.Rev.Lett.* **66** (1991) 2096.

[6] R.Hentschke, R.G.Winkler; *J.Chem.Phys.* **99** (1993) 5528.

[7] O. Venäläinen, T. Ala-Nissilä; *Europhys. Lett.* 25 (1994) 125.

[8] J. DeConinck, U. D'Ortona, J. Koplik, J. R. Banavar; *Phys. Rev. Lett.* **74** (1995) 928.

[9] see, for instance: S.R. deGroot, P. Mazur, 'Non-Equilibrium Thermodynamics'. North-Holland 1969.

[10] R.Kutner, Phys.Lett. **81A** (1981) 239.

OBSERVATION OF ENHANCED VISCOSITY OF WETTING LAYERS OF SMALL MOLECULES

S.Herminghaus, T.Paatzsch, T.Häcker, P. Leiderer
Fakultät für Physik, Universität Konstanz, 78434 Konstanz,
Federal Republic of Germany

The transport kinetics of wetting layers of ethanol and propane on silver substrates is investigated by monitoring the temporal decay of pulsed laser induced spatial thickness modulations. Our method allows to distinguish between different transport mechanisms, such as direct exchange with the vapor phase, viscous flow within the wetting layer, or surface diffusion. In either case, the activation energy found for the lateral transport points to viscous flow as the dominant mechanism in the investigated temperature range. For very thin films, the flow proceeds considerably slower than expected from bulk viscosity data. This suggests that the proximity of the substrate influences the morphology of the liquid, giving rise to an enhanced effective viscosity.

Thin films on solid surfaces have become an attractive field of condensed matter physics. This is not only due to their technological importance but also for the sake of the fascinating dynamical phenomena discovered in surface diffusion, catalytic surface reactions and the dynamics of wetting far from thermodynamical equilibrium[1-5]. For specific investigations of these phenomena, one has to identify the basic transport mechanisms and determine the corresponding transport coefficients, which may be strongly affected by the confined (film) geometry[6,7]. In particular, it has been reported that the viscosity of a few molecular layers of liquid between solid walls may be enhanced by up to six orders of magnitude[8]. Effects of this kind have not yet been investigated in equilibrium wetting layers due to the lack of experimental techniques.

We monitored the decay of pulsed laser induced spatially periodic thickness modulations in wetting layers of liquid ethanol and propane on a silver surface. In the absence of inertial effects, the decay proceeds exponentially in time, with the decay rate depending in a characteristic manner on the wave vector of the thickness modulation, $q=2\pi/\lambda$. If the modulation decays via exchange of molecules with the surrounding vapor, the equilibration proceeds locally and the decay rate does not depend on q [9]. If, however, the decay proceeds via lateral transport mechanisms, such as viscous flow within the film or surface diffusion at the liquid-vapor boundary, the decay rate is proportional to q^2.

The substrate consisted of an evaporated silver film (50 nm thickness) whose surface was characterized by scanning tunneling microscopy. On an atomic lateral scale, the films were smooth with height variations of a few Å. On a lateral length scale of a few hundred Å, variations with typical slopes up to 0.4 were found[10]. The thickness variation of an adsorbed liquid film due to this roughness can be estimated from the known substrate profiles, liquid surface tensions and typical adsorption energies[11]. We obtain a thickness variation of only about 2 Å for a 30 Å ethanol film. We thus do not expect the substrate morphology to have a dramatic impact on the lateral transport in the film.

Experiments were performed with wetting layers adjacent to a vertical substrate. The sample consisted of a closed volume next to the silver coated glass prism which served as the cell window. After filling the cell with a certain amount of material, it was cooled down to the desired temperature. A wetting layer formed within a few hours, in the course of thermal equilibration of the sample. The modulation was created by pulsed laser induced thermal desorption using two crossed Nd:YAG laser beams. From the thermal properties of the involved materials, we can estimate that about 100 μsec after the laser pulse, the amplitude of the temperature modulation at the surface has decayed to less than 10 mK. The spatial average of the surface temperature approaches the equilibrium temperature to within 1 K within a millisecond. For the measurement of the film thickness and detection of the thickness modulation, we used optically excited surface plasmons as described before[12,13]. The observed decay times of the thickness modulations ranged from a few milliseconds to several seconds.

Fig.1. Plot of the modulation decay time vs the wavenumber of the modulation for a 30 Å ethanol film at 150 K. The solid line represents a least squares fit according to $A = a\,q^2 + b$. The error bars indicate the standard deviation of a number of meas-urements.

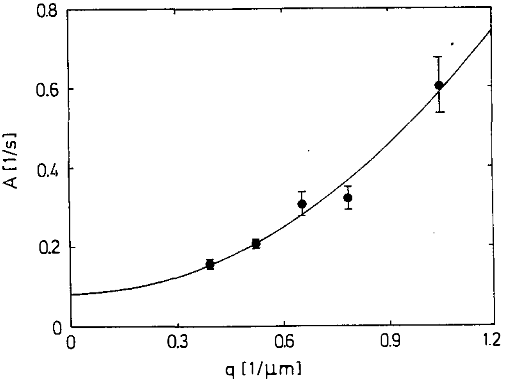

Fig.1 shows the temporal decay constant a of the thickness modulation in an ethanol wetting layer as a function of its wave number, q. At this temperature (T = 150 K), lateral transport seems to play an important role, as the strong q-dependence suggests. The solid line represents a least squares fit of the function $A = aq^2 + b$, where b represents the (q-independent) exchange of material with the vapor and a represents a lateral transport coef-

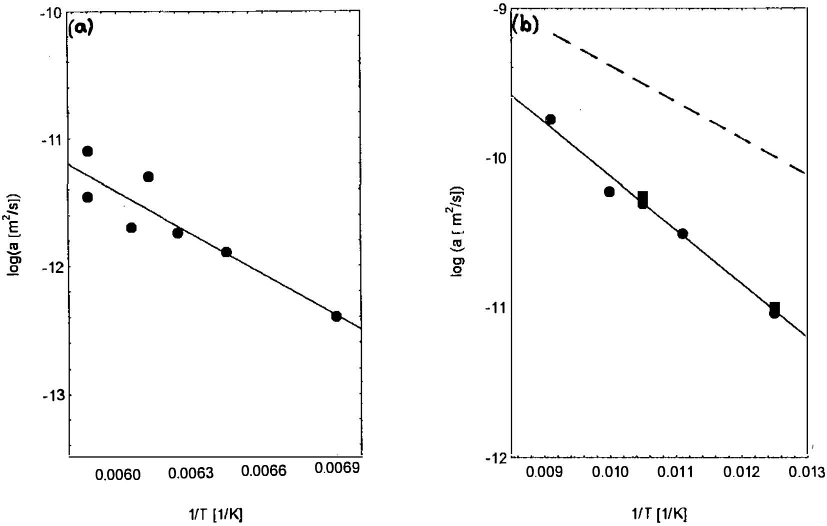

Fig.2. Arrhenius plot of the fit parameter a for ethanol (a) and propane (b) films. The slope, which corresponds to the activation energy of the transport process, suggests that viscous flow is the dominant mechanism. The dashed line represents what one would expect from bulk viscosity data.

ficient. The latter is expected to be inversely proportional to the viscosity of the liquid if viscous flow is the dominant transport mechanism[14)]. An Arrhenius plot of *a* measured with an ethanol film of 30 Å thickness is shown in fig.2a. From the slope of the fitted line, we obtain an activation energy of 220 ± 50 meV, while from reported data for viscous flow[15)] we derived a value of 170 meV. If surface diffusion would play an important role here, we would expect the activation energy to be considerably smaller than the reported value for viscous (bulk) flow. This seems not to be the case here. The deviation to *higher* energies, if considered significant in view of the large experimental scattering, may be due to the high van der Waals pressure within the film, which can be several hundred bars, depending on the interaction potential and the film thickness. Judging from available data for the pressure dependence of th viscosity[15)], it appears possible that this changes the activation energy by the observed amount.

Fig.2b shows our results obtained with propane films of 26 Å thickness. We would like to mention the reproducibility demonstrated by the accordance of the circles with the squares, which were measured in different experimental setups. This lets an influence of contamination effects on our results appear very unlikely. Furthermore, the experimental scattering is considerably less than in the case of ethanol. The slope of the data in the Arrhenius plot yields an activation energy of 73 ± 7 meV, while the reported value for bulk viscous flow is 50 ± 4 meV [16)]. The deviation is similar to what we found for ethanol, pointing again to viscous flow as the dominant transport mechanism, with the activation energy being slightly enhanced probably due to the van der Waals pressure. Surface diffusion does not seem to play an important role.

In order to obtain a prediction not only for the activation energy, but also for the prefactor in the Arrhenius plot, we have to know the Hamaker constant for the interaction of the propane molecules with the substrate. The Hamaker constant does not vary dramatically for different liquids, as long as quantum liquids are disregarded. Even for systems as different as nitrogen, methane and krypton, the calculated Hamaker constants lie within 25 percent[17)]. For the alkanes, the polarizabilities of the C-H bonds can be regarded as additive. We can thus obtain a reasonable estimate for the Hamaker constant of the propane/silver system by appropriate scaling of the value of 23.8×10^3K$Å^3$ reported for the methane/ gold system[17)].

The dashed line in fig.2b represents what one would expect accordingly for the viscous transport in the propane film. As already mentioned, the slope representing the activation energy is quite close to the observation. However, the prefactor of the decay rate differs by more than an order of magnitude. This discrepancy is too large for being explained by the van der Waals pressure in the film. A possible explanation is that the confined geometry of the thin film (i.e., the proximity of the substrate) gives rise to a substantial enhancement of the effective viscosity, similar to what has been observed by other authors for liquid films between solid walls[8)]. In fact, a strong tendency to liquid-crystal-like order near the substrate has been reported for alkanes and other liquids both experimentally[8,18,19)] and theoretically[20)]. An effect of these structures on the transport properties of a wetting layer may be expected, but the crucial test whether this is actually the case is to measure the dependence of the transport kinetics as a function of the liquid film thickness.

This is shown in fig.3, where we have plotted the decay coefficient a vs the film thickness in a log-log plot at T = 90 K. For Poiseuille flow in the film and a van der Waals potential following an inverse-cube law[21)], *a* should vary inversely proportional to the film thickness. This is indicated by the solid line where the Hamaker constant has been estimated as discussed above. As one can see, the discrepancy in the transport rates almost vanishes as the film thickness exceeds 70 Å. On the other hand, it increases steadily as the films become thinner, just as expected in the case of a substrate induced effect.

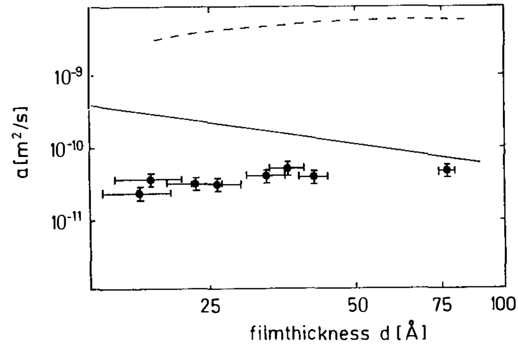

Fig.3 Log-log plot of the decay rate coefficient a vs the film thickness for propane at T = 90 K (a similar behaviour has been observed at T = 110 K). The data show a crossover to bulk viscous transport at film thicknesses above 70 Å when one compares with the usual van der Waals behaviour (solid line). The discrepancy with experimental work on the adsorption potential of similar compounds (dotted line) is even larger.

Finally, we want to discuss the possibility of a non-van der Waals surface potential. In fact, it has been reported that the van der Waals potential might be inadequate for the adsorption behaviour of similar compounds[22,23)], among others pentane, a homologue of propane, and ethanol. In contrast, a potential following approximately an inverse-square law has been found, along with an adsorption energy which exceeded the typical van der Waals energy by orders of magnitude for film thicknesses similar to those investigated in our experiment. If we adopt this (yet unexplained) potential, along with the high binding energies found, we obtain for the decay rate coefficient a the behaviour indicated by the dotted line in fig.3. Although the general trend that a be more or less independent of the film thickness is in accordance with our results, the discrepancy in the absolute value is even larger, and independent of film thickness. A large discrepancy in the apparent viscosity is then found for ethanol as well. As an alternative interpretation of our data, we should thus take into account the possibility that some mechanism which gives rise to the unexplained non-van der Waals potential in the reported isotherms[22,23)] may also be responsible for the (in this case dramatically) enhanced viscosity we have observed.

We are indebted to J.Israelachvili and J.Klein for helpful comments and suggestions and thank G.Reiter and U.Seifert for inspiring discussions. This work was supported by the Deutsche Forschungsgemeinschaft (SFB 306).

References

[1] S.Jakubith, H.H.Rotermund, W.Engel, A.Vonoertzen, G.Ertl, *Phys.Rev.Lett* **65** (1990) 3013.

[2] P.Guenoun, D.Beysens, M.Robert, *Phys.Rev.Lett.* **65** (1989) 2406.

[3] G.Reiter, Phys.Rev.Lett. **68** (1992) 75

[4] J.B.Broszka, F.Brochard-Wyart, F.Rondelez, *Europhys.Lett.* **19** (1992) 97.

[5] J.M.Guerra, M.Srinivasaro, R.S.Stein, *Science* **262** (1993) 1395.

[6] B.V.Deryagin, *Z.Physik* **84** (1993) 675.

[7] K.H.Adlfinger, G.Peschl, *Ber.Bunsenges.* **74** (1970) 347.

[8] M.L.Gee, P.M.Guiggan, J.N.Israelachvili, *J.Chem.Phys.* **93** (1990) 1895.

[9] this is true when the mean free path in the gas is large as compared to the wavelength of the thickness modulation, which was always the case in our experiment.

[10] our findings were consistent with reported tunneling microscopic images obtained on similar films by other authors before. See, for instance J.Vancea, G.Reiss, F.Schneider, K.Bauer, H.Hofmann, *Surf.Sci.* **218** (1989) 108.

[11] M.O.Robbins, D.Andelman, J.F.Joanny, *Phys.Rev.* **A43** (1992) 5760.

[12] H.Musil, S.Herminghaus, P.Leiderer, *Surf.Sci.Lett.* **294** (1993) L919.

[13] S.Herminghaus, U.Sigel, T.Paatzsch, H.Musil, P.Leiderer, *Ber.Bunsenges.* **98** (1994) 443.

[14] E.Ruckenstein, R.K.Jain, *Chem.Soc.Farad.Trans.* **70** (1974) 132.

[15] *'International Critical Tables of Numerical Data, Physics, Chemistry and Technology'*, Vol.**5** p.11 and Vol. **7** p.214, C.J.West edtr., McGraw-Hill 1933.

[16] B.A.Younglove, J.F.Ely, *J.Phys.Chem.Ref.Data* **16** (1987) 577. N.B.Vargaftig, *'Handbook of Physical Properties of Liquids and Gases'* (Springer, Berlin 1975).

[17] E.Cheng, M.W.Cole, *Phys.Rev.* **B38** (1988) 987.

[18] J.P.Rabe, S.Buchholz, *Phys.Rev.Lett.* **66** (1991) 2096.

[19] R.Hentschke, B.L.Schürmann, J.P.Rabe, *J.Chem.Phys.* **96** (1992) 6213.

[20] R.Hentschke, R.G.Winkler, *J.Chem.Phys.* **99** (1993) 5528.

[21] I.E.Dzyaloshinskii, E.M.Lifshitz, L.P.Pitaevskii, *Adv.Phys.* **10** (1961) 165.

[22] D.Beaglehole, E.Z.Radlinska, B.W.Ninham, H.K.Christenson, *Phys.Rev.Lett.* **66** (1991) 2084.

[23] P.S.Vukusic, G.W.Bradberry, J.R.Sambles, *Surf.Sci.Lett.* **277** (1992) L34.

ISLAND FORMATION IN ULTRATHIN ORGANIC MULTILAYERS OF BEHENIC ACID ON SILICONDIOXIDE SURFACES

Hans Riegler, Axel Asmussen and Christoph Merkl, Max-Planck-Institut für Kolloid- und Grenzflächenforschung, Rudower Chaussee 5, 12489 Berlin/Adlershof
Frank Schabert and Jürgen Rabe, Institut für Physik, Humboldt-Universität, Invalidenstraße 110, 10115 Berlin
Alexander Davydov, Oil and Gas Research Institute of the Russian Academy of Sciences, 63 Leninskii Prospect, Moscow, Russia 117 917

Abstract

Organic multilayers of well-defined thicknesses were prepared via Langmuir-Blodgett transfer and serve as model systems to probe the influence of short and long range interactions on the molecular ordering and topology of ultrathin organic films. After their preparation LB-films usually are not in equilibrium.Thin multilayers of behenic acid on silicondioxide surfaces break up irreversibly into islands (dewetting) at elevated temperatures. X-ray reflectivity, polarization microscopy and AFM studies show that these islands have a unique equilibrium height irrespective of the original film thickness. The degree of island coverage increases linearly with increasing original film thickness due to material conservation. Multilayers originally thicker than the equilibrium island height remain closed films. The results are explained with the minimization of the sum of the interface tension and Van-der-Waals energy contributions.

Introduction

The stability and wetting behaviour of ultrathin organic films on solid interfaces is an interesting field of physics and of considerable practical interest for coating and painting applications. Langmuir-Blodgett-films are suitable model systems for such studies because their thickness can be controlled precisely in bilayer increments and their properties can be varied by chemical engineering.

Behenic acid (dodecanoic acid) multilayers were deposited on naturally oxidized silicon wafer surfaces as described in detail elsewhere[1]. Their thermal annealing behaviour, structure and topology was investigated by x-ray reflectivity, polarized reflection microscopy and AFM.

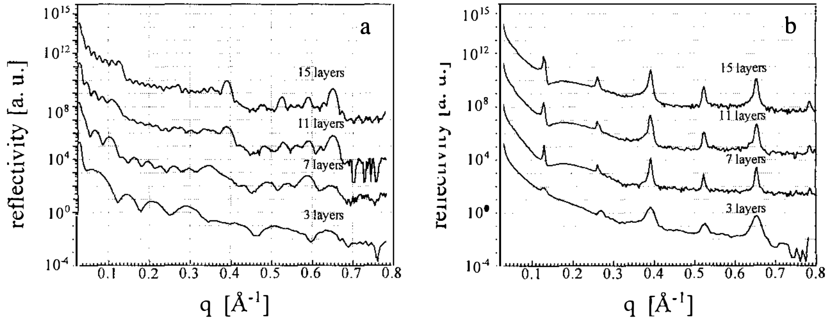

Figure 1: X-ray reflectograms of multilayers of various thicknesses as-deposited (a) and after thermal annealing for 60 hours (3 layers: 8hours) at 70°C (b). For presentation in one graph some intensities were multiplied by factors of 1000.

Experimental Results

The data of Figure 1 show that the thermal treatment changes the internal structure of the multilayer films. A detailed analysis[2] reveals that the samples as-deposited are continuous multilayer films with their number of layers identical to the number of dipping cycles. Films as-deposited consist of micrometer sized (lateral dimension) stacks of bilayers with three different bilayer spacings (55Å, 52Å, 48Å) corresponding to three different molecular tilt angles (21deg, 28deg, 36deg). During the annealing thin films irreversibly rupture into islands of increased layer number and areas of bare monolayer covered substrate surface. The islands consist of stacks of bilayers with uniform spacing (48Å) and molecular tilt (36deg). Polarized reflection microscopy (Fig. 2) and AFM studies (Fig. 3) reveal that the island covered area depends on the original film thickness and the annealing time. Thick samples (>21 layers) remain closed films even after long annealing times (>30 hours). Thinner films break up within a few minutes. After several hours of annealing the island heights of all samples approach a fairly unique value (Fig. 3).

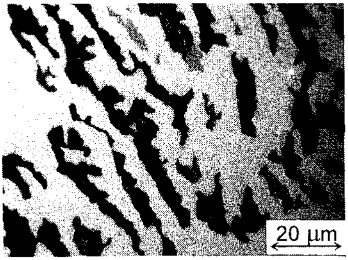

Figure 2: Polarized reflection light micrograph of a 9-layer film after annealing (dark areas = islands).

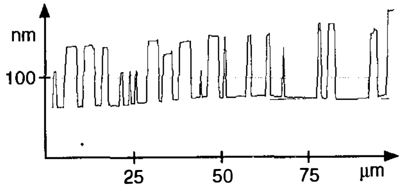

Figure 3: Height profile of an annealed 13-layer sample measured with AFM.

This equilibrium island height is independent of the original film thickness and the relative surface coverage with islands area ρ_e increases linearly with the original film thickness (Figure 5).

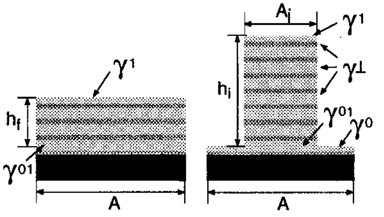

Figure 4: Schematic diagram of the topology of a continuous and annealed film.

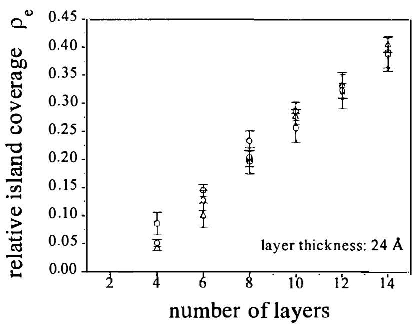

Figure 5: Relative island coverage ρ_e of as function of the original film thickness.

Theory

Figure 4 shows a schematic diagram of the film topology of an area A with a continuous film and an island. For model calculations it is assumed that:

1) the equilibrium topology of the film is determined by the minimum of the sum of the interface (surface tension) and long range (VdW) energy contributions[3,4];

2) the islands have an area of A_i;

3) during the annealing the total amount of material is conserved; it is shuffled from a continuous film of height h_f into islands of height h_i:

$$Ah_f = A_i h_i; \tag{1}$$

4) the ratio ρ of island covered area vs. bare monolayer surface is:

$$\rho = \frac{A_i}{A}; \tag{2}$$

5) short range interactions are represented by interface energy contributions with the spreading coefficient:

$$S_\gamma = \gamma^0 - (\gamma^{01} + \gamma^1); \tag{3}$$

6) long range (VdW) energy contributions for a film of thickness $h = nd$ (n = number of bilayers, d = bilayer thickness) are described by:

$$E_n = -\frac{A_H}{12\pi h^2} = -\frac{A_H}{12\pi n^2 d^2} \tag{4}$$

with A_H as non-retarded Hamaker constant for the interaction of air with the monolayer covered substrate across the multilayer.

The free energy per area for a film with an island coverage ratio ρ and a line tension contribution $\gamma^\perp A^\perp$ ($A^\perp$= boundary area of an island) is:

$$f_i = \frac{F_i}{A} = \gamma^0 - S_\gamma \rho + \gamma^\perp \frac{A^\perp}{A} + E_n \rho \tag{5}$$

With eqs. (1) and (2) this can be written as:

$$f_i = \gamma^0 - S_\gamma \rho + \gamma^\perp \frac{A^\perp}{A} - \frac{A_H}{12\pi h_f^2} \rho^3 \tag{5a}$$

If line tension contributions are neglected eq. (5a) has a minimum of energy per unit area for area ratios ρ_e of:

$$\rho_e = \sqrt{-\frac{4\pi S_\gamma}{A_H}} \cdot h_f \tag{6}$$

Eq. (6) describes an energetic minimum only for positive spreading coefficients ($S_\gamma > 0$) and negative Hamaker constants ($A_H < 0$), i. e. the minimum results from the competition between the interfacial energies, which favour a continuous film and the long range interactions, which tend to thicken the film. The conservation of material leads to island formation. With a typical Hamaker constant ($A_H = -10^{-20}$ J) and experimental values ($\rho_e = 0.3$ for $h_f = 3 \times 10^{-8}$ m) eq. (6) yields $S_\gamma \approx 8 \times 10^{-5}$ mJm^{-2}. Such a small value is not unreasonable, because it is the spreading factor of fatty acid on a fatty acid coated surface.

Discussion

The measured area ratios ρ_e vs. the original multilayer thicknesses h_f show a linear relation as predicted by the simple model (Fig. 5). For a more quantitative analysis, however, additional contributions have to be taken into account: 1) evaporation losses; 2) nucleation and dewetting kinetics; 3) island height distribution; 4) island size distribution; 5) island shape; and 6) line tension contributions.

The data presented in Figure 5 were obtained from samples treated long enough to approximately reach the equilibrium island height h_e. The linear extrapolation of the data does not go through the origin, which points to some loss of material. This can also be observed directly with polarization microscopy during annealing: For the 2-layer films (=monolayer plus bilayer) no area ratio is plotted in Figure 5 although island formation occurs. But while these islands gain height during annealing, evaporation causes the loss of all the material before h_e is reached. The data of Figure 5 and other investigations not presented here indicate that the total amount of material loss is roughly proportional to the annealing time and independent of the original film thickness. Thus, evaporation affects thin films much more than thick multilayers.

At their main transition the multilayer films (multilayer islands) segregate into three-dimensional droplets without internal layered structure. Upon cooling below the main melting temperature these droplets remain and consist of randomly oriented micrograins with bilayered packing.

Annealing is performed at temperatures below the main melting transition. The increased molecular mobility during the annealing is probably caused by the melting of only the chains. The internal bilayer structure is preserved and the films/islands remain highly viscous. The samples approach the equilibrium topology only slowly, with thicker samples taking longer times (>10 hours) than thinner films. The equilibrium thickness of the islands is around 80 - 100 nm. Therefore samples with less than 35 - 40 layers should separate into islands whereas thicker multilayers should retain their continuous film topology. In the experiments however, samples with more than 21 layers have not yet been observed to form islands. This may have energetic and nucleation reasons. In the beginning of the annealing the closed film has to be ruptured. This is probably a nucleation process which has to overcome line tension contributions and the activation energy will roughly be proportional to the film thickness. Surfaces with already thick islands also gain less energy upon increasing their island heights compared to those starting with thinner heights because of the fading VdW-contribution with increasing thickness. Both these effects, the smaller energy gain and the higher activation barrier, may explain why films close to but with still less than the island equilibrium height have hitherto not yet been ob-served to break up. The relatively smaller energy gain per height increase for island heights close to h_e also explains, why there is some variation in the island heights (Figure 3).

Nothing is currently known about details of the molecular transport during the annealing and the mechanisms causing the sizes and shapes of the islands. Nucleation, molecular transport, and line tension will determine these characteristics. In the model calculations the line tension contribution has been neglected because it cannot easily be incorporated into calculations due to the complicated island shapes and size distributions. Experimentally the influence of the line tension is observable. The island shapes tend to become more and more smooth during annealing. Line tension contributions will play a more important role for small islands. For idealized round islands it scales linearly with the island diameter whereas the surface contributions go quadratic. With a typical island diameter of 10μm one obtains perimeter areas of $3\mu m^2$ compared to surface areas of $80\mu m^2$ (for h_e=100nm) and line tension contributions may be negelected in a first approximation.

The observed phenomena and their theoretical interpretation bears strong similarities to the wetting/dewetting behaviour of polymers[5,6,7] and liquids[8]. The internal structure of Langmuir-Blodgett multilayers resembles that of layered block copolymer layers, where also island topologies can be found[9] (however caused by different reasons). A great advantage of Langmuir-Blodgett multilayers is the possibility of preparing films in precise thickness increments of the bilayer spacings. Thus the thickness of the films as-deposited can be controlled within a few Ångströms and series of various film thicknesses can be prepared and investigated. By changing the substance it is further possible to selectively change the geometrical and physical properties.

Acknowledgement

We thank Wacker Burghausen for generously donating the silicon wafers. Helpful discussions with G. Reiter and D. Beaglehole are appreciated.

References:

1) A. Leuthe and H. Riegler, J. Physics D: Appl. Phys. **25**, 1786 (1992)
2) A. Leuthe and H. Riegler, J. Phys. Chem. submitted
3) F. Brochard Wyart and J. Daillant. Can. J. Phys. **68**, 1084 (1990)
4) F. Brochard Wyart, J.-M. diMeglio, D. Quere, and P.-G. deGennes, Langmuir **7**, 335 (1991)
5) G. Reiter, Phys. Rev. Lett. **68(1)**, 75 (1992)
6) G. Reiter, Langmuir **9**, 1344 (1993)
7) G. Reiter, Macromolecules **27**, 3046 (1994)
8) M. P. Valignat, N. Fraysse, and A. M. Cazabat, Langmuir **9**, 3255 (1993)
9) M. Maaloum, D. Ausserre, D. Chateney, and Y. Gallot, Phys. Rev. Lett. **70(17)**, 2577 (1993)

ADHESION BETWEEN AN ELASTOMER AND A GRAFTED SURFACE

L. Léger and E. Raphaël
Laboratoire de Physique de la Matière Condensée,
U.R.A. n° 792 du C.N.R.S.,
Collège de France,
11, Place Marcelin Berthelot,
75231 Paris Cedex 05, France

Abstract. The interface between a flat solid surface and a cross-linked elastomer can be considerably strengthened by the addition of chains (chemically identical to the elastomer) that are tethered by one end to the solid surface. At high grafting densities these coupling chains may, however, segregate from the elastomer and the adhesion may drop substantially. This important problem has been recently considered by de several authors in the case of a monodisperse "brush". In this article, we analyse the adhesion between a polydisperse brush and an elastomer, and we present some recent experiments conducted on polydimethylsiloxane - silica systems.

1 Introduction

Adhesion between a flat solid surface and a cross-linked elastomer is a technologically important problem (a cross-linked elastomer consists of long, flexible chain-like molecules that are interconnected at various points by cross-links to form a molecular network; the polymer medium is locally fluid, but the macroscopic flow of the material is prevented by the cross-links). The interface between the two materials can be strengthened by the addition of chains (chemically identical to the elastomer) that are tethered by one end to the solid surface. As a crack grows along the interface, these coupling chains are progressively pulled-out from the elastomer[1-3]. This "suction" process is expected to occur in an approximately planar *cohesive zone* directly ahead of the crack tip[4].

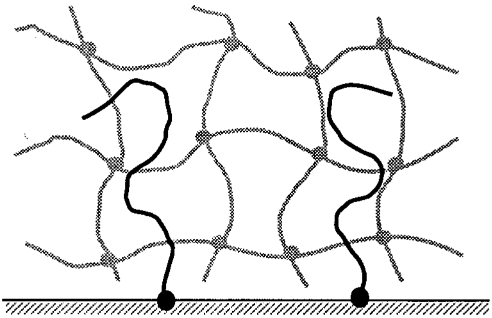

Figure 1. The interface between flat solid surface and a cross-linked elastomer is strengthened by the addition of chains (chemically identical to the elastomer) that are tethered by one end to the solid surface.

A number of models have been proposed to describe the process of chain pull-out and the relation between chain pull-out and interfacial toughness[5-11]. In the model of Raphaël and de Gennes[8-9], the partially pulled-out chains are assumed to form single-chain fibrils. The minimization of the sum of the surface and stretching energies of these chains shows that there is a minimum force f^* required for a fibril to exist even at zero pull-out rate. As the force on a chain that is being pulled-out remains finite as $V \rightarrow 0$, the existence of a threshold toughness G_0 that is larger than the work of adhesion W due to intermolecular interactions (typically van der Waals type) is predicted. For many practical cases, the zero-rate fracture energy G_0 is given by[9-10]

$$G_0 - W \cong kTN\nu \qquad (1)$$

where ν is the number of coupling chains per unit interface area, N their polymerization index, and kT the thermal energy. In what follows we will often use the dimensionless grafting density $\sigma = \nu a^2$, where a is the monomer size.

Equation (1) is valid as long as the interdigitation between the coupling chains and the elastomer is total. For high σ values, however, the coupling chains may segregate (at least partially) from the elastomer and G_0 may reduce to W. This important problem has been recently considered by de Gennes[12] and by Brochard-Wyart *et al.*[13]. The starting point of these studies is the analysis by de Gennes of the equilibrium between a melt of chains (N monomers per chain) and an elastomer cross-linked *in the dry state* (N_c monomers between cross-links)[12]. For a single N chain inside the elastomer, the Flory-type free energy can be written as

$$\frac{F}{kT} \cong \frac{R^2}{a^2N} + \frac{a^3}{N_c}\frac{N^2}{R^3} \tag{2}$$

(all numerical factors being ignored). The first term represents the deformation energy of the chain (R is the coil radius). The second term is the swelling energy of the elastomer. Since the free energy eqn (2) is identical to the free energy of a chain (N monomers) immersed in a melt of shorter, chemically identical chains (N_c monomers per chain)[14], the N-chain conformation is the same in both situations. However, the volume fraction of monomers of the N chains within the elastomer is limited by the elastic energy of the elastomer to a value N_c/N[12]. Similarly, a monodisperse brush* in contact with an elastomer is expected to fully interdigitate the network if the resulting volume fraction of monomers from the brush inside the elastomer, Φ, is smaller than a critical value $\Phi_1 = N_c/N$[13]. The corresponding grafting density is $\sigma_1 = N_c/N^{3/2}$. For $\sigma < \sigma_1$, $G_0 - W$ is a linear function of σ. For $\sigma > \sigma_1$, the interdigitation between the brush and the elastomer is only partial and each grafted chain has only a number $n \cong N_c^{2/3}\sigma^{-1}$ of monomers within the elastomer. As a result, $G_0 - W \cong kTn\nu$ increases more gradualy with σ (like $\sigma^{1/3}$). In this regime, Φ is larger than Φ_1 and reaches a value of order 1 for $\sigma \cong N_c^{-1/2}$. At that point, the interdigitation is lost and $G_0 - W$ falls off to zero[15].

Experimentaly, the formation of a dense polymer brush is a delicate chemical problem: one has to find a system in which the wall has no preferential interaction with the monomers of the chains, except the extremity to be grafted. An example of such a system has been worked out by P. Auroy *et al.*[16], with α-ω

---

* A layer of polymer chains grafted at one end onto a solid surface is usually referred to as a "brush".

hydroxylterminated polydimethylsiloxane (PDMS) chains end grafted on previously modified porous silica beads (by esterification of most of the silanol sites of the surface by pentanol molecules). Another and simpler way of forming dense surface anchored layers of polymer chains has been worked out by M. Deruelle *et al.*[17], through simultaneous adsorption and end grafting of PDMS on untreated silica surfaces. If the naturally oxydised surface of a silicon wafer is used, the layers can be analysed in details through reflectometry techniques such as X-Rays, neutrons reflectivity, or ellipsometry. The dry thikness h_0 of such layers, characterised by ellipsometry and X-Rays reflectivity, follows rather well the scaling law $h_0 \cong a N^{1/2} \Phi_0^{7/8}$. When put into contact with a good solvent, these layers swell, but the thickness saturates at a value smaller than what would have been obtained with a purely end grafted layer made with the same chains, at the same surface density[18]. This is an experimental evidence that the structure of these simultaneously adsorbed and end grafted layers is different from that of a brush. In fact, due to the adsorption, these layers are made of loops, with a large polydispersity of loop sizes, reflecting the statistics of the chains in the reaction bath. The structure of such irreversibly adsorbed layers has been worked out by O. Guiselin[19], and they have been named pseudo-brushes, because they are analogous to highly polydisperse brushes of loops. Since, experimentaly, pseudo-brushes are formed rather easily, it is of some importance to try to estimate the adhesion between a pseudo-brush and an elastomer. This will be done in Section 2. In Section 3 we present experiments conducted on polydimethylsiloxane - silica systems. The paper ends with some concluding remarks.

2 Adhesion between a polydisperse brush and an elastomer

In order to estimate the adhesion energy between a pseudo-brush and an elastomer, we will treat the pseudo-brush as a polydisperse brush of half loops. We assume the polydisperse brush to be characterized by the following distribution:

$$S(n) \cong \frac{\Phi_0^{7/8}}{a^2 n^{1/2}} \qquad 1<n<N \qquad (3)$$

where $S(n)$ is the number (per unit area) of chains made of more than n monomers ($1<n<N$). This distribution is reminiscent of the "pseudo-tail" distribution calculated by Guiselin in the case of a layer prepared by irreversible adsorption from a semi-dilute solution of volume fraction Φ_0[19].

Let us first recall some useful results concerning the behavior of a polydisperse brush (described by the length distribution eqn (3)) exposed to a melt of mobile chains (degree of polymerization N_c, with $N^{1/2} < N_c < N$)[20-21]. (a) In the regime $\Phi_0 > N_c^{-1/3}$, the mobile chains penetrate into the brush to a distance from the wall that corresponds for the tethered chains to the index

$$s \cong N_c \Phi_0^{7/4} \tag{4}$$

(the n-th monomers of all tethered chains larger than n are supposed to be located at the same distance from the surface)[19-21]. Note that s is an increasing function of N_c: decreasing the length of the melt chains increases the stretching of the brush and therefore increases the mixing by providing more volume for the melt. (b) There exists a threshold value of Φ_0 below which the excluded volume interactions cease to be relevant at the brush extremity[20-22]. This threshold value is given by $\Phi_{0T} \cong (N_c/N)^{8/7}$ (see also Ref.12). For $\Phi_0 \cong \Phi_{0T}$, the number of chains per unit area is of the order of $a^{-2}(N_c/N)$ and the average volume fraction of chains of the brush inside the interdigitation zone is of the order of N_c/N.

We now consider what happens when the polydisperse brush is exposed to an elastomer (N_c monomers between cross-links, with $N^{1/2} < N_c < N$). By analogy with the monodisperse brush, we make the conjecture that the network elasticity starts to restrict the interdigitation when $\Phi_0 = \Phi_{0T}$. The use of this criterion is strengthened by the fact that it is also the point when the average volume fraction of brush chains in the network is of the order of N_c/N.

We now consider the situation $\Phi_0 > \Phi_{0T}$ where we expect partial interdigitation: as a result of the brush polydispersity, long enough chains will penetrate into the elastomer while short ones will not. In order to describe qualitatively this partial interdigitation regime, we assume that the number of chains per unit area that enter the network is locked at its value for $\Phi_0 = \Phi_{0T}$, that is at $a^{-2}(N_c/N)$. One can thus define an index m such that the number (per unit area) of chains with more than m monomers is given by $a^{-2}(N_c/N)$:

$$m \cong (N_c/N)^2 \Phi_0^{7/4} \tag{5}$$

The novel feature of the polydisperse brush compared to the monodisperse brush is that we now have two independent mechanisms leading to partial interdigitation: the ‘melt mixing effect’, which imposes the cutoff s, and the elastomer elasticity, which imposes the cutoff m. According to the relative value of s and m (eqns (4) and (5)), two cases must be considered. As long as s is larger than m, that is for $N_C > N^{2/3}$, it is plausible to assume that the elastomer behaves like a melt of N_C chains and penetrates into the brush to a distance from the wall that corresponds to the index s. According to eqn (1), the adhesion energy G_0 is then given by

$$G_0 - W = kT\int_s^N dn\left(-\frac{dS(n)}{dn}\right)(n-s) \tag{6}$$

The integral appearing in eqn (6) corresponds to the number of monomers of the brush present in the elastomer (see eqn (1)). Using eqn (4), we get[23]

$$G_0 - W \cong \frac{kT}{a^2}N^{1/2}\Phi_0^{7/8}\left[1 - \Phi_0^{7/8}(N_c/N)^{1/2}\right]^2 \tag{7}$$

Equation (7) predicts the existence of a maximum in the adhesion energy as $\Phi_0^{7/8}$ increases. This maximum occurs for $\Phi_{0\max}{}^{7/8} = (N/9N_c)^{1/2}$ and $(G_0 - W)_{\max} = kTa^{-2}N^{1/2}(4/9)\Phi_{0\max}{}^{7/8}$. Note that since Φ_0 cannot exceed 1, the maximum disappears if N is larger than $9N_c$.

We now consider the opposite case $N_c < N^{2/3}$. Since m is now larger than s, we expect the elastomer to penetrate into the brush less deeply than a melt of N_c chains. If one postulates that the penetration is controlled by the index m, the adhesion energy G_0 is then given by[23]

$$\begin{aligned} G_0 - W &= kT\int_m^N dn\left(-\frac{dS(n)}{dn}\right)(n-s) \\ &\cong \frac{kT}{a^2}N^{1/2}\Phi_0^{7/8}\left[1 - \Phi_0^{7/8}\left(N^{1/2}/N_c\right)\right]^2 \end{aligned} \tag{8}$$

Equation (8) predicts the existence of a maximum in the adhesion energy as $\Phi_0^{7/8}$ increases. This maximum occurs for $\Phi_{0\max}{}^{7/8} = N_c/\left(3\,N^{1/2}\right)$ and $(G_0 - W)_{\max} = kTa^{-2}N^{1/2}(4/9)\Phi_{0\max}{}^{7/8}$. Note that since Φ_0 cannot exceed 1, the maximum disappears if N is larger than $N_c^2/9$.

It is worth noting that eqns (7) and (8) can be rewritten as[24]

$$\frac{G_0 - W}{(G_0 - W)_{\max}} = \frac{9}{4}\frac{\Phi_0^{7/8}}{\Phi_0^{7/8}{}_{\max}}\left(1 - \frac{1}{3}\frac{\Phi_0^{7/8}}{\Phi_{0\max}{}^{7/8}}\right)^2 \tag{9}$$

According to eqns (7) and (8), the maximal value of the curve $G_0 - W$ versus $\Phi_0^{7/8}$ varies *non monotonically* with N_c:

$$\frac{a^2}{kT}\left(G_0 - W\right)_{max} \cong \left(4/3^3\right)N_c \qquad \text{for} \qquad N^{1/2} < N_c < N^{2/3} \qquad (10)$$

and

$$\frac{a^2}{kT}\left(G_0 - W\right)_{max} \cong \left(4/3^3\right)N\,N_c^{-1/2} \qquad \text{pour} \qquad N^{2/3} < N_c < N \qquad (11)$$

From eqns (10) and (11), one finds that $\left(G_0 - W\right)_{max}$ is optimum for $N_c \cong N^{2/3}$ where it takes the value $\left(4/3^3\right)kT\,a^{-2}\,N^{2/3}$[25].

3 Experiments

Systematic experiments on polydimethylsiloxane - silica systems have been undertaken using the pseudo-brushes presented at the end of Section 2[24][26-28]. Narrow fractions of PDMS chains (α-ω hydroxyl terminated, M_W in the range 20 000 to 700 000, $M_W/M_n = 1.1$) were used at volume fractions Φ_0 ranging from 5 to 100%, to form the layers on the upper surface of silicon wafers.

Two mechanical tests have been developed to extract the adhesion energy: 90° peel tests, conducted on an especially built machine allowing for very low velocities (5 nm/s to 10 mm/s) and the J.K.R. test[29] in which a small elastomer lens is pressed against the substrate; measuring the area of contact as a function of the applied load yields both the adhesion energy and the elastic modulus of the elastomer. Details of the experimental set up and of the results are reported in reference[24][26] for the peel test and in references[27][28] for the JKR test. In order to minimise as much as possible bulk dissipation in the elastomer in the peel test, we have used silk reinforced thin ribbons (200 mm thick), and checked both the thickness and the width dependence of the measured peel force.

On Fig. 2 we have reported the measured adhesion energies obtained at very low velocity (5 nm/s) deduced from peel tests (Fig.2a) and from J.K.R. tests (Fig.2b), on layers formed at fixed molecular weight and increasing Φ_0. In both cases, a maximum in the evolution of the adhesion energy as a function of the surface density of chains, $\sigma \approx \Phi_0^{7/8}$, is clearly visible. On Figure 2a, results obtained with two different elastomers (molecular weights between cross links respectively 10 400 and 24 000) seem to indicate that the position of the maximum is not strongly affected by N_c, the polymerisation index betwen crosslinks, while the adhesion energy at the maximum increases with N_c. Surprisingly enough, the layers with the higher σ (obtained by adsorption and grafting from a polymer melt) do not provide large adhesion energy.

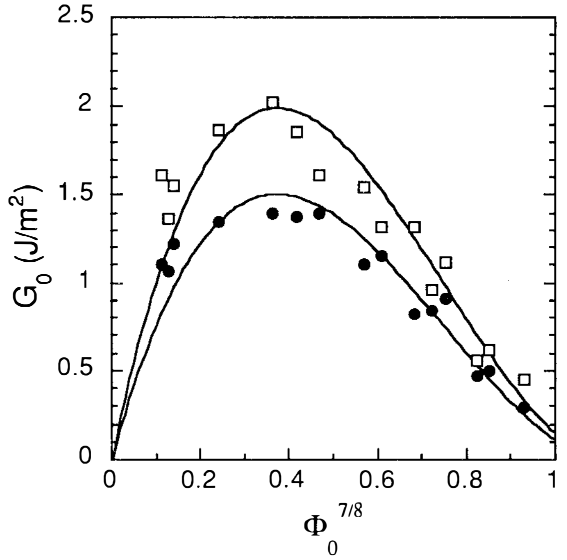

Figure 2a. Measured adhesion energy G_0 as a function of the surface density of the chains in the surface layers (proportional to $\Phi_0^{7/8}$) from peel experiments performed at a velocity $V = 50\,\mathrm{nm\,s^{-1}}$ for elastomers with $M_c = 10000$ (filled symbols) and $M_c = 24000$ (open symbols), and chains in the surface layers with a molecular weight 412000. The full lines are just guides for the eyes.

4. Concluding remarks

The remarkable experimental features presented in the preceeding section are in qualitative agreement with the theoretical predictions of section 2. In fact, the experimental system is more complicated since one deals with loops rather than individual chains. According to Brochard-Wyart *et al.*[13] when a loop (with fixed attachment points on the solid surface) of length $2n$ interdigitates into the elastomer, its conformations are strongly restricted. The corresponding entropy loss is given by $\Delta S \cong \beta(2n/N_c)$, where β is a numerical factor of order unity[13] This effect, referred to as "the cactus effect", is absent when one considers the penetration of two distinct chains of length *n* into the elastomer.

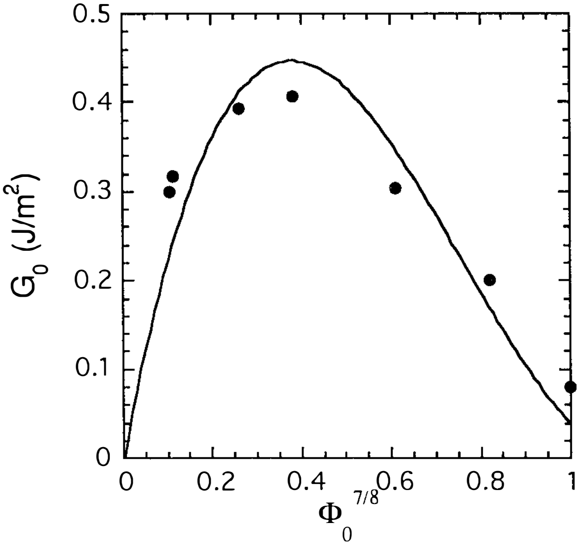

Figure 2b. Measured adhesion energy G_0 as a function of the surface density of the chains in the surface layers from JKR experiments at $V = 10\,nm\,s^{-1}$ for elastomers with $M_c = 10000$ and chains in the surface layers with a molecular weight 412000. The full lines is just a guide for the eyes.

A model taking the cactus effect into account has been recently proposed[24]. This model also leads to the form of eqn (9) but with $\Phi_{0max}{}^{7/8} = 1/3$ and $(G_0 - W)_{max} = kTa^{-2}N^{1/2}(4/9)\Phi_{0max}{}^{7/8}$. All the experimental results obtained with peel tests are reported on Figure 3, along with the master curve eqn (9).

The challenge is at present to obtain sufficiently accurate data to test further the validity of these descriptions. This implies controlling as far as possible the quality and the reproducibility of the elastomers, as the local elasticity in the interdigitated region is the key parameter which limits or allows the connectors to be efficient. A strong advantage of the J.K.R. test is to allow simultaneous measurements of the adhesion energy and of the elastic modulus. It thus reveals to be a unique tool and

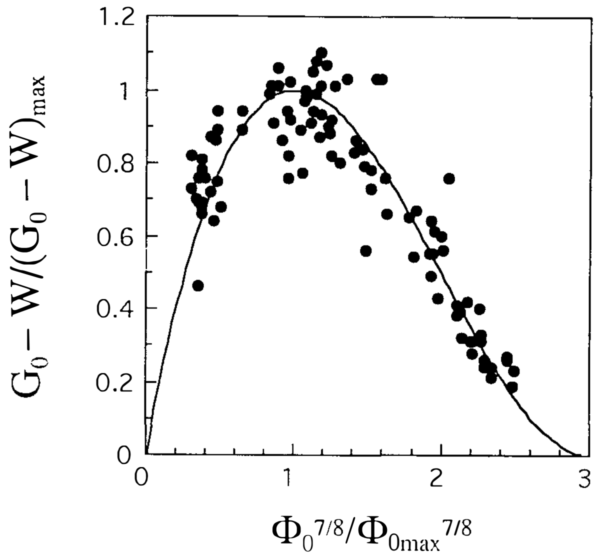

Figure 3. $\frac{G_0 - W}{(G_0 - W)_{max}}$ as a function of $\Phi_0^{7/8}/\Phi_{0max}^{7/8}$: experimental results and master curve eqn (9).

should allow a better understanding of the molecular mechanisms at the origin of the enhancement of the adhesion energy between a solid and an elastomer through connector molecules.

Acknowledgment

We would like to thank M. Aubouy, F. Brochard-Wyart, H. Brown, M. Deruelle, P.-G. de Gennes, H. Hervet and Y. Marciano for very stimulating discussions. We thank Rhône-Poulenc for financial support.

References

1. H. R. Brown, *Ann. Rev. Mat. Sci.*, 21, 463 (1991).
2. H. R. Brown, *Macromolecules,* 26,1666 (1993).
3. Creton C., Brown H. R. and Shull K. R., *Macromolecules,* 27,3174 (1994).
4. A thorough investigation of cohesive zone models can be found in Fager L.-O., Bassani J. L., Hui C.-Y. and Xu D.-B., *Int. J. Fracture Mech.*, 52, 119 (1991).
5. Xu D.-B., Hui C.-Y., Kramer E. J. and Creton C., *Mech. Mater.*, 11, 257 (1991) . This model is aimed mainly at the pull-out process in glassy polymers.
6. De Gennes P.G., *J. Phys. France.*, 50, 2551(1989).
7. De Gennes, *C. R. Acad. Sci. (Paris) II*, 309, 1125 (1989).
8. Raphaël E. and De Gennes P.G., *J. Phys. Chem.*, 96, 4002 (1992).
9. Raphaël E. and De Gennes P.G., in *Soft order in physical systems* , R. Bruisma and Y. Rabin eds, (Plenum Press, N.Y.,1994)
10. Brown H. R., Hui C.-Y. and Raphaël E., *Macromolecules,* 27, 607 (1994).
11. Hong Ji and and De Gennes P.G., *Macromolecules*, 26, 520 (1993) .
12. De Gennes P.G., *C. R. Acad. Sci. (Paris) II*, 318, 165 (1994).
13. Brochard-Wyart, De Gennes P.G., Léger L., Marciano Y. and Raphaël E., *J. Phys. Chem.*, 98, 9404 (1994).
14. De Gennes, *Macromolecules*, 13, 1069 (1980).
15. A natural way to describe the fall of the adhesion in the vicinity of $\sigma \simeq N_c^{-1/2}$ is to replace $G_0 - W \simeq kTn\nu$ by $G_0 - W \simeq kTn\nu(1-\Phi)$. The factor $(1-\Phi)$ is a way of taking into account the fact that a monomer of a tethered chain inside the elastomer sees less and less the network as Φ reaches values of order 1. Note that this argument is somewhat different from the argument of Brochard *et al.* (Ref. 13) which involves a subtle analysis of the surface energy between the elastomer and the passive layer formed by those of the coupling chains that do not penetrate into the network.
16. Auroy P., Auvray L. and Léger L., *Macromolecules* 24, 5158 (1991).
17. Deruelle M., Ober R. and Léger L., submitted to *Macromolecules*
18. Deruelle M., Ondarçuhu T. and Léger L., to be published
19. Guiselin O., *Europhys. Lett.*, 17, 225 (1992).
20. Aubouy M. and Raphaël E., *C. R. Acad. Sci. (Paris) II*, 318, 1081 (1994).
21. Aubouy M. and Raphaël E., *Macromolecules*, 27, 5182 (1994).
22. Ligoure C., unpublished results.
23. Aubouy M., Brown H. R., Léger, L., Marciano, Y. and Raphaël E., To appear in the proceedings of the 53rd International Meeting of Physical Chemistry, Organic Coatings, Paris, January 1995.
24. Marciano, Y, Adhésion entre un élastomère et un couche adsorbée de polydiméthylsiloxane, Thèse, Université Paris XI, 1994.
25. Equations (10) and (11) are valid for not to large values of N ($N<729$). For a more complete discussion, see Ref. 23.

26 Marciano, Y., Hervet, H., Vovelle, L., Léger, L., *to be published*

27 Deruelle, M., Hervet ,H., Léger, L., *to be published*

28 Deruelle, M., Tirrell, M., Marciano, Y., Hervet, H., Léger, L., *Faraday Discuss* **98** (1994)

29. Johnson K.L., Kendall K. and Roberts A.D., *Proc. Roy. Soc. London* 1971, **A** **324**, 301

MODIFICATION OF THE WETTABILITY AND ADHESIVE PROPERTIES OF POLYPROPYLENE BY AN AMMONIA PLASMA TREATMENT . APPLICATION TO ALUMINIUM-PP SYSTEM

N. Shahidzadeh-Ahmadi, M. Tatoulian, F. Arefi-Khonsari, M.M. Chehimi# and J. Amouroux
Laboratoire de Génie des procédés plasmas, ENSCP-Université Pierre et Marie Curie, 11 rue Pierre et Marie Curie, 75005 Paris (France)
Institut de Topologie et de Dynamique des Systèmes de l'Université Denis Diderot Paris7, associé au CNRS (URA34), 1 rue Guy de la Brosse,75005 Paris (France)

Abstract

In order to improve the properties such as adhesion and surface energy the surface of polypropylene (PP) films were modified by ammonia plasma treatment. The physicochemical modification of the treated surfaces was studied in terms of acid-base properties. The ammonia treated PP became more wettable and showed a basic character for treatments of the order of 0.7-1 s. This work points out the importance of the specific basic groups grafted on the surface by an ammonia plasma on the adhesion phenomena with aluminium. However, this basic character of the surface disappeared with ageing leading to an amphoteric one. The latter has been explained by the fact that the polar groups are burried away from the surface and/or are neutralized by atmospheric contaminants. It has been shown that the ageing phenomena can be limited by crosslinking the PP surfaces with helium discharge, before ammonia plasma treatment.

Introduction

The plasma technique is a dry process which can tailor polymers in order to introduce polar functional groups at the surface [1]. The advantage of such treatments is that the modification is restricted to the upper most layers of the substrate. It is clear that the type of polar or non polar groups introduced on the surface depend on the plasma atmosphere chosen for the study. Recently, the classification of "polar" properties in terms of lewis acid-base interactions rather than "polar" interactions seems to be more appropriate [2-4].

In this paper, firstly we characterize the acid-base properties acquired by polypropylene (PP) films (a non polar material) treated by an ammonia plasma. For this, contact angle measurements and X-ray Photoelectron Spectroscopy (XPS) in conjunction with molecular probe are used. Secondly, we study the effect of the ammonia treatment on the adhesion improvement of PP to a thin aluminium coating (≈ 20 nm) as well as the ageing effect of the treated PP before metallization.

I-The acid-base character of "polar" interactions

For fifty years or so intermolecular interactions have been classified as "polar" or "non polar", as a result of the remarkable achievements in the understanding of the nature of the attractive forces in gases. So, It became customary to discuss the dipole-dipole interactions and the dipole induced-dipole interactions for molecules in the liquid or solid state , or at their interfaces. Only very recently has the extrapolation from gases to condensed phases of the dipole interactions been studied, and it is found so far that ***in condensed phases there is no evidence for any measurable dipole interactions energies of cohesion and adhesion*** [5]. Instead it is found that the lewis acid-base interactions occur between the so-called "polar" groups in liquids and solids and that this interactions are quite independent of "polarity" as measured by dipole moment. It is therefore concluded that dipole-dipole interactions in liquids are negligibly small as compared to acid-base interactions or dispersion force interactions [4]. Several compounds usually referred to as "polar" have both acidic and basic sites as in water, alcohols and acetone. Often in these compounds molecules self-associate through acid-base bonds to line up the dipole moments thereby resulting in high dielectric constant.

Generally, the thermodynamic work of adhesion W is defined as the reversible work of adhesion (per unit area) to disjoin the adhesive adherend-interface (i.e solid/liquid) [4]:

$$W=\gamma_1 + \gamma_2 - \gamma_{12} = \gamma_l (1+ \cos \theta) \qquad (1)$$

where $\gamma 1$ and $\gamma 2$ are the surface free enegies of components 1 and 2, $\gamma 12$ is the interfacial free energy of the material. Fowkes has shown that the latter includes two kinds of interactions [5]:

$$W= W^{d} + W^{ab} \qquad (2)$$

W^{d} defines the dispersion or London forces and W^{ab} the non dispersive or acid-base interactions:

$$W^{d} = 2 (\gamma 1 \gamma 2)^{1/2} \qquad W^{ab} = W - W^{d} \qquad (3)$$

To determine the work of adhesion W (eq.1) of treated PP surfaces, we have employed the classical contact angle technique using unbuffered aqueous acidic and basic solutions [6,7].

II-Assessment of acid-base properties of polymer surfaces by XPS

The XPS method for determining acid-base interactions of polymer has been described elsewhere[8-9]. The polymer film is exposed to liquid vapours of known acid-base properties. The polymer film is then allowed to outgas the excess of solute and is transfered into the XPS equipment for surface characterisation. If the polymer-solute acid-base interactions are strong enough, then a residual amount of solute is detected and the molar ratio of solute per polymer repeat unit (%S) is evaluated.

III-Plasma treatments

The plasma reactor used to treat PP films (8μm thick) was a bell jar one with a non symmetrical configuration of electrodes (hollow electrode-earthed cylinder). The reactor was described in detail elsewhere [10]. The working pressure was about 150 Pa and the NH_3 discharge was established with the help of 70 kHz excitation source. The power of the discharge was approximately 70 W. In situ metallisation of pretreated PP films was carried out by thermal evaporation in the same chamber, which avoided any contact of the pretreated polymer with air prior to Aluminium deposition.

IV- Results and discussion

As we have mentioned before, the work of adhesion of treated PP films were determined with different aqueous solutions. The contact angle of these solutions at the surface were measured immediately after the treatment. Figure 1 shows the increase in the total work of adhesion of treated PP films using different test liquids for different treatment times. It should be noted on this figure the basic character of the surface, i.e.W_{sl}= 129 mJ/m^2 for acid pH and W_{sl}= 120 mJ/m^2 for basic pH, for treatment times of the order of 0.7 to 1 s. For longer treatment times, the surface reaches an amphoteric character with the same total work of adhesion for the strongly acidic and basic aqueous solutions.

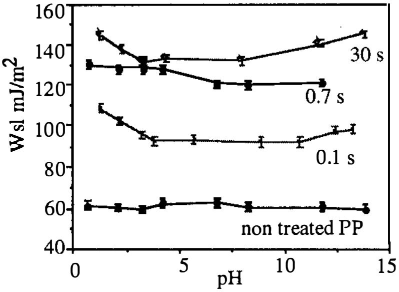

Figure1. Variation of the total work of adhesion with different test liquids for different treatment times:
(a) untreated PP; (b) t=0.1s; (c) t= 0.7s; (d) t=30s

Ammonia plasma treatment produces chemical modification of the PP surface by grafting nitrogen and/or oxygen namely an increase of N/C and O/C ratio around 12% and 5% respectively [11].

In order to confirm the results obtained by wettability measurements, chloroform (TCM) was used as the molecular probe (lewis acid) in conjunction with XPS to interrogate the acid-base properties of ammonia plasma treated PP[8]. Figure 2 shows the adsorption of TCM on ammonia plasma treated PP and not on the untreated PP.

This is interpreted in terms of acid-base interactions between TCM and basic groups (amine, amide) grafted at the surface. The molar ratio of TCM per polymer repeat unit (%S) is evaluated in figure 3. In the first region, i.e. for treatment time shorter than 1 s, the %S has its upper value equal to 5%. In the second region i.e. for treatment time longer than 1 s, %S ratio decreases sharply until 0.7% for a treatment time equal to 30 s.

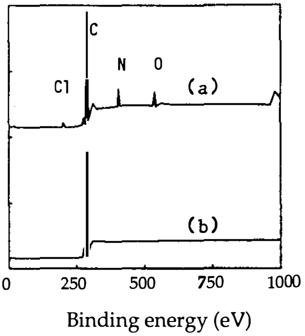

Figure 2. XPS survey spectras of (a) 0.7 s NH_3 treated PP and (b) untreated PP following 10 mn exposure to TCM vapours.

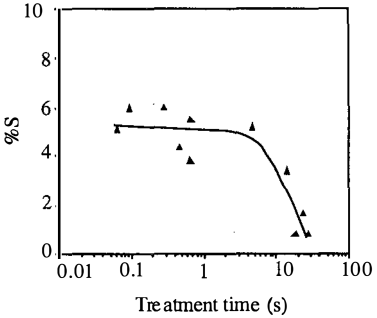

Figure3. %S, the chloroform to nitrogen atom ratio (in %) vs treatment time. The plots shows that optimal treatment time is lower than 1s.

The variation of %S vs treatment time is in complete agreement with the results obtained from contact angle measurements and adhesion measurements of thin aluminium coating to ammonia plasma treated PP.

The metallization process consisted of depositing in situ a thin aluminium coating on the ammonia treated PP films by thermal evaporation at 10^{-3} Pa[12]. Simultaneously with the peel strength recorded, the percentage of the peeled off metal was measured with the help of a video camera and an image processor using the black and white contrast between the covered and non covered areas[10]. The results (figure 4) show a sharp decrease of the aluminuim % peeled off from the begining of the plasma treatment (for 0.023s of treatment time only 4-5 % of Al is peeled off). This percentage remains constant with increasing plasma treatment time and then it increase (20%) for treatments exceeding 1s.

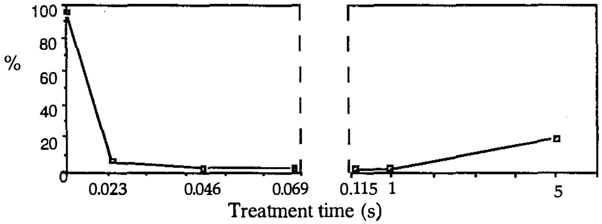

Figure 4 . Evolution of the amount of aluminium peeled off as a function of the treatment time.

In fact, both XPS and adhesion measurements point out that ammonia plasma treated PP interacts favourably with either an acidic molecule (TCM) or an amphoteric element (aluminium) following a short plasma treatment that does not exceed 1s.

However, we have observed the ageing phenomena of the 1 s pretreated film upon exposure to a non polar medium such as air. On the one hand the surface rendered wettable by the treatment is found to revert to a less wettable state with time and on the other hand the adhesion starts to degrade leading to a higher percentage of the peeled off metal [11,12]. Note on Figure 5(c) that with ageing the basic character is no longer clearly observed and the surface becomes amphoteric. Furthermore, Figure 6 shows that the measured percentage of peeled off metal increases in function of the ageing time of ammonia treated PP before mettallization confirming the results discussed above.

One can suggest that the ageing process results firstly, from a reorientation of polar moieties away from the surface into sub-surface giving rise by this way to a lower value of the work of adhesion W_{sl}. Secondly, from a neutralization of basic polar groups by atmospheric contaminants [11].
In order to minimize this reorganization upon contact with air, we have pretreated the surface with a helium plasma before the ammonia treatment [13], because, inert gases are well known to crosslink polymer surfaces [14].The results show in this case that the surface energy remained relatively unchanged since the contact angle of water shown in figure 7 increased very slowly in 4 days (less than 10%) and then remained constant for longer periods. Moreover, no degradation of the adhesion was observed even for treatments exceeding a few seconds considered to be an overtreatment (8-10% for t=5s) [13]. The polymeric surface being crosslinked, the mobility of the polymer segments at the surface decreases and the scissoring effect due to a plasma overtreatment (t=5s) is considerably less, limiting in this way the formation of a weak boundary layer responsible for the adhesion degradation of the Al-PP system[13].

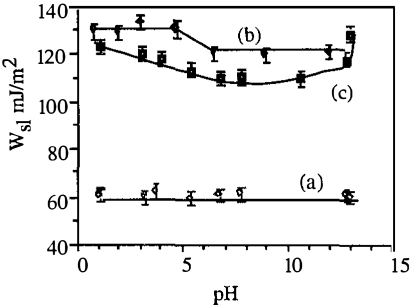

Figure 5. Total work of adhesion W_{sl} of NH_3 treated PP films measured in function of different pH values; (a) untreated PP; (b) freshly treated 0.7s; (c) after 70 days.

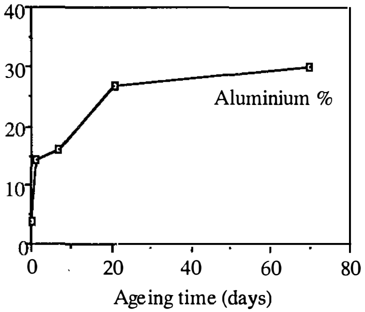

Figure6. Evolution of the percentage of Al peeled off in function of the ageing time.

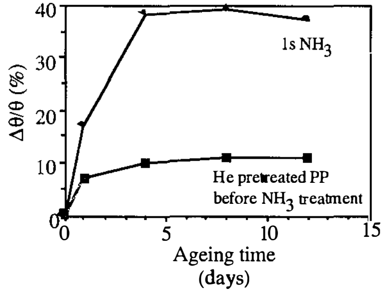

*Figure7.*Role of the helium pretreatment on the contact angle change with ageing.

Conclusion

Adhesion and wettability of polymers to substrates may be enhanced by surface modification. In this aim, The plasma process is a successful tool bringing about acidic and basic groups grafted to the surface. The 'polar' interfacial interactions which are exothermic and enhance adhesion can never be of a dipole-dipole type but are the result of exothermic lewis acid-base interactions.

The acid-base properties of ammonia plasma treated polypropylene were characterize by contact angle measurements and, XPS using chloroform as the lewis acidic probe. The former points out the basic character of the NH3 treated PP explaining in this way the adsorption of chloroform to the surface. The latter has been interpreted in terms of acid-base interactions between chloroform and basic groups grafted on the surface. However, the chloroform/N ratio has its upper value for a treatment time lower than 1s and then decrease sharply for longer treatment times. The results parallel those obtained from the metallization of ammonia plasma treated PP by aluminium.

Nevertheless, the ageing phenomena brings about surface rearrangement and neutralization of basic groups by atmospheric contaminants. Therefore, in order to minimize this phenomenon the surfaces were crosslinked by a helium pretreatment limiting thus the mobility of the polar groups.

References

1-H.Yasuda, *Plasma Polymerisation,* Academic Press, New York 1985.
2- F.M.Fowkes, F.L.Riddle Jr, W.E.Pastore and A.A.Weber , *Colloids & Surfaces,* 43 (1990) 367-387.
3- G.M.Whitesides, H.A. Biebuyck, J.P. Folkers and K.L.Prime, *J.Adhesion Sci. Technol.,* vol 5. No1, (1991) pp 57-69.
4- F.M.Fowkes, *J.Adhesion Sci. Technol.* vol 4, No 8, (1990) pp 669-691.
5- *Surface & Interfacial Aspects of Biomedical Polymers,* Eds J.D.Andrade, Plenum Press, New York and London (1985).
6- K.J.Hüttinger, S.Höhmann-Wien and G.Krekel, *J.Adhesion Sci. Technol.,* 6 (1992) 317.
7- G.M.Whitesides and P.E.Laibinis, *Langmuir,* 6 (1991) 87.
8- N. Shahidzadeh-Ahmadi, M.M.Chehimi, F.Arefi-Khonsari, J.Amouroux and M.Delamar, *J.Plasmas & Polymers,* in the press.
9- M.M.Chehimi, J.F.Watts, S.M.Jenkins and J.E.Castle, *J.Mater.Chem.,* 2(1992) 269.
10- F.Arefi-Khonsari, M.Tatoulian, V.André, J.Amouroux and G.Lorang, *Metallized Plastics3 : Fundamental and Applied Aspects, Edited by K.L.Mittal, Plenum Press, New York 1992.*
11- N. Shahidzadeh-Ahmadi, F.Arefi-Khonsari, J.Amouroux ,*J.Mater.Chem.,* 5(2) (1995) 229-236.
12- M.Tatoulian, F.Arefi-Khonsari, N. Shahidzadeh-Ahmadi, J.Amouroux, *Int.J. of Adhesion & Adhesives,* in the press.
13- M.Tatoulian, F.Arefi-Khonsari, I.Rouger, J.Amouroux, M. Gheorgiu and D. Bouchier, *J.Adhesion Sci. Technol* in the press.
14- Hansen, R.H. and H.Schonhorn.Polym.Lett., 4 (1966) 203.

IMPROVEMENT OF ADHESION AND CORROSION PROTECTION OF METALS , FROM THE GRAFTING OF CONDUCTING POLYMERS VIA PREADSORPTION OF AROMATIC THIOLS

P.Lang, Z.Mekhalif, A.Regis*, F.Garnier,
Laboratoire des Matériaux Moléculaires; CNRS ; 2 rue H.Dunant 94320 THIAIS
*LASIR: same address.

Abstract

The deposition of conducting polymers such as 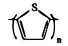 *onto metallic substrates (Pt, Ti ,Al) is performed after a chemical pretreatment of the surface substrate ,using aliphatic* (CH_3-$(CH_2)_n$-SH *n=0 to10) and bipolar thiols (* Φ-$(CH_2)_nSH$*, n=0,1,2,3). The formation of the thiol self-assembled monolayers is optimized towards the blocking of the metal oxidation. The pretreatment with aromatic thiols improves also the polymer film adhesion . Moreover, this procedure leads to dense , long conjugated polymers with few defects.*

INTRODUCTION

The electrodeposition of polymers such as Conducting Polymers (CP) is an area of considerable activity. The process, which involves the oxidation of a monomer at an electrode surface is hindered when the electrode oxidizes before the electropolymerization takes place.

Up to now, noble metals have been mainly choosen as suitable electrodes, but recently some attempts have been undertaken for depositing pyrrole or thiophene onto Fe, Ti , Al...1,2).Generally the metal surfaces are passivated by the solvent or by the supporting salt. In such cases, the polymer films are often of poor quality, of low adherence, and they can aslo contain metal oxide traces. In regard to the potential applications of these electrodeposited polymers as adhesive and protective films against corrosion or as painting primary, this method appears not at all acquainted as the polymer film must be of good quality in regard to two aspects: interfacial properties (adhesion, high coverage...) and also structural properties (density, porosity, morphology, electronic properties).

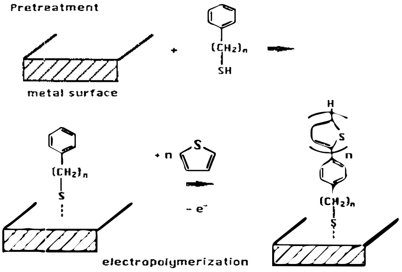

Fig.1

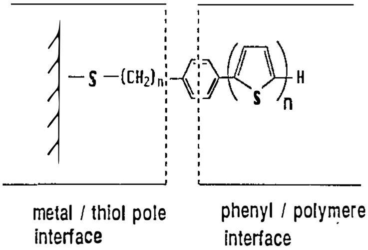

Fig.2

As alternative way for electrodepositing polymers onto oxidable substrates we propose the pretreatment of the metal surface by molecules having a large affinity for metals such as sulfur-based molecules [3,4] possessing two active poles $HS-(CH_2)_n-Y$ .These molecules are designed to contain a pole X (SH, for example) which is intended to adsorb strongly. and the other hand, the Y pole, which must be able to react during the electropolymerization process with the monomer or oligomer in solution and form thus a strong covalent bond (Fig.1). After such pretreatment, polybithiophene can be further electrochemically deposited.

The goals of such pretreatments concern the improvement of :

a) the interfacial properties as adhesion, coverage, charge transfer,...

b) the interesting bulk structural properties of the polymer films towards future utilization, such as density, conductivity, stablity....

We have studied the formation and properties of i) the metal/thiol interface (with $R-\Phi-(CH_2)_nSH$, n=0,1,2,3; R=H, CH_3) and ii) the thiol/polymer interface (Fig.2). With this aim, we have firstly focused the study on a model system, i.e. the platinum/thiol system covered or not by the conducting polymer. We have optimized the properties of the thiol layers in regard to their blocking properties towards H_3O^+, OH^-, and oxygen adsorptions. This step allows not only to show the influence of the pretreatment on the polymer film properties but also to analyze the effect of an adsorbed oxide layer. Secondly, we have applied this process to the case of oxidizable metals.

The preparation of platinum single polyoriented crystals, and the thiol pretreatment have been described elsewhere [3]. The electrode is dipped in an aqueous thiol solution, carefully rinsed with water and acetonitrile. The electropolymerization occurs in a $LiClO_4$ 0,2M - CH_3CN solution containing recristallized bithiophene (0,2M)

I. FORMATION AND CHARACTERIZATION OF ALIPHATIC $CH_3(CH_2)_nSH$ (n=0 to 10) AND AROMATIC ($R-\Phi-(CH_2)_nSH$, n=0 to 3; R=H, CH_3) THIOL MONOLAYERS

High concentrations($>10^{-2}$ M) of the thiols in water with relatively long time of dipping (>1 mn) of the elecrode lead to the best blocking properties .The blocking coefficients x, higher than 95% [3b,d 4] , are measured by the amount of hydrogen that the electrode can adsorb in sulfuric acid medium . The values of capacitive current, the blocking ability towards the metal oxidation and the wetting properties have been also considered. It has been thus shown that the ordering, close-packing , and hydrophobicity of these layers increase with the aliphatic chain length (n), that drives the self-assembling properties of the molecules.

The electrode can also be quenched with deaerated and H_2 saturated water. In this case, the thiol adsorbs onto an oxygen free surface. The blocking coefficient and the hydrophobicity are then higher, due to a closer-packing of the thiol molecules. However the adsorbed oxygen is displaced by the thiol as shown by Auger spectroscopy [3e,4] .The role of oxygen is probably related to the potential taken by the electrode during the thiol adsorption.

II INFLUENCE OF THE CHAIN LENGTH n OF Φ-$(CH_2)_nSH$ (n=0,1,2,3)

II.1.Kinetic of Growth Process

In Figure 3, the electropolymerization curves show important modifications in regard to the molecule used for pretreatment . The curves could be divided in three regions :

-In region I where the monomer is not yet oxidized, the current is due to the capacitive charge or to the residual water oxidation, all the more lowered than the chain length is longer (see inset b): The blocking efficiency towards these processes increases with n.

- In region II, the current concerns mainly the monomer oxidation, the formation of oligomers and of the first nuclei. With the pretreated electrodes, the current begins a little later but increases quicker and clearer (inset b). The current is even lower at the maximum potential Vmax.

- In the last region, the current, connected to the kinetic of film growth, increases quicker when the chain length increases. With bithiophene as monomer, the alkyl chain length of the thiol doesn't limit the growth rate of the polymer film.

II.2 Electrochemical properties of the films

Once the films formed, a doping-undoping process is observed electrochemically (Fig.4). The potential peak of the obtained polybithiophene (PBT) film $E_{ox,p}$ is a parameter expressing the conjugation length of the chain. Its half width at half height (PHWHH) characterizes the distribution of the lengths of the conjugated segments. Negative differences of Δ(Eox,p) and Δ(PHWHH) between pretreated electrode and the bare one indicate an improvement of the film quality.The films deposited on pretreated electrodes show improved characteristics in regard to their electrochemical properties (Fig.5): $\Delta(E_{ox,p})$ and Δ(PHWHH) are negative and decrease with the chain length.The longer the alkyl chain length is, the more improved the electronic films properties are. The role of the alkyl chain appears therefore determining; this effect is probably related to the greater order of the longer chains which show higher close-packed density, as already observed with aliphatic thiols. Let us notice that the improvements of the films have been observed with aliphatic thiols with the same trend . However the practical adhesion of the films is very weak showing the role of the aromatic cycle in the deposition process.

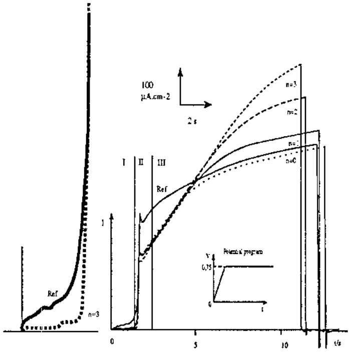

Fig.3: Grafting curves for electrodes pretreated with Φ-$(CH_2)_nSH$ (n=0-3) and for a no pretreated one (——)

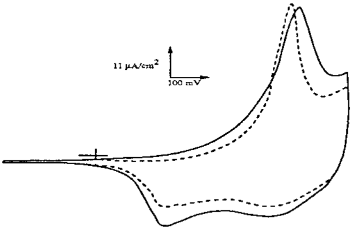

Fig.4: Comparison between voltammogramms of doping-undoping :PBTfilms: (——) without pretreatment; (- -) pretreated with n=3;

Influence of initially adsorbed oxygen

In this case, the thiol adsorbs onto an oxygen free surface. With Φ-SH, the electrochemical properties are better improved as compared to oxidized platinum electrode. Electrochemical parameters decrease of δΔ(E ox,p)= -10mV and δΔ(PHWHH) = -18mV more; As previously shown for the aliphatic thiols $^{2,4)}$, the oxygen hinders a good ordering of the monolayers.

III INFLUENCE OF METHYL SUBSTITUENTS OF THE PHENYL CYCLE OF $(CH3)_m$-Φ-SH (m=0,1,2)

The presence of one methyl substituent still improves the properties of the polymer films (Fig.6). Furthermore, the meta position appears as the best one. In this only position, the electronic effect of both the CH_3 and S substituents add up, activating the positions 2,4,6 Let us notice that the position 4 is also sterically favoured. These results indicate that a chemical reaction -electrophilic substitution type- occurs, leading to the formation of a C-C covalent bond . Moreover the adhesion is much better in the case of aromatic thiols than with aliphatic thiols. Thus the role of the aromatic cycle is confirmed, as previously suggested in Fig. 1.

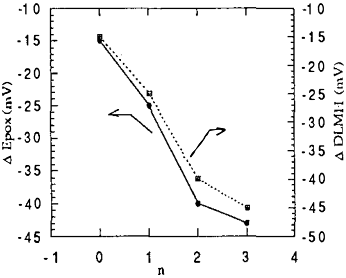

Fig.5 : Δ Epox et Δ DLMH of the polybithiophen grafted onto platinum versus n for Φ-$(CH_2)_nSH$.

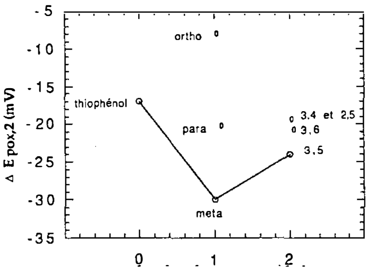

Fig.6: Δ Epox of the polybithiophene grafted onto platinum versus m for $(CH_3)_m$-Φ-SH.

IV PRETREATMENT OF OXIDIZABLE METALS: TITANIUM AND ALUMINIUM

After polishing , the electrode is immediatly dipped into pure thiol, rinsed with CH_3CN and introduced in the cell. Figures 7a and 7b show that, in the presence or not of bithiophene in the solution, the metal oxidation is largely inhibited. In absence of the adsorbed thiol, the polymer grows onto an oxide layer which has been formed at a lower potential . In this last case, the deposition rate is lowered. By electrodepositing the polymer by cyclic voltammetry, the same behaviour is again observed ; moreover the electrochemical properties of the films are improved as for platinum (fig 7). The deposition yield also increases, as for an identical oxidation charge, the amount of deposited film onto pretreated Ti is larger than that on a bare electrode.

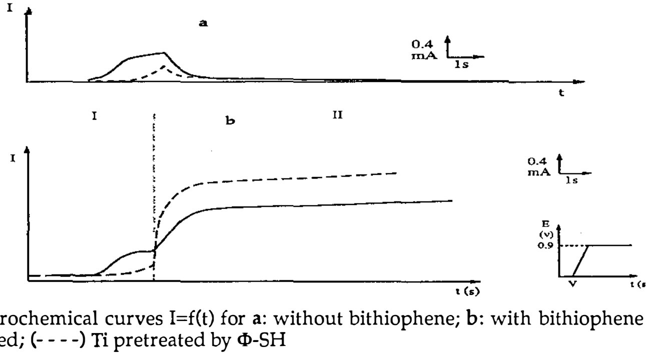

Fig.7: Electrochemical curves I=f(t) for **a**: without bithiophene; **b**: with bithiophene ;(——) Ti no pretreated; (- - - -) Ti pretreated by Φ-SH

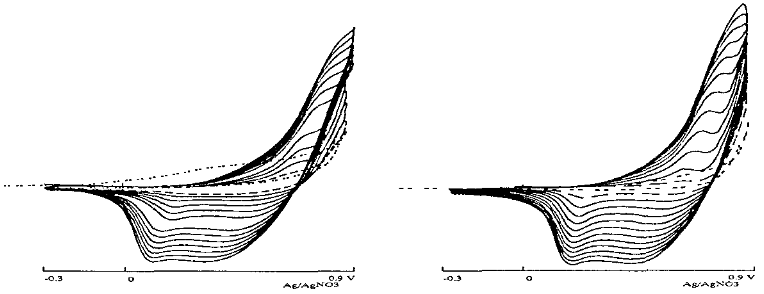

a b

Fig.8 Voltammogram I=f(V) for the electropolymerization of bithiophene on **a**: Ti ; **b**: ΦSH/Ti ;(- - - -) first cycle.

Concerning aluminum electrodes , comparable results were obtained for the blocking properties, growth mechanism and electrochemical properties. Finally, the practical adhesion of these films studied by MEB after a deadhesion test, is strongly enhanced when using an arylthiol pretreatment. This effect is not observed when using aliphatic thiol, demonstrating again the important role played by the phenyl group .

Conclusion

The pretreatment of platinum electrodes by aliphatic aromatic thiols leads to significant modifications in the deposition process kinetic and in the electrochemical properties of polybithiophene films. The longer the alkyl chains are, the better the films are. We interprete this behaviour by the difference in the structure of the thiol monolayers which become highly ordered and close packed with a long chain. With aromatic thiols, such pretreatments has been shown to allow the grafting of conducting polymer with the formation of a .covalent C-C bond improving thus the adhesion of the polymer film deposited onto platinum as well as onto oxidizable metals such as Ti and Al.

REFERENCES

1°) F.Beck, P.Hüler; J. Electroanal Chem., 280 ,159,(1990)

2°) C.A Ferreira, S. Aeiyach, M.Delamar, P.C.Lacaze, J. Electroanal Chem; 284,351,(1990)

3°)a°)P.Lang, F.Chao, M.Costa, F.Garnier; Polymer,28,668,(1987).b) P.Lang, Z.Mekhalif, F.Garnier;J.Chim.Phys. 89,1063(1992); c) Le vide, les couches minces 268(1993); d) Z.Mekhalif, P.Lang, F.Garnier, A.Regis; J.Chim.Phys. (1995) accepted; e) Z. Mekhalif; Ph. D University PARIS VI, 1994

4°)P.Lang, B.Rat, N. Kitakatsu, Z. Mekhalif, F.Garnier, E.Alleno, MG. Barthès, L.Minel, M.R Vilar; Congrés SFP , Coll.I ; 1993, Toulouse, France

SHORT AND LONG CHAINS IN BIOLOGY

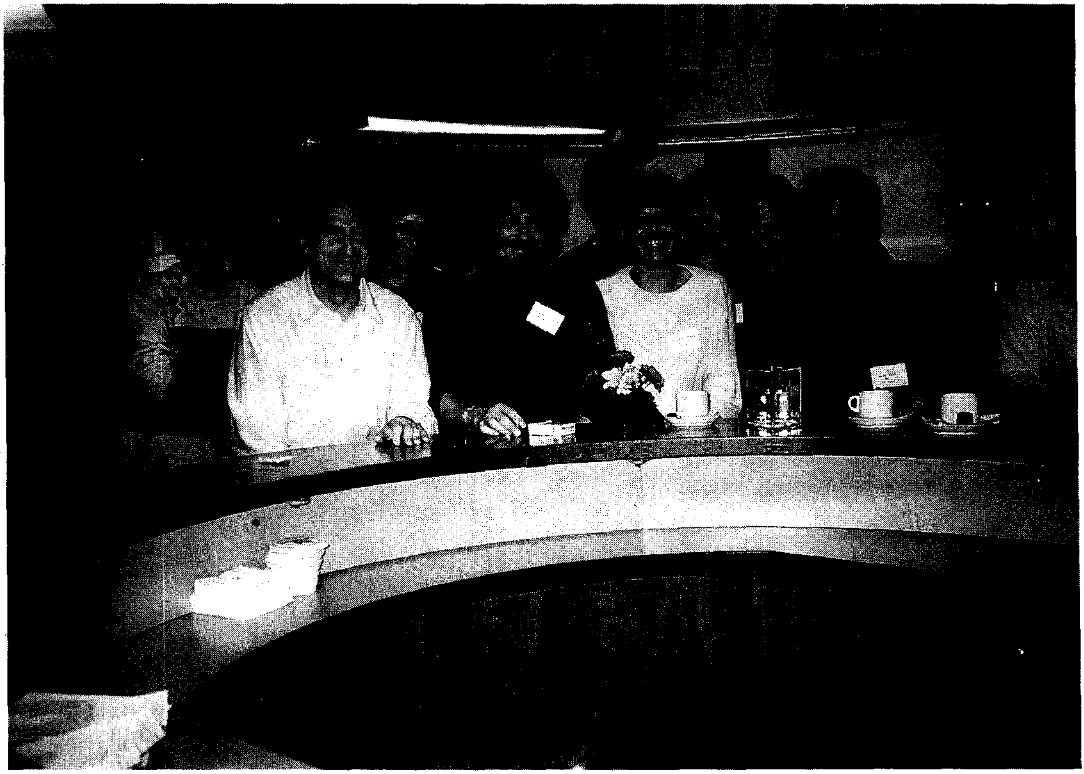

INTERACTION OF LIPID BILAYER MEMBRANES WITH AMPHIPHILIC HELICAL PEPTIDES

Huey W. Huang, Ke He, William Heller and Steve J. Ludtke
Physics Department, Rice University, Houston, Texas 77251-1892, USA

Small amphiphilic helical peptides are antibiotics produced in the host defense systems of animals. They exert their activity directly on the lipid bilayer of cell membrane. How do they attack bacteria without harming the host cells? It turns out that the mechanism of their activity is related to a phase transition like behavior. At low concentrations, they are adsorbed on the membrane surface. Above a critical concentration, they insert into the bilayer. The critical concentration depends on the lipid compostion of the cell membrane. We use the methods of oriented circular dichroism, x-ray diffraction and neutron scattering to study this problem.

Introduction

How is the physical property of a lipid bilayer related to the membrane interaction with proteins? Naturally produced amphiphilic helical peptides provide a simple, well-defined system for studying this problem. These 20-30 amino-acid peptides are antibiotics; the best known examples are megainins$^{1)}$. They rupture bacterial cell membranes but are, at the effective antibacterial concentrations, nonhemolytic. The evidence that these peptides exert their activity directly on the lipid bilayer rather than on some protein targets is threefold: the synthetic enantiomers made of D-amino acids are equally active as the natural L enantiomers$^{2)}$; their effects on artificial membranes are similar to that on cell membranes; and so far no proteins receptors have been found for these peptides. The question then is how do they interact with a lipid bilayer? And how do we account for their biological functions, particularly how do they attack bacteria without harming the host cells? Most of our experiments were performed with magainins and alamethicin.

One expects an amphiphilic helical peptide of about 20 amino acids to either adsorb on the interface between the polar region and the hydrocarbon region of the bilayer or insert in the bilayer as an aggregate such that the exterior surface of the aggregate is hydrophobic. To study such peptide/membrane systems, we prepared the samples into smectic liquid crystals. (All experiments were performed with the lipids in the Lα phase as monitored by polarized microscopy or x-ray diffraction.) We could then distinguish the two above-mentioned states by measuring the orientation of the peptide helices. This was done by the method of oriented circular dichroism$^{3)}$. Our measurements showed that the two distinct states actually represent two thermodynamic phases of the peptide-membrane systems$^{4)}$. In general, at low concentrations, expressed as the peptide-to-lipid molar ratio P/L, the peptides are adsorbed parallel to the membrane surface. Above a critical concentration P/L*, there is a coexistence region in which a fraction of the peptide molecules are inserted perpendicularly in the bilayer, and the rest remain on the surface. The inserted fraction increases (from zero at P/L*) with P/L. In some cases the coexistence region ends at a higher P/L and beyond this concentration all peptide molecules are inserted$^{4,\,5)}$. In other cases, the coexistence region extends to very high P/L's and the completely inserted phase was not detected within the experimental limit. The value of the critical P/L* for a given peptide varies with the lipid composition of the bilayer. In the activity assays, these peptides show critical concentrations for lysis. Thus it was hypothesized$^{5)}$ that the insertion transition is the mechanism of cytotoxicity and the cell selectivity is achieved by the dependence of P/L* on the lipid composition of the cell membranes.

The smectic liquid crystalline samples are also ideal for lamellar diffraction and in-plane scattering. By the x-ray lamellar diffraction study, we found that when the peptides are adsorbed on the membrane surface, the lipid chains become disordered and the bilayer thickness decreases. The decrease of the bilayer thickness is proportional to P/L (as long as it is below P/L*). Since the chain volume is approximately constant, the chain cross section must increase correspondingly, and from this one can calculate the area occupied by the adsorbed peptides. These results reveal a very simple way the peptides interact with bilayers at low concentrations, that leads to peptide insertion at high concentrations.

The inserted peptide molecules in the bilayer can be detected by x-ray or neutron in-plane scattering. Our preliminary neutron in-plane scattering experiment showed that alamethicin forms well defined channels in the "barrel-stave" fashion.

Oriented Circular Dichroism

To determine the orientation of the helices with respect to the planes of the bilayers in our multilayer (smectic L. C.) samples, we employed the method of oriented circular dichroism (OCD) described in Wu et al. (1990)$^{3)}$. This method makes use of the Moffitt theory$^{6)}$ that the peptide's exciton band at 208 nm is polarized parallel to the helical axis$^{7)}$. Thus a normal incident OCD of a multilayer sample shows, for helices parallel to the membranes, a 208 nm amplitude slightly larger than the corresponding vesicular CD, whereas the band disappears if the helices are perpendicular to the membranes. This simple method allowed us to examine the peptide orientation in a matter of minutes using a standard CD spectropolarimeter.

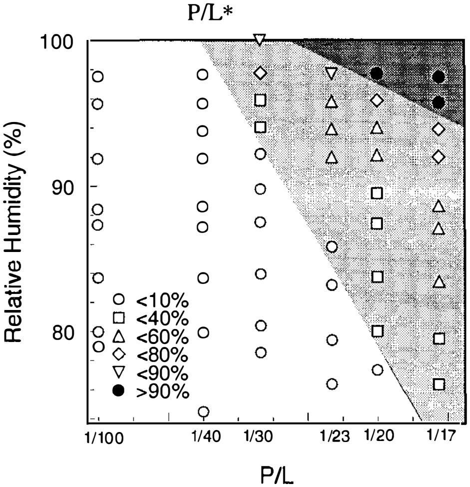

OCD were measured with the multilayer samples equilibrated in a humidity chamber. An example of alamethicin with diphytanoyl phosphatidylcholine is shown above. The phase diagram show three distinct regions: the region where the peptide molecules are practically all inserted (dark), practically all in the surface state (white), and the coexistence region (gray). The symbols denote the fraction of inserted, e.g., Δ means the fraction of insertion is between 40% and 60%. The critical concentration for insertion P/L*~ 1/40. The phase diagram varies with both peptide and lipid.

X-ray lamellar diffraction

Because of the long range thermal undulations, the diffraction patterns of membranes in excessive water are suppressed; as a result, only two or three Bragg orders are detectable. This problem can be overcome by reducing the water content in the multilayer sample but still maintaining the lipids in the Lα phase. 8 to 9 Bragg orders are measurable under such conditions. The electron density profiles of the bilayes showed that peptides in the surface state reduce the bilayer thickness. In all cases the decrease of the bilayer thickness is proportional to P/L8). These results can be interpreted as follows. In a planar bilayer of pure lipid, the polar region and the hydrocarbon chain region must occupy the same cross sectional area. If some peptide molecules are inserted in the polar region, the added cross sectional area in the polar region due to the adsorbed peptide molecules must be matched by a corresponding areal increase in the chain region. In general, the cross sectional area of a lipid is larger if its chains are more disordered. Since the volume of the chains is, to the first order, constant during an order-disorder transition, the fractional increase in the cross section $\Delta A/A_o$ (per peptide) equals the fractional decrease in the thickness. $\Delta S=\Delta A(L/P)$ is then the expanded area due to each adsorbed peptide molecule. The experimental values of ΔS are approximately that of the cross sections of the adsorbed peptides8). This is consistent with the assumption that the peptide is adsorbed at the interface and the adsorbing peptide pushes the lipid head groups laterally to create an additional area of ΔS in the polar region. Furthermore, since the free energy of membrane deformation is proportional to the square of the thickness change, it will increase with $(P/L)^2$.

The critical concentration for insertion can now be understood as follows9). The free energy of adsorption consists of two parts, the energy of binding to the interface and the energy of membrane deformation. At low P/L's, the free energy of insertion is much larger than the free energy of adsorption. However, at a sufficiently high peptide concentration, the energy of adsorption can exceed the energy of insertion. The critical concentration for insertion is the point when these two energies are equal.

Neutron in-plane scattering

Peptides embedded in the bilayers can be detected by in-plane scattering10). To study how inserted alamethicin molecules are distributed in the bilayer, neutron scattering of alamethicin in dilauroyl phosphatidylcholine was measured with Q parallel to the plane of bilayers. Water was replace by D_2O so that, if there is a substantial amount of water associated with inserted alamethicin, D_2O would provide the primary contrast against the lipid-peptide background. An example was shown in Fig. A[11]. The peak at Q~ 0.11Å^{1} is the first order lamellar peak due to smectic defects present in the multilayer sample. The lamellar peak may be removed from the data (Fig. B). The analysis of the scattering curves showed that alamethicin forms cylindrical channels, primarily of eight monomers.

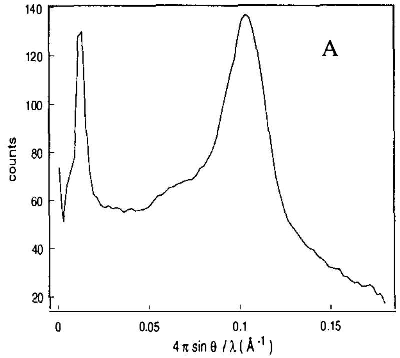

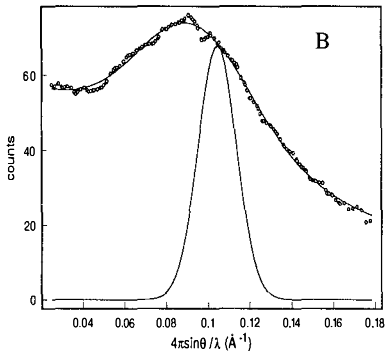

References

1) Zasloff, M., Proc. Natn. Acad. Sci. U.S.A. 84, 5449-5453 (1987).
2) Wade, D. et al., Proc. Natn. Acad. Sci. U.S.A. 87, 4761-4765 (1990)
3) Wu, Y., Huang, H. W. & Olah, G. A., Biophys. J. 57, 797-806 (1990).
4) Huang, H. W. & Wu, Y., Biophys. J. 60, 1079-1087 (1991).
5) Ludtke, S. J., He, K., Wu, Y. & Huang, H. W., Biochim. Biophys. Acta 1190, 181-184 (1994).
6) Moffitt, W., J., Chem. Phys. 25, 467-478 (1956).
7) Olah, G. A. & Huang, H. W., J . Chem. Phys. 89, 2531-2537 (1988).
8) Wu, Y., He, K., Ludtke, S. J. & Huang, H. W., Biophys. J. (June, 1995).
9) Huang, H. W., J. Phys. II France (1995).
10) He, K., Ludtke, S. J., Wu, Y. & Huang, H. W., Biophys. J. 64, 157-162 (1993).
11) He, K., Ludtke, S. J., Huang, H. W. & Worcester, S. L. (1995)

EXCHANGE KINETICS FOR PROTEIN ADSORPTION ON SOLID SURFACES

E. K. Mann,[1,2] V. Ball,[1] Ph. Huetz,[1] L. Heinrich,[2] P. Schaaf,[2] J.-C. Voegel[1]
[1]Centre de Recherches Odontologiques, INSERM Unité 424
Université Louis Pasteur; 1, Place de l'Hôpital 67000 Strasbourg, France
[2]Institut Charles Sadron, ULP-CNRS; 6, rue Boussingault 67083 Strasbourg Cedex

Protein adsorption on solid surfaces plays a fundamental role in the field of biocompatible materials, and is an important consideration for blood compatible surfaces or metallic surgical implants. One of the main differences between adsorption processes of "small" molecules and of macromolecules is that macromolecules can reach the surface by two different mechanisms: by direct adsorption or by a progressive exchange reaction. This exchange mechanism has been investigated for two different cases: (a) homogeneous exchange whereby IgG molecules adsorbed onto latex particles are replaced by IgG molecules from the bulk solution and (b) heterogeneous exchange whereby IgG molecules adsorbed onto a hydrophilic silica surface are replaced by fibrinogen molecules from the solution. Selective ^{125}I radiolabeling was used to distinguish between incoming and outgoing proteins. In the two cases, the replacement at an intermediate time scale (several hours) can be modelled by a first order kinetic reaction with respect to the molecules in solution, similar to that described for homogeneous exchange in polymer systems. Rate constants were determined.

Introduction

Protein adsorption on solid surfaces presents a fundamental challenge: A protein is very different from the simple, stable, point or spherical particles beloved of most theories of adsorption.$^{1)}$ Furthermore, processes allowing the surface configuration to change between different possible states are often be so slow that no equilibrium state is reached, within reasonable experimental times (*i.e.* several days).

The large molecule is in contact with the surface not at one single point, but at many. The interaction energy at any one point may be small but the sum total very large, leading to tight binding of the molecule. This is so strong that the protein solution may be replaced by a pure buffer solution with little observable desorption. However, the protein may be progressively deplaced at the interaction sites by an incoming protein. This process is of interest both simply because it is intrinsically different from the usual, simple adsorption occurring when a surface is first placed in contact with an adsorbate solution, and because during this process the proteins may be forced to change configurations, through irreversible denaturization, more than is necessarily the case for simple adsorption.

The "exchange" process was first proposed for proteins many years ago,$^{2)}$ but so far the only systematic studies performed have involved synthetic polymers.$^{3),4),5)}$ The major difficulty involved, in either case, is that exchange cannot be monitored directly with available techniques. It is however possible to search for general laws governing the adsorption or desorption of the protein molecules, and compare them with the laws expected for exchange processes. This will be attempted here for two different protein systems: Immunoglobulin G (IgG) on the surface, placed in contact with either an IgG solution (homogeneous exchange) or with a fibrinogen (Fib) solution (inhomogeneous exchange). These proteins were chosen in part for their biological importance: IgG is the standard antibody while fibrinogen plays a major role in blood clotting phenomena.

Materials and Methods

IgG (M_w=150 000), provided by the Centre Régional de Transfusion Sanguine (Strasbourg, France), was isolated from human serum. Human fibrinogen (M_w=340 000) was purchased from Kabi Vitrum (Stockholm, Sweden).

Two different substrates were used. The homogeneous exchange experiments used monodisperse polystyrene latex particles, prepared under emulsifier-free conditions, with diameter 790 nm. A Tris/HCl buffer solution (pH 7.35) was chosen in order to avoid flocculation. The particles were placed in individual small tubes and left in contact with the initial protein solution for 4 hours. The protein solution was separated from the particles by centrifugation, the solution was four times removed and replaced with buffer, which was then replaced with a second protein solution. After a given time, the protein solution was removed and tested for radioactivity: the change in activity was assumed to be due either to radiolabeled molecules leaving this solution to adsorb on the surface or to radiolabeled molecules desorbing from the surface, depending on which species was radiolabeled. This method is limited to measurements at discrete time intervals (one for each tube).

For the inhomogeneous exchange experiments, the protein or buffer solutions flowed through a silica tube of inner diameter 0.17 cm and length 21.5 cm, positioned in the center of a circular NaI detector. The inner surface of the tube provided the adsorbing surface, which could thus be monitored continuously.

Further experimental details may be found in references [6] and [7].

Results and Discussion

INITIAL PROTEIN LAYER

The protein molecules are not spherical: the simplest approximation of the Fib molecule would be as a rod of dimension 45x9x6 nm^3 while the IgG molecule in solution is roughly T-shaped, with dimensions 23.5x4.4x4.4 nm^3.[8] The Fib molecule in particular is somewhat flexible; further conformational changes may occur at the surface even without denaturization. Different surface configurations are clearly possible. The initial configuration may depend on the concentration of the protein in solution, shear at the surface during deposition, etc. As long as the conditions are kept constant, a well-defined "adsorption isotherm" may be obtained (see fig. 1a).

The replacement experiments were performed with an initial protein solution of concentration c_1=0.25 g/l, replaced by buffer after 4 hours, leading to an initial surface concentration Γ_1=0.55μg/cm^2. If the buffer is now replaced by a second protein solution, the new proteins may reach the surface by three major mechanisms: they

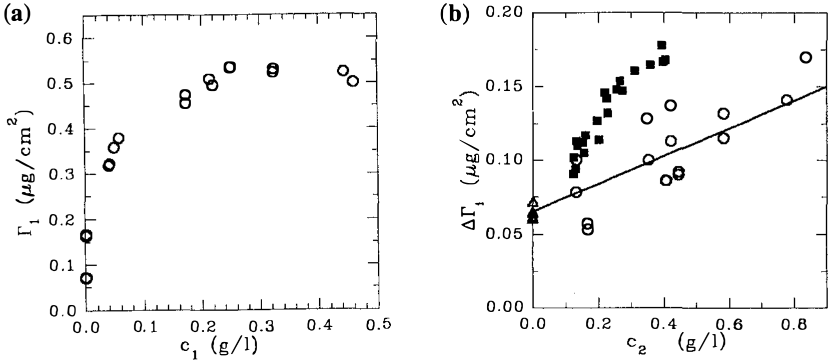

Fig. 1. (a) IgG surface concentration on latex particles after 3 hoursin contact with IgG solution with bulk concentration c_1. (b) Protein replacement on a surface with preadsorbed proteins (surface concentration Γ_1 = 0.54 μg/cm^2). Quantities of protein released from ($\Delta\Gamma_1$: ○) and fixed on ($\Delta\Gamma_2$: ■) latex particles after 4 hours in contact with IgG solution of concentration c_2. Solid line: quantity adsorbed excluding first hour, with finite quantity (△) desorbed for c_2=0 as baseline.

may fill available holes in the surface, they may fill space left by a molecule that leaves the surface spontaneously, or they may reach the surface by a cooperative exchange process. The difficulty is in distinguishing between the three processes.

HOMOGENEOUS REPLACEMENT ONTO LATEX PARTICLES: IGG-IGG

Here we are limited to discrete measurements in time; further, only for adsorption is the signal-to-noise ratio sufficient to determine the surface concentration. Some pure desorption is observed (see figure 1b), calling for direct replacement. Further, the final total protein concentration was found (fig. 2a; by radiolabeling both incoming and outgoing proteins) to be significantly greater than after the first protein adsorption step: this also corresponds to direct adsorption. These two "direct" quantities correspond to a significant fraction of the total protein adsorbed from the second solution, as indicated in figure 2a. However, these processes appear quite rapid, completed within the hour which is also characteristic for the initial protein adsorption. With time, the protein concentration continues to increase (fig. 2a): in analogy with a chemical reaction, the adsorption rate might be expected to follow the law

$$\frac{d\Gamma_2}{dt} = f(\Gamma_1, c_2) \overset{?}{=} k\Gamma_1^{\beta} c_2^{\alpha} \tag{1}$$

where the indices (1,2) indicate the initial and replacement proteins respectively, Γ the surface concentration, and c the bulk concentration. Since the protein concentration in solution and in volume remain constant to a good approximation, this suggests a linear increase in time. The increase was measured for a series of different bulk concentrations c_2 (figure 2b), and found to be linear in this concentration, suggesting an analogy to a first-order chemical reaction, with one and only one protein molecule

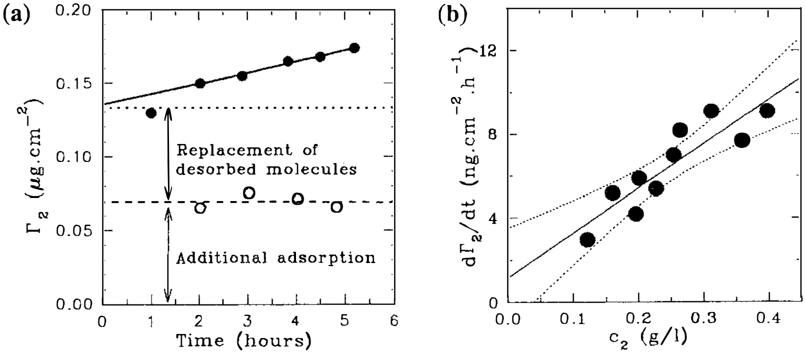

Fig 2 *(a) Replacement-adsorption on latex particles with an initial IgG surface concentration* Γ_1= *0.54 μg/cm²*. ● : *increase with time of surface concentration* Γ_2 *in presence of an IgG solution with bulk concentration* c_2=*0.36 g/l;* ○ *increase of total surface concentration (both incoming and outgoing species labled) Note 0.06 μg/cm² pure desorption (figure 1b), replaced by pure adsorption (b) Rate of change of* $\Delta\Gamma_2$ *with time, in function of* c_2. *Solid line: linear least squares fit, yielding slope 2.3·10⁻⁵ cm/hr. Dashed curves: 95% confidence limits.*

involved in the rate limiting-step of the adsorption. This can be called exchange only if at least one previously-adsorbed molecule is also involved in the adsorption. This cannot be demonstrated directly. However, we do see (figure 1b) that the total desorbed quantity after a given time is consistent with the total adsorbed which is attributed to the exchange process (i.e. not including the net increase in protein concentration during the adsorption-rinsing-readsorption process).

INHOMOGENEOUS REPLACEMENT IN A SILICA TUBE: IGG-FIB

The limitations of the above approach, using adsorption onto particles, are obvious. Adsorption onto the inner surface of a tube, through which a protein or buffer solution may be flowing, has several advantages: the tube may be directly placed in the detector to continuously monitor the desorption (presently only possible if the liquid in the tube is ***not*** radiolabeled) and the flow conditions through the tube are well defined.

We see significant desorption from the initial protein layer, with pure buffer as well as with the second protein solution. The surface concentration can no longer be taken as constant, but neither does it follow a simple exponential law as suggested by eq. 1. The simplest adequate fitting formula

$$\Gamma_1 = Ae^{-K_1 t} + Be^{-K_0 t} + C \tag{2}$$

introduces 3 characteristic time scales: 1/K$_1$, on the order of hours; 1/K$_2$, on the order of 2 days, and a third much longer. This dependence of the replacement rate with time, implying either several (at least three) distinct populations of proteins or an evolution of the protein layer with time, has been observed previously.[3),9)] The short time constant, K$_1$, is again linear with protein bulk concentration, suggesting a first

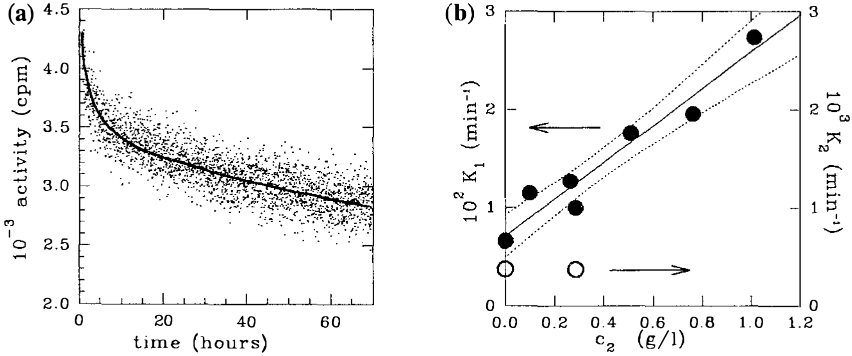

*Fig. 3 Kinetics of desorption-replacement of IgG molecules in the presence of unlabeled Fib, flowing through a silica tube. (**a**) Decrease with time of the activity of an IgG* layer with initial surface concentration* Γ_I– *0.55 μg/cm*^{2}*, in the presence of Fib at bulk concentration* c_2– *0.28 g/l. Solid curve: Best fit to an exponential decrease with three different time constants* K_1, K_2, *and 0 (eq. 2). (**b**) Time constants* K_1 *and* K_2 *vs.* c_2*. Note the order of magnitude difference in the scales for the two variables. Solid curve: least-squares fit to a straight line. Dashed curves: 95% confidence limit.*

order process. K_2 is however independent of bulk concentration. It is the desorption given by K_1 which is a candidate for a true exchange process. One may note that the total adsorbed protein is again approximately equal to the total desorbed quantity.

Another open question is that of possible configurational changes of the protein during the exchange process. One test of this change would be the reactivity of the protein with antibodies directed against the protein. With the radioactivity experiments, it is difficult to distinguish between antibodies which adsorb on the substrate, either directly or by exchange, and those which attach to adsorbed protein molecules.10) Another method, scanning angle reflectometry,11) allows one to measure both the total protein surface concentration and the thickness of the protein layer, which increases significantly when antibodies attach to the proteins, but not during additional adsorption exchange. We observe thus that Fib which replaces IgG on the silica surface remains reactive against anti-Fib, qualitatively to the same extent as Fib directly adsorbed on the surface.

Conclusions

In both cases, several different desorption processes appear to occur at the interface, with widely varying time scales. In the time scale of hours, the exchange rate was shown to follow a first-order equation in the bulk concentration ($\alpha=1$ in eq. 1). Incoming and outgoing proteins balanced during this time scale. The rate constant for what is tentatively identified as an exchange process is $k_e=(5.8\pm1.0)10^3$l/mole hr for replacement of IgG by IgG on the latex particles and $k_e=(3.8\pm0.1)10^5$l/mole hr for the replacement of IgG by Fib on the silica surface. The orders of magnitude difference between the rate constants may reflect a greater ease in the replacement of IgG by Fib than by IgG, but the different surfaces in the two experiments certainly play a role. Further experiments with different protein pairs on the silica surface are in progress.

---

1) Evans, J. W. *Rev. Mod. Phys.* **65** (1993) 1287.

2) Brash, J. L.; Samak, Q. M. *J. Colloid Interface Science* **65** (1978) 495.

3) Peffercorn, E.; Carroy, A.; Varoqui, R. *J. Polymer Sci.* **23** (1985) 1997; Varoqui, R., Pefferkorn, E. *Progr. Colloid Polym. Sci.* **83** (1990) 96.

4) Douglas, J. F.; Johnson, H. E.; Granick, S. *Science* **262** (1993) 2010; Johnson, H. E.; Douglas, J. F.; Granick, S. *Phys. Rev. Lett.* **70** (1993) 3267; Douglas, J. F.; Frantz, P ; Johnson, H. E.; Schneider, H. M., Granick, S. *Colloids Surfaces A.* **86** (1994) 251.

5) de Gennes, P G. *C. R. Acad. Sc. Paris* **306 II** (1985) 1399.

6) Ball, V; Huetz, P.; Elaissari, A.; Cazenave, J.-P., Voegel, J.-C.; Schaaf, P *Proc. Natl. Acad. Sci. USA* **91** (1994) 7330..

7) Huetz, P.; Ball, V.; Voegel, J.-C.; Schaaf, P. submitted.

8) Quash, G. A.; Rodwell, J. D.; in *Covalently Modified Antigens and Antibodies in Diabnosis and Therapy;* (Marcel Dekker, Inc: New York 1989) p 156.

9) Furusawa, K.; Yamamoto, K. *Bull. Chem. Soc. Jpn.,* **56** (1983) 1958; Schmidt, C. F.; Zimmermann, R. M.; Gaub, H. E. *Biophys. J.* **57** (1990) 577.

10) Huetz, P. *Doctoral Thesis* (Université Louis Pasteur, Strasbourg; 1995).

11) Schaaf, P.; Déjardin, P.; Schmitt, A. *Langmuir* **3** (1987) 1131.

HYDRODYNAMICS AND POLYMERS (TURBULENCE, RHEOLOGY)

OSSI
NZANO
NZANO
RICARD
DUVAL
CAMPARI
MARTINI
ARTINI
MARTINI

TURBULENT FLOWS OF POLYMER SOLUTIONS

Hans-Werner Bewersdorff
FH Lausitz, Dept. of Chemical Engineering, Großenhainer Str. 57, D-01968 Senftenberg

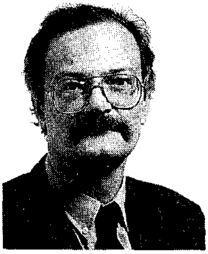

Abstract

The addition of minute amounts of soluble high molecular weight polymers to Newtonian fluids results in a lowering of the friction factor in turbulent pipe flows. In some polymer-solvent systems the polymer concentrations, which are needed to produce the effect, can be lower than 1 ppm. This shows that the effect can occur in ultradilute solutions. Since the lowering of the friction factor is accompanied by a modification of the structure of turbulence the coherent structures of turbulence have to interact with the viscoelastic material properties of the polymer solution.

First, the known different viscoelastic rheological properties of dilute polymer solutions, the shear viscosity behaviour, the non-vanishing normal stress differences in shear flows, and the increased elongational viscosity behaviour are reviewed and discussed with respect to its importance in turbulent flows, before the basics of turbulent drag reduction are presented. The influence of the polymer parameters on the friction behaviour in smoooth pipes is related to changes in the structure of turbulence. In turbulent velocity profiles of drag reducing polymer solutions the buffer layer between the viscous sublayer and the turbulent core expands with increasing drag reduction. In this region the structure of turbulence changes dramatically. A strong damping of the Reynolds shear stresses occurs, the cross-mixing of the flow is reduced, and a deficit in the (Newtonian) momentum balance is found. An attempt is made to relate these changes in the structure of turbulence to the viscoelastic rheological properties of the polymer solution in order to gain information on the mechanism of interaction between the turbulence and the additives which leads to the observed reduction in drag.

Introduction

When minute amounts of suitable high molecular weight polymers are dissolved in a Newtonian fluid, the resulting polymer solution becomes a non-Newtonian fluid and can exhibit elastic effects. In turbulent flows these elastic properties of polymer solutions can interact with the coherent structures of turbulence causing a modification of these structures. This occurs in free turbulent flows as well as in wall-bounded turbulence. In wall-bounded turbulence the interaction of viscoelasticity and turbulence results in a lowering of the wall shear stress at a constant flow-rate. Due to possible energy savings in practical applications of the effect intensive research in this field resulted in more than thousand publications in the last three decades. Only a few publications deal with the modifications of the structure of turbulence in free turbulence in dilute polymer solutions. They are reviewed in [1] and [2]. In general, in these free turbulent flows the polymers cause a suppression of the small-scale turbulence.

However, most publications deal with pipe or channel flows, i.e. with wall-bounded turbulence. In a fully developed pipe flow a force balance between the pressure forces and the frictional forces results in

$$\Delta p \, \frac{d^2}{4} \, \pi = \tau_w \, l \, \pi \, d \ . \tag{1}$$

In this equation $\Delta \mathbf{p}$ is the pressure drop, **d** the pipe diameter, τ_w the wall shear stress, and l the length of the pipe segment. In hydraulics it is common to plot a friction factor

$$f = \frac{2 \, \tau_w}{\rho \, u^2} \ , \tag{2}$$

which is the ratio of the wall shear stress to the pressure head with ρ being the density of the fluid and **u** the bulk velocity, versus the Reynolds number

$$Re = \frac{u \, d}{v} \ . \tag{3}$$

In eq. (3) v denotes the kinematic viscosity of the fluid.

In this plot (see Fig. 1) two flow regimes occur for a pipe flow of a Newtonian fluid. For **Re < 2,320** the flow is laminar with

$$f = 16 / Re \tag{4}$$

which results from Poiseuille's law. In the turbulent flow regime in hydraulically smooth pipes the friction factor is given by

$$1 / \sqrt{f} = 4 \log \left(Re \sqrt{f} \right) - 0.4 \ , \tag{5}$$

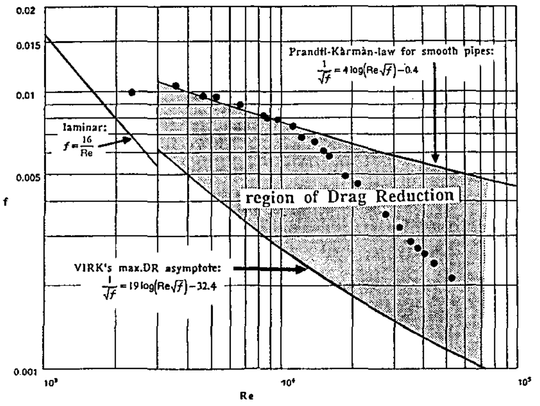

Figure 1: Friction behaviour of a 10 ppm aqueous polyacrylamide solution in a 30 mm pipe

the Prandtl-Kármán-law.

Any lowering of the friction factor in the turbulent flow regime at a constant flow-rate is called drag reduction. It should be mentioned that drag reduction does not only occur in dilute polymer solutions, e.g. as for the dilute polyacrylamide solution in Fig. 1. In general, a distinction is made between drag reduction by active or by passive means. Passive drag reduction can be produced by appropriate changes in geometry, e.g. riblets, outer-layer-manipulators, and convex curvatures [3]. In the area of active drag reduction one has to distinguish between drag reduction by magnetohydrodynamic (MHD) forcing, drag reduction in liquid boundary layers by gas injection, drag reduction by particle injection, drag reduction by surface mass injection [3], and last not least, drag reduction by polymer and surfactant [4] addition.

Drag reduction in turbulent flows of polymer solutions is observed when the molecular weight is larger than about 500,000 g/mol. It occurs in turbulent flows of dilute solutions of flexible and semi-dilute and concentrated solutions of rod-like polymers. Frequently studied polymer-solvent systems are: polyethyleneoxide (PEO) - water, polyacrylamide (PAAm) - water, polystyrene (PS) - toluoene, polyisobutene (PIB) - petroleum, carboxymethylcellulose (CMC) - water, Xanthan Gum - water.

Rheology of polymer solutions

Polymer solutions normally exhibit a shear thinning behaviour in simple shear flows, meaning the shear viscosity decreases with the shear rate. However, since the polymer concentrations needed to produce drag reduction in turbulent flows are extremely low, usually a few ppm, the small deviations in shear viscosity from that of the Newtonian solvent can be neglected in most cases. Consequently, according to Virk [5] in plots of the friction behaviour of drag reducing polymer solutions the Reynolds number is usually based on the solvent viscosity. In polymer solutions in which higher concentrations are needed to produce drag reduction in turbulent flows, the influence of the shear-thinning on the friction behaviour can no longer be neglected. This holds mainly for solutions of relatively stiff rod-like polymer molecules, e.g. for Xanthan Gum and carboxymethylcellulose (CMC) solutions and is discussed in [6].

When a viscoelastic fluid leaves a capillary, the diameter of its jet can increase up to three times of the capillary diameter in contrast to a Newtonian fluid. This flow phenomenon is called die swell effect. The physical reason for such a behaviour is that in the capillary flow of the viscoelastic fluid an extra stress along the streamlines exists. When the fluid leaves the capillary, these normal stresses in flow direction relax, the fluid contracts in axial direction and expands in radial direction. This means that in a capillary flow, which is a shear flow, viscoelastic fluids exhibit normal stresses in contrast to Newtonian fluids. In solutions of flexible polymers, besides of the region at low shear rates, the normal stress difference is higher than the shear stress with a slope of the first normal stress difference as a function of the shear rate between 1 and 2. However, the occurring normal stresses in shear flows of dilute polymer solutions in low viscosity solvents are normally too small to be resolved by commercial rheometers.

Dilute polymer solutions exhibit the most dramatic deviations from Newtonian behaviour in elongational flows. However, the measurement of elongational viacosities is one of the most difficult problems in rheometry, especially for low shear viscosity fluids. Several extensional viscometers have been proposed. However, in most situations no steady state can be reached in these instruments and only transient elongational viscosities, depending on the residence time in the elongational field, can be measured. Nevertheless, in many flow situations, as in the local elongational fields of a turbulent flow, no steady state is reached either. Furthermore, since the actual flow behaviour of viscoelastic materials depends on the deformation history, the flow in an elongational field should be shearfree and the strain history of the test material in the rheometer should have no influence. On the other hand, the elongational fields in the boundary layer are not shearfree either.

The difficulties in measuring elongational viscosities of polymer solutions and the state of the art of the measuring technique are described in a special issue of the Journal of Non-Newtonian Fluid Mechanics, Vol. **35** (1990) 85-470. The influence of pre-shearing on the elongational behaviour of dilute polymer (and surfactant) solutions was studied in [7-9]. In these studies the transient elongational viscosity of drag reducing dilute polymer solutions started to increase from its Newtonian value only when a certain critical shear rate was exceeded. This finds its analogy in the onset behaviour in turbulent pipe flows as we will see later on.

Friction behaviour

Dilute solutions of flexible polymers exhibit a so-called onset phenomenon which means that the deviations in the friction behaviour from that of the Newtonian solvent start to occur when a certain Reynolds number (see Fig. 1), or more accurately when a certain wall shear stress is exceeded which is characteristic for each polymer-solvent system. The critical wall shear stress is independent of the pipe diameter and the polymer concentration. According to [10] the product of the velocity gradient at the wall at onset conditions and the relaxation time of the polymer solution has a characteristic value for polymer solutions. Furthermore there exists a limit of the maximum attainable drag reduction [5] in pipe flows given by

$$1 / \sqrt{f'} = 19 \log (Re \sqrt{f'}) - 32.4 \ . \qquad (6)$$

This means that in the turbulent flow regime a polymer addition can produce drag reduction up to 80 %. However, even at maximum drag reduction conditions the flow is still turbulent and not laminar. In pipes of small diameter no onset behaviour often can be detected. This is due to the fact that in these cases the critical wall shear stress is already exceeded in the laminar flow regime. The influence of the pipe diameter **d** , the polymer concentration c , and the molecular weight **M** on the friction behaviour of dilute solutions of flexible polymers is shown in the Figures 2 - 4.

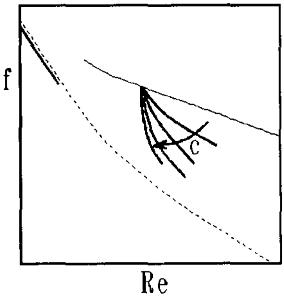

Figure 2: Friction behaviour of dilute polymer solutions of different concentrations

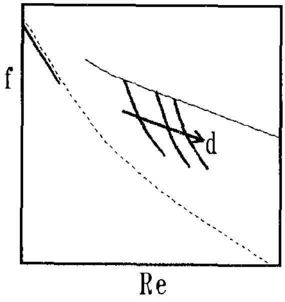

Figure 3: Friction behaviour of dilute polymer solutions in pipes of different diameter

The onset of drag reduction can be related to molecular dimensions of the polymer molecules. As shown by Virk [5] a relationship between the wall shear stress at onset conditions τ_w and the radius of gyration R_G of the polymer molecules exists

$$\tau_w = C / R_G^3 \qquad (7)$$

which means that the onset wall shear stress is inversely proportional to the hydrodynamic volume of the polymer molecule; C is a constant. By changing the quality of the solvent, or the pH-value of the solution in case of polyelectrolytes, the hydrodynamic volume, and therefore the critical wall shear stress at onset conditions change.

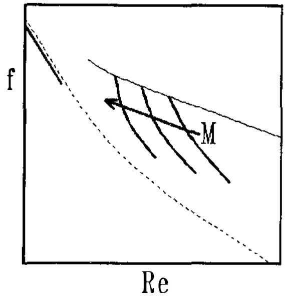

Figure 4: Friction behaviour of dilute polymer solutions of different molecular weight

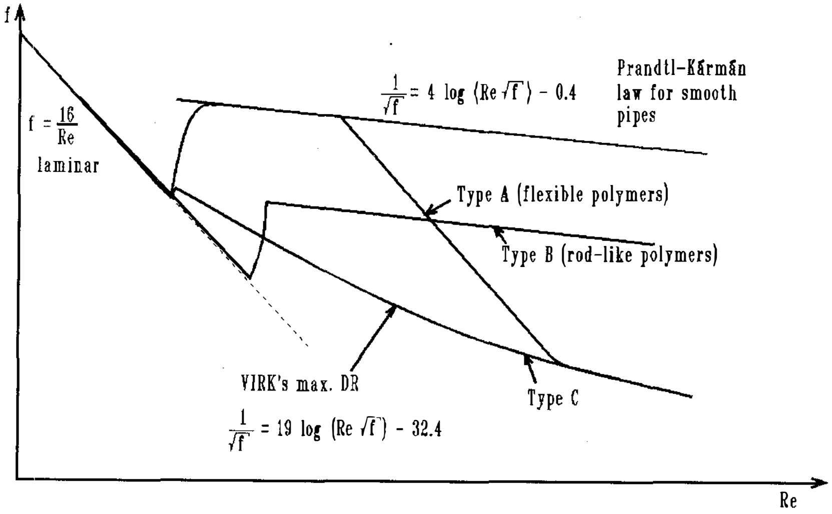

Figure 5: Friction behaviour of polymer solutions

In Fig. 5 type A shows the friction behaviour of dilute solutions of flexible polymers, which was described above, whereas type C elucidates the maximum drag reduction behaviour which is observed when the saturation concentration is reached. Solutions of rod-like polymers (type B) exhibit a so-called retro-onset-behaviour. In the turbulent flow regime the friction first is described by the maximum drag reduction asymptote, eq. (6). When a critical wall shear stress, which depends on the polymer concentration, is exceeded, the friction behaviour is parallel to the Prandtl-Kármán law, eq. (5).

Structure of turbulence

Turbulent velocity profiles are normally presented in terms of wall variables with the non-dimensional velocity

$$U^+ = U / u_\tau \ , \tag{8}$$

with the friction velocity

$$u_\tau = \sqrt{\tau_w / \rho} \ , \tag{9}$$

plotted versus the logarithm of

$$y^+ = y \, u_\tau / \nu \tag{10}$$

where y is the distance from the wall. In case of drag reduction for dilute polymer solutions (see Fig. 6) three different regions in the velocity profile can be distinguished. First near the wall the viscous sublayer with

$$U^+ = y^+ \tag{11}$$

exists which is increased in size in comparison to a Newtonian fluid. Then the velocity profile follows the so-called ultimate profile [5]

$$U^+ = 11.7 \ln y^+ - 17 \tag{12}$$

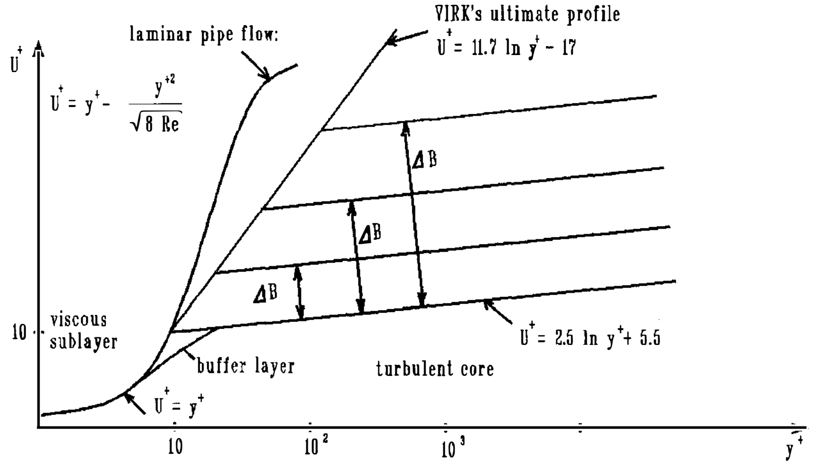

Figure 6: Dimensionless velocity profiles of drag reducing polymer solutions

in the buffer layer, and in the core region it shows a parallel shift to higher U^+ -values in comparison to a Newtonian fluid

$$U^+ = 2.5 \ln y^+ + 5.5 + \Delta B \quad . \tag{13}$$

As the drag reduction increases, the buffer layer expands until, for the case of Virk's [5] maximum drag reduction, no turbulent core exists and the buffer layer reaches the centre of the pipe.

From the velocity profiles it may be concluded that the interaction between the polymer molecules and the turbulent structures takes place in the buffer layer which therefore is also called elastic layer. The same conclusion follows from the measurements of the turbulence intensities and the Reynolds stresses. The maximum intensity of the axial turbulence is shifted, with increasing drag reduction, more and more towards the centre of the pipe whereas the radial turbulence intensity is strongly damped, e.g. [11]. The Reynolds shear stresses which characterize the turbulent momentum transport are also drastically reduced in flows of drag reducing polymer solutions [11]. However, when the solvent viscosity is used for calculating y^+ for drag reducing fluids a Reynolds stress deficit occurs and in dimensionless form

$$- \frac{\overline{u'v'}}{u_\tau^2} = 1 - \frac{y}{R} - \frac{dU^+}{dy^+} - G \tag{14}$$

where G stands for "elastic stresses", as it was called by the first authors [12] recognizing this deficit. The origin of the Reynolds stress deficit is unknown. By calling G elastic stresses one implies that this deficit is due to elastic properties resulting from rheological effects. An alternative would be that the structures of the turbulent flow are altered so that they can be dominated by viscosity up to higher distances from the wall. The quantity G could be interpreted by a wall distance dependent effective viscosity

$$- \frac{\overline{u'v'}}{u_\tau^2} = 1 - \frac{y}{R} - \frac{\nu_{eff}}{\nu_0} \frac{dU^+}{dy^+} - G \tag{14}$$

where ν_{eff} is the effective kinematic viscosity and ν_0 the kinematic viscosity of the solvent. The maximum relative viscosity ν_{eff} / ν_0 increase is between 3.5 and 5.5 [6].

Remarks on the mechanism of interaction

Although many investigations were undertaken on the behaviour of drag reducing polymer solutions the exact mechanism of interaction between the polymers and the turbulent structures is still unknown. Several models have been proposed. However, all these theories are not completely satisfactory in view of the experimental evidences. Lumley [13] showed that the drag reducing effect by polymer additives can be roughly explained by dimensional reasoning. Due to relatively large strain in turbulent boundary layers he assumed an increase in viscosity of the polymer solution which in turn damps the dissipative eddies. Since the molecules are not expanded in the viscous sublayer, this layer is not affected by the polymers which is in agreement with experimental findings. If a dimensionless wave number

$$k^+ = v / u_\tau \eta , \qquad (15)$$

with η as a length scale of the smallest eddies, is introduced, the spectrum of turbulence is limited by

$$y^+ = 2.5 / k^+ , \qquad (16)$$

curve 1 in Fig. 7, which characterizes the largest eddies, and by

$$y^+ = 2.5 / k^{+4} \qquad (17)$$

as the viscous cut-off for the smallest eddies, curve 2 in Fig. 7.

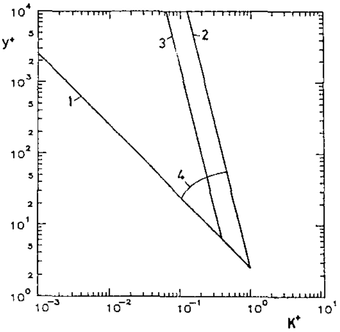

Figure 7: Dimensionless wall distance y^+ as a function of the dimensionless wave number k^+

In case of drag reducing polymer solutions the size of the smallest dissipating eddies increases due to an increased local viscosity, and according to [13] eq. (17) changes to

$$y^+ = \frac{2.5 \; v_0^3}{k^{+4} \; v_{eff}^3} , \qquad (18)$$

curve 3 in Fig. 7. If a wall distance dependent viscosity is assumed [14] which is calcuated from the Reynolds stress deficit, curve 2 changes to curve 4. Curve 4 follows curve 1 up to $y^+ = \mathbf{21}$, which means, supposed the large scale structure remains unchanged, that up to this distance only eddies of one size exist, and that the structures of turbulence are dominated by viscosity up to larger distances from the wall.

Well-known coherent structures in turbulent boundary layers are the counterrotating vortices [15]. These vortices are oriented in flow direction and behave quasi periodic in the spanwise direction. They are responsible for the low speed streaks close to the wall. It is assumed that they are the essential structure responsible for the burst mechanism which is an essential feature of the near-wall turbulence because during bursts 80 % of the time-averaged Reynolds stresses are produced. If these longitudinal vortices are calculated numerically by using the concept of a wall distance dependent effective viscosity [16], their size increases, their centre is shifted to larger wall distance, and their vorticity is decreased considerably. Thus this wall distance dependent viscosity acts like a viscous lid on the boundary turbulence. The boundary layer is stabilized which is in agreement with the experimentally detected reduced burst rate [17].

The movement of the longitudinal vortices creates two instabilities. Firstly these vortices exhibit a instability of themselves, a flapping of them in crossflow direction which results in a vortex breakdown, and secondly they produce an inflexional profile in the region where low speed fluid is lifted up as a result of the vortex motion. In such ejection-type motions a vortex stretching occurs which could be hindered by the increased elongational viscosity of the polymer solution. By a statistical analysis of the momentary values of the velocity fluctuations, e.g. [11], it has been shown that the bursts are suppressed. The same holds for the sweep motions in which high speed fluid is transported to the near-wall region. However, what is missing so far in order to find the exact mechanism of interaction between the polymer molecules and the structures of turbulence, is an information on the orientation and conformation of the polymer molecules in the buffer layer.

References

[1] Giesekus H, Hibberd MF (1987) Turbulence phenomena in drag reducing fluids; In: Majumdar AS, Mashelkar RA (eds.) Advances in Transport Processes, Vol. V, 229, Wiley Eastern, New Dehli

[2] McComb WD (1980) The physics of fluid turbulence, Clarendon Press, Oxford

[3] Bushnell DM, Hefner JN (eds.) (1990) Viscous drag reduction in boundary layers, Progr. in Astronautics and Aeronautics **123**

[4] Bewersdorff HW (1990) In: Gyr A (ed.) Structure of turbulence and drag reduction, Springer, Berlin, 293

[5] Virk PS (1975) AIChE J. **21**, 625

[6] Bewersdorff HW, Berman NS (1988) Rheol. Acta **27**, 130

[7] James DF, McLean BD, Saringer JH (1987) J. Rheology **31**, 453

[8] Wunderlich AM, James DF (1987) Rheol. Acta **26**, 522

[9] Vissmann K, Bewersdorff HW (1990) J. Non-Newtonian Fluid Mech. **34**, 289

[10] Berman NS (1977) Phys. Fluids **20**, S168

[11] Gampert B, Yong CK (1990) In: Gyr, A. (ed.) Structure of turbulence and drag reduction, Springer, Berlin, 223

[12] Schümmer P, Thielen W (1980) Chem. Eng. Commun. **4**, 593

[13] Lumley JL (1973) J. Polymer Sci.: Macromolecular Reviews **7**, 263

[14] Berman NS, Bewersdorff HW (1988) American Institute of Aeronautics and Astronautics, paper 88-3668-CP

[15] Blackwelder RF, Eckelmann H (1979) J. Fluid Mech. **94**, 577

[16] Gyr A, Bewersdorff HW (1990) In: Structure of turbulence and drag reduction, Springer, Berlin, 215

[17] Tiederman WG, Luchik TS, Bogard DG (1985) J. Fluid Mech. **156**, 419

ORIENTATION OF POLYSTYRENE CHAINS IN "STRONG" FLOW

T.Q.Nguyen, G.Yu, H.H.Kausch, Laboratoire de Polymères, Département des Matériaux, Ecole Polytechnique Fédérale de Lausanne, CH-1015 Lausanne, Switzerland

Presented by Tuan Quoc Nguyen

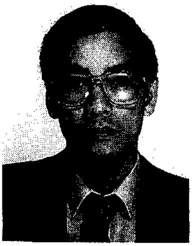

ABSTRACT

The dynamics of segmental orientation in polystyrene has been studied with the technique of polarization-modulated flow birefringence. Two types of flow fields, quasi-steady and transient elongational, have been investigated. In opposed jets flow, the large dispersion in the birefringence curves after correction for molecular weight distribution suggested a gradual increase in segmental orientation with the fluid strain-rate instead of the predicted abrupt coil-to-stretch transition. Segmental orientation was even more gradual in flow through a narrow contraction. Flow-induced degradation was unexpectedly large in this type of flow with a pronounced propensity for midchain scission. Based on the birefringence and degradation results, a coil-to-deformed coil transition in which segmental orientation is significant without an increase in the radius of gyration is proposed to represent chain conformation in strong flows.

1 INTRODUCTION

Flexible chain orientation and extension in flow is an intricate process which depends markedly on the details of the pervading flow field. Its comprehension, however, is fundamental to a molecular interpretation of experimental results in many important areas, such as rheological measurements, flow through porous media, mechanochemical degradation, plastics processing, drag reduction and flow-induced structure formation. Despite some real advances accomplished during the last few years through a combination of theoretical and computer simulation studies, the detailed nature of the process of molecular uncoiling is still largely speculative. The present study focussed on recent experimental results to understand the process of polymer orientation and deformation in strong flow.

THE COIL-STRETCHING TRANSITION IN STRONG FLOW

The coil-to-stretch transition is probably the most striking feature predicted for isolated flexible polymer chains subjected to a strong elongational flow. Very early, it was realized that the inclusion of hydrodynamic interactions can increase the abruptness of the coil-to-stretch transition [1,2] Modeling the chain as a non-free draining slender body, the conditions for flexible chain extension in uniaxial elongational flow have been determined as:

$$\dot{\varepsilon} \geq \dot{\varepsilon}_c = A/\tau_z \sim M^{-3\nu} \qquad (1)$$

$$\text{and} \quad t_r >> \tau_z \qquad (2)$$

($\dot{\varepsilon}$ = fluid strain-rate, τ_z = Zimm's relaxation time for a nondraining chain, t_r = residence time in the high strain rate region, ν = Flory exponent equal to 0.5 in a θ-solvent and 0.6 in a good solvent, A = factor of the order of unity. Elaborated calculations based on the bead-spring model [3] give A = 0.5035 which is just 7% above the value for the Hookean dumbbell). The first condition is imposed by the forces balance equation whereas the second condition is dictated by the amount of accumulated strain necessary for full chain extension. As chain stretching combines two conditions (Eqs. 1 & 2), the experimental requirements for both must be met in order to observe large molecular deformation. The strain-rate condition is easily satisfied with an appropriate pumping system. The large residence time, however, imposes severe restrictions on the flow geometry. In certain elongational flows, which possess a center of symmetry such as at the stagnation point between two opposed jets or in the four-roll mill, a quasi-steady elongational flow can be achieved in the immediate vicinity of the symmetry center. In contrast, transient elongational flows created by forcing a liquid across a narrow contraction have an inherent transient residence time which allows for only modest chain extension. Nevertheless, flow birefringence was readily discerned in this type of flow, indicating a substantial degree of segmental orientation [4]. Other unexpected results observed in transient elongational flow are the sharp midchain scission and the large degradation yields [5].

2. EXPERIMENTAL INVESTIGATION ON POLYMER CHAIN ORIENTATION

2.1. EXPERIMENTAL

- All the experiments were performed at room temperature (23°C).
- Extensional flow fields were created by pumping PS solutions across two sapphire jets in exact opposition (jets ∅ = 500μm, gap distance = 600 μm) for stagnant elongational flow or a single jet for transient elongational flow.

- Sharp PS fractions with molecular weight in the range of $1.13 \bullet 10^6$ to $21 \bullet 10^6$ were dissolved in decalin (poor solvent) or 1-methyl-naphthalene (good solvent) and filtered prior to the experiments.
- The retardation signal (δ') and the orientation angle (α) were mapped across the birefringence domain with a polarization-modulated optical rheometer 6) combined with an X-Y translation stage and an automatic data acquisition system.
- Flow-induced degradation could provide additional information on the stress distribution along the chain at the moment of fracture. Scission yields and molecular weight distribution of degraded polymer were determined by GPC.

2.2. STAGNANT ELONGATIONAL FLOW

The potential applications of elongational flow as the one capable of achieving large degree of coil extension have attracted early researchers' interests. In a series of pioneering experiments 7,8), it has been demonstrated that the birefringence signal in opposed jets flow increased sharply above some critical strain rate ($\dot{\varepsilon}_c$) which scales with polymer molecular weight (M) as:

$$\dot{\varepsilon}_c \cong B \cdot M^{-\beta} \qquad (3)$$

with $\beta = 1.5$ regardless of the solvent quality. Alternatively, Eq.3 can be expressed as:

$$M = (\dot{\varepsilon}_c / B)^{-1/\beta} \qquad (4)$$

Applying Eq.4 and using the birefringence instrument as a molecular weight sensitive analyzer, it was verified that bond scission occurred at a critical strain rate $\dot{\varepsilon}_f$. The observed midchain scission and the measured scaling law $\dot{\varepsilon}_f \propto M^{-2}$ were in perfect agreement with the fully extended chain model and gave further confidence to the coil-to-stretch transition theory. This seemingly coherent picture, however, was challenged by some recent experiments in which the degree of chain orientation and coil expansion are recorded simultaneously as a function of strain-rate 9). Although the birefringence signal reached rapidly saturation above $\dot{\varepsilon}_c$, the degree of coil expansion near the stagnation point remained extremely modest (1.3 to 2 depending on the polymer molecular weight) and was, in any case, well below the limit of full chain extension Similar conclusions have been reached by comparing the birefringence signal with the extensional viscosity 10) With hindsight, it seems that the previous measurements of $\dot{\varepsilon}_c$ from the onset of birefringence are far from being indisputable. This quantity, obviously, depends on the measurement sensitivity and even more drastically on the polymer molecular weight distribution. Another factor which may influence the reliability of birefringence measurements is polymer concentration. Under the dynamic conditions of flow, intermolecular entanglements could be detected at polymer concentrations as low as 100 ppm for a $19 \cdot 10^6$ PS in decalin and 60 ppm for the same sample in 1-methyl-naphthalene. The orientation of the transient network increased the sharpness of the birefringence transition while distorting the retardation profile. The use of a fast polarization-modulation technique in conjunction with signal averaging increased the detection limit by over one order of magnitude in comparison to static-polarization experiments (Fig.1). Retardation could now be determined at polymer concentrations below the 10ppm level. In addition to the gain in sensitivity, the polarization-modulation method provided the capability for real time determination of the absolute values of the retardation (δ') and orientation angle (α) in a single experiment. This feature is particularly valuable in transient elongational flow where α is a function of the flow position.

It can be assessed that the birefringence region is highly localized along the inflow axis with a width <10% of the orifice diameter (Fig.2). It is found, however, that the degree of segmental orientation was not constant but increased from the stagnation point towards the orifice entrances. This effect, particularly visible in good solvents like 1-methyl-naphthalene, indicated that molecular chains did not reach their maximum orientation at the stagnation point.

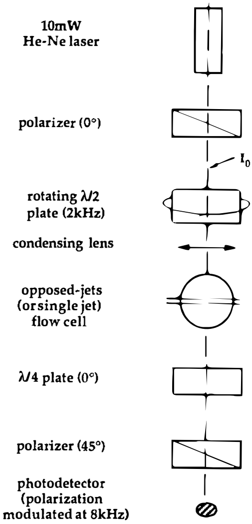

Fig.1 - Diagram of the flow birefringence experiment showing the arrangement of major optical elements.

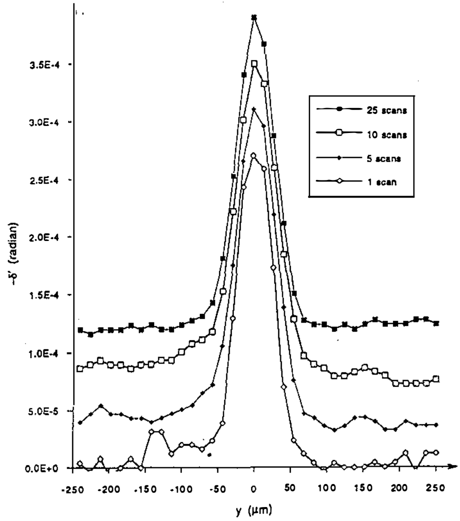

Fig.2 - Retardation profile for a 10 ppm $19\bullet10^6$ PS solution in decalin recorded across the stagnation point.

To circumvent the sample polydispersity problem, $\dot{\varepsilon}_c$ was determined by fitting the birefringence curve transformed according to Eq.4, to the experimental MWD obtained by gel permeation chromatography. In contrast with previous investigations, it was found that $\dot{\varepsilon}_c$ depended on the solvent quality and scaled with polymer molecular weight (M) as ~ $M^{-1.5}$ in a poor solvent (decalin) and as ~ $M^{-1.8}$ in good solvents (toluene and 1-methyl-naphthalene). In addition, the large spreading in the birefringence curves even after appropriate correction for molecular weight distribution, suggested a gradual increase in segmental orientation with fluid strain-rate instead of an abrupt coil-to-stretch transition (Fig. 3).

2.3. TRANSIENT ELONGATIONAL FLOW

Flow across a narrow contraction is characterized by a transient residence time which is usually too short to allow for significant chain extension. Using light scattering technique, it has been assessed that the degree of coil expansion which can be achieved in this type of flow is limited to < 4 even at very high strain rates 11). It has long been conjectured that birefringence would be too low to be detected in fast transient flow.

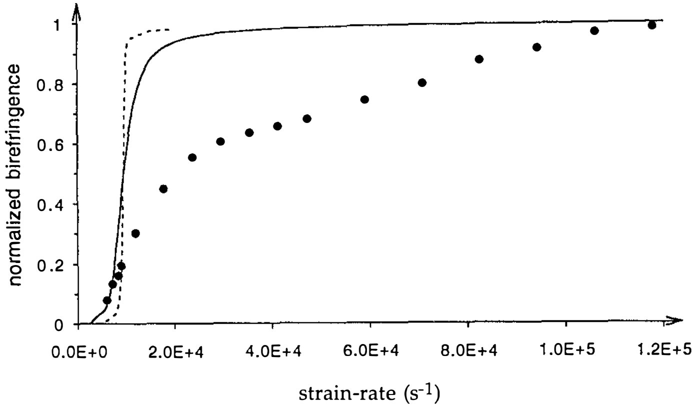

Fig.3 - Birefringence as a function of fluid strain-rate ($\dot{\varepsilon}$) at the stagnation point (●) experimental results; (---) calculated for an hypothetical monodisperse PS sample with M = 3.95•10^6 and (—) for a PS fraction with $\overline{M}_w$ = 3.95•10^6 and $\overline{M}_w/\overline{M}_n$ = 1.10 assuming an abrupt coil-to-stretch transition.

Measurements in our laboratory indicated nevertheless a "cone-like" birefringence region with a maximum intensity at the orifice entrance and extending over less than 1 orifice diameter into the solution (Figs.4a & 4b). This birefringence distribution is in conformity with flow field modelization using the POLYFLOW program. GPC measurements revealed an efficient chain halving process above a critical strain-rate $\dot{\varepsilon}_f$ which depended on M^{-1}. The observed precise midchain scission (Fig.5) is entirely unexpected and raised the intriguing problem on how a partly deformed coil can recognize its center during a fast stretching deformation $^{8)}$.

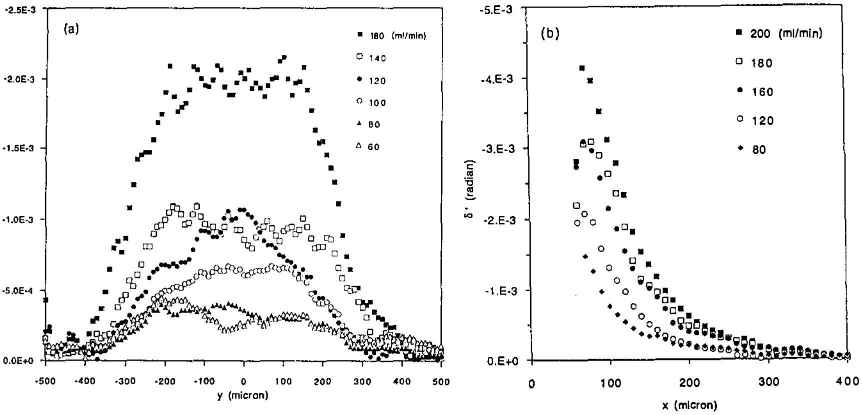

Fig.4 - Retardation profiles in transient elongational flow for a 100 ppm 10.2•10^6 PS solution in decalin, recorded at different flow rates: (a) across the jet entrance at x =100μm; (b) along the flow direction (the orifice entrance is at x = 0).

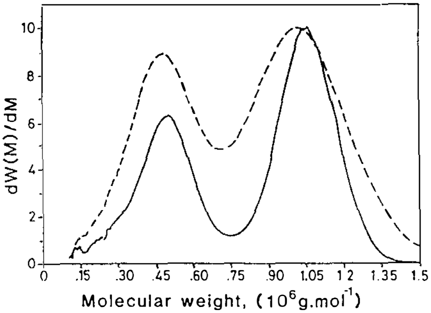

Fig.5 - Molecular weight distribution of a $1.03 \bullet 10^6$ PS degraded in transient elongational flow at $\dot{\varepsilon} = 1.7 \bullet 10^5 \text{ s}^{-1}$ (----) uncorrected and (—) corrected for instrumental broadening.

3. MODELS OF CHAIN DEFORMATION IN "STRONG" FLOW

Experimental data invariably indicate that the degree of shear deformation of an isolated flexible molecular coil is much below the theoretically predicted values. In many respects, a rapidly deforming chain behaves like a rigid body rather than a floppy coil. The origins of kinetic rigidity are complex and can be traced back to the diverse sources of steric and topological hindrances (loosely known as "internal viscosity") present under the dynamic conditions of flow. Based on experimental evidences and recent simulation results 12), it is proposed that a sheared polymer coil passed through a succession of metastable conformations. The presence of self-entanglements delayed further stretching to the very long time limit. During the initial stage of deformation, the molecular coil responded to the flow field by a reorientation of the polymer segments without an increase in the radius of gyration. Instead of the coil-to-stretch transition, the change in coil conformation at $\dot{\varepsilon}_c$ should be more appropriately termed as a coil-to-oriented coil transition. Even for a modestly deformed coil, calculations showed that the maximum stress is concentrated near the middle of the chain 13). This may explain the precise midchain scission observed in both stagnant and transient elongational flow.

ACKNOWLEDGEMENTS

Financial support from the Swiss National Fund is gratefully acknowledged.

REFERENCES

1. P.-G.de Gennes, J.Chem.Phys. 60, 5030, 1974
2. E.J.Hinch, Phys. Fluids 20, S22, 1977
3. J.J.Magda, R.G.Larson, M.E.Mackay, J.Chem.Phys. 89, 2504, 1988
4. D.Hunkeler, T.Q.Nguyen, H.H.Kausch, Polym.Prep. 32 (2), 667, 1991
5. T.Q.Nguyen, H.H.Kausch, Adv.Polym.Sci. 100, 73, 1992
6. G.G.Fuller, Ann.Rev.Fluid Mech. 22, 387, 1990
7. D.P.Pope, A.Keller, Coll.& Polym.Sci. 256, 751, 1978
8. A.Keller, J.Odell, Colloid Polym.Sci. 263, 181, 1985
9. M.J.Menesveta, D.A.Hoagland, Macromolecules 24, 3427, 1991
10. C.A.Cathey, G.G.Fuller, J.Non-Newt.Fluid Mech. 34, 63, 1990
11. R.C.Armstrong, S.K.Gupta, O.Basaran, Poly.Engin.Sci. 20, 466, 1981
12. J.M.Wiest, L.E.Wedgewood, R.B.Bird, J.Chem.Phys. 90, 587, 1989
13. R.G.Larson, J.J.Magda, Macromolecules 22, 3004, 1989

VISCOELASTICITY OF COMPRESSED POLYMER LAYER

P. Sens

Institut Charles Sadron,
6 rue Boussingault, 67083 Strasbourg Cedex, France

ABSTRACT:

We discuss theoretically dynamic measurements with a surface force apparatus composed of a plane and a sphere coated with adsorbed polymer layers in a good solvent. The hydrodynamics are studied within a simple two fluids model where the friction between polymer and solvent is described by the so-called Brinkman approximation. In a steady compression experiment the distance between the sphere and the plane varies at a constant velocity and the polymer layers have a hydrodynamic thickness e_H of the order of their radius of gyration. In a periodic compression experiment, the distance has a periodic modulation of small amplitude at a finite frequency; the results are recast in terms of a complex modulus G. At a low frequency, the modulus has the standard Maxwell behavior ($G' \simeq \omega^2$, $G'' \simeq \omega$). The contribution of the polymer to the loss modulus G'' is small when the polymer layers do not overlap, it is of the same order of magnitude as the pure solvent contribution when they do overlap. The elastic modulus increases with the thickness of the adsorbed layers. At a high frequency, the complex modulus increases as $G \simeq \omega^{2/3}$ and is independent of the thickness of the polymer layers. When the adsorbed polymer layers overlap, there is an intermediate regime where the elastic part of the modulus increases as $G' \simeq \omega^{4/3}$.

I. Introduction

A powerfull way of investigating interactions between surfaces is the surface force apparatus initiated by Israelachvili and Tabor [1], which can measure directly both the static and dynamic forces between two surfaces separated by a thin liquid film. If the liquid film is a polymeric solution, the static force has a repulsive component due to the osmotic pressure of the chains, and an attractive component due to the bridging between the two surfaces [2],[3]. The dynamic force vanishes in the absence of relative motion of the plates and has an hydrodynamic origin. For a Newtonian fluid, it is given by the Reynolds lubrication force. If the two plates are a plane and a sphere of radius R, the force is: $F = 6\pi R^2 \frac{\eta}{h_0}\dot{h}_0$ where h_0 is the minimum distance between the plates and η the viscosity of the fluid (see Fig.1).

The aim of this work is to derive an equivalent expression of the lubrication force for a polymer solution. We consider the case of a irreversibly adsorbed polymers from a good solvent. The bulk solution is washed after adsorption and replaced by pure solvent. We also assume that the polymer moves slowly and does not have time to desorbe during compression.

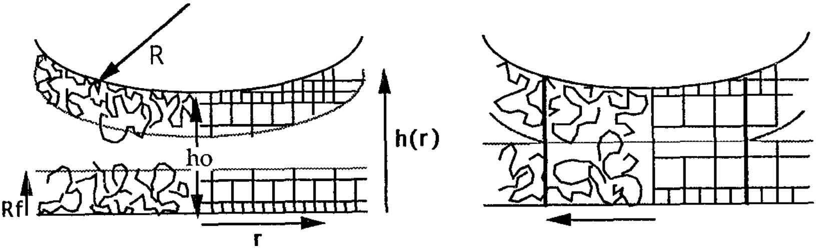

Figure 1 Schematic represenation of a surface force apparatus coated by adsorbed polymer layers. The self similar profil for the adsorbed layer is represented in the nonoverlapping and overlapping cases (1.a and 1.b)

This theoretical work can be compared to experimental studies performed by Pelletier et. al. where the same geometry is used [4]. On their work, an oscillatory motion is imposed to a sphere plan apparatus and the dynamical response of adsorbed polymer layers is measured as a function of the frequency of oscillation. In the case of oscillatory compression, the viscoelastic response of a polymeric fluid can be characterized by the shear relaxation modulus G, which links the shear stress to the shear strain imposed to the sample. For a periodic compression, it is convenient to deal with the complex Fourier transform of the modulus $G^*(\omega) = G' + iG''$, where the real and imaginary parts are the elastic and viscous response of the sample. An analogy of the Reynolds formula for viscoelastic fluids gives $F(\omega) = -6\pi R^2 \gamma G^*(\omega)$

An adsorbed polymer layer are composed by loops of polymer of many sizes separated by trains and tails. The elastic respons of the layer is mainly due to the loops, described using the scaling picture introduced by de Gennes [5] (see Fig.1). The polymer layer is seen as a self similar grid with a characteristic mesh size proportionnal to the distance to the wall $\xi(z) \propto z$ up to a distance from the wall equal to the largest loops of the layer. When the adsorbed layer is in contact with pure solvent, this size is of the order of the Flory radius R_f which increases with the molecular weight of the chains as $R_f \sim N^{3/5}$. As we will see in the following, this length turns out to be the most important size of the problem. The entanglements of the chains lead to a local Young modulus E proportionnal to the osmotic pressure in the layer $E(z) \simeq k_BT/\xi^3$. The oscillatory modes of the chains are characterized by the Zimm relaxation time, which is equal to $\tau(h) \propto \eta h^3/k_BT$ for a chain segment of size h.

The paper is organized as follows. In the next section the hydrodynamic equations for the adsorbed polymer layer are derived using a two fluids model. In section III and IV we study the steady compression and low frequency periodic compression for nonoverlapping layers and overlapping layers (Fig. 1.a and 1.b). In the high frequency limit (section V) we present a new blob model for the adsorbed layer which take into account the internal modes of the polymer loops. The last section presents some concluding remarks and comparisons with experiments.

II. Two Fluids Model

The viscoelastic properties of the confined solution are described within the framework of a two fluids model, where the solvent is caracterized by its viscosity η and the polymer network by a local elastic modulus E. The displacement of the sphere induces a pressure gradient $\partial_r P$ and a flow of the solvent in the radial direction r. The drag of the fluid through the polymer network creates then a viscous dissipation and an elastic strain on the polymer. This effect is described by the Brinkman equation [6], which approximates the polymer solution by a porous medium with a permeability $\eta/\xi(z)^2$.

The hydrodynamic equations to be solved are the stress balance for the solvent and the polymer network. Following Fredrickson and Pincus [7], we write these equations within the lubrication approximation for the case of the gap thickness between the two plates $h(r)$ is much smaller than the radius of the sphere and the r-dependence of the gap thickness is $h(r) \simeq h_0 + h^2/2R$ (see Fig. 1). The time variation of h is expresses with the strain γ: $h(r,t) = h(r) + \gamma h_0$. The viscous and elastic stresses depend on the radial velocity field of the solvent $v_r(z)$ and the radial displacement field of the network $u_r(z)$. The Brinkman dissipation involves the velocity difference of the two fluids $v_r - \dot{u}_r$. In the following equations, we have contracted all the numerical factors in an unique one: the friction parameter l which varies between 1 (no polymer in the gap) and infinity.

For the solvent, the stress balance is:

$$\eta \partial_z^2 v_r - \partial_r P = \eta \frac{l(l-1)}{z^2}(v_r - \dot{u}_r) \tag{1}$$

and for the polymer network, it gives

$$\partial_z \left(\frac{\alpha k_B T}{z^3} \partial_z u_r \right) = -\eta \frac{l(l-1)}{z^2}(v_r - \dot{u}_r) \tag{2}$$

where r and z are the radial and tranverse coordinates.

If we add to these equations the incompressibility relation for the solvent $\partial_z v_z = -1/r \partial_r (r v_r)$, we are able to derive the pressure gradient and the hydrodynamic force given by the integration of the stress tensor over the radial surface:

$$F = 2\pi R \int_{h_0}^{\infty} dh (P(r) - P_\infty - 2\eta \partial_z v_z|_{z=0}) \tag{3}$$

The complex modulus is finally obtained via the Reynolds formula .

III. Nonoverlapping polymer Layer

In the following, we will considere the case of large gap thickness ($h_0 >> R_f$). We separate the gap thickness into three regions, two adsorbed layers of thickness R_f and the free solvent in between. The velocity and displacement fields are found for each regions using the no slip condition at the wall for the solvent and irreversible adsorption for the monomers, as well as no elastic stress at the interface between the layer and the pure solvent region.

III.A Steady Compression

If the compression is slow enough, the polymer network has time to relax toward its equilibrium conformation. In this case, the hydrodynamic force is found to follows the Reynolds lubrication formula, with a correction to the gap thickness twice the so-called hydrodynamic thickness of the adsorbed layer $e_H \simeq \frac{l-1}{l} R_f$

$$F = -6\pi R^2 \eta \frac{\dot{h}}{h_0 - 2e_H} \tag{4}$$

The friction of the solvent on the adsorbed polymer is thus equivalent to an effective reduction of the distance h_0 between the sphere and the plane by the hydrodynamic thickness of the adsorbed layers. This is in agreement with the result of de Gennes for the flow along a wall coated with adsorbed polymer [8].

III.B Periodic Compression

The natural characteristic time of the problem is the Zimm relaxation time of a loop of size $h(r)$, $\tau(h) = \frac{\eta h^3(r)}{\alpha k_B T}$. In order to simplify the equations, this dynamical study is performed in the two asymptotic regimes of low and high frequency. We first described the low frequency limit, which extends up to frequencies ω_f of the order of magnitude of the inverse Zimm time of the biggest loops: $\omega_f = 1/\tau(R_f)$ (see reference [9] for details and exact calculation).

At low frequency, the two adsorbed polymer layers constitute only a small perturbation to the flow and the complex modulus is dominated by the loss modulus of the pure solvent $G''(\omega) = \omega\eta$. The storage modulus $G'(\omega)$ is a correction of higher order in ω. The first order of G'' in R_f/h_0 gives the sam result than the steady compression:

$$G''(\omega) = \omega\eta\left[1 + \frac{2(l-1)}{l}\frac{R_f}{h_0} + O\left(\frac{R_f}{h_0}\right)^2\right] \tag{5}$$

The expansion up to the second order in ω gives the elastic contribution:

$$G'(\omega) = \eta\omega^2\tau_0\left(\frac{(l-1)^2}{4(l+1)(l+3)}\right)\left\{\left(\frac{R_f}{h_0}\right)^4 + O\left(\frac{R_f}{h_0}\right)^5\right\} \propto \frac{\omega^2 R_f^4}{h_0} \tag{6}$$

where $\tau_0 = \frac{\eta\, h_0^3}{\alpha k_B T}$ is the Zimm relaxation time of a chain segment of size h_0.

The frequency dependence of the shear modulus at low frequency ($G' \simeq \omega^2$ and $G" \simeq \omega$) is the standard variation for a Maxwell model for the viscoelastic fluids, which consist of a viscous component of viscosity η coupled with an elastic component of relaxation time τ_m. An interesting point is the $R_f^4 \simeq N^{12/5}$ dependence of the storage modulus, which could be checked experimentally.

This molecular weight dependence can be obtained via the simple following argument. We consider the solution, in the gap of the surface force apparatus as a Maxwell fluid. At low frequency, the real and imaginary parts of the complex modulus are related by $\frac{G'(\omega)}{G''(\omega)} = \omega\tau_m$. To obtain the right scaling behaviour for G', we now choose the relaxation time to be the Zimm time of the largest loops, $\tau(R_f) \propto \frac{\eta R_f^3}{k_B T}$. From the polymer contribution to the loss modulus, we can derive the elastic modulus:

$$G'_p = \omega\eta\frac{R_f}{h_0} \qquad G'(\omega) = \omega^2\eta^2\frac{R_f^4}{k_B T h_0} = \frac{\omega^2\eta^2}{E_0}\frac{R_f^4}{h_0^4} \tag{7}$$

which is the same result as Eq.[6], up to a numerical factor which depends on the friction coefficient l. This simple argument emphasizes the fact that at low frequency, the viscoelastic respons of the layer is dominated by the large loops of size R_f as already found for the effective hydrodynamic thickness of the layers.

IV. Weackly Overlapping Layers

When the two layers weackly overlapped, we have to consider two differents regions in the gap (Fig.1.b). In the central region ($h(r) < h_l = 2R_f$), the layers overlapped and the polymer is everywhere. In the outer region ($h(r) > R_f$) there is still a polymer free region where the solvent can flow, and the problem is similar to the non overlapping case. In the central region, we has to redefine the boudary conditions. the results are given up to functions that depend only in the friction parameter [9].

As in the previous section, the loss and storage modulus are found as the first and second order in the expansion of Eq.[1,2] in omega

$$G'(\omega) = 2\omega^2\eta\tau_0\left\{2\frac{R_f^2}{h_0^2}\gamma(l) - \frac{R_F}{h_0}\delta(l) + \epsilon(l)\right\} \quad G''(\omega) = \omega\eta\left\{\frac{l(l+1)^2}{l+3} + \alpha(l)\frac{h_0}{R_f} + \beta(l)\frac{h_0^2}{R_f^2}\right\} \tag{8}$$

where the l-dependent terms have been calculated either analytically or numerically, and are found to be monotomous and vanishing for $l = 1$. These calculations have shown that the major dissipation occurs in the central region, where the two layers overlapped, and that the elastic respons is mainly due to the junction line between the layers, for $h(r) = 2R_f$. We display in figure 2 the variation of the two modulus with l for different thickness of the gap.

V. Periodic Compression at High Frequency

At a finite frequency ω, all the internal modes of the chains with a relaxation time τ so that $\omega\tau > 1$ are excited. For a portion of chain of size ξ, the typical

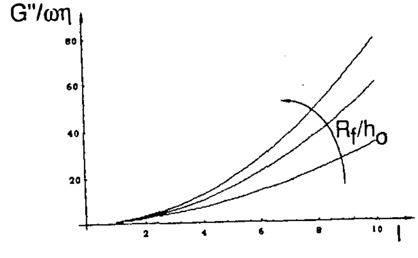

Figure 2 loss modulus for weackly overlapping layers as given by Eq.8. The ratio $G''/\omega\eta$ is represented for three values of the gap thickness: $R_f/h_0 = 1,\ 2,\ 5$

relaxation time is given by the Zimm formula $\tau(\xi) = \eta\xi^3/kT$. We define the length scale $\xi_\omega \propto \left(\frac{k_B T}{\eta\omega}\right)^{\frac{1}{3}}$ such that $\omega\tau(\xi_\omega) = 1$.

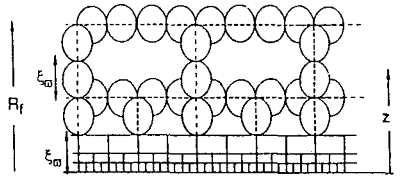

Figure 3 Schematic blob model of an adsorbed polymer layer under periodic compression at high frequency. A caracteristic length ξ_ω is associated at each frequency ω so that $\omega\tau(\xi_\omega) = 1$. The self-similar profil is valid ofr $z < \xi_\omega$. For $z > \xi_\omega$, the layer is equivalent to a solution of blob of constant size ξ_ω

For all sizes ξ of blob smaller than ξ_ω the Brinkman approximation can still be used ($\omega\tau < 1$). For sizes larger than ξ_ω ($\omega\tau > 1$), the monomers are groupped into dynamic blobs of size ξ_ω (see Fig.3). From the hydrodynamic point of view, the blobs can be considered as independent and the friction on each blob is given by Stokes law. A scaling argument allows us to obtain the frequency dependence of the elastic modulus $E(\omega) = k_B T c(z)\omega^{5/9}$ [9], which has also been derived by Doi and Edwards using a slightly different argument [10]. After calculation, it appears that the velocity profil in the ω-layer ($z > \xi_\omega$) is the same as in the free solvent region, plus an exponential decrease over a length ξ_ω. This result shows that the dissipation is weak in this layer, and that we can roughly obtain the high frequency response by replacing R_f by ξ_ω in the solutions of the low frequency limit. We find

$$G'(\omega) \simeq \eta\tau_0^{-1/3}\omega^{2/3} \qquad\qquad G''(\omega) = \omega\eta + \eta\tau_0^{-1/3}\omega^{2/3} \tag{9}$$

The same argument can be used for two overlapping layers ($R_f > h_0$). If $h_0 < \xi_\omega < R_f$ the two layers of thickness ξ_ω overlap and we find the complex modulus from equations [8] by replacing R_f by ξ_ω

$$G'(\omega) = \eta\tau_0^{1/3}\omega^{4/3} \qquad\qquad G''(\omega) = \omega\eta\frac{l(l+1)^2}{l+3} + \eta\tau_0^{1/3}\omega^{4/3} \tag{10}$$

At even larger frequency ($\omega > \omega_0$) the layers of size ξ_ω on the two surfaces no longer overlap and the complex modulus is given by Eq.[9]

VI.Discussion

We have analyzed the viscoelastic behavior of adsorbed polymer layers in an idealized surface force apparatus made of a shere and a plane.

In the steady state experiment, when the two adsorbed polymer layers do not overlap, each polymer layer has a hydrodynamic thickness e_H of the order of the size of the largest loops R_f and the effect of the polymer is equivalent to an effective reduction of the gap between the sphere and the plane by $2e_H$ in agreement with a previous result of de Gennes.

In the finite frequency experiment, the complex modulus has a Maxwell like behavior at low frequency. The real part G' is proportional to ω^2 and the imaginary part G'' varies linearly with ω. When the two adsorbed polymer layers do not overlap, the effect of the polymer on the loss modulus is small, the expression of the imaginary part ($\sim R_f^4$) shows the major role of the biggest loops of size R_f on the elastic response. When the two layers overlap the contribution of the polymer to the loss modulus due to the friction between polymer and solvent is of the same order as the pure solvent contribution. This Maxwell regime is expected until a pulsation ω_f of the order of the inverse Zimm relaxation time of the chains. At higher frequency we predict a contribution of the polymer to the complex modulus proportional to $(i\omega)^{2/3}$ in the non overlapping case. The overlapping case is now related to the value of ξ_ω and vanish at sufficiently high frequency.

Experiments have been performed in the geometry studied here by *Pelletier et al.* [4] with however small differences. At low frequency a Maxwell behavior is observed. At higher frequency, the complex modulus increases with a power of ω lower than 1 and seems to depend weakly on h_0 but the range of h_0 is rather small. The crossover between the low frequency and high frequency regimes occurs at around 10Hz; this roughly agrees with estimates that can be made of ω_0 or ω_f ($\simeq 100Hz$). We hope that further experiments will allow a more quantitative comparison with our theoretical results.

REFERENCES

1. Israelachvili, J.N. *Intermolecular and Surface Forces*, Academic, London (1992).
2. Klein, J. Proceedings of "Liquids at Interfaces", Les Houches 1988.
3. Klein, J. et al. *Macromolecules* **1993**, *26*, 5552.
4. Pelletier, E.; Monfort, J.P.; Loubet, J.L. Tonck, A.; Georges, J.M. to appear in *Macromolecules*
5. de Gennes, P.G. *Macromolecules* **1981**, *14*, 1637.
6. Brinkmann, H.C. *Appl.Sci.Res.* A1, 27, 1947
7. Fredrickson, G.H., Pincus, P. *Langmuir* **1991**, *7*, 786.
8. de Gennes, P.G. *Macromolecules* **1982**, *15*, 492.
9. Sens, P.; Marques, C.M.; Joanny, J.F. *Macromolecules* **1994**, *27*, 3820.
10. Doi, M.; Edwards, S.F. *The Theory of Polymer Dynamics*, Clarendon Press, Oxford (1986).

The Hydrodynamics of Domain Relaxation in a Polymer Monolayer

E. K. Mann,[1,2] S. Hénon,[1] J. Meunier,[1] D. Langevin,[1]
[1]Laboratoire de Physique Statistique de l'E.N.S. 24, rue Lhomond 75231 Paris Cedex
[2]Institut Charles Sadron, ULP-CNRS; 6, rue Boussingault 67083 Strasbourg Cedex

The hydrodynamics of apparently simple movement within a monolayer is complicated by the involvement both of the essentially 2-dimensional monolayer and of the liquid substrate. This question is explored experimentally for domain shape relaxation in a polymer monolayer spread on substrates with varying viscosity, using Brewster angle microscopy to visualize the domains without further additives to the system.

The polymer is PDMS (poly(dimethyl)siloxane), an insoluble polymer which segregates into dense and dilute polymer domains on aqueous glycerol and glucose solutions as well as on pure water. The surface pressure of these polymer films are, before collapse, independent of the glycerol and glucose content of the substrate solutions, permitting the starting hypothesis of a polymer monolayer uninfluenced by the modifier of the bulk viscosity (bulk viscosity $1.2<\eta/\eta_{water}<75$). If deformed, isolated polymer domains relax towards the circular form under the influence of a line tension. This relaxation is linear for the highly-deformed "bola" shape, and exponential for moderate deformations. Relaxation times T_c are measured for domains of size $10\ \mu m<R<80\ \mu m$ and $0.2\ sec<T_c<60$ sec. Relaxation of monolayer domains in the two limits, in which surface or bulk viscosity dominates, is discussed. All data is consistent with dissipation dominated by viscosity in the substrate. The line tension deduced from these experiments is $\lambda = (1.1\pm0.3)10^{-12}$ N.

Introduction

The complicated behavior observed in phase-separated molecular layers at the air-water interface includes the formation of a wide variety of shapes, from circles to stripes to labyrinths.[1] This behavior is believed to be governed by two major static parameters: the line tension, analogous to the three-dimensional surface tension, and the electric dipole moment normal to the layer. The line tension (or line energy) is a parameterization of all short-range forces within the monolayer. The long-range dipolar repulsion, nearly universal in monolayers since virtually any substance which spreads on water is either polar or charged and aligns at the interface, may in many cases be treated as a size- and shape-dependent correction to the line tension.[2]

Most methods used to measure the 3-dimensional surface tension are difficult to imagine extending to the line tension case.[3] One possibility, exploited here, is to measure the relaxation of deformed domains, driven by the Laplace force to minimize their line energy. In order to derive the line energy from these experiments, the hydrodynamic aspects, and in particular the role of both surface and substrate viscosity, must be understood. This is addressed here through the variation of the bulk viscosity over a large range of values.

Materials and Methods

In order to perform the experiment without interference between the relaxation of different domains, it is necessary to produce domains which are isolated one from the other, with a controlled size smaller that the field-of-view of the microscope. This is not attained by the usual deposition methods, which tend to produce one large (i.e. ~cm) polymer domain centered in the dish. A local deposition method was thus developed.[3] A Langmuir-Blodgett method is used to deposit minute quantities of the polymer on a carefully-cleaned stainless needle. If the needle is then drawn through liquid surface under observation, rather than touching it at a point, the dense polymer domains deposited on the surface are elongated, relaxing more or less quickly. It is this relaxation which is studied here. Experimental details can be found in reference (3).

The relaxation times from two different PDMS samples, with molecular weight M_w=10,000 (M_w/M_n=1.13) and M_w=100,000 (M_w/M_n=1.23), were indistinguishable. The glycerol and glucose solutions, analytical grade from Prolabo or Merck, were left in contact with activated charcoal (Prolabo, analytical grade) for several hours and then filtered, to remove surfactant impurities. The viscosity of the solutions was measured with a capillary viscometer. Surface tension measurements were performed by the Wilhelmy method using an open-frame probe.[3] The Brewster Angle Microscope has been discussed elsewhere.[4] It allows studies of the relaxation phenomena without additional additives, which could effect the line tension, but requires a minimum liquid depth of 3 mm; controlling convection for the less viscous substrates presents difficulties.

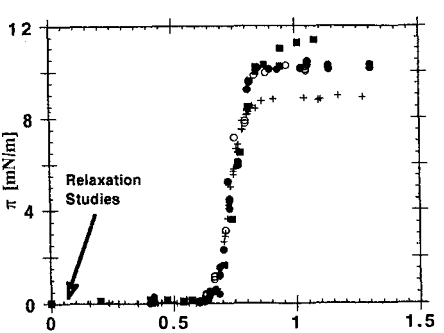

Figure 1. *Surface pressure isotherms, PDMS on pure water (+) and on glucose (20%, solid circles) and glycerol (open symbols; 20%: circles; 80%: squares) solutions.*

Results and discussions

The glycerol and glucose added to the substrate to increase its viscosity could in principle also change the character of the polymer layer. A first test of this possibility is the comparison of the surface tension isotherms for the polymer on various solutions. Such isotherms are presented in figure 1 for the polymer on pure water, on a 20% glucose solution and on 20% and 80% glycerol solutions. Within experimental accuracy, there are no significant differences between the isotherms for surface pressures below about 5 mN/m: In all case the surface pressure (the change in the surface tension in the presence of the polymer) remains unmeasurably low until surface concentrations $C > 0.6$ mg/m^2, when the surface pressure suddenly increases. On all substrates, the same curve is followed with increasing pressure, with deviations occurring as the polymer film begins to collapse out of the monolayer state and the surface pressure begins to levels out to a plateau value. This may indicate the presence of glucose and glycerol in the collapsed film, but these additives have no obvious influence on the monolayer films of interest here (all relaxation measurement are made at $C < 0.1$ mg/m^2.) The relaxation of the polymer domains may however be a more stringent test.

One example of such relaxation is shown in figure 2, along with the definition of

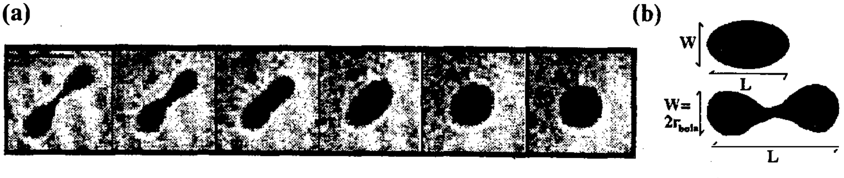

Figure 2. *(a) Relaxation of a dense polymer domain on glucose solution (η_b/η_w=1.4). Bar represents 50 μm. Images are given at 0.4 sec/frame. (b) Definitions for parameters describing domain shape:* Θ=L/W-1; R=(Area/π)$^{1/2}$.

*Table 1. Characteristic speed of relaxation in the various limits: domination by bulk viscosity η_b or surface viscosity η_s; small deformations characterized by an exponential relaxation time T_c, bola relaxation characterized by a constant speed V of the bola ends. The expressions for relaxation dominated by the bulk viscosity assume that both phases of the monolayer are incompressible.*6),7)

	$\eta_s << \eta_b/R$	$\eta_s >> \eta_b/R$
$\theta << 1$; $1/T_c$	$16\lambda / 5\pi\eta_b R^2$	$\lambda / \eta_s R$
$\theta >> 1$; V	$\lambda / 4\eta_b r_{bola}$	---

a simple, easily measured parameter which characterizes the deformation of a domain from a circle. Two regimes are clearly distinguished. Small deformations would be expected to follow an exponential relaxation law, as in fact observed.3),5) The opposite extreme, that of bola, or two heads and a thin connecting strip, has been recently treated by Benvegnu and McConnell6) for the case in which the viscosity is dominated by the substrate. As long as the heads are significantly wider than the connecting strip, the relaxation is observed to occur by simple shortening of the connecting strip, with little change in the size and shape of the heads. In this quasi-steady state, the restoring force of the nearly constant Laplace pressure difference across the domain must be balanced by nearly-constant viscous dissipation, for a nearly constant velocity. The expected behavior of the relaxation in the various limits are given in Table 1.

This is to be compared with the observed behavior. The characteristic relaxation time T_c for small deformations is proportional to the bulk viscosity η_b and to R^2, as predicted for the case when the bulk viscosity dominates (see fig. 3a). The end

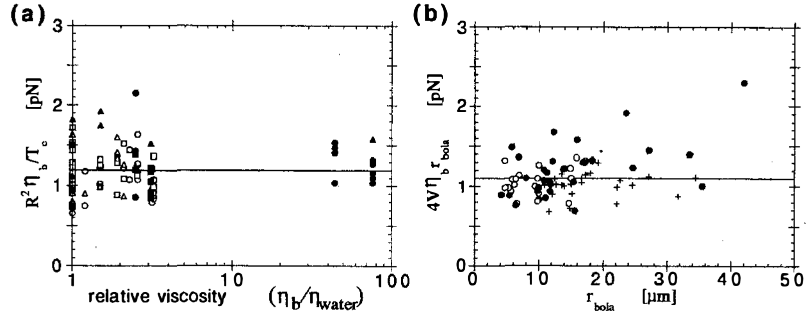

Fig. 3(a) Normalized (by size and viscosity) relaxation rates for moderately deformed polymer domains on glycerol or glucose solutions, vs. bulk viscosity. Open symbols: glucose; closed symbols: glycerol. Divided into size ranges: circles, r< 20 µm; squares: 20<r<30 µm; diamonds: r>30 µm. (b) Relaxation of bola (large deformation limit) on various aqueous substrates: normalized end speed V vs. end radius r_{bola}. Substrates: (●) glycerol, (○)glucose, (+) pure water.

velocity characteristic of bola relaxation is inversely proportional to η_b and R, again as expected when the bulk viscosity dominates (see fig. 3b). Furthermore, the line tensions deduced in the two cases are very close: $\lambda = (1.1\pm0.3)10^{-12}$ N.

This line tension is quite low: it corresponds to a characteristic interaction length within the monolayer of $\delta \approx KT/\lambda = 4$ nm, in comparison with the 0.4 nm characteristic distance between monomers in the dense polymer layer. The origin of this low line tension remains unclear. The contrast in surface concentration between phases and the relatively high monolayer elasticity do not suggest the approach of a critical point.[3] On the other hand, something like a critical point does occur in function of molecular mass: No difference in the line tension is seen between higher molecular weights, here M_w= 10,000 and 100,000. However, no domain separation at all is observed for masses 10 times lower, M_w=1250. Mixtures of low and high molecular weight samples show intermediate behavior: Starting from a homogeneous mixture, the characteristic domain size decreases with increasing proportions of the lower mass.[8] Beginning with a homogeneous layer of the smaller mass, localized additions of the higher mass show fingering and similar shape instabilities, reminiscent of those produced as the line tension decreases to the level of electrostatic effects.[1] This also resembles a spontaneous emulsification, producing smaller and smaller characteristic length scales until these are no longer visible in the microscope. The smaller masses may act as a surfactant to the larger-mass domains. By extension, the terminal ends of the longer chains may also act as a self-surfactant.

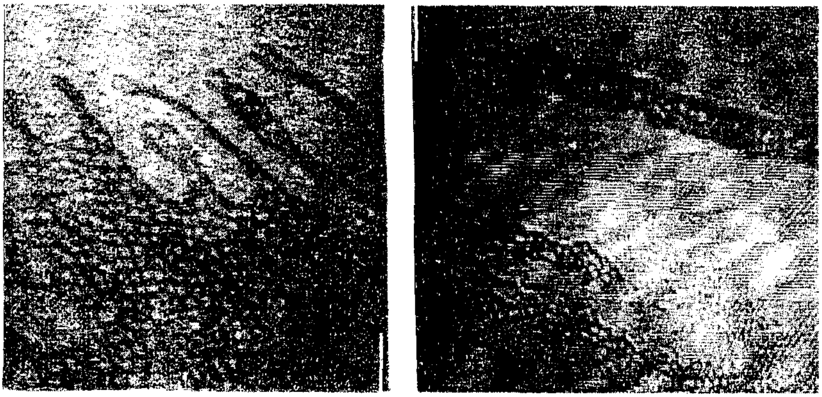

Fig. 4. Spontaneous destabilization of the frontiers of dense (dark) domains of PDMS with M_w=100,000, applied locally to a surface with a uniform surface concentration 0.3 mg/m^2 of PDMS with M_w=1250. Bars: 50 μm.

In all of this analysis we have assumed that the line tension is a well defined quantity, independent of domain shape and size, and in particular that the electrostatic dipole contribution is negligible. In the size range studied (R=10-100 μm), the measured line tension is in fact independent of domain size, and consistent between the two relaxation regimes, with very different domain shapes. The expected electrostatic effects may be estimated, without ambiguity as to the dielectric constant of the interfacial region,[3),9),10)] from measurements of the surface potential difference between phases: λ_e, the contribution to the line energy due to these effects is given by[2)]

$$\lambda_e \approx \frac{(\Delta V)^2 \varepsilon_o}{4\pi} \ln(r/h) = 1 \cdot 10^{-13}\, N$$

for domains with characteristic dimension r in the range 10-100 μm, where the measured potential difference is 0.12 V,[11)] and the molecular parameter h is taken as 0.4 nm, the average distance between monomers in the dense phase. Note that this correction is an order of magnitude less than the measured line tension. It is thus expected to be negligible, as in fact observed.

Conclusions

We demonstrated here that hydrodynamic domain relaxation within one particular polymer monolayer, PDMS on water and sugar solutions, is dominated by the bulk rather than the surface viscosity. A line tension, $\lambda = (1.1 \pm 0.3)10^{-12}$ N, is derived, independent of domain size and consistent between two very different relaxation regimes.

[1)] Seul, M.; Andelman, D. **267** (1995) 476.

[2)] Goldstein, R. E.; Jackson, D. P. *J. Phys. Chem.* **98** (1994) 9626.

[3)] Mann, E.K.; Hénon, S.; Langevin, D.; Meunier, J. *Phys. Rev. E.* to be published.

[4)] Hénon, S.; Meunier, J. *Rev. Sci. Instrum.* **62** (1991) 936.

[5)] Mann, E.K.; Hénon, S.; Langevin, D.; Meunier, J. *J. Phys. II (France)* **2** (1992)1683.

[6)] Benvegnu, D. J.; McConnell, H. M. *J. Phys. Chem.* **96** (1992) 6820.

[7)] Stone, H. A.; McConnell, H. M. *to be published.*

[8)] Mann, E. K. *unpublished.*

[9)] Mann, E. K. *Doctoral Thesis* (Université de Paris VI, 1992).

[10)] Rivière, S.; Hénon, S.; Meunier, J.; Albrecht, G.; Boissonnade, M. M.; Baszkin, A., *submitted.*

[11)] Bernett, M. D.; Zisman, W A., *Macromolecules* **4** (1971) 47.

TRANSPORT COEFFICIENTS OF MICROEMULSIONS AND SPONGE PHASES

G. Gompper[a,b] and M. Hennes[a]
[a] Sektion Physik der Ludwig-Maximilians-Universität München
Theresienstr. 37, 80333 München, Germany
[b] Max-Planck-Institut für Kolloid- und Grenzflächenforschung
Kantstr. 55, 14513 Teltow, Germany

Abstract

Microemulsions and sponge phases are fluids, which are structured on a mesoscopic length scale. The complex internal structure of these phases gives rise to an interesting dynamical behavior. We review recent work on the equilibrium dynamics based on a time-dependent Ginzburg-Landau model consistent with linear hydrodynamics. In particular, the sound dispersion and attenuation, and the complex viscosity are calculated. We discuss the dependence of the typical structural relaxation time on the characteristic length scales of these systems.

Fluids, which are structured on a mesoscopic length scale of the order of 100 – 1000 Å, while the typical sizes of all the molecules involved are only of the order of 10 Å, have been studied intensively over the last few years [1, 2]. Such fluids are microemulsions in ternary amphiphilic systems and sponge phases in aqueous amphiphilic solutions. It is by now well established that the mesoscopic structure of microemulsions, for example, consists of two multiply-connected, intertwined networks of oil and water channels, which are separated by a monolayer of amphiphiles. The average diameter of these channels is given by the mesoscopic length mentioned before. The structure of sponge phases is very similar. Since both networks span the whole volume, these fluids have been denoted "bicontinuous" [3]. Finally, diblock-copolymer melts also form bicontinuous phases, although their molecular architecture is different.

The complicated internal structure of microemulsions, sponge phases and block-copolymer melts gives rise to a interesting dynamical behavior. It has been shown, for example, that shear flow induces a transition to a lamellar phase [4]. We want to review in this paper some recent work on the dynamical behavior of these structured fluids in *thermal equilibrium*, such as the sound dispersion and attenuation [5, 6], and the (complex) viscosity [7, 8, 6]. The dynamic scattering intensity has also been studied in detail [9, 10, 11], but will not be considered here.

The model we consider is an extension of the Siggia, Halperin, and Hohenberg model H [12, 13] consistent with linear hydrodynamics. Our five hydrodynamic variables are the order parameter $\Phi(\mathbf{r}, t)$, which is proportional to the local concentration difference between oil and water, the momentum density $\mathbf{j}(\mathbf{r}, t)$, and a pressure variable $p(\mathbf{r}, t)$. In terms of these variables, the Ginzburg-Landau equilibrium free energy functional reads [5]

$$\mathcal{F} = \int d^3r \left[a(\nabla^2\Phi)^2 + g(\Phi)(\nabla\Phi)^2 + f(\Phi) + \frac{1}{2}\chi_p^{-1}p^2 + \gamma_0 p\Phi^2 + \frac{1}{2}\mathbf{j}^2 \right] . \qquad (1)$$

Here, we assume that the transport of the amphiphile is much faster than all the other transport processes. In this case, the deviation of the amphiphile concentration from its mean value does not have to be included explicitly in our model.

The static behavior of microemulsions can be described very well with the functions [14, 15]

$$g(\Phi) = b_0 + b_2\Phi^2 \qquad (2)$$

$$f(\Phi) = r_2\Phi^2 + r_4\Phi^4 + r_6\Phi^6 , \qquad (3)$$

and $a > 0$. The functions $g(\Phi)$ and $f(\Phi)$ are chosen such that a three-phase coexistence between oil-rich, water-rich and microemulsion phases can be described. The same model can be used to describe sponge phases [16, 2] and diblock-copolymer melts (in the weak segregation regime) [17]. In the microemulsion phase, the static scattering intensity in the Ornstein-Zernike approximation is given by [18]

$$G_{\Phi\Phi}(\mathbf{k}) = \frac{1}{2a\xi^4} \frac{(q\xi)}{(k\xi)^4 + 2(1-(q\xi)^2)(k\xi)^2 + (1+(q\xi)^2)^2}, \tag{4}$$

where $\xi = [\sqrt{r_2/4a} + b_0/4a]^{-1/2}$ is the correlation length, and $q = [\sqrt{r_2/4a} - b_0/4a]^{+1/2}$ is the wavenumber corresponding to the average domain size of coherent oil- and water-regions. For strongly structured microemulsions, the scattering intensity (4) is characterized by a pronounced peak at $k \simeq q$.

The stochastic equations of motion of our Ginzburg-Landau model (1) are [13, 19, 20]

$$\begin{aligned}
\frac{\partial\Phi}{\partial t} &= \Gamma_\Phi \nabla^2 \frac{\partial\mathcal{F}}{\partial\Phi} + g_0 \nabla \left(\Phi \frac{\partial\mathcal{F}}{\partial\mathbf{j}}\right) + \zeta_\Phi && (5)\\
\frac{\partial p}{\partial t} &= \Gamma_p \nabla^2 \frac{\partial\mathcal{F}}{\partial p} + \lambda_0 \nabla \frac{\partial\mathcal{F}}{\partial\mathbf{j}} + \zeta_p && (6)\\
\frac{\partial\mathbf{j}_T}{\partial t} &= \Gamma_T \nabla^2 \left(\frac{\partial\mathcal{F}}{\partial\mathbf{j}}\right)_T + g_0 \left(\Phi \nabla \frac{\partial\mathcal{F}}{\partial\Phi}\right)_T + \boldsymbol{\zeta}_T && (7)\\
\frac{\partial\mathbf{j}_L}{\partial t} &= \Gamma_L \nabla^2 \left(\frac{\partial\mathcal{F}}{\partial\mathbf{j}}\right)_L + \lambda_0 \nabla \frac{\partial\mathcal{F}}{\partial p} + g_0 \left(\Phi \nabla \frac{\partial\mathcal{F}}{\partial\Phi}\right)_L + \boldsymbol{\zeta}_L\,, && (8)
\end{aligned}$$

where the Langevin forces ζ_i have the usual correlations [12],

$$\begin{aligned}
< \zeta_\Phi(\mathbf{r},t)\zeta_\Phi(\mathbf{r}',t') > &= -2\Gamma_\Phi \nabla^2 \delta(\mathbf{r}-\mathbf{r}')\delta(t-t') && (9)\\
< \zeta_{T,\alpha}(\mathbf{r},t)\zeta_{T,\beta}(\mathbf{r}',t') > &= -2\Gamma_T \nabla^2 \delta(\mathbf{r}-\mathbf{r}')\delta(t-t')\delta_{\alpha\beta} && (10)
\end{aligned}$$

etc. The indices $'T'$ and $'L'$ indicate the transverse and longitudinal components of the momentum density $\mathbf{j}$.

When the non-linear terms in the time-dependent Ginzburg-Landau equations (5)-(8) are neglected, the model can be solved easily. In this case, one finds that the sound velocity and damping as well as the viscosity are frequency independent. This property makes these quantities very interesting for the investigation of the dynamical behavior of structured fluids, since the effect of the non-linear terms — which are responsible for the coupling of the momentum density to the structure, for example — can be studied easily by subtracting a frequency-independent background from the measured signal.

In order to calculate the frequency-dependent sound velocity $c(\omega)$ and the damping $D(\omega)$, we use the pole structure of the pp- or the $\mathbf{j}_L\mathbf{j}_L$-correlation function in the hydrodynamic limit (*i.e.* the limit of wavevector k $\to$ 0), where it has the general form

$$G_{pp}(\mathbf{k},\omega) = \frac{N_p(\mathbf{k},\omega)}{|\omega^2 - c(\omega)^2 k^2 + i\omega D(\omega) k^2|^2}\,. \tag{11}$$

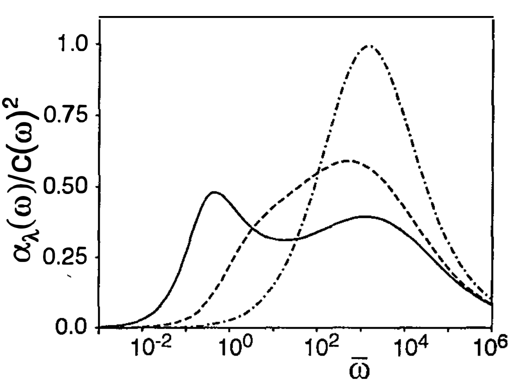

Figure 1: *Sound attenuation* $\alpha_\lambda(\omega)/c(\omega)^2$ *as a function of the scaled frequency* $\overline{\omega} \equiv \omega/\Gamma_\Phi$. *The parameters are* $g_0 = 1$, $\lambda_0 = 1$, $\gamma_0 = 1$, $\chi_p^{-1} = 1$, $a = 1$, $r_2 = 1$, *and* $\Gamma_\phi = \Gamma_p = \Gamma_L = \Gamma_T = 1$. *The dashed-dotted line is calculated for a microemulsion with* $b_0 = 1.95$ *(*$q\xi = 0.113$*), the dashed line for* $b_0 = -1.80$ *(*$q\xi = 3.512$*), and the full line for* $b_0 = -1.95$ *(*$q\xi = 8.888$*).*

Here, $N_p(\mathbf{k},\omega)$ is a polynomial in k^2. The sound attenuation per wavelength $\alpha_\lambda(\omega) = \pi\omega(D(\omega) - D(\infty))/c(\omega)^2$, which is usually measured experimentally, is then easily obtained. The result of a one-loop calculation of the sound attenuation is shown in Fig. 1 for three different values of q and ξ. The internal structure of microemulsions or sponge phases gives rise to the peak at low frequencies. The position of this peak moves to smaller values of ω with increasing domain size q^{-1} and with increasing correlation length ξ.

Similarly, the viscosity $\eta(\omega)$ can be calculated in the hydrodynamic limit from the pole structure of the $\mathbf{j}_T\mathbf{j}_T$-correlation function,

$$G_{j_Tj_T}(\mathbf{k},\omega) = \frac{N_T(\mathbf{k},\omega)}{|i\omega - \eta(\omega)k^2|^2}\,, \tag{12}$$

where $N_T(\mathbf{k},\omega)$ is a polynomial in k^2. The frequency dependence of the real (η') and the imaginary (η'') part of the viscosity, calculated again in the one-loop approximation, is shown in Fig. 2. Our results show the typical behavior of complex fluids. At a characteristic frequency ω^*, the vicosity η' rapidly crosses over from the large zero-shear value to the low value of the solvent viscosity. At the same frequency, a maximum of η'' indicates a strong elastic behavior. The behavior of the viscosity at *small* frequencies is given by [6]

$$\eta'(\omega) - \eta'(0) \sim \omega^2 \tag{13}$$

$$\eta''(\omega) \sim \omega\,. \tag{14}$$

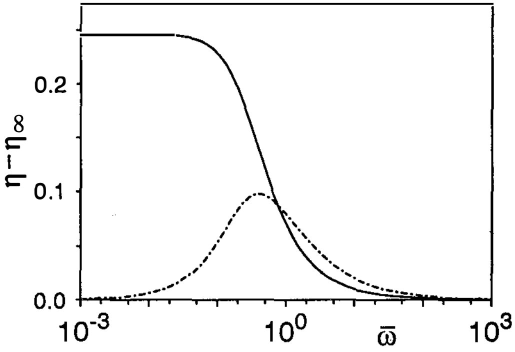

Figure 2: *Complex viscosity* $\eta(\omega)$ *as a function of the scaled frequency* $\bar{\omega} \equiv \omega/\Gamma_\Phi$. *The parameters are the same as in Fig. 1, and* $b_0 = -1.95$ ($q\xi = 8.888$). *The full line is the real part,* η', *the dashed-dotted line the imaginary part,* η'', *of the viscosity.*

Our results for $\eta(\omega)$ in the limit $\omega \longrightarrow 0$ are in agreement with those obtained in Refs. [7] and [8] based on a somewhat different approach (by studying the response of the system to an external shear stress).

More information about the dynamical behavior of a structured fluid is obtained from the structural dependence of the position, ω^*, of the peak of η''. This characteristic frequency is found to have the scaling form [6]

$$\omega^* = \xi^{-6}\Omega(q\xi) \ . \tag{15}$$

The scaling function $\Omega(x)$ approaches a constant quadratically for $x \longrightarrow 0$, and diverges as x^4 for $x \longrightarrow \infty$. Infact, the *same* characteristic frequency also determines the structural dependence of the peak position in the sound attenuation [6].

References

[1] J. Meunier, D. Langevin, and N. Boccara (eds.), *Physics of Amphiphilic Layers*, Springer Proceedings in Physics **21** (Springer, Berlin, 1987); R. Lipowsky, D. Richter, and K. Kremer (eds.), *The Structure and Conformation of Amphiphilic Membranes* (Springer, Berlin, 1992); W.M. Gelbart, D. Roux, and A. Ben-Shaul (eds.), *Micelles, Membranes, Microemulsions, and Monolayers* (Springer, Berlin, 1994).

[2] G. Gompper and M. Schick, in *Phase Transitions and Critical Phenomena*, edited by C. Domb and J. Lebowitz (Academic Press, New York, 1994).

[3] L.E. Scriven, Nature **263**, 123 (1976).

[4] M.E. Cates and S.T. Milner, Phys. Rev. Lett. **62**, 1856 (1989).

[5] G. Gompper and M. Hennes, Europhys. Lett. **25**, 193 (1994).

[6] M. Hennes and G. Gompper, in preparation.

[7] G.H. Fredrickson, R.G. Larson, J. Chem. Phys. **86**, 1553 (1987).

[8] C.J. Mundy, Y. Levin, and K.A. Dawson, J. Chem. Phys. **97**, 7695 (1992).

[9] R. Granek, M.E. Cates, and S. Ramaswamy, Europhys. Lett. **19**, 499 (1992).

[10] R. Granek and M.E. Cates, Phys. Rev. A**46**, 3319 (1992).

[11] G. Gompper and M. Hennes, Phys. Rev. Lett. **73**, 1114 (1994); J. Phys. II France **4**, 1375 (1994).

[12] E.D. Siggia, B.I. Halperin, and P.C. Hohenberg, Phys. Rev. B**13**, 2110 (1976).

[13] P.C. Hohenberg and B.I. Halperin, Rev. Mod. Phys. **49**, 435 (1977).

[14] G. Gompper and M. Schick, Phys. Rev. Lett. **65**, 1116 (1990).

[15] G. Gompper and J. Goos, Phys. Rev. E**50**, 1325 (1994).

[16] D. Roux, C. Coulon, and M.E. Cates, J. Phys. Chem. **96**, 4174 (1992).

[17] T. Ohta and K. Kawasaki, Macromolecules **19**, 2621 (1986).

[18] M. Teubner and R. Strey, J. Chem. Phys. **87**, 3195 (1987).

[19] M. Nolan, Phys. Rev. B**18**, 6334 (1978).

[20] D.M. Kroll and J.M. Ruhland, Phys. Lett. **80A**, 45 (1980).

List of participants

Dr. Alba Michel
DRFMC /SP2M /PI
Bat G1 , CENG,
17 Rue des Martyrs,
38054 Grenoble Cedex
alba@drfmc.ceng.cea.fr

Dr. Amiel Catherine
Ph-Ch. des Biopolymères,
CNRS - UM27
2-8 Rue H. Dunant
94320 Thiais
amiel@glvt-cnrs.fr

Dr. Andrieu Claire
Institut Curie
Physique - chimie, Labo. PSI
11 rue P. et M. Curie
75231 Paris Cedex 05

Dr. Assenheimer Michel
ENS
Lab.de Physique Statistique
24 rue Lhomond
75231 Paris Cedex 05
fnassen@physique.ens.fr

Dr. Auroy Philippe
Institut Curie
URA448
11 rue P. et M. Curie
75005 Paris
auroy@radium.jussieu.fr

Dr. Ausserré Dominique
Université du Maine
Lab. PSPI URA, CNRS 807
BP.535
72017 Le Mans Cedex

Dr. Baltes Hubert
Johannes Gutenberg Universität
Inst. für Physikalische Chemie
Jakob-Weider-Weg 11
D-55099 Mainz
baltes@mzdmza.zdv.uni-mainz.de

Dr. Bassereau Patricia
Institut Curie
Lab. PSI
11 rue P. et M. Curie
75231 Paris Cedex 05
patbass@radium.jussieu.fr

Dr. Bellocq Anne Marie
CRPP
Avenue Dr A. Schweitzer
33600 Pessac

Dr. Berge Bruno
Université Joseph Fourier
Labo. de Spectrométrie Physique
CNRS, BP 87
38402 Saint Martin d'Hères
berge@grenet.fr

Dr. Bergeron Vance
ENS
Lab. de Physique Statistique
24 rue Lhomond
75231 Paris Cedex 05

Prof. Bewersdorff Hans-Werner
FH Lausitz
Chemie ingeniur wesen/Verfahrens technik
Grossenhainer Str. 57
D-01968 Senftenberg

Dr. Bonetti Marco
C.E. Saclay
SPEC
91191 Gif sur Yvette Cedex
bonetti@amoco.saclay.cea.fr

Dr. Bonn Daniel
ENS
Lab. de Physique Statistique
24 rue Lhomond
75231 Paris Cedex 05

Dr. Borisov Oleg
Johannes Gutenberg Universität
Institut für Physik
D-55099 Mainz
borisov@leonardo.physik.uni-mainz.de

Dr. Borukhov Itamar
Tel-Aviv University
School of Physics and Astronomy
69978 Tel-Aviv
itamar@shiva.tau.ac.il

Dr. Braslau Alan
C.E. Saclay
SPEC
91191 Gif sur Yvette Cedex
braslau@amoco.saclay.cea.fr

Dr. Bringezu Frank
Martin Luther Universität
Institut für pharm. Chem.
Weinberweg 15
06120 Halle
qiqb5@mlucom.urz.uni-halle.de

Dr. Cabrerizo Vilchez M. A.
Univ. de Granada,
Fisica Aplicada,(Fluidos)
C/Fuentenueva S/N
18071 Granada
mcabrerizo@ugr.es

Prof. Cohen-Stuart Martinus
Wageningen University
Physical and Colloid Chemistry
Dreienplein 6, PO Box 8038
6700 EK Wageningen
martien@fenk.WAU.nl

Prof. De Coninck Joël
Université de Mons-Hainaut
20 Place du Parc
7000 Mons
joel@gibbs.umh.ac.be

Dr. D'Oliveira Jorge
IST
Fisica Molecular, Complexo I,
Av. Rovisco Pais
1096 Lisboa Cedex
I004@BETA.IST.UTL.PT

Dr. Daillant Jean
C.E. Saclay
SPEC
F-91191 Gif-sur-Yvette Cedex
daillant@amoco.saclay.cea.fr

Prof. Deutsch Moshe
Bar-Ilan University
Dept. of Physics
52900 Bar-Ilan
F67234@barilan.bitnet

Dr. Fontaine Philippe
Institut Curie
Lab. PSI
11 rue P. et M. Curie
75231 Paris Cedex 05
fontaine@radium.jussieu.fr

Dr. Förster Günter
Martin Luther Univ. Halle
Institut Physik Chem.
Mühlpforte 1
D-06108 Halle

Prof. Gallet François
ENS
Labo. de Physique Statistique
24 rue Lhomond
75231 Paris Cedex 05
gallet@physique.ens.fr

Prof. Hochapfel Ambjörg
Université René Descartes
CRPB
45 rue des Saints Pères
75270 Paris
grpb@bisance-citi2.fr

Dr. Gompper Gerhard
MPI-KG
Kantstrasse 55
D-14513 Teltow-Seehof
gompper@micro.stat.physik.uni-muenchen.de

Dr. Gourier Christine
C.E. Saclay
SPEC
91191 Gif sur Yvette Cedex
gourier@amoco.saclay.cea.fr

Dr. Graner François
CNRS
URA 8 ,Lab. de Spectro. Physique
BP 87
38042 Saint Martin d'Hères
graner@grenet.fr

Dr. Guenoun Patrick
C.E. Saclay
SPEC
91191 Gif-sur-Yvette Cedex
guenoun@amoco.saclay.cea.fr

Dr. Herminghaus Stephan
Universität Konstanz
Fakultät für Physik Universitätstrasse 10
D-78434 Konstanz
sherming@spock.physik.uni-konstanz.de

Prof. Huang Huey
Rice University
Physics Department
TX 77251-1892 Houston
huang@ion.rice.edu

Dr. Jacobs Karin
Universität Konstanz
Fakultät für Physik
Postfach 5560
D-78434 Konstanz
karin.jacobs@uni-konstanz.de

Dr. Jada Amane
CNRS
CRPCSS
68200 Mulhouse

Dr. Kaganer Vladimir
Russian Academy of Sciences
Institute of Crystallography, Leninskii Pr. 59
117333 Moscow
kaganer@theory.rc.ac.ru

Dr. Karaborni Sami
Koninklijke/Shell Laboratorium
PO Box 38000
1030 BN Amsterdam
karaborni@ksla.nl

Prof. Knobler Charles M.
UCLA
Dept. of Chem. and Biochem.
CA 90024-1569 Los Angeles
cmk@argon.chem.ucla.edu

Dr. Kornyshev Alexei
Inst. für Energieverfahrenstechnik
Forschungszentrum Jülich GmbH
Postfach 1913
D-52425 Jülich
RBE016@djukfa11.bitnet

Dr. Kramarenko Elena
Moscow State University
Polymer Physics Laboratory
117234 Moscow
kram@polly.phys.msu.su

Dr. Lacaze Emmanuelle
CNRS
Solid Physics group
2 Place Jussieu Tour 23
75251 Paris
lacaze@gps.jussieu.fr

Dr. Lang Philippe
CNRS
Labo. des Matériaux Moléculaires
2-8 rue H. Dunant
94320 Thiais

Dr. Leclerc Emmanuel
C.E. Saclay
Labo. Léon Brillouin ,
Bât. 563
91191 Gif sur Yvette Cedex
LECLERC@bali.saclay.cea.fr

Dr. Lee Lay-Theng
C.E. Saclay
Labo. Léon Brillouin ,
Bât. 563
91191 Gif sur Yvette Cedex
laythen@bali.saclay.cea.fr

Prof. Léger Liliane
Collège de France
Phys. de la Matière Condensée
11 Place Marcelin Berthelot
75231 Paris Cedex 05

Dr. Lesieur Pierre
C.E. Saclay
SCM/LURE
91191 Gif sur Yvette

Dr. Ligoure Christian
Université Montpellier 2,
CNRS, Case 26
Place Eugène Bataillon
34035 Montpellier Cedex 05
smo@gdpc1.univ-montp2.fr

Dr. Maldonado Amir
ENS
Labo. de Physique Statistique
24 rue Lhomond
75231 Paris
amir@physique.ens.fr

Dr. Mann Elizabeth
Institut Charles Sadron
6 rue Boussingault
67083 Strasbourg
mann@ics-crm.u-stasbg.fr

Prof. Mann Jr J.A.
Case West. Reserve Univ.
Dept. of Chemical Engineering
OH 44106 Cleveland
JAM12@PO.CWRU.EDU

Dr. Marchand Jean-Pierre
Rhône Poulenc
RP Industrialisation CRIT-C
85 Av. des Frères Perret, BP62
69192 Saint Fons Cedex

Dr. Marques Carlos
Institut Charles Sadron
6 rue Boussingault
67083 Strasbourg
marques@ics-crm.u-stasbg.fr

Dr. Meunier Jacques
ENS
Labo. de Physique Statistique
24 rue Lhomond
75231 Paris
jmeunier@physique.ens.fr

Dr. Miller Reinhard
MPI
Kolloid u. Grenzflächenforsch.
Rudower chaussee 5
D-92489 Berlin Adlershof
miller@mpikg.fta-berlin.de

Dr. Mougin Nathalie
L'Oréal
1 Av. E. Schueller
93600 Aulnay sous Bois

Dr. Muller Pierre
Institut Charles Sadron
6 rue Boussingault
67083 Strasbourg
muller@ics-crm.u-stasbg.fr

Dr. Nguyen T. Q.
EPFL
PHB- Ecublens
CH-1015 Lausanne

Dr. Ocko Benjamin
Brookhaven National Lab.
510B
NY 11973 Upton
ben@solids.phy.bnl.gov

Dr. Peltonen Jouko
Abo Akademi University
Dept of Physical Chemistry,
Porthansgatan 3
FIN-20500 Turku
JPELTONEN@ABO.FI

Dr. Perez Eric
ENS
Labo. de Physique Statistique
24 rue Lhomond
75231 Paris Cedex 05
perez@physique.ens.fr

Prof. Pincus Philip
UCSB
Physics Dept.
CA 93106 Santa Barbara
FYL@SBPHY.PHYSICS.UCSB.EDU

Dr. Pieranski Pawel
Université Paris Sud - CNRS
Labo. Physique des Solides
91405 Orsay Cedex

Dr. Prost Jacques
ESPCI
Physico chimie théorique
10 rue Vauquelin
75231 Paris Cedex 05
jacques@turner.espci.fr

Dr. Radlinska Ewa
ESPCI
Physico-Chimie Macromolécul.
10 rue Vauquelin
75231 Paris Cedex 05
ewa@physique.ens.fr

Dr. Raphaël Elie
Collège de France
Phys. de la Matière Condensée
11 Place Marcelin Berthelot
75231 Paris Cedex 05

Dr. Reiter Gunther
CNRS
Physico-Chimie des Surf.Solides
68200 Mulhouse
reiter@bali.saclay.cea.fr

Dr. Riegler Hans
MPI
Kolloid und Grenzflächenforschung
Rudower Chaussee 5
12489 Berlin Adlershof

Dr. Rieu Jean-Paul
CNRS
URA 8 , Spectrométrie Physique
BP 87
38402 Saint Martin d'Hères
jp@phase3.grenet.fr

Dr. Rivière Sophie
ENS
Labo. de Physique Statistique
24 rue Lhomond
75231 Paris Cedex 05
rivière@physique.ens.fr

Dr. Saint-Jalmes Arnaud
ENS
Labo. de Physique Statistique
24 rue Lhomond
75231 Paris Cedex 05

Dr. Scalas Enrico
Universität Mainz
Instit. Physikalische Chemie
Welder-weg 11
55099 Mainz
scalas@mwald5.chemie.uni-mainz.de

Dr. Schreyeck Gabriel
Institut Charles Sadron
6 rue Boussingault
67083 Strasbourg Cedex

Dr. Seifert Udo
IFF
Theorie II - KFA
Forschungszentrum
D-52425 Jülich
useifert@iff072.iff.kfa-juelich.de

Dr. Sens Pierre
Institut Charles Sadron
6 rue Boussingault
67083 Strasbourg Cedex
sens@ics-crm.u-stasbg.fr

Dr. Seul Michael
AT&T Bell Labs .
600 Mountain Avenue
PO Box 636
NJ 07974 Murray Hill
seul@physics.att.com

Dr. Shahidzadeh Noushine
Université P. et M. Curie
Génie des Procédés Plasmas
11 rue P. et M. Curie
75231 Paris Cedex

Dr. Shi An-Chang
Xerox
Xerox research centre of Canada
2660 Speakman drive
L5K 2L1 Ontario Mississauga
shi.xrcc@xerox.com

Dr. Steiner Ulrich
Weizmann Institute of Science
Physics of Complex Systems
76100 Rehovot
bpstein@weizmann.weizmann.ac.il

Prof. Sunamoto Junzo
Kyoto University
Division of Synthetic Chemistry
Sakyo-ku, Yoshida Hommachi
606-01 Kyoto
g54111@sakura.kudpc.kyoto-u.ac.jp

Prof. Szleifer Igal
Purdue University
Dept. of Chemistry
IN 47907 West Lafayette
igal@shemesh.chem.purdue.edu

Dr. Tannenbaum Rina
University of Minnesota
Dept. of Chemical Engineering
421 Washington Avenue S.E.
55455 MN Minneapolis
rinatan@epx.cis.umn.edu

Dr. Tiberg Fredrik
Lund University
Physical Chemistry 1,
PO Box 124
22100 Lund
Fredrik.Tiberg@fkem1.lu.se

Dr. Turner Matthew
University of Cambridge
Cavendish Laboratory Madingley Road
CB3 0HE Cambridge
mst10@cus.cam.ac.uk

Prof. Urbach Wladimir
CNRS
Labo. de Physique Statistique
24 rue Lhomond
75231 Paris Cedex 05
urbach@merlin.ens.fr

Dr. Valaulikar Balchandra
ENS
Labo. de Physique Statistique
24 rue Lhomond
75231 Paris Cedex 05
babu@physique.ens.fr

Dr. Valignat Marie Pierre
Collège de France
Phys. de la Matière Condensée
11 Place Marcellin Berthelot
75231 Paris Cedex 05
valignat@ext.jussieu.fr

Dr. Vollhardt Dieter
MPI
Kolloid und Grenzflächenforschung
Rudower chaussee 5
D-12489 Berlin Adlershof
vollh@mpikg.FTA-Berlin.de

Dr. Williams Claudine
Université Paris Sud
CNRS, LURE
Bat 209d
91405 Orsay Cedex
williams@lure.u-psud.fr

Dr. Wong Kenneth
Rhône Poulenc Recherches
52 rue de la Haie Coq
93308 Aubervilliers Cedex

Dr. Wu David
UCSB
Dept. of Chemical Engineering
UCSB
CA 93106-5080 Santa Barbara
wu@cuda.ucsb.edu

Dr. Zeghal Mehdi
Université d'Orsay
Labo. de Physique des Solides
Bât. 510
91405 Orsay Cedex

Dr. Zhulina Ekaterina
Russian Academy of Sciences
Instit. of Macromol. Compounds
Bolshoy prospekt 31
199004 St Petersburg
katya@macro.lgu.spb.su